JOURNAL OF BIOLOGICAL REGULATORS & HOMEOSTATIC AGENTS
Volume 32, No. 6, November - December, 2018

CONTENTS

JOURNAL OF BIOLOGICAL REGULATORS & HOMEOSTATIC AGENTS Vol. 32, no. 6, 1345-1347 (2018)

EDITORIAL

STRESS, INFLAMMATION AND NATURAL TREATMENTS

T.C. THEOHARIDES[1,2,3,4] and M. KAVALIOTI[5*]

*[1]Laboratory of Molecular Immunopharmacology and Drug Discovery, Department of Immunology and Departments of [2]Internal Medicine, [3]Psychiatry and [4]Sackler School of Graduate Biomedical Sciences, Tufts University School of Medicine, Boston, MA, USA; [5]Department of Biomedical Sciences, University of Greenwich, UK - *present address: BiomedAdvice, LLC, Boston, MA, USA*

Received September 15, 2018 - Accepted October 18, 2018

Stress and inflammation have become the curses of our times and are the main pathogenetic factors in multiple diseases that are often comorbid and include allergies and asthma, eczema and psoriasis, fibromyalgia syndrome, mast cell activation syndrome, irritable bowel syndrome, myalgic encephalomyelitis/chronic fatigue syndrome and autism spectrum disorder (ASD). Unfortunately, there are no effective drugs. Cross-talk between mast cells and microglia in the hypothalamus and amygdala could explain stress-induced inflammation. We recently showed that the "alarmin" IL-33 could play a major role through its synergistic action with the neuropeptide substance P to stimulate human mast cell secretion of the pro-inflammatory molecules IL-1β, TNF and VEGF. A new formulation using pure luteolin with Ashwagandha has now been developed and could be of significant benefit to patients suffering from these diseases.

Stress has become the curse of our times, affecting psychosocial, behavioral and general health aspects (1). Geopolitical, socioeconomic and health-related stress has been expanding, leading to an unusually high incidence of suicide and other related neuropsychiatric problems, with tremendous impact on the quality of life, workspace and the economy. For instance, the annual health burden of stress in the US has been estimated at $900 billion (https://www.healthline.com/health-news/stress-health-costs, visited on September 17, 2018). In addition, many other medical conditions are negatively impacted by stress (2), especially allergies and asthma (3), cardiovascular disease (4), fibromyalgia (5, 6), mast cell activation syndrome (7), irritable bowel syndrome (8), migraine (9), multiple sclerosis (10), myalgic encephalomyelitis/chronic fatigue syndrome (11) and autism spectrum disorder (ASD) (12). These conditions add another $400 billion to the annual US health burden; the annual cost of ASD alone was estimated at $268 billion for 2015 and was projected at $416 billion in 2025 (13).

We have demonstrated that a key pathogenetic factor in how stress affects these conditions is the ability of corticotropin-releasing hormone or factor (CRH or CRF), the first hormone secreted from the brain under stress (14) to stimulate the unique tissue immune cell and the mast cell (7), the brain immune cells, the microglia (15). Moreover, mast cells themselves secrete CRH, further potentiating the stress-inflammation axis (16). Mast cells respond to numerous neuroimmune triggers (17) and have

Key words: anxiety, ashwagandha, inflammation, luteolin, natural molecules, stress

Mailing address:
T.C. Theoharides, MS, MPhil, PhD, MD
Department of Immunology, Tufts University School of Medicine,
136 Harrison Avenue, Suite J 304, Boston, MA 02111, USA
Tel.: +1 617 636 6866 Fax: +1 617 636 2456
e-mail: theoharis.theoharides@tufts.edu

0393-974X (2018)

emerged as key immunoregulatory cells (18). An important new finding is that the "alarmin" IL-33 (19) has a synergistic action with the neuropeptide substance P to stimulate human mast cells to secrete impressive amounts of the pro-inflammatory molecules VEGF (20), TNF (21), and IL-1β (22).

Unfortunately, there are no effective drugs to block either the secretion of, or the action of CRH, nor the activation of the mast cells and the microglia. Any formulations that may inhibit these processes would be of great prophylactic and therapeutic importance. We recently reported on the ability of the natural flavonoid luteolin (tetrahydroxyflavone, NOT to be confused with the carotenoid lutein) (23) to inhibit activation of both mast cells (24, 25) and microglia (26), as well as the secretion of TNF (21) and IL-1β (22). Luteolin also has neuroprotective properties (27). It would, therefore, be desirable to combine luteolin with other natural molecules that have anti-stress Traditional Chinese Medicine (TCM) has used various methods in order to relieve stress that ensure the free flow of Liver-Qi (the flow of energy through the liver). TCM includes a number of natural molecules with reported anti-stress activity (Table I).

Table I. *Chinese anti-stress molecules.*

- Ashwagandha
- Cynorium herb
- Dang gui root
- Duanwood reishi
- Ginseng
- Ju Hua (Chrysanthemum tea Rehmannia root)
- Jujube date
- Licorice root
- Polygonum root
- Polyrachis ant
- Yehmannie reishi

There is little hard evidence of the effectiveness of these compounds, except for Ginseng and especially the Ayurvedic herb Ashwaganda (Withania somnifera) (28), which has GABAergic activity (29). Other molecules with calming properties include valerian tea extract, hydroxybutyrate, 5-hydroxytryptophan (5-HTP) or S-adenosyl methionine (SAMe).

A new formulation of the anti-inflammatory luteolin (PureLut™) with Ashwagandha has now been developed (www.algonot.com) and will be available soon under the trade name NormoStres™.

Disclosure: TCT is the recipient of US Patent No 7,906,153 covering the use of flavonoids in neuroinflammatory conditions. The authors report no conflicts of interest.

REFERENCES

1. Schneiderman N, Ironson G, Siegel SD. Stress and health: psychological, behavioral, and biological determinants. Annu Rev Clin Psychol 2005; 1:607-28.
2. Theoharides TC. Atopic conditions in search of pathogenesis and therapy. Clin Ther 2013; 35(5):544-47.
3. Theoharides TC, Enakuaa S, Sismanopoulos N, et al. Contribution of stress to asthma worsening through mast cell activation. Ann Allergy Asthma Immunol 2012; 109(1):14-9.
4. Theoharides TC, Sismanopoulos N, Delivanis DA, Zhang B, Hatziagelaki EE, Kalogeromitros D. Mast cells squeeze the heart and stretch the gird: Their role in atherosclerosis and obesity. Trends Pharmacol Sci 2011; 32(9):534-42.
5. Theoharides TC, Tsilioni I, Arbetman L, et al. Fibromyalgia, a syndrome in search of pathogenesis and therapy. J Pharmacol Exp Ther 2015; 355(2):255-63.
6. Mastrangelo F, Frydas I, Ronconi G, et al. Low-grade chronic inflammation mediated by mast cells in fibromyalgia: role of IL-37. J Biol Regul Homeost Agents 2018; 32(2):195-98.
7. Theoharides TC, Valent P, Akin C. Mast cells, mastocytosis, and related disorders. N Engl J Med 2015; 373(2):163-72.
8. Theoharides TC. Mast cells in irritable bowel syndrome and ulcerative colitis: function not numbers is what makes all the difference. Dig Dis Sci 2014; 59(5):897-98.
9. Theoharides TC, Donelan J, Kandere-Grzybowska K, Konstantinidou A. The role of mast cells in migraine pathophysiology. Brain Res Brain Res Rev

2005; 49(1):65-76.
10. Karagkouni A, Alevizos M, Theoharides TC. Effect of stress on brain inflammation and multiple sclerosis. Autoimmun Rev 2013; 12(10):947-53.
11. Hatziagelaki E, Adamaki M, Dimitriadis G, Tsilioni I, Theoharides TC. Myalgic encephalomyelitis/ chronic fatigue syndrome-metabolic diseases or disturbed homeostasis? JPET 2018; In press.
12. Theoharides TC., Tsilioni I, Patel AB, Doyle R. Atopic diseases and inflammation of the brain in the pathogenesis of autism spectrum disorders. Transl Psychiatry 2016; 6(6):e844.
13. Leigh JP, Du J. Brief Report: Forecasting the Economic Burden of Autism in 2015 and 2025 in the United States. J Autism Dev Disord 2015; 12:4135-39.
14. Theoharides TC, Donelan JM, Papadopoulou N, Cao J, Kempuraj D, Conti P. Mast cells as targets of corticotropin-releasing factor and related peptides. Trends Pharmacol Sci 2004; 25(11):563-68.
15. Zhang X, Wang Y, Dong H, Xu Y, Zhang S. Induction of microglial activation by mediators released from mast cells. Cell Physiol Biochem 2016; 38(4):1520-31.
16. Kempuraj D, Papadopoulou NG, Lytinas M et al. Corticotropin-releasing hormone and its structurally related urocortin are synthesized and secreted by human mast cells. Endocrinology 2004; 145:43-48.
17. Theoharides TC. Neuroendocrinology of mast cells: Challenges and controversies. Exp Dermatol 2017; 26(9):751-59.
18. Caraffa A, Conti C, Ovidio D et al. New concepts in neuroinflammation: mast cells pro-inflammatory and anti-inflammatory cytokine mediators. J Biol Regul Homeost Agents 2018; 32(3):449-54.
19. Theoharides TC, Petra AI, Taracanova A, Panagiotidou S, Conti P. Targeting IL-33 in autoimmunity and inflammation. J Pharmacol Exp Ther 2015; 354(1):24-31.
20. Theoharides TC, Zhang B, Kempuraj D et al. IL-33 augments substance P-induced VEGF secretion from human mast cells and is increased in psoriatic skin. Proc Natl Acad Sci U S A 2010; 107(9):4448-53.
21. Taracanova A, Alevizos M, Karagkouni A, et al. SP and IL-33 together markedly enhance TNF synthesis and secretion from human mast cells mediated by the interaction of their receptors. Proc Natl Acad Sci U S A 2017; 114(20):E4002-9.
22. Taracanova A, Tsilioni I, Conti P, Norwitz ER, Leeman SE, Theoharides TC. Substance P and IL-33 administered together stimulate a marked secretion of IL-1beta from human mast cells, inhibited by methoxyluteolin. Proc Nat Acad Sci 2018; 115(40):E9381-90.
23. Middleton E Jr, Kandaswami C, Theoharides TC. The effects of plant flavonoids on mammalian cells: implications for inflammation, heart disease, and cancer. Pharmacol Rev 2000; 52(4):673-751.
24. Weng Z, Patel AB, Panagiotidou S, Theoharides TC. The novel flavone tetramethoxyluteolin is a potent inhibitor of human mast cells. J Allergy Clin Immunol 2015; 135(4):1044-52.
25. Patel AB, Theoharides TC. Methoxyluteolin Inhibits Neuropeptide-stimulated proinflammatory mediator release via mTOR activation from human mast cells. J Pharmacol Exp Ther 2017; 361(3):462-71.
26. Patel AB, Tsilioni I, Leeman SE, Theoharides TC. Neurotensin stimulates sortilin and mTOR in human microglia inhibitable by methoxyluteolin, a potential therapeutic target for autism. Proc Natl Acad Sci U S A 2016; 113:E7049-58.
27. Theoharides TC. Luteolin as a therapeutic option for multiple sclerosis. J Neuroinflammation 2009; 6:29.
28. Dar PA, Singh LR, Kamal MA, Dar TA. Unique Medicinal Properties of Withania somnifera: Phytochemical Constituents and Protein Component. Curr Pharm Des 2016; 22(5):535-40.
29. Savage K, Firth J, Stough C, Sarris J. GABA-modulating phytomedicines for anxiety: A systematic review of preclinical and clinical evidence. Phytother Res 2018; 32(1):3-18.

EDITORIAL

DOES THE PURINERGIC SYSTEM AFFECT EXTRACELLULAR MATRIX FUNCTIONS IN THE CENTRAL NERVOUS SYSTEM?

M. ZUCCARINI[1,2*], M. CARLUCCIO[1,2*], S. ZIBERI[1,2], P. GIULIANI[1,2], S. BUCCELLA[1,2], C. CONTI[3], R. CICCARELLI[1,2] and P. DI IORIO[1,2]

[1]Department of Medical, Oral and Biotechnological Sciences, "G. d'Annunzio" University of Chieti-Pescara, Chieti, Italy; [2]Aging Research Center, Ce.S.I.Me.T., "G. d'Annunzio" University Foundation, Chieti, Italy; [3]Department of Psychological, Health, and Territorial Sciences, "G. d'Annunzio" University of Chieti-Pescara, Chieti, Italy

Received June 6, 2018 – Accepted August 27, 2018

*These Authors contributed equally to this work

Exracellular matrix (ECM) consists of a plethora of proteins and polysaccharides, which aggregate into an organized network connected to the surface of the producing cells. It is structurally and functionally present in all components of tissues and organs and represents the substrate on which cells adhere, migrate, proliferate and differentiate, influencing their survival, shape and function. In response to acute (trauma) or chronic (degenerative) insults, brain ECM modifies its composition and function, actively contributing to "scar forming" gliosis or tissue degeneration/remodelling. Moreover, morphological changes in dendritic spines associated with extracellular matrix remodeling play key roles in rewiring synaptic circuitry pertinent to memory formation. In the present report, we collected the main acquisitions on the functional interplay between ECM alterations and the adenine-/guanine-based purine system with particular regard on how purine compounds and their respective receptors may affect and be affected by changes of the cerebral ECM.

Composition and function of extracellular matrix in normal brain

The extracellular matrix (ECM) composition of the central nervous tissue and spinal cord, widely reviewed in a recent excellent report (1), differs from that of peripheral tissues as it is richer in glycoproteins and proteoglycans. These molecules include glycoproteins such as tenascins, mainly tenascin-C (TnC) and tenascin-R (TnR), and chondroitin sulphated proteoglycans (CSPGs), stabilized by link proteins (known as hyaluronan and proteoglycan link protein, HAPLN).

Further matrix components include molecules found in the basal laminae such as laminin, fibronectin and collagen. Laminins are heterotrimeric glycoprotein cell adhesion molecules forming a substratum for neuronal migration and axonal pathfinding in development. Fibronectin is a large dimeric protein composed of three distinct tandem repeats (I, II and III), wherein there are functional domains like laminin, enabling polymerization and interactions with cell surface receptors and other ECM components. It is now accepted that fibronectin plays a central role in migration, morphogenesis and proliferation (2).

Key words: brain extracellular matrix, acute and chronic neurodegenerative diseases, extracellular purines, guanosine and guanine

Mailing address:
Prof. Renata Ciccarelli,
Department of Medical,
Oral and Biotechnology Sciences,
Section of Pharmacology,
Via dei Vestini 29, 66100 Chieti, Italy
Tel.: +39 0871 3554015 - Fax: +39 0871 3554011
e-mail: renata.ciccarelli@unich.it

0393-974X (2018)

DISCLOSURE: ALL AUTHORS REPORT NO CONFLICTS OF INTEREST RELEVANT TO THIS ARTICLE.

In adult brain, the ECM helps in maintaining the shape, the correct function and the plasticity of the nervous tissue, which are important for synaptic and network stabilization and homeostasis.

Composition and function of extracellular matrix (ECM) in injured brain

After brain injury, the composition of the ECM dramatically changes, this alteration mostly depending on the type of cells concurring to damage repair. In spinal trauma or cortical stab injuries there is a large contribution of fibroblasts deriving from disrupted meninges, which secrete collagen, fibronectin and laminin, and also of endothelial cells (3). Astrocytes, activated by a pro-inflammatory environment, first proliferate and then become hypertrophic, extending processes and exhibiting changes in gene expression, i.e. the increased expression of glial fibrillary acidic protein (GFAP) (4). Reactive astrocytes have important roles in restoring extracellular homeostasis following injury, by releasing pro- and anti-inflammatory cytokines, and by promoting scar formation.

Also microglia and oligodendrocyte precursor cells (OPCs) concur to the injury response and glial scar formation. Upon injury, microglia proliferate and undergo morphological changes, release cytokines, reactive oxygen species/free radicals and also acquire a phagocytic phenotype (5). Despite the beneficial role in maintaining homeostasis and sealing-off areas of central nervous sytem (CNS) damage, glial scar formation is also associated with regeneration failure. The latter has been partially attributed to the presence of the dense barrier of reactive astrocytes that would prevent growth cone elongation, but is also due to the accumulation of a number of inhibitory ECM molecules, in particular CSPGs (6). Therefore, strategies able to manipulate the ECM may be applied following brain or spinal cord injuries.

Composition and function of extracellular matrix in neurodegenerative diseases

The ECM molecules may play an important role also in the pathogenesis of various CNS diseases. In particular, ECM components are implicated in the pathology of Alzheimer's disease (AD). Proteoglycans co-localize with amyloid β deposits and are implicated in amyloid β fibrillogenesis. Accordingly, the proteolytic degradation of amyloid β by apolipoprotein E is impaired by Heparan sulfate proteoglycan (HSPG) expression within plaques (7).

The ECM is also involved in the regulation of OPC migration, proliferation and differentiation into myelinating oligodendrocytes. In particular, laminin-2, the expression of which is upregulated in multiple sclerosis lesions, is implicated in OPC survival, differentiation and extension of myelinating processes via integrin, contactin and dystroglycan receptor interactions. In contrast, fibronectin expression is increased and impairs remyelination (8). Thus, it could be of great interest to determine whether ECM modification strategies in different acute or chronic CNS disorders may improve disease pathology and lead to functional repair.

Role of adenine- and guanine-based purines in the function of extracellular matrix

Adenine- and guanine-based purines are part of the so-called "purinome" consisting of nucleotides, nucleosides, nucleobases, their derivatives, and different classes of purine receptors [P1 and P2 receptors activated by adenosine or adenosine triphosphate (ATP)/adenosine diphosphate (ADP) nucleotides, respectively], bi-directional transporters and enzymes involved in purinergic transmission (9). These enzymes comprise the family of nucleotide hydrolases, i.e. ectonucleoside triphosphate diphosphohydrolase, ecto-nucleotide pyrophosphatase/phosphodiesterase, ecto-5'-nucleotidase, alkaline phosphatases (AP), adenosine deaminase (ADA), purine nucleoside phosphorylase (PNP), guanine deaminase, xanthine oxidase (10, 11).

To date, the role of purines in the ECM organization in the CNS has been poorly investigated.

Neurons and astrocytes, and in part microglia, express purine receptor subtypes involved in synaptic transmission, neuronal-astroglial communication, proliferation, synaptic plasticity, differentiation and migration (12).

A characteristic hallmark of neurodegenerative disorders, i.e. Alzheimer's disease and Parkinson's

disease, is the alteration of ECM accompanied by a decline in neural transmission, wherein guanine-based purines stand out as key regulators of neuron-glia interactions (13, 14).

In glial cells, PC12 and hippocampal neurons, guanosine (GUO) and guanosine monophosphate (GMP) have been shown to exert a neurotrophic and neuroprotective activity by preventing glutamate-mediated excitotoxicity (15, 16). Furthermore, GUO has been demonstrated to induce neurite outgrowth and dendrite arborization, likely by inducing nerve-growth factor (NGF) release (17). Neurite outgrowth has been reported to be also affected by ECM components such as laminin and fibronectin, the latter exerting a neuroprotective effect on neural cells by interacting with integrins and many neurotrophic factors. Decker and coworkers (2007) investigated the role of guanine derivatives in ECM modulation and demonstrated that extracellular GMP and GUO were able to alter ECM astrocyte organization but had no effect on laminin and fibronectin expression levels (18). Importantly, as GMP is hydrolyzed to GUO in neural cells in a few minutes, it is plausible that its effect is due to its conversion into GUO. Specifically, GUO would interact with a Gi/o-protein coupled receptor and activate different signaling pathways [i.e. Protein Kinase C (PKC), Protein Kinase A (PKA); Mitogen-Activated Protein Kinase (MAPK)/Extracellular signal-Regulated Kinase (ERK), Ca2+/Calmodulin-dependent protein Kinase II (CaMKII)] all responsible for laminin and fibronectin organization from punctuate to fibrous. In this study, cell treatment with GMP or GUO promoted an increased number of cerebellar neurons in a neuron-astrocyte coculture model, without altering the neuritogenesis or the proliferation rate of neurons, this ECM reorganization being favorable towards neuron-astrocyte connections.

Interestingly, we found that, in C6 glioma cells, guanine (GUA) treatment for 24 up to 48 hours induced a marked increase in fibronectin but not laminin expression level (unpublished data), and this effect might be responsible for its role in synaptic plasticity. Indeed, as we previously reported, GUA would activate Phosphoinositide 3-Kinase (PI3K)/_ Protein Kinase B (PKB)/Nitric Oxide (NO)/soluble Soluble Guanylyl Cyclase (sGC)/cyclic GMP (cGMP)/Protein Kinase G (PKG)/ERK signaling cascade and exert a mnesic effect in working memory (19, 20). As for GUO, GUA plausibly activated a Gi/o-protein coupled receptor since its effect was prevented by cell pre-treatment with pertussis toxin (21).

Fibronectin is able to induce cell survival and neuronal differentiation by activating MAPK signaling pathway via α5β1 and α5β3 receptors in cerebrovascular endothelial cells (22), or to promote axonal regeneration in adult white matter.

Noteworthy, fibronectin plays a key role in the pathogenesis of neuropathic pain following peripheral nerve injury. Indeed, fibronectin seems to stimulate microglia to induce Interferon Regulatory Factor-5 (IRF5) which, in turn, would activate P2X4R expression. In these cells, fibronectin binds to α5β1 integrin receptor and activate PI3K/PKB/MAPK/ERK signaling cascade resulting in enhanced IRF5 and increased P2X4R *de novo* expression (23).

After spinal cord injury, fibronectin stimulates spinal cord astrocyte proliferation by enhancing P2Y1-mediated PI3K/PKB/ERK/cAMP Response Element-Binding protein (CREB)/Signal Transducer and Activator of Transcription 3(STAT3) signaling cascade or ATP-induced release of arachidonic acid and prostaglandin-E2 (24). In a model of CNS trauma, P2 and P1 receptor activation by increased extracellular ATP or uridine triphosphate (UTP), elicited an increase of thrombospondin (TSP)-1 expression, a multidomain glycoprotein promoting synaptogenesis via p38MAPK/PKB pathway (25).

Overwhelming experimental evidence points to a significant role of purine-converting enzymes in ECM organization, namely ecto-5'-nucleotidase or CD73 and guanine deaminase (also called cypin).

CD73 is a bifunctional Glycosyl Phosphatidyl Inositol (GPI)-anchored membrane protein with an enzymatic activity (conversion of ribo- and deoxyribonucleoside 5'-monophosphates to their corresponding nucleosides) (26) and with a non-enzymatic activity, being a membrane receptor for extracellular matrix protein. Intriguingly, depending on which ECM component it interacts with, CD73 might negatively or positively affect cell migration

or adhesion. Indeed, CD73 binding to tenascin C or fibronectin and laminin would trigger cell migration or cell adhesion, respectively (27).

In a similar way, compared to CD73, guanine deaminase or cytosolic PSD-95 interactor (cypin) shows a bi-functional activity, either metabolizing guanine into xanthine or accounting for ECM alterations. This enzyme is considered one of the "intrinsic factors" involved in dendrite arborization and microtubule assembly, as it directly binds tubulin heterodimers, thus promoting the microtubule assembly via cytoskeletal rearrangement (28). These authors showed that knocked down of cypin protein levels by using a mutant RNA (U1 small nuclear RNA) decreased dendrite number in neurons.

Strong evidence from studies of neurite outgrowth supports the hypothesis that both adenine- and guanine-based nucleosides are responsible for Brain-Derived Neurotrophic Factor (BDNF)-mediated increase of dendrite branching. That is, activation of A2AR with the selective agonist CGS 21680 stimulated neuronal regeneration after brain injury (29).

Neurotrophic factors, such as BDNF or NGF, have been shown to be modulated by the nucleoside GUO. Specifically, GUO would enhance neurite outgrowth in PC12 cell line via Heme Oxygenase (HO-1)/ Carbon Monoxide (CO)/sGC/cGMP signaling pathway (30). Based on the aforementioned data, GUA would activate cGMP signaling as much as GUO but their effects rely on different neurological functions. Indeed, if cGMP activated by GUA is associated to its mnesic effect and involves NO production, cGMP derived from GUO signaling is part of a neuroprotective program after brain injury events, i.e. ischemic stroke, oxygen and glucose deprivation, neuroinflammation.

In this work, we provide an updated overview of studies on ECM-related CNS events under pathophysiological conditions and we explored the potential neuroprotective mechanism of guanine-based purines.

In this regard, it is conceivable that guanine derivatives elicit important functional roles in both the central and the peripheral nervous system through the main activation of PI3K/PKB/ERK1/2 signaling, and by engaging cGMP more than cyclic 3′,5′-adenosine monophosphate (cAMP) as second messenger in these effects. GUO and GUA emerged as the major players in this complex network, acting as extracellular signaling molecules triggering a series of cellular events leading to neuroprotection or cognitive improvement, respectively. These effects are likely the result of an interaction of guanine derivatives to metabotropic receptors coupled to Gi/o-protein since they are reversed by pertussis toxin pre-treatment. Moreover, the presence has been reported of a single high affinity binding site for [3H]-GUO in rat brain membranes (21) that would suggest the existence of specific transmembrane receptors, not yet identified also for guanine-based purines.

In conclusion, the contributions of guanine-based purines to ECM composition are embodied in different functional roles but all converge on favoring a dynamic neuron-glia network, which is a common feature of many brain-related disorders, i.e. Alzheimer's disease or Parkinson's disease. For this reason, uncovered molecular mechanisms underlying purine-mediated ECM modulation may bring about a greater understanding of identifying a potential pharmacological target for some age-related and neurological disorders.

ACKNOWLEDGEMENTS

The study was in part supported by grants to P. Di I. and R.C. from the Italian Government and University of Chieti-Pescara (Research Funds ex 60%).

REFERENCES

1. Song I, Dityatev A. Crosstalk between glia, extracellular matrix and neurons. Brain Res Bull 2018; 136:101-8.
2. Singh P, Carraher C, Schwarzbauer JE. Assembly of fibronectin extracellular matrix. Annu Rev Cell Dev Biol 2010; 26:397-419.
3. Shearer MC, Fawcett JW. The astrocyte/meningeal cell interface – a barrier to successful nerve regeneration? Cell Tissue Res 2001; 305:267-73.
4. Sun D, Jakobs TC. Structural remodeling of astrocytes in the injured CNS. Neuroscientist 2012; 18:567-88.
5. Streit WJ, Walter SA, Pennell NA. Reactive

microgliosis. Prog Neurobiol 1999; 57:563-81.
6. Fitch MT, Silver J. CNS injury, glial scars, and inflammation: inhibitory extracellular matrices and regeneration failure. Exp Neurol 2008; 209:294-301.
7. Ariga T, Miyatake T, Yu RK. Role of proteoglycans and glycosaminoglycans in the pathogenesis of Alzheimer's disease and related disorders: amyloidogenesis and therapeutic strategies – a review. J Neurosci Res 2010; 88:2303-15.
8. Stoffels JM, de Jonge JC, Stancic M, et al. Fibronectin aggregation in multiple sclerosis lesions impairs remyelination. Brain 2013; 136 (Pt 1):116-31.
9. Burnstock G, Krugel U, Abbracchio MP, Illes P. Purinergic signalling: from normal behavior to pathological brain function. Prog Neurobiol 2011; 95:229-74.
10. Yegutkin GG. Nucleotide- and nucleoside-converting ectoenzymes: Important modulators of purinergic signalling cascade. Biochim Biophys Acta 2008; 1783(5):673-94.
11. Giuliani P, Zuccarini M, Buccella S, et al. Evidence for purine nucleoside phosphorylase (PNP) release from rat C6 glioma cells. J Neurochem 2017; 141:208-21.
12. Neary JT, Zimmermann H. Trophic functions of nucleotides in the central nervous system. Trends Neurosci 2009; 32:189-98.
13. Di Liberto V, Mudò G, Garozzo R, et al. The guanine-based purinergic system: the tale of an orphan neuromodulation. Front Pharmacol 2016; 7:158.
14. Lanznaster D, Mack JM, Coelho V, et al. Guanosine prevents anhedonic-like behavior and impairment in hippocampal glutamate transport following amyloid-β1-40 administration in mice. Mol Neurobiol 2017; 54(7):5482-96.
15. Dal-Cim T, Ludka FK, Martins WC, et al. Guanosine controls inflammatory pathways to afford neuroprotection of hippocampal slices under oxygen and glucose deprivation conditions. J Neurochem 2013; 126:437-50.
16. Di Iorio P, Ballerini P, Traversa U, et al. The antiapoptotic effect of guanosine is mediated by the activation of the PI 3-kinase/AKT/PKB pathway in cultured rat astrocytes. Glia 2004; 46:356-68.
17. Gysbers JW, Rathbone MP. Guanosine enhances NGF-stimulated neurite outgrowth in PC12 cells. Neuroreport 1992; 3:997-1000.
18. Decker H, Francisco SS, Mendes-de-Aguiar CB, et al. Guanine derivatives modulate extracellular matrix proteins organization and improve neuron-astrocyte co-culture. J Neurosci Res 2007; 85(9):1943-51.
19. Zuccarini M, Giuliani P, Frinchi M, et al. Uncovering the signaling pathway behind extracellular guanine-induced activation of NO system: new perspectives in memory-related disorders. Front Pharmacol 2018; 21(9):110.
20. Giuliani P, Buccella S, Ballerini P, et al. Guanine-based purines modulate the effect of L-NAME on learning and memory in rats. Panminerva Med 2012; 54(S4):53-8.
21. Traversa U, Bombi, Di Iorio P, Ciccarelli R, Werstiuk ES, Rathbone MP. Specific [3H]-guanosine binding sites in rat brain membranes. Br J Pharmacol 2002; 135:969-76.
22. Hansen SM, Køhler LB, Li S, et al. NCAM derived peptides function as agonists for the fibroblast growth factor receptor. J Neurochem 2008; 106:2030e41.
23. Inoue K. Purinergic signaling in microglia in the pathogenesis of neuropathic pain. Proc Jpn Acad Ser B Phys Biol Sci 2017; 93(4):174-82.
24. Xia M, Zhu Y. Fibronectin enhances spinal cord astrocyte proliferation by elevating P2Y1 receptor expression. J Neurosci Res 2014; 92(8):1078-90.
25. Tran MD, Neary JT. Purinergic signaling induces thrombospondin-1 expression in astrocytes. Proc Natl Acad Sci U S A 2006; 103(24):93212-6.
26. Yegutkin GG. Enzymes involved in metabolism of extracellular nucleotides and nucleosides: functional implications and measurement of activities. Crit Rev Biochem Mol Biol 2014; 49(6):473-97.
27. Adzic M, Nedeljkovic N. Unveiling the role of ecto-5′-nucleotidase/cd73 in astrocyte migration by using pharmacological tools. Front Pharmacol. 2018; 9:153.
28. Akum BF, Chen M, Gunderson SI, Riefler GM, Scerri-Hansen MM, Firestein BL. Cypin regulates dendrite patterning in hippocampal neurons by promoting microtubule assembly. Nat Neurosci 2004; 7:145-52.
29. Ribeiro FF, Xapelli S, Miranda-Lourenço C, et al. Purine nucleosides in neuroregeneration and neuroprotection. Neuropharmacology 2016; 104:226-42.
30. Bau C, Middlemiss PJ, Hindley S, et al. Guanosine stimulates neurite outgrowth in PC12 cells via activation of heme oxygenase and cyclic GMP. Purinergic Signal 2005; 1:161-72.

JOURNAL OF BIOLOGICAL REGULATORS & HOMEOSTATIC AGENTS Vol. 32, no. 6, 1355-1360 (2018)

EDITORIAL

STIMULATED MAST CELLS RELEASE INFLAMMATORY CYTOKINES: POTENTIAL SUPPRESSION AND THERAPEUTICAL ASPECTS

G. VARVARA[1], L. TETTAMANTI[2], C.E. GALLENGA[3], Al. CARAFFA[4], C. D'OVIDIO[5], F. MASTRANGELO[6], G. RONCONI[7], S.K. KRITAS[8] and P. CONTI[9]

[1]Department of Medical, Oral and Biotechnological Sciences, University "G. d'Annunzio" of Chieti-Pescara, Chieti, Italy; [2]Department of Medical and Morphological Science, University of Insubria, Varese, Italy; [3]Department of Biomedical Sciences and Specialist Surgery, Section of Ophthalmology, University of Ferrara, Italy; [4]School of Pharmacy, University of Camerino, Camerino, Italy; [5]Section of Legal Medicine, Department of Medicine and Aging Sciences, "G. d'Annunzio" University of Chieti–Pescara, Italy; [6]Department of Medical Science and Biotechnology, University of Foggia, Foggia, Italy; [7]UOS Clinica dei Pazienti del Territorio, Policlinico Gemelli, Rome, Italy; [8]Department of Microbiology and Infectious Diseases, Aristotle University of Thessaloniki, Macedonia, Greece; [9]Immunology Division, Postgraduate Medical School, University of Chieti-Pescara, Chieti, Italy

Received November 2, 2018 – Accepted December 4, 2018

Mast cells (MCs) are derived from bone marrow precursors and are immune cells involved in acute and chronic inflammation. MCs are ubiquitous and play a crucial role in innate and acquired immunity. They are activated through cross-linking of their surface high affinity receptors (FcεRI), leading to immediate secretion of stored inflammatory mediators, and late production and release of pro-inflammatory cytokines/chemokines without degranulation. Therefore, MCs are important in inflammatory responses. Members of the interleukin (IL)-1 cytokine family, such as IL-1 and IL-33, and various antigens markedly increase IL-1 and tumor necrosis factor (TNF) expression and secretion from MCs. One of the latest cytokines is IL-33, an IL-1 family member acting via its ST2/IL-1R4, which has been shown to regulate MCs. IL-1 and IL-33 are cytokines found to be implicated in many inflammatory disorders including rheumatoid arthritis, atherosclerosis and psoriasis. In general, IL-1 family member cytokines play a pro-inflammatory role and increase the pathological state. IL-37 is a member of the IL-1 family with anti-inflammatory activity through inhibition of pro-inflammatory cytokines. IL-37 particularly suppresses IL-1-mediated innate inflammatory response, but also acts on the acquired immune response. IL-37 is activated by pro-inflammatory agents and cytokines, playing a protective role against inflammation. This cytokine is a natural regulator of immunity and is a therapeutic promise against inflammatory diseases. Since IL-1 is produced by and activates MCs to release IL-33 and TNF, here we hypothesize that MCs can be inhibited by IL-37 and therefore reduce their pro-inflammatory activity. However, the maturation, transport and secretion of IL-37 remain to be clarified.

Mast cells

In 1878, Paul Ehlich for the first time, identified the presence of mast cells (MCs) on aniline-based preparations. MCs derive from the hematopoietic cells, migrate and mature into various tissues including nerves, blood vessels, skin, gastrointestinal

Key words: mast cells, cytokines, inflammation

Mailing address:
Prof. Pio Conti,
Postgraduate Medical School,
University of Chieti,
Viale Unità d'Italia 73, Chieti, Italy
Tel./Fax: +39 0871 574136
e-mail: pconti@unich.it

0393-974X (2018)

DISCLOSURE: ALL AUTHORS REPORT NO CONFLICTS OF INTEREST RELEVANT TO THIS ARTICLE.

tract and brain (1). They can be stimulated by various compounds, including antigens, and IgE, neuropeptides, cytokines, drugs and toxins, but the classic activation occurs with the aggregation of the FcεRI receptor with the consequent release of inflammatory mediators including cytokines and chemokines (2). Furthermore, MCs can respond to pharmacological stimuli and compounds derived from the environment, mediating immunological and inflammatory phenomena (3). MC-mediators can be distinguished in preformed stored compounds in the cytoplasmic granules, and *de novo* synthesized mediators (Table I) (4).

The interaction of anti-IgE to the high-affinity receptor FcεRI on MC surface initiates important cascade biochemical events leading to degranulation (1).

Table I. *Biological mediators released by mast cells.*

Stored and secreted biological mediators from cytoplasmatic granules.
- Tryptase
- Histamine
- Phospholipases
- Heparin
- Chymase
- Carboxypeptidase A
- Hydrolases
- Peroxidases
- Kinogenases
- TNF
De novo synthesized
- Arachidonic acid products: LTB4, LTC4, PGD2, PGE2.
- Cytokines:IL-1,2,3,4,5,6,9,10,13,31,33
-Chemokines: RANTES, CXCL8, CCL2, MCP-3, MCP-4
- Growth factors: Vascular permeability factor (VPF) fibroblast growth factor (FGF-2), vascular endothelial growth factor (VEGF)
- Peptides: Substance P (SP), Pro-neurotensin, Corticotropin-Releasing Hormone (CRH), Vasoactive Intestinal Peptide (VIP).

The MC receptor FcεRI is formed by one α-subunit, four β, and two γ (1). The alpha subunit binds the IgE antibody which subsequently binds the antigen and thus the MC is stimulated, initiating the phosphorylation, with the activation of the tyrosine kinase. Subsequently, the phospholipase C (PKC) is activated, with calcium release and formation of IP3 and diacillglycerol (DAG) and activation of the mitogen-activated protein kinase (MAPK), c-Jun N-terminal kinase (JNK) and p38 (5). The cascade ends with the generation of cytokines and phospholipases A2 (6).

The stimuli of the MCs are many and can also be of different nature, as shown in Table II.

Table II. *Triggers of mast cells.*

Cytokines: 1, 33, TNF, SCF, TGF- β1
Neuropeptides: Substance P, NGF, CRH, Neurotensin
Biochemical toxins: LPS, Borrelia, mold
Drugs: Polymyxin B, and others

There are many cytokines involved in the activity of MCs, here we will limit ourselves to study only some of them, especially those pro- and anti-inflammatory of IL-1 family members (7).

IL-1

Interleukin (IL)-1 is a classical pro-inflammatory cytokine of innate immunity of which there are different types (IL-1α, IL-1β, IL-18, IL-33, IL-36 α, β, and γ, IL-37, and IL-38) and receptors (8). IL-1 has multiple biological effects including the induction of cyclooxygenase type 2, increased cell expression of adhesion molecules, nitric oxide synthesis and cytokine/chemokine production (9). The IL-1 family is involved in a broad spectrum of both immunological and inflammatory diseases including arthritis, atherosclerosis, Alzheimer's (the most common cause of dementia), and skin diseases such as psoriasis (10). IL-1 is produced by many types of cells, but mostly by monocytic cells (11). IL-1 (distinct in IL-α and IL-1-β) is a soluble mediator of inflammation with extracellular biological activity (8). In this study we will refer to IL-1-β, which is the most present in man in extracellular form.

IL-1 is found in the cytosol in immature form (35-kDa) and is transformed into a mature form (17-kDa) from the caspase IL-1-converting enzyme (ICE) in the active form IL-1-β. The release of IL-1-β is induced by extracellular macrophage ATP (8).

In vitro, MCs stimulated with IgE through the receptor FcεRI, produce various cytokines including TNF, IL-6, IL-31, IL-33 and IL-1, suggesting that there are links between the mediated IgE allergic phenomena and the stimulation of inflammatory cytokines (12). IL-1 stimulates human MCs to secrete IL-6 without tryptase.

In allergic diseases, MCs interact with IL-33 that can be induced by IL-1 which is recognized by different types of cells (13). Therefore, the blockade of IL-1 can certainly produce relief in allergic diseases.

TNF

Tumor necrosis factor (TNF) was first described in activated macrophages, and there is evidence that resident mouse peritoneal MCs constitutively contain large amounts of TNF (14). It was recently reported that substance P plus IL-33 produces massive amounts of TNF (12). Therefore, MCs produce a broad panel of multifunctional cytokines including TNF, a multifunctional cytokine that influences physiological and pathological mechanisms (15).

In addition to the newly synthesized TNF secretion (in several hours), MCs are the only immune cells that store and rapidly secrete (in about 10 minutes after IgE stimulation) preformed TNF. Therefore, MCs activated with IgE *in vitro* produce extracellular TNF and exhibit higher levels of TNF messenger RNA. Thus MCs have a preformed TNF and an immunologically inducible TNF (16).

TNF is a cytokine which has been implicated in inflammatory processes and TNF gene is expressed in cultured human LAD2 and primary MCs derived from umbilical cord blood (12).

It has been noted that some tissues exposed to substance P (or other neurotransmitters) and other stimulators, produce TNF, both preformed and inducible, which can play the role of recalling other inflammatory cells such as neutrophils and macrophage granulocytes, and it can also activate the T cell receptor (17). In addition, TNF induces adhesion molecules such as ICAM-1 and ELAM-1 involved in the recruitment of inflammatory immune cells. TNF-derived MCs stimulates fibroblasts in the production of collagen, playing an important role in allergic reactions (17). Moreover, the production of TNF by MCs also has an anti-tumor role since the number of cytokines produced by MCs is higher in cancer. Therefore, IL-33 can also play a protective immune role, as it stimulates TH2 cells to produce cytokines and increases the type 2 lymphoid cells (17).

IL-33

IL-33 is a member of the family of IL-1 ST2/IL-1R4 receptor involved in a number of diseases and is considered a cytokine "alarmin", as a recognized signaling mediator of inflammation not due to infections, but to trauma and stress (sterile inflammation) (18). The immature form of IL-33 is cleaved by a caspase-1 which makes cytokines active. To date, it is known that from the proteases of MCs some mature forms of IL-33 derive that activate lymphoid cells which also participate in the inflammatory process (17).

IL-33 is a pro-inflammatory cytokine and is found to augment mainly allergic diseases, as well as being involved in rheumatoid arthritis, atherosclerosis, psoriasis, inflammatory bowel disease, neurological disorders, etc. However, the nuclear suppression of IL-33 proves a systemic inflammation that can also be lethal, demonstrating that this cytokine also plays an anti-inflammatory role (18).

We and other authors have already reported that IL-33 is a cytokine which acts through the ST2 receptor that belongs to the toll like receptor (TLR)/IL1R super family. IL-33 is primarily expressed by different types of structural cells including dendritic cells, macrophages, endothelial cells, intestinal epithelial cells, fibroblasts, adipocytes, smooth muscle cells, bronchial and osteoblast (18).

MCs also produce many cytokines (including IL-33) and chemokines, as reported in Table I, and may also promote the maturation of $CD34^+$ cell, which is an MC progenitor. In fact, IL-33 plays a role in the maturation of MCs which, in turn, can produce mediators for the maturation of IL-33 from the immature form (17).

IL-33 increases the production of IL-31 released by MCs without allergic stimulation (17). IL-31, which is involved in tissue remodeling, induces pro-inflammatory cytokines, regulates cell proliferation, and is very pruritogenic. IL-31 and IL-33 work

together and their expression is involved in disease severity. In fact, IL-33 activates MCs without degranulation and therefore, without the release of stored chemical mediators. Moreover, this cytokine is capable of increasing non-allergic stimuli such as the neurotransmitter substance P, intervening in non-allergic inflammatory diseases (19) In addition, IL-33 increases the effect of IgE on MCs and TNF gene expression, favoring allergic reactions.

We recently reported that IL-33 has been implicated in the pathogenesis of psoriasis via keratinocyte and MC activation (14).

IL-18

IL-18 possesses an IL-18Rα receptor inducible (which binds IL-18) and IL-18Rβ which is expressed constitutively and mediates signal transduction (20). Members of IL-1R family with TIR domain are shared with TLRs. Cytoplasmic TIR domains cooperate with the MyD88 factor which activates the nuclear factor NF-κB and generate cytokines (20)

IL-18 is involved in many immune and inflammatory mechanisms. It is expressed essentially by macrophages, dendritic cells, epithelial cells, keratinocytes and other cells, participating in the innate and adaptive immune responses. IL-18 is important in the defense of the human body against bacteria and parasites, but also participates in allergic diseases, where MCs play a crucial role (17). In fact, IL-18 contributes to the activation and degranulation of MCs and its level is high in allergic phenomena. IL-18 was originally called IFN-γ-inducing factor (IGIF) and it was reported that it may also be activated in an inflammasome-independent manner by proteases, such as proteinase 3 and chymase. This cytokine can also play a chemotactic role, causing inflammatory cell recruitment, including macrophages, neutrophils and basophils (17).

It is known that IL-18 promotes the response of TH2 cells involved in both sensitization and later response to allergens, autoimmune diseases and cancer. However, IL-18 does not directly stimulate TH2 cells, which mediate allergic responses induced by antigens and produce many effects on inflammatory cells. Therefore, activated APC cells, release IL-18, provoking TH2 cell and granulocyte recruitment (20). In addition IL-18 causes cell proliferation, cytotoxic and B cell activity in hypersensitive state

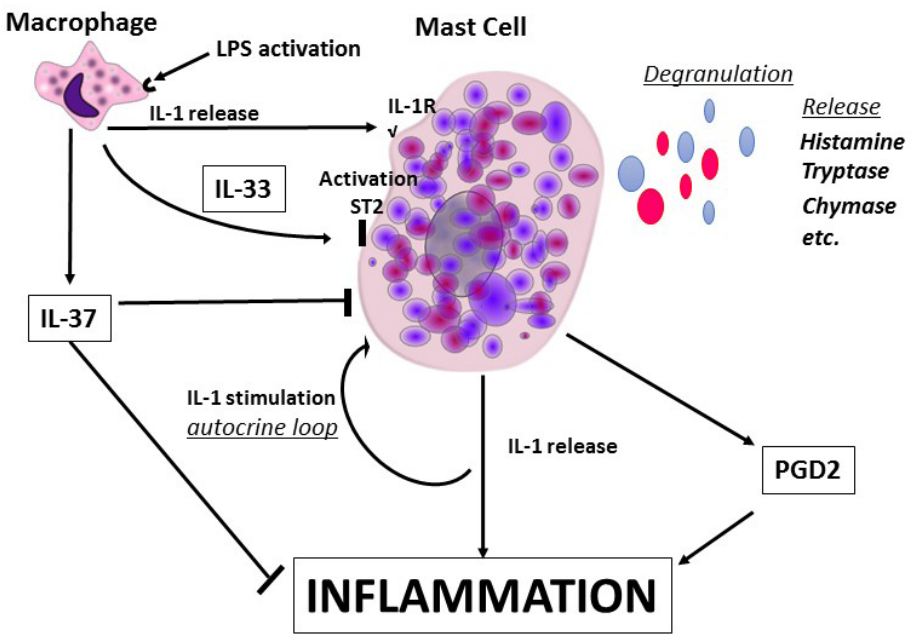

Fig. 1. *This figure depicts that LPS activates macrophages and releases IL-1 and IL-33 which induce mast cell activation mediating inflammation. In addition, macrophage produces also IL-37 which inhibits mast cell IL-1 release and inflammation.*

and other disorders. In allergic reaction, IL-18 increases IL-5, influences eosinophilia, and induces cell differentiation in rodents. Moreover, IL-18 stimulates eosinophilia in asthma and activates CXC and CC chemokine generation. On MCs, IL-18 binds to its IL-18R receptor, provoking the release of IL-4, IL-13 and histamine, similar to the activation of MCs with the allergen that binds FcεRI receptor (17).

Inhibition of the actions of this cytokine would certainly provide relief both to individuals suffering from allergic diseases and to those with acute and chronic inflammatory disorders. IL-18 can be inhibited by both IL-18BP found in nature, and by IL-37, which down-regulates signal transduction and responses caused by IL-18 and, therefore, inhibits inflammation (20).

IL-37

IL-37, previously called IL-1 family member 7 (IL-1F7), is a cytokine of the IL-1 family which includes IL-1α, IL-1β, IL-1RA, IL-18 and IL-33, and can improve inflammatory response (21). IL-37 is a natural suppressor of both innate and acquired immune responses. IL-37 is expressed in a variety of tissues and cells, including monocytes, endothelial cells and epithelial cells. It has been reported that IL-37 inhibits many inflammatory states, suppressing monocytes and macrophages, but may also increase after a pro-inflammatory stimulus caused by LPS (22). IL37 binds IL-18Rα chain, acts with an intracellular mechanism translocating to the nucleus, which inhibits the expression of pro-inflammatory signals cJun, MAP kinase p38, STAT transcription factors and p53.

IL-37 acts by inhibiting the inflammatory signals NF-κB, and transcription factors AP-1, which lead to the production of pro-inflammatory cytokines of the IL-1 family.

Activated MCs produce pro-inflammatory cytokines, including IL-1 and TNF (23-24). IL-37 possesses a pleiotropic anti-inflammatory activity with inhibition of macrophage activation, leukocyte adhesion, metalloproteinase production and IL-1-inducing TNF generation in MCs.

TNF is induced by many pro-inflammatory proteins including IL-1. Furthermore, IL-1 possesses the autocrine property of inducing itself (Fig. 1). Hence, IL-1 induces IL-1 and TNF in macrophages and MCs. Since IL-37 blocks IL-1 and IL-1-induced TNF, these inhibitory effects could be of great benefit in the treatment of inflammatory disorders including those mediated by MCs (25-26). It will be important to develop IL-37 formulation that can deliver it selectively to the cell target including MCs and macrophages.

REFERENCES

1. Galli SJ, Kalesnikoff J, Grimbaldeston MA, Piliponsky AM, Williams CM, Tsai M. Mast cells as "tunable" effector and immunoregulatory cells: recent advances. Annu Rev Immunol 2005; 23:749-86. Review.
2. Theoharides TC, Stewart JM, Taracanova A, Conti P, Zouboulis CC. Neuroendocrinology of the skin. Rev Endocr Metab Disord 2016; 17(3):287-94. Review.
3. Theoharides TC, Petra AI, Taracanova A, Panagiotidou S, Conti P. Targeting IL-33 in autoimmunity and inflammation. J Pharmacol Exp Ther 2015; 354(1):24-31.
4. Conti P, Caraffa A, Ronconi G, et al. Mast cells participate in allograft rejection: can IL-37 play an inhibitory role? Inflamm Res 2018;6 7(9):747-55.
5. Conti P, Caraffa A, Mastrangelo F, et al. Critical role of inflammatory mast cell in fibrosis: Potential therapeutic effect of IL-37. Cell Prolif 2018; 51(5):e12475.
6. Conti P, Caraffa A, Ronconi G, Kritas SK, Mastrangelo F, Tettamanti L, Theoharides TC. Impact of mast cells in mucosal immunity of intestinal inflammation: Inhibitory effect of IL-37. Eur J Pharmacol 2018;818:294-99.
7. Conti P, Carinci F, Lessiani G, et al. Potential therapeutic use of IL-37: a key suppressor of innate immunity and allergic immune responses mediated by mast cells. Immunol Res 2017; 65(5):982-86.
8. Dinarello CA. Introduction to the interleukin-1 family of cytokines and receptors: Drivers of innate inflammation and acquired immunity. Immunol Rev 2018; 281(1):5-7.
9. Tettamanti L, Kritas SK, Gallenga CE, et al. IL-33 mediates allergy through mast cell activation:

Potential inhibitory effect of certain cytokines. J Biol Regul Homeost Agents 2018; 32(5):1061-65.
10. Caraffa A, Conti C, D'Ovidio C, et al. New concepts in neuroinflammation: mast cells pro-inflammatory and anti-inflammatory cytokine mediators. J Biol Regul Homeost Agents 2018; 32(3):449-54. Review.
11. Dinarello CA, Conti P, Mier JW. Effects of human interleukin-1 on natural killer cell activity: is fever a host defense mechanism for tumor killing? Yale J Biol Med 1986; 59(2):97-106.
12. Taracanova A, Tsilioni I, Conti P, Norwitz ER, Leeman SE, Theoharides TC. Substance P and IL-33 administered together stimulate a marked secretion of IL-1β from human mast cells, inhibited by methoxyluteolin. Proc Natl Acad Sci U S A 2018; 115(40):E9381-90.
13. Mastrangelo F, Frydas I, Ronconi G, et al. Low-grade chronic inflammation mediated by mast cells in fibromyalgia: role of IL-37. J Biol Regul Homeost Agents 2018; 32(2):195-98.
14. Taracanova A, Alevizos M, Karagkouni A, et al. SP and IL-33 together markedly enhance TNF synthesis and secretion from human mast cells mediated by the interaction of their receptors. Proc Natl Acad Sci U S A 2017; 114(20):E4002-E4009. doi: 10.1073/pnas.1524845114.
15. Conti P, Lessiani G, Kritas SK, Ronconi G, Caraffa A, Theoharides TC. Mast cells emerge as mediators of atherosclerosis: Special emphasis on IL-37 inhibition. Tissue Cell 2017; 49(3):393-400.
16. Sibilano R, Gaudenzio N, DeGorter MK, et al. A TNFRSF14-FcεRI-mast cell pathway contributes to development of multiple features of asthma pathology in mice. Nat Commun 2016; 7:13696. doi: 10.1038/ncomms13696.
17. Mukai K, Tsai M, Saito H, Galli SJ. Mast cells as sources of cytokines, chemokines, and growth factors. Immunol Rev 2018; 282(1):121-50.
18. Dinarello CA. Overview of the IL-1 family in innate inflammation and acquired immunity. Immunol Rev 2018; 281(1):8-27. doi: 10.1111/imr.12621. Review.
19. Theoharides TC, Leeman SE. Effect of IL-33 on de novo synthesized mediators from human mast cells. J Allergy Clin Immunol 2018. doi: 10.1016/j.jaci.2018.09.014.
20. Dinarello CA, Kaplanski G. Indeed, IL-18 is more than an inducer of IFN-γ. J Leukoc Biol 2018; 104(2):237-38.
21. Cavalli G, Dinarello CA. Suppression of inflammation and acquired immunity by IL-37. Immunol Rev 2018; 281(1):179-90.
22. Kritas SK, Gallenga CE, D Ovidio C, et al. Impact of mold on mast cell-cytokine immune response. J Biol Regul Homeost Agents 2018; 32(4):763-68.
23. Theoharides TC, Tsilioni I, Arbetman L, Panagiotidou S, Stewart JM, Gleason RM, Russell IJ. Fibromyalgia syndrome in need of effective treatments. J Pharmacol Exp Ther 2015; 355(2):255-63.
24. Hatziagelaki E, Adamaki M, Tsilioni I, Dimitriadis G, Theoharides TC. Myalgic encephalomyelitis/chronic fatigue syndrome-metabolic disease or disturbed homeostasis due to focal inflammation in the hypothalamus? J Pharmacol Exp Ther 2018; 367(1):155-67.
25. Conti P, Ronconi G, Kritas SK, Caraffa A, Theoharides TC. Activated mast cells mediate low-grade inflammation in Type 2 diabetes: Interleukin-37 could be beneficial. Can J Diabetes 2018; 42(5):568-73.
26. Tsilioni I, Russell IJ, Stewart JM, Gleason RM, Theoharides TC. Neuropeptides CRH, SP, HK-1, and inflammatory cytokines IL-6 and TNF are increased in serum of patients with fibromyalgia syndrome, implicating mast cells. J Pharmacol Exp Ther 2016; 356(3):664-72.

CYCLIN-DEPENDENT KINASE 7 IS A POTENTIAL THERAPEUTIC TARGET IN PAPILLARY THYROID CARCINOMA

Y. GONG, J. YANG, F. LIU, Z. LI, R. GONG and T. WEI

Department of Thyroid and Parathyroid Surgery Center, Sichuan University West China Hospital, China

Received May 17, 2018 – Accepted September 18, 2018

Given the pathological incidence of metastases or radioiodine-refractory papillary thyroid carcinoma (PTC) is increasing worldwide, patients have little alternatives when choosing effective drugs. Therefore, it is necessary to develop new therapeutic targets for PTC treatment. CDK7 is a member of the cyclin-dependent protein kinase (CDK) family, which plays an important role in various types of cancers. In this study, we found CDK7 were upregulated in PTC cell lines compared to normal thyroid cells using qRT-PCR and Western blot. Furthermore, using cell counting kit-8 (CCK-8) assay and 5-ethynyl-2-deoxyuridine (EdU) assay, we discovered cell growth ratio was positively correlated to the expression level of CDK7. Cell cycle analysis showed that the cells with higher CDK7 expression levels were prone to be in S phase. More importantly, we tested the inhibitory effects of BS-181 on CDK7 both *in vitro* and *in vivo*. Results obtained from this study indicated that BS-181 not only suppressed the cell proliferation *in vitro*, but also inhibited the tumor growth in nude mouse without changing mRNA and protein levels of CDK7. In conclusion, our study might provide a novel potential target for PTC therapy.

Papillary thyroid carcinoma (PTC) accounts for more than 90% of all thyroid cancer cases (1), and has been considered as the most common type of thyroid cancer in past decades. Although the majority of PTC patients have shown good prognosis after receiving a combination of surgery and radioiodine therapy, the remaining patients with metastases or radioiodine-refractory cancers usually exhibit very poor prognosis (2). Therefore, it is necessary to investigate the mechanisms of PTC with the aim of developing novel therapeutic targets for PTC therapy. Cancer cells are characterized with uncontrolled cell division due to their aberrant regulation of cell cycles. Various researches have revealed hyper-activation of CDKs could lead to increased growth rate of cells(3). Thereby, the important role of CDKs in the cell cycle regulation makes it a potential target for the treatment of PTC.

CDK7 was discovered as a regulator of mRNA transcription in *Saccharomyces cerevisiae,* and its homologs in vertebrates has been reported to influence the cell cycle progression (4). In mammals, CDK7 functions as a cyclin-dependent kinase activating kinase (CAK), which activates the downstream CDKs in the cell cycle by forming complexes with cyclin H and Mat1, including CDK1, CDK2, CDK4 and CDK6 (5-7). Many studies have shown that hyper-activation of CDK7 was involved in various types of cancers, such as blood cancers (8), prostate cancers (9), glioma (10), lung cancers (11) as well

Key words: CDK7, papillary thyroid carcinoma, xenograft

Mailing address:
Dr. Tao Wei,
No.37 Guo Xue Xiang,
Wuhou District, Chengdu, Sichuan,
P.R.China, 610041
Fax: +86 2885422467 - Tel.: +86 28 85422467
e-mail: wiitaoscljmc01@126.com

0393-974X (2018)

as breast cancers (12). Interestingly, inhibition of CDK7 in these cancers have been evaluated to be effective in pre-clinic trials. These studies suggest that aberrant expression of CDK7 was involved in occurrence and development of malignancies. To date, little is known about the role of CDK7 in PTC.

In this study, we firstly determined the mRNA and protein levels of CDK7 in PTC by quantitative RT-PCR and Western blot, respectively. Then, effects of CDK7 on cell proliferation and cell cycles were analyzed through CCK-8 assay, EdU assay and flowcytometry assay in PTC cells treated by CDK7 over expression plasmid transfection, shRNA mediating CDK7 knock-down plasmid transfection and adding a CDK7 specific inhibitor BS-181. Moreover, we evaluated the potentiation of CDK7 as a therapeutic target for PTC, using shRNA lentivirus system and BS-181 on xenograft model in nude mice.

MATERIALS AND METHODS

Cell culture

Human PTC cell lines TPC-1 (BNCC337912, BeNa Culture Collection, Beijing, China) and MDA-T120 (CRL-3355, American Type Culture Collection, USA), human normal thyroid cell line Nthy-ori 3-1 (BNCC340487, BeNa Culture Collection, Beijing, China) were maintained in DMEM (Hyclone, GE Healthcare Life Sciences, Piscataway, NJ, USA) supplemented with 10% FBS (Gibco, Thermo Fisher Scientific, Waltham, MA, USA), 100 units of penicillin/mL and 100 ng of streptomycin/mL at 37°C in 5% CO_2 incubator.

Plasmid construction

For CDK7 over-expression, full length of CDK7 CDS was amplified by PCR and cloned into the pcDNA3.1 vector. PCR primer sequences were as follows: *CDK7*-EcoRI, CGGAATTCATGGCTCTGGACGTGAAGTCTCGand*CDK7*-HindIII, AAGCTTTTAGTTTCTTGGGCAATCCTCCTTG (Restriction enzyme cutting sites were underlined). For CDK7 knock-down, shRNA of CDK7 were designed and annealed into PLKO.1 vector. The shRNA target sequences of CDK7 were as follows: sh1: GGGCAAAGCGTTATGAGAAGCTGGA; sh2: GGGCAAAGCGTTATGAGAAGCTGGA, and sh3: ACATGTTGATGACTCTTCAAGGATT. The recombinant plasmids were transfected into cells using Lipofectamine 2000 Transfection Reagent (Invitrogen, Thermo Fisher Scientific, Waltham, MA, USA).

Lentivirus production

For lentivirus production, the recombinant shRNA plasmid was transfected into 293T cells (CRL-3216, ATCC, USA) together with psPAX2 packaging plasmid and pMD2.G envelope plasmid (Addgene). Sixty-four hours after transfection, supernatants were harvested, and viral particle was pelleted by centrifugation. Then the viral titer was estimated and MOI of 0.4 was used.

Real-time quantitative PCR (RT-qPCR)

Total RNA was isolated with TRIzol reagent (Invitrogen, Thermo Fisher Scientific, Waltham, MA, USA) and quantified by Nanodrop 2000. 1 μg total RNA was reverse transcribed into cDNA with oligodT primers. RT-qPCR was carried out on an ABI Prism 7500 fast System (Applied Biosystems, USA) with SYBR Premix Ex TaqTM (Takara, Dalian, China). Primer sets used were as follows: for β-actin, 5′-GTGGACATCCGCAAAGAC-3′, 5′-AAAGGGTGTAACGCAACTA-3′and for CDK7, 5′- ATGGCTCTGGACGTGAAGTCT -3′ (forward), 5′-GCGACAATTTGGTTGGTGTTC -3′ (reverse). Data analysis was performed using the $2^{-\Delta\Delta Ct}$ method.

Western blot

Cells were collected and washed with ice-cold PBS, lysed with ice-cold RIPA lysis buffer (Thermo Fisher Scientific, Waltham, MA, USA). Total protein concentrations were determined using the BCA Protein Assay Kit (Pierce Biotechnology, Thermo Fisher Scientific, Waltham, MA, USA, Catalogue number 23235). 20 μg total protein were loaded and separated by SDS-PAGE. Then, proteins were transferred to PVDF membrane and incubated with rabbit anti-CDK7 (ab216437, abcam, USA) and rabbit anti-GAPDH (Proteintech, Chicago, IL, USA) overnight at 4°C. After washing with TBST three times, bands were then incubated with HRP-conjugated antibody. Signals were developed with ECL. GAPDH was used as the internal standard.

Cell counting kit-8 (CCK-8) assay

The effect of CDK7 on cell viability was analyzed using the CCK-8 assay (Beyotime, Hangzhou, China). Briefly, 1×10^4 cells were reseeded in sextuplet in 96-well

plates and transfected with plasmids or incubation with 20 μM BS-181. Transfected cells were further cultured for indicated times. CCK-8 was then added and incubated for another 2 hours. Then, OD_{490} was measured.

IT Click-iT EdU cell proliferation assay

IT Click-iT EdU (5-ethynyl-2-deoxyuridine) cell proliferation assay was performed with Click-iT Plus EdU Imaging Kits (Invitrogen, Thermo Fisher Scientific, Waltham, MA, USA). 1×10^4 cells were reseeded in sextuplet in 96-well plates and transfected with plasmids or incubated with 20 μM BS-181 and further cultured for 48 hours. Then, the cells were labeled with Click-iT® Plus reaction cocktail, fixed and permeabilizated, and then treated with Click-iT® reaction cocktails. After 30 min incubation, the cell nucleus was further stained with DAPI and visualized under a fluorescence microscope. The EdU positive cells were counted and the percentages of EdU positive cells were defined as the proliferation rates.

Cell cycle analysis

Cells were collected by centrifugation, and the pellets were washed twice with PBS and then fixed in ice-cold 70% ethanol overnight at 4°C. Then the cells were resuspended in PBS containing 10% FBS and filtered through a 400-mesh sieve, and permeated with propidium iodide solution (propidium iodide, 50 μg/mL, 100 μg/mL RNase in PBS) at 37°C in the dark for 30 min. Finally, the cells were subjected to FACS Caliber cytometry (BD Biosciences) for the cell cycle phase analysis. The cells at various phases of the cell cycle were counted.

Animal preparation and human tumor xenografts

All of the procedures were included in a protocol approved by the Animal Care and Use Committee. Female athymic nude mice 4-6 weeks old were purchased and maintained under specific pathogen free (SPF) conditions. Each experimental group included 10 female athymic nude mice. TPC-1 cells or lentivirus infected TPC-1 cells were collected, washed and re-suspended in PBS. After mixing with an equal volume of matrigel (BD Biosciences, Franklin Lakes, NJ, USA), 106 cells were injected s.c. into the flank of the mice. When tumors were approximately 0.5 cm3, the mice were treated with the inhibitors. BS-181 was dissolved in 10% dimethyl sulfoxide/50 mM HCl/5% Tween 20/85% saline and each mouse received intraperitoneal injection of 5 mg/kg/d BS-181 twice daily. Tumor dimensions length (l) and width (w) were measured and tumor volume was calculated as $V(tumor)=\pi lw2/6$. Then, the animals were sacrificed and tumors were removed for Western blot, HE staining and ki67 immunohistochemistry analysis.

Statistical analysis

Statistical analysis was performed using the SPSS 20.0 software (SPSS, Inc., Chicago, IL, USA). Experiments were performed for at least three times and data were expressed as mean±SEM. Statistically significant differences between groups were evaluated using Student's t-test for two groups or Tukey's multiple comparisons test after ANOVA test for three or more groups. The results were determined to be significant when $P<0.05$ was obtained.

RESULTS

CDK7 is highly expressed in thyroid cancer cell lines

It is well known that Cyclin-dependent kinase plays an important role in controlling the cell cycle and it is hypothesized to be a significant target for cancer treatment (13, 14). In the screening of the expression profiles of thyroid cancer in the Gene Expression Omnibus (GEO) data, we found the mRNA level of CDK7 seemed to be up-regulated. We first determined the expression level of CDK7 in PTC cell lines (TPC-1 and MDA-T120). We found the mRNA levels of CDK7 were significantly upregulated in PTC cells compared to normal human thyroid cells (Nthy-ori 3-1) (Fig. 1A). Similar results were also found in Western blot analysis, the protein levels of CDK7 were significantly upregulated in PTC cells (Fig. 1, B and C). These results showed that the expression of CDK7 was indeed up-regulated in PTC cell lines.

Knock-down of CDK7or BS-181 treatment can selectively inhibit CDK7 expression and suppress cell proliferation

To evaluate the function of CDK7 in PTC cell proliferation, we constructed and determined the efficiency of CDK7 over-expression and shRNA mediating knock-down plasmids.

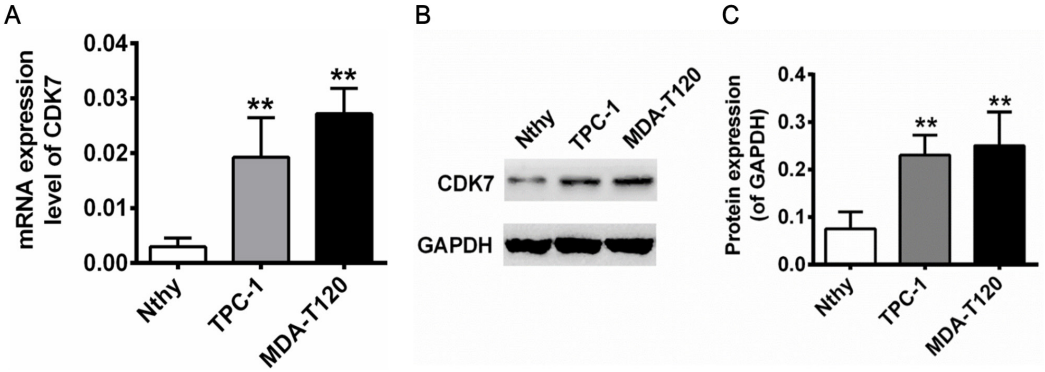

Fig. 1. *CDK7 was up-regulated in PTC cells.* ***A)*** *mRNA levels of CDK7 were determined by qRT-PCR in PTC cell lines (TPC-1 and MDA-T120) and normal human thyroid cell line (Nthy-ori 3-1, Nthy).* ***B)*** *Protein levels of CDK7 were determined by Western blot. Representative images of Western blot were shown, bands were quantitated by densitometry and normalized to GAPDH. (n=3, **p<0.01, compared to Nthy).*

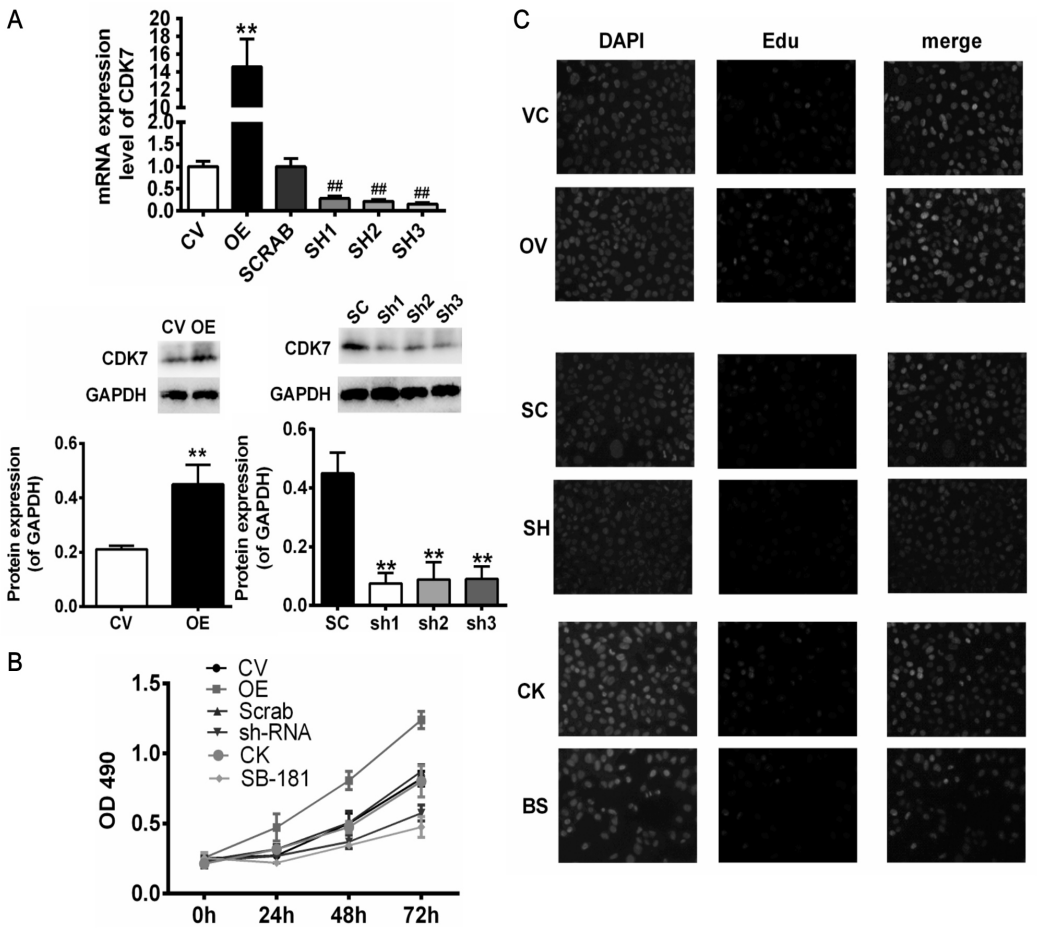

Fig. 2. *Inhibition of CDK7 suppressed TPC-1 proliferation.* ***A)*** *qRT-PCR and Western blot were used to validate the efficiency of CDK7 over-expression or shRNA-mediated knock-down plasmids.* ***B)*** *Growth curves of each group were obtained by CCK-8 assay. OD_{490} was measured at 0, 24, 48, 72 hours after transfection.* ***C)*** *EdU assay were performed. Cell in dividing could be labeled by EdU and cell nucleus was labeled by DAPI. (n=3, **p<0.01, compared with CV or Scramble).*

As shown in Fig. 2A, both the mRNA and protein levels of CDK7 were markedly up-regulated/down-regulated in the cells transfected with over-expression/knock-down plasmids. We also determined the effect of CDK7 on cell proliferation using CCK-8 assay and EdU assay in TPC-1 cells. The results showed that the TPC-1 cells with over-expressed CDK7 grew faster than the cells transfected with CV and had more dividing cells, whereas knock-down of CDK7 by shRNA decreased the cell proliferation rate. More importantly, we also found the proliferation of TPC-1 was significantly inhibited by BS-181 (a specific CDK7 inhibitor) (15) (Fig. 2, B and C). These results indicated that CDK7 promoted cell proliferation in PTC cells and selective inhibition of CDK7 could suppress cell proliferation.

Altering expression levels of CDK7 or BS-181 treatment may change the cell cycles

Given CDK7 could function as CAK and activate CDKs that regulate cycle cells, the cell cycle distributions were analyzed by flow cytometry in the TPC-1 cells with different CDK7 expression levels.

TPC-1 cells with over-expressed CDK7 showed an increase in the numbers of cells in S phase, accompanied by a reduction of cell population in G1 phases, whereas knock-down of CDK7 by shRNA or inhibition of CDK7 by BS-181 showed an opposite effect. Inhibition of CDK7 increased the percentages of cells in G1 phase and decreased the percentages of cells in G2/M plus S phases (Fig. 3). These results indicated altering the expression levels of CDK7 could change the cell cycles.

Knock-down of CDK7 or BS-181 treatment may suppress xenograft tumor growth

Our *in vitro* studies suggested CDK7 involved in cell cycle and cell proliferation regulation and inhibition of CDK7 could slow down the growth of TPC-1 cells. Thereby, we further determined the effects of CDK7 on the tumorigenic potential *in vivo*.

TPC-1 cells infected with lentivirus expressing the shRNA of CDK7 or scramble (CK) were injected into nude mice. For BS-181 treatment, the mice received intraperitoneal injection of 5 mg/kg/d BS-181 twice daily after injection with TPC-1 cells. The results showed that tumors derived from the cells with shRNA mediating CDK7 knock-down or receiving the BS-181 grow much slower than CK (Fig. 4A). HE staining showed both the shRNA group and BS-181 group had condensed chromatin and necrotic mass, while the CK group had large and round cell nucleus (Fig. 4B). More importantly, we performed immunohistochemistry for Ki-67, a specific indicator of the tumor cell proliferation levels (Scholzen and Gerdes 2000). The results showed that both the shRNA and SB-181 group had much less signaling of Ki67 than the CK group (Fig. 4C). These results indicated knock-down of CDK7 or inhibition of CDK7 by BS-181 decreased the tumorigenesis. Finally, we determined the expression levels of CDK7 in tumors. Western blot showed that the expression levels of CDK7 in receiving BS-181 group were similar to the CK group, whereas the shRNA group had significantly decreased CDK7 expression levels. Taken together, these results showed the inhibition of CDK7 by shRNA mediated knock-down or BS-181 treatment indeed impaired the tumor growth.

DISCUSSION

We demonstrated for the first time that the expression levels of CDK7 were upregulated in PTC cells. Experimental results showed that both the mRNA and protein levels were upregulated in PTC cell lines (TPC-1 and MDA-T120) compared to normal human thyroid cells. Besides PTC cells, over-expressions of CDK7 have also been found in many other cancers, such as breast cancer (16), gastric cancer (17), and ovarian cancer(18). These results suggested overexpression of CDK7 might be common in cancers and may function as a biomarker for prognosis. And indeed, up-regulation of CDK7 could predict poor prognosis in gastric cancer (19). However, in breast cancer, expression of CDK7 was positively associated with ER expression and inversely proportional to poor prognostic factors (16). Thereby, the exact meaning of the upregulation of CDK7 in the prognosis of PTC needs further study.

We then found the expression of CDK7 in PTC cells can promote cell proliferation. Further cell cycle

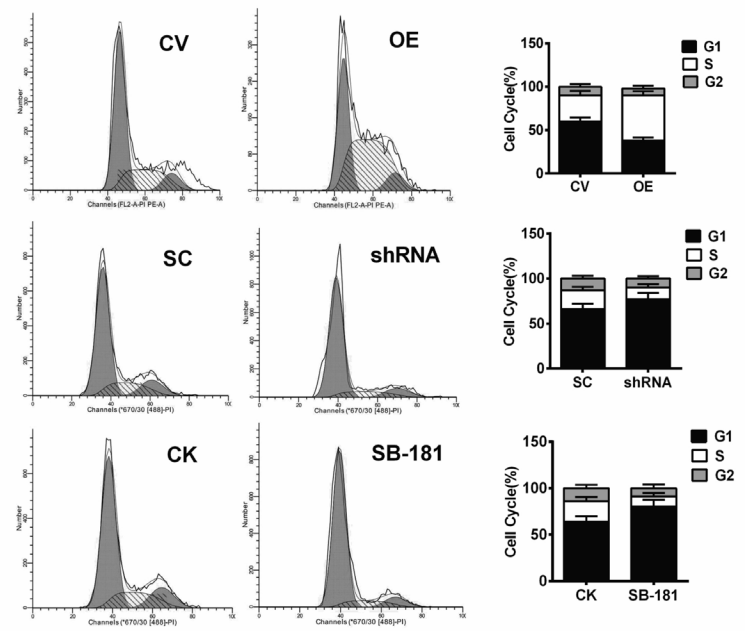

Fig. 3. *Expression of CDK7 affected cell cycle in TPC-1 cells. Cell cycle was analyzed by flow cytometry and the percentages of the cell population of each subsets (G0/G1, S and G2/M) are shown.*

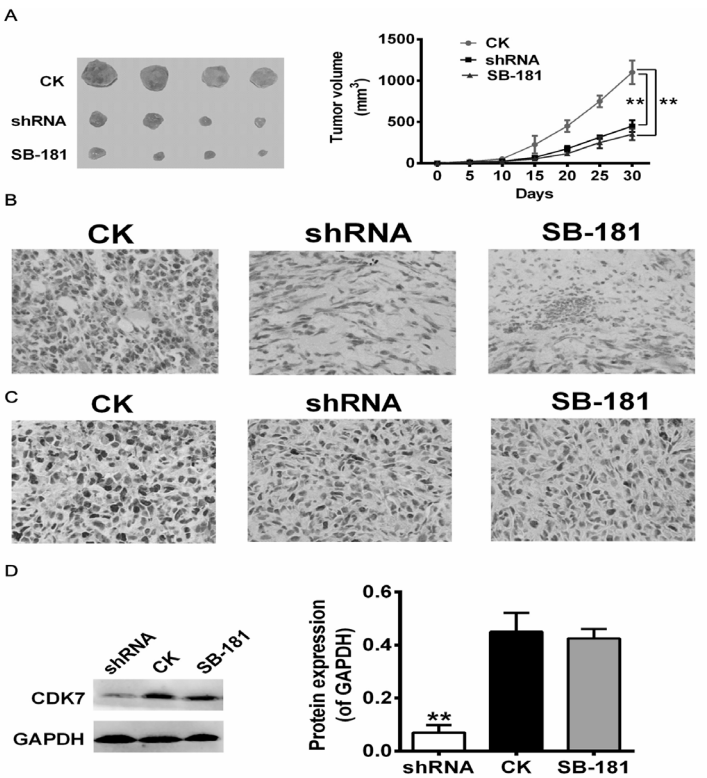

Fig. 4. *Inhibition of CDK7 impaired tumor growth in vivo.* ***A)*** *Representative images of tumor xenografts and tumor growth curves.* ***B)*** *Representative images of HE staining (magnification ×200).* ***C)*** *Representative images of immunohistochemistry for ki67 (magnification, ×200).* ***D)*** *Protein levels of CDK7 in each group were determined by Western blot. (n=3, **p<0.01, compared with CK).*

analysis showed the cells with over-expressed CDK7 were aberrantly accumulated in S phage, which indicated that the dysregulation of CDK7 could affect cell cycles. Similar phenomenon was also observed in breast cancer cells, and gastric cancer cells (17, 19), prostate cancer cells (9), esophageal squamous cell carcinoma (20). These results suggested CDK7 mediated cell cycle dysfunction might be a common pathway in tumorigenesis.

Based on the above, we tested the effect of a special CDK7 inhibitor, BS-181, on PTC cells, and the results showed BS-181 inhibited the growth of PTC cells both *in vitro* and *in vivo*. BS-181 is a pyrazolo [1, 5–*a*] pyrimidine-derived compound, first synthesized in 2010, and it can inhibit the growth and promote apoptosis of MCF-7 breast cancer cells (15). Wang et al. (2016) also reported BS-181 could inhibit cell growth and induce cell cycle arrest and apoptosis in gastric cancer(17). In addition to BS-181, another CDK7 inhibitor, THZ1, showed anti-tumor effects in small cell lung cancer, triple-negative breast cancer, and high grade-glioma (10). These results suggested CDK7 could be a novel cancer therapy target. However, in mammals, CDK7 not only functions as a CAK to active CDK1, CDK2, CDK4 and CDK6, but also can regulate the gene expression by phosphorylating RNA Polymerase II or other transcription factors, including p53 (21-24). Thus, the exact mechanisms of how the inhibition of CDK7 suppresses the tumor growth both *in vitro* and *in vivo* should be further studied. In conclusion, upregulation of CDK7 is crucial in PTC. Using BS-181 as a model inhibitor, we confirm that CDK7 is a new target for PTC therapy.

ACKNOWLEDGEMENTS

This study was supported by the grants from the Department of Sichuan Province, Science and Technology Support Program (Grant No.2018SZ0215).

REFERENCES

1. Hinson AM, Massoll NA, Jolly LA, Stack BC, Jr., Bodenner DL, Franco AT. Structural alterations in tumor-draining lymph nodes before papillary thyroid carcinoma metastasis. Head Neck 2017; 39:1639-46.
2. Liu FH, Kuo SF, Hsueh C, Chao TC, Lin JD. Postoperative recurrence of papillary thyroid carcinoma with lymph node metastasis. J Surg Oncol 2015; 112:149-54.
3. Santo L, Siu KT, Raje N. Targeting cyclin-dependent kinases and cell cycle progression in human cancers. Semin Oncol 2015; 42:788-800.
4. Luo J, Cimermancic P, Viswanath S, et al. Architecture of the human and yeast general transcription and DNA repair factor TFIIH. Mol Cell 2015; 59:794-806.
5. Fisher RP. The CDK Network: linking cycles of cell division and gene expression. Genes Cancer 2012; 3:731-38.
6. Ganuza M, Saiz-Ladera C, Canamero M, et al. Genetic inactivation of Cdk7 leads to cell cycle arrest and induces premature aging due to adult stem cell exhaustion. EMBO J 2012; 31:2498-510.
7. Schachter MM, Merrick KA, Larochelle S, et al. A Cdk7-Cdk4 T-loop phosphorylation cascade promotes G1 progression. Mol Cell 2013; 50:250-60.
8. Bose P, Simmons GL, Grant S. Cyclin-dependent kinase inhibitor therapy for hematologic malignancies. Expert Opin Investig Drugs 2013; 22:723-38.
9. Li J, Zhang Z, Xiong L, et al. SNHG1 lncRNA negatively regulates miR-199a-3p to enhance CDK7 expression and promote cell proliferation in prostate cancer. Biochem Biophys Res Commun 2017; 487:146-52.
10. Greenall SA, Lim YC, Mitchell CB, et al. Cyclin-dependent kinase 7 is a therapeutic target in high-grade glioma. Oncogenesis 2017; 6:e336.
11. Christensen CL, Kwiatkowski N, Abraham BJ, et al. Targeting transcriptional addictions in small cell lung cancer with a covalent CDK7 inhibitor. Cancer Cell 2014; 26:909-22.
12. Wang Y, Zhang T, Kwiatkowski N, et al. CDK7-dependent transcriptional addiction in triple-negative breast cancer. Cell 2015; 163:174-86.
13. Sanjeev KS, Sunil KT, Nigus D, Poonam S. Cyclin dependent kinase as significant target for cancer treatment. Curr Cancer Ther Rev 2012; 8:225-35.
14. VanArsdale T, Boshoff C, Arndt KT, Abraham RT. Molecular Pathways: Targeting the Cyclin D–CDK4/6 Axis for Cancer Treatment. Clin Cancer Res 2015; 21:2905.
15. Ali S, Heathcote DA, Kroll SHB, et al. The development

of a selective cyclin-dependent kinase inhibitor that shows antitumor activity. Cancer Res 2009; 69:6208-15.
16. Patel H, Abduljabbar R, Lai CF, et al. Expression of CDK7, Cyclin H, and MAT1 is elevated in breast cancer and is prognostic in estrogen receptor-positive breast cancer. Clin Cancer Res 2016; 22:5929-38.
17. Naseh G, Mohammadifard M, Mohammadifard M. Upregulation of cyclin-dependent kinase 7 and matrix metalloproteinase-14 expression contribute to metastatic properties of gastric cancer. IUBMB Life 2016; 68:799-805.
18. Francavilla C, Lupia M, Tsafou K, et al. Phosphoproteomics of primary cells reveals druggable kinase signatures in ovarian cancer. Cell Rep 2017; 18:3242-56.
19. Wang Q, Li M, Zhang X, et al. Upregulation of CDK7 in gastric cancer cell promotes tumor cell proliferation and predicts poor prognosis. Exp Mol Pathol 2016; 100:514-21.
20. Zhang J, Yang X, Wang Y, et al. Low Expression of CyclinH and Cyclin-dependent Kinase 7 can decrease the proliferation of human esophageal squamous cell carcinoma. Dig Dis Sci 2013; 58:2028-37.
21. Merrick KA, Larochelle S, Zhang C, Allen JJ, Shokat KM, Fisher RP. Distinct activation pathways confer cyclin-binding specificity on Cdk1 and Cdk2 in human cells. Mol Cell 2008; 32:662-72.
22. Kelso TW, Baumgart K, Eickhoff J, et al. Cyclin-dependent kinase 7 controls mRNA synthesis by affecting stability of preinitiation complexes, leading to altered gene expression, cell cycle progression, and survival of tumor cells. Mol Cell Biol 2014; 34:3675-88.
23. Larochelle S, Amat R, Glover-Cutter K, et al. Cyclin-dependent kinase control of the initiation-to-elongation switch of RNA polymerase II. Nat Struct Mol Biol 2012; 19:1108.
24. Lu H, Fisher RP, Bailey P, Levine AJ. The CDK7-cycH-p36 complex of transcription factor IIH phosphorylates p53, enhancing its sequence-specific DNA binding activity in vitro. Mol Cell Biol 1997; 17:5923-34.

17β-ESTRADIOL INHIBITS HEPATIC iNOS VIA THE ACTIVATION OF THE ESTROGEN RECEPTOR ER-α AND INHIBITION OF ERK1/2-miR-221 AXIS

A. PANIC[1], J. STANIMIROVIC[1], M. OBRADOVIC[1], S. ZAFIROVIC[1], E. SUDAR-MILOVANOVIC[1], N. PETROVIC[1,2] and E.R. ISENOVIC[1]

[1]Vinca Institute of Nuclear Sciences, University of Belgrade, Laboratory of Radiobiology and Molecular Genetics, Belgrade, Serbia; [2]Institute for Oncology and Radiology of Serbia, Belgrade, Serbia

Received June 8, 2018 – Accepted September 25, 2018

17β-Estradiol (E2) is known to negatively regulate inducible nitric oxide (NO) synthase (iNOS) expression via estrogen receptor alpha (ER-α) activation in aortic vascular smooth muscle cells. Therefore, we sought to determine whether E2 can inhibit iNOS *in vivo* in hepatic tissue via the activation of ER-α and whether extracellular signal-regulated kinases 1/2 (ERK1/2)-miR-221 axis is involved in this process. Male Wistar rats were treated with a bolus injection of E2 intraperitoneally (40 μg/kg), and 24 hours after treatment the animals were sacrificed and the livers excised. The protein levels of iNOS, p50 and p65 subunits of nuclear factor κB (NFκB), ERα, ERK1/2 and protein kinase B (Akt), as well as the association of ERα/Src in liver lysates were assessed by Western blot. The expression of hepatic miR-221 was analyzed by qRT-PCR. Results show that E2 reduced hepatic iNOS protein expression ($p < 0.01$), the protein level of ERα ($p < 0.05$), ERK1/2 ($p < 0.05$), Akt phosphorylation ($p < 0.001$) and miR-221 expression ($p<0.05$). In contrast, hepatic ERα/Src kinase association level ($p < 0.05$) increased after E2 treatment. Our results indicate that E2 inhibits hepatic iNOS via molecular mechanisms involving the activation of the ER-α and inhibition of ERK1/2-miR-221 axis.

Estrogens are considered female sex hormones regulating female reproductive physiology and behavior. The most biologically relevant form of estrogens is 17β-estradiol (E2). Diverse estrogen functions are mediated by their specific estrogen receptors (ER), including classic nuclear receptors ERα and ERβ, and membrane-bound receptors G protein-coupled ER (GPER, also known as GPR 30) and membrane-associated ERα and ERβ variants. All the ER subtypes are expressed in the livers of male and female humans and rodents, but at a lower level compared with reproductive organs. ERα has been shown to be responsible for the E2-mediated regulation of inducible nitric oxide (NO) synthase (iNOS) expression in the liver and protection against inflammation (1).

The liver represents an important participant in the systemic inflammatory networks by experiencing activation of inflammatory pathways within its local cells. Proinflammatory cytokines induce increased production of iNOS in the liver (2). A growing body of evidence implicates that iNOS expression and the excessive production of NO is involved in the development of various types of liver diseases

Key words: estradiol, inducible nitric oxide synthase, Src kinase, extracellular signal-regulated kinase, miR-221

Mailing address:
Esma R. Isenovic, Ph.D.
Vinca Institute of Nuclear Science, University of Belgrade
Department of Radiobiology and Molecular Genetics
P.O.Box 522, 11000 Belgrade, Serbia
Tel./Fax: +38111-3408147
e-mail: isenovic@yahoo.com

0393-974X (2018)

(3). iNOS has the highest capacity among all of the NOS isoforms to generate NO (2), an essential gaseous signaling molecule that regulates numerous physiological processes. However, excessive production of NO may potentiate cytotoxicity through its reaction with superoxide anion and nitration of tyrosine residues of proteins (3).

A central role in E2-ER cytoplasmic signaling has non-receptor intracellular Tyr kinase Src (4). Association of ER and Src may initiate signaling through some intracellular kinases, including extracellular signal-regulated kinases 1/2 (ERK1/2) (5) and protein kinase B (Akt) (6). Phosphorylated ERK1/2 and Akt are capable of phosphorylating and activating nuclear transcription factors, such as nuclear factor kappa B (NFκB) (7). Activation of ERK1/2 is required for induction of miR-221 (8), a member of microRNAs (miRNAs) family of small non-protein coding RNAs, that modulates an inflammatory response by controlling the NFkB activity (9). Regulation of iNOS expression via miRNA in various cell types, such as hepatocytes (10), has been demonstrated. Also, E2-regulated miRNA expression and miRNA regulation of ERα and its downstream response to E2 have recently been reported (11).

The overall hypothesis of this study is that E2 can inhibit iNOS *in vivo* in hepatic tissue via the activation of ER-α and that ERK1/2-miR-221 axis is involved in this process. Given the complexity of the physiological effects of E2 and the limited data related to the effects of E2 on the regulation of iNOS *in vivo*, in this study, we examined whether administration of a bolus injection of E2 24 h before sacrifice caused changes in hepatic iNOS protein expression in rats. Also, we assessed whether these changes could be related to changes in ER-α and ERK1/2 activation, and miR-221 expression.

MATERIALS AND METHODS

Animals and experimental treatment

For this study, we used eight-week-old, adult male Wistar rats (150 g-200 g), bred at the Institute of Nuclear Sciences (Vinca, Belgrade). The animals were kept under a 12:12-hour light/dark cycle at 22°C±2°C and were divided into two experimental groups: a control group and a group treated intraperitoneally with a bolus injection of a 40 μg/kg of 17β-estradiol (Sigma-Aldrich Corporation, St. Louis, MO, USA) dissolved in 1% ethanol in phosphate-buffer solution (PBS). The control group was injected with the same volume of 1% ethanol in PBS, 24 h before euthanasia. All rats were sacrificed under deep ether anesthesia (ether was purchased from Lek, Ljubljana, Slovenia) and blood was collected by cardiac puncture. The livers from each animal were excised, measured, snap frozen in liquid nitrogen and stored at −70°C until further experiments. The official Vinca Institute Ethics Committee for Experimental Animals approved all experimental protocols.

Liver lysate preparation.

The liver from each animal was removed and then homogenized on ice using an Ultra-Turrax homogenizer in lysis buffer (150 mM NaCl, 20 mM Tris, 2 mM EDTA, 2 mM DTT, 1% Triton X-100, 10% glycerol, pH 7.4) containing protease (Complete Ultra Tablets, Mini, EDTA-free, EASYpack) and phosphatase inhibitor cocktail (PhosSTOP) (Roche, Mannheim, Germany), and 2 mM sodium orthovanadate. Homogenates were incubated for 60 min with constant rotation at 4°C and then centrifuged for 30 min at 100,000 × g at the same temperature. Total protein concentration in supernatants was determined using the Lowry assay. The final lysates were stored at -70°C until further experiments.

Sodium dodecyl sulfate-polyacrylamide gel electrophoresis (SDS-PAGE) and Western blotting

Total cell protein lysates (80 μg/lane) were separated on 10% or 12% SDS-polyacrylamide gel and transferred to polyvinylidene difluoride (PVDF) membranes. Thereafter, the membranes were blocked with 5% bovine albumin and probed with rabbit polyclonal anti-ERα, anti-NFkB-p65 (Santa Cruz, CA, USA), anti-phospho-p44/42 ERK1/2 (Thr^{202}/Tyr^{204}), anti-total-p44/42 ERK1/2, anti-phospho-Akt (Ser^{473}), anti-total-Akt (Cell Signaling Technology, Beverly, MA USA), anti-iNOS (Abcam, Cambridge, UK), goat polyclonal anti-NFkB-p50, or mouse monoclonal anti-β-actin (Santa Cruz, CA, USA) antibodies. After washing with TBS-t, the membranes were incubated with the appropriate secondary anti-rabbit, anti-goat and anti-mouse IgG horseradish peroxidase-linked antibodies

(Santa Cruz, CA, USA) and used for subsequent detection with the electrochemiluminescence (ECL) method (GE Healthcare Life Sciences, Buckinghamshire, UK). Following analysis of phospho forms of p44/42 ERK1/2 and Akt, the membranes were stripped and reblotted with antibodies detecting the total p44/42 ERK1/2 and Akt contents. To ensure that protein loading was equal in all samples, the blots were reprobed with the mouse anti-β-actin monoclonal antibody and appropriate anti-mouse secondary antibody. For quantification of the signals on membranes, Image J 1.45s software (National Institutes of Health, USA) was used.

Co-immunoprecipitation

Liver tissue lysates were normalized for protein content (500 mg of protein) and incubated overnight with 2 mg of anti-ERα antibody. Immunocomplexes were absorbed with protein A/G-sepharose (previously prepared by manufacturer instructions, Santa Cruz Biotechnology) overnight at 4ºC and then recovered by centrifugation (2500 × g; 5 min), washed three times with lysis buffer, and separated on SDS-PAGE gel, transferred to a PVDF membrane, and then probed with an anti-Src antibody (Cell Signaling Technology, Beverly, MA). Obtained signals were detected and quantified using Image J 1.45s software.

Total RNA isolation and quantitative real-time PCR (qPCR)

Total RNA (including mRNA and miRNA) from liver tissue was extracted using Trizol reagent (Invitrogen Life Technologies, Paisley, GB) according to the procedure recommended by the manufacturer. RNA concentration and purity were determined by measuring the absorbance at 260 nm/280 nm using BioSpec-nano-Spectrophotometer (Shimadzu, USA). To ensure that isolated RNA was not degraded, RNA samples were analyzed by 1.2% agarose gel electrophoresis.

For reverse transcription of miR-221, we used 10 ηg of total RNA, TaqMan MicroRNA Reverse Transcription Kit (Applied Biosystems, Foster City, California, USA), TaqMan Universal master mix 2x, No UNG amperase, according to the manufacturer's protocol.

The expression level of miR-221 in the liver was measured by the qPCR assay performed on 7500 Real-Time PCR System (Applied Biosystems, Foster City, CA, USA). miR-221 expression levels were expressed as relative quantity (RQ) values and normalized to endogenous control U6B. For miR-221 and small nuclear RNA-U6B amplification, we used TaqMan microRNA assays (Thermo Fisher Scientific). RQ values were calculated with 7500 System SDS Software by comparative the $2^{-\Delta\Delta Ct}$ method.

Statistical analysis

Results are expressed as the mean ± standard error of the mean (SEM). Two-tailed Student's *t-test* was used to evaluate the statistical significance of the data. A p-value <0.05 was considered as statistically significant.

RESULTS

Effects of estradiol on the regulation of hepatic iNOS protein expression

Since NO has important roles in the regulation of numerous physiological processes and since we have previously shown that E2 *in vitro* stimulates NO production (12), we next examined whether E2 affects regulation of hepatic iNOS protein level. The results show that the level of hepatic iNOS protein level decreased after E2 treatment ($p < 0.01$) (Fig. 1A).

Effect of estradiol on the hepatic p50 and p65 subunits of NFκB protein

Since the promoter of the iNOS gene contains the binding site for NFκB transcription factor (2), we further examined whether this transcription factor is involved in E2-mediated regulation of hepatic iNOS expression by measuring protein levels of p50 and p65 subunits of NFκB. The results show that there were no significant differences in the levels of either p50 (Fig. 2A) or p65 (Fig. 2C) proteins in E2-treated rats compared with control rats.

Effect of estradiol on the hepatic ERα protein level and ERα/Src association

Since effects of E2 are mediated by specific binding to the ER and that E2 reduces iNOS expression via ERα/NFκB interaction (1), we next examined the level of hepatic ERα protein expression after treatment with E2. The results

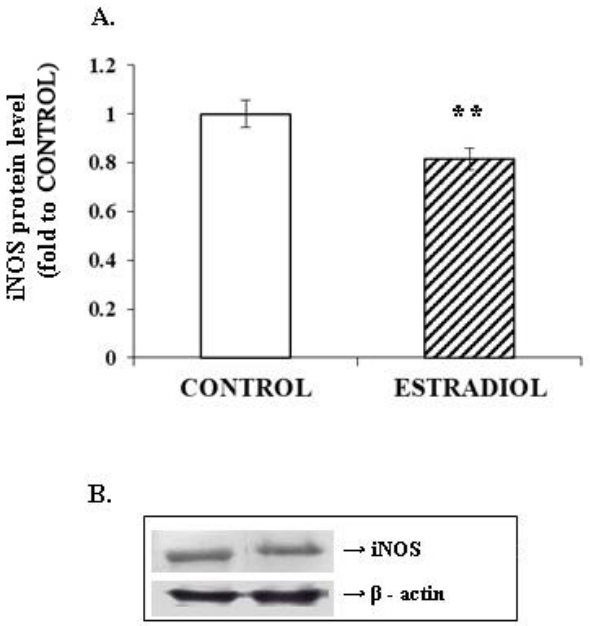

Fig. 1. *Effects of estradiol on the regulation of hepatic iNOS expression. **A)** Densitometry data for 6 separate Western blots (each bar is mean ± SEM). The Y-axis represents iNOS protein level expressed as - fold change to control (control arbitrary set at 1), and the X-axis represents treatment. **B)** Representative Western blot. **p<0.01 indicates a significant difference.*

indicate that E2 treatment induces a significant decrease ($p < 0.05$) of ERα protein level (Fig. 3A). As ER does not possess kinase activity, E2 cannot activate any signaling pathway in the cytoplasm after binding to ER. To activate any signaling pathway in the cytoplasm, ER needs to interact with some other molecules, such as Src tyrosine kinase (4). Here, we examined the effects of E2 on ERα/Src association in the liver. The results of co-immunoprecipitation of ERα and Src revealed that E2 treatment induced an increase in hepatic ERα/Src association ($p < 0.05$) compared with control (Fig. 3C).

Effect of estradiol on the phosphorylation of hepatic ERK1/2 on Thr^{202}/Tyr ^{204} and Akt on Ser^{473}

We previously reported that activation of hepatic iNOS involves phosphorylation of ERK1/2 and Akt (13). In the current study, we further examined the effect of E2 on ERK1/2 phosphorylation at Thr^{202}/Tyr^{204} (Fig. 4A) and on phosphorylation of Akt at Ser^{473} (Fig. 4C). Results show that E2 treatment significantly decreased both the phosphorylation of ERK1/2 ($p < 0.05$) and phosphorylation of Akt ($p < 0.001$).

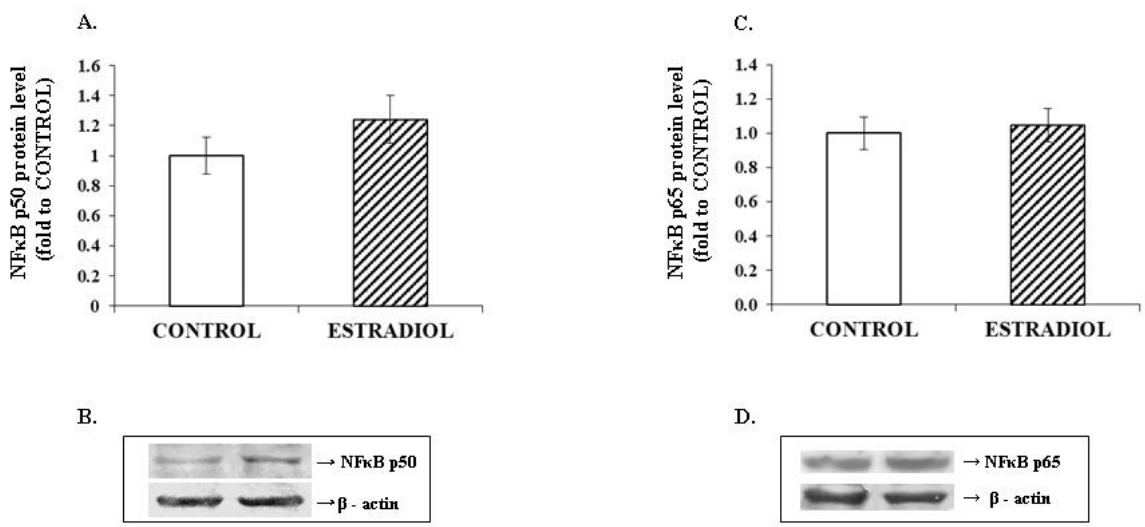

Fig. 2. *Effect of estradiol on the hepatic p50 and p65 subunits of NFκB protein. **A)** Densitometry data for 6 separate Western blots (each bar is mean ± SEM). The Y-axis represents p50 protein level expressed as - fold change to control (control arbitrary set at 1), and the X-axis represents treatment. **B)** Representative Western blot. **C)** Densitometry data for 5 separate Western blots (each bar is mean ± SEM). The Y-axis represents p65 protein level expressed as - fold change to control (control arbitrary set at 1), and the X-axis represents treatment. **D)** Representative Western blot.*

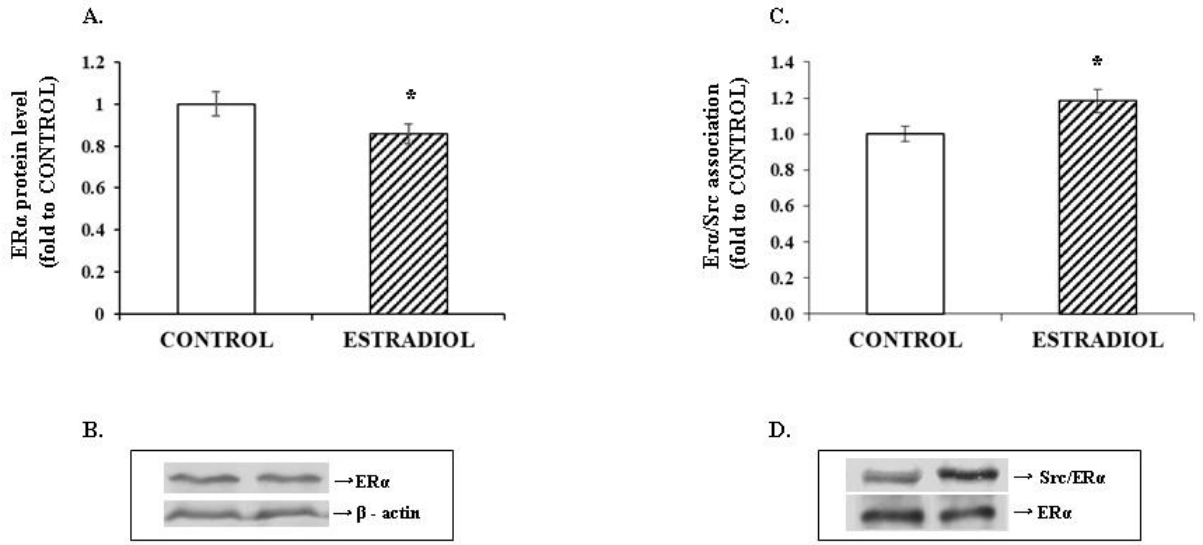

Fig. 3. *Effect of estradiol on the hepatic ERα protein level and ERα/Src association.* ***A)*** *Densitometry data for 7 separate Western blots (each bar is mean ± SEM). The Y-axis represents ERα protein level expressed as fold change to control (control arbitrary set at 1), and the X-axis represents treatment.* ***B)*** *Representative Western blot. *p<0.05 indicates a significant difference.* ***C)*** *Densitometry data for 4 separate Western blots (each bar is mean ± SEM). The Y-axis represents Src protein level in association with ERα expressed as - fold change to control (control arbitrary set at 1), and the X-axis represents treatment.* ***D)*** *Representative Western blot. *p<0.05 indicates a significant difference.*

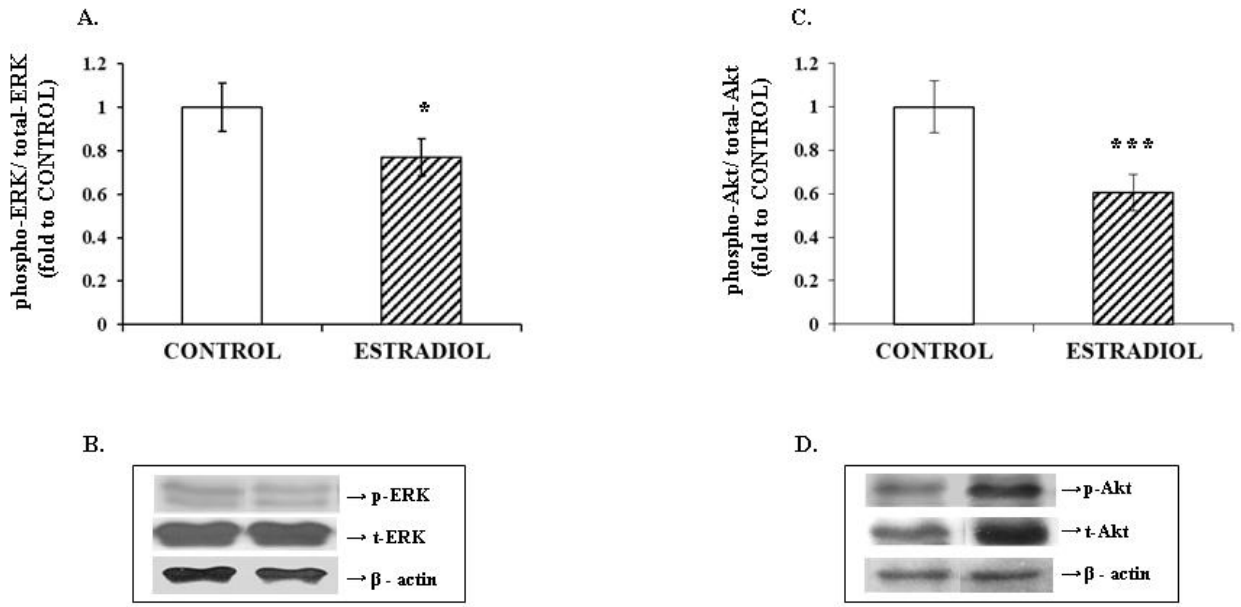

Fig. 4. *Effect of estradiol on the phosphorylation of hepatic ERK1/2 on Thr^{202}/Tyr ^{204} and Akt on Ser^{473}.* ***A)*** *Densitometry data for 7 separate Western blots (each bar is mean ± SEM). The Y-axis represents the ratio of phosphorylated and total ERK1/2 expressed as - fold change to control (control arbitrary set at 1), and the X-axis represents treatment.* ***B)*** *Representative Western blot. *p<0.05 indicates a significant difference.* ***C)*** *Densitometry data for 7 separate Western blots (each bar is mean ± SEM). The Y-axis represents the ratio of phosphorylated and total Akt expressed as fold change to control (control arbitrary set at 1), and the X-axis represents treatment.* ***D)*** *Representative Western blot. ***p<0.001 indicates a significant difference.*

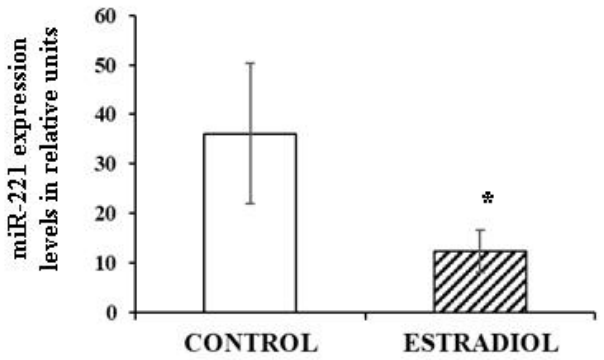

Fig. 5. *Effects of estradiol on the hepatic miR-221 expression. The level of miR-221 gene expression. The Y-axis represents miR-221 level expressed in relative units (each bar is mean ± SEM), and the X-axis represents treatment. *p<0.05 indicates significant differences.*

Effects of estradiol on the hepatic miR-221 expression

Some miRNAs affect the expression of iNOS in various cell types, including hepatocytes (10). To determine whether E2 influenced the miR-221, we measured the level of hepatic miR-221 expression. The results presented in Fig. 5. show that E2 treatment induced a significant decrease of miR-221 ($p < 0.05$) compared with control rats.

DISCUSSION

The principal new finding of the present study is that E2 regulates hepatic iNOS expression *in vivo* via molecular mechanisms involving ER-α and ERK1/2-miR-221 axis. These data extend our previous finding where we showed that E2 *in vitro* stimulates NO production (12). The expression of iNOS can be induced in a wide range of cells and tissues by cytokines and other inflammatory agents (2). The results from our study demonstrate that E2 treatment decreases hepatic iNOS protein level in male rats. Similarly to our results, others also reported that protein expression of iNOS was reduced by E2 treatment (14). In this study we used male rats, to avoid variations in circulating estradiol levels. Also, using female rats would require bilateral ovariectomy followed by decrease of endogenous estradiol which could lead to the development of insulin resistance, obesity and inflammation (15).

Contrary to inhibition of iNOS expression, in our study an increase in nitrite/nitrate plasma concentration following E2 treatment (data not shown) was observed suggesting increased plasma NO level. An increased NO level in the plasma may be responsible for decreased hepatic iNOS protein level, as NO can diffuse rapidly into cells and inhibit iNOS protein expression and activity through coordination with the heme of the iNOS enzyme (16). Because of iNOS inducible nature, regulation of its transcription is a primary step in the control of iNOS activity/expression (2). Analysis of the 5' region of the iNOS gene revealed that it contains redox-sensitive elements including NFκB-responsive element. Mammary NFκB mainly consists of p50 and p65 subunits. Heterodimers consisting of p50 and p65 proteins are involved in the activation of inflammatory genes, with iNOS being one of the main p65 downstream targets. Inhibition of iNOS expression by numerous agents results from inhibition of NFκB activation (17). The results from this study surpassingly show that protein levels of both p50 and p65 NFκB subunits were not changed after E2 administration. These results can be explained by the fact that E2 also affects some of the transcription factors, besides NFκB, responsible for regulation of iNOS (18).

ERα represents the primary ER responsible for E2-mediated regulation of iNOS expression in the liver (1). The results of this study show a significant decrease in ERα protein level. Acute degradation of ERα followed by E2-dependent transcriptional activation of ERα gene is a general response to E2, whereby ERα ubiquitylation and proteolysis are intimately linked to ERα-dependent transcriptional activity (19). In our experiments, rats were treated with a single bolus injection of E2 and sacrificed 24 h after the treatment, whereas literature data showed that long-term exposure to E2 maintains the non-reproductive estrogen target tissues, such as liver, in an estrogen-responsive condition by up-regulating steady-state ERα levels (20). Since ERs do not possess kinase activity, some other molecules are needed to transmit information from E2-ER binding to stimulate cytoplasmic signaling. A central role in E2 cytoplasmic signaling has the

intracellular Tyr kinase Src, a key proximal signaling molecule in multiple pathways (4). Src is a non-receptor kinase belonging to the Src family kinases that phosphorylate a Tyr residue on their target proteins, and their own activity is regulated by Tyr autophosphorylation. The Src kinase family is basally inactive because the catalytic domain is constrained in an inactive state through intramolecular interactions. Catalytic activation requires the release of the constraints by binding of Src protein to other phosphorylated Tyr residues. ERα has been reported to be Tyr phosphorylated by c-Src or other enzymes and to interact with the SH2-domain of c-Src (4). Our results show that E2 treatment increases the association of ERα and Src protein compared with controls, indicating a positive effect of E2 on Src activation. Additionally, ERα/Src crosstalk may not only stimulate ERα-mediated transcription but also appears to activate ERα proteolysis (21). We assume that in our study E2-induced Src activation contributed to the ERα proteolytic degradation and to the detected decrease of ERα protein level.

Association of ligand-bound ER and Src rapidly initiates crosstalk with mitogenic signaling cascades, including ERK1/2 (5) and Akt (6). The role of ERK1/2 in the induction of iNOS has been demonstrated (22). The role of ERK1/2 signaling in E2-regulation of hepatic iNOS in our study was demonstrated by measuring the level of ERK1/2 phosphorylation. The results indicate that E2 leads to decreased hepatic Thr^{202}/Tyr^{204} phosphorylation of ERK1/2. Gaben et al. (23) reported that E2 does not induce rapid ERK phosphorylation, but it induces the transcription of its target genes rapidly and efficiently despite the down-regulation of the receptor. This is in accordance with our current results demonstrating decreased protein level of ERα and decreased ERK1/2 Thr^{202}/Tyr^{204} phosphorylation. Also, the ERα can be activated in a ligand-independent manner in response to peptide growth factors, that activate ERK (24) and Akt signaling pathways (25). Apart from growth factors that utilize the protein kinase Akt to activate ERα (25), E2 also activates Akt. Stoica et al. (26) reported that E2 via ERα activates Akt, which in return phosphorylates ERα leading to the modulation of its genomic effects. However, in this study, we show a reduction of Akt phosphorylation. Similarly to our results, Lobenhofer et al. (27) also detected no phosphorylation of Akt after E2 treatment. Based on the results of our study together with results from others, we hypothesize that there is a connection between unchanged NFκB protein levels and decreased Akt activation after E2 treatment.

As a part of this study, we also examined the effects of E2 on the hepatic miR-221 expression. To the best of our knowledge, there are no published studies exploring the role of miR-221 in the E2-mediated regulation of hepatic iNOS expression. miRNAs are 21–23 nucleotide long non-coding RNA molecules that modulate the stability and/or the translational efficiency of target mRNAs. miRNAs are frequently dysregulated in a variety of pathological conditions, including liver diseases (28). Additionally, E2-regulated miRNA and regulation of ERα by miRNA and its downstream transcriptional response to E2 have also been reported (29). miR-221 overexpression leads to significant increases in NFκB and mitogen-activated protein kinase (MAPK) activation which is associated with the augmented production of proinflammatory cytokines (9). Decreased miR-221 expression after blockading NFκB activation was reported (30), suggesting an NFκB-dependent induction of miR-221. Our results indicate that E2 treatment leads to the reduction of miR-221 expression level. The decreased level of miR-221 expression in our study supports our data showing that E2 treatment did not change levels of NFκB p65 and p50 proteins. Also, since the activation of ERK1/2 is required for induction of miR-221 (8), observed reduction of ERK1/2 phosphorylation after E2 treatment in our study could be a possible explanation for decreased miR-221. Furthermore, it is possible that E2 induces changes in hepatic iNOS via ERK1/2 and miR-221 signaling pathways by affecting some of the transcription factors involved in iNOS regulation without activation of NFκB, such as activator protein-1 (AP-1) (18). Therefore the aim of future investigations should be directed to identify the potential involvement of AP-1 in the E2-mediated regulation of iNOS expression.

In summary, our results indicate that *in vivo* treatment of male rats with E2 modulates iNOS

expression via molecular mechanisms involving increased ERα-Src interaction, decreased ERK1/2 and Akt activation and unchanged transcriptional activation of p65 NFκB protein. Our results also suggest the involvement of miR-221 in the regulation of iNOS expression possibly influencing ERK1/2 activation. Increasing our understanding of the molecular mechanisms responsible for the effects of E2 on hepatic iNOS regulation could be of great interest for future clinical trials related to different hepatic diseases.

ACKNOWLEDGEMENTS

This work was supported by the grants No. 173033 (to E.R.I) and No.175099 (to A.N.) from the Ministry of Education, Science and Technological Development, Republic of Serbia.

REFERENCES

1. Shimizu T, Yu HP, Suzuki T, et al. The role of estrogen receptor subtypes in ameliorating hepatic injury following trauma-hemorrhage. J Hepatol 2007; 46:1047-54.
2. Taylor BS, Alarcon LH, Billiar TR. Inducible nitric oxide synthase in the liver: regulation and function. Biochemistry (Mosc) 1998; 63:766-81.
3. Stanimirovic J, Obradovic M, Zafirovic S, et al. Effects of altered hepatic lipid metabolism on regulation of hepatic iNOS. Clinical Lipidology 2015; 10:167-75.
4. Shupnik MA. Crosstalk between steroid receptors and the c-Src-receptor tyrosine kinase pathways: implications for cell proliferation. Oncogene 2004; 23:7979-89.
5. Migliaccio A, Di Domenico M, Castoria G, et al. Tyrosine kinase/p21ras/MAP-kinase pathway activation by estradiol-receptor complex in MCF-7 cells. EMBO J 1996; 15:1292-300.
6. Castoria G, Migliaccio A, Bilancio A, et al. PI3-kinase in concert with Src promotes the S-phase entry of oestradiol-stimulated MCF-7 cells. EMBO J 2001; 20: 6050-59.
7. Dan HC, Cooper MJ, Cogswell PC, Duncan JA, Ting JP, Baldwin AS. Akt-dependent regulation of NF-{kappa}B is controlled by mTOR and Raptor in association with IKK. Genes Dev 2008; 22:1490-500.
8. Dai R, Li J, Liu Y, et al. miR-221/222 suppression protects against endoplasmic reticulum stress-induced apoptosis via p27Kip1- and MEK/ERK-mediated cell cycle regulation. Biol Chem 2010; 391:791.
9. Zhao D, Zhuang N, Ding Y, Kang Y, Shi L. MiR-221 activates the NF-kappaB pathway by targeting A20. Biochem Biophys Res Commun 2016; 472:11-18.
10. Guo Z, Shao L, Zheng L, et al. miRNA-939 regulates human inducible nitric oxide synthase posttranscriptional gene expression in human hepatocytes. Proceedings of the National Academy of Sciences 2012; 109:5826-31.
11. Rao X, Di Leva G, Li M, et al. MicroRNA-221/222 confers breast cancer fulvestrant resistance by regulating multiple signaling pathways. Oncogene 2011; 30:1082-97.
12. Isenovic ER, Divald A, Milivojevic N, Grgurevic T, Fisher SE, Sowers JR. Interactive effects of insulin-like growth factor-1 and beta-estradiol on endothelial nitric oxide synthase activity in rat aortic endothelial cells. Metabolism 2003; 52:482-87.
13. Stanimirovic J, Obradovic M, Jovanovic A, et al. A high fat diet induces sex-specific differences in hepatic lipid metabolism and nitrite/nitrate in rats. Nitric Oxide 2016; 54:51-59.
14. Nweze IC, Smith JW, Zhang B, Lakshmanan J, Klinge CM, Harbrecht BG. 17β-Estradiol attenuates cytokine-induced nitric oxide production in rat hepatocyte. J Trauma Acute Care 2012; 73:408-12.
15. Zhu L, Brown WC, Cai Q, et al. Estrogen treatment after ovariectomy protects against fatty liver and may improve pathway-selective insulin resistance. Diabetes 2013; 62:424-34.
16. Griscavage JM, Rogers NE, Sherman MP, Ignarro LJ. Inducible nitric oxide synthase from a rat alveolar macrophage cell line is inhibited by nitric Oxide. J Immunol 1993; 151: 6329-37.
17. Jeon YJ, Han SH, Lee YW, Yea SS, Yang KH. Inhibition of NF-kappa B/Rel nuclear translocation by dexamethasone: mechanism for the inhibition of iNOS gene expression. Biochem Mol Biol Int 1998; 45:435-41.
18. Paech K, Webb P, Kuiper GG, et al. Differential ligand activation of estrogen receptors ERalpha and ERbeta at AP1 sites. Science 1997; 277: 1508-10.

19. Reid G, Hubner MR, Metivier R, et al. Cyclic, proteasome-mediated turnover of unliganded and liganded ERalpha on responsive promoters is an integral feature of estrogen signaling. Mol Cell 2003; 11:695-707.
20. Donaghue C, Westley BR, May FE. Selective promoter usage of the human estrogen receptor-alpha gene and its regulation by estrogen. Mol Endocrinol 1999; 13:1934-50.
21. Chu I, Arnaout A, Loiseau S, et al. Src promotes estrogen-dependent estrogen receptor α proteolysis in human breast cancer. J Clin Invest 2007; 117:2205-15.
22. Hou CH, Lin J, Huang SC, Hou SM, Tang CH. Ultrasound stimulates NF-kappaB activation and iNOS expression via the Ras/Raf/MEK/ERK signaling pathway in cultured preosteoblasts. J Cell Physiol 2009; 220:196-203.
23. Gaben AM, Saucier C, Bedin M, Redeuilh G, Mester J. Mitogenic activity of estrogens in human breast cancer cells does not rely on direct induction of mitogen-activated protein kinase/extracellularly regulated kinase or phosphatidylinositol 3-kinase. Mol Endocrinol 2004; 18:2700-713.
24. Improta-Brears T, Whorton AR, Codazzi F, York JD, Meyer T, McDonnell DP. Estrogen-induced activation of mitogen-activated protein kinase requires mobilization of intracellular calcium. Proc Natl Acad Sci U S A 1999; 96: 4686-91.
25. Martin MB, Franke TF, Stoica GE, et al. A role for Akt in mediating the estrogenic functions of epidermal growth factor and insulin-like growth factor I. Endocrinology 2000; 141:4503-11.
26. Stoica GE, Franke TF, Moroni M, et al. Effect of estradiol on estrogen receptor-alpha gene expression and activity can be modulated by the ErbB2/PI 3-K/Akt pathway. Oncogene 2003; 22:7998-8011.
27. Lobenhofer EK,Marks JR. Estrogen-induced mitogenesis of MCF-7 cells does not require the induction of mitogen-activated protein kinase activity. J Steroid Biochem Mol Biol 2000; 75:11-20.
28. Callegari E, Elamin BK, Giannone F, et al. Liver tumorigenicity promoted by microRNA-221 in a mouse transgenic model. Hepatology 2012; 56:1025-33.
29. Castellano L, Giamas G, Jacob J, et al. The estrogen receptor-alpha-induced microRNA signature regulates itself and its transcriptional response. Proc Natl Acad Sci U S A 2009; 106:15732-37.
30. Galardi S, Mercatelli N, Farace MG, Ciafrè SA. NF-kB and c-Jun induce the expression of the oncogenic miR-221 and miR-222 in prostate carcinoma and glioblastoma cells. Nucleic Acids Res 2011; 39:3892-902.

ROLE AND INFLUENCE OF P75 NTR RECEPTOR ON ANTIOXIDATIVE DAMAGE OF RETINAL PIGMENT EPITHELIAL CELLS

HW. LIU[1*], Y. MENG[1*], J. ZHANG[1], YB. REN[1], YC. LI[1], Y. WANG[2] and JJ. WANG[3*]

[1]Department of Ophthalmology, First Affiliated Hospital of Jiamusi University, Jiamusi, Heilongjiang, China; [2]Department of Pharmacology and Toxicology, Wright State University, Fairborn, OH, USA; [3]Department of Immunology, College of Basic Medicine, Jiamusi University, Jiamusi, Heilongjiang, China

Received June 28, 2018 – Accepted October 11, 2018

*These authors contributed equally to this work

The study aimed to investigate the role and mechanism of the p75 NTR receptor in the oxidative damage of retinal pigment epithelial cells (RPE). RPE cells transfected with the p75 NTR receptor were used as the experimental group, and the untransfected RPE cells as the control group. BrdU (5-Bromo-2-deoxyUridine) was used to detect cell proliferation activity; PI/Annexin V-FITC (fluorescein isothiocyanate, FITC) double staining was used to detect the apoptosis rate of the cells. The expression of reactive oxygen species (ROS) in cells was observed by laser microscope, and the expression of ROS, mitochondrial markers, and C expression of cytochrome in cells was detected by flow cytometry. Western blot was used to detect the Fas protein, pyrolysis Caspase-3, and expression level of the vascular endothelial growth factor 165 (VEGF165) protein. The results showed that the proliferation activity of RPE cells in the experimental group decreased gradually with the increase of transfection time, and the apoptosis rate of RPE cells in the experimental group increased gradually with the increase of transfection time, and the apoptosis rate of RPE cells at each time point was significantly higher than that of the control group. The fluorescence intensity of ROS in the experimental group was significantly stronger than that in the control group (P<0.01). The fluorescence intensity of cytochrome C in the RPE cells in the experimental group was significantly higher than that in the control group, while the number of positive mitochondria markers in the experimental group was less than that of the control group and the fluorescence intensity was weakened. The expression of Fas protein, Caspase-3 and VEGF165 protein in the experimental group was significantly higher than that in the control group (P<0.01). In conclusion, p75 NTR receptor may be a cause of oxidative damage in RPE cells.

Choroidal neovascularization (CNV) is common in macular degeneration (1, 2), which can cause different degrees of damage to human vision (3). Retinal pigment epithelial (RPE) cells can be degenerative under certain specific factors (4), and CNV is a chronic and hereditary retinal degeneration with poor prognosis (5, 6). The oxidative damage of RPE cells may be the pathological basis for the occurrence and development of age-related macular degeneration (AMD) (7). Reactive oxygen species (ROS), which are produced by oxidative stress, reduce the metabolic capacity of RPE cells and accelerate the occurrence and development of AMD (8). It has been found that oxidative damage in RPE

Key words: p75 NTR receptor, retinal pigment epithelial cells, anti-oxidant damage, proliferation, apoptosis

Mailing address:
Dr Jianjie Wang,
Department of Immunology, College of Basic Medicine,
Jiamusi University, No. 148 Xuefu Street,
Xiangyang District, Jiamusi, 154007,
Heilongjiang, China
e-mail: jmsdx_jianjie@163.com

0393-974X (2018)

cells can activate the p75 NTR receptor of the tumor necrosis factor superfamily, and thus cause vascular endothelial cell proliferation (9, 10). p75 NTR receptors can activate cell death domains by binding to ligands (11), and cell damage can be mediated by caspase, cell cycle inhibition, and other pathways without ligand binding (12,13). RPE cells were used to study the mechanism of p75 NTR receptor in the oxidative damage of RPE.

MATERIALS AND METHODS

Materials

Cells were from ARPE-19 (ARPE19) (Shanghai Gaining Biological Technology Co., Ltd., China).

Main reagents were: p75 NTR receptor expression plasmid (Wuhan Miaoling Biological Science and Technology Co., Ltd., China); BrdU Kit (Swiss Roche Company); PI/AnnexinV-FITC detection kit, ROS detection kit, mitochondrial marker detection kit, and cytochrome C detection kit (American ATCC company); rabbit anti-human Fas antibody, rabbit anti-human Caspase-3 antibody, and rabbit anti-human VEGF165 antibody (American Invitrogen Company).

Main instruments were : CO_2 constant temperature incubator (Shanghai Qi Qian Electronic Technology Co., Ltd.); fluorescence microscope (Shanghai Cai Kang Optical Instrument Co., Ltd.); flow cytometry (American Fas Calibur, Becton Dickeinson Company); electrophoretic instrument (Shanghai Da Ping Instrument Co., Ltd.).

RPE cell culture and transfection

RPE cells were placed into the medium containing 10% fetal bovine serum and cultured in the incubator (37 DEG C, 50mL/L CO_2). RPE cells transfected with p75 NTR receptor were the experimental group, and the untransfected RPE cells were the control group. The transfection A solution was prepared with solution (10 μg p75 NTR receptor expression plasmid DNA was added to 50 μL serum-free medium); B solution (2 μL liposome2000 transfection solution was added with 50 μL serum-free culture medium). After mixing A and B liquid, it remained static for 30 min at room temperature; for cell transfection RPE cells were added with A and B solutions, and culture medium, and then cultured in the incubator for 6 h; cells stably expressing the p75 NTR receptor were selected, transferred, and amplified for culture. The expression of green fluorescent protein was detected under the fluorescence microscope. When the transfection efficiency reached 80%, it showed that the transfection was successful, as shown in Fig.1.

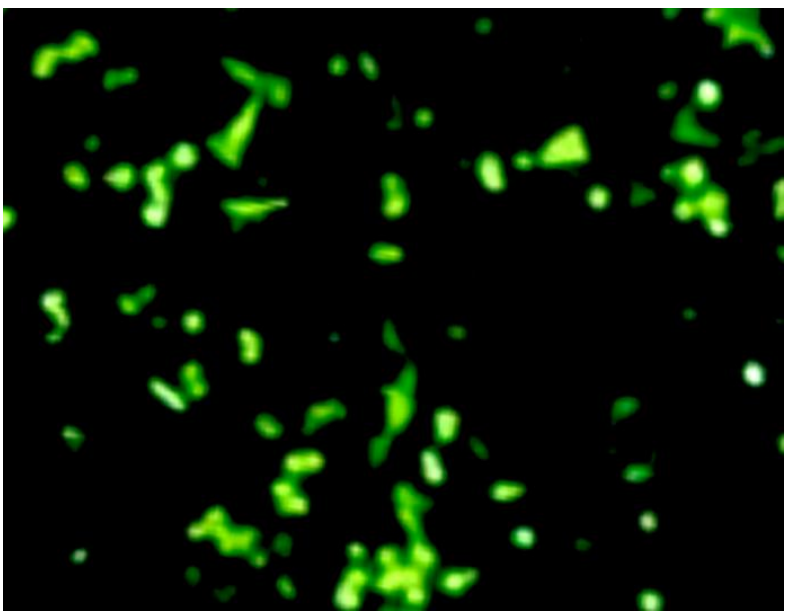

Fig. 1. *RPE cells (x 200) transfected with p75 NTR receptor.*

Detection of cell proliferation by BrdU

The two groups of RPE cells were seeded on 96 well plates at a density of 2 x 10^4/mL, 100 μL per WELL. After culture of 1, 2, 3 and 4 days, 10 μL BrdU solution was added to culture for 3 h. After removing the liquid from each pore, 200 μL of cell immobilized liquid was fixed for 25 ~ 35 min. The fixative of each pore was discarded, then 200 μL anti-BrdU-POD liquid was added to culture for 85 ~ 95 min. PBS rinses were performed 2~4 times, 100 μL substrate chromogenic solution was added, and the absorbance (A) value was determined at a wavelength of 450nm. The experiment was repeated 3 times, and the average value was taken. Cell activity rate = $A_{\text{experimental group}}/A_{\text{control group}} \times 100\%$.

Detection of apoptosis rate by PI/AnnexinV-FITC double staining

Two groups of RPE cells were seeded on 6 well plates with 2 x 10^4 wells. The cells were collected after culturing for 1, 2, 3, and 4 days, and 450 μL sample buffer was added. Then, 10 μL PI and 5 μL Annexin V-FITC were added, and incubated for 3 ~ 6 min after mixing. Flow cytometry was employed (ex/em=488 nm/530 nm), and Annexin V was determined by FITC (FLl). PI was detected by PE (FL2). The percentage of apoptosis was sum of the percentages of early and late apoptotic cells. Five pores were set up for each group. The experiment was repeated for three times, and the average value was taken.

Observation of intracellular ROS level by laser microscope

RPE cells were inoculated in Petri dish (diameter 60 mm) for 1.5 to 2 d by 1 x 10^4 wells. The medium was discarded and rinsed PBS for 1~3 times, 3~6 min each time. 1 mL DCFH-DA working fluid was added and incubated for 30 min. The liquid was discarded, PBS rinsed for 1~3 times, 3~6 min/times and the ROS fluorescence staining was observed in the cells under the laser microscope, and ROS showed green fluorescence.

Observation of mitochondria in cells by laser microscope

RPE cells were inoculated in a Petri dish (diameter 60 mm) for 1.5 to 2 d by 1 x 10^4/wells. Discarded supernatant and PBS rinsed 2 times, for 3~6 min each time. Added 1 ml 500 nm TMRM (Tetramethylrhodamine methyl ester) working fluid and incubated in incubator at 37°C for 30 min, discarded supernatant and PBS rinsed for 2 times, 3~6 min/time. 1 ml PBS was added to each Petri dish, and the images were observed and captured by laser microscope. After TMRM entered mitochondria, strong fluorescence was emitted.

Observation of expression of cytochrome C in cells by laser microscope

The RPE cells were seeded on the cover glass (each cover glass seeded 2000 cells), and the cover glass was placed in the 6 well plates for 1.5 d to 2 d; 30 min before the termination of culture, the supernatant was discarded and 1ml/well of 200 nm was added to the MitoTracker and incubated at 37°C for 30 min. The cell tablets were removed and 4% paraformaldehyde was added to immobilize for 15 min. After rinsing, ice formaldehyde was added to the surface of tablets and processed on the ice for 5 min. After the goat serum was closed, the cytochrome C-antibody was incubated overnight at 4°C; and the FITC-labeled donkey anti-mouse fluorescence was incubated for 1 h at room temperature and Hoechst 33342 (1:1000) was added for dye nuclear for 5 min. Under the laser microscope, cytochrome C expression was observed to be green fluorescence.

Detection of expression levels of ROS, mitochondrial markers, and cytochrome C by flow cytometry

RPE cells were seeded on 6 hole plates and cultured for 1.5 to 2d with 2 x 10^4 holes. The cells were collected, each tube had 500 μL 1μmol/L H_2DCFDA overhanging cells added, and then were incubated in the incubator at a temperature of 37°C for 30 min. Centrifugation was used to remove the supernatant and after 500 μL PBS overhanging cells, flow cytometry was carried out. The hydrolyzed H_2DCFDA was detected by FITC channel (FLl). The experiment was repeated at least 3 times. The percentage of intracellular ROS positive (%) = ROS positive number/control group ROS positive number × 100%. Then, according to the mitochondrial markers test box, cytochrome C test kit operating instructions, operation, and machine test were conducted. Five pores were set up for each group and the experiment was repeated 3 times.

Detection of expression levels of Fas, Caspase-3, and VEGF165 proteins by Western blot

RPE cells were seeded in Petri dishes at 2 * 10^5/mL and cultured for 1.5 to 2 d. The protein concentration was determined by the Bicinchoninic (BCA) acid method.

SDS-PAGE gel electrophoresis was conducted for 2 h, and trans-membrane to PVDF membrane. The cells were incubated with skim milk powder and incubated overnight at 4°C (rabbit anti human Fas antibody, rabbit anti human Caspase-3 antibody, and rabbit anti-human VEGF165 antibody). TBST rinsed 2~4 times, added the corresponding two-anti and incubated for 0.8 ~ 1.2 h. Rinsed TBST for 2~4 times, detected the expression of protein by exposure method, and analyzed the gray value of the strip by Image J software. Five pores were set up for each group and the experiment was repeated 3 times.

Statistical analysis

The data obtained were analyzed by SPSS 20.0. χ^2 test was used to count data, and Levene test was performed in all groups. Measurement data was represented by $\bar{x} \pm s$, LSD (Least-Significant Difference) test was used in comparison between groups, and the difference was statistically significant when $P<0.05$.

RESULTS

Cell proliferation activity and apoptosis rate

As shown in Table I, the proliferation activity of RPE cells in the experimental group gradually decreased with the prolongation of the transfection time. The proliferation activity of each transfection time was significantly different ($P<0.05$), but all were significantly lower than that of the control group ($P<0.05$).

The apoptosis rate of RPE cells in the experimental group increased gradually with the prolongation of the transfection time. There was a significant difference in the apoptosis rate of RPE cells between

Table I. *Comparison of proliferative activity ($\bar{x} \pm s$, %)*

Groups	Transfection time	RPE cell proliferation activity
Experimental group	Transfect 1d	92.18±0.71 g
	Transfect 2d	89.03±0.68 a,g
	Transfect 3d	71.44±0.74 a,e,g
	Transfect 4d	61.27±1.01 a,c,e,g
Control group	-	100.00±0.00

Experimental group: transfected RPE cells of p75 NTR receptor; the control group: Untransfected RPE cells. a: P<0.05 vs transfect 1d; c: P<0.05 vs transfect 2d; e: P<0.05 vs transfect 3d; g: P<0.05 vs control group.

Table II. *Comparison of apoptosis rate ($\bar{x} \pm s$,%)*

Groups	Transfection time	RPE cell proliferation activity
The experimental group	Transfect 1d	4.84±0.45 h
	Transfect 2d	9.57±1.08 b,h
	Transfect 3d	17.18±1.25 b,d,h
	Transfect 4d	22.24±2.33 b,d,e,h
The control group	-	0.80±0.09

Experimental group: transfected RPE cells of p75 NTR receptor; control group: untransfected RPE cells. b: P<0.01 vs transfect 1d; d: P<0.01 vs transfect 2d; e: P<0.05 vs transfect 3d; h: P<0.01 vs control group.

the different transfection time points (P<0.01) which were significantly higher than those of the control group (P<0.01) (Table II).

Expression of ROS, mitochondrial markers and cytochrome C

As shown in Fig. 2, the ROS green fluorescence signal in the experimental group was obviously stronger than that in the control group. The red fluorescence signal of the mitochondria markers in the control group was obviously stronger than that in the experimental group (Fig. 3). The red fluorescence of the mitochondrial markers in the experimental group was close to that of the control group, and the green fluorescence of the cytochrome C was obviously enhanced. However, the green fluorescence of cytochrome C was not found in the control group (Fig. 4).

Detection of expression levels of ROS, mitochondrial markers and cytochrome C by flow cytometry

The level of ROS in the RPE cells of the control group (100±0%) was significantly different (P<0.01) from that of the experimental group (223.15±21.62%). The positive rate of mitochondrial markers in the RPE cells of the experimental group (37.22±1.89%) was also significantly different (P<0.01) from that of the control group (100%±0%). The expression level of cytochrome C in the experimental group (55.18±5.03%) was significantly higher than that in the control group (15.43±1.83%) (Fig. 5).

Detection of apoptosis-related protein expression in two groups of RPE cells by Western blot

As seen in Table III and Fig. 6, the expression of three proteins in the experimental group was significantly higher than that in the control group (P<0.01).

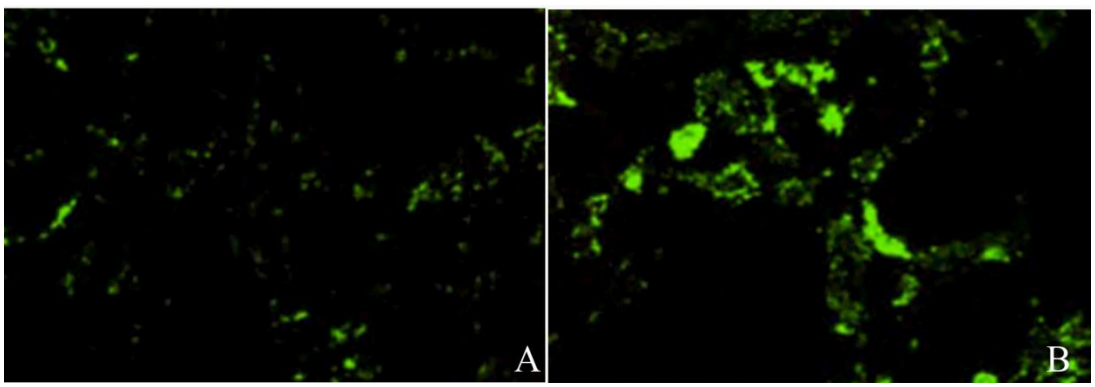

Fig. 2. *The results of ROS fluorescence staining under laser microscope (x 400). **A)** control group; **B)** experimental group).*

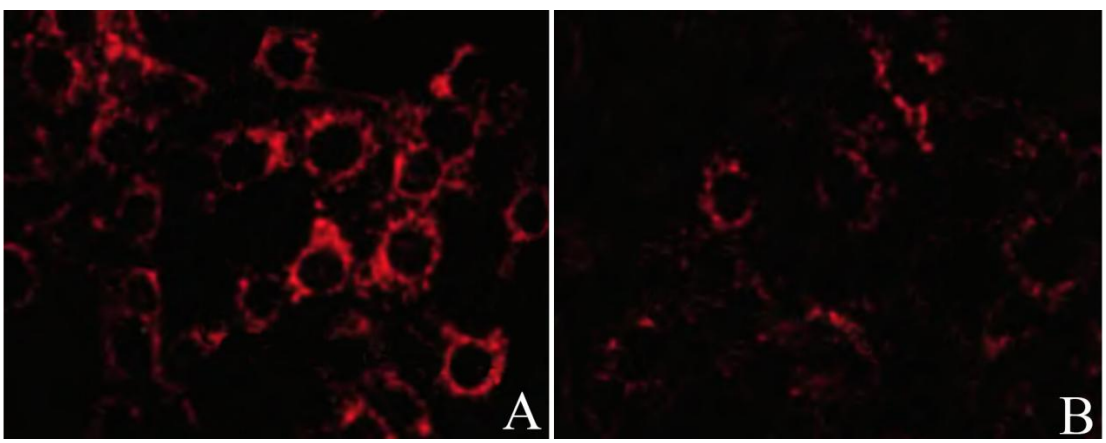

Fig. 3. *Fluorescent staining results of mitochondrial markers under laser microscope. **A)** control group; **B)** experimental group) (wavelength of TMRM: 10 um).*

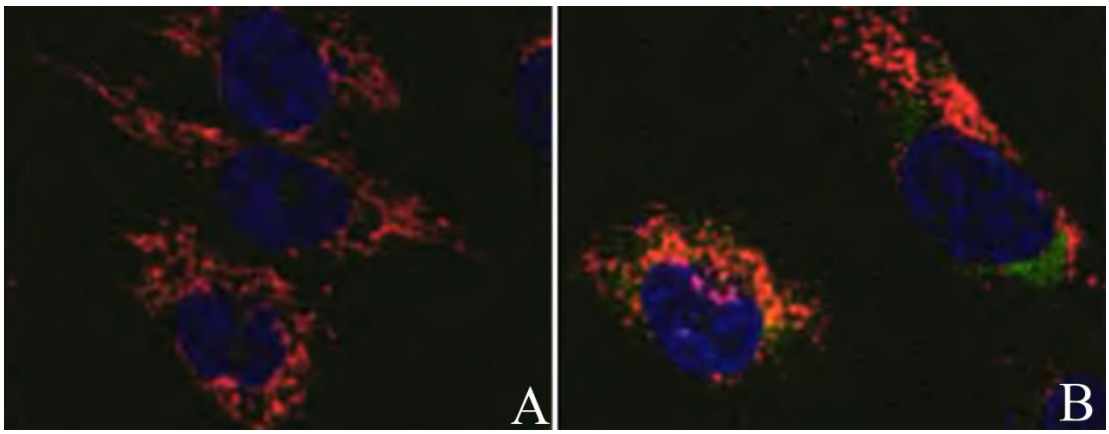

Fig. 4. *Cytochrome C expression under a laser microscope. **A**) Control group; **B**) experimental group) (wavelength of FITC: 10 um).*

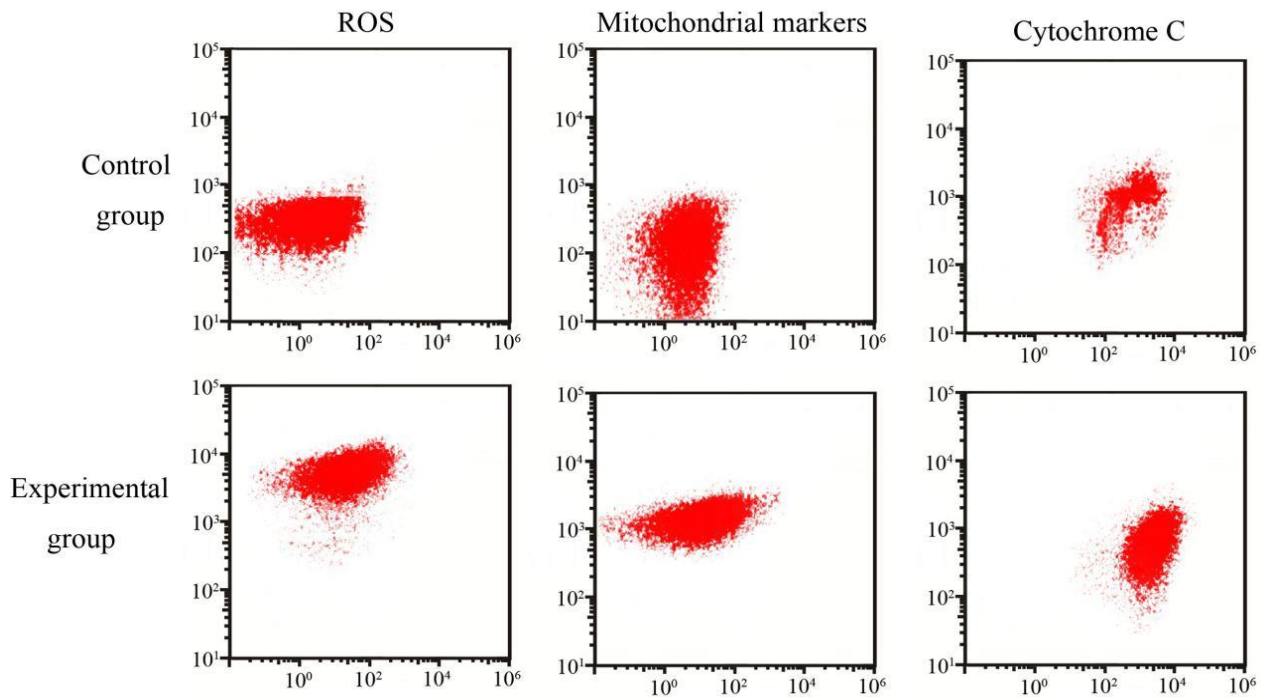

Fig. 5. *Flow cytometry detection.*

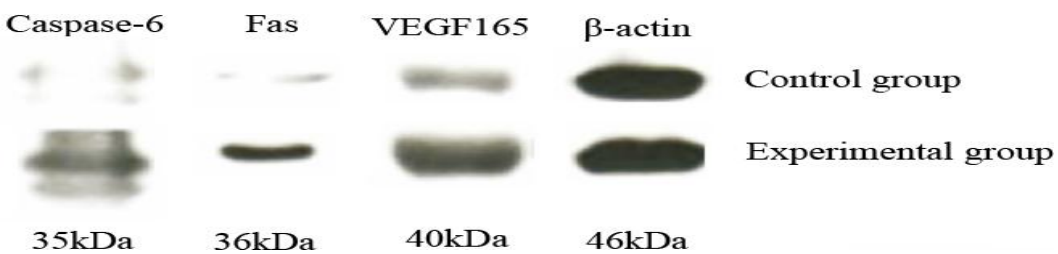

Fig. 6. *Detection of expression levels of Fas, Caspase-3, and VEGF165 proteins by Western blot.*

Table III. *Comparison of gray value of apoptosis-related protein bands*

Groups	Caspase-2	Fas protein	VEGF165 protein
The control group	112.14±9.65	108.96±12.65	133.28±13.82
The experimental group	351.48±27.64	542.94±47.38	639.17±52.74
T	13.10	14.51	15.63
P	<0.01	<0.01	<0.01

DISCUSSION

The oxidative damage of RPE is one of the main factors in the formation of choroidal neovascularization (14, 15). Because RPE cells are often related to the physiological metabolic function of the human retina, the important goal is to neutralize the photon energy to produce ROS (16-18). According to Antyborzec et al. (19), ROS production is increased among RPE cells as they age. This is because the phagocytosis of RPE becomes weaker as age increases. When ROS reacts with lysosome in the human body to synthesize phagosome, it is more likely to lead to the production of lipofuscin precursor, resulting in more ROS. The studies of Ragunathan et al. (20) showed that the metabolic function of the body is reduced as they age, which results in more and more waste from the base. If these metabolic wastes cannot be removed in time, the Bruch film will be thickened. This thickening will lead to the formation of warts on the vitreous membrane, promote the occurrence of oxidative damage, and eventually lead to the formation of CNV.

p75 NTR receptor is lowly expressed in RPE cells of the human body (21), but when the body suffers damage, it will present a high expression state (22, 23). The relationship between p75 NTR receptor and RPE oxidative damage was studied. It was found that the longer the p75 NTR receptor transfection time is, the lower the cell viability is and the higher the apoptosis rate will be. The positive rate of mitochondrial markers in the experimental group is far lower than that of the control group ($P<0.01$). Because the mitochondrial membrane potential changes in the early stage of apoptosis, if the mitochondrial membrane potential is depolarized the cytochrome C and ROS will be increased (23), and the mitochondrion itself will become the target of the oxidative damage of ROS. A vicious circle will further aggravate oxidative damage (24, 25). At the same time, once cytochrome C is released from mitochondria into the cytoplasm, it will lead to Caspase cascade reaction, which will make cell apoptosis more serious (26).

To summarize, the overexpressed p75 NTR receptor can cause damage to the cell mitochondria of the RPE, and also promote cell apoptosis reaction and eventually lead to the formation of choroidal neovascularization. Thus, it is possible to speculate that the p75 NTR receptor is one of the factors that cause damage of RPE.

REFERENCES

1. Mathieu B, Isaico R, Ramel JC, Bron AM, Creuzot-Garcher C. Treatment of high myopic choroidal neovascularisation with intravitreal bevacizumab. J Fr Opthalmol 2014; 37(1):54-57.
2. Zhou Q, Gallagher R, Ufret-Vincenty R, Li X, Olson EN, Wang S. Regulation of angiogenesis and choroidal neovascularization by members of microRNA- 23-27-24 clusters. Proc Natl Acad Sci U S A 2011; 108(20):8287-92.
3. Saishin Y, Saishin Y, Takahashi K, et al. VEGF-TRAPR1R2 suppresses choroidal neovascularization and VEGF-induced breakdown of the blood–retinal barrier. J Cell Physiol 2003; 195(2):241-8.
4. Kokkinaki M, Sahibzada N, Golestaneh N. Human induced pluripotent stem-derived retinal pigment

epithelium (RPE) cells exhibit ion transport, membrane potential, polarized vascular endothelial growth factor secretion, and gene expression pattern similar to native RPE. Stem Cells 2011; 29(5):825-35.
5. Falkner-Radler CI, Krebs I, Glittenberg C, Povazay B, Drexler W, Graf A, Binder S. Human retinal pigment epithelium (RPE) transplantation: outcome after autologous RPE-choroid sheet and RPE cell-suspension in a randomised clinical study. Br J Ophthalmol 2011; 95(3):370-75.
6. Kanemura H, Go MJ, Shikamura M, et al. Tumorigenicity Studies of Induced Pluripotent Stem Cell (iPSC)-Derived Retinal Pigment Epithelium (RPE) for the Treatment of Age-Related Macular Degeneration. PLoS One 2014; 9(1):e85336.
7. Tezel TH, Del Priore LV, Berger AS, Kaplan HJ. Adult retinal pigment epithelial transplantation in exudative age-related macular degeneration. Am J Ophthalmol 2007; 143(4):584-95.
8. Lois N, McBain V, Abdelkader E, Scott NW, Kumari R. Retinal pigment epithelial atrophy in patients with exudative age-related macular degeneration undergoing anti-vascular endothelial growth factor therapy. Retina 2013; 33(1):13-22.
9. Zhang J, Zhao J, Bai Y, Huang L, Yu W, Li X. Effects of p75 neurotrophin receptor on regulating hypoxia-induced angiogenic factors in retinal pigment epithelial cells. Mol Cell Biochem 2015; 398(1-2):123-34.
10. Hollborn M, Kohen L, Wiedemann P, Enzmann V. The influence of pro-inflammatory cytokines on human retinal pigment epithelium cell receptors. Graefes Arch Clin Exp Ophthalmol 2001; 239(4):294-301.
11. Tuffereau C, Bénéjean J, Blondel D, Kieffer B, Flamand A. Low-affinity nerve-growth factor receptor (P75NTR) can serve as a receptor for rabies virus. EMBO J 1998; 17(24):7250-59.
12. Casademunt E, Carter BD, Benzel I, Frade JM, Dechant G, Barde YA. The zinc finger protein NRIF interacts with the neurotrophin receptor p75 (NTR) and participates in programmed cell death. EMBO J 1999; 18(21):6050-61.
13. Quann EJ, Khwaja F, Zavitz KH, Djakiew D. The aryl propionic acid R-flurbiprofen selectively induces p75NTR-dependent decreased survival of prostate tumor cells. Cancer Res 2007; 67(7):3254-62.
14. Shadrach KG, Rayborn ME, Hollyfield JG, Bonilha VL. DJ-1-Dependent Regulation of Oxidative Stress in the Retinal Pigment Epithelium (RPE). PLoS One 2013; 8(7):e67983.
15. Wang CH, Cao GF, Jiang Q, Yao J. TNF-α promotes human retinal pigment epithelial (RPE) cell migration by inducing matrix metallopeptidase 9 (MMP-9) expression through activation of Akt/mTORC1 signaling. Biochem Biophys Res Commun 2012; 425(1):33-8.
16. King A, Gottlieb E, Brooks DG, Murphy MP, Dunaief JL. Mitochondria-derived reactive oxygen species mediate blue light–induced death of retinal pigment epithelial Cells. Photochem Photobiol 2004; 79(5):470-5.
17. Yang D, Elner SG, Bian ZM, Till GO, Petty HR, Elner VM. Pro-inflammatory cytokines increase retinal pigment epithelial cell reactive oxygen species production through mitochondria and NADPH oxidase. Exp Eye Res 2007; 85(4):462-72.
18. Feng L L, Luan J, Fu M. Effects of high glucose condition on the proliferation and reactive oxygen species expression cultured human retinal pigment epithelial cells in vitro. Int J Ophthalmol 2010; 10(3):453-55.
19. Antyborzec I, O'Leary VB, Dolly JO, Ovsepian SV. Low-affinity neurotrophin receptor p75 promotes the transduction of targeted lentiviral vectors to cholinergic neurons of rat basal forebrain. Neurotherapeutics 2016; 13(4):859-70.
20. Ragunathan YT, Madhavan NR, Mohan SP, Kumar SK. Immunohistochemical detection of p75 neurotrophin receptor (p75-NTR) in follicular and plexiform ameloblastoma. J Clin Diagn Res 2016; 10(8):ZC63-6.
21. Ghazi-Nouri SM, Assi A, Limb GA, et al. Laser photocoagulation alters the pattern of staining for neurotrophin-4, GFAP, and CD68 in human retina. Br J Ophthalmol 2003; 87(4):488-92.
22. Ginsberg SD1, Che S, Wuu J, Counts SE, Mufson EJ. Down regulation of Trk but not p75NTR gene expression in single cholinergic basal forebrain neurons mark the progression of Alzheimer's disease. J Neurochem 2006; 97(2):475-87.
23. Kuner P, Hertel C. NGF induces apoptosis in a human neuroblastoma cell line expressing the neurotrophin receptor p75NTR. J Neurosci Res 1998; 54(4):465-74.
24. Chakravarthy R, Mnich K, Gorman AM. Nerve growth factor (NGF)-mediated regulation of p75 (NTR)

expression contributes to chemotherapeutic resistance in triple negative breast cancer cells. Biochem Biophys Res Commun 2016; 478(4):1541-7.

25. Gibon J, Kang MS, Aliaga A, et al. Towards the PET radiotracer for p75 neurotrophin receptor: [(11)C] LM11A-24 shows biological activity in vitro, but unfavorable ex vivo and in vivo profile. Bioorg Med Chem 2016; 24(19):4759-65.
26. Khodorova A, Nicol G D, Strichartz G. The p75 NTR, signaling cascade mediates mechanical hyperalgesia induced by nerve growth factor injected into the rat hind paw. Neuroscience 2013; 254: 312-23.

APOPTOSIS OF HEPATOCARCINOMA CELLS $HepG_2$ INDUCED BY *HUAIER* EXTRACT THROUGH REGULATION OF HBx and CEACAM1 GENE EXPRESSION

LH. ZHONG[1], LY. ZHU[1], YY. ZHAO[2], W. WANG[3], BL. LU[1], Y. WANG[4], Y. CHENG[1] and YJ. MA[1]

[1]Department of Infectious Disease, The Fourth Hospital of Harbin Medical University, Harbin, China; [2]Department of Medical Oncology, The Fourth Hospital of Harbin Medical University, Harbin, China; [3]National Institute for Communicable Disease Control and Prevention, Chinese Center for Disease Control and Prevention, Beijing, China; [4]Department of Pharmacology and Toxicology, Wright State University, Fairborn, OH, USA

Received September 11, 2018 – Accepted October 1, 2018

Huaier **can effectively inhibit the growth of tumor cells by enhancing the immune system. However, the mechanism of its function is still not clear. The current study aimed to explore the possible mechanism of *Huaier* in inhibiting human hepatocarcinoma cells by observing its effect on proliferation and invasion in hepatocarcinoma cells, $HepG_2$ and $HepG_2$-X, which stably express the HBx gene, and by comparing the levels of mRNA transcription and protein expression of HBx and CEACAM1 in $HepG_2$ cells and $HepG_2$-X cells when treated with different concentrations of *Huaier*. $HepG_2$ cells and $HepG_2$-X cells were treated with 0, 1.5, 3.0, and 6.0 g/L-1 *Huaier* extract *in vitro*. MTT assay was used to measure the inhibition of cell proliferation. The transwell cell model coated with Matrigel glue was used to detect the invasion of $HepG_2$ and $HepG_2$-X cells *in vitro*. Flowcytometry was used to observe changes in cell cycle. Real-time PCR and Western blot were used to detect HBx and CEREAM1 mRNA transcription and protein expression separately. *Huaier* extract can inhibit $HepG_2$ and $HepG_2$-X cell proliferation in a time- and dose-dependent manner. The A value of $HepG_2$-X cells in each group was higher than that of $HepG_2$ cells. Compared with the control group, the invasion ability of $HepG_2$ and $HepG_2$-X cells decreased significantly after treatment with *Huaier* extract, in a dose-dependent manner. The cell cycle of $HepG_2$ and $HepG_2$-X was arrested at S phase. The distribution of G0/G1 phase decreased gradually with the increase of the concentration of *Huaier* extract, and the proportion of G0/G1 phase distribution declined. After treating with *Huaier* extract, mRNA transcription and protein expression of HBx in $HepG_2$ and HepG2-X declined, while those of CEACAM1 increased, reflecting a dose-dependent manner ($P<0.05$). Therefore, we concluded that the inhibitory effect of *Huaier* extract on hepatocarcinoma cell proliferation might function through down regulation of HBx gene expression and upregulation of CEACAM1 gene expression.**

In China, approximately 85%-90% hepatocarcinoma (HCC) is associated with hepatitis B virus (HBV) infection, which is HBV-related liver cancer (1, 2). To date, the most effective treatment is radical surgical removal in the early stage of hepatocarcinoma, even in the intermediate and late stages (3). However, the intrahepatic recurrence is the major reason hampering the long-term survival of patients after hepatectomy (1, 2, 4). Studies have reported that about 70% of patients suffered

Key words: hepatocarcinoma, HBx, CEACAM1, Huaier extract, apoptosis

Mailing address:
Dr. Yingji Ma,
Department of Infectious Disease,
The Fourth Hospital of Harbin Medical University,
No. 37, Yiyuan Street, Nangang District,
Harbin, 150001, China
e-mail: yingjima679@126.com

0393-974X (2018)

from recurrence within two years after surgery, which directly impacted patient quality of life (3, 5). The HBx gene is within X open reading frames (ORFs), which mainly codes for X protein (6). HBx transactivation can activate multiple signaling pathways, regulate gene expression, DNA repair, cell apoptosis and cell cycle (7-9). HBx is an independent predictive factor in chronic hepatitis B and occurrence of HCC and the further development of HCC (10). Carcinoembryonic antigen-related cell adhesion molecule 1(CEACAM1) is a transmembrane glycoprotein, one of the members of the carcinoembryonic antigen (CEA) gene family with different roles in different types of malignant tumors (11). In HBV-associated hepatocarcinoma, CEACAM1 is a tumor suppressor gene whose downregulation by HBx promotes the development of hepatocarcimona (12, 13).

Huaier extract is a fungal species thought to strengthen and consolidate body resistance and promote blood circulation (14). It is recommended for patients with primary HCC (15, 16). *Huaier* extract can effectively inhibit the growth of tumor cells by enhancing the immune system and inhibiting angiogenesis (17, 18). However, there is no study showing its clinical application in treating HBV-associated HCC. In this paper, we studied the effect of *Huaier* extract on inducing apoptosis and on gene regulation of CEACAM1 in $HepG_2$-X which has a stable transfection of the HBx gene.

MATERIALS AND METHODS

Experimental materials

Human hepatocarcinoma cell line HepG2 and $HepG_2$-X (Institute of Biochemistry and Cell Biology, Shanghai, China); *Huaier* extract (Qidong Gai Tian Li Pharmaceutical Co., Ltd., Jiangsu, China); Eagles MEM (GIBCO, New York, USA); Fetal calf serum (FCS) (HYCLONE, LA, USA); MTT and Hoechst 33342 (Sigma, US); Fetal bovine serum and DMEM (Gibco, BRL, USA); RNA extraction kit and Trizol kit (Invitrogen, USA); Fluorescence quantitative PCR kit (TaKaRa, Dalian, China); Mouse anti human HBx monoclonal antibody and rabbit anti CEACAM1 monoclonal antibody (Epitomics, USA). Horseradish peroxidase labeled mouse anti rabbit secondary antibody (Boster Biological Technology Co., Ltd., USA); ECL Chemiluminescence kit (Bi Yun Tian Company, Beijing).

Cell culture and medicine preparation

Cells from the liquid nitrogen were thawed in a 40°C water bath. After centrifuge, the cell pellet was resuspended and was routinely cultured at 37°C with 5% CO_2. Twenty-four hours ahead of the experiment, cells were seeded at the concentration of 1×10^5 cells /ml in 96-well plates. *Huaier* extract (16 g) was dissolved in 1000 ml of RPMI1640 medium and was then filtered through a 0.22 μm filter to obtain the 100 mg/ml stock solution, which was stored at 4°C. The stock solution was diluted into 1.5, 3.0, 6.0 g/L^{-1} working concentrations before use. The control solution was the same volume of RPMI1640 medium.

MTT method detecting $HepG_2$ and $HepG_2$-X cell proliferation

$HepG_2$ and $HepG_2$-X cells were seeded in 96-well plates at the concentration of 1×10^5 cells/ml. Medium was replaced by 1.5, 3.0, 6.0 g/L^{-1} of *Huaier* extract solution and the control group had only medium. Every treatment was repeated 5 times. After 24 h, 48 h, and 72 h, the supernatant was replaced by 150 μL of dimethyl sulfoxide (DMSO) in each well. The absorbance (A) value of the cells at 595 nm wave length was detected. The final A value, which was the mean value from five repeats, was used for the growth curve of the cells. Cell growth inhibition rate (IR) was detected by MTT method. The higher IR value was correlated with stronger inhibition of cell growth.

Transwell analysis of cell invasion

Liquid gel was made from serum-free RPMIl640 and Matrigel at the ratio of 1:1, and 60 μL of liquid gel was added to each well in the Transwell plate, which was then maintained at 37°C for 3 h for solidification. Then cells that hadbeen pre-incubated with *Huaier* extract were resuspended in RPMIl640 at the concentration of 5×10^5/mL in the Transwells at the final volume of 200 μL. 600 μL of RPMIl640 with serum was added to the lower well. The plate was then incubated at 37°C for 48 h. The cells that transferred through the gel were fixed by paraformaldehyde for 30 min before Giemsa dyeing. For observation of cells undera microscope (×400

magnification), 5 fields were randomly selected. The experiments were repeated 4 times. The average number of transferred cells was used to evaluate the cell invasion.

Flowcytometry analysis of cell cycle changes

$HepG_2$ cells and $HepG_2$-X cells were seeded in 96-well plates at the concentration of 1×10^5 cells/ml. Cells were treated in the conditions described above in Material and Methods 1.3. After 24 h, the cells were permeabilized by 70% ethanol for 12 h. RNAse A was added before propidium iodide (PI) staining. Within 60 min, cells were analyzed by flow cytometry to monitor changes in cell cycle.

Real-time PCR analysis of mRNA expression of HBx and CEACAM1

$HepG_2$ cells and $HepG_2$-X cells were treated with different concentrations of *Huaier* extract and the control medium. Every condition was represented by three replicates. Forty-eight hours later after cell culture at 37 with 5% CO_2 supply, cells were collected, and the total RNA was extracted by RNA extraction kit (Invitrogen, USA). Primers (Table I) were synthesized by Takara Bio Group, Dalian, China. The RNA was reverse transcribed into complementary (c) DNA. mRNA HBx and CEACAM1 was detected by using Real-time PCR kit (TaKaRa, Dalian, China). ^{CT} method was used to calculate relative quantity of the target gene expression.

Western blot analysis of HBx and CEACAM1 protein expression

$HepG_2$ cells and $HepG_2$-X cells were treated with different concentrations of *Huaier* extract, as described above. Total proteins were extracted from the cells through the Trizol method. Protein concentration was measured by the BCA kit. Protein samples were then subjected to sodium dodecyl sulfate-polyacrylamide gel electrophoresis and resolved on a 12% gel. Proteins were transferred onto a polyvinylidene difluoride membrane under 23V at 4°C. The membrane was incubated in a blocking solution with 5% fat free milk powder for 60 min and was then incubated with the primary antibody for 12 h at 4°C. Following three washes with Tris-buffered saline containing Tween 20 (TBST), the membrane was incubated with the secondary antibody for 60 min at room temperature. After another three washes of TBST, the blot was developed by ECL chemiluminescence kit and the results were detected using the Gel Imaging System for protein expression analysis.

Statistical analysis

All statistical analyses were conducted using SPSS version 19.0. The measurement data were expressed by the mean ± standard deviation, and two independent samples *t*-test was used to compare the mean values between each two groups. The mean variance between groups was analyzed by one-way ANOVA. The homogeneity of variance between two groups was analyzed by the LSD method, and the heterogeneity of variance was analyzed by Dennett T3 method. The *chi*-squared independence test was used for testing if two categorical variables were related. $P<0.05$ was considered a statistically significant difference.

RESULTS

Inhibitory effect of Huaier extract on hepatocarcinoma cell proliferation

The results from the MTT test showed that the A values of $HepG_2$-X cells in each group were

Table I. *Real-time PCR primers.*

Gene		Primer sequence
HBx	For	5'-GCCAATTGGCTACCGTGCTACCGTCTG-3'
	Rev	5'-GGGTCCAGCCGTTCAGTGGTGGACGT-3'
CEACAM1	For	5'-TTCGCACCTCGCAGATCT-3'
	Rev	5'-GCTTCTGCGCTAGGATTCGTAGCA-3'

significantly higher than those of $HepG_2$ cells at different time points (P<0.05), suggesting that the growth rate of $HepG_2$-X cells was faster than that of $HepG_2$ cells and that HBx plays a positive role in cell proliferation of $HepG_2$-X cells. After treatment with *Huaier* extract, the A values decreased gradually. Furthermore, the decrease of A value was more significant in the groups treated with a higher concentration of *Huaier* extract and with longer times of treatment. The A value difference between the experimental groups and the negative control group was statistically significant (P<0.05), suggesting an inhibitory effect of *Huaier* extract on hepatocarcinoma cell proliferation with a significant positive correlation with concentration and time (Tables II, III and Fig. 1).

Transwell analysis of cell invasion

Both $HepG_2$ cells and $HepG_2$-X cells have strong invasion ability with 100% migration rate. After treatment with *Huaier* extract, the invasion is weakened with a significantly lower migration rate compared with control groups (P<0.05). The migration rate of $HepG_2$-X cells was higher than that of $HepG_2$ cells under the treatment of various concentrations of *Huaier* extract, suggesting that the expression of HBx could promote the migration and invasion of the cells, while *Huaier* extract could inhibit the expression of HBx in varying degrees (Table IV).

Effect of Huaier extract on cell cycle distribution $HepG_2$ cells and $HepG_2$-X cells

After treatment of *Huaier* extract, $HepG_2$ cells and $HepG_2$-X cells were arrested at S phase, and the distribution of G0/G1 phase decreased significantly. By increasing the concentration of *Huaier* extract, the distribution of G0/G1 phase decreased. At a concentration of 6.0 $g \cdot L^{-1}$, the proportion of G0/G1 phase was statistically higher than that of the control group (P<0.05). After treatment with *Huaier* extract at varying concentrations, the apoptotic rate in $HepG_2$ cells was significantly higher than that of untreated HepG2 cells (P<0.05) (Table V). Similarly, $HepG_2$-X

Table II. *The A Value and the growth inhibition rate of different concentrations of Huaier extract on $HepG_2$ cells at different times.*

Huaier extract ($g \cdot L^{-1}$)	24h		48h		72h	
	$A_{595\ nm}$	Inhibition rate (%)	$A_{595\ nm}$	Inhibition rate (%)	$A_{595\ nm}$	Inhibition rate (%)
0	0.82±0.06	0	0.76±0.05	0	0.65±0.04	0
1.5	0.64±0.05	21.6*	0.55±0.03	27.6*	0.47±0.02	28.3*
3.0	0.45±0.03	45.2*#	0.38±0.02	49.5*#	0.35±0.03	46.7*#
6.0	0.30±0.04	63.7*#▲	0.27±0.04	65.1*#▲	0.23±0.04	64.2*#▲

*Note: Compared with 0 $g \cdot L^{-1}$, *P<0.05; Compared with 1.5 $g \cdot L^{-1}$, #P<0.05; Compared with3.0 $g \cdot L^{-1}$, ▲P<0.05。*

Table III. *The A Value and the growth inhibition rate of different concentrations of Huaier extract on $HepG_2$-X cells at different times.*

Huaier extract ($g \cdot L^{-1}$)	24h		48h		72h	
	$A_{595\ nm}$	Inhibition rate (%)	$A_{595\ nm}$	Inhibition rate (%)	$A_{595\ nm}$	Inhibition rate (%)
0	0.89±0.05	0	0.90±0.06	0	0.83±0.03	0
1.5	0.77±0.03	13.2*	0.75±0.02	16.2*	0.60±0.05	28.3*
3.0	0.61±0.04	31.7*#	0.58±0.03	35.1*#	0.54±0.03	34.5*#
6.0	0.48±0.02	45.6*#▲	0.47±0.04	47.3*#▲	0.44±0.02	46.9*#▲

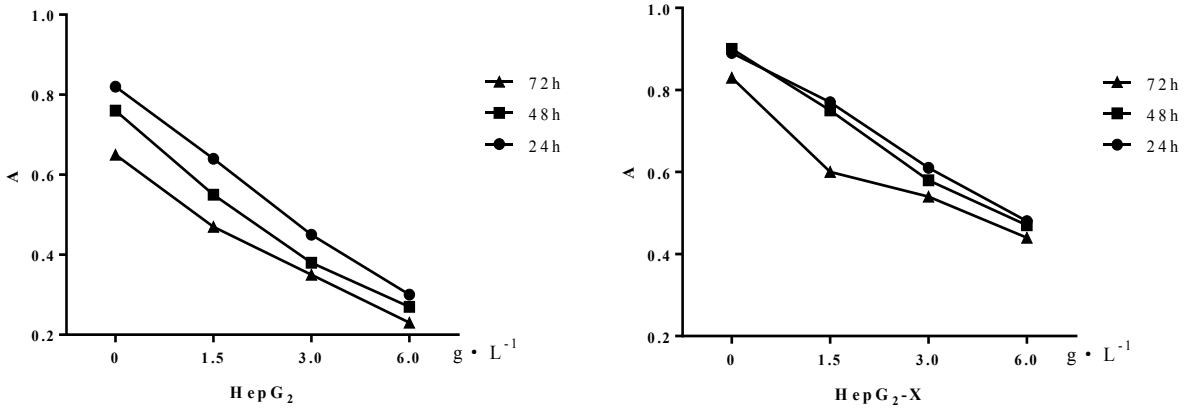

Fig. 1. *The inhibitory effect of Huaier extract at different concentrations on proliferation of $HepG_2$ cells and $HepG_2$-X cells*

cells treated with *Huaier* extract also showed a dose-dependent increase in apoptotic rate compared with the untreated cells (P<0.05) (Table VI).

The effect of Huaier extract on mRNA expression of HBx and CEACAM1

The results of Real-time PCR showed that, compared with the control group, HBx mRNA was down regulated in $HepG_2$ cells and $HepG_2$-X cells which were treated with different concentrations of *Huaier* extract, whereas CEACAM1 mRNA was up regulated, in a dose-dependent manner (P<0.05). The highest concentration of *Huaier* extract treatment was most effective on promoting CEACAM1 mRNA expression and on inhibiting HBx mRNA transcription (Table VII and Fig. 3).

The effect of Huaier extract on protein expression of HBx and CEACAM1

Western blot showed that, compared with the control group, HBx protein expression was down regulated while CEACAM1 protein expression was up regulated in $HepG_2$-X cells after treatment of *Huaier* extract (P<0.05). The highest concentration of *Huaier* extract led to the most significant enhancement of CEACAM1 protein expression and to the most significant inhibition of HBx protein expression (Fig. 4).

DISCUSSION

Huaier extract is the effective component extracted from a medicinal fungus (14). The major active ingredient of *Huaier* extract is a proteoglycan (14, 18). Modern pharmacological studies showed that it has a role in inhibition of different types of cancer cells and in induction of cell apoptosis (17-20). *Huaier* extract can effectively inhibit colon cancer SW480 cell invasion and migration. The mechanism may be related to the inhibition of

Table IV. *Effect of Huaier extract on $HepG_2$ and $HepG_2$-X cell invasion at different concentrations.*

Huaier extract（$g \cdot L^{-1}$）	$HepG_2$-X cells	$HepG_2$ cells
0	100%	100%
1.5	68.09%*	56.21%*
3.0	49.22%*#	41.43%*#
6.0	23.46%*#▲	16.09%*#▲

*Note: Compared with 0 $g \cdot L^{-1}$, *P<0.05; compared with 1.5 $g \cdot L^{-1}$, #P<0.05; compared with 3.0 $g \cdot L^{-1}$, ▲P<0.05.*

Table V. *The effect of different concentrations of Huaier extract on HepG2 cell apoptosis (%).*

Huaier extract (g·L^{-1})	G0/G1phase	S phase	G2/M phase	Apoptotic rate
0	58.21±2.29	20.39±1.15	21.37±1.52	6.51±0.12
1.5	57.13±2.25	21.56±1.74	21.31±2.16	6.78±0.36
3.0	55.37±2.72	22.79±1.13	21.84±1.95	6.82±0.25*
6.0	52.91±2.87*	23.51±1.18*	23.58±2.23	6.92±0.23*

*Note: Compared with 0 g·L-1, *P<0.05.*

Table VI. *The effect of different concentrations of Huaier extract on HepG$_2$-X cell apoptosis (%).*

Huaier extract (g·L^{-1})	G0/G1 Phase	S Phase	G2/M Phase	Apoptotic rate
0	58.62±1.51	20.25±1.23	21.13±1.26	5.16±0.27
1.5	57.53±2.32	21.32±1.21	21.15±2.13	6.57±0.21*
3.0	55.47±1.53*	22.15±2.05	22.38±1.91	6.81±0.23*
6.0	53.48±1.38*	22.87±1.15*	23.65±1.27	6.84±0.26*

*Note: Compared with 0 g·L$^{-1,}$ *P<0.05.*

epithelial-mesenchymal transition (21, 22). *Huaier* extract can inhibit human oophoroma SKOV-3 cell proliferation and induce cell apoptosis *in vitro* (23). Combined with chemotherapeutic drugs (24), *Huaier* extract can significantly increase the apoptosis rate of cancer cells. The curative effect is significantly better than that of chemotherapeutic drugs alone (24, 25). Importantly, a recent multicenter, controlled, randomized phase IV clinical trial revealed that Huaier granule significantly reduced the extrahepatic recurrence and prolonged the recurrence free survival in hepatocarcinoma patients (16).

The results from this study showed that the A value of HepG$_2$ cells deceased after treatment with *Huaier* extract. With increasing concentrations of *Huaier* extract and longer incubation times, the A value declined with significant reduced invasion and migration, compared with the control group. Hoechst33342 staining results showed that cells treated with *Huaier* extract had significant apoptosis, indicating that *Huaier* extract has a good inhibitory effect on hepatocarcinoma cells by promoting cell apoptosis and inhibiting migration and invasion. Thus, there is a significant positive correlation with time and concentration.

It is well known that HBV is an important factor in inducing HCC. The HBx gene plays a critical role during the process of HBV replication and spreading, which impinges on the development of chronic hepatitis B and HCC (26). The location of the HBx gene lies in the open reading frame of the X region of the HBV genome (10, 26). HBx encodes X protein which can transactivate cell proliferation and invasion (6). HBx promotes the proliferation and apoptosis of hepatocarcinoma cells by activating multiple signaling pathways, including: Ras-Raf/MAPK (Mitogen-Activated Protein Kinase) signaling pathway, NF (Nuclear Factor)-B signaling pathway, PKC (Protein Kinase C) signaling pathway, JAK-STAT signaling pathway, EOK/CR signaling pathway, and JNK signaling pathway (7, 8, 27, 28). HBx can also inhibit tumor suppressor genes, such as p53 and CEACAM1, to promote cancer development (10). Carcinoembryonic antigen-related cell adhesion molecule 1 (CEACAM1) is an important transmembrane protein, which is a member of the family of carcinoembryonic antigen (CEA) (11). Studies have shown that, HBx can promote the development of hepatocarcinoma cells by inhibiting the expression of CEACAM1 (13, 29).

The results from the MTT method showed that the A values of HepG$_2$-X cells at different time points

Table VII. *Effects of different concentrations of Huaier extract on HBx and CEACAM1 mRNA transcription.*

Huaier extract (g·L^{-1})	$HepG_2$ cells		$HepG_2$-X cells	
	HBx	CEACAM1	HBx	CEACAM1
0	5.31±0.23	3.21±0.19	7.25±0.16	3.25±0.15
1.5	4.27±0.25*	3.75±0.23*	5.36±0.13*	3.61±0.21*
3.0	3.89±0.21$^{*\#}$	4.02±0.21*	4.12±0.23$^{*\#}$	3.98±0.23*
6.0	3.41±0.23$^{*\#\blacktriangle}$	4.39±0.27$^{*\#\blacktriangle}$	3.56±0.27$^{*\#\blacktriangle}$	4.23±0.25$^{*\#}$

Note: Compared with0 g·L^{-1}, $^{*}P<0.05$; compared with1.5 g·L^{-1}, $^{\#}P<0.05$; compared with 3.0 g·L^{-1}, $^{\blacktriangle}P<0.05$.

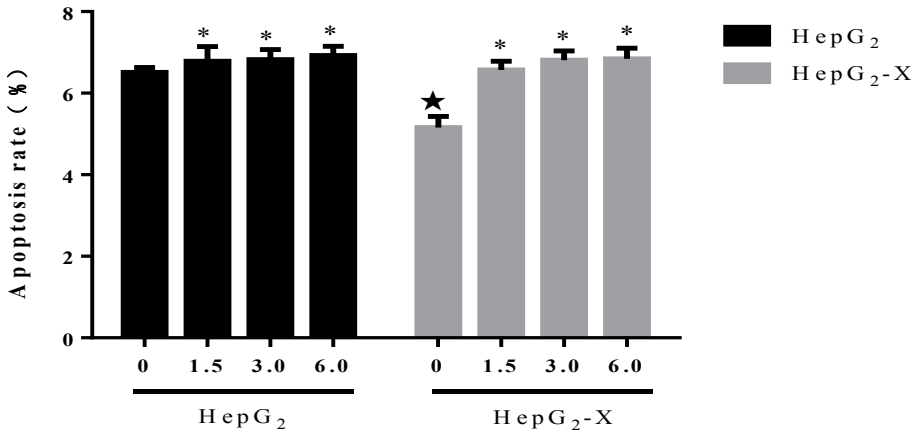

Fig. 2. *The effect of different concentrations of Huaier extract on the apoptotic rate of $HepG_2$ cells and $HepG_2$-X cells (Note: $^{*}P<0.05$ compared with $HepG_2$ 0 g·L^{-1}. *P<0.05□HepG2-X 0 g·L-1compared with $HepG_2$ 0 g·L^{-1})*

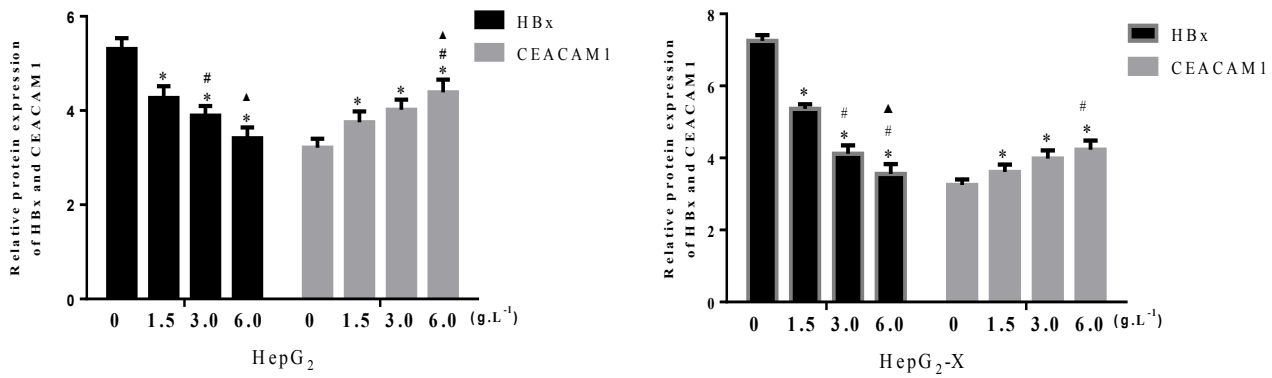

Fig. 3. *Effects of different concentrations of Huaier extract on HBx and CEACAM1 mRNA transcription (Note: Compared with 0 g·L^{-1}, $^{*}P<0.05$; compared with1.5 g·L^{-1}, $^{\#}P<0.05$; compared with 3.0 g·L^{-1},$^{\blacktriangle}P<0.05$).*

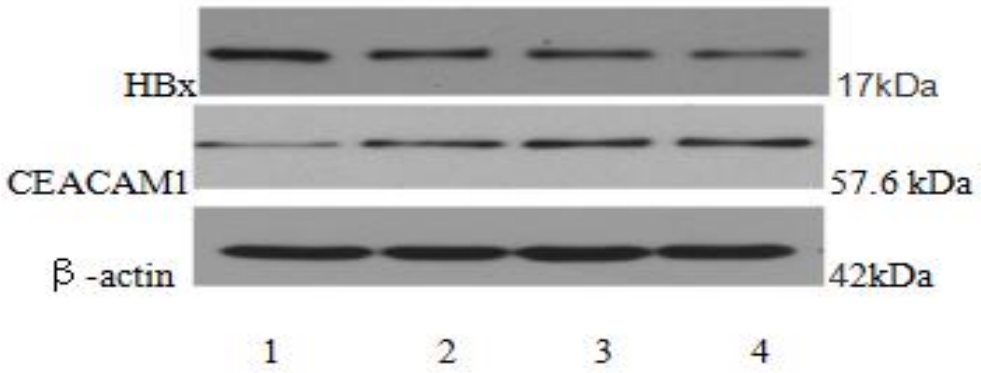

Fig. 4. *Effects of Huaier extract on the protein expression of HBx and CEACAM1 (Note: Lane 1: 0 g·L^{-1}, Lane 2: 1.5 g·L^{-1}, Lane 3: 3.0 g·L^{-1}, Lane 4: 6.0 g·L^{-1}).*

were significantly higher than those of $HepG_2$ cells ($P<0.05$), indicating that HBx could promote the proliferation of $HepG_2$-X cells. The apoptosis rate of $HepG_2$-X cells was lower than that of $HepG_2$ cells before *Huaier* extract treatment, while the migration of $HepG_2$-X cells was higher than that of HepG2 cells after treatment of *Huaier* extract, suggesting that the expression of HBx could promote the migration and invasion of cells and reduce the apoptosis of cells. *Huaier* extract inhibited the expression of HBx, thereby preventing the migration of HepG2 cells. Meanwhile, the $HepG_2$ cells and $HepG_2$-X cells were arrested in the S phase after *Huaier* extract treatment, with a significant reduced distribution of G0/G1 phase. By increasing of the concentration of *Huaier* extract, the proportion of the G0/G1 phase distribution decreased, demonstrating that cell viability was inhibited.

The mRNA expression of HBx and CEACAM1 in $HepG_2$ cells and $HepG_2$-X cells was also measured. The results showed that the mRNA expression of HBx was down regulated by *Huaier* extract, and mRNA expression of CEACAM1 was upregulated, following a dose-dependent manner ($P<0.05$). Furthermore, high dose of *Huaier* extract increased the expression of CEACAM1 mRNA and inhibited the expression of HBx mRNA, which was consistent with the results from Western blot, suggesting that *Huaier* extract inhibited cell migration and invasion and promoted apoptosis by inhibiting the expression of HBx and enhancing the expression of CEACAM1.

In conclusion, HBx may promote the proliferation and migration of hepatocarcinoma cells. *Huaier* extract can inhibit the proliferation and promote apoptosis of hepatocarcinoma cells. The mechanism may be related to inhibiting the expression of HBx and promoting the expression of CEACAM1. However, the specific pathways of its action remains to be further elucidated.

REFERENCES

1. El-Serag HB, Rudolph KL. Hepatocellular carcinoma: epidemiology and molecular carcinogenesis. Gastroenterology 2007; 132(7):2557-76.
2. Trepo C, Chan HL, Lok A. Hepatitis B virus infection. Lancet 2014; 84(9959):2053-63.
3. Li ZQ, Hu CL, Yu P, et al. The development of hepatocarcinoma after long-term antivirus treatment of Chinese patients with chronic hepatitis B virus infection: Incidence, long-term outcomes and predictive factors. Clin Res Hepatol Gastroenterol 2017; 41(3):311-18.
4. Jung SW, Kim DS, Yu YD, Han JH, Suh SO. Risk factors for cancer recurrence or death within 6 months after liver resection in patients with colorectal cancer liver metastasis. Ann Surg Treat Res 2016; 90(5):257-64.
5. Li T, Qin LX, Gong X, et al. Hepatitis B virus surface antigen-negative and hepatitis C virus antibody-negative hepatocellular carcinoma: clinical characteristics, outcome, and risk factors for early and

late intrahepatic recurrence after resection. Cancer 2013; 119(1):126-35.
6. Holotnakova T, Tylkova L, Takacova M, Kopacek J, Petrik J, Pastorekova S, Pastorek J. Role of the HBx oncoprotein in carbonic anhydrase 9 induction. J Med Virol 2010; 82(1):32-40.
7. Chen JY, Chen YJ, Yen CJ, Chen WS, Huang WC. HBx sensitizes hepatocellular carcinoma cells to lapatinib by up-regulating ErbB3. Oncotarget 2016; 7(1):473-89.
8. Zhu M, Li W, Lu Y, et al. HBx drives alpha fetoprotein expression to promote initiation of liver cancer stem cells through activating PI3K/AKT signal pathway. Int J Cancer 2017; 140(6):1346-55.
9. Wang MD, Wu H, Huang S, et al. HBx regulates fatty acid oxidation to promote hepatocellular carcinoma survival during metabolic stress. Oncotarget 2016; 7(6):6711-26.
10. Mao CS, Yin H, Ning HB, Peng Z, Li K, Ding GQ. Levels of HBx, VEGF, and CEACAM1 in HBV-related hepatocellular carcinoma and their correlation with cancer prognosis. Eur Rev Med Pharmacol Sci 2017; 21(17):3827-33.
11. Dankner M, Gray-Owen SD, Huang YH, Blumberg RS, Beauchemin N. CEACAM1 as a multi-purpose target for cancer immunotherapy. Oncoimmunology 2017; 6(7):e1328336.
12. Ramakrishnan SK, Khuder SS, Al-Share QY, et al. PPARalpha (Peroxisome Proliferator-activated Receptor alpha) activation reduces hepatic CEACAM1 protein expression to regulate fatty acid oxidation during fasting-refeeding transition. J Biol Chem 2016; 291(15):8121-29.
13. Yamaguchi S, Yokoyama S, Ueno M, et al. CEACAM1 is associated with recurrence after hepatectomy for colorectal liver metastasis. J Surg Res 2017; 220:353-62.
14. Song X, Li Y, Zhang H, Yang Q. The anticancer effect of Huaier (Review). Oncol Rep 2015; 34(1):12-21.
15. Lei JY, Yan LN, Zhu JQ, Wang WT. Hepatocellular carcinoma patients may benefit from postoperative Huaier aqueous extract after liver transplantation. Transplant Proc 2015; 47(10):2920-4.
16. Chen Q, Shu C, Laurence AD, et al. Effect of Huaier granule on recurrence after curative resection of HCC: a multicentre, randomised clinical trial. Gut 2018; 67(11):2006-16.
17. Li C, Wu X, Zhang H, et al. A Huaier polysaccharide inhibits hepatocellular carcinoma growth and metastasis. Tumour Biol 2015; 36(3):1739-45.
18. Bao H, Liu P, Jiang K, Zhang X, Xie L, Wang Z, Gong P. Huaier polysaccharide induces apoptosis in hepatocellular carcinoma cells through p38 MAPK. Oncol Lett 2016; 12(2):1058-66.
19. Chen Y, Wu H, Wang X, et al. Huaier Granule extract inhibit the proliferation and metastasis of lung cancer cells through down-regulation of MTDH, JAK2/STAT3 and MAPK signaling pathways. Biomed Pharmacother 2018; 101:311-21.
20. Qi W, Sun M, Kong X, et al. Huaier extract synergizes with tamoxifen to induce autophagy and apoptosis in ER-positive breast cancer cells. Oncotarget 2016; 7(18):26003-15.
21. Sun WW, Dou JX, Zhang L, Qiao LK, Shen N, Zhao Q, Gao WY. Killing effects of Huaier Granule combined with DC-CIK on nude mice transplanted with colon carcinoma cell line. Oncotarget 2017; 8(28):46081-9.
22. Xu Z, Zheng G, Wang Y, et al. Aqueous huaier extract suppresses gastric cancer metastasis and epithelial to mesenchymal transition by targeting twist. J Cancer 2017; 8(18):3876-86.
23. Yan X, Lyu T, Jia N, Yu Y, Hua K, Feng W. Huaier aqueous extract inhibits ovarian cancer cell motility via the AKT/GSK3beta/beta-catenin pathway. PLoS One 2013; 8(5):e63731.
24. Zhao GS, Liu Y, Zhang Q, et al. Transarterial chemoembolization combined with Huaier granule for the treatment of primary hepatic carcinoma: Safety and efficacy. Medicine (Baltimore) 2017; 96(29):e7589.
25. Hu Z, Yang A, Fan H, et al. Huaier aqueous extract sensitizes cells to rapamycin and cisplatin through activating mTOR signaling. J Ethnopharmacol 2016; 186:143-50.
26. Cheng ST, Ren JH, Cai XF, Jiang H, Chen J. HBx-elevated SIRT2 promotes HBV replication and hepatocarcinogenesis. Biochem Biophys Res Commun 2018; 496(3):904-10.
27. Kim JY, Song EH, Lee HJ, et al. HBx-induced hepatic steatosis and apoptosis are regulated by TNFR1- and NF-kappaB-dependent pathways. J Mol Biol 2010; 397(4):917-31.

28. Klein NP, Schneider RJ. Activation of Src family kinases by hepatitis B virus HBx protein and coupled signaling to Ras. Mol Cell Biol 1997; 17(11):6427-36.

29. Xu J, Liu B, Ma S, et al. Characterizing the tumor suppressor role of CEACAM1 in multiple myeloma. Cell Physiol Biochem 2018; 45(4):1631-40.

SOX2 GENE EXPRESSION AND ITS ROLE IN TRIPLE NEGATIVE BREAST CANCER TISSUES

GD. YAO, YY. NIU, KX. CHEN, HX. MENG, HT. SONG, ZN. TIAN, JS. GENG and MY. FENG

Department of Pathology, Harbin Medical University Cancer Hospital, Harbin, Heilongjiang Province, China

Received September 30, 2018 – Accepted December 6, 2018

The aim of this work was to study the expression of SOX2 gene in triple negative breast cancer and its role. One hundred and twenty specimens of paraffin-embedded triple negative breast cancer (TNBC) tissues were collected from Harbin Medical University Cancer Hospital, Heilongjiang, China between January 2014 and March 2018. The expression of SOX2 was detected using immunohistochemistry, and the relationship between the expression of SOX2 and clinical features was analyzed. Breast cancer cell lines (normal group, SOX2 interference group, SOX2 overexpression group) were cultured *in vitro* to detect the proliferation and cloning ability of the cell lines. The expression of SOX2 was related to lymph node metastasis and stage of breast cancer ($P < 0.05$), but was not related to age, menopause or tumor size ($P > 0.05$); the expression of SOX2 in the overexpression group was significantly greater than that in the normal group after 72 hours, and no significant difference between the overexpression group and the interference group was observed. The number of clone cells with a diameter of 0.5 mm in the interference group was lower compared to the normal group, and that of the overexpression group was higher, but not significant. SOX2 is associated with the high invasiveness of breast cancer and can be used as a therapeutic target to inhibit the metastasis of cancer cells. SOX2 can promote the proliferation of breast cancer cells and affect the size of clone cells in its involvement in clone.

Breast cancer is a commonly seen malignant tumor among women (1). The age of onset has become lower in recent years, and possibilities of recurrence and metastasis increase under the influence of multiple factors (2).

Cancer cells have the similar function characteristics as steam cells; hence the theory of cancer stem cell (CSC) (3) was proposed, which regards cancer cells as a special kind of embryonic stem cells. SOX gene is a transcription factor which participates in the development of sex organs, blood cells and the nervous system. It can reprogram differentiated somatic cells into pluripotent stem cells and is also a key factor to maintain the basic characteristics of stem cells (4). SOX2 is not expressed in normal somatic cells, but has an expression in cancer cells, and the proliferation and cloning of cancer cells is closely related to SOX2 gene (5). Piconruiz et al. (6) found that cancer cells cultured with cytokines or immature adipocytes

Key words: triple negative breast cancer; SOX2; clinical features; fluorescence polymerase chain reaction

Mailing address:
Jingshu Geng, Meiyan Feng,
No. 150, Haping Road,
Nangang district,
Harbin, Heilongjiang,
150081, China
e-mails: jingshugeng@hrbmu.edu.cn, meiyanf@yeah.net

0393-974X (2018)

promoted the up-regulation of SOX2, c-Myc and Nanog through activating Src. Zhou et al. (7) explored the effect of SOX2-targeted microRNAs-590-5P on breast cancer cell lines by flow cytometry, further analyzed the regulatory effect of microRNAs-590-5P on SOX2 by Western blotting, and found that microRNAs-590-5P could significantly reduce the number of breast cancer cells. Liu et al. (8) studied the role of SOX2 in breast cancer metastasis by wound healing, cell culture, colony formation, shRNA-mediated knockout, xenotransplantation, transporous cavity and tail vein injection. They found that SOX2 could control the proliferation and migration of breast cancer cells by regulating microRNAs and the diffusion and migration of cancer cells were inhibited after SOX2 gene was knocked out. One hundred and twenty complete paraffin-embedded female cancer tissue specimens were collected from Harbin Medical University Cancer Hospital, Heilongjiang, China, between January 2014 and March 2018. The expression of SOX2 was detected using the immunohistochemical method, and the relationship between the expression of SOX2 and clinical characteristics was analyzed. Breast cancer cell lines (normal group, SOX2 interference group, SOX2 overexpression group) were cultured *in vitro*. SOX2 influence on the cloning, proliferation and migration ability of cell lines was studied through direct counting method, plate cloning and Western blot.

MATERIALS AND METHODS

Research subjects

One hundred and twenty complete paraffin-embedded cancer tissues which were reserved after resection of triple negative breast cancer (TNBC) in Harbin Medical University Cancer Hospital, Heilongjiang, China between January 2014 and March 2018 were collected. All the samples came from females aged 30~70 years and had complete medical records. The subjects were informed regarding the content of the study, and approval was obtained from the ethics committee of the hospital.

Three stable cell lines, human breast ductal carcinoma cell line ZR7530 with normal expression of SOX2, overexpression of SOX2 and interfered expression of SOX2 were prepared.

Instruments and reagents

Main instruments included slicing machine, constant temperature blast drying oven, ultra-pure water meter, optical microscope, high pressure steam boiler, refrigerator, water bath pot, centrifuge and cell incubator.

Main reagents included rabbit two-step immunohistochemical detection reagent (9), diaminobenzidine (DAB) color developing kit, citrate buffer, SOX2 rabbit anti-Human monoclonal antibody, xylene, neutral gum, phosphate buffer solution (PBS), 0.05% Ethylene Diamine Tetraacetic Acid (EDTA) trypsin (9) embryonic bovine serum, complete culture medium, penicillin and streptomycin.

Detection of SOX2 expression

As shown in Fig. 1, the paraffin-embedded cancer tissues were cut into slices, deparaffinized, then added with 3% hydrogen peroxide, incubated at room temperature for 20 min, and finally washed by PBS. Antigen was restored by microwave heating (10). Rabbit serum was added and preserved at room temperature. Thirty min later, the serum was removed, and SOX2 antibody working solution was added. Then they were incubated at 37°C for 2 h. After that, they were washed by PBS, added with biotin antibody working solution, preserved at room temperature for 30 min, washed by PBS, added with DAB color development reagent, washed by ultra-pure water, redyed, washed, and mounted with neutral balsam (11). Finally they were observed under an optical microscope.

Cell proliferation

Three stable ZR7530 cell lines were firstly added to complete medium which contained 10% embryonic bovine serum, 40 U/mL penicillin, 100 U/mL streptomycin and then cultured in an incubator at 37°C, 5% CO_2. At logarithmic phase, 0.05% trypsin was added to the medium, shaken (12-13) and centrifuged, and then the cell lines were counted. After that, the dispersion liquid of the three cell lines were absorbed by a pipette and inoculated to a 6-well plate. Each kind of cell line had three copied wells. The 6-well plate was incubated in an incubator under the same conditions. Twenty-four hours later, the proliferative cells were digested using 0.05% trypsin and counted, once every 24 hours, for 4 times. The operation was repeated for three times on each kind of cell line.

Cell clone

Firstly, the three stable cell lines were cultured as before, and the cell line which grew to logarithmic phase was digested using 0.05% EDTA trypsin and centrifuged (14). The concentration of the cell lines was adjusted to 30,000 cells/mL with the culture medium. Then the cell lines were inoculated into a 6-well plate with a pipette. After the addition of the culture medium, they were cultured in an incubator with the same conditions. New culture medium was used to replace the old one every two days. The cloning process was observed once a day. When the clone was visible to the naked eye, the culture was over. Then they were washed by PBS twice, fixed with 4% paraformaldehyde solution (PFA) for 20 min, stained at room temperature, washed with distilled water after 25 min, and dried. The total number of cloned cells was counted first, and cloned cells with diameters greater than 0.5 mm were also counted. The operation was repeated for three times on each kind of cell line.

Detection of SOX expression with reverse transcription PCR amplification.

Cell lines on the culture medium were added with 1 ml of Trizol, mixed, incubated at room temperature for 5 min to make the nucleic acid protein complex completely separated and transferred to an Ep tube. After incubation, they were centrifuged at 4°C and 12,000 rpm for 10 min. There were three layers. The top layer which contained RNA was transferred into a new Ep tube, and white membrane at the boundary phrase was avoided; 1 ml of Trizol and 75% ethanol were added to wash sediment, and then it was processed by centrifugation at 12,000 rpm and 4°C for 10 min. After the removal of the supernatant, the Ep tube was inverted on clean filter paper for 10 min. Then 30 μl of RNase-free water was added to dissolve RNA (15). An ultraviolet spectrophotometer was used to detect the content of RNA. The purity was good if the content was between 1.8 and 2.0, and RNA needed to be re-extracted if the content was smaller than 1.8 or larger than 2.0. Then 1 μg of RNA sample, 10 μg of forward primer (5'-CTCCGGGACATGATCAGC-3') and 2 μg of reverse primer (5'-CTGGGACATGTGAAGTCTGC-3') were taken for reverse transcription PCR. The operation was carried out under 42°C for 10 min, 30°C for 20 min, 99°C for 5 min and 4°C for 5 min. Finally complementary DNA (cDNA) was obtained. The 15 μl of cDNA was mixed with 1 μL of double labeled probe, and then was cycled for 40 times at 50°C for 2 min, 95°C for 10 min, and 60°C for 1 min. Finally, it was observed using a PCR instrument.

Determination method

SOX2 which locates inside cell nucleus showed yellow after staining, and the score was given according to the staining degree (16). 0 points were given if there were no stained cells; the score increased with the deepening of color; the highest score was 3. Ten fields of the sample were randomly selected under 400 amplification. The cells were counted taking 100 each field as the standard. The average number of positive cells in the 10 fields was taken for calculation of percentage, and the staining score was also calculated. Three points were given when there was more than 50% positive cells, 2 points were given if there was 25% ~ 50% positive cells, 1 point was given if there was less than 25% cells, and 0 points were given if there was no positive cells. The sum of the score of the percentage of positive cells and the score of staining degree was taken as the staining index of the sample. When the staining index was larger than 3, SOX2 was considered having a high expression (17).

Statistical analysis

The collected data was processed by *Chi*-squared test using SPSS (12). Enumeration data was expressed as $\bar{x} \pm s$ and processed by independent *t*-test. Difference was considered significant if the value of P was less than 0.05.

RESULTS

The relationship between the expression of SOX2 and clinical features in TNBC

Cells with no expression of SOX2 showed blue-purple color after staining, and the nuclei and cytoplasm were stained (Fig. 2). There were only blue-purple cells in Fig. 2, and no yellow positive cells were observed.

When positive cells with SOX2 expression were stained, the nucleus and cytoplasm were yellow (Fig. 3). The deeper the yellow, the higher the expression level of SOX2. Most of the cells in Fig. 2 were yellow and positive, and few were blue-purple, with no

expression of SOX2. According to the above criteria, they had high expression of SOX2. It was also found that normal cells with no expression of SOX2 also existed in cancer tissues with high expression of SOX2.

As can be seen in Table I, SOX2 was considered having a high expression when the staining index of the sample was higher than 3 points. 55.54% of the patients under 35 years old had high expression of SOX2 and 51.23% of the patients over 35 years old had high expression of SOX2, suggesting no significant difference ($P = 0.819 > 0.05$); hence there was no correlation between the high expression of SOX2 and age of patients. 43.15% of the patients with tumor diameter smaller than 3 cm and 65.57% of the patients with tumor diameter larger than 3 cm had high expression of SOX2, suggesting no significant difference ($P = 0.174 > 0.05$); hence SOX2 expression was not associated to the size of tumor. 16.17% of the patients with stage 1 cancer cell histology, 32.15% of the patients with stage 2 cancer cell histology and 47.55% of the patients with stage 3 cancer cell histology had high expression of SOX2, suggesting no significant difference ($P = 0.174 > 0.05$). The difference between the three groups was insignificant ($P = 0.114 > 0.05$); hence the histological stage of cancer cells was not related to the expression of SOX2. 23.18% of the patients without lymph node metastasis and 62.89% of the patients with metastasis of lymph node had high expression of SOX2, showing a significant difference ($P = 0.012 < 0.05$), which indicated that the expression of SOX2 was in a correlation with lymph node metastasis. 12.21% of patients who had stage 1 breast cancer, 45.16% of patients who had stage 2 and 60.15% of patients who had stage 3 had high expression of SOX2; the difference was significant ($P=0.011 < 0.05$), which suggested that the expression of SOX2 was related to the stage of TNBC.

Cell proliferation experiment

The normal group was human breast duct

Table I. *The relationship between high expression of SOX2 in TNBC and clinical features.*

Clinical features		Percentage of patients with high expression of SOX2/%	χ^2	P value
Age	Under 35 years	55.54	0.055	0.819
	Over 35 years	51.23		
Diameter of tumor	Smaller than 3 cm	43.15	1.854	0.174
	Larger than 3 cm	65.57		
Histological stage	Stage 1	16.17	2.461	0.114
	Stage 2	32.15		
	Stage 3	47.55		
lymph node metastasis	No	23.18	6.023	0.012
	Yes	62.89		
Stage of TNBC	Stage 1	12.21	6.054	0.011
	Stage 2	45.16		
	Stage 3	60.15		

cancer cell ZR7530 without additional treatment, the overexpression group was breast cancer cells added with more SOX2 fragments by transgenic or other means, and the SOX2 interference group was breast cancer cell with SOX2 fragments knocked out by transgenic or other means. After multiple generations of culture and detection, the three cell lines are expressed (Fig. 4).

Twenty-four hours after inoculation, there was no significant difference in the number of cells in the overexpression group and the interference group compared with the normal group; 48 hours after inoculation, the number of cells in the overexpression group and the interference group were insignificantly different from those in the normal group; 72 hours after inoculation, there was a significant difference between the overexpression group and the normal group, but there was still no significant difference between the interference and normal groups. A very significant difference was observed between the overexpression group and the normal group after 96 hours.

Cell cloning experiment

The number of cloned cells in the overexpression and interference groups was not significantly different from that in the normal group; the number of cloned cells with diameter larger than 0.5 mm in the interference group was significantly lower than that in the normal group ($P < 0.05$) (Fig. 5). Although the number of cloned cells in the overexpression group was higher than that in the normal group, the difference was not significant. This indicated that SOX2 was related to cell clone and could directly affect size of cloned cells.

Detection of SOX2 expression with fluorescence reverse transcription PCR

As shown in Fig. 6, SOX2 expression was 300 bp. It was observed that the overexpression group had higher expression of SOX2 and bright strip compared to the normal group and there was nearly no expression of SOX2 in the cancer tissues in the interference group. The gray analysis on some strips of SOX2 suggested that there were significant differences between the three groups, which further verified the inheritance stability of cell lines which were adjusted by transgenic technology and the correlation between SOX2 and proliferation and clone of cancer cells.

DISCUSSION

Breast cancer is similar to other types of cancer (18). Although it can be cured by surgery or chemotherapy, metastasis or recurrence of cancer cells may occur according to the malignancy degree. In order to cure breast cancer better, many scholars are looking for and studying the prognostic markers of breast cancer.

"Triple negative" in TNBC means that epidermal growth factor receptor, progesterone receptor,

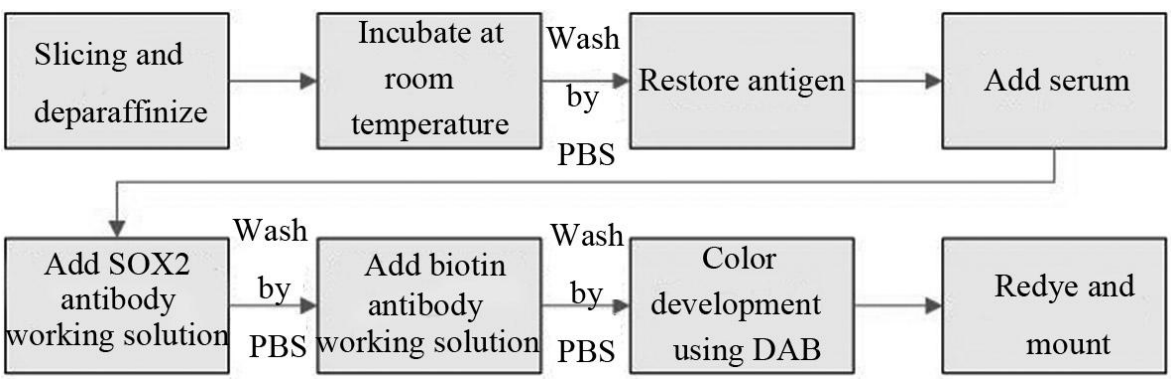

Fig. 1. *The detection flow of SOX2 expression in TNBC*

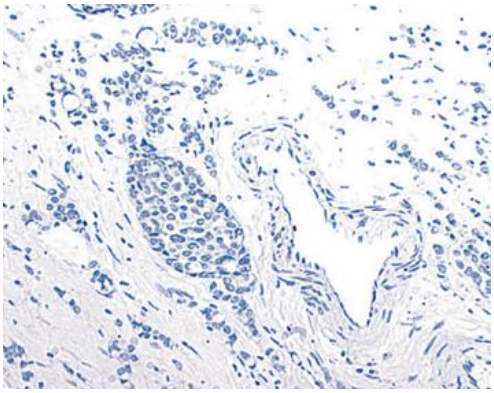

Fig. 2. *Cells with no expression of SOX2.*

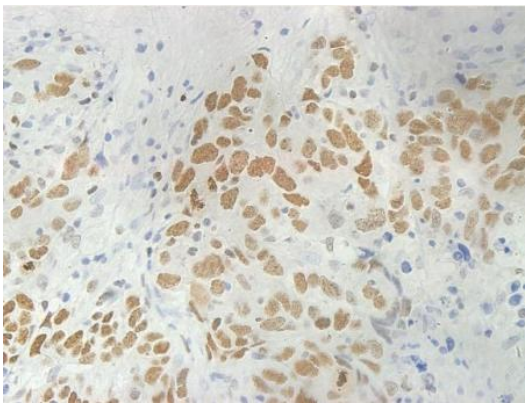

Fig. 3. *Cells with high expression of SOX2.*

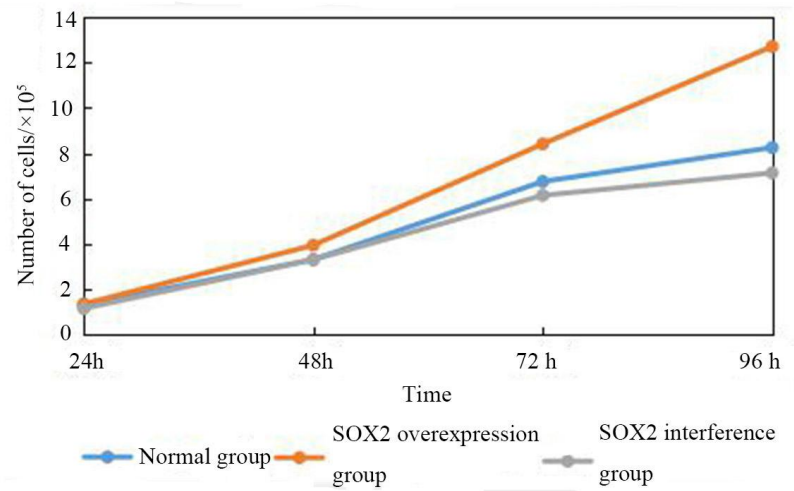

Fig. 4. *Count results of breast cancer cells with different expression levels of SOX2 at different time points.*

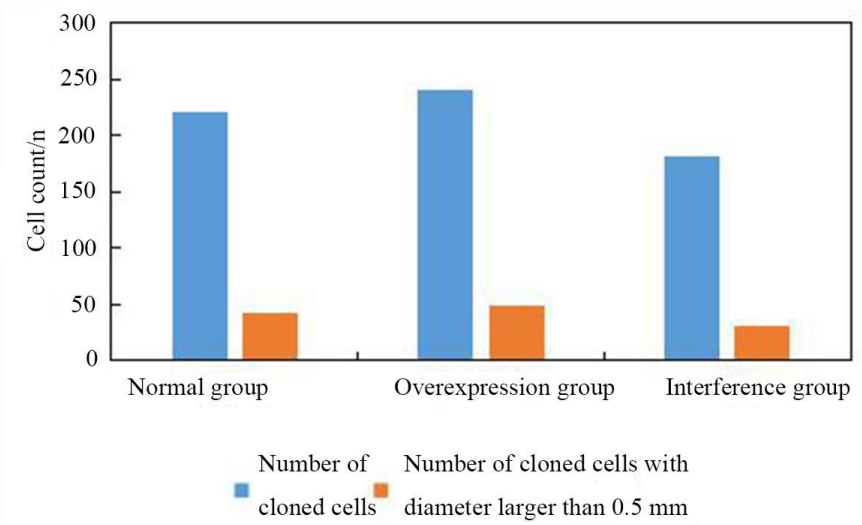

Fig. 5. *Count result of cloned cells under different expression levels of SOX2.*

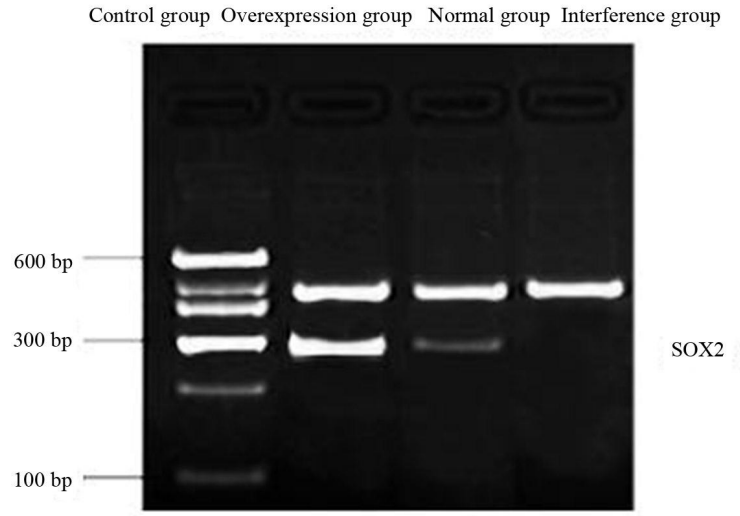

Fig. 6. *Detection of expression of SOX2 based on fluorescence reverse transcription PCR.*

and estrogen receptor (19) are negative. SOX2, a transcription factor in SOX gene, can help to maintain stemness of cells, and cancer cells are a kind of uncontrolled undifferentiated stem cells; therefore SOX2 and cancer cells are related. In the present study, the high expression of SOX2 in breast cancer cells was in connection with TNM stage (20) and lymph node metastasis of cancer, and the high expression of SOX2 promoted the diffusion and metastasis of cancer cells. Therefore, SOX2 expression in prognostic patients can be used as a reference predictor of diffusion and metastasis of breast cancer cells.

In this study, 120 specimens of paraffin-embedded breast cancer tissues were collected from the Harbin Medical University Cancer Hospital, Heilongjiang, China, and the expression of SOX2 and the relationship between SOX2 expression and clinical characteristics were detected by immunohistochemistry. Moreover, breast cancer cell lines (normal group, SOX2 interference group, overexpression group) were cultured *in vitro*. The effects of SOX2 on the proliferation and cloning ability of the cell lines were studied using direct counting, plate cloning and fluorescence reverse transcription PCR. The overexpression of SOX2 was found as being related to lymph node metastasis and TNM stage. SOX2 could promote the proliferation and cloning of breast cancer cells, and the overexpression of SOX2 in the overexpression group was stronger in PCR detection. After 72 hours, the proliferation ability of cancer cell lines with overexpressed SOX2 strengthened significantly, but the proliferation ability of cancer cell lines with SOX2 knocked out was inhibited, but not significant. The results of the fluorescence reverse transcription PCR for the three cell lines demonstrated that the expression of SOX2 in the overexpression group was extremely strong and SOX2 had nearly no expression in the interference group, which further verified that SOX2 could promote the proliferation and cloning of breast cancer cells.

REFERENCES

1. Mou W, Xu Y, Ye Y, et al. Expression of Sox2, in breast cancer cells promotes the recruitment of M2 macrophages to tumor microenvironment. Cancer Lett 2015; 358(2):115-23.
2. Jung K, Gupta N, Wang P, et al. Triple negative breast cancers comprise a highly tumorigenic cell subpopulation detectable by its high responsiveness to a Sox2 regulatory region 2 (SRR2) reporter. Oncotarget 2015; 6(12):10366-73.

3. Liu K, Xie F, Gao A, et al. SOX2 regulates multiple malignant processes of breast cancer development through the SOX2/miR-181a-5p, miR-30e-5p/TUSC3 axis. Mol Cancer 2017; 16(1):62.
4. Tang X, Gao Y, Yu L, Zhou G, Cheng L, Sun K, Zhu B, Xu M, Liu J. Correlations between lncRNA-SOX2OT polymorphism and susceptibility to breast cancer in a Chinese population. Biomark Med 2017; 11(3):277-84.
5. Gopal K, Gupta N, Zhang H, et al. Oxidative stress induces the acquisition of cancer stem-like phenotype in breast cancer detectable by using a Sox2 regulatory region-2 (SRR2) reporter. Oncotarget 2016; 7(3):3111-27.
6. Piconruiz M, Pan C, Drewselger K, et al. Interactions between adipocytes and breast cancer cells stimulate cytokine production and drive Src/Sox2/miR-302b-mediated malignant progression. Cancer Res 2016; 76(2):491-504.
7. Zhou L, Zhao L C, Jiang N, Wang XL, Zhou XN, Luo XL, Ren J. MicroRNA miR-590-5p inhibits breast cancer cell stemness and metastasis by targeting SOX2. Eur Rev Med Pharmaco 2017; 21(1):87.
8. Liu K, Xie F, Gao A, et al. SOX2 regulates multiple malignant processes of breast cancer development through the SOX2/miR-181a-5p, miR-30e-5p/TUSC3 axis. Mol Cancer 2017; 16(1):62.
9. Zheng Y, Qin B, Li F, Xu S, Wang S, Li L. Clinicopathological significance of Sox2 expression in patients with breast cancer: a meta-analysis. Int J Clin Exp Med 2015; 8(12):22382.
10. Wang Y, Zhou J, Wang Z, Wang P, Li S. Upregulation of SOX2 activated LncRNA PVT1 expression promotes breast cancer cell growth and invasion. Biochem Biophys Res Commun 2017; 493(1):429-436.
11. Liu P, Tang H, Song C, Wang J, Chen B, Huang XJ, Pei XQ, Liu LZ. SOX2 promotes cell proliferation and metastasis in triple negative breast cancer. Front Pharmacol 2018; 9:942.
12. Lillo MA, Nichols C, Seagroves T N, Mirandacarboni GA, Krum SA. Bisphenol A induces Sox2 in ER +, breast cancer stem-like cells. Horm Cancer 2017; 8(2):1-10.
13. Zeng H, Wang L, Wang J, et al. microRNA-129-5p suppresses Adriamycin resistance in breast cancer by targeting SOX2. Arch Biochem Biophys 2018; 651:52-30.
14. Xu Y, Dong X, Qi P, et al. Sox2 Communicates With Tregs Through CCL1 To Promote The Stemness Property Of Breast Cancer Cells. Stem Cells 2017; 35(12):2351-65.
15. Zhang J M, Wei K, Jiang M. OCT4 but not SOX2 expression correlates with worse prognosis in surgical patients with triple-negative breast cancer. Breast Cancer 2018; (10074):1-9.
16. Kamarlis RK, Lubis MN, Hernowo BS, Kar AS. Immunoexpression of P63 and SOX2 in triple-negative breast cancers, Indonesia. F1000research 2017; 6:1780.
17. Gupta N, Jung K, Wu C, et al. High Myc expression and transcription activity underlies intra-tumoral heterogeneity in triple-negative breast cancer. Oncotarget 2017; 8(17):28101-15.
18. Samanta S, Sun H, Goel HL, et al. IMP3 promotes stem-like properties in triple-negative breast cancer by regulating SLUG. Oncogene 2015; 35(9):1111.
19. Lehmann B D, Jovanović B, Chen X, et al. refinement of triple-negative breast cancer molecular subtypes: implications for neoadjuvant chemotherapy selection. Plos One 2016; 11(6):e0157368.
20. Yeganeh SM, Vasei M, Tavakoli R, Kia V, Paryan M. The effect of miR-340 over-expression on cell-cycle-related genes in triple-negative breast cancer cells. Eur J Cancer Care 2017; 26(6).

LONGITUDINAL STUDY ON THE EFFECT OF ORAL HYGIENE MEASURES ON THE SALIVARY COUNT OF MICROBIAL SPECIES WITH CARIOGENIC POTENTIAL

S. ESIN[1], M. PASINI[2], M. MICELI[2], G. COSSEDDU[2], M.R. GIUCA[2] and G. BATONI[1]

[1]Department of Translational Research and New Technologies in Medicine and Surgery, University of Pisa, Pisa, Italy; [2]Department of Surgical, Medical, Molecular and Critical Area Pathology, Unit of Pediatric Dentistry, University of Pisa, Pisa, Italy

Received June 2, 2018 – Accepted October 11, 2018

The effect of oral hygiene education measures and professional tooth cleaning on the salivary levels of microbial species with high cariogenic potential (i.e. *Streptococcus mutans*, *Lactobacillus* spp. and *Candida albicans*) was evaluated at different time points. At time 0, high salivary carriage rates were recorded in the study group (n=30). Fifty percent of the subjects harbored all three species in their saliva, 27% harbored 2 species, and 23% only one species. At 3 months after oral hygiene measures, a statistically significant reduction was observed in salivary count of *S. mutans* and *Lactobacillus* spp. The percentage of subjects harboring all three species was also highly reduced, along with an overall improvement of clinical and risk factors parameters. At 8 months after oral hygiene measures, *S. mutans* and *Lactobacillus* spp. load was still statistically lower than that recorded at time 0, although an increment in bacterial load and a partial worsening of clinical and risk factors parameters were observed. *S. mutans* count in saliva inversely correlated with salivary pH, while it positively correlated with *C. albicans* salivary levels. The results obtained suggest that strengthening of the motivation and administration of oral hygiene instructions and professional tooth cleaning every 6-8 months, might be necessary to control salivary levels of cariogenic species.

Dental caries is a preventable infectious disease continuing to affect millions of individuals worldwide, particularly those belonging to low-income and underprivileged groups. In most industrialized countries 60-90% of schoolchildren and the vast majority of adults are affected by the disease (1). The global goals of oral health by the year 2020 aim to: increase, over the regional, local, or national baseline levels, the proportion of caries-free 6-year-old children; reduce the decayed, missing, and filled-teeth (DMFT) index, particularly the D component, at age 12 years; and lower the number of teeth extracted due to dental caries at ages 18, 35-44 and 65-74 years (2). Such goals will hardly be accomplished without the implementation of oral disease prevention programs and the promotion of oral health as an important component of general health and quality of life (3, 4).

It is well established that dental caries is a multifactorial process caused by a cariogenic microbiota that produces acid from the fermentation of dietary carbohydrates in a susceptible host (5). Key risk factors are primarily behavioral-based and include frequent sugar consumption, insufficient or

Key words: dental caries, oral hygiene, Streptococcus mutans, Lactobacillus, Candida albicans

Mailing address:
Prof. Giovanna Batoni,
Department of Translational Research
and New Technologies in Medicine and Surgery,
Via S. Zeno 35-39, 56123, Pisa, Italy
Tel.: +39 050 2213696 - Fax: +39 050 2213711
e-mail: giovanna.batoni@med.unipi.it

0393-974X (2018)

inadequate oral hygiene and, in the case of children, lack of parental involvement in the child's tooth cleaning (6). Therefore, large-scale educational programs, provided by highly qualified personnel, and aimed at correcting wrong habits and motivating the patients to perform regular dental home-care, are key pillars of oral disease preventive approaches.

A number of studies have pointed to a major role of *Streptococcus mutans* and other "mutans streptococci" (e.g. *S. sobrinus*) in tooth decay initiation, both in children and in adults (7-10). The cariogenic potential of such bacteria relies on their marked aciduric and acidogenic properties, as well as on their ability to produce intracellular and extracellular polysaccharides that promote bacterial attachment on the tooth surface. Although *S. mutans* has been long regarded as a specific etiological agent of dental caries, the actual view consider caries as a polymicrobial infection in which diverse species of microorganisms of the oral biofilm may interact with each other and provide synergistic effect in the etiopathogenesis of the disease (11). In addition to "mutans streptococci", lactobacilli have also been implicated in dental caries. Due to their poor ability to adhere to smooth surfaces and high aciduric properties, *Lactobacillus* spp. are believed to colonize the oral cavity only in the presence of retentive, partially anaerobic and low pH niches (e.g. caries lesions), where they may ferment carbohydrates and represent major contributors to caries progression rather than caries initiation (12). Recently, the possible spectrum of cariogenic microorganisms has expanded to include representatives of the fungi kingdom such as *Candida albicans*. Although this fungus is found as commensal in the oral cavity of a high proportion of individuals, it is highly acidogenic and aciduric. Furthermore, it has the ability to ferment and assimilate dietary sugar, to adhere to dental surfaces such as enamel and exposed dentine, and to produce collagenolytic proteinases, all factors indicative of a cariogenic potential (13). The cariogenicity of the fungus has been demonstrated in animal models (14), while high *C. albicans* infection rates were reported in children with severe early childhood caries (ECC) (15, 16) further supporting the cariogenic potential of the fungus.

The microflora attaching to the teeth is continuously shed into the saliva so that salivary microbiota has been regarded as the "fingerprint" of the oral microbiota associated to the oral surfaces (17). Many studies have demonstrated that high "mutans streptococci" and lactobacilli loads in saliva significantly correlate with caries prevalence and/or caries risk development (15, 18-20). Similarly, higher levels of *C. albicans* in saliva, dental plaque or dentin of children with ECC have been reported as compared to caries-free children (15, 21, 22). A bacterial load equal to or greater than 10^5 CFU/ml of saliva of both *S. mutans* and *Lactobacillus* is considered predictive of individual susceptibility to dental decay (23). Preventive measures aimed at reducing *S. mutans*' salivary levels in mothers (e.g. oral antiseptic treatment) delay or prevent colonization by the bacterium of the oral cavity of their children and this, in turn, results in a reduction in dental caries (24, 25). Therefore, identification of factors capable of affecting the salivary level of species with high cariogenic potential can help in planning caries control interventions in the population.

The aim of the present study was to evaluate, at different time points, the effect of oral hygiene instruction and professional tooth cleaning on the salivary count of three species with high cariogenic potential (*S. mutans*, *Lactobacillus* spp. and *C. albicans*). Evaluation of clinical parameters of oral health status or caries susceptibility was also performed at the same time-points.

MATERIALS AND METHODS

Study groups

The subjects included in the study were recruited at the Oral Hygiene Surgery of the University Hospital of Pisa, Italy. At time 0, the study group consisted of 30 subjects with ages between 4 and 75 years. Ten were children (4-10-yr, group A), 10 adolescents (11-18-yr, group B) and 10 adults (>30 yr, group C). The study group included 18 females and 22 males subdivided as follows: 5 males and 5 females in group A, 4 males and 6 females in group B, 3 males and 7 females in group C. Group A included 8 foreigners (children of immigrants permanently resident

in Italy); no foreigner was present in group B and one foreigner was present in group C. The vast majority (8/10) of the subjects in group B were carriers of mobile or fixed orthodontic devices. At 3 months, 9/10 children of group A, 9/10 adolescents of group B and 7/10 adults of group C were available for the follow-up, for a total of 25 subjects. At 8 months, the study group was made up of 18 subjects (7 children, 7 adolescents, 4 adults). The Human Ethics Committee approved the study and all patients provided their informed consent to participate in the study.

Clinical examination

Each patient underwent a careful intra-oral examination to evaluate the oral health status through the assessment of the plaque index (PI), the decayed, missing and filled teeth index (dmft for deciduous dentition and DMFT for permanent dentition) and the International Caries Detection and Assessment System (ICDAS) index. A single operator carried out the examination in all the subjects, using a mouth mirror and an explorer.

The PI was assessed by evaluating the presence of plaque (soft deposits) on four surfaces of each tooth: distal, mesial, lingual, buccal. The PI (%) was calculated according to the formula: (Number of sites with plaque)/ Total number of sites) x100 where the total number of sites was obtained multiplying the number of teeth present by four. Third molars and incompletely erupted teeth were not scored.

The DMTF/dmtf index was calculated by evaluating for each patient: the number of decayed teeth (D) (white spot lesions excluded); the number of missing teeth (M) (teeth absent for exchange, for agenesis or not erupted were not considered in the calculation; if there was an implant the tooth was considered lost); the number of filled teeth (F). The sum of these values was divided by the total number of teeth according to the formula: DMFT(or dmft) = (D + M + F) / (total number of teeth present).

For each patient, caries detection and assessment was also evaluated by the ICDAS index. ICDAS detection codes for coronal caries were attributed according to Gugnani et al. (26) and ranged from 0 (sound tooth surface) to 6 (extensive distinct cavity with visible dentin) depending on the severity of the lesion.

Saliva collection and processing

Each patient was asked to collect the saliva inside a sterile 50 ml tube for 3 min. Saliva samples were collected 2 h after last meal/tooth brushing in a mid-morning session, stored in ice and transferred to the Microbiology laboratory within 2 h from collection. Upon arrival at the laboratory, some drops of saliva were placed on litmus paper detecting the pH in the range between 6 and 7.7. The salivary flow assessment (ml/min.) was performed by measuring the total volume of saliva with graduated pipettes and dividing it by the collection time (3 min).

Measures of oral hygiene education and motivation of the patients

At time 0, once salivary sampling and clinical examination were performed, the patients underwent a professional oral hygiene session. Children with completely erupted and healthy molar teeth were subjected to sealing of furrows and dimples. Education and motivation procedures were aimed at informing the patients about the state of their oral health and to encourage them to implement a personalized home therapy based on the individual caries risk or protective factors emerging from the anamnesis. In general, the therapeutic plan could include tooth brushing 3 times a day with a manual or electric brush. Advice was given to the patients or, in case of minors, to the parents regarding the choice of the most suitable manual or electric toothbrush. Correct procedures on electric toothbrush usage or manual tooth brushing technique were taught (taking into account the age of the subject, his/her manual ability, the subject's peculiarities of the oral cavity, and/or the presence of orthodontic appliances). In the case of children under the age of 6, the parents were actively involved in the brushing. Advice on the home-usage of fluorine chemicals (toothpaste and mouthwashes) were also given, including the use of toothpaste with at least 1000 ppm of fluorine under the age of 12, and with at least 1400 ppm of fluorine over 12 years. The use of fluorinated mouthwash (500 ppm of fluorine) was recommended from 7 years of age. Finally, advice regarding the implementation of correct eating habits was given which included: to avoid taking more than 5 meals a day; limit or avoid consumption of solid/ liquid fermentable carbohydrates (sugars and starches) and food of a sticky consistency. Sporadic intake of sugary soft drinks, fruit juices, coffee or tea, was allowed but always followed by the intake of a glass of water. Furthermore, subjects were advised to consume foods that promote tooth mineralization such as dark-green leafed vegetables,

cheese, milk, cod-liver oil, oyster mushrooms, eggs and certain species of wild salmon. No subject used probiotics. In the case of children, parental involvement was asked to increase the compliance to the indicated diet.

Table I. *Clinical parameters and caries risk factors of the study groups at time 0.*

Patient group		A (n=10)	B (n=10)	C (n=10)	P value
Mean PI (%)		55.73±11.79	72.02±9.97	71.34±11.16	>0.05
Mean dmft/DMFT		0.37±0.13	0.03±0.02	0.85±0.19	A *vs* B **P<0.05** B *vs* C **P<0.001**
Total number of active lesions/total number of teeth		48/215	6/262	22/217	-
Total number of tooth reconstruction/total number of teeth		15/215	15/262	77/217	-
ICDAS codes*	1	3	4	0	-
	2	2	0	4	-
	3	0	2	1	-
	4	5	0	2	-
	5	19	0	12	-
	6	19	0	3	-
Salivary pH (range); (mean)		(6.4-7.3); (6.86±2.17)	(6.7-7.4); (7.12±2.25)	(6.0-7.4); (6.67±2.11)	>0.05
Salivary flow (range); (mean)		(0.04-0.66); (0.42±0.13)	(0.30-1.1); (0.53±0.17)	(0.13-0.97); (0.51±0.16)	>0.05

Values indicate mean±standard error of the means where applicable
PI: plaque index;
**for each ICDAS code the total number of lesions of each type is reported for each group of subjects*

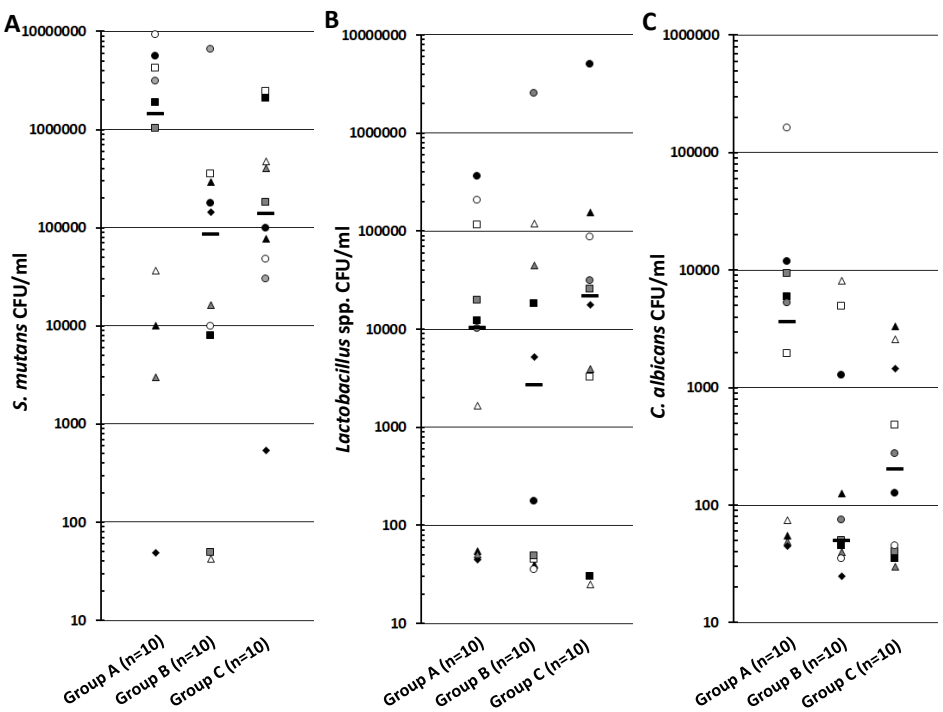

Fig. 1. *Salivary levels of S. mutans (**A**), Lactobacillus spp. (**B**) and C. albicans (**C**) at time 0 in children (Group A), adolescents (Group B), and adults (Group C). Each dot represents the salivary level detected in one subject. Within each group, dots of the same color/shape refer to the same subject. Black lines indicate median values. No statistically significant differences were found among groups (Mann Whitney U-test).*

Enumeration of S. mutans, Lactobacillus spp. and C. albicans in saliva

Selective culture media for the isolation of the 3 microbial species under examination were prepared according to the manufacturer's instructions. Mitis salivarius agar (MSA) (Sigma Aldrich, Milano, Italy), containing potassium tellurite (1 ml of a 1% solution in 1000 ml medium), bacitracin (final concentration 0.2 U/ml) and sucrose (final concentration 150 g/l) was used for the selective recovery of *S. mutans*. For the isolation of *Lactobacillus* spp. Rogosa agar (Sigma Aldrich) adjusted at pH 5.5 with glacial acetic acid and added with 10 ml of a sterile 10% Tween 80 solution per liter was used. For selective isolation of *C. albicans*, the *Candida* ident Agar medium (Sigma Aldrich), supplemented with 100 mg of gentamicin per liter, was used.

Saliva samples were vigorously vortexed for 2 min. to disperse clumps and ten-fold diluted with physiological solution from 1:10 to $1:10^4$. Two-hundred microliters of each dilution were plated in duplicates on the surface of selective solid media in 6 cm diameter Petri dishes. Plates were incubated for 48 h at 37°C and for 24 h at room temperature to allow growth of *S. mutans* and *Lactobacillus* spp. or for 24 h at 30°C to obtain colonies of *C. albicans*. At the end of the incubation period, the identification of the three species was carried out on the basis of colony morphology, microscopic appearance after Gram staining and, in case of doubtful results, analysis of the biochemical profile with standard identification galleries or MALDI-TOF. The colonies were counted and the number of colony forming units (CFU) per ml of saliva was determined.

Statistical analysis

The statistical significance of the data was evaluated by Student's *t*-test for paired samples, the non-parametric Mann Whitney U-test, Wilcoxon signed-rank test, *Chi*-squared or Fisher's exact test. Correlation between variables was evaluated using the Spearman's Rho correlation test. A P value <0.05 was considered significant.

RESULTS

Evaluation of microbiological and clinical parameters, and caries risk factors at time 0

At time 0 the study group consisted of 30 subjects including 10 children (Group A), 10 adolescents (Group B), and 10 adults (Group C). The microbiological analysis at time 0 showed high rates of salivary colonization by the three cariogenic species in the study group as a whole. Indeed, 90% of subjects had *S. mutans* in saliva, 73% *Lactobacillus* spp. and 63% *C. albicans* (data not shown). Salivary multi-species colonization was also frequently recorded. In fact, only 23% of the subjects in the study group was colonized by only one of the 3 cariogenic species, while 27% harbored two species in saliva and as much as 50% all three species. *S. mutans* salivary count was particularly high in the children's group (Fig. 1): 6 out of 10 children had levels of *S. mutans* greater than 1 million per ml, a value well above the level of 100,000 per ml, considered a risk factor for caries development. Interestingly, all children with *S. mutans* higher than 100,000 per ml harbored also *C. albicans* in saliva. Lactobacilli levels were similar in the three groups (around 10,000/ml), while higher levels of *C. albicans* were recorded in the children's group as compared to adolescents and adults, albeit the differences did not reach statistical significance.

Table I shows the clinical parameters and caries risk factors of the study groups at time 0. In agreement with the high levels of salivary colonization, the mean PI exceeded 50% in all three groups of subjects being particularly high in the adolescents and adults (higher than 70%). Caries experience evaluated as DMFT/dmft index was particularly severe in adults, followed by children. The value greatly influencing the DMFT value of C group was the number of filled or lost teeth, although in the subjects of this group there were also numerous active lesions (Table I). In contrast, in group A, the greatest contribution to the DMTF/dmft index was given by the high number of active carious lesions that were particularly severe in this group of subjects, as assessed by the ICDAS score (Table I).

The average unstimulated salivary flow was between 0.42 and 0.53 ml/min in the 3 groups of subjects, while the average pH of saliva was mild acidic in the group of children and adults and close to neutrality in the adolescent group (Table I).

Evaluation of microbiological and clinical parameters, and caries risk factors at 3 months

The evaluation of the microbiological and

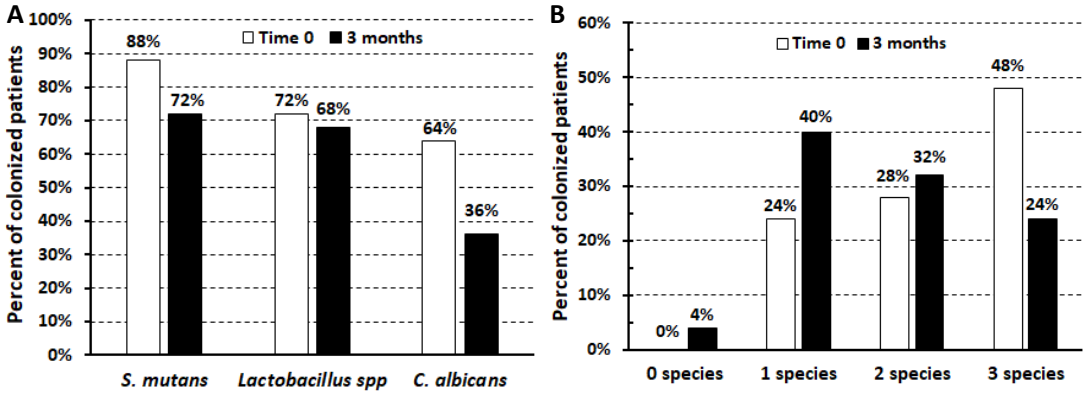

Fig. 2. ***A)*** *Percentage of subjects carrying S. mutans, Lactobacillus spp. or C. albicans in their saliva.* ***B)*** *Percentage of subjects carrying 0, 1, 2, or 3 cariogenic species in their saliva. At both time points data presented refer to the 25 subjects who were available for the follow-up at 3 months.*

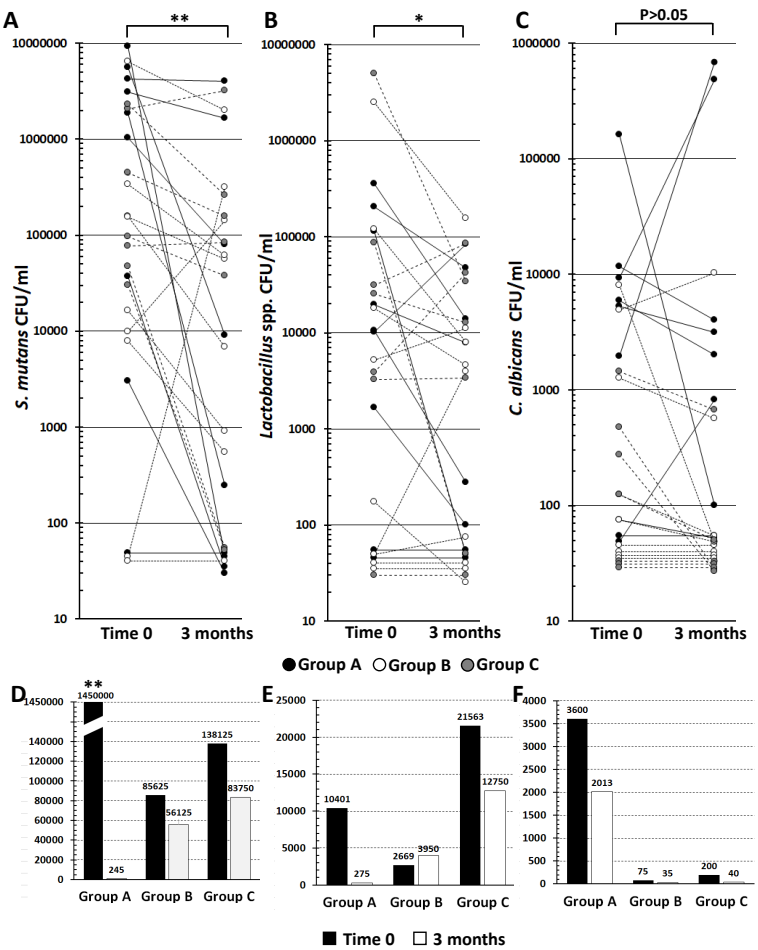

Fig. 3. *Salivary levels of S. mutans (**A**), Lactobacillus spp (**B**), and C. albicans (**C**) at 3 months as compared to time 0 in children (Group A, n=9), adolescents (Group B, n=9) and adults (Group C, n=7). See text for details. At both time points data presented refer to the 25 subjects who were available for the follow-up at 3 months. Median salivary levels (CFU/ml) of S. mutans (**D**), Lactobacillus spp. (**E**), and C. albicans (**F**) at 3 months as compared to time 0 in children (Group A), adolescents (Group B) and adults (Group C). Statistical analysis was performed for each bacterial species considering the three groups of subjects as a whole (panels A, B, C) or separately (panels D, E, F). ** P<0.01, *P<0.05, Wilcoxon signed-rank test.*

clinical parameters was repeated 3 months after the professional oral hygiene session and the administration of rules of oral hygiene and alimentary behavior. As five patients did not attend the 3-month follow-up, the study group consequently consisted of 25 subjects (9 children, 9 adolescents and 7 adults).

As shown in Fig. 2, at 3 months, a decrease in the percentage of patients positive for *S. mutans* (from 88 to 72%) and for *C. albicans* (from 64 to 36%) was recorded. A slight decrease in the percent of patients positive for lactobacilli was also observed (from 72 to 68%). Regarding multiple salivary colonization, although there was a drastic reduction (from 48 to 24%) in the percentage of the patients colonized by all three species, this did not reach statistical significance (P=0.07, *Chi*-squared test, n=25). The percentage of patients not colonized or carrying only one or two cariogenic species in their saliva increased as compared to time 0 (Fig. 2).

Fig. 3 shows the number of CFUs of the 3 microbial species per ml of saliva in the three groups of patients at time 0 and at 3 months. Each patient is represented by a dot (black, white or grey) corresponding to the group he/she belongs to. A line combines, for each patient, the CFU value at time 0 and at 3 months. Considering the study group as a whole, a statistically significant reduction was observed in both the *S. mutans* and *Lactobacillus* spp. salivary count after 3 months compared to time 0 (Fig. 3A and B). In particular, the number of *S. mutans* CFU/ml was reduced in 19 patients out of 25; 2 patients not colonized at time 0, remained

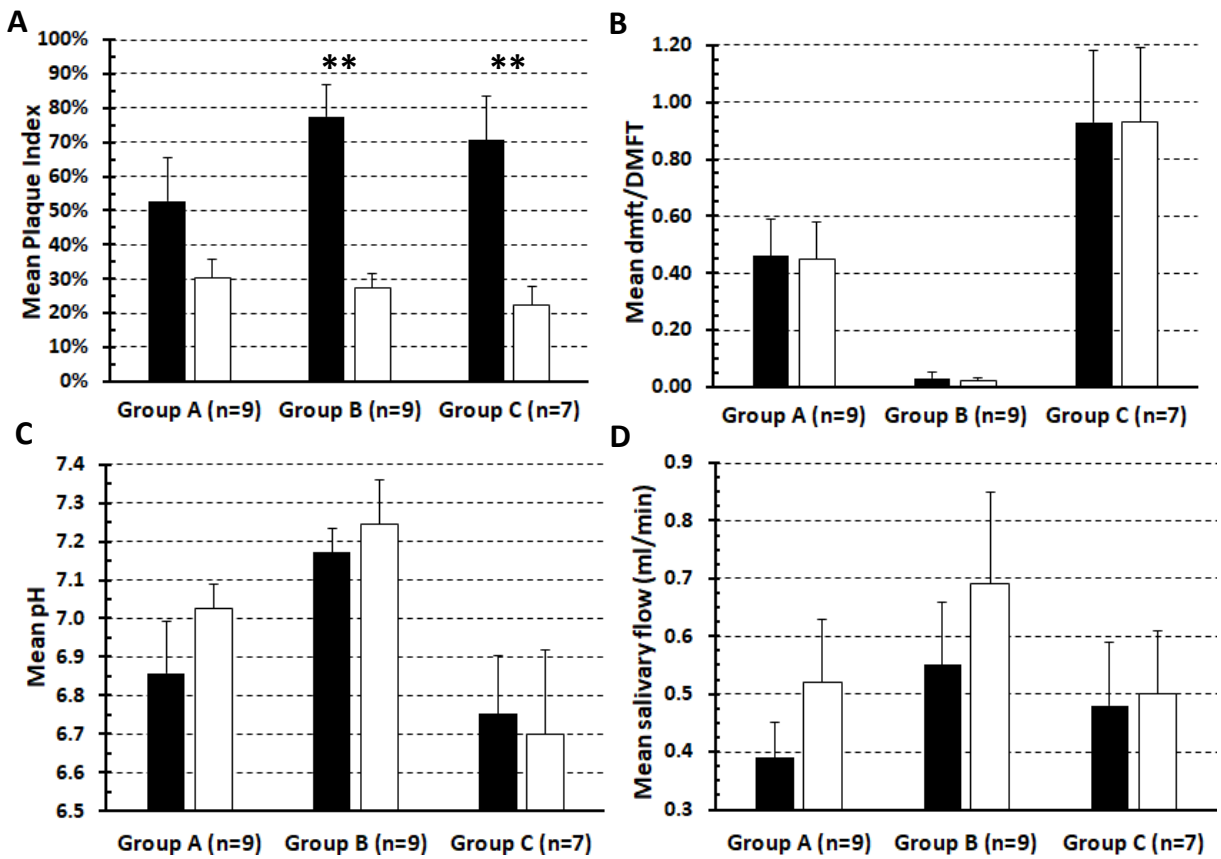

Fig. 4. *Clinical parameters (**A**, **B**) and caries risk factors (**C**, **D**) at time 0 (black bars) and 3 months (white bars) in children (Group A), adolescents (Group B) and adults (Group C). At both time points data presented refer to the 25 subjects who were available for the follow-up at 3 months. ** P<0.01, Student's t-test for paired samples.*

negative for *S. mutans* at 3 months, while 4 patients showed an increase in *S. mutans* salivary count (in 2 of them the increase in CFU/ml was rather marked, while in 2 it was very mild). A consistent decrease in the median value of *S. mutans* CFU/ml was evident above all in the group of children (P<0.01; Fig. 3D).

For *Lactobacillus* spp., a decrease in CFU/ml of saliva was recorded in 13/25 patients; in 6 patients (of whom 5 were not colonized at time 0) the CFU remained unchanged, while in 6 patients there was an increase in CFU/ml. The reduction in the median values of *Lactobacillus* CFU/ml (Fig. 3E) was particularly evident in the group of children and adults (although not statistically significant), while in the adolescent group the median remained almost unchanged (Fig. 3E). Finally, with regard to *C. albicans*, in 13 patients out of 25 a salivary charge reduction was observed at 3 months compared to

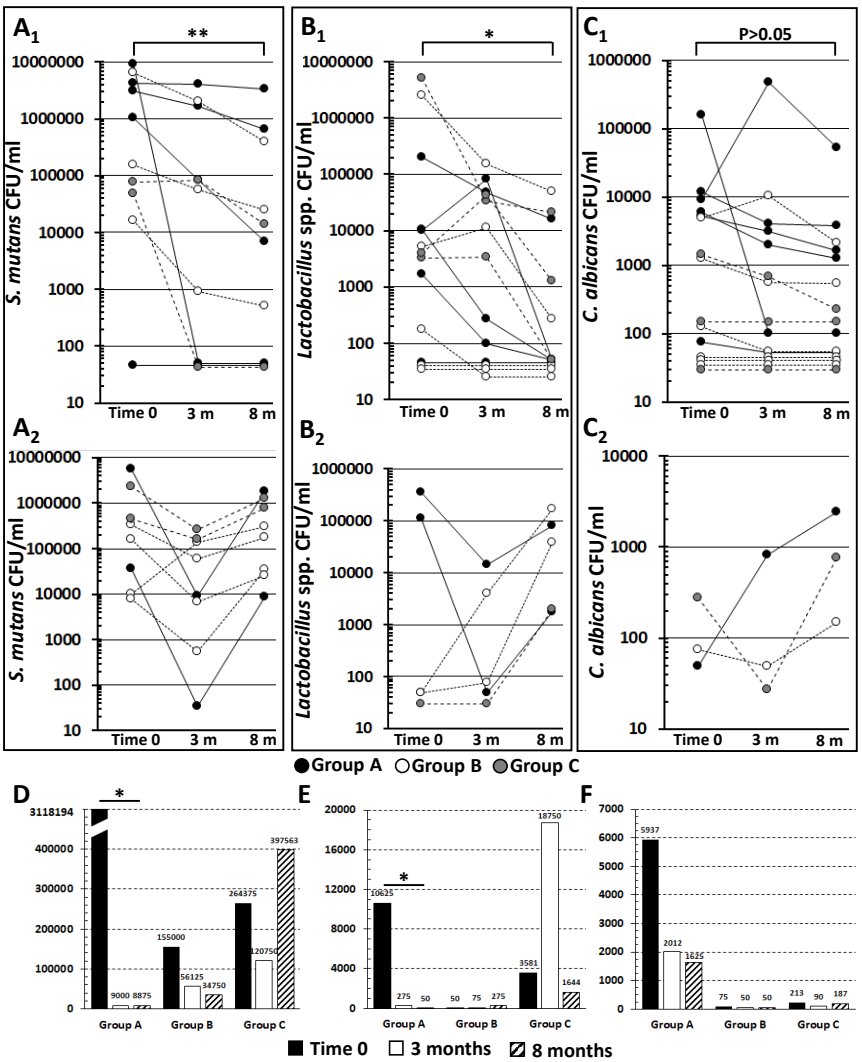

Fig. 5. *Salivary levels of S. mutans (**A1**, **A2**), Lactobacillus spp. (**B1**, **B2**) and C. albicans (**C1**, **C2**) at 8 months as compared to time 0 and 3 months in children (Group A), adolescents (Group B) and adults (Group C). See text for details. At each time point, data presented refer to the 18 subjects who were available for the follow-up at 8 months. Median salivary levels (CFU/ml) of S. mutans (**D**), Lactobacillus spp. (**E**), and C. albicans (**F**) at 3 and 8 months as compared to time 0 in children (Group A), adolescents (Group B) and adults (Group C). Statistical analysis was performed for each bacterial species considering the three groups of subjects as a whole (panels A, B, C) or separately (panels D, E, F). ** P<0.01, *P<0.05, Wilcoxon signed-rank test.*

time 0; 8 non-colonized patients at time 0 remained as such at 3 months, whereas in 4 patients an increase in the CFU/ml was observed. The difference between time 0 and 3 months was not statistically significant (Fig. 3C), even if the median values decreased, especially in the group of children (Fig. 3F).

In accordance with the reduction in the percentage of colonization and the number of CFUs, the comparison of mean plaque indexes between 0 and 3 months showed a significant reduction in plaque accumulation in adolescents and adults while in children it did not reach statistical significance (Fig. 4A). DMTF/dmtf scores remained unchanged (Fig. 4B), while an overall tendency to salivary pH and flow increment was observed (Fig. 4C and D).

Evaluation of microbiological and clinical parameters and caries risk factors at time 8 months

The microbiological and clinical analysis was repeated at 8 months from the oral hygiene/education measures, when the study group, due to drop-outs, consisted of 18 patients (7 children, 7 adolescents and 4 adults).

Fig. 5 shows the quantitative analysis of the number of CFUs of *S. mutans* (A1, A2), *Lactobacillus* spp. (B1, B2) and *C. albicans* (C1, C2) at the three time points of the study. For clarity, data have been divided into two panels for each species. As shown in the upper panel of each series (A1, B1 and C1) in most patients, the number of CFU/ml decreased or remained constant from 3 to 8 months. In contrast, for the remaining patients (lower panels A2, B2 and C2) an increase in the number of CFUs was observed, as compared to the 3-month time period. Analyzing the 18 patients as a whole, the difference in the number of CFU/ml was not statistically significant between 3 and 8 months, indicating globally that the trend in the reduction of the salivary count of the cariogenic species observed between 0 and 3 months was interrupted. Despite this, the 8-month CFU/ml numbers of *S.*

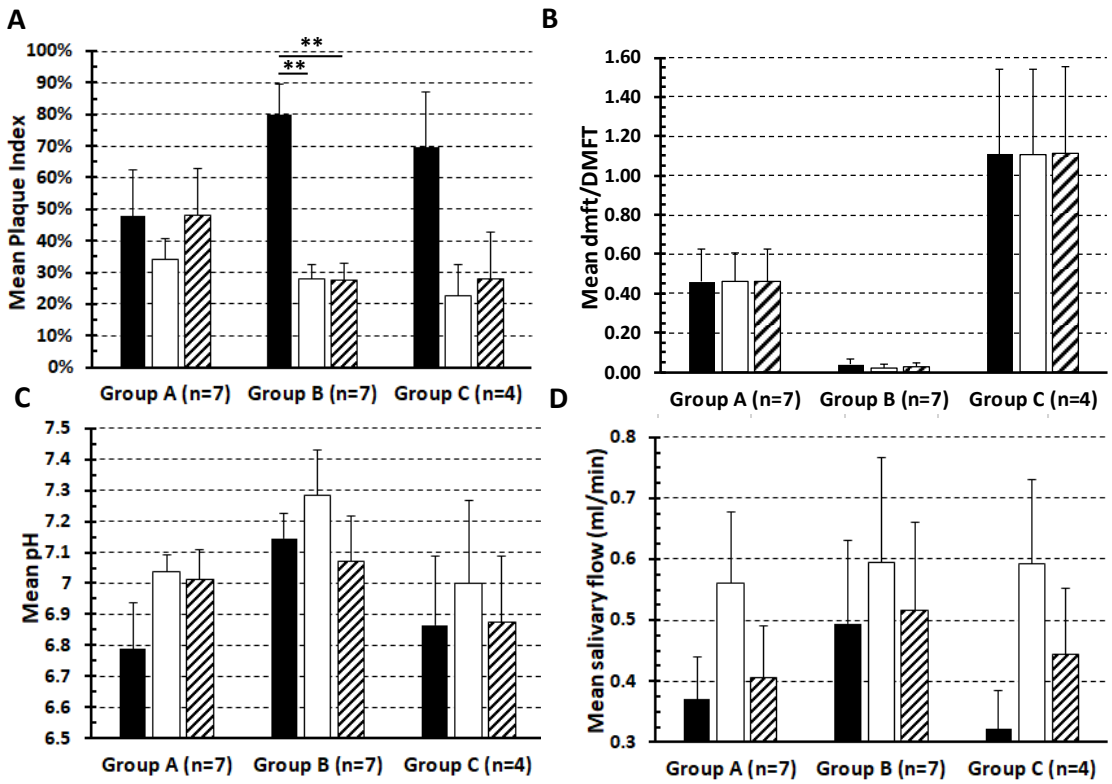

Fig. 6. *Clinical parameters (**A**, **B**) and caries risk factors (**C**, **D**) at time 0 (black bars), 3- (white bars) and 8-months (dashed bars) in children (Group A), adolescents (Group B), and adults (Group C). At each time point, data presented refer to the 18 subjects who were available for the follow-up at 8 months. ** P<0.01, Student's t-test for paired samples.*

mutans and *Lactobacillus* spp. were statistically lower than those recorded at time 0, suggesting, globally, the persistence of a positive effect of the hygiene/oral education measures given at time 0, on the salivary levels of cariogenic species. A decrease in the median CFU/ml value of *S. mutans* (Fig. 5D) as well as *Lactobacillus* spp. (Fig. 5E) was evident in the group of children ($P<0.05$). In the case of *C. albicans,* there was an increase in the number of CFU (panel C2) only for 3 patients, but the difference compared to time 0 remained non-significant, probably due to the high number of non-colonized patients at the 3 tim- points considered (panel C1 and F).

The analysis of the clinical parameters showed that at 8 months the mean PI, which was reduced at 3-months in all three groups of subjects, was increased particularly within group A where it reached levels similar to the ones recorded at time 0 (Fig. 6A). For Groups B and C mean PI at 8 months remained at levels similar to 3 months. DMFT/dmft indexes of the study group remained stable over 8 months (Fig. 6B), while the pH and saliva flow increased in all 3 groups at 3 months, but at 8 months they tended to decrease (Fig. 6C and D).

Correlation between salivary S. mutans levels and pH

Due to the marked ability of *S. mutans* to generate and tolerate acid we wanted to assess whether there was a statistically significant relationship between the load of *S. mutans* in saliva and the pH of saliva itself, considering the study group as a whole. Fig. 7 depicts, for each subject and for each time-point considered, the salivary count of *S. mutans* (in Log, y axis) and the salivary pH of the same patient (x axis). The two variables were found to be inversely correlated with a decrease in the CFU/ml along with an increment in the pH value in a statistically significant manner ($R=-0.27$, $P<0.05$, Spearman's Rho correlation test).

Correlation between S. mutans and C. albicans salivary levels

Due to the recently described association between *S. mutans* and *C. albicans* in oral biofilms, we evaluated the existence of a correlation between *S. mutans* and *C. albicans* salivary levels in the study population. As shown in Fig. 8A, when the subjects who presented salivary *S. mutans* counts above the risk level of $1x10^5$ CFU/ml were included

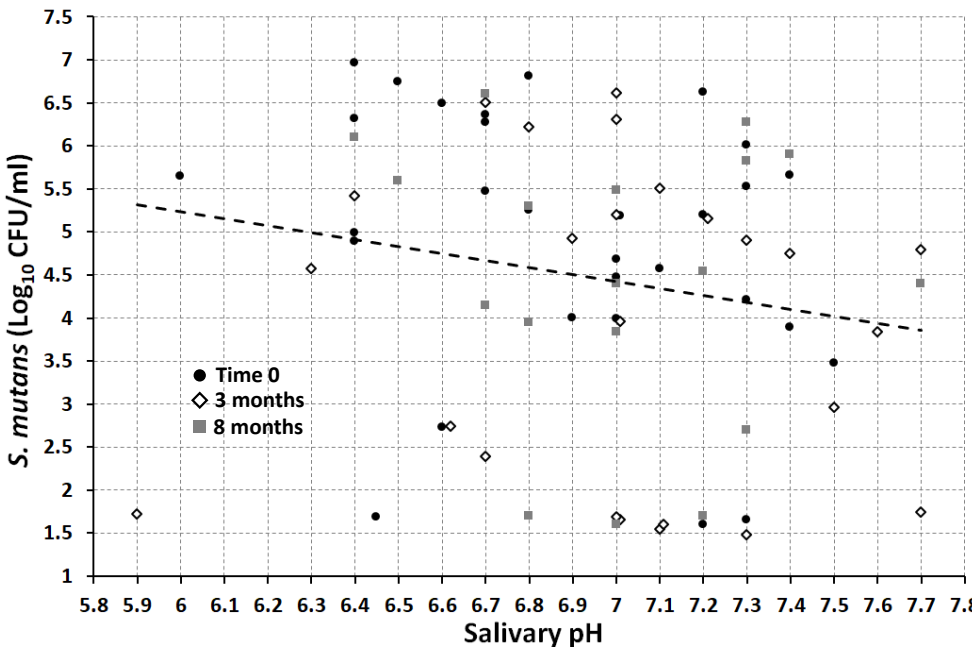

Fig. 7. *Inverse correlation between salivary S. mutans levels and pH in the 3 groups of subjects at all 3 time points considered. R=-0.27, P<0.05 Spearman's Rho correlation test.*

in the analysis, a positive and statistically significant correlation was found with the CFU number of *C. albicans* per ml of saliva (R=0.62, P<0.001 Spearman's Rho correlation test). Furthermore, when at all time-points the clinical parameters were compared between the patients who presented both *S. mutans* and *C. albicans* in saliva, and those that had only one or neither of them, a greater number of lesions and a higher PI was detected in the first group of subjects compared to the latter (Fig. 8B and C).

DISCUSSION

It is increasingly recognized that management of caries should not only rely on restorative treatments, but should also aim to prevent, by adequate oral health education actions, the ecological factors that promote the selection of a cariogenic microbiota (e.g. inadequate oral hygiene procedures and high dietary sugar intake) (27). In addition to microbial factors, host factors such as salivary flow and buffering capacity also play crucial roles in caries development (28).

The present longitudinal study aimed at evaluating the effectiveness of oral health education/hygiene measures, given by highly qualified personnel, on the salivary count of microbial species with high cariogenic potential as well as on clinical parameters indicative of oral health status and caries risk factors.

High frequencies of carriage and salivary levels of microbial species associated with dental caries were detected in the study population at time 0. These parameters were particularly severe in the group of children and correlated with severe clinical indexes (PI, DMTF, ICDAS index) and presence of susceptibility factors associated with a higher risk of caries (acidic pH, low saliva flow rates). These data indicate that despite the spread of caries control programs and the greater awareness of the importance of oral health compared to the

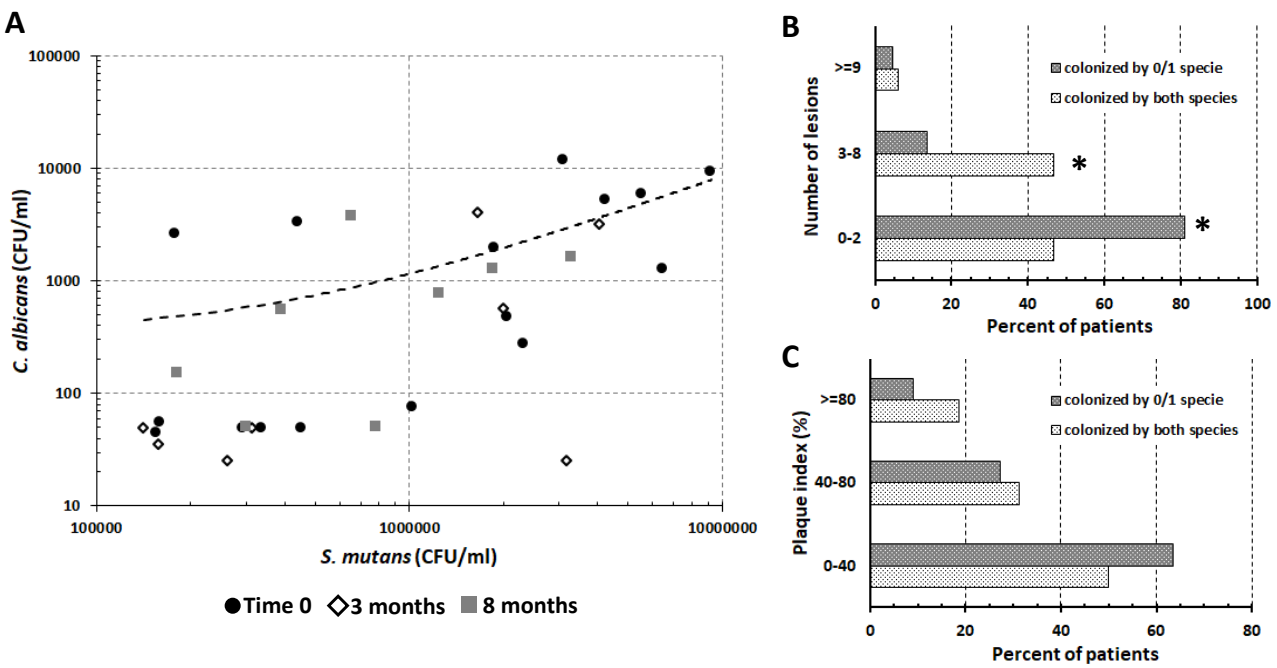

Fig. 8. *Positive correlation between salivary levels of S. mutans and C. albicans in the 3 groups of subjects at all 3 time points considered (**A**). Only subjects carrying salivary S. mutans levels ≥ 1x10^5 CFU/ml were included in the analysis. R=0.62, P<0.001 Spearman's Rho correlation test. Number of caries lesions (**B**), and plaque index (**C**) in subjects carrying both species (S. mutans ≥ 1x10^5 CFU/ml and C. albicans) in their saliva as compared to subjects carrying none or only one of the two species. *P<0.05, Fisher's exact test.*

past, dental caries remain widespread among the population. The percentage of subjects colonized by more than one cariogenic microbial species was also high at time 0 with about 50% of the subjects carrying all three cariogenic species analyzed in their saliva. This supports the current view that considers caries a polymicrobial infection in which both individual predisposing factors and the metabolic activity of different microbial species that synergistically interact with each other contribute to the pathogenesis of the disease.

At time 0 each subject underwent a careful intraoral examination to evaluate the degree of oral hygiene and health status as well as the presence of risk factors and the plaque distribution at different oral sites. The disclosure of these data allowed to define an individual-based therapeutic plan, which included advice on the most appropriate brushing method for the subject and indications of the areas in which he/she had to pay more attention during home cleansing.

After 3 months from the education/oral hygiene measures a statistically significant reduction was observed in the salivary load (CFU/ml) of *S. mutans* and *Lactobacillus* spp. which was associated with an overall improvement in clinical parameters (decrease in PI), and in caries risk factors (increase in pH and salivary flow). These data indicate that the professional removal of plaque and adequate education actions given by highly specialized personnel, aimed to correct incorrect brushing and dietary habits, have a positive impact on the salivary levels of species with high cariogenic potential at least in a 3-month time-span.

At 8 months from the education/oral hygiene measures, in many patients there was a further drop or stagnation of the salivary levels of *S. mutans* and *Lactobacillus*, while in others the microbial load tended to rise again. Despite this, globally, the salivary load of these bacterial species was still statistically lower than at time 0. Such microbiological data were associated, overall, with a worsening of clinical parameters compared to 3 months and a partial return of risk factors at less favorable levels. This could mean that, while for particularly motivated patients the oral education measures given at time 0 continued to have the desired effect even after relatively long periods, in patients less receptive or exhibiting individual risk factors it is necessary to repeat the education and motivation at shorter time intervals to root the habit of correct oral and alimentary hygiene.

In agreement with a previous report (29), the reduction of *S. mutans* in saliva correlated inversely, in a statistically significant manner, with the saliva pH, suggesting that the measurement of pH can be a parameter of easy and rapid determination to be used to identify subjects at a particularly high risk.

Interestingly, a statistically significant positive correlation was found between the levels of *S. mutans* and *C. albicans* in saliva. Furthermore, carriers of both microbial species exhibited more severe clinical parameters (high number of active lesions, elevated PI) than subjects harboring only one or none of the two species. These data support recent studies that suggest a marked inter-kingdom synergistic effect between *S. mutans* and *C. albicans* in the colonization of the oral cavity/pathogenesis of caries. These data also suggest that future caries control measures should be directed not only towards the bacterial component, but also towards the fungal one of the oral microbiota (30). The synergistic interaction between *S. mutans* and *C. albicans* seems to occur at several levels. For instance, it has been reported that the two species provide each other with sites for adhesion and that physical co-adhesion of *S. mutans* and *C. albicans* and cross-kingdom biofilm formation is highly enhanced in the presence of sucrose (31, 32). In addition, lactate secreted by *S. mutans* can be utilized as a carbon source by the fungus, which in turn reduces oxygen tension to levels preferred by the bacterium (32). Interestingly, coinfection of rats with *S. mutans* and *C. albicans* have been demonstrated to enhance the colonization and carriage of both organisms *in vivo* and markedly increase the biofilm formed on rodent dentition, leading to the development of rampant carious lesions (33). These findings support our results of more critical clinical parameters recorded in double-carriers as compared to single-carrier or non-colonized subjects.

Overall, the results obtained suggest that large-scale oral hygiene education programs could be

beneficial in reducing the salivary counts of species involved in the onset/progression of dental caries in a medium to long-term time-span (3-8 months). As suggested (34), the optimal frequency for dental checkups should be evaluated on the basis of individual factors, but our results indicate that strengthening of the motivation and administration of oral hygiene instruction and professional tooth cleaning every 6-8 months might be necessary to control the salivary levels of cariogenic species. Although *S. mutans* has been largely accepted as the etiologic agent of dental caries, our results support recent evidence indicating high prevalence for *S. mutans* in dental biofilms where the fungal pathogen *C. albicans* resides, suggesting that the interaction between these diverse species may mediate caries development.

ACKNOWLEDGEMENTS

This work was supported by funds from the University of Pisa (Rating di Ateneo).

REFERENCES

1. Petersen PE. The World Oral Health Report 2003: continuous improvement of oral health in the 21st century--the approach of the WHO Global Oral Health Programme. Community Dent Oral Epidemiol 2003; 31(suppl 1):3-23.
2. Hobdell M, Petersen PE, Clarkson J, Johnson N. Global goals for oral health 2020. Int Dent J 2003; 53:285-88.
3. Petersen PE, Kwan S. Evaluation of community-based oral health promotion and oral disease prevention--WHO recommendations for improved evidence in public health practice, Community Dent Health 2004; 21(4 suppl):319-29.
4. Petersen PE. Global policy for improvement of oral health in the 21st century--implications to oral health research of World Health Assembly 2007, World Health Organization. Community Dent Oral Epidemiol 2009; 37:1-8.
5. Selwitz RH, Ismail AI, Pitts NB. Dental caries. The Lancet 2007; 369:51-59.
6. Wagner Y, Heinrich-Weltzien R. Risk factors for dental problems: Recommendations for oral health in infancy. Early Hum Dev 2017; 114:16-21.
7. Batoni G, Ota F, Ghelardi E, et al. Epidemiological survey of *Streptococcus mutans* in a group of adult patients living in Pisa (Italy). Eur J Epidemiol 1992; 8:238-42.
8. Pannu P, Gambhir R, Sujlana A. Correlation between the salivary *Streptococcus mutans* levels and dental caries experience in adult population of Chandigarh, India. Eur J Dent 2013; **7**:191-95.
9. Nanda J, Sachdev V, Sandhu M, Deep-Singh-Nanda K. Correlation between dental caries experience and mutans streptococci counts using saliva and plaque as microbial risk indicators in 3-8 year old children. A cross Sectional study. J Clin Exp Dent 2015; **7**:114-18.
10. Colombo NH, Kreling PF, Ribas LFF, et al. Quantitative assessment of salivary oral bacteria according to the severity of dental caries in childhood. Arch Oral Biol 2017; 83:282-88.
11. Simón-Soro A, Mira A. Solving the etiology of dental caries. Trends Microbiol 2015; 23:76-82.
12. Caufield PW, Schön CN, Saraithong P, Li Y, Argimón S. Oral Lactobacilli and dental caries: A model for niche adaptation in humans. J Dent Res 2015; 94 (9 suppl):110S-18S.
13. Pereira D, Seneviratne DJ, Koga-Ito CY, Samaranayake LP. Is the oral fungal pathogen *Candida albicans* a cariogen? Oral Dis 2018; 24:518-26.
14. Klinke T, Guggenheim B, Klimm W, Thurnheer T. Dental caries in rats associated with *Candida albicans*. Caries Res 2011; 45:100-106.
15. De Carvalho FG, Parisotto TM. Presence of *Candida* spp. in infants' oral cavity and its association with early childhood caries. Brazilian J Oral Sci 2007; 6:1249-53.
16. Xiao J, Moon Y, Li L et al. *Candida albicans* carriage in children with severe early childhood caries (S-ECC) and maternal relatedness. PLoS One 2016; 11:e0164242.
17. Fábián TK, Fejérdy P, Csermely P. Salivary genomics, transcriptomics and proteomics: the emerging concept of the oral ecosystem and their use in the early diagnosis of cancer and other diseases. Curr Genomics 2008; 9:11-21.

18. Al Shukairy H, Alamoudi N, Farsi N, Al Mushayt A, Masoud I. A comparative study of *Streptococcus mutans* and lactobacilli in mothers and children with severe early childhood caries (SECC) versus a caries free group of children and their corresponding mothers. J Clin Pediatr Dent 2006; 31:80-85.
19. Crossner CG. Salivary lactobacillus counts in the prediction of caries activity. Community Dent Oral Epidemiol 1981; 9:182-90.
20. Raja M, Hannan A, Ali K. Association of oral candidal carriage with dental caries in children. Caries Res 2010; 44:272-76.
21. Moalic E, Gestalin A, Quinio D, Gest PE, Zerilli A, Le Flohic AM. The extent of oral fungal flora in 353 students and possible relationship with dental caries. Caries Res 2001; 35:149-55.
22. Lozano Moraga CP, Rodríguez Martínez GA, Lefimil Puente CA, Morales Bozo IC, Urzúa Orellana BR. Prevalence of *Candida albicans* and carriage of *Candida* non-albicans in the saliva of preschool children, according to their caries status. Acta Odontol Scand 2017; 75:30-35.
23. Leal SC, Mickenautsch S. Salivary *Streptococcus mutans* count and caries outcome – a systematic review. J Minim Interv Dent 2010; 3:137-47.
24. Kohler B, Bratthall D, Krasse B. Preventive measures in mothers influence the establishment of the bacterium *Streptococcus mutans* in their infants. Arch Oral Biol 1983; 28:225-31.
25. Kohler B, Andreen I, Jonsson B. The earlier the colonization by mutans streptococci, the higher the caries prevalence at 4 years of age. Oral Microbiol Immunol 1988; 3:14-17.
26. Gugnani N, Pandit IK, Srivastava N, Gupta M, Sharma M. International Caries Detection and Assessment System (ICDAS): A New Concept. Int J Clin Pediatr Dent 2011; 4:93-100.
27. WHO Information Series on School Health, Oral Health Promotion: An Essential Element of a Health-Promoting School, Geneva: World Health Organization, http://www.who.int/oral_health/media/en/orh_school_doc11.pdf?ua=1 2003.
28. Guo L, Shi W. Salivary biomarkers for caries risk assessment. J Calif Dent Assoc 2013; 41:107-18.
29. Abbate GM, Borghi D, Passi A, Levrini L. Correlation between unstimulated salivary flow, pH and *Streptococcus mutans*, analysed with real time PCR, in caries-free and caries-active children. Eur J Paediatr Dent 2014; 15:51-54.
30. Koo H, Bowen WH. *Candida albicans* and *Streptococcus mutans*: a potential synergistic alliance to cause virulent tooth decay in children. Future Microbiol 2014; 9:1295-97.
31. Ellepola K, Liu Y, Cao T, Koo H, Seneviratne CJ. Bacterial GtfB augments *Candida albicans* accumulation in cross-kingdom biofilms. J Dent Res 2017; 96:1129-35.
32. Metwalli KH, Khan SA, Krom BP, Jabra-Rizk MA. *Streptococcus mutans*, *Candida albicans*, and the human mouth: a sticky situation. PLoS Pathog 2013; 9:e1003616.
33. Falsetta ML, Klein MI, Colonne PM et al. Symbiotic relationship between *Streptococcus mutans* and *Candida albicans* synergizes virulence of plaque biofilms in vivo. Infect Immun 2014; 82:1968-81.
34. Hahn TW, Kraus C, Hooper-Lane C. Clinical Inquiries: What is the optimal frequency for dental checkups for children and adults? J Fam Pract 2017; 66:699-700.

IMPACT OF TREATMENTS ON FECAL MICROBIOTA AND FECAL METABOLOME IN SYMPTOMATIC UNCOMPLICATED DIVERTICULAR DISEASE OF THE COLON: A PILOT STUDY

L. LAGHI[1*], P. MASTROMARINO[2*], W. ELISEI[3], D. CAPOBIANCO[2], C.-L. ZHU[1], M. PICCHIO[4], G. GIORGETTI[5], G. BRANDIMARTE[6] and A. TURSI[7]

[1]Centre of Foodomics, Department of Agro-Food Science and Technology, University of Bologna, Bologna, Italy; [2]Department of Public Health and Infectious Diseases, Section of Microbiology, Sapienza University, Rome, Italy; [3]Division of Gastroenterology, ASL RM6, Albano Laziale, Rome, Italy; [4]Division of Surgery, "P. Colombo" Hospital, ASL RM6, Velletri Rome, Italy; [5]Digestive Endoscopy and Clinical Nutrition Unit, "S. Eugenio" Hospital, Rome, Italy; [6]Division of Internal Medicine and Gastroenterology, "Cristo Re" Hospital, Rome, Italy; [7]Gastroenterology Service, ASL BAT, Andria (BT), Italy

Received June 18, 2018 – Accepted September 6, 2018

*These Authors contributed equally to this article

Symptomatic uncomplicated diverticular disease (SUDD) affects 50% of people having diverticulosis. We performed a pilot study assessing the effect of current treatments on fecal microbiota and metabolome in SUDD. Thirteen consecutive females with SUDD were treated with a 2-week therapeutic trial of 30 g/day fiber supplementation (3 patients), 1.6 g/day of mesalazine (3 patients), 900 billion/day of probiotic mixture VivoMixx® (3 patients), or 800 mg/day of rifaximin (4 patients). Stool samples were collected at entry (T0), at the end of the 2-week therapeutic course (T1), and 30 (T2) and 60 days (T3) after the end of the therapeutic course. Real-time PCR quantified targeted microorganisms. Fecal metabolome patterns were studied by high-resolution proton NMR spectroscopy. At cumulative analysis, symptoms significantly decreased at each time point during follow-up ($p<0.0001$), and only left-lower quadrant pain increased again at T3. The overall bacterial quantity was not altered by the treatments. The amount of *Akkermansia muciniphila* species was significantly reduced at T1 ($p=0.017$) and at T2 ($p=0.026$), while at T3 the reduction was not significant in comparison to enrollment ($p=0.090$). Fecal molecular profile showed significant changes at T1 and T2, while at T3 it became similar to that of T0. Differences were found for 18 of the quantified molecules (tryptophan, phenylalanine, tyrosine, 4-hydroxyphenylacetate, urocanate, X-6.363, X-5.779, uridylate, galactose, X-4.197, threonine, sarcosine, methionine, 2-oxoisocaproate, 5-aminolevulinate, alanine, leucine, valerate). Metabolome and microbiota changed in patients with SUDD under treatment, confirming a possible role of dysbiosis/dysmetabolome in the pathology.

Diverticulosis of the colon is the most common anatomic alteration found by colonoscopy (1). Its symptomatic form, called symptomatic uncomplicated diverticular disease (SUDD), affects one-fifth of the people with diverticulosis (1). Although the pathogenesis is not completely

Key words: diverticular disease, fecal metabolome, fecal microbiota, treatment

Mailing address:
Antonio Tursi, MD
Servizio di Gastroenterologia Territoriale,
DSS n°4, ASL BAT
Via Torino, 49 76123 Andria (BT), Italy
Tel.: +39 0883 551094 - Fax: +39 0883 1978210
e-mail: antotursi@tiscali.it

0393-974X (2018)

understood, it has been suggested that a changed gut microbiota composition is a plausible etiopathogenetic factor in diverticular disease (2). Indeed, recent papers indicated that the diversity of the *Proteobacteria* phylum was significantly higher in fecal samples of patients compared to controls (3) while some *Clostridium* clusters, *Fusobacterium* and Lactobacillaceae were reduced in symptomatic versus asymptomatic patients (4). Moreover, a significant increase of *Akkermansia muciniphila* in symptomatic and asymptomatic patients in comparison to healthy controls has been reported (5).

Metabolic profiling is a powerful exploratory tool for understanding interactions between nutrients, intestinal metabolism and microbiota composition in health and disease and for gaining deeper insight in the metabolic pathways altered by diseases. Currently, metabolomic technologies are increasingly used to discover gastrointestinal disease signatures and have been applied for the screening of different pathological conditions that are linked with a metabolic imbalance (6). Besides microbial imbalance, differences in fecal metabolome have also been observed in diverticular disease (4, 5).

Several treatments are currently proposed in order to treat symptoms in SUDD patients. Typically, pharmacological treatments, such as rifaximin and mesalazine or dietary supplements (fibers and probiotics), share some features like the ability to modify the intestinal microbiota and antiinflammatory activity, however, there is no information whether those treatments are also able to influence fecal microbiota in relation to metabolome in SUDD patients. The aim of this pilot study was therefore to assess variation of fecal microbiota and fecal metabolome in SUDD patients after treatment, assessing also whether there was a relationship between symptom expression, fecal microbiota and fecal metabolome in the subjects under treatment.

MATERIALS AND METHODS

Setting and participants

SUDD was defined as the presence of symptoms in patients with diverticulosis, in absence of signs and/or symptoms and laboratory and/or endoscopy and/or radiology according to acute diverticulitis, and in absence of any other complication (stenosis, abscesses, fistulas) (7).

From June to December 2015, 13 consecutive patients, undergoing colonoscopy and suffering from SUDD according to the above-mentioned criteria, were enrolled according to the following characteristics: middle-aged female patients; birth by vaginal delivery and with exclusive breastfeeding; living in the same geographical area (Castelli Romani, located south of Rome, Italy, and >600.000 population); body mass index (BMI) in the range 20-34; no use of antibiotics in the three months previous to enrolment; ongoing or past acute complicated and uncomplicated diverticulitis; absence of bacterial and/or parasitic intestinal diseases (assessed by stool analysis) and of lactose malabsorption (assessed by lactose H_2 breath test); no intestinal surgical procedure.

The protocol was approved by the Ethic Committee of the ASL Roma C, Italy (approval number 6/2012). This study is registered with www.ClinicalTrials.gov., number NCT01831323. Written informed consent was obtained from all subjects.

According to Tursi et al. (8, 9), left lower quadrant abdominal pain for more than 24 h, the main symptom characterizing SUDD (7, 8), was assessed using a 10-point scale, assigning numerical values of 0 for absence of pain, 1–4 for mild pain, 5–7 for moderate pain and 8–10 for severe pain. The same scale was also used to evaluate other symptoms assessed in this study, namely lower abdominal pain, upper abdominal pain, rectal bleeding, sensation of incomplete evacuation, bloating and mucus in stool. Symptoms were assessed at entry (T0), at the end of the 2-week therapeutic trial (T1), 30 (T2) and 60 (T3) days after the end of the therapeutic trial, as depicted in Fig. 1. Fecal calprotectin (FC) expression was also assessed in all SUDD patients by a semi-quantitative test (CalDetect®, SOFAR S.p.A., Trezzano Rosa (MI), Italy) at the time of enrolment (T0).

Since fibers, rifaximin, mesalazine and probiotics are currently used as cyclic treatment for SUDD (7), we treated patients with a two-week therapeutic course of 30 g/day of soluble fiber supplementation (Psyllium, 3 patients), 1.6 g/day of mesalazine Eudragit L (3 patients), 900 billion/day of probiotic mixture VivoMixx® (3 patients), or 800 mg/day of rifaximin (4 patients). The probiotic product contains 4 strains of lactobacilli (*L. plantarum*, *L. paracasei*, *L. delbrueckii* subsp. *bulgaricus*,

L. acidophilus), 3 strains of bifidobacteria (*B. breve, B. longum, B. infantis),* and 1 strain of *Streptococcus thermophilus*. We choose these treatments because fiber, rifaximin, probiotics and mesalazine are the most common treatments prescribed in treating symptomatic SUDD (7).

Fecal samples collection

Stool samples were collected for at least four weeks following colonoscopy, at T0, T1, T2 and T3. They were collected early morning at home, in sterile plastic tubes, transported on ice to the laboratory within 2 h and stored at −80°C until analysis.

Fecal microbiota assessment

Bacterial DNA from fecal samples was extracted using the QIAamp Fast DNA Stool Mini Kit (Qiagen, Hilden, Germany). Approximately 200 mg of feces were cut from frozen samples using sterile disposable scalpels, resuspended in 1 ml of InhibitEX lysis buffer from the stool kit, added with glass beads (150-212 μm Sigma-Aldrich, USA) and homogenized thoroughly. The suspension was incubated at 95°C for 5 min and DNA was purified according to the manufacturer's instructions. Purified DNA aliquots were stored at –20ºC until analysis. Real-time PCR was used to quantify total bacteria, *Bifidobacterium* and *Lactobacillus* genera, and *Akkermansia muciniphila,* using primers and conditions described by Nadkarni et al. (10), Matsuki et al. (11), Štšepetova et al. (12), and Collado et al. (13), respectively. PCR amplification and detection were performed on optical-grade 96-well plates using the Applied Biosystems 7500 Real-Time PCR System. The reaction mixture (25 μl) was composed of SensiMix SYBR PCR Master Mix (Bioline), 500 nM primers for total bacteria, 500 nM primers for *Bifidobacterium* genus, 200 nM for *Lactobacillus* genus and 200 nM for *Akkermansia muciniphila*, respectively, and 2.5 μl of template DNA. The fluorescent products were detected at the last step of each of 40 cycles. A melting curve analysis was made after amplification to distinguish the targeted PCR product from the PCR products not targeted. Standard curves were created using serial ten-fold dilutions of bacterial DNA extracted from *Bacteroides fragilis* for total bacteria*, Bifidobacterium breve* and *Lactobacillus brevis* for *Bifidobacterium* and *Lactobacillus* genera, respectively, and from *Akkermansia muciniphila*. All samples were analyzed in duplicate in two independent real-time PCR assays.

Fecal metabolome assessment

Fecal samples were prepared for NMR analysis by vortex mixing for 5 min 80 mg of stool with 1 ml of deionized water. The obtained mixes were then centrifuged for 15 min at 18630 g and 4°C. 700 μl of supernatant were added to 100 μl of a D_2O solution of 3-(trimethylsilyl)-propionic-2,2,3,3-d4 acid sodium salt (TSP) 10 mM, used as NMR chemical-shift reference, buffered at pH 7.00 by means of 1M phosphate buffer. Finally, the so obtained samples were centrifuged again at the above conditions.

^{1}H-NMR spectra were recorded at 298 K with an AVANCE III spectrometer (Bruker, Milan, Italy) operating at a frequency of 600.13 MHz. Following Ventrella et al. (14), the signals from broad resonances originating from large molecules were suppressed by a CPMG-filter composed by 400 echoes with a τ of 400 μs and a 180° pulse of 24 μs, for a total filter of 330 ms. The HOD residual signal was suppressed by means of presaturation. This was done by employing the cpmgpr1d sequence, part of the standard pulse sequence library. Each spectrum was acquired by summing up 256 transients using 32 K data points over a 7184 Hz spectral window, with an acquisition time of 2.28s. In order to apply NMR as a quantitative technique (15), the recycle delay was set to 5s, keeping into consideration the relaxation time of the protons under investigation. ^{1}H-NMR spectra baseline-adjusted by means of the peak detection according to the "rolling ball" principle (16) implemented in the baseline R package (17). A linear correction was then applied to each spectrum to make the points pertaining to the baseline randomly spread around zero. No manual alignment of the signals was necessary, differently from previous investigations (4). Differences in water and fiber contents among samples were taken into consideration by probabilistic quotient normalization (18), applied to the entire spectra array.

The signals were assigned by comparing their chemical shift and multiplicity with the Human Metabolome Database (19) and Chenomx software data bank (Chenomx Inc., Canada, ver 8.1). Molecules with unknown chemical structure were also detected and quantified. Following Ventrella et al. (14), they will be referred to throughout the text with an x followed by the chemical shift in ppm of their signal used for quantification (i.e. x-4.197).

Statistical methods

Clinical scores and microorganism or molecule concentrations varying independently from the treatments applied were looked for by paired Wilcoxon test, by accepting a p-value limit for significance of 0.05. Molecules, the concentrations of which varied in relation to the treatments were looked for by means of non-parametric analysis of variance by Kruskal-Wallis test (20). To highlight any trend in the data, for this test a p-value limit for significance of 0.1 was accepted.

To highlight the overall trends characterizing the samples, principal component analysis models (PCA) and their sparse counterparts (sPCA) (21) were employed, by means of the corresponding algorithms implemented in R mixOmics package (22). For this purpose, clinical scores or molecules and microorganisms concentrations were centered and scaled to unity variance. For each PCA model, we calculated the score plot, the projection of the samples in the PC space, tailored to highlight the underlying structure of the data. Besides, we calculated the correlation plot, according to Pearson, relating the concentration of each variable to the components of PCA model, therefore tailored to highlight the correlations among molecules and microorganisms. To consider that the same subjects were followed along the entire experiment, giving rise to a repeated measurement data structure, molecules and microorganisms concentrations at time point T0 were subtracted from every time point, as suggested by Ndagijimana et al. (23).

RESULTS

Characteristics of the study population

The characteristics of the study group are reported in Table I. The median age of the studied population was 64 (range 52-70) years, and the median BMI was 25.6 (range 21.6-33.7). All patients had left lower quadrant pain for more than 24 hours. With the exception of abdominal pain, the most frequent symptom was abdominal bloating, occurring in 10 patients (76.9%). According to the manufacturer's instructions, all of them showed over-expression of fecal calprotectin which was between 15 and 60 μg in 10 patients (64.7%), and ≥60 μg in 3 patients (35.3%).

To highlight symptoms that could reveal at best the health conditions of the patients independently from the kind of treatment explored, we set up a one-tailed paired Wilcoxon test comparing T0 with the following time points for the 13 subjects studied. Pain in the lower abdomen, pain in the left lower abdomen and meteorism showed statistically significant decreases ($p<0.01$) at T1, that lasted till the end of the observation (Fig. 2, A and B). Moreover, we found that left lower quadrant pain decreased significantly in the studied population at T1 and T2, but increased again at T3 (without reaching T0 levels).

To gain an overview of the highlighted symptoms, a PCA model was calculated (Fig. 3). In the score plot (Fig. 3A), PC 1, accounting for 56.3% of the total variance among the subjects, offered an effective summary of the clinical scores, with subjects at T0 appearing at high values and subjects at the other time points appearing at lower values. The corresponding correlation plot (Fig. 3B) revealed that the symptom that mostly contributed to such trend was lower abdomen pain, followed by left lower abdomen pain and meteorism. Each symptom showed a correlation with its importance on PC 1 higher than 0.5. To gain an insight on the peculiar consequences of the tested treatments on these symptoms, the median position of the groups along PC 1 was calculated at each time point (Fig. 3C). This representation made clear that each treatment led to an improvement of the symptoms between T0 and T1 which was confirmed for each treatment by the following time points, so that the difference between samples obtained at T0 and those obtained at the following time points, cumulatively considered, was statistically significant ($p<0.05$). The evolution of symptoms over time seemed nevertheless to differentiate the treatments. On the one hand, in the treatment with probiotics the symptoms went on linearly improving in the T1-T3 time-lapse ($p<0.05$), so that their median score along PC 1 at T3 was the furthest from that at T0. On the other hand, such improvement tended to partially fade in subjects treated with rifaximin and mesalazine, so that their median scores along PC 1 at T2 and T3 were between those at T0 and T1.

Analysis of fecal microbiota

In order to gain information about the health status of the subjects from a microbiome point of view,

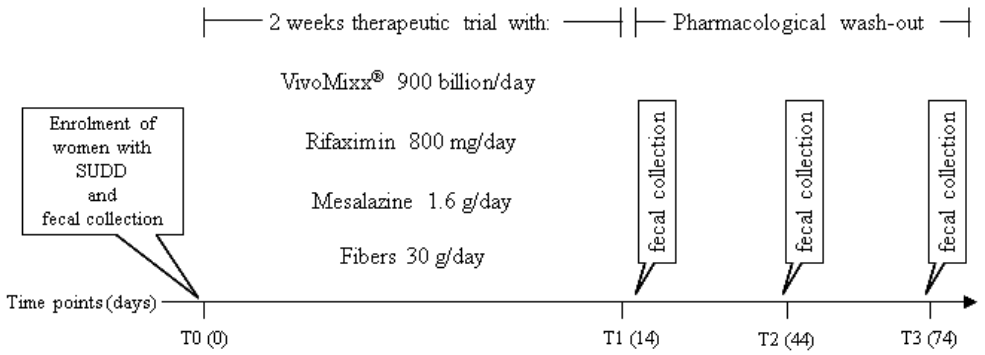

Fig. 1. *Flow-chart of the study.*

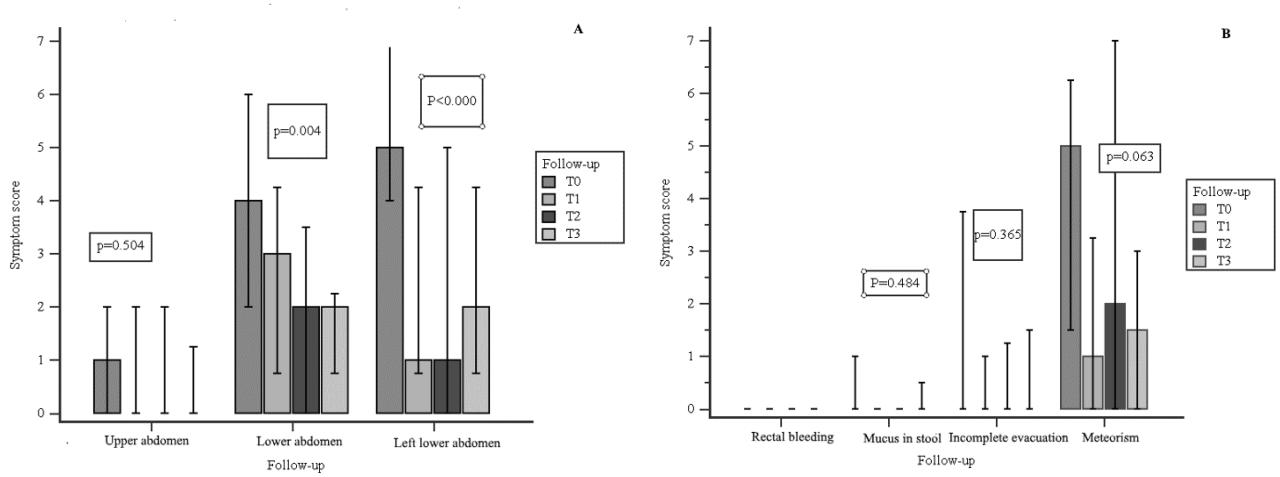

Fig. 2. *Clinical symptom scores assessed at baseline and during follow-up. **A)** Abdominal pain; **B)** Other symptoms.*

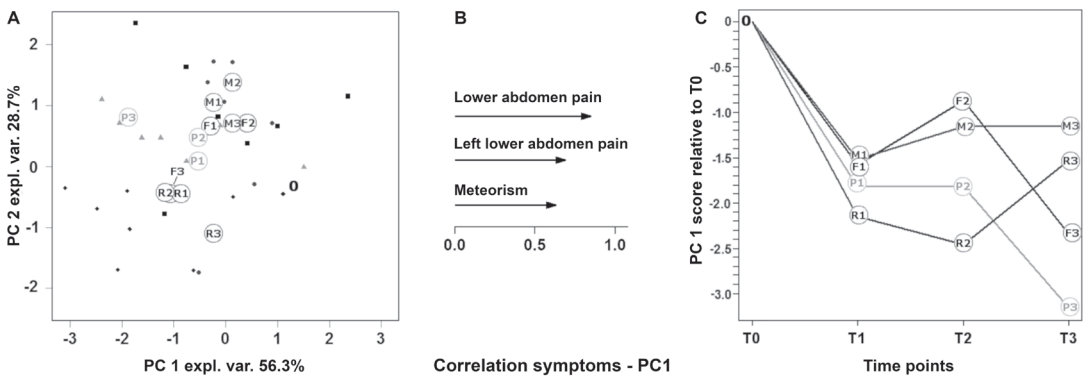

Fig. 3. *PCA model calculated on the clinical scores of Fig. 2, centered and scaled to unity variance. **A)** Scoreplot of the model, with triangles, squares, diamonds and circles representing samples from subjects treated with probiotics (P), fibers (F), rifaximin (R) and mesalazine (M), respectively. For each group, the median position in the scoreplot is indicated with the initial letter of the treatment followed by the time point. Samples at T0 are superimposed and are indicated with a 0 number. **B)** Correlation between clinical scores and their importance along PC 1. **C)** Median position of the groups of subjects along PC 1.*

lactobacilli and bifidobacteria, usually considered substantial components of healthy gut microbiota, were quantified. Neither showed statistically significant trends along the tested time points, either as absolute amounts or after normalization in respect to total bacteria. A linear positive

Table I. *Characteristics of the study population.*

Patient	Age	BMI	Localization of diverticula	Left lower abdominal quadrant pain	Diffuse lower abdominal pain	Diffuse upper abdominal pain	Abdominal bloating	Sensation of incomplete evacuation	Mucus in the feces	Blood in the feces	Fecal calprotectin	Type of therapy
Patient 1	66	33.7	Sigma	4	2	0	7	6	0	0	>15<60 µg	Fibers
Patient 2	52	21.6	Sigma	4	2	2	5	6	0	0	>15<60 µg	Mesalazine
Patient 3	70	31.3	Sigma	7	8	0	2	1	0	0	>15<60 µg	Probiotics
Patient 4	64	29.7	Sigma	7	2	2	5	0	0	0	>60 µg	Rifaximin
Patient 5	66	24.7	Sigma	5	6	1	8	0	0	0	>15<60 µg	Rifaximin
Patient 6	66	25.5	Sigma	4	5	2	6	3	2	0	>60 µg	Probiotics
Patient 7	65	28.8	Sigma	4	3	3	8	10	1	0	>15<60 µg	Fibers
Patient 8	61	22.3	Sigma	5	4	1	2	1	2	0	>15<60 µg	Probiotics
Patient 9	65	25.6	Sigma	7	7	2	0	0	0	0	>15<60 µg	Fibers
Patient 10	61	27.9	Sigma	5	5	0	6	0	0	0	>15<60 µg	Rifaximin
Patient 11	61	33.3	Sigma	7	0	0	0	0	0	0	>60 µg	Mesalazine
Patient 12	59	25.0	Sigma	6	6	0	6	0	0	0	>15<60 µg	Rifaximin
Patient 13	66	33.7	Sigma	5	1	0	0	0	1	0	>15<60 µg	Mesalazine

Table II. *Concentration of the molecules that were found to differ significantly between T0 and the other time-points.*

Organic acids				
Formate	$9.66x10^{-5} \pm 4.43x10^{-5}$	$1.85x10^{-4} \pm 7.89x10^{-5**}$	$1.48x10^{-4} \pm 1.08x10^{-4*}$	$1.87x10^{-4} \pm 1.27x10^{-4**}$
2-Hydroxy-3 methylvalerate	$4.39x10^{-4} \pm 2.68x10^{-4}$	$2.27x10^{-4} \pm 8.46x10^{-5**}$	$2.57x10^{-4} \pm 9.82x10^{-5}$	$3.45x10^{-4} \pm 3.24x10^{-4}$
3-Hydroxy phenylacetate	$8.97x10^{-4} \pm 8.87x10^{-4}$	$9.08x10^{-4} \pm 7.91x10^{-4}$	$7.98x10^{-4} \pm 7.85x10^{-4}$	$4.85x10^{-4} \pm 5.48x10^{-4*}$
Valerate	$7.85x10^{-4} \pm 3.01x10^{-4}$	$7.42x10^{-4} \pm 4.18x10^{-4}$	$6.37x10^{-4} \pm 3.22x10^{-4**}$	$7.52x10^{-4} \pm 5.58x10^{-4*}$
Aminoacids				
Phenylalanine	$1.10x10^{-3} \pm 2.76x10^{-4}$	$1.58x10^{-3} \pm 6.60x10^{-4**}$	$1.27x10^{-3} \pm 5.67x10^{-4}$	$1.61x10^{-3} \pm 1.07x10^{-3**}$
Glycine	$1.74x10^{-3} \pm 5.73x10^{-4}$	$2.26x10^{-3} \pm 1.00x10^{-3**}$	$1.98x10^{-3} \pm 7.56x10^{-4}$	$2.23x10^{-3} \pm 9.14x10^{-4*}$
Aspartate	$4.09x10^{-4} \pm 2.29x10^{-4}$	$5.58x10^{-4} \pm 2.42x10^{-4**}$	$4.59x10^{-4} \pm 2.59x10^{-4}$	$5.11x10^{-4} \pm 2.62x10^{-4*}$
Valine	$2.25x10^{-3} \pm 7.50x10^{-4}$	$2.77x10^{-3} \pm 9.23x10^{-4*}$	$2.90x10^{-3} \pm 1.54x10^{-3}$	$3.59x10^{-3} \pm 2.55x10^{-3**}$
Leucine	$6.47x10^{-3} \pm 2.03x10^{-3}$	$7.78x10^{-3} \pm 2.47x10^{-3*}$	$7.63x10^{-3} \pm 2.81x10^{-3**}$	$9.68x10^{-3} \pm 5.81x10^{-3**}$
Isoleucine	$1.66x10^{-3} \pm 5.45x10^{-4}$	$2.01x10^{-3} \pm 6.37x10^{-4*}$	$1.95x10^{-3} \pm 6.84x10^{-4}$	$2.44x10^{-3} \pm 1.32x10^{-3**}$
Proline	$1.37x10^{-3} \pm 5.74x10^{-4}$	$1.23x10^{-3} \pm 5.24x10^{-4}$	$1.73x10^{-3} \pm 7.57x10^{-4*}$	$1.64x10^{-3} \pm 6.93x10^{-4}$
Methionine	$6.84x10^{-4} \pm 1.81x10^{-4}$	$7.67x10^{-4} \pm 2.31x10^{-4}$	$7.64x10^{-4} \pm 3.10x10^{-4}$	$8.65x10^{-4} \pm 2.45x10^{-4*}$
Threonine	$1.98x10^{-3} \pm 5.47x10^{-4}$	$2.26x10^{-3} \pm 7.58x10^{-4**}$	$1.91x10^{-3} \pm 3.04x10^{-4}$	$2.51x10^{-3} \pm 1.60x10^{-3}$
Alanine	$4.75x10^{-3} \pm 1.47x10^{-3}$	$5.35x10^{-3} \pm 1.52x10^{-3}$	$5.45x10^{-3} \pm 1.89x10^{-3}$	$5.97x10^{-3} \pm 2.71x10^{-3*}$
Taurine	$2.74x10^{-3} \pm 2.45x10^{-3}$	$3.00x10^{-3} \pm 2.03x10^{-3*}$	$3.31x10^{-3} \pm 2.68x10^{-3}$	$2.80x10^{-3} \pm 2.65x10^{-3}$
Alcohols				
Methanol	$1.26x10^{-3} \pm 1.21x10^{-3}$	$3.80x10^{-4} \pm 2.51x10^{-4**}$	$6.68x10^{-4} \pm 9.75x10^{-4*}$	$4.87x10^{-4} \pm 3.64x10^{-4**}$
Ethanol	$2.79x10^{-3} \pm 2.09x10^{-3}$	$8.80x10^{-4} \pm 7.58x10^{-4*}$	$6.51x10^{-4} \pm 4.36x10^{-4**}$	$1.20x10^{-3} \pm 1.27x10^{-3*}$
Others				
Nicotinate	$2.38x10^{-4} \pm 5.30x10^{-5}$	$1.97x10^{-4} \pm 5.53x10^{-5**}$	$2.51x10^{-4} \pm 6.26x10^{-5}$	$2.32x10^{-4} \pm 1.29x10^{-4}$
Urocanate	$1.01x10^{-4} \pm 6.14x10^{-5}$	$7.25x10^{-5} \pm 4.80x10^{-5}$	$6.43x10^{-5} \pm 3.71x10^{-5*}$	$1.03x10^{-4} \pm 8.19x10^{-5}$
3-Methylglutarate	$4.18x10^{-4} \pm 2.59x10^{-4}$	$4.10x10^{-4} \pm 2.12x10^{-4}$	$4.86x10^{-4} \pm 2.70x10^{-4**}$	$4.61x10^{-4} \pm 3.26x10^{-4}$
m-Cresol	$7.20x10^{-4} \pm 6.07x10^{-4}$	$7.32x10^{-4} \pm 5.90x10^{-4}$	$7.07x10^{-4} \pm 5.14x10^{-4}$	$4.52x10^{-4} \pm 3.18x10^{-4*}$
Uridine	$1.40x10^{-4} \pm 9.06x10^{-5}$	$1.02x10^{-4} \pm 1.19x10^{-4}$	$1.13x10^{-4} \pm 7.63x10^{-5}$	$8.52x10^{-5} \pm 9.11x10^{-5*}$
x-4.199	$1.14x10^{-3} \pm 7.11x10^{-4}$	$7.07x10^{-4} \pm 4.26x10^{-4**}$	$1.02x10^{-3} \pm 5.73x10^{-4}$	$1.04x10^{-3} \pm 5.72x10^{-4}$
x-3.953	$8.01x10^{-4} \pm 3.09x10^{-4}$	$7.86x10^{-4} \pm 3.12x10^{-4}$	$9.64x10^{-4} \pm 4.22x10^{-4*}$	$8.92x10^{-4} \pm 3.09x10^{-4}$
x-3.061	$1.83x10^{-4} \pm 8.39x10^{-5}$	$2.32x10^{-4} \pm 9.22x10^{-5**}$	$2.27x10^{-4} \pm 9.66x10^{-5}$	$1.99x10^{-4} \pm 5.25x10^{-5}$
x-0.782	$9.85x10^{-5} \pm 9.04x10^{-5}$	$6.26x10^{-5} \pm 3.46x10^{-5*}$	$5.51x10^{-5} \pm 2.17x10^{-5}$	$1.30x10^{-4} \pm 2.39x10^{-4}$

*Concentration of the molecules is reported as mmol/L. Significant differences with respect to T1 are indicated with * (P<0.1) and ** (P<0.05)*

correlation between fecal levels of lactobacilli and bifidobacteria was observed across the entire study (R=0.34, p=0.013). To highlight other species that could reveal the health conditions of the patients independently from the kind of treatment explored, we set up a two-tailed Wilcoxon test comparing T0 and T1 time points for the 13 studied subjects. *A. muciniphila* showed a decrease with a high level of significance (p=0.0017), as shown in Fig. 4. The latter trend was confirmed also when T0 was compared with T2 (p=0.026). Interestingly, *A. muciniphila* and lactobacilli were found to be inversely correlated across the entire study (p<0.01). In this context, analysis of variance revealed that the tested treatments did not have different effects on the concentration of *A. muciniphila* or on the *A. muciniphila* /lactobacilli ratio.

Analysis of fecal metabolome

To understand how the treatments under consideration could affect the fecal molecular profile, a metabolomics investigation was set up by means of ^{1}H-NMR. Sixty-five molecules could be quantified, pertaining to the chemical groups of amino acids, short chain fatty acids, organic acids and monomeric carbohydrates. Six molecules more could be quantified, with a partially unclear structure, and therefore denoted with the location in the NMR spectrum, expressed in ppm. To highlight the effects that the four tested treatments had in common, we set up a two-tailed Wilcoxon test comparing T0 against the other time points for the 13 studied subjects (Table II). The molecular profile at T1 differed from the one at T0 in the concentration of 16 molecules. As many as 6 aminoacids and the non-proteinogenic aminoacid taurine resulted significant in this comparison. Interestingly, all were found to increase along time. In addition, these trends were confirmed by the T0-T2 and T0-T3 comparisons. The concentration of formate was found to increase as a consequence of the treatments, both immediately and in the long term, while the opposite was found for valerate and its derivative 2-hydroxy-3-methylvalerate.

Comparison of fecal microbiota – fecal metabolome

To highlight peculiarities in the effect of the studied treatments on the microbiota and on the molecular profile, we set up a three-step protocol. Firstly, for each quantified molecule the concentration changes between T0 and T1 were calculated for each subject. Secondly, a Kruskal-Wallis test revealed that these changes were significantly related (p<0.1) to the tested treatments for 18 molecules, namely tryptophan, phenylalanine, tyrosine, 4-hydroxyphenylacetate, urocanate,

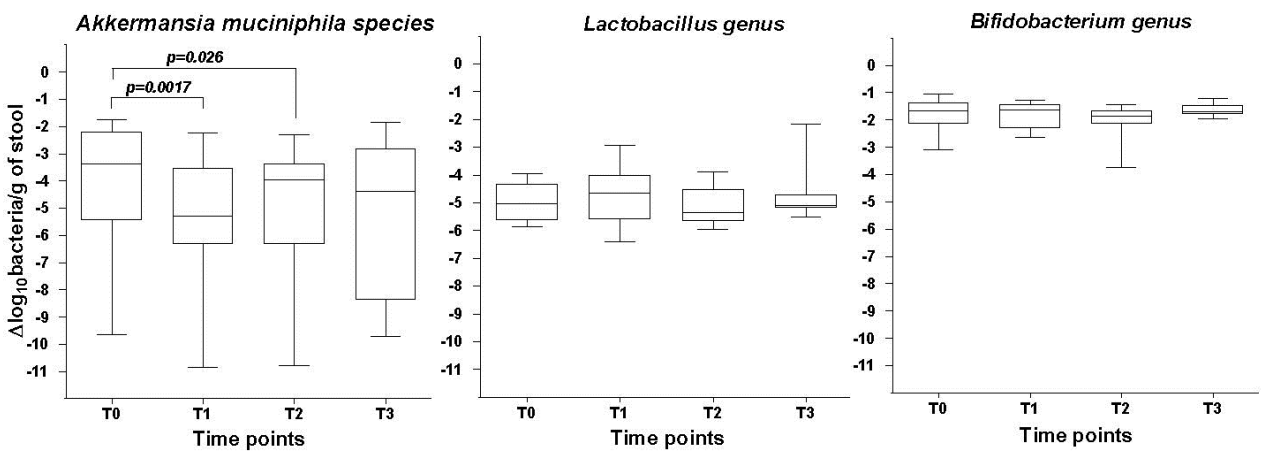

Fig. 4. *qPCR results for A. muciniphila, lactobacilli and bifidobacteria in SUDD patients at enrolment (T0), after 14 days of therapy (T1), and after 30 (T2) and 60 (T3) days of washout. The amount of each bacterial group was normalized for each subject and calculated as the log number of targeted bacteria minus the log number of total bacteria.*

X-6.363, X-5.779, uridylate, galactose, X-4.197, threonine, sarcosine, methionine, 2-oxoisocaproate, 5-aminolevulinate, alanine, leucine and valerate. Finally, the centered and scaled concentrations of these molecules and of lactobacilli, bifidobacteria and *A. muciniphila* were employed to calculate a PCA model (Fig. 5). Its correlation plot (Fig. 5B) showed that the concentrations of microorganisms were scarcely related to PC 1, while deeply influencing PC 2, representing 13.7% of the total variance of the data. In particular, while *A. muciniphila* appeared as positively correlated with PC 2, bifidobacteria and, at a much higher extent, lactobacilli were negatively correlated with it. The distribution of samples along PC 2 of the score plot therefore represented a handy method to observe how the molecular profile co-evolved with microbiota in response to the tested treatments. For this reason, the median position of the samples along PC 2 is more conveniently highlighted in Fig. 5C. In subjects treated with probiotics and, to a lower extent, with rifaximin, the metabolite profile showed at T1 a positive correlation with lactobacilli/*A. muciniphila* ratio, the latter being higher than that at T0. Subjects treated with fibers and, to a lower extent, with mesalazine showed an opposite correlation with such ratio. From T2 onward subjects treated with probiotics moved steadily towards an even more favorable lactobacilli/*A. muciniphila* ratio, so that samples obtained in the time lapse T1-T3, cumulatively considered, showed PC 2 scores lower than those at T0 ($p<0.05$). Contrarily, subjects treated with rifaximin remained stable. Remarkably, during the same time lapse, subjects treated with mesalazine and fibers showed a marked movement towards positive values of lactobacilli/*A. muciniphila* ratio, so that each of the treatments led to a median condition at T3 that could be considered as more favorable that that at T0.

The correlation plot of Fig. 5B allowed ranking the molecules according to their influence over the trends. Molecules that mainly contributed to the distribution of the samples were further highlighted by applying the sparsity principle (21). Leucine and alanine therefore appeared as the most important molecules in determining the samples' trends along PC 1, while threonine and 4-hydroxyphenilacetate appeared as the most important in determining the samples' trends along PC 2.

Comparison between symptoms fecal microbiota and fecal metabolome

In order to highlight possible relationships

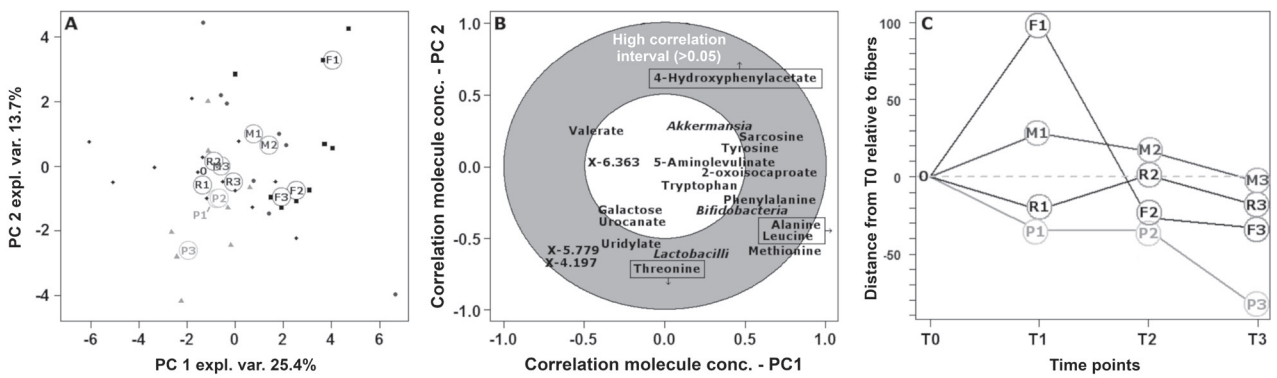

Fig. 5. *PCA model built on the space constituted by lactobacilli, bifidobacteria and A. muciniphila concentrations together with the concentration of the molecules resulted significant from a Kruskal-Wallis test between time points T0 and T1. In the scoreplot (**A**), samples from people treated with probiotics (P), fibers (F), rifaximin (R) and mesalazine (M) are represented with triangles, squares, diamonds and circles, respectively. For each group, the median position in the scoreplot is indicated with the initial letter of the treatment followed by the time point. Samples at T0 are superimposed and are indicated with a 1 number. In the correlation plot (**B**), the concentric circles highlight a correlation between molecule concentrations and molecule importance in the model of 0.5 and 1, respectively. The molecules are surrounded by a square when selected according to the principle of sparsity along PC 1 (horizontal arrow) or PC 2 (vertical arrow). **C**) Median position of the samples along PC 2. To ease a visual comparison across groups, each position has been scaled to the greatest, that of the fibers group at T1, set to 100 arbitrary units.*

between SUDD symptoms and the overall information obtained on microbiota and metabolome from the corresponding PCA model, we calculated the correlations between the PC 2 scores reported in Fig. 5A and the scores of lower abdomen pain, left lower abdomen pain and meteorism. None resulted as significant, and only left lower abdominal pain seemed to show a trend towards a relationship with *A. muciniphila* and metabolome. Contrarily, when the single clinical scores were substituted by their overall trend, summarized by PC 1 in Fig. 3A, then a highly significant correlation was found ($p<0.01$).

DISCUSSION

Current data on microbiota in diverticulosis/diverticular disease are quite conflicting. For example, *Proteobacteria* phylum seems to be increased in diverticulosis (24) but not in acute diverticulitis (3), while characteristics of microbiota in diverticular disease change significantly among the studies, probably due to different and difficult sampling and low number of patients enrolled (4, 5, 25-27). The only datum currently shared is that no clear evidence of substantial associations between the microbial community and diverticulosis among cases and controls can be found (4, 5, 24).

In our study, clinical, microbiological and metabolomic changes in SUDD patients after treatment were analyzed. In spite of the small sample size of the study population, our results revealed for the first time that the most frequently employed treatments for SUDD bring common changes to the fecal microbiota and metabolome composition, correlated to the improvements of clinical symptoms. In light of these findings, several interesting considerations can be pointed out.

This study showed for the first time that there is a relationship between symptoms expression, fecal microbiota imbalance and fecal metabolome expression in SUDD patients. Interestingly, there was no specific symptom significantly linked with fecal microbiota and fecal metabolome, even if left lower abdominal pain was the symptom that best characterized SUDD. On the contrary, when single symptom analysis was substituted by their overall trend, a highly significant correlation was found. A possible explanation of this finding is that SUDD has a multi-factorial pathogenesis, ranging from microbiota imbalance to colonic motility imbalance and low-grade mucosal inflammation (7). Each of these components could regulate the symptoms and, at the same time, influence fecal metabolome expression.

The second strength of this study is that fecal amounts of *A. muciniphila*, a mucus-degrading species (28), could represent a biomarker of SUDD. We recently found a significant increase of *A. muciniphila* relative abundance in fecal samples of SUDD patients in comparison with healthy controls (5). The present study found that *A. muciniphila* significantly decreased at the end of treatment, and was still significantly lower 30 days later, however, the reduction was not significant at the end of the observational period. A reduced fecal level of *Akkermansia* relative abundance has been recently reported in subjects over 49 years of age in comparison to younger patients (29). A great advantage of our study was the reduced age range of patients. Indeed, all the patients included in our study were over 50 years of age. The age-related amount of this species could also explain why the previous studies on gut microbiota in diverticular disease did not report variations in the level of *A. muciniphila* (3, 4). From our results it is not possible to know whether the fecal increase of *A. muciniphila* is due to an increased multiplication of this species in the gut or to shedding of intestinal mucosal layer containing the microorganism in SUDD patients. We can only hypothesize that *A. muciniphila* could represent a biomarker of SUDD occurrence in patients having diverticula. It is noteworthy that the relative abundance of *A. muciniphila* in SUDD seems to be inverse to that occurring in ulcerative colitis (30). This means that the increase or reduction of the same bacterial species may characterize different colonic diseases, sharing an inflammatory pathway but having a different pathogenetic mechanism (31). On the other hand, the relative abundance of *A. muciniphila* was recently positively correlated with damaged histopathology and colonic inflammation in an experimental colitis model (32) and exacerbated

gut inflammation in *Salmonella* Typhimurium-infected gnotobiotic mice (33).

Moreover, we found that *A. muciniphila* and lactobacilli were inversely correlated across the entire study ($p<0.01$) and this inverse relationship confirms the protective value of lactobacilli abundance in the occurrence of SUDD, and may explain the efficacy of lactobacilli supplementation in controlling symptoms in SUDD patients (9). Interestingly, rifaximin, besides its typical antimicrobial effect, promotes the growth of beneficial bacteria, such as bifidobacteria and lactobacilli of the gut microbial community (34, 35).

The third strength of this study is that fecal metabolome in those patients showed an overall trend that paralleled those of symptoms and fecal microbiota. We found that fecal metabolome clearly changed after SUDD treatment, with a trend towards restoration during the observational period. Several molecules significantly changed during the follow-up. The presence of ethanol has been linked to yeast overgrowth as well as bacteria synthesis by the Embden-Meyerhof pathway (36). Formate and some amino acids, including valine, have been recognized as substrates for microorganism fermentation, leading to the production of short chain fatty acids (SCFAs), one of which is valerate (37). The increase we noticed in concentration of formate and 6 aminoacids, paralleled by the decreased concentration of valerate, seems to suggest that the conversion of the former in SCFAs is reduced by each of the treatments applied. It is worth noticing, in this context, that fibers increased consumption is generally recognized to be associated to an increase of SCFAs (38). The opposite trend we find here is therefore coherent with the observation that we here face a different phenomenon, peculiar to the microbiota linked to SUDD. In the quest to identify such mechanism, it is interesting to observe that SCFA production from peptides has been found to be depleted, in *in-vitro* systems, by the increase of several saccharides (39). If we observe the trend of the most important molecules arising from the PCA analysis of microbiota/metabolome (see Fig. 5B), we can see that SCFA production from peptides and organic acids, mediated by saccharides, seems to be the most important metabolic parameter for metabolome restoration. SCFA seems therefore to play a mainstay role in the complex metabolic pathway characterizing SUDD patients, as hypothesized in the past (7) but not clearly confirmed until now. Going into detail regarding the effect of each treatment on the fecal metabolome, we found that fibers, mesalazine and probiotic mixture VivoMixx® were able to modify it considerably in the short term, with a return to the initial levels during the follow-up. On the contrary, rifaximin was not able to significantly modify fecal metabolome in those patients, but why this occurs is unknown.

In conclusion our results indicate that, as expected, each treatment reduces clinical symptoms at the end of product administration, however only probiotics are able to maintain and reinforce such improvement 60 days after the end of the therapeutic trial. Probiotic administration also resulted the only treatment producing a linear improvement in the T1-T3 time-lapse of metabolome/microbiological data.

The main limits of this study are the small number of subjects enrolled and fecal assessment of microbiota, with no possibility to conclude whether fecal abundance of *A. muciniphila* is due to actual changes in bacterial numbers, or alterations of the mucosal layer and gut architecture in SUDD patients. Indeed, microbiota in the mucus layer differs from that of the intestinal lumen, and *A. muciniphila* is closely associated to the gut mucosal layer (40). Also fecal metabolites may arise from mucosal rather than fecal microbiota activity. Finally, assessing symptoms depending on therapy could be influenced by investigators' judgment. A randomized, double-blind study would be the preferred design in assessing this specific point, and further studies have to adopt this specific design. Although no definitive conclusions can be drawn, this pilot study shows clearly that fecal metabolome and microbiota changed in patients with SUDD under treatment, suggesting a possible role of dysbiosis/dymetabolome in the pathology and suggesting that further larger studies are needed to confirm these results.

REFERENCES

1. Strate LL, Modi R, Cohen E, Spiegel BM. Diverticular disease as a chronic illness: evolving epidemiologic

and clinical insights. Am J Gastroenterol 2012; 107:1486-95.
2. Daniels L, Philipszoon LE, Boermeester MA. A hypothesis: important role for gut microbiota in the etiopathogenesis of diverticular disease. Dis Colon Rectum 2014; 57:539-43.
3. Daniels L, Budding AE, de Korte N, et al. Fecal microbiome analysis as a diagnostic test for diverticulitis. Eur J Clin Microbiol Infect Dis 2014; 33:1927-36.
4. Barbara G, Scaioli E, Barbaro MR, et al. Gut microbiota, metabolome and immune signatures in patients with uncomplicated diverticular disease. Gut 2017; 66:1252-61.
5. Tursi A, Mastromarino P, Capobianco D, et al. Assessment of fecal microbiota and fecal metabolome in symptomatic uncomplicated diverticular disease of the colon. J Clin Gastroenterol 2016; 50:S9-S12.
6. De Preter V, Verbeke K. Metabolomics as a diagnostic tool in gastroenterology. World J Gastrointest Pharmacol Ther 2913; 4: 97-107.
7. Tursi A, Papa A, Danese S. The pathophysiology and medical management of diverticulosis and diverticular disease of the colon. Aliment Pharmacol Ther 2015; 42:664-84.
8. Tursi A, Elisei W, Picchio M, Giorgetti GM, Brandimarte G. Moderate to severe and prolonged left lower-abdominal pain is the best symptom characterizing symptomatic uncomplicated diverticular disease of the colon: a comparison with fecal calprotectin in clinical setting. J Clin Gastroenterol 2015; 49:218-21.
9. Tursi A, Brandimarte G, Elisei W, et al. Randomised clinical trial: mesalazine and/or probiotics in maintaining remission of symptomatic uncomplicated diverticular disease–a double-blind, randomised, placebo□controlled study. Aliment Pharmacol Ther 2013; 38:741-51.
10. Nadkarni MA, Martin FE, Jacques NA, Hunter N. Determination of bacterial load by real-time PCR using a broad-range (universal) probe and primers set. Microbiology 2002; 148:257-66.
11. Matsuki T, Watanabe K, Fujimoto J, Takada T, Tanaka R. Use of 16S rRNA gene-targeted group-specific primers for real-time PCR analysis of predominant bacteria in human feces. Appl Environ Microbiol 2004; 70:7220-28.
12. Štšepetova J, Sepp E, Kolk H, Lõivukene K, Songisepp E, Mikelsaar M. Diversity and metabolic impact of intestinal Lactobacillus species in healthy adults and the elderly. Brit J Nutr 2011; 105:1235-44.
13. Collado MC, Derrien M, Isolauri E, de Vos WM, Salminen S. Intestinal integrity and Akkermansia muciniphila, a mucin-degrading member of the intestinal microbiota present in infants, adults, and the elderly. Appl Environ Microbiol 2007; 73:7767-70.
14. Ventrella S, Laghi L, Barone F, Elmi A, Romagnoli N, Bacci ML. Age-related 1H NMR characterization of Cerebrospinal Fluid in newborn and young healthy piglets. Plos One 2016; 11:e0157623.
15. Simmler C, Napolitano JG, McAlpine JB, Chen SN, Pauli GF. Universal quantitative NMR analysis of complex natural samples. Curr Opin Biotechnol 2014: 25:51-59 .
16. Kneen M, Annegarn H. Algorithm for fitting XRF, SEM and PIXE X-ray spectra backgrounds. Nucl Instrum Methods Phys Res 1996; 109:209-13.
17. Liland KH, Almøy T, Mevik BH. Optimal choice of baseline correction for multivariate calibration of spectra. Appl Spectrosc 2010; 64:1007-16.
18. Dieterle F, Ross A, Schlotterbeck G, Senn H. Probabilistic quotient normalization as robust method to account for dilution of complex biological mixtures. Application in 1H NMR metabonomics. Anal Chem 2006; 78:4281-90.
19. Wishart DS, Tzur D, Knox C, et al. HMDB: the human metabolome database. Nucleic Acids Res 2007; 35:D521-D526.
20. Hollander M, Wolfe DA, Chicken E. Nonparametric statistical methods: Wiley; New York, 2013.
21. Shen H, Huang JZ. Sparse principal component analysis via regularized low rank matrix approximation. J Multivariate Anal 2008; 99:1015-34.
22. Rohart F, Gautier B, Singh A, Lê Cao KA. mixOmics: An R package for 'omics feature selection and multiple data integration. PLoS Comput Biol 2017; 13:e1005752.
23. Ndagijimana M, Laghi L, Vitali B, Placucci G, Brigidi P, Guerzoni ME. Effect of a synbiotic food consumption on human gut metabolic profiles evaluated by 1H Nuclear Magnetic Resonance spectroscopy. Int J Food Microbiol 2009; 134:147-153.
24. Jones RB, Fodor AA, Peery AF, et al. An aberrant

microbiota is not strongly associated with incidental colonic diverticulosis. Sci Rep 2018; 8:4951.
25. Lopetuso LR, Petito V, Graziani C, et al. Gut microbiota in health, diverticular disease, irritable bowel syndrome, and inflammatory bowel diseases: time for microbial marker of gastrointestinal disorders. Dig Dis 2018; 36:56-65.
26. Kvasnovsky CL, Leong LEX, Choo JM, et al. Clinical and symptom scores are significantly correlated with fecal microbiota features in patients with symptomatic uncomplicated diverticular disease: a pilot study. Eur J Gastroenterol Hepatol 2018; 30:107-11.
27. Linninge C, Roth B, Erlanson-Albertsson C, Molin G, Toth E, Ohlsson B. Abundance of Enterobacteriaceae in the colon mucosa in diverticular disease. World J Gastrointest Pathophysiol 2018; 9:18-27.
28. van Passel MW, Kant R, Zoetendal EG, et al. The Genome of *Akkermansia muciniphila*, a dedicated intestinal mucin degrader, and its use in exploring intestinal metagenomes PLoS One 2011: 6:e16876.
29. Dao MC, Everard A, Aron-Wisnewsky J, et al.; MICRO-Obes Consortium. Akkermansia muciniphila and improved metabolic health during a dietary intervention in obesity: relationship with gut microbiome richness and ecology. Gut 2016; 65:426-36.
30. Vigsnæs LK, Brynskov J, Steenholdt C, Wilcks A, Licht TR. Gram-negative bacteria account for main differences between faecal microbiota from patients with ulcerative colitis and healthy controls. Benef Microbes 2012; 3:287-97.
31. Dai L, King DW, Perera DS, Lubowski DZ, Burcher L, Liu L. Inverse expression of prostaglandin E2-related enzymes highlights differences between diverticulitis and inflammatory bowel disease. Digest Dis Sci 2015; 60:1236-46.
32. Castro-Mejía J, Jakesevic M, Krych Ł, et al. Treatment with a Monoclonal Anti-IL-12p40 Antibody Induces Substantial Gut Microbiota Changes in an Experimental Colitis Model. Gastroenterol Res Pract 2016; 2016:4953120.
33. Ganesh BP, Klopfleisch R, Loh G, Blaut M. Commensal Akkermansia muciniphila exacerbates gut inflammation in *Salmonella* Typhimurium-infected gnotobiotic mice. PLoS One 2013; 8:e74963.
34. Brigidi P, Swennen E, Rizzello F, Bozzolasco M, Matteuzzi D. Effects of rifaximin administration on the intestinal microbiota in patients with ulcerative colitis. J Chemother 2002; 14:290-95.
35. Ponziani FR, Scaldaferri F, Petito V, et al. The role of antibiotics in gut microbiota modulation: the eubiotic effects of rifaximin. Dig Dis 2016; 34:269-78 .
36. Garner CE, Smith S, de Lacy Costello B, et al. Volatile organic compounds from feces and their potential for diagnosis of gastrointestinal disease. FASEB J 2007; 21:1675-88.
37. Blaut M, Clavel T. Metabolic diversity of the intestinal microbiota: implications for health and disease. J Nutr 2007; 137:751S-755S.
38. Cummings JH, Pomare EW, Branch WJ, Naylor CP, Macfarlane GT. Short chain fatty acids in human large intestine, portal, hepatic and venous blood. Gut 1987; 28:1221-27.
39. Mortensen PB, Holtug K, Rasmussen HS. Short-chain fatty acid production from mono-and disaccharides in a fecal incubation system: implications for colonic fermentation of dietary fiber in humans. J Nutr 1988; 118:321-25.
40. Van den Abbeele P, Roos S, Eeckhaut V, et al. Incorporating a mucosal environment in a dynamic gut model results in a more representative colonization by lactobacilli. Microb Biotechnol 2012; 5:106-15.

ONE-YEAR FOLLOW-UP SHOWING EFFECTS OF SINGLE INTRA-ARTICULAR INJECTION OF HYALURONIC ACID (1,500-2,000 kDa) IN SYMPTOMATIC KNEE OSTEOARTHRITIS

A. MIGLIORE[1], B. FREDIANI[2], G. GIGLIUCCI[1], S.E. ANICHINI[1], M. CASSOL[3], S. CRIMALDI[4], O. DE LUCIA[5], G. IOLASCON[6] and C. FOTI[7]

[1]Rheumatology Unit, S. Pietro FBF Hospital, Rome, Italy; [2]Department of Medicine, Surgery and Neurosciences, Rheumatology Section, University of Siena; Osteo-Articular Diagnostic Procedures Hospital, Siena, Italy; [3]Internal Medicine Department, S. Pietro FBF Hospital, Rome, Italy; [4]Orthopaedics 2, Orthopaedic Mininvasive Surgery and New Technologies, Humanitas Hospital, Castellanza, Italy; [5]Rheumatology Department, ASST Gaetano Pini-CTO Orthopedic and Traumatology Specialist Center, Milan, Italy: [6]Department of Medical and Surgical Specialties and Dentistry, University of Campania "Luigi Vanvitelli", Naples, Italy; [7]Department of Physical and Rehabilitation Medicine, Clinical Sciences and Translational Medicine Department, Tor Vergata University, Rome, Italy

Received July 23, 2018 – Accepted September 25, 2018

Clinical evidence on knee osteoarthritis suggests that intra-articular administration of hyaluronic acid may be useful in the management of patients with persistent pain. This study assesses the duration of effectiveness of a single intra-articular hyaluronic acid injection in a large population of patients with knee osteoarthritis. This retrospective post-marketing cohort study collected data from the ANTIAGE Registry (http://www.antiagefbf.it/registro), selecting patients of age ≥ 40 years, with symptomatic knee osteoarthritis (Kellgren-Lawrence grade I-III) of ≥ 12 months duration, and ≥ 12 months of follow-up. Patients had received a single intra-articular injection of high molecular weight hyaluronic acid (1,500-2,000 kDa) at baseline. WOMAC Osteoarthritis Index total scores measured using the LK 3.1 scale and 10 cm VAS pain scores were evaluated before IA Injection and at 6, 9, 10, 11 and 12 months. Blood cell counts, uricemia, erythrocyte sedimentation rates and levels of C-reactive protein were measured at baseline and 12 months. Time from initial treatment to second injection up to 12 months was recorded to assess event-free survival. Included patients (n = 187) were 53.5% female and had a mean (±SD) age at baseline of 62 (±16.6) years and mean (±SD) body mass index of 26.2 (±2.5) kg/m². Mean (±SD) WOMAC index total score and VAS pain scores were 60.9 (±7.1) and 5.9 cm (±1.8), respectively. There were statistically significant reductions compared to baseline in mean WOMAC index total score and VAS pain score at all time points ($p < 0.01$ at 6 and 9 months; $p < 0.05$ at 10, 11 and 12 months for both parameters). These results support the clinical effectiveness and safety of hyaluronic acid for up to 12 months for pain relief and function improvement in patients with knee osteoarthritis, confirming previous data on intra-articular administration of hyaluronic acid as chronic therapy in the management of knee osteoarthritis.

Key words: knee osteoarthritis, viscosupplementation, intra-articular injection, hyaluronic acid

Mailing address:
Prof. Alberto Migliore,
Rheumatology Unit,
San Pietro, Fatebenefratelli Hospital,
Via Cassia 600, 00189, Rome, Italy
Tel.: +06 3358 5802
e-mail: migliore.alberto60@gmail.com

0393-974X (2018)

Osteoarthritis (OA) is a common cause of joint pain in adults, and its incidence is expected to increase with increases in lifespan and obesity (1). OA often causes physical impairment and social isolation, especially when the hip or knee is involved. Synovial fluid from patients with knee OA contains reduced concentration and molecular weight of the glycosaminoglycan hyaluronic acid (HA) (2, 3). Several studies suggest that intra-articular (IA) administration of HA may be useful in the management of patients with persistent knee pain associated with OA (4).

This treatment has generally been accepted in OA management guidelines; however, there are discrepancies between guidelines and clinical practice (5). It was not recommended in the 2014 NCC-CC guidelines (6), nor in the 2013 AAOS guidelines (7), and received a rating of 'uncertain' in the 2014 OARSI statement (8). It has been suggested that the conflicting results of some of the meta-analyses that informed these decisions may have resulted from methodological differences or flaws (9, 10). In particular, some guidelines do not differentiate among HA-based products, but considered them as a single class of compounds. However, HA-based preparations for intra-articular administration vary in concentration, molecular weight and injection protocol. Their molecular structure can also vary, including native HA, and HA derivatives engineered to increase viscoelasticity and IA residence time.

Clinical experience with a high molecular weight HA (1,500–2,000 kDa) fraction is summarised in a meta-analysis by Guidolin et al. (11). The authors review treatment of a variety of different joints, with a focus on knee and hip, and conclude that the IA injection of HA (1,500–2,000 kDa) reduces symptoms, and improves both function and quality of life. Priano et al. (12). conducted a multicentre, randomised, open label, controlled study on 100 patients undergoing arthroscopic meniscectomy, showing that post-operative administration of high molecular weight (1,500-2,000 kDa) HA was associated with significantly better clinical outcomes, both in terms of function and pain symptoms, compared with the surgical procedure alone. Recently, a prospective study of 168 patients treated with a single IA injection of the same high molecular weight (1500-2000 kDa) linear HA fraction showed significant improvement in symptom outcome measures and knee function for up to 6 months (13).

In the present study, we evaluated the long-term effectiveness and safety of IA injections of this high molecular weight HA (1,500-2,000 kDa) fraction in patients with symptomatic knee OA using improvement in Western Ontario and McMaster Universities Osteoarthritis (WOMAC) index total scores and VAS pain scores as clinical outcomes. Our hypothesis was that the effectiveness of a single IA injection of high molecular weight (1500-2000 kDa) may extend beyond 6 months.

MATERIALS AND METHODS

Study design

This is a retrospective analysis of data from the multicentre ANTIAGE osteoarthritis registry (http://www.antiagefbf.it/registro). We identified patients with mild to moderate knee OA who had received IA injections of a highly purified solution of sodium hyaluronate with a molecular weight (MW) of 1,500–2,000 kDa in the affected knee, with the first injection between January 2015 and November 2016.

Study population

Included patients were ≥ 40 years of age with an X-ray-confirmed diagnosis of mild to moderate knee OA of Kellgren-Lawrence (KL) grade 1-3 in the treated knee and moderate to severe walking pain with 10 cm visual analogue scale (VAS) pain scores between 4 and 8 cm in the treated knee, who had received IA injections of high molecular weight HA (1,500-2,000 kDa) and had complete follow-up data in the ANTIAGE osteoarthritis registry. All data were obtained with prior ethics committee approval and presented following the STROBE checklist for cohort studies. Patients gave written informed consent to participate in the study.

Exclusion criteria were: severe OA (KL grade 4); concomitant use of oral anticoagulant therapy, severe comorbidities (e.g., rheumatologic disease, low back pain, femoral head osteonecrosis), significant varus or valgus deformity requiring surgical correction, inflammatory diseases that might affect joints, positive history of sepsis or subacute infection in any joint, relevant lymphatic stasis in the treated knee, hypersensitivity to any component of the HA-based preparation, treatment with HA or HA derivatives in the previous 6 months or with IA steroids in the previous 3 months.

We enrolled 187 patients meeting all criteria. Mean age was 62 (±16.6) years and there was a tendency toward

overweight. Most patients had moderate knee OA (93.6% KL grade 2 or 3) affecting only one knee (unilateral 89.6%). Characteristics of the study cohort at baseline are presented in Table I.

Procedures

Radiological evaluations using the KL OA scale were made on an X-ray taken no more than 6 months prior to treatment. Pain was evaluated on a 10-cm VAS. The WOMAC Osteoarthritis Index (WOMAC) total score was assessed with the WOMAC LK 3.1 scale, which provided a composite measure of pain, function and joint stiffness. Changes from baseline greater than 16 points were considered clinically significant (14). Data from patient records matching the above-mentioned inclusion and exclusion criteria were extracted from the ANTIAGE registry. Clinical history and demographic information had been recorded at baseline, when all patients had received a single 4 ml (60 mg) IA injection in the affected knee of HyalOne® (second brand name Hyalubrix®60), a viscoelastic solution containing HA sodium salt with a molecular weight range of 1,500–2,000 kDa obtained by bacterial fermentation (Hyalubrix®60 package insert: http://www.hyalubrix.it/foglietto_illustrativo_hyalubrix_60.pd). Additional injections were administered if clinically requested during follow-up. Data were collected on follow-up visits at 6, 9, 10, 11 and 12 months after injection, when VAS pain and WOMAC OA index were assessed.

A blood sample routinely collected at baseline and yearly thereafter was used to assess blood cell counts, uricemia, erythrocyte sedimentation rates and levels of C-reactive protein; patients with clinically significant abnormalities are not injected and are examined and/or treated for comorbidities. Time to second injection was recorded to perform an event-free survival analysis, defined as the time from initial treatment to retreatment.

Study endpoints

The primary endpoint was the change from baseline in the WOMAC total score. Secondary endpoints included duration of symptom relief after a single IA injection of

Table I. *Characteristics of the study cohort at baseline.*

Patients (n)	**187**
Men	87 (46.5%)
Women	100 (53.5%)
Age, years, mean (±SD)	62 (±16.6)
BMI, mean (±SD)	26.2 (±2.5)
Weight, kg, mean (±SD)	74.7 (±10.9)
Height, cm, mean (±SD)	168.3 (±7.8)
Smokers, n (%)	48 (26%)
WOMAC index total score, mean (±SD)	60.9 (±7.1)
10 cm VAS Pain, mean (±SD)	5.9 (±1.8)
NSAID intake, mean days/month (±SD)	6.4 (±6.2)
Diabetes mellitus, n (%)	12 (6.4%)
Knee affected, n (%)	
Right	80 (42.7%)
Left	86 (45.9%)
Bilateral	21 (11.4%)
Kellgren-Lawrence radiological index, n (%)	
Grade I	12 (6.4%)
Grade II	79 (42.2%)
Grade III	96 (51.4%)

HyalOne®, measured with VAS pain score, time to second injection, safety of single or repeated IA injections and changes in hematochemical tests.

Statistical analysis

After the first IA HA injection at baseline, data were collected on follow-up visits at 6, 9, 10, 11 and 12 months. All included patients had attended the baseline visit and all 5 follow-up visits. Data for continuous variables are expressed as mean ±standard deviation (SD), whereas those for discrete variables are reported as counts and proportions. WOMAC index total score and VAS pain scores were recorded at each study visit, and changes from baseline were assessed using the Wilcoxon test for paired data. Significance was defined as $p < 0.05$. Statistical analyses were carried out using Stata software version 13 (StataCorp, College Station, TX, USA). Data on blood cell counts and serum values were compared at baseline and study end using Pearson's tests.

RESULTS

Over the 12 months of follow-up, pain scores and WOMAC total scores were lowest at the 6-month time point, before gradually increasing during the subsequent 6 months for patients not yet requiring a second intra-articular injection of HA (Fig. 1).

We assessed the time to treatment failure, when a second IA injection of HyalOne® was administered. The effect duration was approximately 9 or 10 months in 62% of patients, whereas the effect duration in the remaining 38% was between 11-12 months. At 9, 10, 11 and 12 months, the second injection was administered to 60 (32%), 56 (30%), 39 (21%) and 32 (17%) patients. Event-free survival after the first injection was assessed using Kaplan–Meier analysis of the time to second injection up to 12 months (Fig. 2).

The clinical course of patients receiving HA injections was followed by assessing pain, stiffness and physical function at each visit, up to treatment failure. The 10 cm VAS pain and WOMAC total scores at treatment failure, when patients with knee OA required a second IA HA injection, are presented in Table II.

Blood values for markers of inflammation were in the normal range at both baseline and after up to 12 months of follow-up, without statistically significant

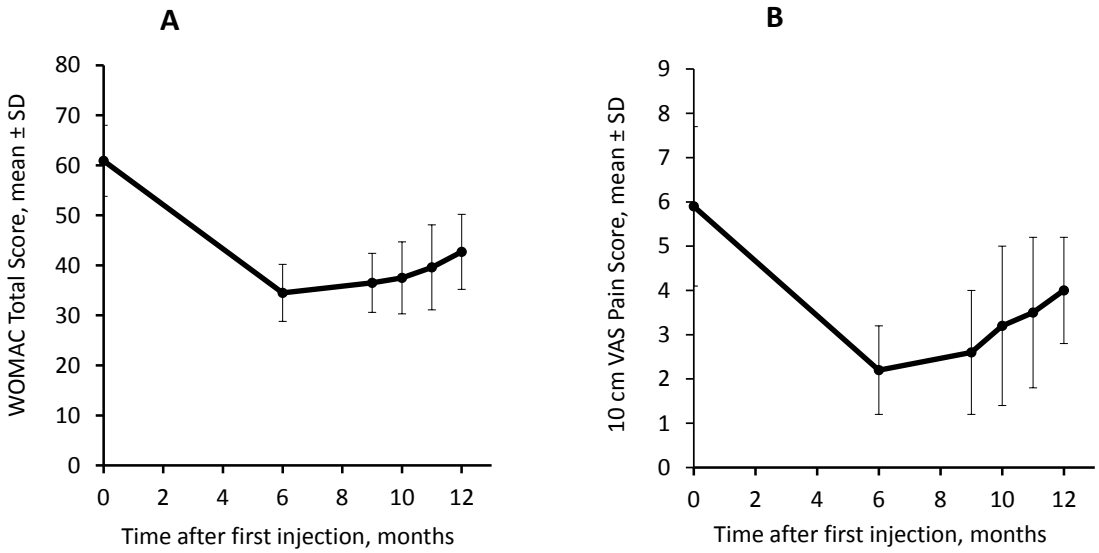

Fig. 1. *Changes in WOMAC total score (**A**) and pain (**B**) over 12 months of follow-up for patients not yet requiring a second intra-articular injection of hyaluronic acid. There were 187 patients at baseline, 6, and 9 months, 127 patients at 10 months, 72 patients at 11 months and 32 patients at 12 months.*

differences (Table III). However, there was a non-significant trend toward reduction in the level of CRP after 12 months.

Safety

No systemic or severe local side effects were reported after the first or the second injection. In 8 cases, there was a sensation of pain lasting from several hours to a few days, regressing spontaneously without requiring medical intervention.

DISCUSSION

IA injection of HA and HA derivatives has gained consensus among practitioners who recognize this approach as a safe and effective treatment of OA (15, 16). Meta-analysis of 54 eligible trials that included 7545 patients demonstrated the effectiveness of this treatment for knee OA, with improvements in pain scores, function and patient global assessment (17).

The molecular weight of HA is an important characteristic that influences its physical and biological properties. HA molecular weight fractions between 500 and 2000 kda are associated with improved lubrication and resistance to surface wear in *in vitro* tests. In addition to improving the rheological properties of synovial fluid, high molecular weight HA has long-term anti-inflammatory effects that are not observed with low molecular weight (< 40 kDa) HA fractions (18,19). Higher molecular weight HA has longer residence time in synovial fluid. HA molecular weight can be increased through cross linking to provide higher viscosity, improve rheological properties and longer joint residency times; however, cross-linked preparations are associated with a higher frequency of adverse events (20).

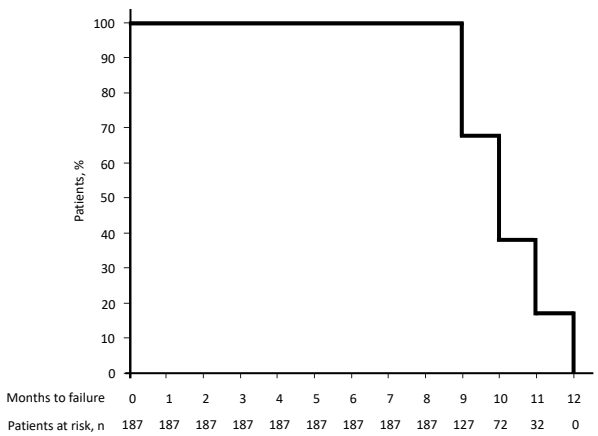

Fig. 2. *Kaplan-Meier survival analysis of time to second IA Injection of high molecular weight hyaluronic acid (HyalOne®), in 187 patients who received more than one injection.*

Researchers have sought to improve and prolong the effectiveness of IA HA by combining HA with other agents, including polyols, corticosteroids and platelet-rich plasma (PRP). The addition of a polyol such as mannitol or sorbitol is thought to increase viscosity and prolong residency time by reducing the oxidative degradation of HA that occurs after IA injection (21). The efficacy and safety of IA HA combined with mannitol has been tested in a double-blind, controlled clinical trial and found to be similar to IA HA alone (22). Corticosteroids have been combined with HA for OA. High doses of IA corticosteroids are indicated for severe acute inflammatory flares not responding to treatment with NSAIDs (23); however, they are not suitable for long-term therapy. A meta-analysis of 7 trials comparing IA corticosteroids with IA HA revealed that corticosteroids are more effective during the first 4 weeks, after which IA HA provides superior benefits that continue for months (24). A preliminary controlled study comparing IA HA with or without a much lower dose of corticosteroid (10 mg triamcinolone acetonide) revealed earlier onset of pain relief with the combination (25), however these preliminary results require confirmation in a larger study. Platelet-rich plasma (PRP), a source of growth factors that influence chondrocyte proliferation and extracellular matrix production, has also been combined with IA HA for treating knee OA. Clinical studies have had mixed results, with one study showing no additive effect (26), and another study showing a synergistic effect between PRP and HA (27).

It has been suggested that data from controlled trials of IA HA treatment should be integrated with data from the real-world setting and from studies with longer follow-up (5). We report data on the

impact of a single IA injection of a 1.5% formulation of natural HA with MW in the range 1500-2000 kDa in a real-world setting, showing control of symptoms and functional improvement in a large cohort of patients followed retrospectively for one year.

Previously, Vetro et al. (13) conducted a 6-month open study on a prospective cohort of 168 patients treated with a single IA injection of the same high molecular weight (1500-2000 kDa) linear HA fraction, demonstrating a significant improvement from baseline in all symptom outcome measures and an improvement in knee function confirmed by results on both the WOMAC index and Knee injury and Osteoarthritis Outcome Score (KOOS) instruments that was maintained through 6 months. The study population in that cohort was younger than ours (mean age 54 *vs* 62 years), had more severe knee OA (VAS pain scores 77 *vs* 59 mm) and a shorter follow-up (6 months *vs* 12 months). Our results show that the findings of significant continuing response after a single IA injection of high molecular weight (1500-2000 kDa) in the 6-month study conducted by Vetro et al. (13) may be extended for several months beyond the six-month time point. This has important

Table II. *VAS pain and WOMAC total scores from baseline to the time of the second intra-articular injection of high molecular weight hyaluronic acid (HyalOne®) for knee osteoarthritis.*

Time of second injection (pts., n)	Study visit					
	Baseline	6 months	9 months	10 months	11 months	12 months
9 months (60)						
VAS Pain	6.5±2.1	1.8±1.3*	2.4±1.4*			
WOMAC	63.4±6.3	38.2±4.3*	39.1±5.2*			
10 months (56)						
VAS Pain	7.3±1.8	2.6±1.5*	2.8±1.7*	3.2±2.4**		
WOMAC	58.7±7.2	34.3±6.3*	35.3±5.5*	38.1±6.1**		
11 months (39)						
VAS Pain	5.9±1.4	2.1±0.9*	2.8±1.6*	3.1±1.8**	3.3±1.7**	
WOMAC	61.3±8.1	31.1±6.2*	34.2±5.9*	35.3±7.1**	38.1±8.1**	
12 months (32)						
VAS Pain	6.8±1.2	2.4±0.4*	2.7±0.7*	3.4±1.3*	3.8±1.6**	4.0±1.2**
WOMAC	59.5±6.8	33.7±5.9*	36.4±7.2*	39.3±8.4*	41.4±8.8**	42.7±7.5**

*Scores are expressed as mean ±SD: before treatment and then after 6, 9, 10, 11 and 12 months. *Significant difference compared to baseline (p <0.01). **Significant difference compared to baseline (p <0.05).*

Table III. *Biochemical values for serum markers of inflammation at baseline and after up to 12 months of follow-up.*

	Baseline	Follow-up	p-value	Reference value
Hematocrit, %	47±6	45±7	0.631	38-54
Red blood cells/µl	5.20±2.1 x 10^6	5.32±2.2 x 10^6	0.761	4.0-5.6 x 10^6/µl
White blood cells/µl	5.600±3.700	6.100±3.900	0.568	4.000-11.000/µl
CRP, mg/dl	1.8 ±1.3	1.1 ±0.7	0.074	< 3 mg/dl
ESR, mm/h	18.4 ±11,8	18.1 ±13,4	0.713	< 25 mm/h
Uric Acid, mg/dl	4.3±1.7	4.1±1.5	0.589	< 6 mg/dl

CRP: C-reactive protein; ESR: erythrocyte sedimentation rate.

implications for the timing of subsequent injections, and may mean that it is possible delay retreatment, with associated cost savings over the course of long-term treatment.

In our study population, the effect duration, determined by the timing of a request for a second injection, was between 9 and 10 months in 62% of our patients. The remaining 38% of patients required retreatment more than 11 months after the first injection. Putting this in perspective, it means that IA HA treatment in patients with KL radiological grade 1-3 knee OA results in 2 out of 3 patients requiring a second treatment after 9 to 10 months, and 1 out of 3 patients requiring a second treatment after 10 months.

In the future, it would be useful to identify factors that predict the timing of the need for retreatment with HA. There was a rapid effect at 6 months in all patients, corresponding to a clinically significant improvement in the WOMAC total score, followed by a modest progressive worsening of outcome measures that did not return to initial baseline levels during the observation period, and more importantly, the improvement remained clinically significant throughout follow-up. The non-significant trend toward reduction of CRP level after 12 months (Table III) could be compatible with a reduction in the local level of inflammation, which would also be supported by the reduction of NSAID consumption and absence of flares during follow-up. The anti-inflammatory effects of IA injection of HA in knee OA have been attributed to interactions mediated by the cell surface receptors CD-44, toll-like receptors 2 and 4, intercellular adhesion molecule-1, and layilin (19).

Limitations of this study include the retrospective design and absence of a control arm with placebo or active comparator. Moreover, we did not assess the effectiveness of subsequent injections on outcomes. However, long-term follow-up of patients with symptomatic OA of the hip treated with IA injection of HA at least every six months supported the continuing effectiveness after 7 years of follow-up. In that study, patients were evaluated with the Lequesne index, pain VAS, NSAIDs intake, global medical and patient assessments every six months from baseline. Patients were categorized by age class, gender and body mass index (BMI), and all groups had statistically significant reductions ($p < 0.05$) at all time points compared to baseline for the Lequesne index, pain VAS, NSAIDs intake and global medical and patient assessments, confirming the long-term efficacy and safety of HA in the treatment of osteoarthritis (28). This is also reflected in the findings from a retrospective cohort of 182,000 patients with a diagnosis of knee OA identified in an administrative claims database (29). Patients who had received IA HA injections had a significantly longer time to total knee replacement ($p < 0.0001$). Moreover, there was a dose-dependent increase in the mean time to knee replacement: no HA, 0.7 years; one cycle, 1.4 years ($p < 0.0001$); ≥5 cycles 3.6 years ($p < 0.0001$). These results were confirmed in a similar study of 267,345 patients with incident knee OA from a Medicare database. Receiving IA HA was associated with a median 8.7-month delay in total knee replacement compared to patients not receiving HA (95% CI 8.3-9.1 months; $P < 0.001$) (30).

Our results support the clinical effectiveness and safety of IA injections of high molecular weight HA (1,500-2,000 kDa) in patients with symptomatic knee OA. After 9 months of follow-up, a second injection was requested by 60 patients (32%), at 10 months by 56 (30%), at 11 months by 39 (21%) and at 12 months by 32 (17%) patients, demonstrating the long-term effectiveness of intra-articular HyalOne® injection therapy, which was associated with a clinically significant improvement in WOMAC total scores.

Declaration of Conflicting Interests. AM received grants or fees from Pfizer, MSD, Fidia, Sanofi, IBSA.

REFERENCES

1. Cross M, Smith E, Hoy D, et al. The global burden of hip and knee osteoarthritis: estimates from the global burden of disease 2010 study. Ann Rheum Dis 2014;73:1323-30.
2. Band PA, Heeter J, Wisniewski HG, et al. Hyaluronan molecular weight distribution is associated with the risk of knee osteoarthritis progression. Osteoarthritis Cartilage 2015; 23:70-76.
3. Kosinska MK, Ludwig TE, Liebisch G, et al. Articular joint lubricants during osteoarthritis and rheumatoid

arthritis display altered levels and molecular species. PLoS One 2015; 10:e0125192.
4. Roman-Blas JA, Bizzi E, Largo R, Migliore A, Herrero-Beaumont G. An update on the up and coming therapies to treat osteoarthritis, a multifaceted disease. Expert Opin Pharmacother 2016; 17:1745-56
5. Migliore A, Bizzi E, Herrero-Beaumont J, Petrella RJ, Raman R, Chevalier X. The discrepancy between recommendations and clinical practice for viscosupplementation in osteoarthritis: mind the gap! Eur Rev Med Pharmacol Sci 2015;19:1124-29.
6. NICE Clinical Guidelines, No. 177. Osteoarthritis: Care and Management in Adults. National Clinical Guideline Centre (UK) London: National Institute for Health and Care Excellence (UK); 2014 Feb.
7. Brown GA. AAOS clinical practice guideline: treatment of osteoarthritis of the knee: evidence-based guideline, 2nd edition. J Am Acad Orthop Surg 2013; 21:577-79.
8. McAlindon TE, Bannuru RR, Sullivan MC, et al. OARSI guidelines for the non-surgical management of knee osteoarthritis. Osteoarthritis Cartilage 2014; 22:363-88.
9. Bannuru RR, Vaysbrot EE, McIntyre LF. Did the American Academy of Orthopaedic Surgeons osteoarthritis guidelines miss the mark? Arthroscopy 2014; 30:86-89.
10. Henrotin Y, Raman R, Richette P, et al. Consensus statement on viscosupplementation with hyaluronic acid for the management of osteoarthritis. Semin Arthritis Rheum 2015: 45:140-9.10.
11. Guidolin D, Franceschi F. Viscosupplementation with high molecular weight native hyaluronan. Focus on a 1500-2000 KDa fraction (Hyalubrix®). Eur Rev Med Pharmacol Sci 2014: 18:3326-38.
12. Priano F, Guelfi M. Efficacy of intra-articular hyaluronic acid (Hyalubrix) in arthroscopy. Artroscopia 2017; 8:3-12.
13. Vetro A, Iovane A, Di Gesù M, Giordan N, Mantia F, Mantia R. Pain relief and functional recovery over a six-month period after intra- articular injection with sodium hyaluronate (MW 1500- 2000 KDA) in osteoarthritis of the knee. Eur Journal of Musculoskeletal Diseases 2014; 1:25-33.
14. Hmamouchi I, Allali F, Tahiri L, et al. Clinically important improvement in the WOMAC and predictor factors for response to non-specific non-steroidal anti-inflammatory drugs in osteoarthritic patients: a prospective study. BMC Res Notes 2012;5:58.
15. Miller LE, Block JE. US-Approved intra-articular hyaluronic acid injections are safe and effective in patients with knee osteoarthritis: systematic review and meta-analysis of randomized, saline-controlled trials. Clin Med Insights Arthritis Musculoskelet Disord 2013; 6:57-63.
16. Bannuru RR, Vaysbrot EE, Sullivan MC, McAlindon TE. Relative efficacy of hyaluronic acid in comparison with NSAIDs for knee osteoarthritis: a systematic review and meta-analysis. Semin Arthritis Rheum 2014; 43:593-99.
17. Bannuru RR, Natov NS, Dasi UR, Schmid CH, McAlindon TE. Therapeutic trajectory following intra-articular hyaluronic acid injection in knee osteoarthritis--meta-analysis. Osteoarthritis Cartilage 2011; 19:611-19.
18. Petrey AC, de la Motte CA. Hyaluronan, a crucial regulator of inflammation. Front Immunol 2014; 5:101.
19. Altman R, Bedi A, Manjoo A, Niazi F, Shaw P, Mease P. Anti-Inflammatory Effects of Intra-Articular Hyaluronic Acid: A Systematic Review. Cartilage 2018; 1:1947603517749919.
20. Yan CH, Chan WL, Yuen WH, et al. Efficacy and safety of hylan G-F 20 injection in treatment of knee osteoarthritis in Chinese patients: results of a prospective, multicentre, longitudinal study. Hong Kong Med J 2015; 21:327-32.
21. Conrozier T, Mathieu P, Rinaudo M. Mannitol preserves the viscoelastic properties of hyaluronic acid in an in vitro model of oxidative stress. Rheumatol Ther 2014; 1:45-54.
22. Conrozier T, Eymard F, Afif N, Balblanc JC, Legré-Boyer V, Chevalier X; Happyvisc Study Group. Safety and efficacy of intra-articular injections of a combination of hyaluronic acid and mannitol (HAnOX-M) in patients with symptomatic knee osteoarthritis: Results of a double-blind, controlled, multicenter, randomized trial. Knee 2016; 23:842-48.
23. Bruyère O, Cooper C, Pelletier JP, et al. An algorithm recommendation for the management of knee osteoarthritis in Europe and internationally: a report from a task force of the European Society for Clinical and Economic Aspects of Osteoporosis and Osteoarthritis (ESCEO). Semin Arthritis Rheum

2014; 44:253-63.
24. Bannuru RR, Natov NS, Obadan IE, Price LL, Schmid CH, McAlindon TE. Therapeutic trajectory of hyaluronic acid versus corticosteroids in the treatment of knee osteoarthritis: a systematic review and meta-analysis. Arthritis Rheum 2009; 61:1704-11.
25. Petrella RJ, Emans PJ, Alleyne J, Dellaert F, Gill DP, Maroney M. Safety and performance of Hydros and Hydros-TA for knee osteoarthritis: a prospective, multicenter, randomized, double-blind feasibility trial. BMC Musculoskelet Disord 2015; 16:57.
26. Abate M, Verna S, Schiavone C, Di Gregorio P, Salini V. Efficacy and safety profile of a compound composed of platelet-rich plasma and hyaluronic acid in the treatment for knee osteoarthritis (preliminary results). Eur J Orthop Surg Traumatol 2015; 25:1321-26.
27. Lana JF, Weglein A, Sampson SE, et al. Randomized controlled trial comparing hyaluronic acid, platelet-rich plasma and the combination of both in the treatment of mild and moderate osteoarthritis of the knee. J Stem Cells Regen Med 2016; 12:69-78.
28. Migliore A, Massafra U, Frediani B, et al. HyalOne® in the treatment of symptomatic hip OA - data from the ANTIAGE register: seven years of observation. Eur Rev Med Pharmacol Sci 2017; 21:1635-44.
29. Altman R, Lim S, Steen RG, Dasa V. Hyaluronic acid injections are associated with delay of total knee replacement surgery in patients with knee osteoarthritis: evidence from a large U.S. Health Claims Database. PLoS One 2015; 10:e0145776.
30. Ong KL, Anderson AF, Niazi F, Fierlinger AL, Kurtz SM, Altman RD. Hyaluronic acid injections in medicare knee osteoarthritis patients are associated with longer time to knee arthroplasty. J Arthroplasty 2016; 31:1667-73.

LETTER TO THE EDITOR

MOLECULAR MECHANISM OF ACTION OF VALPROATE ACID ALONE OR IN COMBINATION WITH CHLORPROMAZINE IN THE EPIGENETIC REGULATION OF SCHIZOPHRENIA

YM. GENG[1], JT. XUE[1], JP. SU[2] and HY. LI[3]

[1]Department of Clinical Psychology, School of Public Health of Mudanjiang Medical University, MuDanJiang City, Heilongjiang Province, China; [2]Department of Medical Psychology, School of Public Health of Mudanjiang Medical University, Mudanjiang City, Heilongjiang Province, China; [3]Quality Control and Supervision Office, Affiliated Hongqi Hospital of Mudanjiang Medical University, Mudanjiang City, Heilongjiang Province, China

Received July 4, 2018 – Accepted August 8, 2018

This study aimed to assess the molecular mechanism of the histone deacetylase inhibitor (HDACI) valproate acid (VPA) alone or in combination with the antipsychotic drug chlorpromazine in the epigenetic regulation of schizophrenia. A total of 60 perinatal CD-SD rats were divided in a control group (16 animals) and a schizophrenia model group (44 animals). For the schizophrenia model group the rats received phencyclidine (PCP) 10 mg/kg/day by intradermal injection on days 7, 9, and 11 after birth. The model was confirmed by the Morris water test in 40 rats. The control and model rats were divided into 7 groups. The Real Time PCR assay was used to detect the mRNA expression changes of GABA system gene [GABBR1 (GABA B receptor 1)], GAD1 (glutamic acid decarboxylase1), GAD2 (glutamic acid decarboxylase2), Lipase metabolic key enzyme LPL (lipoprotein lipase) gene, glutamate neurotransmitter gene GRIA2 (AMPA subtype glutamate receptors 2), inward rectifier potassium channel members KCNJ4 (potassium voltage-gated channel subfamily J member 4) and neuropeptide signal gene TAC1 (tachykinin precursor 1,TAC1) in four brain regions: the prefrontal cortex (PC), the amygdala (AM), the caudate-putamen (CPU) and the hippocampus (HIP). The platform arrival time of PMV and PMVC groups was significantly reduced compared to the PM group, the reduction being more significant in the PMV group. In the four brain regions of the epigenetic animal model of schizophrenia, the expression of GABBR1, GAD1, and GAD2 genes increased significantly. Following administration of HDACI VPA, the mRNA expression of this gene in the four brain regions decreased or approached normal levels. GABBR1 GAD1 and GAD2 are likely to be the target genes affected by the HDACI VPA.

To the Editor,

Schizophrenia is a neurodevelopmental disorder. Histone modification is one of the epigenetic mechanisms caused by the dual influence of genetic and environmental factors (1, 2). It has been reported that the role of histone deacetylases (HDACs) to inhibit gene expression is likely to be involved in the pathogenesis of schizophrenia (3-5). HDACIs can regulate the expression of genes by inhibiting the ability of HDAC enzymes to regulate the level of histone and non-histone acetylation (6). It has been reported that the histone deacetylase inhibitor (HDACI) valproic

Key words: HDACI valproate acid, chlorpromazine, schizophrenia, genetic regulation

Mailing address:
Dr Huayang Li,
Quality Control and Supervision Office,
Affiliated HongQi Hospital of MuDanJiang Medical University,
No 5 TongXiang Road, Mudanjiang City 157011,
Heilongjiang Province, China
e-mail: lhuayang2008@163.com

0393-974X (2018)

acid (VPA) can effectively induce DNA demethylation and chromatin remodeling in the preclinical model of psychosis (7). Its mechanism may be related to the enhancement of gamma aminobutyric acid (GABA) levels and the inhibition of the N-methyl-D-aspartic acid (NMDA) receptor (8).

In the present study, genes associated with the GABA axis, such as GABBR1, GAD1, GAD2, LPL, GRIA2, SYN2, KCNJ4, and TAC1 were selected as candidate genes. Some studies have reported that the changes in the expression levels of the above gene may be associated with the onset of schizophrenia (9). Initially, an epigenetic animal model of schizophrenia was established, and the effect of the HDACI VPA alone and in combination with a standard antipsychotic drug was investigated. Thus, the study aimed to elucidate the possible molecular mechanisms of VPA with regard to the epigenetic regulation of schizophrenia by identifying the possible target genes.

MATERIALS AND METHODS

Main experimental reagents and equipment

The reagents used were as follows: chlorpromazine (Zhangjiakou Yunfeng Pharmaceutical Co., Ltd.); phencyclidine (PCP), methionine, valproic acid (American Sigma); anhydrous ethanol, isopropanol, chloroform, sodium chloride (Shanghai Lu Shi Chemical Co., Ltd.); First Strand cDNA Synthesis Kit, RNA extraction reagent, Fluorescent quantitative PCR kit, PCR primers (Britain Thermo Scientific), diethy pyrocarbonate (Beijing Baiao Laibo Technology Co. Ltd.); and deionized water (Shandong Sihai Water Treatment Equipment Co., Ltd.).

The equipment used was the following: Mx3000P Real-Time PCR (American Stratagene); Epoch nucleic acid protein concentration analyzer (American BioTek); 2700PCR analyzer (Shanghai Qiqian Electronic Technology Co., Ltd.); Vortex-Genie2 vortex mixer (Shanghai Damu Industrial Co., Ltd.); X-RAD 320ix X-ray deep irradiating instrument (Provided by China Huijia Biological Shares Co., Ltd.); TGL-16G high-speed desktop centrifuge (Changsha Xiang Rui Centrifuge Co., Ltd.); GAX-9240 drying box (Wuxi Marret Technology Co., Ltd.).

Model preparation

A total of 60 perinatal CD-SD rats were included in the study and were kept in strict accordance with the experimental requirements. After birth the animals were kept in standard conditions of 25±1°C, humidity of 40±5% and 12-hour light/dark cycle. The animal experiment was approved by the ethics committee of the School of Public Health of Mudanjiang Medical University. The animal model of schizophrenia was designed using phencyclidine (PCP) (10). A total of 16 rats received no treatment and they were classified as controls and the remaining 44 rats were used for schizophrenia model preparation. This group of rats received PCP at doses of 10mg/kg/day by intradermal injection on days 7, 9, and 11 days after birth. After reaching adulthood (9 weeks), the animal model was successfully confirmed in 40 rats using the Morris water rat test. Methionine administration was performed in order to influence the DNA methylation process and these epigenetic DNA modifications were shown to play a role in schizophrenia development (10). In the present study methionine administration was used to induce epigenetic changes related to schizophrenia. Following modeling, the rats were divided into 7 groups (8 rats per group) as follows:

- Control group (CON) that received no treatment during the study period;
- Methionine group (MET) that received only methionine at doses of 2mL/kgbw/day 2 times/day for 15 consecutive days during adulthood;
- Schizophrenia model group (PCP) that received PCP at doses of 10mg/kg/day by intradermal injection on days 7, 9, and 11 after birth, and during adulthood was administered normal saline solution at a dose of 0.1mL/100g 2 times per day for 15 consecutive days;
- Epigenetic schizophrenia model group (PM) that received PCP at doses of 10 mg/kg/day by intradermal injection on days 7, 9, and 11 after birth, and during adulthood was administered methionine at a dose of 2mL/kgbw/day 2 times per day for 15 consecutive days;
- Treatment group with valproic acid (PMV group) that received PCP at doses of 10mg/kg/day by intradermal injection on days 7, 9,

and 11 after birth, and during adulthood was administered methionine at the dose of 2mL/kgbw/day. Valproic acid was also administered at a dose of 20mg/kgbw/day 2 times per day for 15 consecutive days by subcutaneous injection;

- Treatment group with chlorpromazine (PMC group) that received PCP at doses of 10 mg/kg/day by intradermal injection on days 7, 9, and 11 after birth, and during adulthood was administered methionine at a dose of 2mL/kgbw/day and chlorpromazine at a dose of 20mg/kgbw/day 2 times per day for 15 consecutive days by subcutaneous injection;
- Treatment group with valproic acid plus chlorpromazine (PMVC group) that received PCP at doses of 10mg/kg/day by intradermal injection on days 7, 9, and 11 after birth. and during adulthood was administered methionine at doses of 2mL/kgbw/day and valproic acid (20mg/kgbw/day) plus chlorpromazine (20mg/kgbw/day) 2 times per day for 15 consecutive days by subcutaneous injection.

Following treatment, the groups were evaluated by the Morris water test.

Morris water maze experiment

A circular stainless-steel sink (180 cm in diameter, 50 cm height and 60 cm depth) was prepared, and the water level was controlled at 35 cm. The water temperature was 23±0.5°C. An appropriate amount of milk powder was added to the water to make the water cloudy and opaque. The sink was divided into four equal quadrants according to the east, south, west, and north directions. They are denoted NE, SE, NW and SW, respectively, and four entry points were marked at the edge of the sink. A platform (28 cm high and 11 cm in diameter) was placed in the center of the SE quadrant. Various rich references**?** were placed around the sink. The space marks provided by the canopy, the surrounding walls, and the objects around the labyrinth were always fixed. One water entry point was selected, and the rats were put into the sink. Each time the rats were put into the labyrinth, the rats' sight was obstructed. The time to find the platform with a maximum time of 3 min was recorded, that is, the escape latency of the hidden platform. If the rat could not find the platform in the - min period, then the rat was led to the platform and retained for 20 s, so that it could learn and memorize the way and position of the platform. The activity was carried out twice a day, and each action was repeated 3 times. After two days, the average results were taken as the experimental data, and statistical analysis was carried out.

Extraction of total RNA and the determination of its purity and concentration

Following establishment of all the animal models, the animals were sacrificed by cervical dislocation and the brain tissues were separated by aseptic operation. This surgical procedure included 4 brain regions: the prefrontal cortex (PC), the amygdala (AM), the caudate-putamen (CPU) and the hippocampus (HIP). The brain extracts were stored in the EP tubes containing Trizol and were stored at -80°C. Total RNA was subsequently extracted. A total of 2 μl of RNA was extracted, and the purity and concentration (ng/ μl) were detected by the Epoch nucleic acid protein concentration analyzer.

The reverse transcriptase step was carried out in strict accordance with the Thermo Fisher Scientific kit Rever Aid First Stand cDNA. The sample mass of RNA was 5 ng, and the volume of RNA was calculated according to the measured concentration. The total sample volume was 12 μl.

The selection of the candidate genes was as follows: GABA system gene [GABBR1 (GABA B receptor 1), GAD1 (glutamic acid decarboxylase1), GAD2 (glutamic acid decarboxylase2)], Lipase metabolic key enzyme LPL (lipoprotein lipase) gene; glutamate neurotransmitter geneGRIA2 (AMPA subtype glutamate receptors 2); inward rectifier potassium channel members KCNJ4 (potassium voltage-gated channel subfamily J member 4) and neuropeptide signal gene TAC1 (tachykinin precursor 1, TAC1).

The gene sequences of GAD1, TAC1, GAD2, LPL, GABBR1, GRIA2, KCNJ4, and GAPDH were all referenced to GenBank, and the primers were designed and synthesized by Primer 5. The Primer Correspondence Sequence: GAD1-F:ATGGGTGTGCTGCTCCAGTG; GAD1-

R:GTCATACTGGTCTGGCTGGAA; TAC1-F:ACTGGTCCGACAGTGACCAAATC; TAC1-R:CCCGTTTGCTTAATCCA; GAD2-F:TGACGCACTGCCAAACAACTC; GAD2-R:TGCTGCTAATCCAACCATATCCAA; LPL-F:AGTGACCAGGGACATGTGACTTTG; LPL-R:GACTAAGGGTCAGGAATCCACGAG; GABBR1-F:CGAAACCAAGAGCGTGTCCA; GABBR1-R:AAAGGCTGCGTCCTGCTGA; GRIA2-F:TACGGCATCGCCACACCTAA; GRIA2-R:ACCAACAGGCCTTGTTCATTCA; KCNJ4-F:ACAGCGGCCAAACCGTGTA; KCNJ4-R:ACTGGACAACCACTGCGATGAC; GPADH-F:GGCACAGTCAAGGCTGAGAATG; GPADH-R:ATGGTGGTGAAGACGCCAGTA.

In addition, the expression of the candidate genes was detected by real time fluorescence quantitative PCR. The cDNA of the control group was used as a template to analyze the dissolution curve and the standard curve of the fluorescence quantitative PCR. When the dissolution curve corresponded to a single peak, the peak position was consistent with the annealing temperature (95°C) and the experimental results were effective. Using GAPDH as a reference, gene expression analysis was carried out. All cDNA samples were diluted 4 times, and the number of each sample number was n≥6. The reaction conditions were as follows: 95°C, 10 min→(95°C, 30s→55°C, 1min→72°C, 1min).

Statistical analysis

The data obtained were statistically analyzed by SPSS19.0. The data were expressed in the form of mean ± standard deviation ($\bar{x} \pm s$). The paired *t*-test was used for comparison between groups, and the differences were statistically significant when $P<0.05$.

RESULTS

Morris water maze behavior test

The modification in the animal behavior by the Morris water maze test indicated the following results: compared with the control group (30.21±13.22), the platform arrival time of the PCP group (89.32±56.43) was significantly higher (*P<0.05). No difference in the arrival time of the MET group (31.61±12.59) was noted. The arrival time of the PM group (107.22±33.41) was three times higher compared with that noted in the control group. Compared with the PM group, the arrival time of the PMC group (55.16±43.17) was significantly lower. Compared to the PM group, the arrival time of the PMV and PMVC groups (34.26±19.33, 53.07±22.31) was significantly reduced ($^{\&\&}P<0.05$, $^{\&}P<0.01$) (Fig. 1).

Validation of candidate gene expression

Real-time PCR was used to detect the expression of candidate genes. Using GAPDH as an internal

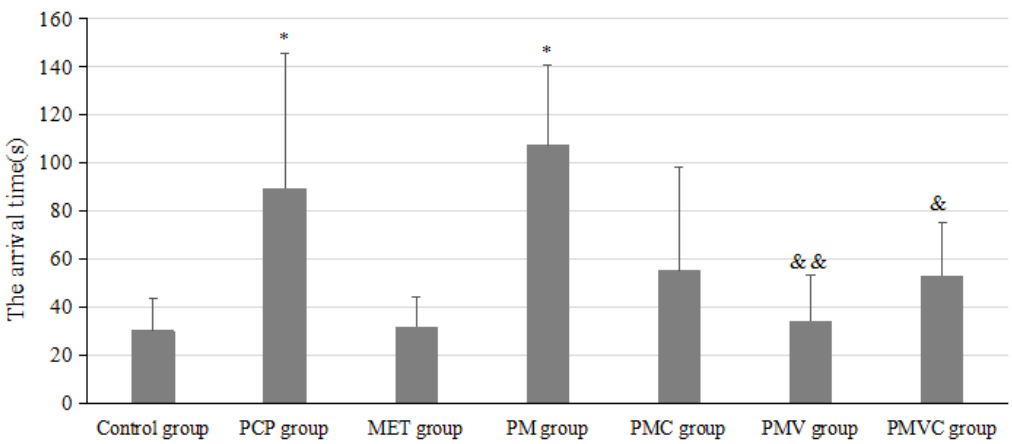

Fig. 1. *Platform arrival time of each group (*P<0.05 vs control group; $^{\&}P<0.05$ and $^{\&\&}P<0.01$ vs PM group.*

reference, the candidate and reference genes showed a single peak, according to the MxPro software analysis. However, no specific peak was noted. In addition, the peak position was consistent with the annealing temperature, indicating that the primer and cDNA models could be combined specifically. In addition, the RSq values and amplification efficiency of the candidate gene and the reference gene are shown in Table I.

As shown in Table I, the RSq values of the candidate genes were approximately 0.990 and the amplification efficiency was estimated to 99%. The RSq values of the reference gene were 0.992, and the amplification efficiency was 99.6%. The amplification efficiency of the candidate and reference genes was no more than 5%, which could be compared by relative quantification.

Changes in mRNA expression of candidate genes

In Fig. 2, the changes in the mRNA expression of the candidate genes in different the brain regions of the rats are presented. In the PCP, the MET and the PM groups, the mRNA expression levels of the GABBR1 gene increased ($^{*}P<0.05$, $^{**}P<0.01$) in PC, AM and CPU. In the PMV and PMVC groups, the mRNA expression levels decreased in the PC and AM ($^{\&\&}P<0.01$). In CPU, the mRNA expression levels decreased in the PMV group ($^{\&}P<0.05$), and increased in the PMVC group ($^{\&\&}P<0.01$).

In the PCP, the MET group, and the PCP+MET groups, the mRNA expression levels of the GAD1 gene increased in the three brain regions of the AM, CPU, and HIP (**P<0.01), indicating that this gene was related to the epigenetic molecular mechanism of schizophrenia. The mRNA expression levels of the GAD1 gene decreased in both the VPA group and the VPA+CPZ combined medication group ($^{\&\&}P<0.01$) in the three brain regions. In the PCP, MET, and PCP+MET groups, the results of the present study indicated that the mRNA expression levels of the GAD2 gene increased in the four brain regions of the PC, AM, CPU, and HIP (**P<0.01). In the VPA group, the mRNA expression levels decreased in the AM, CPU, and HIP ($^{\&\&}P<0.01$). In the VPA+CPZ combined medication group, the mRNA expression levels decreased in the PC, AM, and CPU brain regions ($^{\&\&}P<0.01$).

In the PCP group, the expression levels of the LPL gene increased in the CPU brain region (**P<0.01). In the MET group, the expression levels of mRNA decreased in the PC and HIP brain regions (*P<0.05, **P<0.01), whereas it increased in the CPU brain region (**P<0.01). In the PCP+MET model group, the mRNA expression levels decreased in the PC brain region (*P<0.05) and increased in the CPU and HIP brain regions (**P<0.01). This result highlighted that the expression of the LPL gene varied in the different models. In the VPA group, the mRNA expression levels increased in the PC brain region ($^{\&\&}P<0.01$) and decreased in the CPU

Table I. *RSq value and amplification efficiency of candidate genes and reference genes.*

Gene name	RSq	Amplification efficiency (%)
GABBR1	0.989	107.5
GAD1	0.998	100.8
GAD2	0.986	105.2
LPL	0.999	114.6
GRIA2	0.993	98.9
KCNJ4	0.990	110.9
TAC1	1.000	96.7
GAPDH	0.993	99.7

and HIP brain regions ($^{\&}P<0.05$, $^{\&\&}P<0.01$). In the VPA+CPZ combined medication group, the mRNA expression levels increased in the PC brain region ($^{\&}P<0.05$) and decreased in the CPU and HIP brain regions ($^{\&\&}P<0.01$).

The mRNA expression of GRIA2 gene in the PCP, MET, and PCP+MET groups increased in the CPU brain region (**P<0.01). In the individual VPA group, the mRNA expression levels decreased in the CPU brain region ($^{\&\&}P<0.01$). In the VPA+CPZ combined medication group, the expression of mRNA significantly increased ($^{\&\&}P<0.01$). However, compared with the CPZ group, the reverse direction was changed. In the PCP group, MET group, and PCP+MET group, the expression levels of the KCNJ4 mRNA increased in the PC and HIP brain regions (**P<0.01) and decreased in the AM and CPU brain regions (**P<0.01). In the VPA group, the mRNA expression levels decreased in the PC and HIP brain regions ($^{\&}P<0.05$, $^{\&\&}P<0.01$) and increased in the AM and CPU brain regions ($^{\&\&}P<0.01$). In the VPA+CPZ combined medication group, the expression of mRNA decreased in the PC brain region ($^{\&\&}P<0.01$) and increased in the HIP brain region ($^{\&\&}P<0.01$). However, compared with the single CPZ, the gene expression in the HIP region exhibited an opposite pattern. In the PCP group, the mRNA expression levels of the TAC1 gene

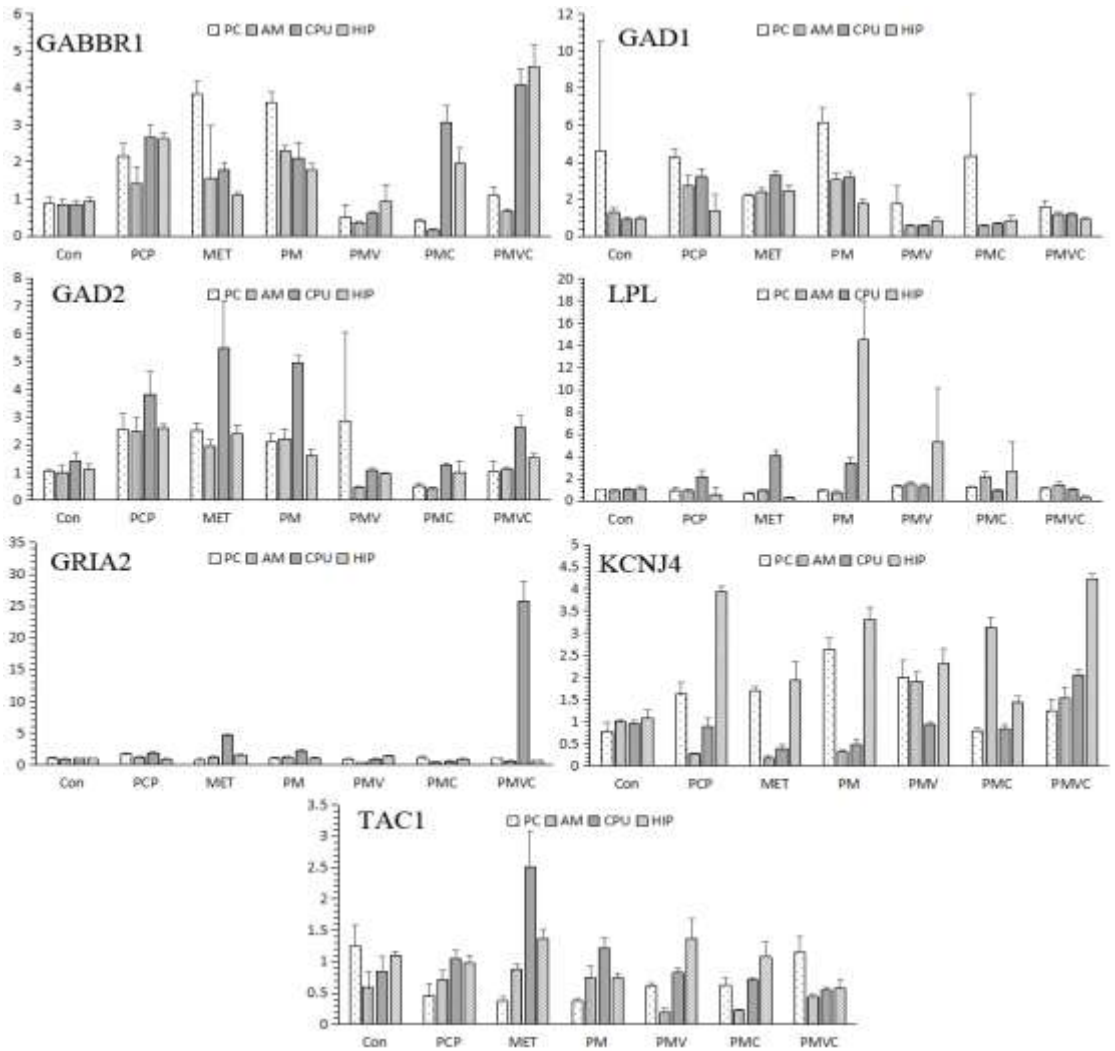

Fig. 2. *Analysis of mRNA expression of candidate genes.*

decreased in the PC brain regions (**P<0.01). In the MET group, the expression levels of the mRNA decreased in the PC brain region (**P<0.01) and increased in the HIP brain region (*P<0.05). In the PCP+MET model group, the expression levels of the mRNA decreased in the PC and HIP brain regions (**P<0.01) and increased in the CPU brain region (*P<0.05). In the individual VPA group, the mRNA expression levels increased in the PC and HIP brain regions ($^{\&\&}$P<0.01) and decreased in the CPU brain region ($^{\&\&}$P<0.01). In the VPA+CPZ combined medication group, the expression levels of the TAC1 gene increased in the PC brain region ($^{\&\&}$P<0.01) and decreased in the CPU and HIP regions ($^{\&}$P<0.05, $^{\&\&}$P<0.01).

DISCUSSION

The Morris water maze is an experimental method applied to the study of brain learning and memory mechanism (11). In the present study, the results of the Morris water maze experiment indicated that VPA may have a certain impact on cognitive impairment in schizophrenia and that the combined use of drugs may have synergistic effects.

The GABBR1 gene is considered to be a potentially sensitive gene locus involving the cause of schizophrenia (12). The results of the present study confirm that the expression levels of GABBR1 are associated with schizophrenia and GABBR1 gene might be the target of VPA. The expression levels of the GAD1 and GAD2 genes could be effectively changed following the use of VPA alone. This suggested that the HDACI VPA could affect the expression levels of the genes GAD1 and GAD2. Therefore, it could be assumed that the gene may be the action target of VPA. When VPA was administered, the expression levels of the LPL gene were also effectively reversed. Therefore, it was hypothesized that the HDACI VPA was associated with the epigenetic regulation of schizophrenia. These results suggest that the GRIA2 gene is closely related to the onset of schizophrenia, and may be related to the epigenetic molecular mechanism of schizophrenia. Following treatment with VPA alone, the expression of the KCNJ4 gene was also effectively reversed. This suggested that the HDACI VPA could affect the expression levels of the KCNJ4 gene in the epigenetic inheritance of schizophrenia. The results of this experiment indicated that in the three brain regions, TAC1 gene mRNA expression levels were related to learning, memory, cognition, and emotional function. This suggests that the TAC1 gene may be involved in the epigenetic molecular mechanism of schizophrenia.

In conclusion, the GABBR1, GAD1 and GAD2 genes are likely to be the target genes for the HDACI VPA.

REFERENCES

1. Sekar A, Bialas AR, de Rivera H, et al. Schizophrenia risk from complex variation of complement component 4. Nature 2016; 530(7589):177-83.
2. Gavin DP, Sharma RP. Histone modifications, DNA methylation, and schizophrenia. Neurosci Biobehav Rev 2010; 34(6):882-88.
3. Pang B, Wang J, Zhang W, Gao Y, Zhang J, Su Y, Kou C. Increased histone deacetylase activity in peripheral blood mononuclear cells of patients with schizophrenia. Psychiatry Res 2016; 245:105-7.
4. Penney J, Tsai LH. Histone deacetylases in memory and cognition. Sci Signal 2014; 7(355):re12.
5. Simonini MV, Camargo LM, Dong E, Maloku E, Veldic M, Costa E, Guidotti A. The benzamide MS-275 is a potent, long-lasting brain region-selective inhibitor of histone deacetylases. Proc Natl Acad Sci U S A 2006; 103(5):1587-92.
6. Bassett SA, Barnett MPG. The role of dietary histone deacetylases (HDACs) inhibitors in health and disease. Nutrients 2014; 6(10):4273-301.
7. Savickiene J, Treigyte G, Jazdauskaite A, Borutinskaite VV, Navakauskiene R. DNA methyltransferase inhibitor RG108 and histone deacetylase inhibitors cooperate to enhance NB4 cell differentiation and E-cadherin re-expression by chromatin remodelling. Cell Biol Int 2012; 36(11):1067-78.
8. Andonie DA, Seremet OC, Stefanescu E, Zanfirescu A, Grosan A, Osz BE, Dogaru MT. The pharmacological effect of valproic acid, levetiracetam, carbamazepine and the coadministration of valproic acid-

levetiracetam and carbamazepine-levetiracetam on tactile sensitivity, motor activity and the formation of conditioned reflex in rats. Farmacia 2018; 66(2):267-74.

9. Licheri V, Talani G, Gorule AA, Mostallino MC, Biggio G, Sanna E. Plasticity of GABAA receptors during pregnancy and postpartum period: from gene to function. Neural Plast 2015; 2015:170435.
10. Neill JC, Barnes S, Cook S, et al. Animal models of cognitive dysfunction and negative symptoms of schizophrenia: focus on NMDA receptor antagonism. Pharmacol Ther 2010; 128(3):419-32.
11. Saroja SR, Sase A, Kircher SG, et al. Hippocampal proteoglycans brevican and versican are linked to spatial memory of Sprague-Dawley rats in the Morris water maze. J Neurochem 2014; 130(6):797-804.
12. Fatemi SH, Folsom TD, Thuras PD. Deficits in GABAB receptor system in schizophrenia and mood disorders: a postmortem study. Schizophr Res 2011; 128(1-3):37-43.

JOURNAL OF BIOLOGICAL REGULATORS & HOMEOSTATIC AGENTS Vol. 32, no. 6, 1451-1455 (2018)

LETTER TO THE EDITOR

TANSHINONE IIA PROTECTS AGAINST CARDIAC FIBROSIS THROUGH INHIBITION OF β-TUBULIN EXPRESSION

Y. ZHANG[1*], S. ZHANG[1*] and X. CHEN[2]

[1]Department of Cardiology, The First Clinical Medical College, Affiliated Integrated Chinese and Western Medicine Hospital of Jiangsu Province, Nanjing University of Chinese Medicine, Nanjing, Jiangsu, China; [2]Department of Cardiology, Jiangsu Province Hospital of TCM, Nanjing, Jiangsu, China

Received July 27, 2018 – Accepted August 27, 2018

[*]These authors contributed equally to this work

Cardiac fibrosis is a significant global health problem that occurs after pathological stimuli to the cardiovascular system. Previous researchers have shown the protective role of *Salvia miltiorrhiza* Bunge (Danshen) as well as its extracted compound Tanshinone IIA (Tan IIA) against cardiac fibrosis. However no previous work has shown the effects of Tanshinone IIA on cardiac cytoskeleton or the possible relations with its role on cardiac fibrosis. The present study confirms that Tan IIA inhibits the proliferation of mouse cardiac fibroblasts in cultures by MTT assay. It was also observed that Tan IIA decreases β-tubulin expression, especially in the perinuclear area of fibroblasts. Furthermore, we presented by Western blot that TanII A attenuates VEGF expression through HIF-1α and Keap1-Nrf2 pathways, which could be the underlying mechanisms of the Tan IIA's role on cardiac fibrosis. This work demonstrated, for the first time, that the protective role of TanII A against cardiac fibrosis through inhibition of cardiac β-tubulin involves regulation on the antioxidant pathways.

To the Editor,

Myocardial fibrosis, one of the most common histologic features of the late stages of diverse cardiac disease, is caused by a variety of changes in the myocardial collagen network that occur as a response to cardiac ischemic insults, inherited cardiomyopathy mutations, or other systemic diseases affecting the circulatory system. Alterations in myocardial architecture associated with fibrotic remodeling lead to deranged heart function and eventually to heart failure and death (1, 2). Danshen, the dried root of *Salvia miltiorrhiza bunge*, has been successfully utilized by traditional Chinese medicine practitioners to treat patients suffering from myocardial infarction, coronary artery diseases, angina pectoris, stroke, diabetes, liver malfunction, and other conditions (3-6). Tanshinone IIA (TanII A), the compound extracted from Danshen, is regarded as one of the main ingredients of *Salvia miltiorrhiza* for cardioprotective effect. Cardiac fibrosis is characterized by a disproportionate accumulation of extracellular matrix and increased myofibroblast activity that leads to remodeling of the myocardium, and eventually heart failure and death.

Previous studies have shown that cardiac function is inversely correlated with microtubule

Key words: Tanshinone IIA, cardiac fibrosis, β-tubulin, VEGF, HIF-1α, Keap1-Nrf2

Mailing address:
Dr Xiaohu Chen,
Department of Cardiology,
Jiangsu Province Hospital of TCM,
155 Hanzhong Road, Nanjing,
Jiangsu, 210029, China
e-mail: chen_xiaohuxh@163.com

0393-974X (2018)

densification and contributes to heart failure. The tubulin expression and microtubule network density were substantially increased in maladaptive hearts in rodents (7). Here, the direct evidence shows that TanII A inhibits cardiac fibroblast proliferation in cultured mouse fibroblasts and suppresses the expression of β-tubulin. Furthermore, the attenuated VEGF expression through HIF-1α and Keap1-Nrf2 pathway by TanII A was confirmed, which might suggest a novel mechanism for the protective role of TanII A against cardiac fibrosis that has not been addressed previously.

MATERIALS AND METHODS

Primary culture of mouse cardiac fibroblast cells

Primary cardiac fibroblast cells were isolated from the ventricular of neonatal C57BL/6 mice using the enzymatic digestion and selective plating methods as previously described (8). Briefly, the hearts were removed from the sterilized mouse with 75% ethanol and then washed with cold PBS for three to four times, the left ventriculars were then minced before incubation with 0.1% collagenase at 37°C for ~6 min. The digested cell suspension was then transferred to 50 ml tube and mixed with DMEM containing 20% fetal bovine serum to stop digestion and then centrifuged (250-300 g, 10 min, 4 C°) and suspended again. After several rounds of repeated digestions, the fibroblasts were separated from myocytes and other cells by selective planting for 90 min. The isolated cardiac fibroblasts were cultured in HG-DMEM containing 10% fetal bovine serum. Cultured fibroblasts of the third passage were used for further experiments. The identity of cardiac fibroblast cells was assessed by morphology examination.

Treatment of Tanshinone IIA on cultured cardiac fibroblasts

Cultured fibroblasts from the mouse heart were studied at 70% confluence. After cells were attached, Tanshinone IIA was diluted at 1, 5, 10, 25, 50, 100, 200, 500 ug/ml by culture media and added for periods of 24-72 h.

MTT cell proliferation assay

The viability of cultured cardiac fibroblasts was analyzed using the MTT [3-(4,5-dimethylthiazol-2-yl)-2,5- diphenyltetrazolium bromide] method (9). In brief, 100 μl of MTT (OD490) (Beyotime Biotechnology, Shanghai, China) was added to the 96-well plates at a final concentration of 0.5 g/ml for 4 h. After 4 h of incubation, the media was removed and 100 ul DMSO was added, the absorbance value for each well was measured using a microplate reader at a wavelength of 490 nm (1681130-4A, Bao-Cheng Biotec, Inc, Nanjing, China).

Western blotting

Western blotting was performed according to methods established previously. Briefly, the cell lysis were mixed with sample buffer containing 50 mM Tris-HCl (pH 7.6), 2% SDS, 10% glycerol, 10 mM DTT, and 0.2% bromophenol blue and boiled for 5 min. The concentration of the protein samples were determined by using DC™ protein assay kit (5000112, Bio-Rad, CA, USA). The proteins were separated by 10% SDS-polyacrylamide gel electrophoresis (PAGE) and then transferred to PVDF membrane. The membrane was then dried and blocked in 10% non-fat milk for 1 h at room temperature. Incubations with antibodies to KEAP1 (1:1000, 60027-1-Ig, Proteintech, Wuhan, China), NRF-2 (1:1000, 16396-1-AP, Proteintech, Wuhan, China), HIF-α (1:1000, #36169T, Cell Signaling Technology, MA, USA), VEGF (1:1000, #2463, Cell Signaling Technology, MA, USA) and GAPDH (1:1000, #5174, Cell Signaling Technology, MA, USA) were performed at 4°C overnight. The target proteins were detected using horseradish peroxidase-linked anti-rabbit or anti-mouse IgGs (#7074/#7076, Cell Signaling Technology, MA, USA) at 1:5,000 dilution, then visualized by the enhanced chemiluminescence kit (Pierce Chemical Company, Rockford, IL, USA). Immunoreactive bands were quantitatively analyzed by Quantity One 1-D Analysis Software. This experiment was repeated three times.

Immunocytochemistry

Cells were fixed in 4% paraformaldehyde for 20 min at room temperature, blocked by 1% BSA at 37C° for 20 min, and incubated with a primary antibody against β-tubulin (#2416, Cell Signaling Technology, MA, USA) overnight and secondary antibodies were conjugated with Alexa 488 (Molecular Probes) and DAPI (Invitrogen). The fluorescence intensity of β-tubulin was measured by image J software. In each experiment, the numbers

of immunopositive cells were counted in six randomly selected fields, and 500-1000 fibroblasts were counted in total. The immunohistochemical staining was repeated for four times.

Statistical analysis

Results are presented as mean ± SEM. The significance of the difference was performed using one-way/two-way analysis of variance (ANOVA) with Tukey's procedure for post-hoc comparisons or the Student's *t*-test. A value of $P < 0.05$ was considered statistically significant.

RESULTS

Tan IIA inhibits cardiac fibroblasts proliferation in dose- and time-dependent manners

To evaluate the role of TanII A on cardiac fibrosis, we performed TanII A on cultured cardiac fibroblasts at various doses of 1, 5, 10, 25, 50, 100, 200, and 500 ug/ml and assessed the morphology change as well as the cell viability after 24, 48 and 72 h. As shown in Fig. 1A of the phase-contrast micrographs, the cells became hypercontracted (abnormally shaped, considered non-viable) compared with control cells that have a thin and triangular profile under light microscope (rod-shaped, data not shown here). The viability of cardiac fibroblasts was further confirmed by MTT cell proliferation assay.

Cell viability was decreased at 24, 48, and 72 h after TanII A performance compared with the untreated group, and maintained at the platform levels at high doses of TanII A by Two-way ANOVA (Fig. 1, B and C). High dose of TanII A treatment at 500 μg/ml for 72 h on isolated mouse cardiac fibroblasts inhibited ~80% of the cell viability. Overall, these results indicate that TanII A inhibits cardiac fibroblasts proliferation.

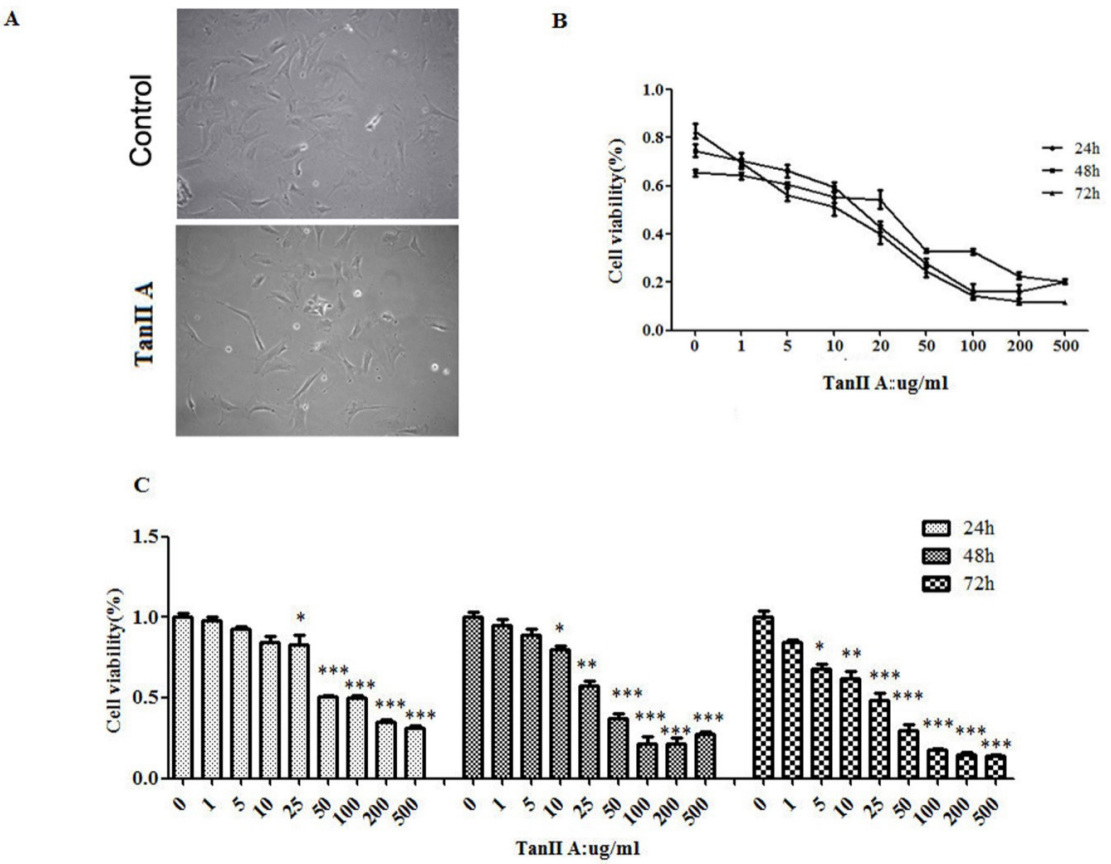

Fig. 1. *Tan IIA inhibits cardiac fibroblast proliferation*.

Tan IIA decreases β-tubulin expression, especially in the perinuclear area of fibroblasts

Cardiac fibrosis is regarded as the consequence of an increased microtubular density, especially in the perinuclear area. To further investigate the underlying mechanism that mediated the protective role of TanII A, we measured the expression of β-tubulin after TanII A treatment in cultured cardiac fibroblasts by immunocytochemistry. Compared with control, the intensity of β-tubulin in fibroblasts was significantly decreased by 72-h treatment of TanII A, and the immunocytochemical localization of β-tubulin demonstrated a decreased density of microtubules in most of the perinuclear area (Fig. 2, A and B).

TanII A attenuates VEGF expression through HIF-1α and Keap1-Nrf2 pathways

Previous works have confirmed that oxidative stress mediates cardiac fibrosis, we therefore further evaluated whether the oxidative stress-related molecular pathways are changed by TanII

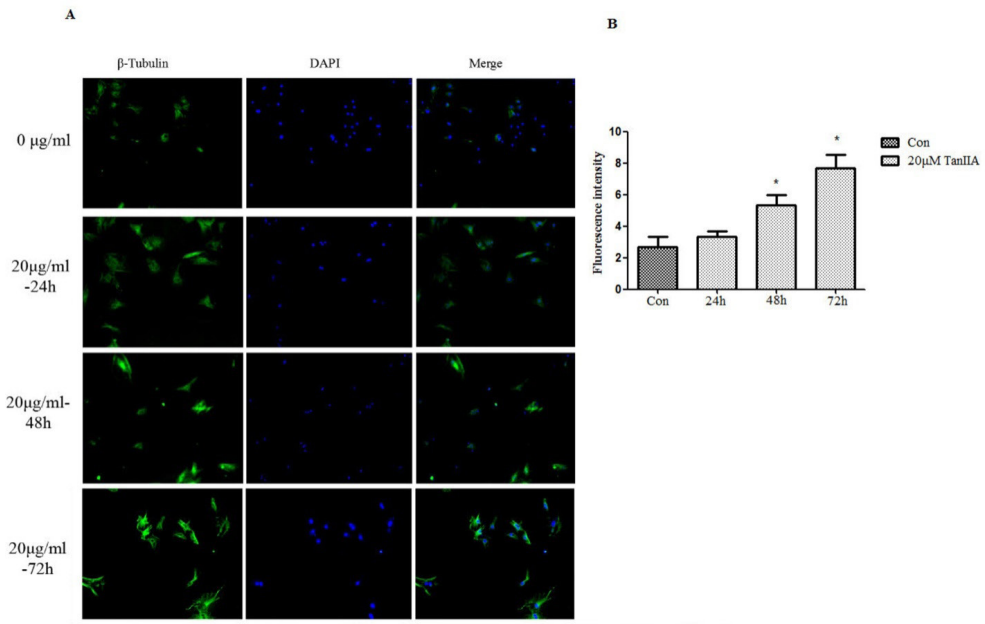

Fig. 2. *Tan IIA decreases β-tubulin expression in cultured cardiac fibroblasts.*

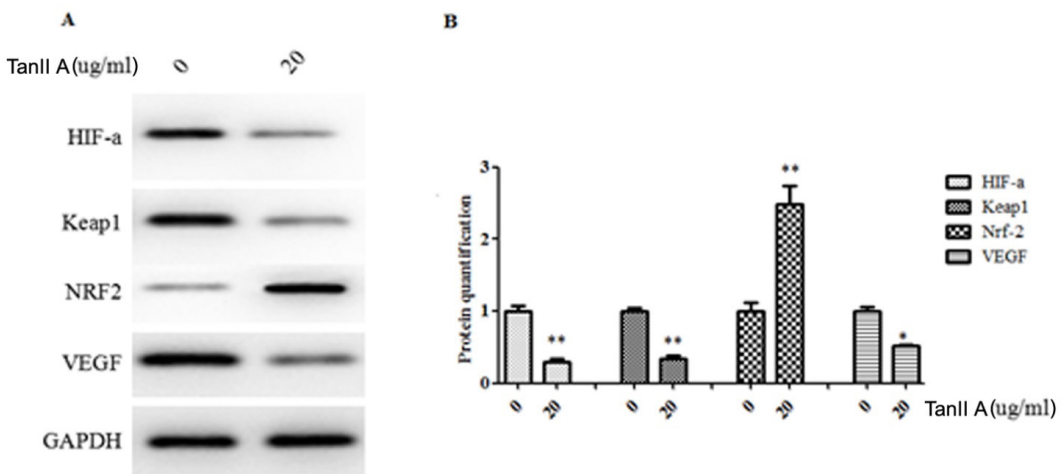

Fig. 3. *TanII A attenuates VEGF expression via regulating HIF-1α and Keap1-Nrf2 pathways.*

A performance in cultured cardiac fibroblasts. By Western blot analyses, we observed that the expressions of HIF-a, and Keap1 as well as VEGF were decreased by 20 ug/ml of TanII A, while the level of NRF2 was significantly increased (Fig. 3).

DISCUSSION

Although less lethal, cardiovascular disease is still the most common cause of global death and its prevalence is incessantly increasing, according to the reports from World Health Organization. The protective roles of Danshen on circulatory disturbance-related diseases are due to its multiple pharmacological actions, including anti-coagulation, anti-inflammation, and free radical scavenging. Cardial reactive oxygen species (ROS) generation and apoptosis contribute to interstitial fibrosis and perivascular fibrosis. Angiotensin II can stimulate ROS and collagen synthesis in cardiac fibroblasts, which suggests that specific pharmacological intervention to reduce ROS can probably be an approach against myocardial fibrosis. Tan IIA has widely shown to depress the intracellular generation of ROS, nicotinamide adenine dinucleotide phosphate (NADPH) oxidase activity, and subunit p47 (phox) expression. Evidence of intracellular ROS generation and VEGF expression in retinal endothelial cells mediated by activation of NADPH oxidase has also been shown. ROS inhibits the enzyme PHD2, which leads to the stabilization of hypoxia-inducible factor-1α (HIF-α) and the formation of the active transcription factor HIF and is involved in the regulation of cell proliferation (10). On the other hand, the Keap1-Nrf2 pathway is the major regulator of cytoprotective responses to oxidative and electrophilic stress (11) and it is regarded as a potential pathway for cardiac protection (12). Here, we further demonstrated that the VEGF expression was significantly decreased by TanII A, along with the significantly increased level of NRF2 and decreased levels of HIF-α and Keap1. To our knowledge, this is the first research on characterizing the protective role of Tan IIA against cardiac fibrosis through the regulation of β-tubulin and cardiac cytoskeleton via HIF-1α and Keap1-Nrf2 pathways.

REFERENCES

1. Tian J, An X, Niu L. Myocardial fibrosis in congenital and pediatric heart disease. Exp Ther Med 2017; 13(5):1660-64.
2. Gyöngyösi M, Winkler J, Ramos I, et al. Myocardial fibrosis: biomedical research from bench to bedside. Eur J Heart Fail 2017; 19(2):177-91.
3. Wu B, Liu M, Zhang S. Dan Shen agents for acute ischaemic stroke. Cochrane Database Syst Rev 2004; (4):CD004295.
4. Oh SH, Cho KH, Yang BS, Roh YK. Natural compounds from Danshen suppress the activity of hepatic stellate cells. Arch Pharm Res 2006; 29(9):762-67.
5. Lee CY, Sher HF, Chen HW, et al. Anticancer effects of tanshinone I in human non-small cell lung cancer. Mol Cancer Ther 2008; 7(11):3527-38.
6. Zhou L, Zuo Z, Chow MS. Danshen: an overview of its chemistry, pharmacology, pharmacokinetics, and clinical use. J Clin Pharmacol 2005; 45(12):1345-59.
7. Sequeira V, Nijenkamp LL, Regan JA, van der Velden J. The physiological role of cardiac cytoskeleton and its alterations in heart failure. Biochim Biophys Acta 2014; 1838(2):700-722.
8. Tao H, Yang JJ, Shi KH, Li J. Epigenetic factors MeCP2 and HDAC6 control alpha-tubulin acetylation in cardiac fibroblast proliferation and fibrosis. Inflamm Res 2016; 65(5):415-26.
9. Ivey MJ, Tallquist MD. Defining the cardiac fibroblast. Circ J 2016; 80(11):2269-2276.
10. Chen QM, Maltagliati AJ. Nrf2 at the heart of oxidative stress and cardiac protection. Physiol Genomics 2018; 50(2):77-97.
11. Villacorta L, Zhang J, Garcia-Barrio MT, Chen XL, Freeman BA, Chen YE, Cui T. Nitro-linoleic acid inhibits vascular smooth muscle cell proliferation via the Keap1/Nrf2 signaling pathway. Am J Physiol Heart Circ Physiol 2007; 293(1):770-76.
12. Choi SH, Park S, Oh CJ, Leem J, Park KG, Lee IK. Dipeptidyl peptidase-4 inhibition by gemigliptin prevents abnormal vascular remodeling via NF-E2-related factor 2 activation. Vascul Pharmacol 2015; 73:11-19.

JOURNAL OF BIOLOGICAL REGULATORS & HOMEOSTATIC AGENTS Vol. 32, no. 6, 1457-1459 (2018)

LETTER TO THE EDITOR

BRASSINOSTEROID BIOSYNTHESIS, STRESS RESISTANCE IN PLANTS, AND APPLICATION OF BRASSINOSTEROIDS IN PLANT BIOTECHNOLOGY

M.M. ALI, M.A. IHSAN, H. ZAFAR, Q.A. RAUF and M.K. AKHTAR

Institute of Biochemistry and Biotechnology,
University of Veterinary and Animals Sciences, Lahore, Pakistan

Received June 2, 2018 – Accepted September 6, 2018

Brassinosteroids (BRs) are newly discovered plant hormones that protect the plants from biotic and abiotic stress. Plants produce these hormones at all times, however, the quantity and location of their production vary. It has been demonstrated that BRs help the plants to regulate their response to stress conditions and make them more resistant to pest attack, extreme hot or cold environment, water scarcity, and salinity, among other types of stress. Manipulation of genes involved in the synthesis of BRs in different plants is a feasible strategy for genetic improvement of crop production and stress tolerance.

To the Editor,

Plants, being sessile, are vulnerable to environmental stress. However, nature has endowed them with several mechanisms to resist environmental stress by hormonal regulation of different genes. Brassinosteroids (BRs) are the sixth class of plant hormones and are present ubiquitously throughout the plant kingdom. They control the activity of plants under stress conditions; for example, under cold stress, they interact with the CBF gene to provide chilling resistance, whereas under heat stress, they bind to Phytochrome Interacting Factor-4 (PIF-4) to reduce the effect of temperature. In recent times, there has been an increased research focus on generating high yielding and resistant plant varieties by incorporation of genes that are involved in biotic and abiotic stress tolerance. Genes involved in the production of BRs are also considered as candidate genes for improving the yield and resistance of crop plants to environmental stresses.

Signaling pathway of brassinosteroids

Brassinolide (BL), which is a type of BR, binds to brassinosteroid-insensitive1 (BRI-1) and induces a series of biochemical events, such as phosphorylation of BRI-1 and dissociation of many inhibitory proteins (1). It negatively regulates Brassinazole Resistant 1 (BZR-1) and BRI1-EMS-suppressor-1 (BES-1) through Brassinosteroid-Insensitive-2 (BIN-2). BIN-2 inhibits the activities of BES-1 and BZR-1 (2, 3). If the phosphorylation of BIN-2 occurs, there is no BR activation; however, in its dephosphorylated form, BIN-2 molecule becomes inactivated, as a result of which there is an activation of Bri1 Suppressor-1 (BSU-1) that leads to the accumulation and activation of BZR-1 and BES-1. The activated BZR-1 directly binds to the BR promoter gene region and affects its expression. The majority of BR-regulated genes are involved in plant growth, cell wall modification, and cytoskeleton formation (4). BES-1 and MYB-30 (a factor that regulates cell death response and

Key words: brassinosteroid, BZR1, environmental stress, exogenous application, hormone regulation, genetic manipulation

Mailing address:
Dr. Muhammad Muddassir Ali,
Institute of Biochemistry and Biotechnology,
University of Veterinary and Animals Sciences,
Outfall Lahore, Lower MJall Road, Lahore, Punjab, Pakistan
Tel.: +923336252189
e-mail: muddassir.ali@uvas.edu.pk

0393-974X (2018)

flowering time) bind to conserved regions in the promoter of the BR gene and enhance its expression. An understanding of the interaction between BES-1 and BZR-1 should reveal the mechanism involved in the control of BR gene expression.

Role of BRs in cold stress

Under favorable conditions, BRs are not present in cells. When plants encounter cold stress, they initiate a cascade of intracellular reactions that helps them tolerate the stress by producing BRs, which combine with the BRI-1 cell surface receptor, and activate the BRI-1 kinase that degrades BIN-2, a repressor of BZR-1 and BES-1. Because of the degradation of BIN 2, BZR 1 and BES-1 are dephosphorylated and activated and start accumulating in the nucleus. The activated BZR 1 can induce cold tolerance in plants either through CBF-dependent or CBF-independent pathways. In both the cases, the ultimate target genes belong to the COR family. BZR-1 and its homolog, BES-1, bind to the BRRE and R-box motifs in the promoter regions of CBF-1 and CBF-2 genes (5). Furthermore, BZR-1 also acts as an inducer of CBF-1 and CBF-2 genes and enhances their translation rate. These proteins provide immunity to plants against cold stress.

It is assumed that BRs also respond to the cold stress by regulating genes other than CBF, such as *PLY-6*, *WRKY-6*, *SAG-21*, *JMT*, and *ESM-1*. BZR-1 binds specifically to the promoters of WRKY-6, SOC-1, and JMT genes and induces cold acclimation. When WRKY mutants were subjected to freezing tolerance assay they showed hypersensitivity towards low temperature as compared to the wild-type plants. These results suggest that BZR-1 regulates both CBF and COR genes to provide cold acclimation in plants.

Role of BRs against water scarcity stress

BRs help the plants in adapting to water scarcity in multiple ways, for example, by increasing the length of their roots so as to increase water absorption or by enhancing root nodulation. Root nodulation increases with the increase in BR concentration. BRs also affect the concentration of Abscisic acid (ABA) and cytokinin. BL inhibits the entry of sugars into the cells under drought conditions. This blockage of the entry of sugars inside the cell influences the intracellular concentration of salt and ABA in plants. The increased salt concentration in cells results in endosmosis and avoidance of water loss. Under conditions of water scarcity, the density of chlorophyll is decreased by activated BRs (6). HomoBL stimulates drought tolerance. Its presence in the cell causes an increase in water content and nitrate reductase levels, as well as in photosynthesis. HomoBL also decreases the activity of reactive oxygen species (ROS), produced during drought stress, and increases the stability of cellular membranes. Results of experiments carried out on sugar beet, rice, and wheat indicate that the growth of plants exposed to stress is substantially less as compared to non-stressed plants (7). However, if plants are treated with BRs, there is an improvement in their growth as a result of drought tolerance.

Role of BRs in salinity stress

Zea mays seeds treated with 28-homobrassinolide (28-BL) showed mitigation of salinity stress induced by varying concentrations of NaCl and an obvious increase in seedling growth was observed as a result of an increase in the activity of antioxidant and cell wall loosening enzymes and reduction in the loss of chlorophyll (8, 9). The exogenous application of 28-BL increases the levels of antioxidant enzymes such as superoxide dismutase (SOD), catalase (CAT), guaiacol peroxidase (POD), ascorbate peroxidase (APOX), and glutathione reductase (GR).

BRs improve the salt tolerance in rice plants by significantly increasing the levels of CAT and SOD (10). Studies on *Eucalyptus camalduienis* suggest that the application of 24-epi brassinolide (24-epi BL), which is a BR, improves the seed germination and seedling growth in the presence of salt (1). Moreover, the application of BRs in *Oryza sativa* removes the inhibitory effects on seed germination caused by salinity stress.

Role of BRs in plant biotechnology

Plants engineered for the expression of BRs show desirable characteristics including increased height, weight, yield, and stress resistance (11). The overexpression of DWF-4 gene was shown to double

the number of branches and production of seeds in transgenic plants. In these engineered plants, the grain yield increased from 15% to 44% as a result of the increase in seed weight, seed number, and tiller number. In cotton, the exogenous application of BRs improved the cotton fiber number by 22.6% and fiber length by 10.7% (12).

Moreover, 24-epi BL helps the plants in regulating photosynthesis in their leaves. It was demonstrated that exogenous application of BRs on cucumber increased the photosynthetic rates within a week. Recent investigations revealed that the BR gene confers environmental stress resistance in plants and improves their growth by enhancing the rate of photosynthesis and increasing their adaptability to the stress. Thus, exogenous application of BRs can induce desirable improvements in plants.

Conclusion

Brassinosteroids are involved in the protection of plants against both biotic and abiotic stresses. They provide protection by activating different mechanisms depending upon the nature of stress; for example, BRs protect against oxidative and salinity stress by stimulating the release of ROS scavenging enzymes. BRs have a great potential to genetically improve important crops around the world. The introduction of BR and other yield-related genes in plants through biotechnological methods results in enhanced resistance to environmental stress and increased yield. This helps researchers to produce a variety of plants that have the resistance gene and thus increased production.

REFERENCES

1. Wang X, Kota U, He K, et al. Sequential transphosphorylation of the BRI1/BAK1 receptor kinase complex impacts early events in brassinosteroid signaling. Develop Cell 2008; 15(2):220-35.
2. Vert G, Chory J. Downstream nuclear events in brassinosteroid signaling. Nature 2006; 441(7089):96-100.
3. Gampala SS, Kim TW, He JX, et al. An essential role for 14-3-3 proteins in brassinosteroid signal transduction in Arabidopsis. Develop Cell 2007; 13(2):177-89.
4. Vert G NJ, Geldner N, Hong F, Chory J. Molecular mechanisms of steroid hormone signaling in plants. Cell Dev Bio 2005; 21:177-201.
5. Li H, Ye K, Shi Y, Cheng J, Zhang X, Yang S. BZR1 Positively regulates freezing tolerance via CBF-dependent and CBF-independent pathways in arabidopsis. Mol Plant 2017; 10(4):545-59.
6. Zhu JK. Salt and drought stress signal transduction in plants. Annu Rev Plant Biol 2002; 53:247-73.
7. Si J. Variation in the antioxidant metabolism of young and mature leaves of Arabidopsis thaliana subjected to drought. Plant Sci 2003; 166:459-66.
8. Arora A SR, Srivastava GC Oxidative stress and antioxidative system in plants. Curr Sci 2002; 82:1227-38.
9. Anuradha S, S. Seeta Ram Rao. Application of brassinosteroids to rice seeds (Oryza sativa L.) reduced the impact of salt stress on growth, prevented photosynthetic pigment loss and increased nitrate reductase activity. Plant Growth Reg 2003; 40:29-32.
10. J.M. Sasse RS, I. Hudson. Effect of 24-epibrassinolide on germination of seed of Eucalyptus camaldulensis in saline conditions. Plant Growth Regul 1995; 22:136-41.
11. Sun Y, Veerabomma S, Abdel-Mageed HA, Fokar M, Asami T, Yoshida S, Allen RD. Brassinosteroid regulates fiber development on cultured cotton ovules. Plant Cell Physiol 2005; 46(8):1384-91.
12. Koh SLS, Kim MK, Koh JH, Lee S, An G, Choe S, Kim SR. T-DNA tagged knockout mutation of rice OsGSK1, an orthologue of Arabidopsis BIN2, with enhanced tolerance to various abiotic stresses. Plant Mol Biol 2007; 4(65):1158-64).

LETTER TO THE EDITOR

CORRELATION BETWEEN RHEUMATOID ARTHRITIS AND IMMUNOLOGICAL CHANGES IN A RHEUMATOID ARTHRITIS RAT MODEL

S. WU[1], Z. MENG[1] and Y. ZHANG[2]

[1]Zhejiang Chinese Medical University, Hangzhou, China; [2]Department of Hematology, First Affiliated Hospital of Zhejiang Chinese Medical University, Hangzhou, China

Received July 24, 2018 – Accepted September 10, 2018

Rheumatoid arthritis is an autoimmune disease characterized by the synovitis of joints and the modulation of chronic inflammation determined by increased levels of inflammatory cytokines. This study aimed to investigate the characteristics of the immunological profile of the cells of the synovial membrane and the expression of IL-10 and IL-17 in a rheumatoid arthritis rat model in order to provide a target-directed treatment for immunological control. Eighty female Wistar rats were randomly divided into a rheumatic arthritis model group (model group) and a control group, 40 animals per group. After the successful rheumatoid arthritis rat model was obtained, 10 animals were sacrificed from each group every week starting from the third week till the sixth week and the expression levels of CD3, CD21, and CD68 in the synovial region along with the blood level of IL-10 and IL-17 were assessed. At the four stages after modeling, the expression of CD3 in the model group increased compared with the control group ($P<0.05$). The expression of CD21 was different between the model group and the control group, but the difference did not reach statistical significance ($P>0.05$). The expression of CD68 determined at weeks 4 and 5 after modeling was increased compared to the control group ($P<0.05$). At 6 week after modeling, IL-10 levels in the model group were higher than those in the control group ($P<0.05$). At weeks 4 and 5 after modeling, the level of IL-17 in the model group increased compared to the control group ($P<0.05$). The level of IL-17 increased with the increase of synovial inflammation in the rheumatoid arthritis-induced rats, and the level of IL-10 increased as the inflammation subsided, which shows that both cytokines are related to the occurrence and development of rheumatoid arthritis and its inflammation.

To the Editor,

Rheumatoid arthritis is an autoimmune disease characterized by the synovitis of joints and the modulation of chronic inflammation determined by increased levels of inflammatory cytokines. Clinical symptoms include swelling, pain, and deformity of the joints (1). Currently, the pathogenesis of rheumatoid arthritis is not completely clear. Most studies focus on the overall disruption of the body's immune system (2). To date, some studies have shown that immune cells, cytokines and their inhibitors play an important role in the development of rheumatoid arthritis lesions (3-5). The Th2 cells are a subset of lymphocytes that secrete IL-10 anti-inflammatory cytokine which has a major role in enhancing the humoral immune response mediated by B lymphocytes (6). In rheumatoid arthritis, IL-10 can inhibit Th17 cell-mediated inflammatory response, reduce joint swelling and inhibit the development of arthritis. IL-10 has immunosuppressive and immunoregulatory

Key words: rheumatoid arthritis, joint synovial membrane, inflammatory factors, immunity

Mailing address:
Dr Yu Zhang,
Department of Hematology,
First Affiliated Hospital
Zhejiang Chinese Medical University,
54#YouDian Road, Hangzhou, 310006, China
e-mail: zyzhangyu66@163.com

0393-974X (2018)

DISCLOSURE: ALL AUTHORS REPORT NO CONFLICTS OF INTEREST RELEVANT TO THIS ARTICLE.

functions (7). IL-17 is a pro-inflammatory factor that binds to human IL-17 receptor and exerts its effect (8). It can induce and synergize the expression of other pro-inflammatory factors, mediate inflammatory cells to cause local infiltration and tissue damage, exert its inflammatory effect, and has a high level of expression in the advanced stage of inflammation (9, 10). Therefore, IL-10 and IL-17 and their interrelationships are closely related to the occurrence and development of RA. This study aimed to assess the expression of CD3, CD21, and CD68 in synovial cells and the serum levels of IL-10 and IL-17 cytokines in serum and their associated effects on a rheumatoid arthritis rat model in order to clarify the immunological mechanism of rheumatoid arthritis and to provide a new perspective for immunologically targeted therapy.

MATERIALS AND METHODS

Animals

Eighty 5-week old female Wistar rats with a median weight of 131.05±14.72 g were purchased from the Guangdong Medical Experimental Animal Center. The animals were acclimatized for one week to the new laboratory conditions with standard conditions of 23±1°C temperature, humidity between 40±5° and 12 hour light/dark cycle. After acclimatization the animals were randomly divided into two groups: a model group and a control group, 40 rats per group. The animals received food and water *ad libitum*. This study was approved by the ethics committee of Zhejiang Chinese Medical University, and all the animal experiments were in accordance with International law regarding animal studies.

Rheumatoid arthritis rat model

A rheumatoid arthritis rat model was designed as following. After acclimatization, the rats from the model group received intradermally in the right hind foot 0.1 ml Freund's complete adjuvant (CFA), and after the foot was soaked in cold water at 4°C for 40 min associated with 4 levels of wind, every day for 2 weeks. The rats from the control group received intradermally the same quantity of normal saline solution and no other treatment was applied.

Experimental method

From the first day of modeling, 10 rats of each group were randomly selected on the last day of the 3rd, 4th, 5th, and 6th week from the beginning of the modeling. The degree of joint swelling in rats was measured and recorded, and spleen coefficient and proliferation rates of spleen cells were calculated. The rats were anesthetized with 10% chloral hydrate (3mL/kg) injected intraperitoneally and were then sacrificed by cervical vertebra luxation. The tread joints of the right hind limbs of both groups of rats were taken and decalcified to make a pathological wax block for sectioning and HE (Hematoxylin-erosion) staining. Synovial tissue lesions were observed. Through the above indicators, the modeling results were evaluated.

The expression of CD3, CD21, and CD68 in the synovium of the two groups was detected by immunohistochemistry. On the last day of the 3rd, 4th, 5th, and 6th week after the rats were modeled, the right hind limb ankle of about 2 cm long was taken from 10 rats in the model group and the control group, and the decalcified dehydration was prepared. The treated bare joints were tissue-embedded and sectioned. Each ankle wax block was sliced and attached to three immunohistochemical adhesion slides for CD3, CD21, and CD68 immunohistochemical staining. The staining of the cells was observed under an optical microscope and the percentage of CD3, CD21, and CD68 expression was calculated.

For the detection of IL-10 and IL-17 levels in the serum an ELISA method was used according to the manufacturer's instructions using IL-10 ELISA kit (Biotech Biotech Co., Ltd.) and IL-17 ELISA kit (US Biosciences).

Statistical analysis

SPSS11.5 software was used for statistical analysis. The data were expressed as mean± standard deviation. A comparison of multiple groups was made using one-way analysis of variance. The *t*-test was used to compare the mean values of the two groups. The test level that was taken on both sides was α =0.05. The difference was statistically significant when $P<0.05$

RESULTS

Comparison of joint swelling between the two groups of rats

After three days of modeling, the joints of the model group began to have red swelling, and the degree of joint swelling became more pronounced with the prolongation of modelling time. At 3 weeks, 4 weeks, 5 weeks and 6 weeks from the beginning of the modeling, the degrees of joint swelling in the model group were (10.88±0.60)mm, (10.18±1.28) mm, (11.37±0.84)mm and (10.53±1.02)mm, respectively; and the degrees of joint swelling in the control group were (8.21±0.41)mm, (8.63±0.44)mm, (8.93±0.32)mm and (8.95±0.58)mm, respectively. The joint swelling of rats in the model group was increased compared to the control group ($P<0.05$).

Spleen cell proliferation rate and spleen coefficient in the two groups

Splenic lymphocytes in the control group had small cell volume and high nucleus-cytoplasm ratio cytoplasm. In the model group, rat spleen lymphocytes became large. The cytoplasm was enlarged and the nuclear chromatin was loose. Obvious nucleoli were found. The model group rats had the highest spleen cell proliferation rate at the 4th week after modeling (99.2±0.5%). Lymphocyte transformation was evident with the exacerbation of rheumatoid arthritis in rats. In the 4th week, when the joint swelling was more severe, splenocyte proliferation rate reached the highest value. The proliferation rate of spleen cells in the model group was increased compared to the control group at all four points of determination ($P < 0.05$). No significant differences between the two groups were observed regarding spleen coefficient ($P>0.05$).

Pathological morphology of joint synovial tissue in two groups

The pathological morphology of joint synovium in the two groups of rats is shown in Fig. 1. The synovial cells of the control group were monolayered. Macrophages, collagen fibers, blood vessels, and lymphatic vessels are clearly visible. At the third week after model establishment, chronic

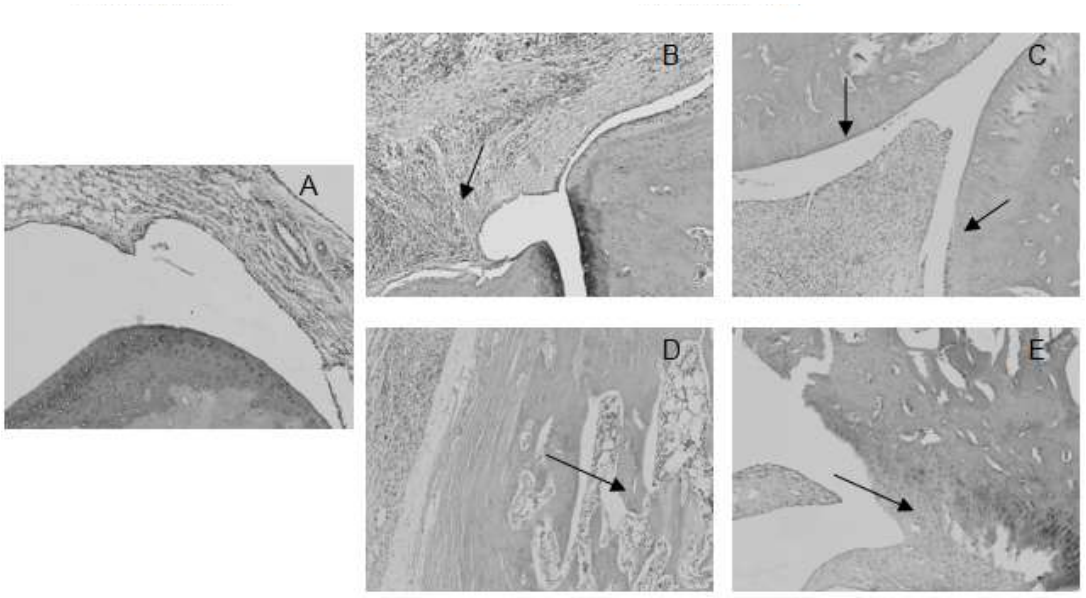

Fig. 1. *Pathological morphology of joint synovium in two groups (staining with hematoxylin and eosin (HE), 400X).* ***A****) Pathological morphology of synovial tissue in the control group.* ***B****) Synovial tissue morphology at the third week in the model group;* ***C****) synovial tissue morphology at the 4th week in the model group;* ***D****) synovial tissue morphology at the 5th week in the model group;* ***E****) synovial tissue morphology at week 6 in the model group.*

synovial inflammation appeared in the model group. The number of cell layers increases. Neutrophils, lymphocytes, and plasma cells exuded in large quantities. In the fourth week, the synovial membrane became a stratified layer. Hyperplasia occurred in the tissue with a large number of lymphocytes and plasma cell infiltrates. Chronic inflammation was evident. After the fifth week, the number of synovial layers increased. The synovial mesenchyme was fibrotic. The joint space became narrow. After the sixth week, there was an exfoliative lesion in the articular cartilage, and the joint cavity was disordered and some inflammatory cells were still visible.

Expression of CD3, CD21, and CD68 in synovial membrane of rats in two groups

In the control group the percentage of CD3, CD21, and CD68 in the synovial tissue was very low. The percentage of CD3 expressions and some CD21 and CD68 expressions were observed in synovial tissue of rats in the model group. In the model group, the cell membrane of CD3 positive cells contained dark brown granules; the positive expression of CD21 was mainly distributed in the cell membrane, partially distributed in the other lymphocytes outside the follicle; CD68 cells were dispersed in the lymphoid follicles, with dark brown granules. The average expression rate of CD3, CD21, and cells in the model group increased gradually during the four periods after modeling. At the 6th week, the maximum value was reached. In the four periods after modeling, the expression rate of CD3 in the model group rats was higher than that in the control group ($P<0.05$). The expression of CD21 in the model group rats was higher than that in the control group ($P>0.05$). The expression rate of CD68 in the model group rats was higher in the 4th and 5th weeks than in the control group ($P<0.05$). The specific results are shown in Fig. 2 and Table I.

The serum levels of IL-10 and IL-17 in the two groups

The serum levels of IL-10 and IL-17 in the two groups are also shown in Table I. Compared with the control group, the IL-10 level in the model group increased at the 6th week ($P>0.05$). The serum level

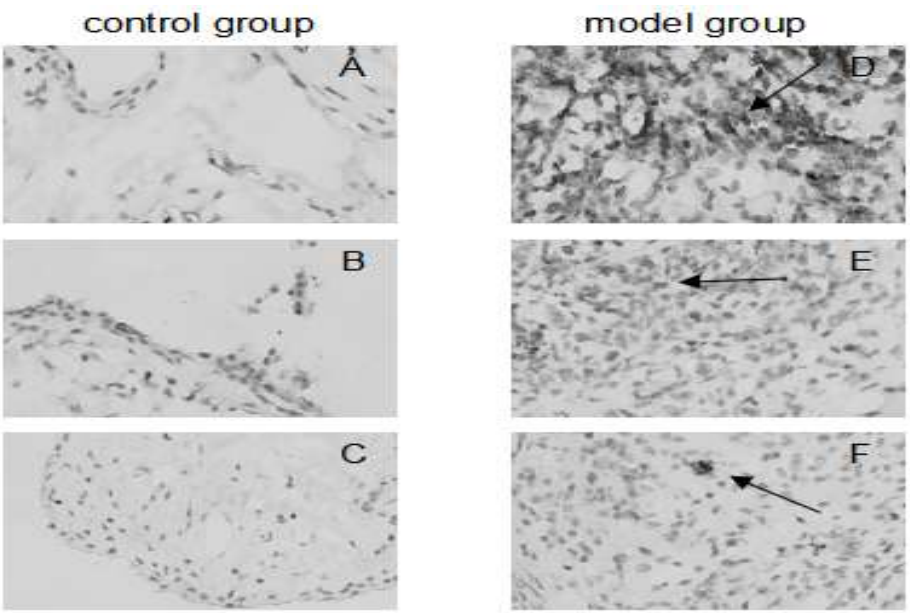

Fig. 2. *Expression of immunohistochemical staining of CD3, CD21 and CD68 in synovial tissue of rats in two groups (staining with hematoxylin and eosin, 400X).* ***A)*** *CD3 expression in the synovial tissue of the control group;* ***B)*** *CD21 expression in the synovial tissue of the control group;* ***C)*** *CD68 expression in the synovial tissue of the control group;* ***D)*** *CD3 expression in the synovial tissue of the model group;* ***E)*** *CD21 expression in the synovial tissue of the model group;* ***F)*** *CD68 expression in the synovial tissue of the model group.*

Table I. *Changes of synovial tissue CD3, CD21, and CD68 in the two groups of rats.*

Detection object	Period	Control group	Model group	t	P
CD3 (%)	Week 3	3.1±1.5	53.7±7.3*	14.884	0.000
	Week 4	3.7±1.7	60.5±17.2*	7.329	0.002
	Week 5	3.1±1.6	73.9±16.9*^#	9.139	0.001
	Week 6	1.9±0.9	83.5±10.2*^#	17.583	0.000
CD21 (%)	Week 3	28.7±20.3	22.9±11.1	-0.553	0.594
	Week 4	36.5±9.6	34.7±9.2	-0.301	0.772
	Week 5	37.5±14.2	43.7±8.5*	0.838	0.429
	Week 6	22.3±8.4	50.9±4.8*#	6.631	0.000
CD68 (%)	Week 3	26.1±26.7	17.1±5.9	-0.735	0.502
	Week 4	10.3±5.8	28.1±15.3*	2.439	0.042
	Week 5	5.9±2.4	29.9±4.0*	11.340	0.000
	Week 6	16.1±20.2	31.1±9.5^	1.496	0.173
IL-10 (pg/ml)	Week 3	45.21±5.81	60.95±13.47	2.385	0.058
	Week 4	53.24±18.29	57.71±4.28	0.535	0.603
	Week 5	45.47±17.56	57.89±8.02	1.433	0.192
	Week 6	35.55±5.26	66.04±7.12*	7.534	0.000
IL-17(pg/ml)	Week 3	33.61±3.18	48.79±2.63*#	8.035	0.000
	Week 4	38.87±1.94	59.52±7.38*	5.906	0.003
	Week 5	30.92±1.25	43.55±4.15*#	6.467	0.003
	Week 6	35.51±2.97	43.21±3.09*#	4.091	0.004

(mean ± standard deviation)

** Compared with the control group P<0.05, ^ compared with the third week P<0.05, # compared with the fourth week P<0.05.*

of IL-17 in the model group reached the highest level at the 4th week after model establishment. It indirectly shows that the arthritis of rats in the model group was most severe at the 4th week, and IL-17 played a major role. The serum level of IL-17 in the model group rats at the 4th and 5th week was higher than that of the control group (P>0.05). The specific data is shown in Table IV.

DISCUSSION

The change of each index in this study suggested that the course of the rats in the model group changed significantly. This is similar to human rheumatoid arthritis. The success of the model is consistent with the study of Hu et al. (11).

The experimental results showed that there were a large number of T lymphocytes in the synovial tissue, and the effect of T lymphocyte inflammatory cells increases with the increase of the CD3 expression rate. There is no direct relationship between the B lymphocytes and the synovial tissue damage in rheumatoid arthritis. Macrophages may be involved in the formation and development of inflammation. This is consistent with reports such as that of Fabien Depis (12). Both T lymphocytes and macrophages are involved in the development of joint synovial inflammation, but T lymphocytes are the major inflammatory factors.

In this study, regarding the expression of IL-10 and IL-17 in serum of two groups of rats, it has been shown

that under the regulation of the body's autoimmunity, the arterial soft tissue inflammation of the model group decreased, the anti-inflammatory factors slowly restored immune regulation, the level of IL-10 increased, the effect of pro-inflammatory factors is suppressed, and in turn causes a decrease in the level of IL-17.

In summary, T lymphocytes are the main immune cells in the synovial region of rheumatoid arthritis. The study shows that the serum level of IL-17 and the level of IL-10 are closely related to the occurrence and development of rheumatoid arthritis and its inflammation. This will help to further explore the pathogenesis of rheumatoid arthritis.

ACKNOWLEDGEMENTS

This work was supported by the Natural Science Foundation of China (NO. 81603573).

REFERENCES

1. Singh JA, Cameron C, Noorbaloochi S, et al. Risk of serious infection in biological treatment of patients with rheumatoid arthritis: a systematic review and meta-analysis. Lancet 2015; 386(9990):258-65.
2. Kubota K, Ito K, Morooka M, et al. FDG PET for rheumatoid arthritis: basic considerations and whole-body PET/CT. Ann N Y Acad Sci 2011; 1228:29-38.
3. Xia T, Zheng XF, Qian BH, et al. Plasma interleukin-37 is elevated in patients with rheumatoid arthritis: its correlation with disease activity and Th1/Th2/Th17-related cytokines. Dis Markers 2015; 2015:795043.
4. Nakano S, Morimoto S, Suzuki S, Tsushima H, Yamanaka K, Sekigawa I, Takasaki Y. Immunoregulatory role of IL-35 in T cells of patients with rheumatoid arthritis. Rheumatology (Oxford) 2015; 54(8):1498-506.
5. Koo J, Kim S, Jung WJ, Lee YE, Song GG, Kim KS, Kim MY. Increased lymphocyte infiltration in rheumatoid arthritis is correlated with an increase in LTi-like cells in synovial fluid. Immune Netw 2013; 13(6):240-58.
6. Kimmig S, Baumgrass R. Biological switches: the all-or-none principle in T-cell activation. Z Rheumatol 2009; 68(7):560, 562-65.
7. Huber S, Gagliani N, Esplugues E, et al. Th17 cells express ninterleukin-10 receptor and are controlled by $Foxp3^-$ and $Foxp3^+$ regulatory $CD4^+$ T cells in an interleukin-10-dependent manner. Immunity 2011; 34(4):554-65.
8. Ito H, Yamada H, Shibata TN, Mitomi H, Nomoto S, Ozaki S. Dual role of interleukin-17 in pannus growth and osteoclastogenesis in rheumatoid arthritis. Arthritis Res Ther 2011; 13(1):R14.
9. van Hamburg JP, Corneth OB, Paulissen SM, Davelaar N, Asmawidjaja PS, Mus AM, Lubberts E. IL-17/Th17 mediated synovial inflammation is IL-22independent. Ann Rheum Dis 2013; 72(10):1700-707.
10. Cho KA, Kim JY, Woo SY, Park HJ, Lee KH, Pae CU. Interleukin-17 and Interleukin-22 Induced Proinflammatory Cytokine Production in Keratinocytes via Inhibitor of Nuclear Factor κB Kinase-α Expression. Ann Dermatol 2012; 24(4):398-405.
11. Hu Y, Cheng W, Cai W, Yue Y, Li J, Zhang P. Advances in research on animal models of rheumatoid arthritis. Clin Rheumatol 2013; 32(2):161-65.
12. Dépis F, Hatterer E, Lamacchia C, et al. Long-term amelioration of established collagen induced arthritis achieved with short term therapy combining anti-CD3 and anti-tumor necrosis factor treatments. Arthritis Rheum 2012; 64(10):3189-98.

LETTER TO THE EDITOR

miR-200b PROMOTES CELL PROLIFERATION AND INVASION IN T-CELL ACUTE LYMPHOBLASTIC LEUKEMIA THROUGH NOTCH1

F. NING[1], Q. ZHOU[2] and X. CHEN[3]

[1]Department of Hematology, Zhejiang Provincial People's Hospital, People's Hospital of Hangzhou Medical College, Hangzhou, China; [2]Department of Internal Medicine, Zhejiang Provincial People's Hospital, People's Hospital of Hangzhou Medical College, Hangzhou, China; [3]Department of Respiratory Medicine, Zhejiang Provincial People's Hospital, People's Hospital of Hangzhou Medical College, Hangzhou, China

Received July 4, 2018 – Accepted September 12, 2018

MicroRNA-200b (miR-200b) functions as an oncogenic regulator in human lung cancer. However, the effect of miRNA-200b on the development and progression of T-Cell acute lymphoblastic leukemia (T-ALL) remains largely unknown. In this study, we evaluated the impact of miR-200b in T-ALL cell proliferation, survival and invasion using gain and loss of function approaches. Human Jurkat cells, a widely used *in-vitro* T-ALL cell model, were transfected with miR-200b mimic or miR-200b inhibitor. miR-200b mimics substantially inhibited Jurkat cell proliferation and invasion while significantly stimulating cell apoptosis compared to the control miRNA-treated cells. In contrast, Jurkat cells treated with anti-miR200 demonstrated induction of cell growth and invasion but repression of cell apoptosis. Such effect was accompanied by the corresponding alteration in NOTCH1 expression, suggesting that NOTCH1 might be the target gene for miR-200b function in Jurkat cells. In summary, our findings demonstrate that miR-200b may serve as a potential therapeutic target for T-ALL by negatively regulating the NOTCH1 signaling pathway.

To the Editor,

T-Cell acute lymphoblastic leukemia (T-ALL) is an aggressive cancer derived from the malignant transformation of immature T-cell progenitors (1). T-ALL is initiated by the activation of oncogene and deactivation of the tumor suppressor, followed by aberrant cell proliferation, inhibition of cell apoptosis and abnormal differentiation. The finding that aberrant, constitutive activation of NOTCH1 signaling presents in over 60% of T-ALL patients (2) generates enormous enthusiasm to develop molecularly-tailored therapies. NOTCH1 is a member of the NOTCH family of conserved transmembrane receptors that regulate T-lymphocyte differentiation, proliferation and apoptosis by targeting the crucial signaling pathways and genes such as nuclear factor-κB (NF-κB), MYC, IGF-1R, and IL-7R (3, 4).

NOTCH1 signaling in T-ALL is regulated by MicroRNAs (miRNA)which are small non-coding RNA molecules that function as post-transcriptional gene regulators. Aberrant expression of miRNAs can function as either oncogenes or tumor suppressors in T-ALL (5). MiR-200 has been identified as a novel therapeutic target duet to its important roles in cancer

Key words: miR-200b, NOTCH1, T-ALL, microRNA

Mailing address:
Dr Fangying Ning,
Department of Hematology,
Zhejiang Provincial People's Hospital,
People's Hospital of Hangzhou Medical College,
No.158 Shangtang Road, Xiacheng District,
Hangzhou 310000, China
e-mail: ningfangying2011@126.com

0393-974X (2018)

initiation, metastasis, and relapses (6). MiR-200 family genes also impact the tumor cell metastasis by targeting on tumor cell survival, angiogenesis and invasion to surrounding tissues (7). Due to its potent roles in all aspects of tumor development, miR-200 family had been considered as a potential diagnostic and prognostic marker. However, the function of the miR200 family in T-ALL remains largely unknown. Therefore, in this study we propose to investigate the impact of miR-200b expression on lymphocyte proliferation and apoptosis in Jurkat cells. As expected, overexpression of miR-200b inhibited Jurkat cell proliferation and invasion while stimulating apoptosis. Such effect is likely through the inhibition of NOTCH1 signaling.

MATERIALS AND METHODS

Cell culture and transfection

Human T-ALL Jurkat cell lines were purchased from the American Type Culture Collection (ATCC, Manassas, VA, USA). Jurkat cells were cultured in RPMI 1640 (RPMI1640; Life Technology, Shanghai, China) supplemented with 10% fetal bovine serum. All cells were incubated in a humidified incubator with 5% CO2 at 37°C. MiR-200b mimics, anti-miR 200b and its negative control RNA (miR-NC) were synthesized by Life Technology (Shanghai, China). For transfection, Jurkat cells were seeded in 24-well plates at 3×10^5 cells/wells and incubated overnight, after which 200 nM miR-200b mimics, anti-miR200b or miR-NC were transfected into cells using Lipofectamine 2000 according to the manufacturer's instructions (Invitrogen, Shanghai, China). All constructs were confirmed by DNA sequencing.

RNA extraction and quantitative real-time polymerase chain reaction (qPCR)

Total RNA was extracted from the cells by using TRIzol reagent (Invitrogen, Shanghai, China) according to the manufacturer's instructions. To quantify the miR-200 expression, complementary DNA (cDNA) was synthesized with miScript Reverse Transcription Kit (Qiagen, Hilden, Germany) and then amplified using SYBR Premix Ex Taq™ (TaKaRa, Otsu, Shiga, Japan). The reaction conditions were as follows: one cycle of pre-denaturation at 95°C for 30S, followed by 40 cycles of denaturation at 95°C for 5S, annealing and extension at 60°C for 30S. An RT-qPCR platform (ABI PRISM 7300 system, ABI, USA) was used for detection. U6 was used as an internal control. The sequence for the primer pairs were: miR-200b forward: 5'-UAAUACUGCCUGGUAAUGAUGA-3'; miR-200b reverse: 5'-AUCAUUACCAG-GCAGUAUAAAU-3'; U6 forward 5'-CTCGCTTCGGCAGCACA-3', U6 reverse 5'-AACGCTTCACGAATTTGCGT-3'. Gene expression was measured in triplicates, quantified using the $2^{-\Delta\Delta CT}$ method, and normalized to a control. qPCR assays were performed on an iQ5 real-time PCR Detection System (Bio-Rad, CA, USA).

Cell proliferation assay

Cell proliferation was determined by Cell Counting Kit-8 (CCK-8; Dojindo Laboratories, Kumamoto, Japan). Jurkat cells were seeded into 24-well plates at a density of 3×10^5 cells per well. After 24 h culture in complete growth medium, cells were allowed to grow in serum-free medium (100μL/well) for another 24 h. Cells were then transfected with miR-200b mimic, anti-miR-200b or miR-NC and then incubated with a dye solution (CCK-8 solution diluted with serum-free medium at 1:10) at 37°C for 60 min. The number of viable cells was determined according to the color conversion measured by microplate reader with absorbance at 450 nm. Proliferation rates were determined at 24, 48 and 72 h after transfection.

Apoptosis determination

Apoptosis assay was performed using Annexin V-fluorescein isothiocyanate (FITC) Apoptosis Detection Kit I (BD Bioscience, San Diego, CA, USA) following the manufacturer's instruction. After 48 h of transfection with RNA oligonucleotides, Jurkat cells were harvested, centrifuged, and resuspended in 100 μl of FITC-binding buffer. Approximately 5 μl of ready-to-use Annexin V-FITC (BD Bioscience, CA, USA) and 5 μl of PI were added to the mixture. Cells were incubated for 30 min. Annexin V-FITC and PI fluorescence were assessed by BD FACS Calibur flow cytometer (BD Technologies) and analyzed by CellQuest software (BD Bioscience).

Cell invasion assays

Cell invasion was measured in 12-well transwell chambers with 8-μm pore-size (Corning, Shanghai,

China). Briefly, a total of 8×10^4 cells was suspended in 500 µL of serum-free medium and added to the upper chamber of Transwells pre-coated with Matrigel (200 µg/ml, 37°C for 40 minutes) (BD Bioscience). The lower chamber was filled with 1.5 mL culture medium containing 100 ng/ml CXCL12 which served as a chemoattractant. After 24 h of incubation, the filters were fixed in methanol for 30 min. Cells that failed to invade through the pore were carefully moved by cotton swabs and the bottom surface of the membrane was stained with 0.1% crystal violet for 20 min. Five random fields were counted per chamber under microscope (Carl Zeiss, Berlin, Germany).

Western blotting

Total protein was extracted from cultured cells using Ripa buffer supplemented with protease inhibitor cocktail (Sigma, ST. Louis, MI, USA). Protein concentration was determined by bicinchoninic acid (BCA) protein assay kit (Nanjing KeyGEN Biotech, Jiangsu, China). Cell lysates were re-suspended in SDS sample loading buffer, separated by 10% SDS-PAGE gel and transferred onto PVDF membrane (Millipore, Bedford, MA, USA). The membranes were blocked in Tris-buffered saline with 0.2 % of Tween 20 (TBST) containing 5% w/v non-fat milk. Western blotting was performed with primary antibodies targeting NOTCH1 (Millipore, Bedford, MA, USA) and β-actin (Abnova, Taiwan, China), followed by the secondary antibody conjugated with horseradish peroxidase (Sigma). Immunobands were visualized using ECL and Bio-rad Image station (Bio-rad, CA, USA).

Statistical analysis

Data are expressed as means ± standard deviation (SD) of quadruplicates. Statistical analysis was determined by one-way ANOVA and difference between two groups was assayed by student's *t*-test. $P < 0.05$ was considered statistically significant.

RESULTS

Mir-200b impacts Jurkat cell proliferation, survival and invasion

The impact of miR-200 in acute Lymphocyte leukemia was examined in Jurkat cells. Jurkat cells were transfected with miR-200b mimics as well as anti-miR-200b inhibitors to examine the gain and loss of function. Efficient modulation of miR-200 gene expression was confirmed by real time RCR determination; as indicated in Fig. 1A, Jurkat cells receiving miR-200b showed 3-fold increase in miR-200b gene expression. In contrast, anti-miR-200b treatment induced over 60% decrease in miR-200b gene expression.

Using these cell models, we further evaluated the impact of miR-200b expression on tumor cell proliferation, apoptosis and invasion. CCK-8 proliferation assay was used to evaluate cell proliferation during a 4-day period. In agreement with reports on other tumor cell lines, miR-200b expression in Jurkat cells significantly inhibited the cell growth, as illustrated by attenuated cell proliferation in miR-200 mimic transfected cells compared with cells receiving control miRNA. Conversely, stimulated cell growth was observed in cells receiving miR-200b inhibitor (Fig. 1B).

Similar experimental approaches were adopted to determine the effect of miR-200b on tumor cell apoptosis (Fig. 1C) and invasion (Fig. 1D), crucial processes for tumor cell chemoresistance and metastasis. Over-expression of miR-200b using miR-200b mimics markedly stimulated Jurkat cell apoptosis while impeded cell invasion and migration, whereas attenuation of miR-200b expression by the application of miR-200b inhibitor prevented Jurkat cells from apoptosis and enhanced Jurkat cell invasion. Findings obtained from these experiments further confirmed miR-200b as a therapeutic target in T-ALL.

miR-200 modulates NOTCH1 expression in T-ALL

In general, microRNAs exert their functions through the regulation of a cluster of target genes crucial for the physiological pathways. To explore the molecular mechanism linked to the miR-200b function, we screened several intracellular signaling pathways and identified that NOTCH1 signaling might be targeted by miR-200b. As we can see from Fig.2, NOTCH1 expression is prone to miR-200b regulation, reflected by a substantial decrease in NOCH1 protein expression in response to miR-200 activation versus a marked increase in NOCH1 expression to miR-200b inhibition.

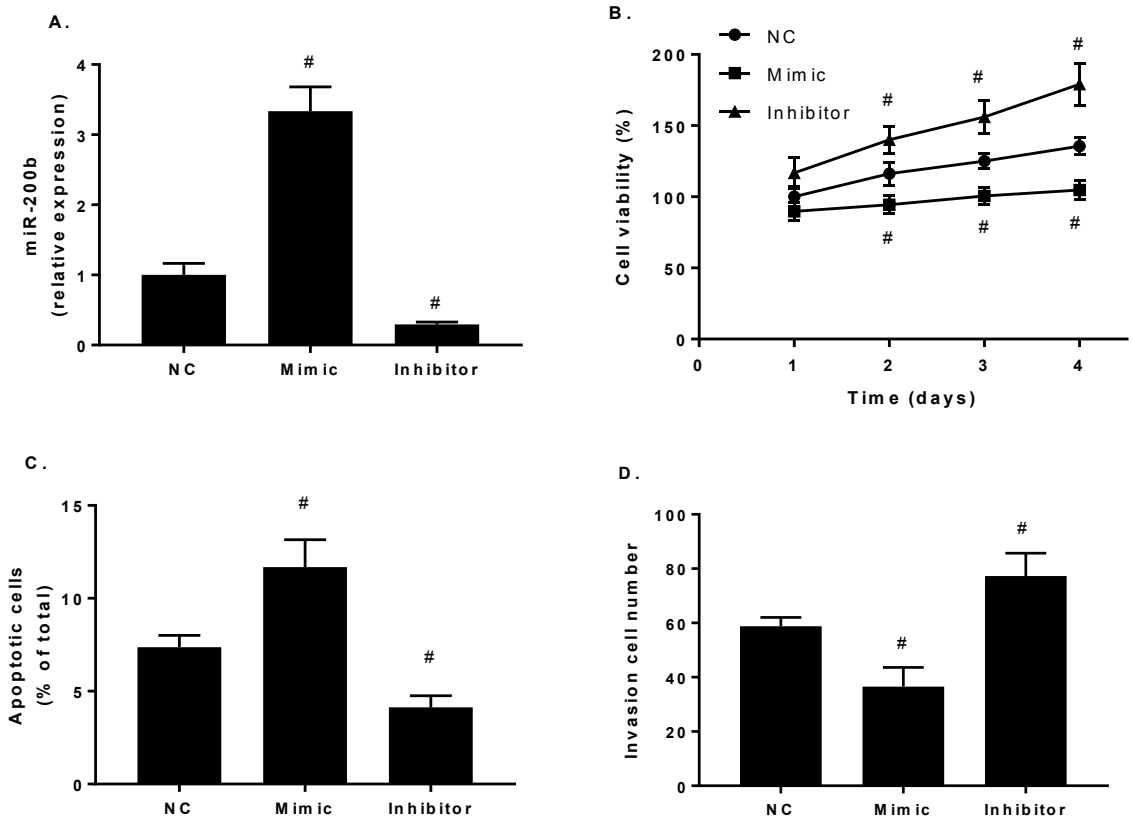

Fig. 1. *miR-200b affects the proliferation, survival and invasion of Jurkat cells. Jurkat cells were transfected with miR-200b mimic or inhibitors. Cells transfected with negative control miRNA were used as negative control (NC).* ***A)*** *miR-200b expression determined by QPCR. Values shown are relative expression normalized to U6.* ***B)*** *Cell growth rate was determined by CCK-8 assay.* ***C)*** *Cell apoptosis. The percentage of apoptotic cells was calculated by analyzing Annexin V/PI double staining followed by flow cytometry.* ***D)*** *Cell invasion was determined by transwell invasion assay. Similar results were observed in three separate experiments. #, P<0.05.*

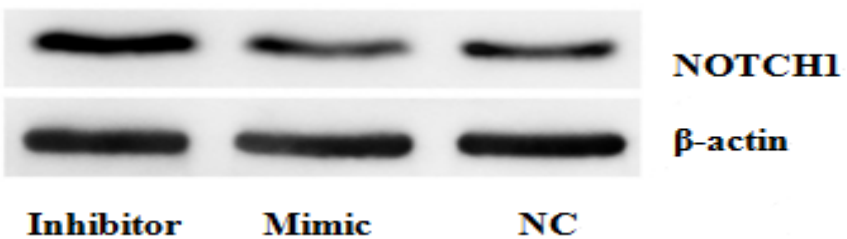

Fig. 2. *NOTCH1 protein was down-regulated by miR-200b. Jurkat cells were transfected with miR-200b mimics or inhibitors. Cells transfected with negative control miRNA were used as control (NC). Cells were harvested, and total protein was isolated from cell lysates. NOTCH1 protein expression was determined by Western blotting analysis. β-actin was used as reference protein. Similar results were observed in two separate experiments.*

DISCUSSION

In this study, we were able to define that miR-200b mimics substantially inhibited Jurkat cell proliferation and invasion while significantly stimulating cell apoptosis compared to the control miRNA-treated cells. In contrast, Jurkat cells treated with anti-miR200 demonstrated induction of cell growth and invasion but repression of cell apoptosis. Such effects were accompanied by the corresponding alteration in NOTCH1 expression, suggesting that NOTCH1 might be the target gene for miR-200b modulated leukemia cell growth and invasion.

The identification of the NOTCH1 signaling as miR-200b target gene further indicates that miR-200b might be a potent modulator for the progression of acute T-cell leukemia. It has been reported that sustained NOTCH1 signaling controls the cell growth, proliferation and survival in T-ALL through modulating the intracellular pathways, such as PI3K/AKT, NF-κB, cAMP/PKA, and JAK/STAT which subsequently impact a broad array of downstream target genes (8). NOTCH1 signaling impacts T-lineage-specific IL-7Rα gene expression in leukemia (9). Sustained NOTCH1 activation promotes leukemic cell growth by directly inducing the expression of c-myc (10). In addition to promoting anabolic cell growth, NOTCH1 signaling has shown to directly promote proliferation via increased G1/S cell cycle progression in T-ALL (11). More importantly, NOTCH1 signaling is pivotal in chemoresistance in T-ALL, as illustrated by the finding that NOTCH1 inhibition by gamma secretase inhibitors reverse resistance to glucocorticoids in T-ALL (12). In summary, our findings suggest that miR-200b might be a potential therapeutic target for T-ALL through its inhibition of the NOTCH1 signaling. Future mechanistical analysis will be focused on elucidating the molecule signaling pathway of miR200/NOTCH1 and its implications in the chemoresistance in T-ALL.

ACKNOWLEDGEMENTS

This work was supported by Zhejiang Medical and Health Science and Technology Project (2018KY242).

REFERENCES

1. Van Vlierberghe P, Ferrando A. The molecular basis of T cell acute lymphoblastic leukemia. J Clin Invest 2012; 122(10):3398-406.
2. Weng AP, Ferrando AA, Lee W, et al. Activating mutations of NOTCH1 in human T cell acute lymphoblastic leukemia. Science 2004; 306(5694):269-71.
3. Roti G, Stegmaier K. New approaches to target T-ALL. Front Oncol 2014; 4:170.
4. Vilimas T, Mascarenhas J, Palomero T, et al. Targeting the NF-kappaB signaling pathway in Notch1-induced T-cell leukemia. Nat Med 2007; 13(1):70-77.
5. Humphries B, Yang C. The microRNA-200 family: small molecules with novel roles in cancer development, progression and therapy. Oncotarget 2015; 6(9):6472-98.
6. Tellez CS, Juri DE, Do K, et al. EMT and stem cell-like properties associated with miR-205 and miR-200 epigenetic silencing are early manifestations during carcinogen-induced transformation of human lung epithelial cells. Cancer Res 2011; 71(8):3087-97.
7. Sun Y, Shen S, Liu X, et al. MiR-429 inhibits cells growth and invasion and regulates EMT-related marker genes by targeting Onecut2 in colorectal carcinoma. Mol Cell Biochem 2014; 390(1-2):19-30.
8. Tzoneva G, Ferrando AA. Recent advances on NOTCH signaling in T-ALL. Curr Top Microbiol Immunol 2012; 360:163-82.
9. González-García S, García-Peydró M, Martín-Gayo E, et al. CSL-MAML-dependent Notch1 signaling controls T lineage-specific IL-7R{alpha} gene expression in early human thymopoiesis and leukemia. J Exp Med 2009; 206(4):779-91.
10. Medyouf H, Gusscott S, Wang H, et al. High-level IGF1R expression is required for leukemia-initiating cell activity in T-ALL and is supported by Notch signaling. J Exp Med 2011; 208(9):1809-22.
11. Joshi I, Minter LM, Telfer J, et al. Notch signaling mediates G1/S cell-cycle progression in T cells via cyclin D3 and its dependent kinases. Blood 2009; 113(8):1689-98.
12. Wang Z, Li Y, Ahmad A, et al. Targeting Notch signaling pathway to overcome drug resistance for cancer therapy. Biochim Biophys Acta 2010; 1806(2):258-67.

JOURNAL OF BIOLOGICAL REGULATORS & HOMEOSTATIC AGENTS Vol. 32, no. 6, 1473-1477 (2018)

LETTER TO THE EDITOR

DIFFERENTIAL EXPRESSION OF CYP2J2 GENE AND PROTEIN IN *CAMELUS DROMEDARIUS*

S. KAMEL, M. IBRAHIM, E.T. AWAD, H.M.A. EL-HINDI and S.A. ABDEL-AZIZ

Biochemistry and Chemistry of Nutrition Department, Faculty of Veterinary Medicine, Cairo University, Giza, Egypt

Received June 16, 2018 – Accepted September 12, 2018

CYP2J2 is a member of the cytochrome P450 superfamily. It had been described in different mammalian species; however, no studies have described this gene in *Camelus dromedarius*. CYP2J2 is an epoxygenase enzyme which oxidizes various fatty acids, mainly arachidonic acid, via NADPH-dependent epoxidation to generate epoxyeicosatrienoic acids (EETs). It is a multi-functional enzyme that plays crucial roles in inflammation, cancer, drug metabolism, and embryo development. It controls the water re-absorption in the kidney and maintains the blood pressure and glucose homeostasis. This study is considered the first report investigating the differential expression profiles of the CYP2J2 mRNA and protein in the liver, heart, and kidney of *Camelus dromedarius*. A total of 30 samples were used to determine the expression of both CYP2J2 mRNA and protein using qRT-PCR and western blotting methods, respectively. The mRNA level of *CYP2J2* was significantly elevated in the liver compared to that in the heart and kidney. The tissue distribution of the CYP2J2 protein was coherent to its transcript level in the kidney, but not in the liver and heart samples. The difference between the CYP2J2 mRNA and protein distributions in the three studied organs may be attributed to the mechanism by which the CYP2J2 might be involved in the adaptability of the camel to the arid environment.

To the Editor,

The *Camelus dromedarius* has well-developed adaptive mechanisms that maintain the physiological and productive processes to the hostile environment of arid and desert areas (1). CYP2J2 is a member of the cytochrome P450 epoxygenase enzymes. It is encoded by the *CYP2J2* gene. It metabolizes the arachidonic acid mainly via NADPH-dependent epoxidation to produce four regioisomers of epoxyeicosatrienoic acids (EETs) (2). The formed EETs are rapidly metabolized by soluble epoxide hydrolase (sEH) to produce the corresponding fatty acid diols, dihydroxyeicosatrienoic acids (DHETs). Therefore, inhibition of sEH activity can be used as a means of studying the biological functions of EETs (3). CYP2J2 is a multifunctional enzyme that plays vital roles in inflammation, cancer (3), drug metabolism (4), and embryo development (5). It controls the water re-absorption in the kidney (6) and maintains the blood pressure (7) and glucose homeostasis (8). EETs are vasodilators and natriuretic substances that increase the sodium excretion and lower the arterial pressure (7). EETs, inhibit inflammation via blocking the nuclear factor-κB (NF-κB) pathway (3). The current study aimed to determine the level of expression of the CYP2J2 mRNA and protein in three organs (liver, heart, and kidney) of *Camelus*

Key words: camel, CYP2J2, epoxygenase, EETs, expression, liver, kidney, heart

Mailing address:
Dr Shaimaa Kamel,
Biochemistry and Chemistry of Nutrition Department,
Faculty of Veterinary Medicine,
Cairo University,
Giza, Egypt
e-mail: vetsh85@gmail.com

0393-974X (2018)

dromedarius. This is the first report dealing with this determination. The comparative mRNA expression levels of the *CYP2J2* in the different tissues may elucidate the regulation of this gene in the camel and improve our understanding of the genetic profile of the *CYP2J2* in the three major organs and to identify new potential highlight useful for further studies. Then, the CYP2J2 protein expression levels in the same tissues may reveal the functional regulation of this protein according to the environmental requirements for camel adaptation in the deserts.

MATERIALS AND METHODS

Sampling

Thirty fresh different tissues samples (liver, kidney, and heart) were collected, from slaughterhouses in Cairo, from ten clinically normal adult male Arabian camels (Age: 3-5 years; weight: 350-550 kg). Samples were collected from highly cellular regions of the different tissues and from the cellular part at the cortical-medullary junctions in the kidney samples. Each sample was divided into two portions; one part for transcriptomic analysis and the other for proteomic analysis of the CYP2J2. The consent was obtained from the Institutional Animal Care and Use Committee (IACUC) prior to carrying out the experimental procedures on the camel. Certification for this work has been assigned (CU II F C 63 18).

Transcriptional expression of the CYP2J2 gene in different tissues

Real-time reverse transcription (qRT)-PCR was used to analyze the expression of the putative gene at the mRNA level in the liver, heart, and kidney of the camel. Total RNA was isolated from 30 mg of the studied tissues using the GF-1 Total RNA Extraction Kit (Vivantis, Cat. No. GF-TR-050) according to the manufacturer's instructions. RNA quality and quantity were assessed using a Nanodrop ND-1000 spectrophotometer (Nanodrop Technologies). The cDNA was generated using Viva 2-steps RT-PCR Kit (Vivantis, Product No. RTPL 12) according to the provided protocol and the mRNA levels were detected using qRT-PCR, performed with the SYBR green kit (TaKaRa). The qRT-PCR primers, amplifying a 212-bp fragment were designed based on multiple sequence alignment of the *CYP2J2* sequences for human (AB080265.1), rat (NM_175766.3), sheep (NM_001077210.1) and the three camel species predicted sequences [*Camelus dromedarius* (XM_010988583.1), *Camelus bacterianus* (XM_010949871.1), and *Camelus ferus* (XM_006187584.2)]. The primer pairs were designed in the most conserved regions among the different species. The primers were as follows: 5'-CCCTACACCAACGCTGTCAT-3' (sense) and 5'-CCATTCTCCAGAAAGTGCTC-3' (antisense). The cycle conditions were as follows: 95°C for 3 min; 40 cycles of 95°C for 15 s, 62°C for 30 s, and 72°C for 15 s. Each qRT-PCR was conducted in triplicate. The GAPDH gene was used as an internal control (accession No. EU331417.1). The data obtained from the qRT-PCR were analyzed using CT, ΔCT, ΔΔCT MxPro QPCR Software (Stratagene) (9). The PCR products were analyzed on 2% agarose gel electrophoresis to confirm the amplification specificity and amplicon size, purified and sequenced. The sequencing result was analyzed by using the blast database to verify that the amplified products were the *CYP2J2* gene.

Extraction of total proteins

Total proteins were extracted from the liver, heart, and kidney by using the NP-40 lysis buffer which is a popular buffer for studying proteins that are cytoplasmic or membrane-bound, or for whole cell extracts to reach the membrane-bound CYP2J2 protein (http://www.abcam.com/protocols/sample-preparation-for-western-blot) in combination with proteases and phosphatases inhibitors mix (Catalog#BWR1022). The purified protein concentration was determined.

Western blot assay

The Western blotting analysis was conducted as follows. Approximately 20 mg of protein from each sample were loaded onto a 10% SDS polyacrylamide gel and transferred onto PVDF membranes. The membranes were blocked for 1 h at room temperature with PBS/0.05 Tween 20 containing 5% powdered milk. The membranes were then probed with primary antibodies raised against anti-human CYP2J2 polyclonal antibodies (Santa Cruz Biotechnology, USA) using the mini trans-blot system (Bio-Rad). The predicted CYP2J2 protein (*Camelus dromedarius* XP_010986885.1) from the gene bank database give high similarity with the amino acids sequence

as the immunogen of the human CYP2J2 antibody from Santa Cruz. The membranes were blocked with 5% fat-free milk in TBST (Tris-buffered saline including 0.1% Tween) and incubated with the blocking solution using the optimized dilutions overnight at 4°C. The membranes were washed and treated for 1 h at 25°C with a secondary antibody (horseradish peroxidase conjugate). The results were confirmed through three independent assays. The protein bands were quantified by densitometry using Quantity One software (Bio-Rad, Hercules, CA, USA).

Statistical analysis

All data are presented as mean ± SEM. Statistical analysis was carried out using the SPSS software program version 24 (SPSS Inc., USA). Shapiro Wilk test was conducted to confirm the normal distribution. One way analysis of variance (ANOVA) was used to assess the significant differences among the different groups at $P< 0.05$.

RESULTS

Tissue distribution of the CYP2J2 mRNA

The qRT-PCR experiments examined the tissue distribution of the *CYP2J2* mRNA among the studied camel tissues. A prominent fragment of the predicted size (212 bp) was amplified from the RNA extracted from the three tissues of adult healthy camels (heart, liver, and kidney). The *CYP2J2* gene was expressed in all the examined tissues and particularly in the liver. The heart showed the least mRNA level compared to both liver and kidney. Our results recorded a significant difference in the *CYP2J2* mRNA level between the liver and kidney and between the liver and heart, while a non-significant difference was observed between the kidney and heart (Fig. 1).

Tissue expression of the CYP2J2 protein

The Western blot assay using polyclonal antibodies anti-human CYP2J2 showed a cross-reactive band with an expected molecular weight of 51334.89 Da (Authors' study under publication). This molecular weight comes in agreement with the calculated molecular weight of the purified recombinant protein (56707 Da) in the predicted *Camelus dromedarius* CYP2J2 (XP_010986885.1) and (57480 Da) in the Human CYP2J2 protein (NP_000766.2). Anti-CYP2J2 IgG recognized discrete bands from the heart, liver and kidney of the camel. The CYP2J2 protein expression was significantly different between the different tissues (liver, kidney, and heart) of *Camelus dromedarius* (Fig. 2).

DISCUSSION

Our comparative investigation of the CYP2J2 mRNA and protein expression levels delivered

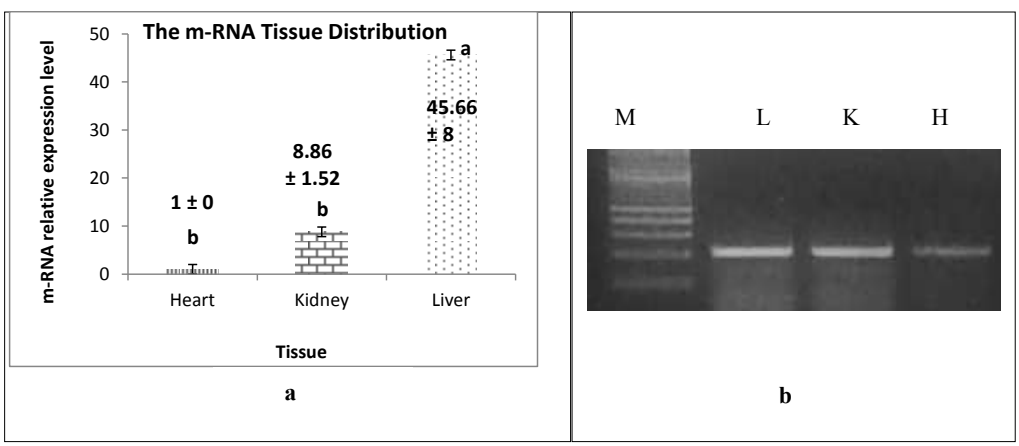

Fig. 1. *CYP2J2 mRNA relative expression level in different tissues of Camelus dromedarius.* ***a****) Fold change of mRNA expression of CYP2J2 in different tissues of Camelus dromedarius. Data are represented as mean ± SEM. Groups having different superscripts letters are significantly different from each other at P < 0.05. Groups having similar superscript letters are non-significantly different from each other at P < 0.05.* ***b****) PCR products of 212 bp of CYP2J2 in different tissues of Camelus dromedarius were separated by electrophoresis on 2% agarose gel and stained with ethidium bromide. M: Marker; L: Liver; K: Kidney; H: Heart.*

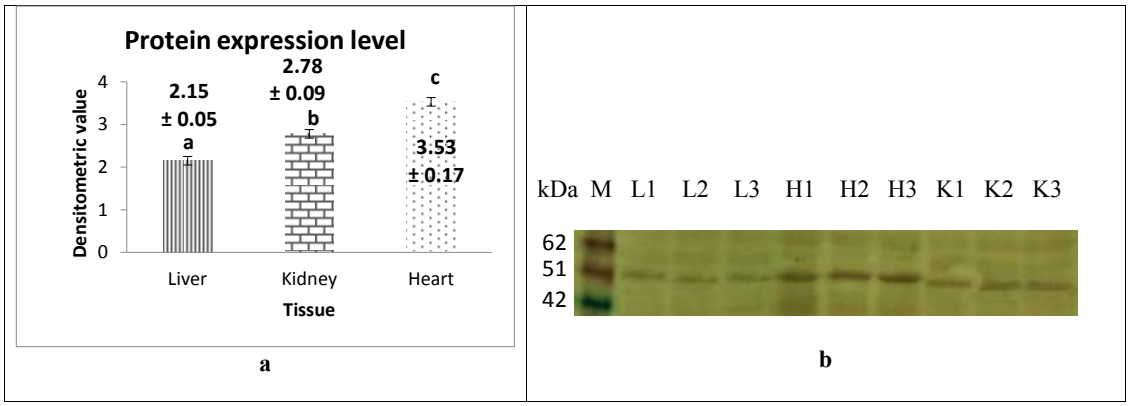

Fig. 2. *CYP2J2 protein expression level in different tissues of Camelus dromedarius.* ***a)*** *The densitometric values of various protein bands. Data are represented as mean ± SEM. Groups having different superscript letters are significantly different from each other at P < 0.05.* ***b)*** *The PVDF membrane of the western blot of the CYP2J2 protein of expected size of 51334.89 Da in different tissues of Camelus dromedarius. M: Marker. L1, L2, L3: Liver samples. H1, H2, H3: Heart samples. K1, K2, K3: Kidney samples.*

concerns about their distribution among the three major organs in the Arabian camel. The current findings recorded a significantly elevated level of the *CYP2J2* mRNA in the liver compared to the kidney and heart which showed a non-significant variation between each other. It was reported previously that the *CYP2J2* gene expression level is higher in the liver than the heart in cattle (10) and sheep (5). The abundant *CYP2J2* mRNA in the liver may be attributed to the critical role played by the CYP superfamily for xenobiotic metabolism. Our study expanded to find out whether the differences reported in the mRNA expression of the *CYP2J2* among the three tissues are related to the protein levels. The protein expression was studied by Western blot in the same tissues. The CYP2J2 protein level recorded the highest value in the heart followed by the kidney and liver, respectively. The CYP2J2 protein was reported to be the most abundant isoform in the human heart (11), while in the liver, the CYP2J2 abundance is less than 1% of the total CYP450 content. The ultimate expression of the CYP2J2 protein in the heart is attributed to its essential role in the blood homeostasis which might explain the vital function of the CYP2J2 for camel adaptation in the desert. The expression of the CYP2J2 protein is relatively high in the kidney. This elevation may be related to its central role in the water re-absorption and natriuresis. The lowest expression of the CYP2J2 protein in the liver may be attached to the minor function of the liver CYP2J2 in drug metabolism for the camel. However, both mRNA and protein expressions were detected in the three tissues under study, their expression levels were not mirrored in each tissue. We detected abundant *CYP2J2* mRNA in the liver using qRT-PCR but not the protein by Western blot. Controversially, the mRNA of the heart was low compared to the prominent protein level detected.

In conclusion, a clear variation in the CYP2J2 expression at the mRNA and protein levels was recorded among the liver, heart, and kidney of *Camelus dromedarius.* The current results may be supportive in expanding the fundamental knowledge of the potential physiological functions of the CYP2J2 protein. Additionally, our findings can be beneficial for future studies on the mechanistic role of the CYP2J2 in the Arabian camel.

REFERENCES

1. Bouâouda H, Achâaban MR, Ouassat M, et al. Daily regulation of body temperature rhythm in the camel (Camelus dromedarius) exposed to experimental

desert conditions. Physiol Rep 2014; 2(9).
2. Xu X, Li R, Chen G, Hoopes SL, Zeldin DC, Wang DW. The role of cytochrome P450 epoxygenases, soluble epoxide hydrolase, and epoxyeicosatrienoic acids in metabolic diseases. Adv Nutr 2016; 7(6):1122-28.
3. Zhang G, Kodania S, Hammock BD. Stabilized epoxygenated fatty acids regulate inflammation, pain, angiogenesis, and cancer. Prog Lipid Res 2014; 53:108-23.
4. Zanger UM, Schwab M. Cytochrome P450 enzymes in drug metabolism: Regulation of gene expression, enzyme activities, and impact of genetic variation. Pharmacol Ther 2013; (138):103-41.
5. Messina A, Nencioni S, Gervasi PG, Gotlinger KH, Schwartzman ML, Longo V. Molecular cloning and enzymatic characterization of sheep CYP2J. Xenobiotica 2010; 40(2):109-18.
6. Jirimutu, Wang Z, Ding G, et al. Genome sequences of wild and domestic Bactrian camels. Nat Commun 2012; 3:1202.
7. Imig JD. Epoxyeicosatrienoic acid, 20-hydroxyeicosatetraenoic acid, and renal microvascular function. Prostaglandins Other Lipid Mediat 2013; 104-105:2-7.
8. Chen L, Fan C, Zhang Y, et al. Beneficial effects of inhibition of soluble epoxide hydrolase on glucose homeostasis and islet damage in a streptozotocin-induced diabetic mouse model. Prostaglandins Other Lipid Mediat 2013; 104-105:42-48.
9. Morgan AM, Ibrahim MA, Hussien AM. The potential protective role of akropower against atrazine induced humoral immunotoxicity in rabbits. Biomed Pharmacother 2017; 96:710-15.
10. Grassoa E, Longob V, Coceania F, Gervasi PG. Cytochrome P450 expression and catalytic activity in coronary arteries and liver of cattle. Biochim Biophys Acta 2005; 1722:116-23.
11. Michaud V, Frappier M, Dumas MC, Turgeon J. Metabolic activity and mRNA levels of human cardiac CYP450s involved in drug metabolism. PLoS One 2010; 5(12):e15666.

JOURNAL OF BIOLOGICAL REGULATORS & HOMEOSTATIC AGENTS Vol. 32, no. 6, 1479-1483 (2018)

LETTER TO THE EDITOR

CARBON MONOXIDE MODULATES MELATONIN SYNTHESIS IN PORCINE PINEAL CELLS *IN VITRO*: A PRELIMINARY STUDY

M. ROMEROWICZ-MISIELAK[1], A. KOZIOROWSKA[2], O. KUSAK[1], A. GÓRKA[3], D. BRODA[4], E.M. WASZKIEWICZ[5] and M. KOZIOROWSKI[3]

[1]Laboratory of Bioelectromagnetism, Faculty of Biotechnology, University of Rzeszow, Rzeszow, Poland; [2]Laboratory of Bioelectromagnetism, Faculty of Mathematics and Natural Sciences, University of Rzeszow, Rzeszow, Poland; [3]Department of Physiology and Reproduction of Animals, Faculty of Biotechnology, University of Rzeszow, Rzeszow, Poland; [4]Laboratory of Molecular Biotechnology, Faculty of Biotechnology, University of Rzeszow, Rzeszow, Poland; [5]Department of Animal Anatomy and Physiology, Faculty of Biology and Biotechnology, University of Warmia and Mazury in Olsztyn, Olsztyn, Poland

Received May 28, 2018 – Accepted September 17, 2018

Two main isoforms of heme oxygenase (HO-1 and HO-2), the main enzyme of heme metabolism, were identified in the pineal gland. This suggests possible interactions between the melatonin synthesis pathway and the HO system. The aim of this study was to investigate the participation of carbon monoxide (CO), an HO by-product, on the melatonin synthesis pathway. Tests were carried using primary cell cultures of porcine pineal glands. The tricarbonyldichlororuthenium (II) dimer (CORM-2) compound was used as a CO donor at concentrations of 1 and 3 μM, as low concentrations of CORM-2 affect the regulation of the melatonin synthesis pathway in pineal cells *in vitro*. In addition, the presence of Sn-protoporphyrin-IX, an HO inhibitor, changed the melatonin response of pineal cells. These results suggest the existence of an intermediate mechanism in the pineal gland, which is associated with HO activity, that is involved in the modulation of melatonin synthesis.

To the Editor,

Information on the environmental lighting condition is neuronally encoded by the retina and converted into elevated nocturnal synthesis of the hormone melatonin as a darkness message for the body. The key regulatory enzyme in rhythmic melatonin biosynthesis is arylalkylamine N-acetyltransferase (AANAT) (1). This enzyme is subject to transcriptional (2), posttranscriptional (mRNA degradation) (3) and posttranslational (proteolysis) (4) regulatory mechanisms. The increased production of melatonin during the night reflects increased AANAT activity and, in many species, increased *Aanat* transcription (5). Heme oxygenase (HO) plays an important role in regulating the intracellular heme level by catalysing heme degradation, which results in the formation of biliverdin, carbon monoxide (CO) and free iron (6). Jacobs et al. showed that mRNA for two isoforms of HO, *Ho-1* and *Ho-2,* were present in the pineal glands of rats but that neither isoform was photoregulated (7). Melatonin increases HO-1

Key words: melatonin, carbon monoxide, arylalkylamine N-acetyltransferase, hydroxyindole-O-methyltransferase, pineal cells, heme oxygenase

Mailing address:
Dr Maria Romerowicz-Misielak,
University of Rzeszow, Laboratory of Bioelectromagnetism,
Faculty of Biotechnology, Al. Rejtana 16c,
35-959 Rzeszow, Poland
Tel./Fax: +48 17 851 87 64
e-mail: m_romer@interia.pl

0393-974X (2018)

activity and contributes to the restriction of oxidative tissue damage (8). The activation of both HO-1 and HO-2 within areas primarily involved in melatonin synthesis suggests a possible interaction between the melatonin synthesis pathway and the HO system. The importance of CO in regulating melatonin release was previously assessed *in vivo* (9). It is difficult to determine the effective local concentration of exogenous CO added to biological systems as CO is a diffusion molecule with many high-affinity biological targets, therefore, these studies have been simplified in this research model. The aim of this study was to undertake preliminary investigations to characterise the participation of CO, a by-product of the HO system, in the modulation of melatonin release by pineal cells.

MATERIALS AND METHODS

Pinealocyte culture

Primary pinealocyte cultures were prepared from the pineal glands of adult male pigs as previously described (10) with some modifications. Briefly, pinealocytes were obtained by trypsinisation (0.25%, 37°C, 15 min) followed by mechanical dispersion in the presence of a trypsin inhibitor (chicken egg white). After centrifugation (15 min, 1000 x g), the cells were resuspended in Dulbecco's Modified Eagle's Medium (DMEM) supplemented with 7.5% fetal bovine serum (FCS), 7.5% horse serum, 100 U/mL of penicillin and 100 µg/mL of streptomycin. The total number of cells and survival were estimated by Trypan blue exclusion. The survival rate was ≥90%. Cells (0.5 x 10^5/cm^2) were seeded on six-well plates and maintained at 37°C and 5% CO_2 for 18 h prior to the experimental procedure.

In vitro treatments

In this study, the CO-releasing molecule, tricarbonyldichlororuthenium dimer (CORM-2; Sigma-Aldrich), and the commonly-used competitive HO-1 inhibitor, tin protoporphyrin-IX (SnPPIX; Sigma-Aldrich), were used to assess the effects and potential mechanisms of locally-released CO in the modulation of melatonin synthesis. SnPPIX is synthetic heme analog that selectively inhibits HO-1 over HO-2. It also weakly inhibits nitric oxide synthase and soluble guanyl cyclase. CORM-2 was prepared in dimethyl sulfoxide (DMSO) at a stock solution of 15 mM, while the stock solution (15 mM) of SnPPIX was dissolved in 0.1 M NaOH. Both substances were then diluted in culture medium at the desired working concentration. In control experiments, cells were treated with the same concentration of DMSO or NaOH, and the former did not exhibit any significant activity on either melatonin release from pinealocyte cells or *Aanat* and *Hiomt* expression. The concentrations of CORM-2 and SnPPIX used were based on a previous report that used these compounds in cell culture experiments (11). CORM-2 was used at working concentrations of 1 and 3 µM and either applied alone or in combination with SnPPIX (5 µM). The effect of CO on melatonin synthesis parameters was assessed 24 h after the addition of test compounds.

Gene expression

RNA isolation and reverse transcription

Total RNA was extracted from cell cultures using the

Table I. *Sequences of the primers used in the PCR reaction.*

Genes	Forward primer	Reverse primer
Hiomt	CATGGTGTCCCAGGTTCTCT	CAGCTTCAGGGACACACAGA
Aanat	TGGATGTGACCAGCCATAGA	TGGAACAGCTTGCTTCATTG
Gapdh	CGTCCCTGAGACACGATGGT	CCCGATGCGGCCAAAT

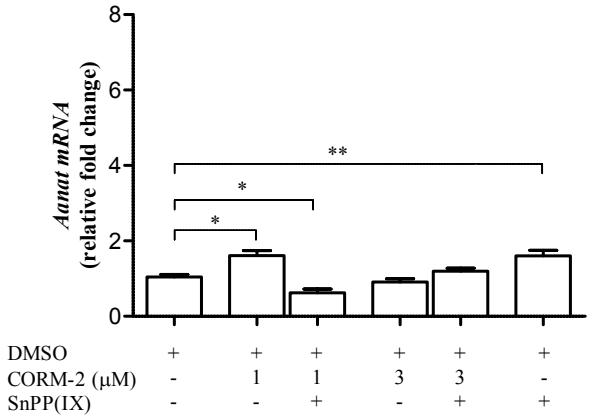

Fig. 1. *Relative Aanat gene expression level in the pineal cells of Sus scrofa. Cells were untreated (control) or stimulated with test compounds for 24 h. The results are presented as mean ± SEM. *P ≤ 0.05; **P ≤ 0.01.*

Total RNA Kit (A&A Biotechnology). Each RNA pellet was dissolved in RNase-free water, and the quantity and quality of RNA was assessed spectrophotometrically at 260 and 260/280 nm, respectively (NanoDrop, Thermo Scientific). Extracted RNA (1 μg) was reverse transcribed using a High Capacity cDNA Reverse Transcription kit (Applied Biosystems).

Expression of Hiomt and Aanat genes

Messenger RNA (mRNA) levels of *Hiomt* and *Aanat* were determined by real-time quantitative PCR using the SYBR Green method (Power SYBR Green Master Mix, Applied Biosystems). Oligonucleotide primer pairs (Table I) were constructed based on the GenBank sequence using Primer3 software. The results were analysed on the StepOnePlus System (Applied Biosystems) and normalised against the housekeeping gene, glyceraldehyde-3-phosphate dehydrogenase.

Melatonin analysis

The concentration of melatonin released into the cell medium by pinealocytes was measured using high-performance liquid chromatography (HPLC). Analysis was performed using a Dionex UltiMate 3000 equipped with an electrochemical coulometric array detector (Esa CoulArray (ESA Inc.). The HPLC equipment used in the experiment included a pump and autosampler (Dionex, Sunnyvale, CA, USA) and ACE 5 C18 column 4.6 x 250 mm (particle size 5 μm, pore size 100 Å) connected to an ACE 5 C18 guard column (Advanced Chromatography Technologies LTD, Scotland). The analysis was carried out by injecting 20 μl of the culture medium samples, or standard, filtered through a syringe filter (0.40 μm), with isocratic mode using acetonitrile-acetate buffer (50 mM sodium acetate, 100 mM acetic acid, pH 5, 0.1 mM EDTA) (25:75, v/v) as a mobile phase at a flow rate of 1 ml min^{-1}, and the column temperature 25°C. Compounds were defined by comparing the value of their potentials, and the correct signal was read at 600 mV. All measurements were performed with Chromeleon Chromatography Data System 6.8 software. Analysis of each sample was performed in triplicate and depended on the incubation time of pinealocytes with CORM. Melatonin stock solution was prepared by dissolving previously weighed amounts of melatonin in HPLC-grade methanol. This stock solution was next diluted with HPLC-grade water which provided melatonin working standards at concentrations of 2000, 5000, 10000, 20000 pg/ml.

Statistical analysis

Statistical analysis was performed using GraphPad Prism 6.0 using a one-way analysis of variance, followed by Bonferroni's post hoc test. Results are presented as mean ± standard error of the mean (SEM). $P < 0.05$ was considered a statistically significant difference.

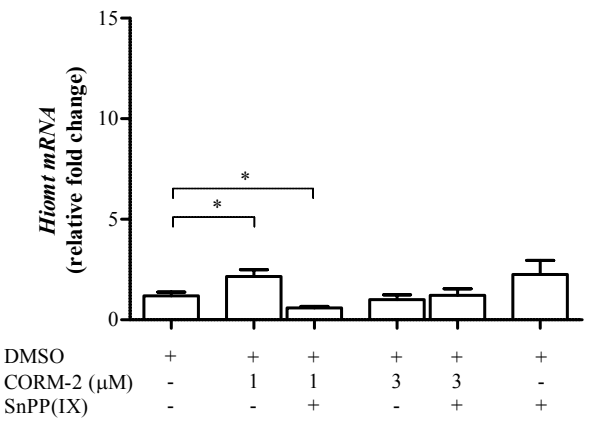

Fig. 2. *Relative Hiomt gene expression level in the pineal cells of Sus scrofa. Cells were untreated (control) or stimulated with test compounds for 24 h. The results are presented as mean ± SEM. *P ≤ 0.05.*

RESULTS

Effects on Aanat mRNA levels

The concentration of *Aanat* mRNA in pineal cells differed significantly depending on the test compound treatment. A significant increase in *Aanat* mRNA levels was observed when CORM-2 treatment (1 μM) ($P \leq 0.05$) or SnPPIX treatment was used alone ($P \leq 0.01$). A significant decrease in *Aanat* mRNA levels was detected after the addition of CORM-2 (1 μM) in combination with SnPPIX ($P \leq 0.05$). The treatment of pineal cells with 3 μM CORM-2 alone or in combination with SnPPIX did not have an effect on *Aanat* mRNA levels

Effects on Hiomt mRNA levels

Treatment of pineal cells with CORM-2 (1 μM) increased *Hiomt* mRNA levels ($P \leq 0.05$). Conversely, incubation with CORM-2 (1 μM) in combination with SnPPIX decreased the expression of *Hiomt* ($P \leq 0.05$). Treatment of pineal cells with 3 μM CORM-2 alone or in combination with SnPPIX did not affect *Hiomt* mRNA levels (Fig. 2).

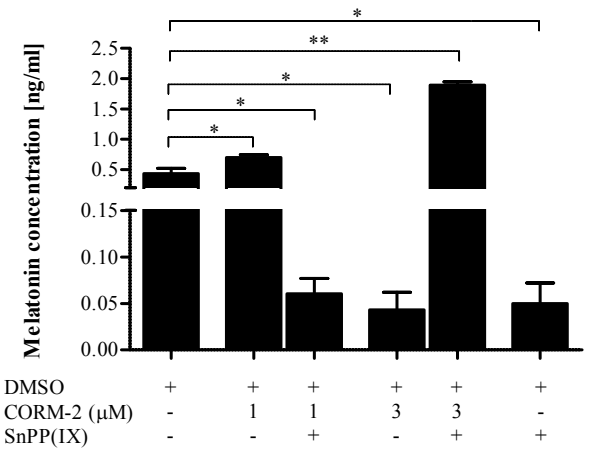

Fig. 3. *Melatonin concentration (ng/mL in culture medium) from the pineal cells of Sus scrofa. Cells were untreated (control) or stimulated with test compounds for 24 h. The results are presented as mean ± SEM. *P ≤ 0.05; **P ≤ 0.01 versus control.*

Effects on melatonin secretion

Analysis of the culture medium revealed that 24-h treatment with 3 μM CORM-2, SnPPIX or a combination of 1 μM CORM-2 and SnPPIX significantly decreased the melatonin content ($P \leq 0.05$). However, melatonin synthesis in pineal cells was four-fold higher when incubated with CORM-2 (3 μM) and SnPPIX when compared with the control ($P \leq 0.01$). Incubation of pineal cells with CORM-2 (1 μM) also increased melatonin synthesis ($P \leq 0.05$).

DISCUSSION

Previous studies conducted on a hybrid of domestic pig and wild boar showed that a two-fold increase in CO in blood flowing into the brain area affected the expression level of the AANAT enzyme in a manner dependent on the length of daylight. At the same time, parallel changes in melatonin levels were observed in the general circulation (9). In the literature, the CO concentrations used vary widely due to a lack of data on the physiological intracellular concentration of CO. Additionally, the expression levels of *Ho-1* and *Ho-2* are different depending on the tissue (12), and may vary depending on HO-1 activity. In this study 1 μM CORM-2 concentration alone or in the presence of the inhibitor changed *Aanat* and *Hiomt* gene expression levels and led to parallel changes in the melatonin concentration in the culture fluid. An increase in the CORM-2 concentration to 3 μM did not cause changes at the mRNA level; however, significant changes were observed in the concentration of melatonin in the culture medium. No marked variation in *Aanat* and *Hiomt* mRNA levels were observed after 3 μM CORM-2 was used alone or in concert with SnPPIX, and changes in the melatonin concentration did not correlate with the expression of these enzymes. This indicates that the regulation of melatonin production could occur by inhibiting cAMP degradation by proteasomal proteolysis of AANAT (4). Coincubation of pineal cells with CORM-2 and a HO inhibitor changed the degree of melatonin synthesis compared to incubation with CORM-2 alone. Melatonin increases HO-1 activity and contributes to the restriction of oxidative tissue damage (8). The blockade of

Ho-1 expression with SnPPIX, an HO-1 inhibitor, probably attenuated HO-1 induction by melatonin. In conclusion, these results suggest the existence of an intermediate mechanism in the pineal gland, which is associated with HO activity, that is involved in the modulation of melatonin synthesis.

REFERENCES

1. Coon SL, Roseboom PH, Baler R, Weller JL, Namboodiri MA, Koonin EV, Klein DC. Pineal serotonin N-acetytransferase: expression cloning and molecular analysis. Science 1995; 270:1681-83.
2. Baler R, Covington S, Klein DC. The rat arlalkylamine N-acetyltransferase gene promoter. cAMP activation via a cAMP-responsive element-CCAAT complex. J Biol Chem 1997; 272:6979-85.
3. Kim TD, Kim JS, Kim JH, et al. Rhythmic serotonin N-acetyltransferase mRNA degradation is essential for the maintenance of its circadian oscillation. Mol Cell Biol 2005; 25:3232-46.
4. Gastel JA, Roseboom PH, Rinaldi PA, Weller JL, Klein DC. Melatonin production: Proteasomal proteolysis in serotonin N-acetyltransferase regulation. Science 1998; 279:1358-60.
5. Ganguly S, Coon SL, Klein DC. Control of melatonin synthesis in the mammalian pinela gland: the critical role of serotonin acetylation. Cell Tissue Res 2002; 309:127-37.
6. Maines MD. Heme oxygenase: function, multiplicity, regulatory mechanisms, and clinical applications. FASEB J 1988; 2(10):2557-68
7. Jacobs RA, Schaad NC, Vanecek J, et al. Pineal nitric oxide synthase, but not heme oxygenase, mRNA is suppressed by continuous exposure to light. Brain Res Mol Brain Res 1999; 70(2):264-72.
8. Kwon KJ, Kim JN, Kim MK, et al. Melatonin synergistically increases resveratrol-induced heme oxygenase-1 expression through the inhibition of ubiquitin-dependent proteasome pathway: a possible role in neuroprotection. J Pineal Res 2011; 50(2):110-23.
9. Romerowicz-Misielak M, Oren DA, Sowa-Kucma M, Tabecka-Lonczynska A, Gilun P, Stefanczyk-Krzymowska S, Koziorowski M. Changes in melatonin synthesis parameters after carbon monoxide increase in the cavernous sinus. J Physiol Pharmacol 2015; 66(4):505-14.
10. Ferreira ZS, Garcia CR, Spray DC, Markus RP. P2Y(1) receptor activation enhances the rate of rat pinealocytes-induced extracellular acidification via calcium-dependent mechanism. Pharmacology 2003; 69(1):33-37.
11. Errico S, Shohreh R, Barone E, Pusateri A, Mores N, Mancuso C. Heme oxygenase-derived carbon monoxide modulates gonadotropin-releasing hormone in immortalized hypothalamic neurons. Neurosci Lett 2010; 471(3):175-78
12. Weber CM, Eke BC, Maines MD. Corticosterone regulates heme oxygenase-2 and NO synthase transcription and protein expression in rat brain. J Neurochem 1944; 63(3):953-62.

LETTER TO THE EDITOR

INFLUENCE OF SERUM HMGB1 LEVEL ON THE INCIDENCE OF RESPIRATORY DISTRESS SYNDROME IN NEONATES

F. XUE[1], C. LIU[1] and S. WANG[2]

[1]Department of Critical Care Medicine, Tianjin Baodi Hospital, Baodi Clinical College of Tianjin Medical University, Tianjin, China; [2]Neonatal Intensive Care Unit, Women and Children Health Institute Futian, University of South China, Shenzhen, China

Received June 28, 2018 – Accepted September 19, 2018

The aim of this study was to analyse the correlation between high mobility group protein B1 (HMGB1) and neonatal respiratory distress syndrome (NDS), and to provide a theoretical basis for its diagnosis and prognosis. Sixty cases of neonates with respiratory distress syndrome were selected and designated as a survival group (36 cases) and a death group (24 cases) according to their prognosis. Sixty healthy neonates were also selected and designated as the control group. Peripheral venous blood and related clinical data of the neonates were collected 12-24 h after birth. Enzyme-linked immunosorbent assay (ELISA) was used to detect the level of HMGB1 in the sera of the two groups. SPSS 17 software was used for statistical analysis of the experimental data. The test results showed that the serum HMGB1 levels of those in the study group were significantly higher than those of the control group, and the difference was statistically significant (P<0.05); the serum HMGB1 levels of those in the death group was significantly higher than those in the survival group, and the difference was statistically significant (P<0.05). Serum HMGB1 level predicts the area under curve (AUC) value of NRDS as 0.872. A serum HMGB1 level of 625.2198pg/mL represents the best boundary value for predicting NRDS. The serum HMGB1 level predicts the AUC of death from NRDS children as 0.912, and a level of 786.7643pg/mL represents the best boundary value for predicting patient death. In conclusion, the level of HMGB1 in the sera of newborns can better predict the occurrence and death of NRDS, and can therefore be considered as a marker for its diagnosis, evaluation and prognosis.

To the Editor,

Neonatal respiratory distress syndrome (NRDS) is an important factor leading to respiratory failure and death in neonates (1). Since the early clinical manifestations of NRDS are not typical, and affected neonates have progressive symptoms 6-12 h after birth, the condition often fails to be clearly diagnosed in a timely fashion and therefore often cannot be actively and effectively treated (2-4). Thus, the rapid and objective diagnosis of NRDS, as well as early assessment of the condition and prognosis, are of great significance for improving the outcome, including reducing mortality, decreasing the incidence of sequelae and improving the overall prognosis.

High mobility group protein B1 (HMGB1) is an active cell factor that can be released from the nucleus to the extracellular space. In recent years,

Key words: respiratory distress syndrome, high mobility group protein B1, neonates, enzyme-linked immunosorbent assay

Mailing address:
Dr Shaohua Wang,
Neonatal Intensive Care Unit,
Women and Children Health Institute Futian,
University of South China, No. 2002 Jintian South Road,
Futian District, Shenzhen 518045, China
e-mail: wangshaohua_usc@163.com

0393-974X (2018)

many reports have shown that HMGB1 is involved in the inflammatory processes of sepsis, acute lung injury, arthritis and other diseases (5, 6). Suda et al. (7) found that HMGB1 levels were significantly elevated in blood and lung epithelial stroma of mice with LPS-induced acute lung injuries. Kokkola et al. (8) showed that HMGB1 plays an important role in the pathogenesis of arthritis. At present, there are few studies on the relationship between HMGB1 and NRDS. Therefore, by examining the correlation between NRDS and serum HMGB1 levels in normal and NRDS neonates, the present study seeks to find biological markers for the diagnosis and evaluation of the severity and prognosis of NRDS.

MATERIALS AND METHODS

Study subjects

Sixty cases of NRDS treated in Tianjin Baodi Hospital from May 2016 to November 2017 were selected as the study group. Following-up for 6 months and depending on the prognosis, patients in the study group were apportioned into a survival group (cured neonate) and a death group (eventual death). Chest radiographic findings and acidosis are the main diagnostic criteria of NRDS (9). Sixty healthy neonates born in Tianjin Baodi Hospital during the same period were selected as the control group. Clinical data including hospitalization number, gestational age, gender, mode of birth, age of onset, laboratory examination and prognosis were recorded. The guardians of all participating neonates provided informed consent, and the study was approved by the Ethics Committee of Tianjin Baodi Hospital.

2 mL peripheral venous blood samples were collected from the two groups of neonates 12 ~ 24h after birth and were placed immediately into drying tubes. After 30 min at room temperature, the blood was centrifuged at 3000rpm/min for 10 min. 1 mL of each serum sample was placed into an EP tube and stored at -80°C. Enzyme linked immunosorbent assay (ELISA) was used to detect the content of HMGB1 in the sera of the two groups of neonates. The experiment was carried out in accordance with the high mobility group protein B1 ELISA kit instructions (Wuhan Elrite Biotech Co., Ltd.).

Prior to the test, HMGB1 ELISA kit was used for thawing at room temperature, and concentrated washing liquid was diluted to 1:25 by double distilled water for preservation; 8 EP tubes were prepared and labeled; standard sample and 1.0 mL dilution liquid were added to the freeze-dried standard, and mixed (2000pg/mL). Then, , these were diluted to 2000, 1000, 500, 250, 125, 62.5, 31.25, or 0 pg/mL, where the standard and sample dilution solution was 0 pg/mL, and the biotinylated antibody was diluted to 1:100 for preservation. The concentrated enzyme conjugates were diluted to 1:100 and set aside; additionally, 2 sets of newborn serum specimens were taken out and conserved at room temperature after thawing.

100 ul sample diluent, 100 ul standard sample and 100 ul tested sample were 100 added to the ELISA plate, respectively. After shaking, the membrane was coated with the enzyme standard plate, and incubated at 37°C for 90 min. The liquid was discarded and the plate dried; 100 uL biotinylated antibody working fluid was added to each well; the sample was then film-coated with the enzyme plate, and incubated for 1 h at 37°C. The liquid was then discarded and the plate dried; the plate was washed 3 times and dried.100 uL of the working fluid was then added to each well and the membrane was incubated at 37°C for 30 min. The liquid in the well was discarded, and the plate was dried and washed 5 times. 90 uL substrate solution (TMB) was added to each well, the enzyme-labeled board coated with film and incubated at 37°C in the dark for 15 min. 50 uL terminating liquid was added to each well, causing a color change to yellow. The order in adding terminating liquid was consistent with the order in adding substrate solution. The OD value for each well was measured at 450 nm with an enzyme-labeling instrument (Bio-Rad, USA). The ELISAcalc.exe software was applied with the standard concentration as the abscissa, and the standard curve was drawn with the OD value measured as the ordinate. Sample concentrations were obtained from the equation of the best-fit standard curve.

Statistical analysis

After the experiment, the SPSS 17 software was used to analyze the data; measurement data was expressed as ($x \pm S$), and the groups were compared using the *t*-test. The count data was expressed with the rate (%), and the χ^2 test was used in group comparison. Evaluation of diagnostic value utilized the Receiver-Operating Characteristics (ROC) curve analysis, and the determination of appropriate points used the Youden index maximum method. The difference was statistically significant when $P< 0.05$.

RESULTS

Comparison of general clinical data and serum HMGB1 levels between two groups of neonates

The general clinical data and serum HMGB1 levels of the two groups of neonates are shown in Table I. There were 60 neonates in the experimental group, including: 32 males and 28 females; 33 caesarean sections and 27 vaginal deliveries; an average birth weight of 2.81±0.95 kg; and an average gestational age of 35.19±3.43 weeks. There were 60 neonates in the normal control group, including: 33 males and 27 females; 21 caesarean sections and 39 vaginal deliveries; and an average birth weight of 3.15±0.45 kg; and an average gestational age of 36.01±1.07 weeks. There were perceptible differences in gender, mode of birth and birth weight between the two groups, but the differences were not statistically significant (P>0.05). The average serum HMGB1 level of the neonates in the experimental group was 784.93±171.86 pg/mL, which was significantly higher than the HMGB1 levels in the serum samples of the control group, and the difference was statistically significant (P<0.05).

Comparison of general clinical data and serum HMGB1 levels between survival group and death group

The general clinical data and serum HMGB1 levels of those in the survival and death subgroups of the study group are shown in Table II. There were 36

Table I. *Comparison of the general clinical data and serum HMGB1 levels of the two groups of neonates ($\bar{x}$ ±S).*

Groups	Cases	Mode of birth		Gender		Birth weight (g)	Gestational age(week)	HMGB1 (pg/ml)
		Cesarean section	Natural childbirth	Male	Female			
Experimental group	60	33	27	32	28	2.81±0.95	35.19±3.43	784.93±171.86
Control group	60	21	39	33	27	3.15±0.45	36.01±1.07	569.78±76.32
Statistics		3.673		0.176		-1.971	-1.980	7.216
P		0.091		0.842		0.053	0.052	0.000

Table II. *Comparison of the general clinical data and serum HMGB1 levels between the survival group and the death group.*

Groups	Cases	Mode of birth		Gender		Birth weight (g)	Gestational age(Week)	HMGB1 (pg/ml)
		Cesarean section	Natural childbirth	Male	Female			
Survival group	36	22	14	19	17	2.97±1.12	35.89±2.77	679.48±126.16
Death group	24	11	13	13	11	2.41±0.68	34.13±3.02	942.12±148.39
Statistics		1.502		0.062		1.905	1.972	-6.351
P		0.239		1.003		0.061	0.057	0.000

cases in the survival group, including: 19 males and 17 females; 22 cesarean sections and 14 cases of vaginal childbirth; an average birth weight of 2.97±1.12 kg; and an average gestational age of 35.89±2.77 weeks. There were 24 cases in the death group, including: 13 males and 11 females; 11 caesarean sections and 13 cases of vaginal childbirth; an average birth weight of 2.41±0.68 kg; and an average gestational age of 34.13±3.02 weeks. There were perceptible differences in gender, birth weight and mode of birth between the survival group and the death group, but these differences were not statistically significant ($P<0.05$). Comparison of serum HMGB1 levels between the survival group and the death group showed that the serum HMGB1 levels of those in the death group were 942.12±148.39 pg/mL, which was significantly higher than those of the survival group, and these differences were statistically significant ($P<0.05$).

Diagnostic value and prognostic value of serum HMGB1 level in neonatal respiratory distress syndrome

ROC curve was used to analyze the diagnostic value of serum HMGB1 level in neonatal respiratory distress syndrome. The area under curve (AUC) value of NRDS diagnosis was 0.872. When Youden index (YI) was 0.600, serum HMGB1 level was 625.2198pg/mL. The sensitivity and specificity of serum HMGB1 in diagnosing NRDS were 77.7% and 82.1%, respectively. The wrong-diagnosis rate was 22.1%, and the missed diagnosis rate was 17.7%, and the AUC for predicting the mortality risk of NRDS was 0.913. When YI was 0.758, serum HMGB1 level was 786.7643pg/mL. The sensitivity and specificity of serum HMGB1 level in predicting the prognosis of NRDS were 83.2% and 92.5%, respectively. The wrong-diagnosis rate was 16.6% and the missed diagnosis rate was 7.3%, as shown in Fig. 1.

DISCUSSION

The results showed that the serum HMGB1 levels in neonates in the experimental group were much higher than those of the control group ($P<0.05$). This may be due to the lack of pulmonary surfactant (PS) in neonates with NRDS, causing alveolar collapse, obstruction of gas exchange, damage to pulmonary vasculature and the release of inflammatory factors, thus provoking an inflammatory response. These inflammatory factors can induce activated immune cells to release HMGB1. At the same time, damaged lung tissue cells may passively release HMGB1. The two actions together result in an increase in serum

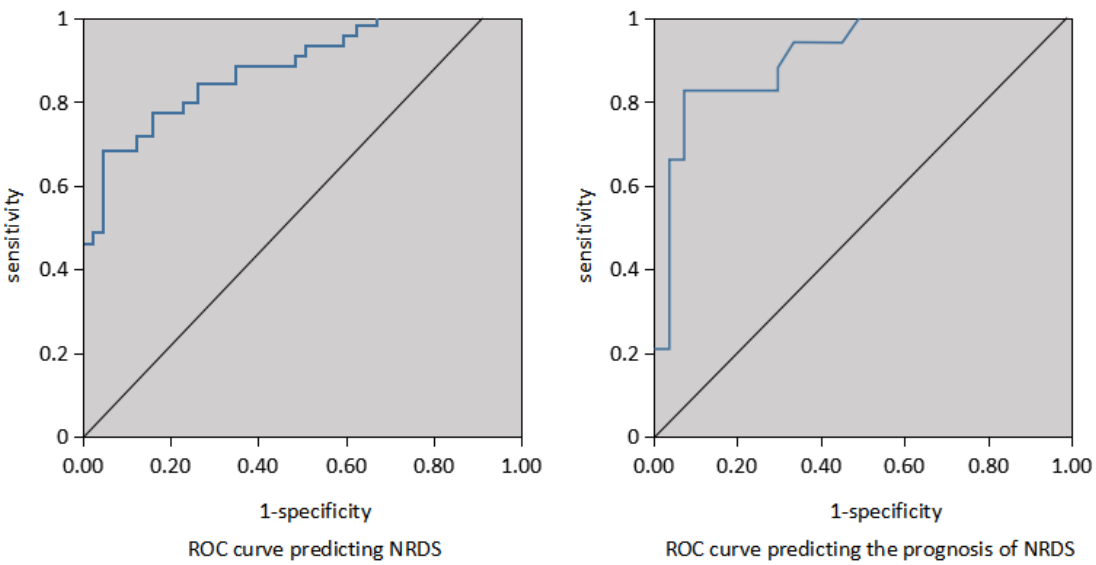

Fig. 1. *ROC curve of HMGB1 in predicting NRDS and its prognosis.*

HMGB1 level in neonates with NRDS (10).

The results showed that there was a distinct difference in serum HMGB1 levels between the survival group and the death group, and the difference was statistically significant ($P<0.05$). These results demonstrated that serum HMGB1 level is related to the severity and prognosis of NRDS, which was consistent with the finding of Jiang et al. (11). The cause of this result may be related the role of HMGB1 pro-inflammatory factors. The released HMGB1 can be bound by receptors on the cell surfaces, thus initiating a signal transduction pathway, leading to produce a series of inflammatory factors which can also promote the release of HMGB1, exacerbate lung injury, cause NRDS disease aggravation, and affect the prognosis. The detection of serum HMGB1 level in neonates shows a good predictive value and may be helpful in the diagnosis and prognosis of NRDS.

In summary, HMGB1 may play an important role in the pathogenesis and progression of NRDS and serum HMGB1 level is of great value to the diagnosis, as well as evaluation of severity and prognosis, of NRDS.

ACKNOWLEDGEMENTS

This work was supported by Shenzhen health and family planning system research project in 2015 (Project No.: 201505022): Mechanism of hyperoxia lung injury, scarless repair and signal transduction in neonatal rats.

REFERENCES

1. Edwards MO, Kotecha SJ, Kotecha S. Respiratory distress of the term newborn infant. Paediatr Respir Rev 2013; 14(1): 29-36; quiz 36-7.
2. Britt RD Jr, Velten M, Tipple TE, Nelin LD, Rogers LK. Cyclooxygenase-2 in newborn hyperoxic lung injury. Free Radic Biol Med 2013; 61:502-11.
3. Speer CP. Neonatal respiratory distress syndrome: an inflammatory disease? Neonatology 2011; 99(4):316-19.
4. Bhargava R, Janssen W, Altmann C, et al. Intratracheal IL-6 protects against lung inflammation in direct, but not indirect, causes of acute lung injury in mice. PLoS One 2013; 8(5):e61405.
5. Wang X, Guo Y, Wang C, Yu H, Yu X, Yu H. MicroRNA-142-3p inhibits chondrocyte apoptosis and inflammation in osteoarthritis by targeting HMGB1. Inflammation 2016; 39(5):1718-28.
6. Jessop F, Holian A. ExtracelluLar HMGB1 regulates multi-walled carbon nanotube-induced inflammation in vivo. Nanotoxicology 2015; 9(3):365-72.
7. Suda K, Takeuchi H, Ishizaka A, Kitagawa Y. High-mobility-group box chromosomal protein 1as a new target for moduLating stress response. Surg Today 2010; 40(7):592-601.
8. Kokkola R, Sundberg E, Ulfgren AK, et al. High mobility group box chromosomal protein 1: a novel proinflammatory mediator in synovitis. Arthritis Rheum 2002; 46(10):2598-603.
9. Kusuda S, Fujimura M, Sakuma I, et al. Neonatal Research Network, Japan. Morbidity and mortality of infants with very low birth weight in Japan: center variation. Pediatrics 2006; 118(4):e1130-38.
10. Park JS, Arcaroli J, Yum HK, et al. Activation of gene expression in human neutrophilsby high mobility group box 1 protein. Am J Physiol Cell Physiol 2003; 284(4):C870-9.
11. Jiang Z, Zhou Q, Gu C, Li D, Zhu L. Depletion of circulating monocytes suppresses IL-17 and HMGB1 expression in mice with LPS-induced acute lung injury. Am J Physiol Lung Cell Mol Physiol 2017; 312(2):L231-L242.

LETTER TO THE EDITOR

EFFECT OF PROPRANOLOL ON PROLIFERATION AND APOPTOSIS OF HEMANGIOMA ENDOTHELIAL CELLS IN INFANTS AND YOUNG CHILDREN

S. XU[1] and E. GUO[2]

[1]Pediatric Surgery, Jinhua Central Hospital, Jinhua, Zhejiang, China; [2]Department of Hand Surgery and Reconstructive Surgery, Zhejiang Provincial People's Hospital (People's Hospital of Hangzhou Medical College), Hangzhou, Zhejiang, China

Received July 11, 2018 – Accepted September 17, 2018

The aim of this study was to investigate the effects of propranolol on the proliferation and apoptosis of hemangioma endothelial cells in infants and young children, and to explore the molecular mechanism of hemangioma treatment. Infant HemEC was cultured *in vitro*. HemEC cells were treated with different concentrations of propranolol (0umol/L, 25umol/L, 50umol/L, 75umol/L, 100umol/L, 125umol/L). After 24, 48 and 72 hours, the viability of the cells was examined by MTT {3-(4, 5-Dimethylthiazol-2-yl)-2,5-diphenyltetrazolium bromide} method. The apoptosis rate of the cells was measured by flow cytometry using Annexin V. The propranolol concentration was 25umol/L. After 24 h and 48 h, HemEC could slightly proliferate (P<0.05). With the concentration of ≥100umol/L, the survival time of HemEC decreased when the action time was longer than 24 h. Within a certain range, the drug efficacy was positively correlated with drug concentration and action time (P<0.05). When propranolol concentration was ≥100umol/L, it could cause HemEC apoptosis. With the increase of drug concentration and the prolongation of intervention time, the apoptosis rate increased (P<0.05). In conclusion, the inhibition of hemangiomas by propranolol may be related to the inhibition of HemEC proliferation and its promotion of apoptosis.

To the Editor,

The incidence of hemangioma during infancy is 5-10% (1). Its characteristic pathological change is hyperproliferation of hemangioma endothelial cells (HemEC) (2, 3). Propranolol is a nonselective β-adrenoceptor blocker that blocks the β-receptor in the heart muscle. It is usually used for the treatment of arrhythmias and diseases such as hypertension (4). When propranolol is used to treat hemangiomas, it has the advantages of rapid onset, good effect, less adverse reactions, and small individual differences (5). Propranolol has a good therapeutic effect, but its mechanism is still unclear. At present, it is thought that it may be related to inhibiting HemEC proliferation and promoting its apoptosis. HemEC was cultured *in vitro* by Chim, et al. (6). After intervention with propranolol, the cell viability and migration ability decreased, and the higher the concentration, the more obvious the effect. In addition, after drug intervention, the expression of vascular endothelial growth factor (VEGF) and -1(hypoxia inducible factor-1, HIF-1α) was significantly down regulated. Annabi et al. (7) cultured human brain microvascular endothelial cells *in vitro*, and the angiogenesis and MMP-9 secretion were significantly decreased after propranolol intervention. It was hypothesized

Key words: propranolol, hemangioma endothelial cells, proliferation, apoptosis

Mailing address:
Dr Sheng Xu,
Pediatric Surgery,
Jinhua Central Hospital,
No. 351 Mingyue Street,
Jinhua, 321000, Zhejiang, China
e-mail: xushengxs00@163.com

0393-974X (2018)

DISCLOSURE: ALL AUTHORS REPORT NO CONFLICTS OF INTEREST RELEVANT TO THIS ARTICLE.

that propranolol inhibiting hemangioma growth was related to inhibiting MMP-9 secretion and endothelial cell production. The effect of propranolol on the proliferation and apoptosis of hemangioma endothelial cells was investigated, and the molecular mechanism of propranolol treatment of hemangiomas was analyzed.

MATERIALS AND METHODS

Experimental instruments and materials

Fluorescence inverted microscope (Shanghai Caikang Optical Instrument Co., Ltd., China); enzyme detector (Meigu Molecular Instrument (Shanghai) Co., Ltd., China); high-speed refrigerated centrifuge (Eppendorf, Germany); microcentrifuge (Fisher Scientific Co., Ltd., USA); flow cytometry BD FACsort (Boao Pak Biological Technology Co., Ltd., Beijing); 2.0 ml cryopreservation tube; 1.5 ml centrifuge tube; 1.5 ml cryovial; six-well, multi-well culture plates (Corning, USA); LS separation column; MACS magnetic bead sorter receptacle (Miltenyi, Germany).

Main reagents

EGM-2 MV cell culture medium (Lonza, Switzerland); DMEM high glucose cell culture medium; collagenase; fibronectin; 0.25% trypsin; fetal bovine serum; bovine serum albumin (BSA) (Gibco, USA); CD31 immunomagnetic beads (Miltenyi, Germany); dispase II, isolate protease II(Sigma, USA); streptomycin double resistance (Gibco, USA); vWF antibody and fluorescent secondary antibody(Abcam, USA); MTT reagents (Shanghai Crystal Anti Bioengineering Co., Ltd., China); DMSO and propranolol hydrochloride(Sigma, USA); apoptosis kits (Miltenyi, Germany); 0.25% trypsin (without EDTA) (Sigma, USA).

Culture and identification of HemEC in vitro

A total of 15 samples were collected from infants with hemangiomas undergoing neonatal surgery or general surgery in Jinhua Central Hospital from March 2017 to April 2018. Twelve samples were cultivated successfully. The inclusion criteria were: children aged ≤ 6 months diagnosed as hemangioma clinically and pathologically; the tumor was proliferating and had no complications such as bleeding, ulceration, or infection. A portion of the surgically resected hemangiomas was used for pathological examination, and the other part was placed in a 50 ml sterile centrifuge tube (containing serum-free DMEM medium to prevent accelerated cell aging, while using cryogenic storage and transport). The patients' families gave their informed consent for the study which was approved by the Ethics Committee of Jinhua Central Hospital.

Enzymatic digestion of hemangiomas

The hemangiomas in the centrifuge tube were transferred to a petri dish, and the tissues were repeatedly washed with PBS containing a double antibody followed by rinsing with sterile PBS. The tissue was cut into 1cm^3 pieces. After washing in PBS, the tissue mass was transferred to a 15-ml centrifuge tube. Five ml of 2.4μg/ml dispase II solution was added and the mixture was digested overnight at 4°C. On the second day, the centrifuge tube was removed and the dispase II solution was removed and washed twice in PBS. The epidermis and dermis were removed. The tissue was cut into 1mm^3 size and placed in a 15-ml centrifuge tube. Ten ml of 0.2% type I collagenase was added to the 37°C water bath, and the centrifuge tube was vortexed every 15 min for a total of 2-3 h until milky. The remaining tissue was removed using a 70 um filter. The filtrate was centrifuged at 1000 rpm for 5 min and the supernatant was discarded. The cells were resuspended in 5 ml of 0.1% BSA and centrifuged at 800 rpm for 3 min. Then 5 ml of 0.1% BSA solution was resuspended and mixed by pipetting. The hemocytometer was used for counting.

The cell suspension was centrifuged at 800 rpm for 5 min and the supernatant discarded. Every 1×10^7 cells were resuspended by adding 60 μl of 0.1% BSA solution; 30 μl of FcR inhibitor was added and mixed; 30 μl of CD31 magnetic beads were added and incubated at 4°C for 15 min. One ml 0.1%BSA solution was added to every 1×10^7 cells, and the LS column was prepared for magnetic separation. The LS column was mounted on the cell sorter, and then connected to the 50-ml centrifuge tube. The 3 ml 0.1% BSA solution was added to the LS column for washing. When the liquid was fast flowing into the cell suspension, the cell suspension labeled CD31 magnetic beads was added and washed with 3 ml 0.1%BSA. When the liquid was drained off, 0.1% BSA was added and the cells were washed three times. The LS column was removed and placed in a 15 ml sterile centrifuge tube. Then 6 ml of 0.1% BSA was added to rapidly drain the liquid from the LS column. The cell suspension in the

centrifuge tube was a CD31 positive cell labeled HemEC. Then, it was centrifuged at 1000 rpm for 5 min and the supernatant was discarded.

Culture and passage of hemangioma endothelial cells

Four ml of EGM-2/20% FBS was used to resuspend completely for cell counting. A 25cm^2 cell culture flask was pre-laminated with 1 ug/ml fibronectin solution. The cells were placed in culture flasks at a density of 5 x 10^3 cells/cm^2. After 48 h, the medium was changed and then every 3 days for 20-25 days, then passaged 1:3 after being overgrown, and passed to a 25cm^2 culture flask preliminarily containing 1 μg/ml fibronectin solution.

Identification of hemangioma endothelial cells

HemEC specifically expresses von Willebrand Factor (vWF) antigen. HemEC was used as an experimental group to create cell slides. Immunofluorescence staining with vWF antibody was performed for identification. First, the cover glass was placed in a 6-well plate with a cover glass in each well. The cell concentration was adjusted to 3×10^4 / ml, cell suspension was added dropwise onto a cover glass, and the cells were cultured for 0.5 h until cell adhesion. The complete medium of 2 ml was added to culture for 10 h to remove the substrate. Then, it was washed 3 times with PBS for 3 min each time. After acetone was fixed for 10 min, PBS was washed 3 times, and each time was 5 min. 50 ul solution was added to the round coverslip and incubated for 10 min at room temperature. Then, it was washed 3 times with PBS for 5 min/time. After removing the PBS solution, 50 ul of the 1:200 diluted vWF antibody was added to each well and 50 ul of PBS was added to the blank control group and left overnight at 4°C. The coverslip was washed 3 times for 5 min each time with PBS. The PBS was removed, and 50 ul of the 1:100 fluorescent secondary antibody was added to each slide and incubated for 30 min at room temperature and then was washed 3 times in the dark for 5 min each time with PBS. PBS was removed. 50 ul of diluted Hochest 33242 staining 1:10000 was added to each hole, and was incubated for 10 min at room temperature to avoid staining nuclei and then was photographed by a fluorescent microscope after being washed by PBS 3 times.

Detection of HemEC survival after intervention with propranolol

The HemEC experimental group was divided into 6 subgroups according to the concentration of propranolol from low to high during experimental drug intervention: 25umol/L group, 50umol/L group, 75umol/L group, 100umol/L group, 125umol/L group, and 150umol/L group. The control group received only the same amount of EGM-2/0.5% FBS medium (no growth factor added).

Drug configuration steps: 50 mg propranolol was put in an aseptic centrifuge tube and 1ml PBS was added. After dissolution, the concentration was 50mg/ml drug solution and was stored at -20°C. Six sterile centrifuge tubes were selected. EGM-2/0.5% FBS was used to mix the diluted mother liquor. The drug solution was prepared at concentrations of 25, 50, 75, 100, 125 and 150umol/L.

MTT test

Logarithmic growth HemEC cells were selected. After trypsinization, HemEC cells were centrifuged at 1000rmp for 5 min and the supernatant was removed. EGM-2/20% FBS medium was used for resuspending and mixing by pipetting. The cells were then counted. Cell suspension was adjusted to a density of 1 x 10^5 cells/ml. 200ul/well was added to the 96-well plate and incubated for 24 h before removing the supernatant. 200ul/well of different concentrations of drugs were added separately. The blank control group was added with 200 ul of EGM-2/0.5% FBS medium without drug and incubated for 24-72 h. Two h after addition of the drug, the state of the cells was observed under a microscope and photographed. After 24 h, 48 h, and 72 h, 50 μl/well of 5 mg/ml MTT solution was added in three batches and culture was continued for 4 h. The red-purple formazan around the cells could be seen under the microscope. The supernatant was removed and 200 μl of DMSO solution was added to each well to dissolve formazan. After 15 min on a horizontal shaker, the optical density (OD) was measured with a microplate reader. Based on the OD value of each well, the cell survival rate was calculated for each concentration and for each period. Calculation formula: Cell survival rate =1-[|experimental port OD-zero port OD|-|control port OD- zero port OD|]/| control port OD- zero port OD|.

Detection of apoptosis rate of HemEC after intervention with propranolol

The logarithmic growth HemEC was selected and digested with EDTA-free trypsin, centrifuged at 1000rmp for 5 min, and cells were collected. EGM-2/20% FBS

medium was used to resuspend the cells. The cells were counted. The cell density was adjusted to 1 x 10^5 cells/ml. In a 6-well plate, each well was 2 ml. The 6-well plate was placed in a CO_2 incubator. After 12 h, the cells were adhered, and the medium was aspirated. EGM-2/0.5%FBS medium 2 ml with different concentrations of drugs was added to each well. In the blank control group, the EGM-2/0.5%FBS medium containing no medicine was added to each well, and 2 ml was added into the incubator to cultivate 24-72 h, respectively. After 24 h, 48 h and 72 h, the medium was removed, PBS was rinsed once, and 0.5ml was digested without EDTA trypsin. After 1 min, 1 ml of complete medium was added to stop the digestion. Resuspend was blown gently. The cell suspension was collected in a flow tube and centrifuged at 1000 rpm for 5 min to remove the supernatant and 3 ml PBS was added. The cells were resuspended once and centrifuged for 5 min at 800rmp and the supernatant was removed, after which 200 ul Binding Buffer suspension cells were added. Annexin V-FITC 5 uL was added and incubated for 15 min at room temperature in the dark, and then 5 uL PI staining was added 5 min before the flow cytometer. It was detected within 1 h.

Statistical analysis

The data was analyzed using SPSS 22.0 software. Measurement data is expressed in $\bar{x} \pm s$. Univariate method analysis and independent sample *t*-test were applied. $P<0.05$ indicates that the results are statistically different.

RESULTS

Observation of cell morphology

The prophase of primary cell proliferation is slow.

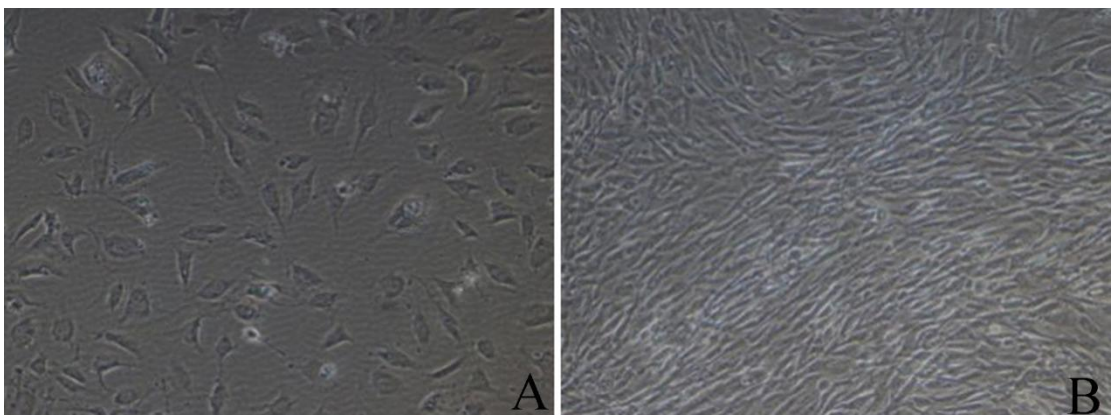

Fig. 1. *HemEC cell morphology observation (×200 times). **A**) Form at the 14th day; **B**) Form at the 20th day)*

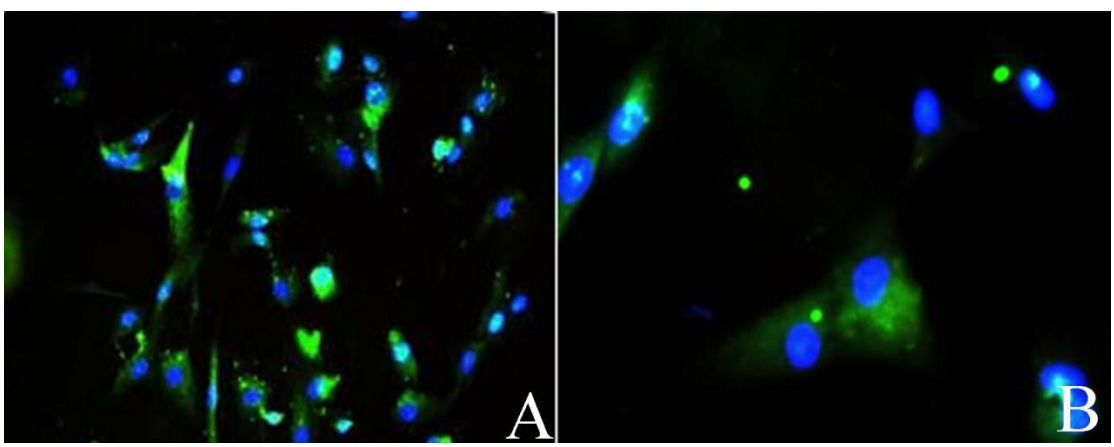

Fig. 2. *A) The cytoplasmic vWF staining of HemEC was positive (×200); **B**) HemEC. Cytoplasmic vWF staining was positive (×400)*

On the 14th day, the density of adherent cells growing on the bottom of the culture flask was still sparse (Fig. 1A). After 14 days, the proliferative power accelerated. On the 20th day, HemEC could be observed under the microscope and swirled. The arrangement was more orderly and dense. At this point, growth reached 90% confluence (Fig. 1B). After passage, the proliferation of cells was also very strong.

Cellular immunofluorescence

As can be seen from Fig. 2, the cytoplasm of the experimental group showed green fluorescence mainly distributed around the nucleus. vWF antibody immunofluorescence staining was positive, indicating that the cell is indeed HemEC.

Cellular morphology after drug intervention

HemEC (0, 25, 50, 75, 100, 125, 150 umol/L) was treated with different concentrations of propranolol and observed after 2 h. HemEC morphology gradually changed with increasing drug concentrations. It was seen that the cells began to shrink and become round, and at high concentrations the outline of the cells disappeared. When the concentration was ≥100umol/L, the cells began to shrink and become round, with a little detachment. Fig. 3 shows the morphology of the HemEC under the microscope.

Cell proliferation test results

HemECs were treated with different concentrations of 0, 25, 50, 75, 100, 125, 150 umol/L propranolol. As seen from the data in Table I, the concentration of propranolol of 25umol/h caused slight proliferation of HemEC after 24 h and 48 h ($P<0.05$). When the concentration was ≥100umol/L, the survival time of HemEC was decreased after the treatment time ≥24 h, and it was concentration-dependent and time-dependent within a certain range ($P<0.05$).

Apoptosis

Propranolol 100-150umol/L could induce apoptosis of HemEC after intervention for 24 h, 48 h, and 72 h, and was positively correlated with drug concentration and action time ($P<0.05$). The data is shown in Table II.

DISCUSSION

Léauté-Labrèze et al. (8) used propranolol to treat two children with heart disease and hemangioma. They found that the atrophy of the hemangioma decreased. Later, researcher used propranolol again in 9 other cases of hemangiomas and achieved the same results. In this study, the propranolol concentration was 25umol/L.

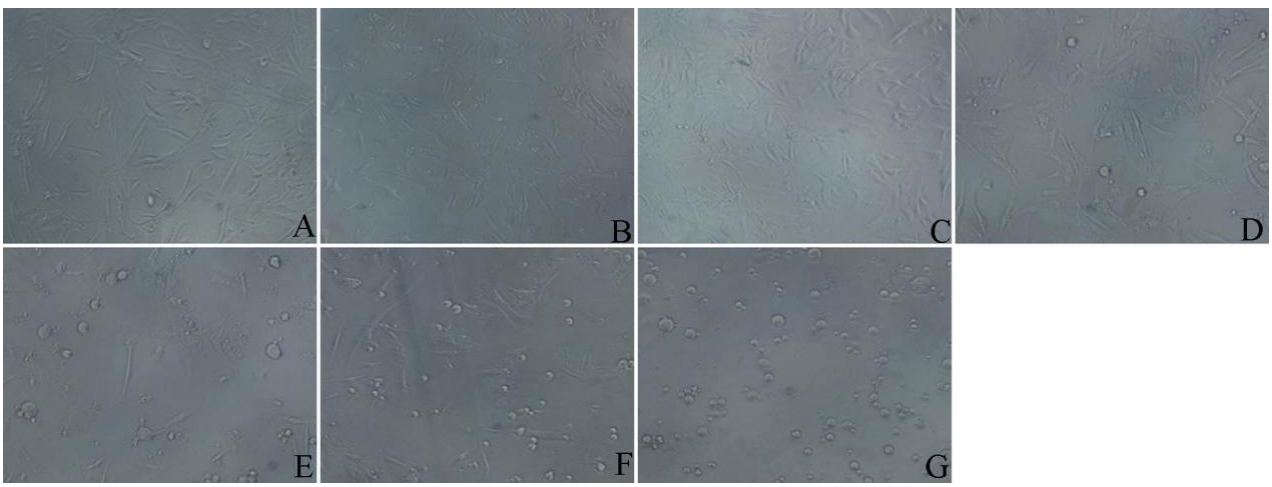

Fig. 3. *HemEC form (×100). A) control group;* ***B****) 25umol/L;* ***C****) 50umol/L;* ***D****) 75umol/L;* ***E****) 100umol/L;* ***F****) 125umol/L;* ***G****) 150umol/L.*

After 24h-48h of intervention, HemEC caused slight proliferation (P<0.05). When the drug concentration was ≥100umol/L and the action time was > 24h, the survival rate of HemEC decreased. The drug efficacy was positively correlated with drug concentration and duration of action (P<0.05). This is similar to the results obtained by other researchers (9, 10). This shows that low concentrations of propranolol can promote the proliferation of HemEC, and high concentration of propranolol can inhibit the proliferation of HemEC.

In addition, the apoptosis of endothelial cells in hemangiomas treated with different concentrations of propranolol was explored. The results showed that the drug can cause apoptosis of hemangioma endothelial cells at ≥100umol/L. With a continuous increase of the action time and drug concentration, the apoptotic rate gradually increased. Other studies (11, 12) have shown that propranolol can cause apoptosis in capillary endothelial cells and pancreatic cancer cells when the concentration is within the range of 10 to 100 μmol/L with actuation duration of 24 ~ 72h. This is similar to the results of this experiment. However, it is still unclear whether its mechanism of action is the same as the mechanism that causes HemEC apoptosis.

In summary, low concentrations of propranolol have a certain role in promoting the proliferation of hemangioma endothelial cells. However, high concentrations of propranolol have inhibitory effects on the proliferation of hemangioma endothelial cells. In addition, propranolol may inhibit the growth of hemangiomas by inhibiting the proliferation of hemangioendothelioma cells and promoting their apoptosis.

Table I. *Cell survival rate of HemEC after drug intervention*

Concentration (μmol/L)	24h	48h	72h
0	1.00±0.00	1.00±0.00	1.00±0.00
25	1.26±0.11**	1.16±0.11*	1.09±0.11
50	1.03±0.13	1.11±0.12	0.99±0.12
75	0.92±0.09	0.82±0.08**	0.93±0.11
100	0.68±0.13*	0.51±0.07**	0.42±0.08**
125	0.61±0.12**	0.33±0.05**	0.20±0.05**
150	0.30±0.08**	0.12±0.03**	0.05±0.02**

*Note: Compared with the blank control group, *P<0.05, **P<0.01*

Table II. *Apoptosis of HemEC after drug intervention*

Concentration (μmol/L)	24h	48h	72h
0	2.61±0.07	3.34±0.31	5.32±0.11
25	4.75±0.19	6.88±0.33	9.14±0.36
50	9.53±0.31	10.96±1.53	12.76±0.42
75	13.13±1.12*	18.36±3.13	18.76±1.14*
100	19.13±1.57*#	45.18±7.13*#	58.16±4.33*#
125	22.21±1.94*#	55.92±6.84*#	64.88±1.17*#
150	32.38±2.34*#	61.93±5.97*#	71.05±3.75*#

*Note: The apoptosis rate of the two groups was *P<0.05 at the same concentration and different time points, and the apoptosis rate of the two groups was #P<0.05 at the same time point and different concentrations.*

REFERENCES

1. Haggstrom AN, Drolet BA, Baselga E, et al. Prospective study of infantile hemangiomas: clinical characteristics predicting complications and treatment. Pediatrics 2006; 118(3):882-87.
2. Garzon MC, Drolet BA, Baselga E, et al. Comparison of infantile hemangiomas in preterm and term infants: a prospective study. Arch Dermatol 2008; 144(9):1231-32.
3. Dosanjh A, Chang J, Bresnick S, Zhou L, Reinisch J, Longaker M, Karasek M. In vitro characteristics of neonatal hemangioma endothelial cells: similarities and differences between normal neonatal and fetal endothelial cells. J Cutan Pathol 2010; 27(9):441-50.
4. Poynard T, Lebrec D, Hillon P, et al. Propranolol for prevention of recurrent gastrointestinal bleeding in patients with cirrhosis: a prospective study of factors associated with rebleeding. Hepatology1987; 7(3):447-51.
5. Bonanno C, Paccanaro M, Fontanellilea A. Propranolol for severe hemangioma of infancy. J Cardiovasc Med (Hagerstown) 2011; 12(1):73.
6. Chim H, Armijo BS, Miller E, Gliniak C, Serret MA, Gosain AK. Propranolol induces regression of hemangioma cells through HIF-1α-mediated inhibition of VEGF-A. Ann Surg 2012; 256(1):146-56.
7. Annabi B, Lachambre MP, Plouffe K, Moumdjian R, Béliveau R. Propranolol adrenergic blockade inhibits human brain endothelial cells tubulogenesis and matrix metalloproteinase-9 secretion. Pharmacol Res 2009; 60(5):438-45.
8. Léauté-Labrèze C, Dumas de la Roque E, Hubiche T, Boralevi F, Thambo JB, Taïeb A. Propranolol for severe hemangiomas of infancy. N Engl J Med 2008; 358(24):2649-51.
9. Zhu Y, Tuerxun A, Hui Y, Abliz P. Effects of propranolol and isoproterenol on infantile hemangioma endothelial cells in vitro. Exp Ther Med 2014; 8(2):647-51.
10. Tu JB, Ma RZ, Dong Q, et al. Induction of apoptosis in infantile hemangioma endothelial cells by propranolol. Exp Ther Med 2013; 6(2):574-78.
11. Barron TI, Connolly RM, Sharp L, Bennett K, Visvanathan K. Beta blockers and breast cancer mortality: a population- based study. J Clin Oncol 2011; 29(19):2635-44.
12. Albiñana V1, Villar Gómez de Las Heras K2, Serrano-Heras G, et al. Propranolol reduces viability and induces apoptosis in hemangioblastoma cells from von Hippel-Lindau patients. Orphanet J Rare Dis 2015; 10:118.

JOURNAL OF BIOLOGICAL REGULATORS & HOMEOSTATIC AGENTS Vol. 32, no. 6, 1499-1505 (2018)

LETTER TO THE EDITOR

SUPPLEMENTATION WITH L-ARGININE AFFECTS ITS METABOLIZING PATHWAYS IN RAT LIVER SUBJECTED TO BILE DUCT LIGATION

V.P. NIČKOVIĆ[1], T. NOVAKOVIĆ[2], Z.M. PETKOVIĆ-MIRKOVIĆ[2], J.B. ŽIVKOVIĆ[2], A. ANDREJEVIĆ[1], L.A. ANDREJEVIĆ[2], D. SOKOLOVIĆ[3] and D.T. SOKOLOVIĆ[4]

[1]Clinical-Hospital Center, Pristina, Gracanica, Serbia; [2]Medical Faculty in Kosovska Mitrovica, Univeristy of Priština, Kosovska Mitrovica, Serbia; [3]Institute for Blood Transfusion in Nis, Clinical center Nis, Serbia; [4]Department of Biochemistry, Faculty of Medicine, University of Niš, Niš, Serbia

Received July 15, 2018 – Accepted October 1, 2018

Liver cholestasis is known to accompany several major liver disorders and is adequately mimicked in rats by ligation of the bile duct (BDL). L-arginine is a semi-essential amino acid which is involved in several important metabolic pathways that are significantly affected during cholestasis. This study was conducted in order to contribute to the understanding of the enrolment of L-arginine supplementation in cholestatic liver function. This was carried out by estimation of serum and liver tissue arginase activity, along with liver tissue citrulline, nitric oxide (NO) and polyamine concentrations. Rats subjected to BDL were treated for nine days with L-arginine (150 mg/kg) or remained without any treatment. Animals from two control groups were either subjected to medial laparotomy (sham/opened group) or were without any surgical treatment and received only L-arginine. Application of L-arginine prevented a significant increase in plasma bile acid and bilirubin concentrations, as well as enzyme biochemical markers that were increased after BDL. It is worth mentioning that L-arginine was able to cause a decrease in arginase activity and liver tissue NO concentrations that were found to be significantly altered during cholestasis. On the other hand, the changes occurring in the concentration of liver polyamines (putrescine, spermidine and spermine) and the activity of polyamine metabolizing enzymes were not notably affected by the administered L-arginine. The results of the present study revealed that exogenous L-arginine was able to ameliorate or prevent changes occurring in its metabolism in liver during cholestasis.

To the Editor,

Numerous studies have provided substantial information regarding the function of liver tissue affected by cholestasis, which accompanies several major liver disorders (1). These studies extensively evaluated the role of bile acids and their hepatocyte damaging mechanisms, which include direct cytotoxicity, and pro-apoptotic action, as well as tissue lipid peroxidation and oxidative damage (2).

L-arginine is a semi-essential amino acid which is involved in several important metabolic pathways, serving as either donor of guanidine group or as a starting molecule for nitric oxide (NO) and polyamine synthesis, etc. (2). Polyamines, especially putrescine, spermidine and spermine, are omnipresent intracellular molecules tightly related to numerous sophisticated cellular processes. The disturbance in exogenous L-arginine availability leads to the alterations in spermatogenesis and urea cycle, and to a dramatic reduction in tissue and circulating levels of arginine and ornithine (3), however, it does not affect polyamine synthesis (4).

Keywords: L-arginine, bile duct ligation, nitric oxide, polyamines

Mailing address:
Dr Dušan T. Sokolović,
Department of Biochemistry,
Faculty of Medicine, University of Niš,
Zorana Đinđića 81, 18000 Niš, Serbia
Tel.: +381 642136478 - Fax: +381 18238770
e-mail: dusantsokolovic@gmail.com

0393-974X (2018)

Since the arginine is a building block molecule and is involved in several metabolic pathways one can speculate that a significant alteration in the quantity of metabolic pathway end-product would occur during cholestasis.

In order to contribute to the understanding of the enrolment of L-arginine in cholestatic liver tissue, we evaluated how a nine-day supplementation with L-arginine (at a dose of 150 mg/day) to rats subjected to BDL affects the metabolism of this amino acid. This was carried out by estimating serum and liver tissue arginase activity, along with liver tissue citrulline and nitric oxide (NO) concentrations. Also, liver polyamine (putrescine, spermidine and spermine) contents and enzymes involved in their metabolism were also estimated.

MATERIALS AND METHODS

Drugs and chemicals

All drugs were purchased from Sigma (St. Louis, MO, USA) and were of the highest commercial quality available, while the chemicals used were of analytical grade. Drug and reagent solutions were prepared fresh daily and filter sterilized if necessary.

Animals and housing

Forty disease and pathogen-free four-month-old male Wistar rats (weighing 250–300 g) were obtained from the Vivarium of the Institute of Biomedical Research, Faculty of Medicine, University of Niš, Niš, Serbia. During the course of the experiment all animals were kept under standard laboratory conditions at 22±2°C and 60% humidity, 12-h light and dark cycle, with food and water available *ad libitum*. Seven days prior to the experiment, the animals were randomly divided into experimental groups consisting of 10 animals each. All experimental procedures with the animals were conducted in compliance with the declaration of Helsinki and European Community guidelines for the ethical handling of laboratory animals (EU Directive of 2010; 2010/63/EU).

Bile duct ligation

Experimental cholestasis, previously described in great detail (3), was induced by BDL using a surgical thread, under ketamine anesthesia (50 mg/kg), following the rules of asepsis. In animals belonging to the sham-opened group only midline laparotomy was performed, without any surgical procedures, in order to eliminate potential effects of operation procedure on the evaluated biochemical parameters.

Treatment protocol

After appropriate surgical protocol, the animals were divided into three groups consisting of 10 animals each, while the fourth group served as a control. The experimental groups were treated as follows:

Group I: Sham/opened group, treated daily, for nine days, via intraperitoneal (*i.p.*) with saline (10 ml/kg).

Group II: L-arginine treated control group, was not subjected to surgical treatment, received *i.p.* injection of L-arginine (150 ml/kg) once daily for nine days.

Group III: BDL group, animals with cholestasis induced by BDL, treated with *i.p.* injection of saline (10 ml/kg) once daily for nine days.

Group IV: BDL and L-arginine group, animals with cholestasis induced by BDL, treated with *i.p.* injection of L-arginine (150 mg/kg) once daily for nine days.

All animals were sacrificed, 9 days following BLD, under ketamine anesthesia, after 15 h of starvation. The sample blood was collected by heart puncture after medial laparotomy and the liver tissue was quickly removed, washed and frozen.

Serum biochemical analysis

Tubes containing anticoagulant (heparin) were used for blood sampling from the animals' abdominal aorta. The obtained blood was centrifuged at 3000 rpm for 15 min and the plasma collected was stored frozen at –20°C until further analysis. Plasma alanine transaminase (ALT alkaline phosphates (ALP) and gamma-glutamyltransferase (γ-GT) activities, as well as total (TB) and direct bilirubin (DB), were determined using automated biochemical analyzer BTS-370 (BioSystems). Total plasma bile acids level were determined using a direct spectrophotometric method previously described by Mashige and co-workers (2).

Tissue homogenate preparation

Dissected liver tissue was immediately frozen and chopped into small pieces that were further used for homogenate preparation. Homogenates (10%, w/v),

prepared with ice-cold distilled water, were centrifuged at 12000 rpm for 10 min at 4°C in order to obtain clear supernatants that were used for further experiments. Protein content in the supernatants was determined using a Lowry's method (2) and the results were calculated based on the bovine serum albumin standard curve.

Arginase activity determination

Plasma and liver homogenate arginase activity was determined following a standard protocol, utilizing ninhydrin as a reagent, which estimates the amounts of formed ornithine after the reaction between arginase and arginine. The absorbance of the reaction mixture was measured at 515 nm and the values obtained were corrected with those obtained from the control (2).

Citrulline concentration measurement

The amount of L-citrulline in liver tissue homogenates was determined using a colorimetric assay that utilizes diacetyl monooxime and thiosemicarbazide (2). The reaction was terminated by adding trichloroacetic acid and the color was developed after incubation at 100°C for 5 min. The absorbance of the solution was measured at 530 nm and the results were presented as μmol/mg of proteins.

Nitrite measurement

After sample deproteinization, liver tissue NO production was evaluated by measuring nitrite and nitrate concentrations (NO_2^-+NO_3^-). Nitrates were previously transformed into nitrites by the cadmium reduction method. Nitrites were assayed directly spectrophotometrically at 492 nm, using Griess reagent (1.5% sulfanilamide in HCl with 0.15% *N*-(1-naphthyl) ethylenediamine dihydrochloride). The results were expressed as nmol/mg of liver tissue.

Determination of liver polyamine content

Polyamine content (putrescine, spermine and spermidine) was determined in a sample obtained after the homogenates were extracted with n-butanol. Separation of amines was performed using electrophoresis (80 V/cm for 1.5 h) under acidic conditions (pH 4.3), where the three amines were separated with no overlap and negligible streaking. Finally, the concentration of a single band was determined spectrophotometrically after its reaction with ninhydrin at 505 nm (2). The amounts of each of the polyamines was calculated using a standard curve.

Polyamine metabolizing enzymes activity determination

The activity of polyamine oxidase (PAO) and diamine oxidase (DAO)was determined spectrophotometrically in a reaction of PAO or DAO with a specific substrate, i.e. spermine tetrahydrochloride and putrescine dihydrochloride, respectively. The reaction is based on the determination of formed amounts of amino aldehydes (2). Enzyme activity was expressed as U/mg of protein present in liver tissue homogenate.

Statistical analysis

Data presented as mean±SD were compared using one-way analysis of variance (ANOVA), followed by Tukey's post hoc test for multiple comparisons (GraphPad Prism, ver. 5.03; San Diego, CA, USA). Probability values (p) less than 0.05 were considered to be statistically significant.

RESULTS

Plasma bilirubin levels (total, direct and indirect) were found to be significantly increased in groups of rats subjected to BDL (Fig. 1A). The bilirubin levels in the group that received arginine after BDL were significantly less increased compared to the control (Fig. 1A). The same trend of changes in bile acids levels was observed as well (Fig. 1B). Also, parameters reflecting cholestatic liver damage (ALT, γ-GT and ALP) were found to be significantly increased in rats subjected to BDL compare to the control group (Table I). The levels of γ-GT and ALP were only slightly affected by a nine-day L-arginine treatment, while the levels of ALT remained the same as in the sham/opened group (Table I), i.e. they were not significantly different from those from the control group.

Plasma arginase activity was found to be significantly increased in the groups of rats with BDL and BDL and L-arginine compared to the control group, while the liver arginase activity in the same groups was found to be significantly decreased compared to the control group (Table I). Application of L-arginine after BDL prevented such significant increase/decrease in plasma and liver arginase activity, respectively (Table I).

The amount of NO and citrulline was determined in liver tissue homogenates of animals from all four

Table I. *Plasma and liver biochemical parameters determined for rats from different experimental groups.*

Parameter/Group	Sham/opened (I)	L-arginine treated (II)	BDL (III)	BDL + L-arginine (IV)
ALT (U/L) (P)	45±12.4	58±9.9	101.5±14.5*	62.7±14.2#
γ-GT (U/L) (P)	5.27±0.2	3.37±0.2	19.9±3.4*	6.3±2.1*
ALP (U/L) (P)	194.2±12.3	139.3± 18.4	340.5± 45.2*	258±34.3*,#
Arginase (U/L) (P)	0.9±0.2	0.84±0.2	25.5±3.4*	7.5±1.5*,#
Arginase (U/L) (H)	25.1±0.5	28.0±0.8	18.8±0.7*	23.4±1.4*,#
PAO (U/mg of proteins) (H)	2.1±0.33	1.6±0.15*	1.1±0.09*	1.5±0.13*
DAO (U/mg of proteins) (H)	1.8±0.12	1.7±0.11	1.1±0.18*	1.6±0.02*

*P: plasma; H: homogenate; Values are given as means±SD, n=10. One-way ANOVA followed by Tukey's test was used to compare the groups. *p<0.001 vs sham/opened group, #p<0.001 vs BDL group.*

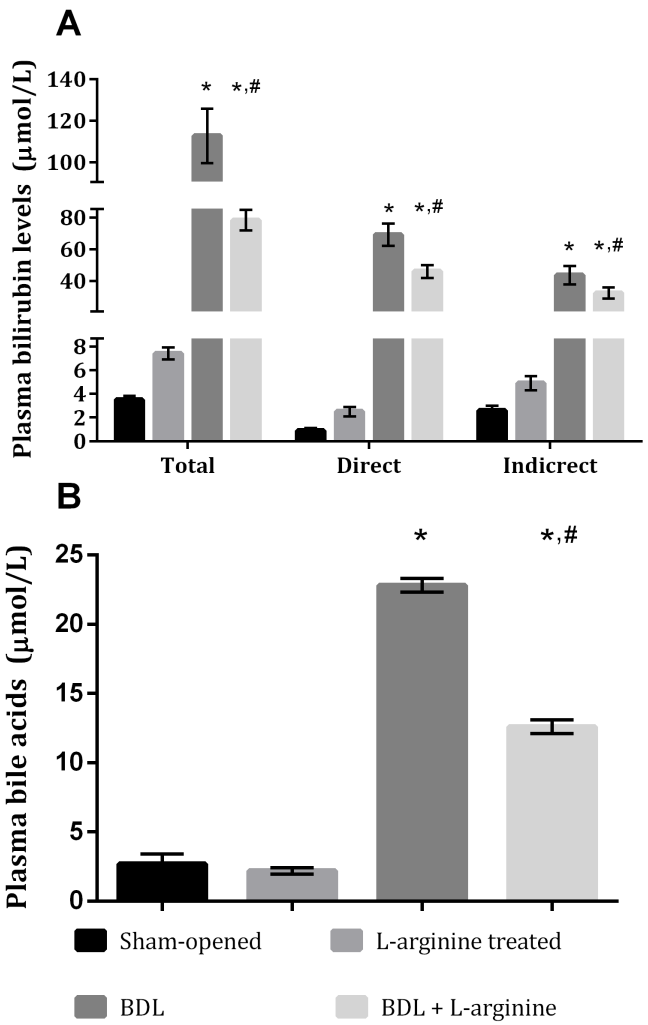

Fig. 1. *Plasma bilirubin (**A**) and bile acid (**B**) levels measured in animals from different experimental groups. Values are given as means±SD, n=10. One-way ANOVA followed by Tukey's test was used to compare the groups. *p<0.001 vs sham/opened group, #p<0.001 vs BDL group.*

experimental groups (Fig. 2). Statistical comparison of the results revealed significant changes in NO concentrations between the compared groups, while the citrulline concentrations remained unchanged. Ligation of the bile duct caused a significant increase in liver NO concentrations in all animals subjected to this surgical procedure. In the group that received L-arginine after BDL for nine days the concentrations of NO were found to be significantly different compared to both THE sham/opened and BDL groupS (Fig. 2).

The treatment of healthy animals with L-arginine (group II) did not affect the levels of polyamines (Fig. 3) in rat livers compared to the control group,.

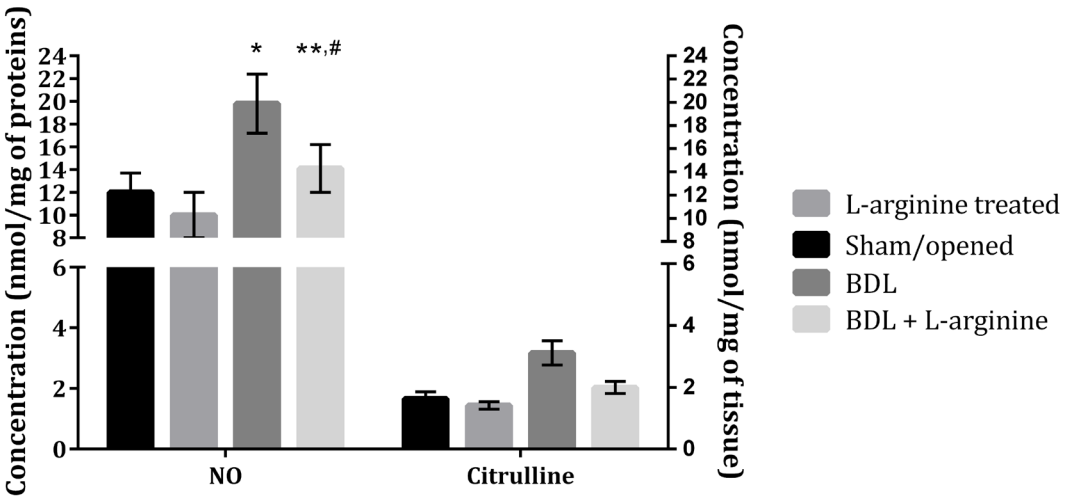

Fig. 2. *Liver tissue NO and citrulline concentrations obtained from control and experimental rats. Values are given as means±SD, n=10. One-way ANOVA followed by Tukey's test was used to compare the groups. *p<0.001 vs sham/opened group, #p<0.001 vs BDL group.*

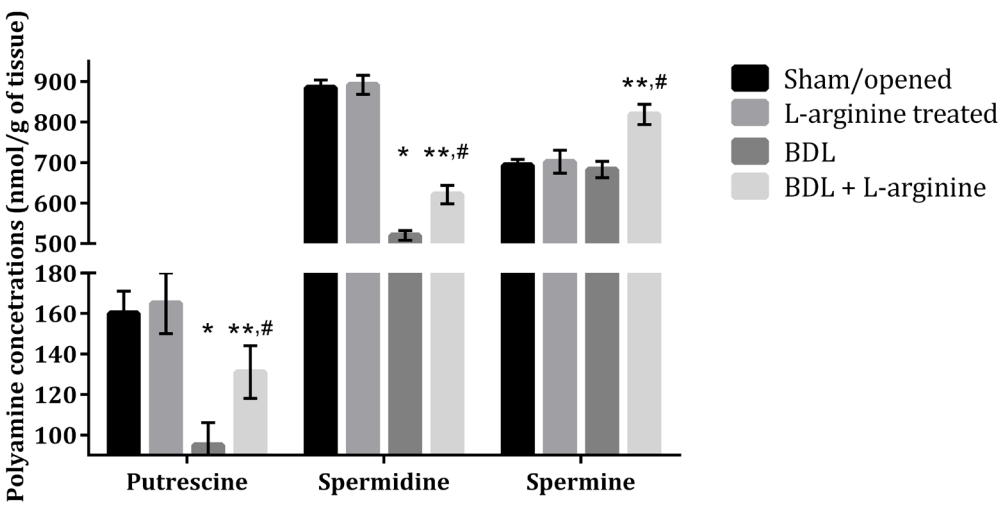

Fig. 3. *Polyamine concertation (nmol/g of tissue) in liver tissue of control and experimental rats. Values are given as means±SD, n=10. One-way ANOVA followed by Tukey's test was used to compare the groups. **p<0.01; *p<0.001 vs sham/opened group, #p<0.001 vs BDL group.*

In group III of rats (those subjected to BDL) liver amounts of putrescine and spermidine were found to be statistically significantly decreased compared to the sham/opened group (Fig. 3). A significant decrease in the levels of polyamines in rats subjected to BDL was prevented by a nine-day L-arginine treatment (Fig. 3).

During the course of experiment, application of L-arginine led to a significant decrease in liver tissue PAO activity compared to the sham/opened group, while the DAO activity remained unaffected (Table I). A nine-day L-arginine treatment was able to significantly prevent BDL-induced PAO and DAO decrease in rat liver (Table I), but the activity was still insignificantly different from both the sham/opened and BLD groups of rats.

DISCUSSION

The beneficial properties of high doses of L-arginine in BDL model have been previously published (5, 6), additionally, we found that L-arginine application to rats with BDL resulted in a significant decrease of bile acid concentration, which accumulates during cholestasis and causes significant damage to the liver (2), compared to rats subjected to BDL. The course of cholestasis hepatic dysfunction partially depends on NO (5-8) and the results of this study showed for the first time that the application of L-arginine during cholestasis led to a decrease in NO production. Other enzymes (arginase) and products of enzymatic reaction [citrulline (9)] were found to be significantly affected also by L-arginine application during cholestasis. These results are somewhat unexpected since arginine is a source molecule for NO generation (10).

Polyamine levels were significantly decreased during cholestasis and we found that liver tissue polyamine, where their concertation is highest (11), are mainly unaffected by L-arginine, except for spermine. These results are in good correlation with the theory that NO inhibits polyamine synthesis (12). Also, the PAO and DAO, main polyamine catabolizing enzymes (10), that are decreased during cholestasis induced by BDL were found to be poorly affected by L-arginine treatment, which might not be completely non-beneficial, since by the decrease in their activity the amounts of polyamines could remain stable (constant) and the pro-apoptotic molecules arising from their activity would not be generated (10).

The obtained results contribute to the pool of knowledge related to the involvement of L-arginine as a hepatoprotective agent by mitigating the harmful effects of bile during cholestasis, affecting NO-urea cycle and by maintaining liver tissue polyamine concentrations.

ACKNOWLEDGEMENTS

This work was supported by the Ministry of Education, Science and Technological Development of the Republic of Serbia (Project 43012).

REFERENCES

1. Wang H, Vohra BP, Zhang Y, Heuckeroth RO. Transcriptional profiling after bile duct ligation identifies PAI-1 as a contributor to cholestatic injury in mice. Hepatology 2005; 42:1099-08.
2. Sokolović D, Bjelaković G, Nikolić J, et al. Effect of L-arginine on metabolism of polyamines in rat's brain with extrahepatic cholestasis. Amino Acids 2010; 38:339-45.
3. Morris JG. Nutritional and metabolic responses to arginine deficiency in carnivores. J Nutr 1985; 115:524-31.
4. Teixeira D, Santaolaria ML, Meneu V, Alonso E. Dietary arginine slightly and variably affects tissue polyamine levels in male Swiss albino mice. J Nutr 2002; 132:3715-20.
5. Ozsoy Y, Coskun T, Yavuz K, Ozbilgin K, Var A, Ozyurt B. The effects of L-arginine on liver damage in experimental acute cholestasis an immunohistochemical study. HPB Surg 2011; 2011:306069.
6. Muriel P, González P. Liver damage induced by acute cholestasis in the rat is ameliorated partially by L-arginine. Comp Biochem Physiol C Pharmacol Toxicol Endocrinol 1998; 120:421-4.
7. Iwakiri Y, Kim MY. Nitric oxide in liver diseases. Trends Pharmacol Sci 2015; 36:524-36.

8. Muriel P. Regulation of nitric oxide synthesis in the liver. J Appl Toxicol 2000; 20:189-95.
9. Wu G, Bazer FW, Davis TA, et al. Arginine metabolism and nutrition in growth, health and disease. Amino Acids 2009; 37:153-68.
10. Nikolic J, Stojanovic I, Pavlovic R, Sokolovic D, Bjelakovic G, Beninati S. The role of L-arginine in toxic liver failure: interrelation of arginase, polyamine catabolic enzymes and nitric oxide synthase. Amino Acids 2007; 32:127-31.
11. Sokolovic D, Bjelakovic G, Nikolic J, Kocic G, Pavlovic D, Stojanovic I, Effect of L-methionine as hepatoprotective agent on polyamine metabolism in experimental cholestasis. Jugoslov Med Biohem 2006, 25:54.
12. Bjelakovic G, Pavlovic D, Jevtovic T, et al. Vitamin B12 and folic acid effects on polyamine metabolism in rat liver. Pteridines 2006; 17:90-94.

LETTER TO THE EDITOR

CONTINUOUS NURSING INTERVENTION ON RECOVERY OF DIABETIC PATIENTS

S. CHI[1], JL. LIU[1], HC. KANG[1] and DM. LV[2]

[1]Endocrinology Unit 5, The Second Affiliated Hospital of Harbin Medical University, Harbin, Heilongjiang, China; [2]Department of Nursing, The Second Affiliated Hospital of Harbin Medical University, Harbin, Heilongjiang, China

Received September 25, 2018 – Accepted October 16, 2018

The aim of this study was to probe the influence of continuous nursing intervention on recovery of diabetic patients. From October 2016 to June 2017, 80 diabetic patients who received treatment in our hospital were selected and randomly divided into an intervention group and a control group. The intervention group received continuous nursing care including indirect follow-up, health education and home visit. The self-care ability and blood sugar of the two groups were compared three months later. The score of self-care ability in the intervention group was 89.64±1.64 and that in control group was 72.68±2.47, and a significant difference was observed (P < 0.001). The fasting blood glucose level in the intervention group was 6.62±0.86 MMOL/L, and the 2-hour post-meal blood glucose level was 8.47±1.32 MMOL/L, which were both lower than those in the control group. Continuous nursing can help monitor the recovery of patients after discharge. It is helpful to improve the self-care ability of patients, control blood sugar level, and promote recovery. It is worth wide promotion.

To the Editor,

Diabetes, a common chronic disease, is a metabolic disorder related to blood glucose level (1) and is accompanied by complications such as neuropathy and retinopathy (2, 3), which can seriously affect the life quality of diabetic patients. The treatment of diabetes is a relatively long process. Many diabetic patients do not maintain good habits after discharge and have insufficient understanding of or give lack of attention to their condition, leading to the deterioration of the disease. Providing a long-term medical service for patients is an important issue in medical care nowadays. Continuous nursing is a type of nursing that provides patients with consistent medical help after they leave the hospital, and can effectively promote their recovery. Zhang et al. (4) studied the impact of continuous nursing on the living capacity and quality of life of patients with hypertensive intracerebral hemorrhage and found that continuous nursing could effectively improve the living capacity of patients after surgery, reduce the probability of complications, and improve their quality of life. Li et al. (5) found that patients who received continuous care were superior to those who did not receive continuing care in terms of nursing methods, nursing skills and health knowledge one year after discharge, indicating that continuous care had a significant effect on improving the patients' self-care ability. Otaghi et al. (6) studied the effect of continuous nursing on sleep quality and found that the sleep quality of hemodialysis patients was significantly improved after one month of nursing intervention compared with patients without continuous nursing. That article discussed the

Key words: diabetes, continuous nursing, nursing intervention, nursing effect

Mailing address:
Dr Dongmei Lv,
Department of Nursing, The Second Affiliated Hospital ,
Harbin Medical University, No. 248, Xuefu Road,
Nangang District,
Harbin, Heilongjiang, 150086, China
e-mail: dongmeilvhr@yeah.net

0393-974X (2018)

influence of continual nursing on the recovery of patients with diabetes.

In the present study, 80 patients with diabetes were divided into an intervention group and a control group; patients in the intervention group received continuous nursing including indirect follow-up, health education and home visits. The effect of continuous nursing on diabetic patients was analyzed by comparing the self-nursing ability and blood glucose control of patients in the two groups.

MATERIALS AND METHODS

General data

Eighty diabetic patients who came to our hospital for treatment between October 2016 and June 2017 were randomly selected as the study subjects. Patients or their family members could communicate via Wechat or QQ, and volunteered to join the study and signed informed consent. The 80 patients were randomly divided into an intervention group and a control group, and continuous nursing care was given to the intervention group. The age of the subjects was between 30 and 80 years, and the proportion of men and women in the two groups was similar and most of them lived with their families. Medical insurance was the main payment form for medical expenses. The general data such as age, sex, job, educational background were compared between the two groups, but no significant difference was found ($P > 0.05$), thus the results of the two groups could be compared. The comparison of general data between the two groups is shown in Table I.

Continuous nursing method

Nursing staff was organized to set up a continuous nursing team. Patients in the control group were given conventional nursing, while patients in the intervention group were given continuous nursing. The content of the nursing is shown below.

Indirect follow-up

The patients were followed up via telephone, WeChat and QQ, 30 min each time. They were followed up at the 1st, 2nd, 4th, 8th and 12th week after discharge. With regard to diet, the daily calorie necessity was calculated; the daily intake of carbohydrates was controlled between 50% and 60%, protein between 15% and 20%, and fat lower than 30%; meals were arranged regularly; proper fruits were selected; smoking and wine were forbidden. Regarding medication, patients were asked to follow the doctor's advice and keep the medication time, dosage and possible adverse reactions in mind. For blood glucose, the patients were informed of the correct blood glucose monitoring method; the monitoring time was set according to actual conditions of patients; they were shown how to accurately record the monitoring results of blood glucose and were informed regarding matters needing attentions. The patients were asked to carry out regular moderate exercise, and carry their diabetes first aid card during exercise. In the aspect of foot care, the water temperature was lower than 37°C; nails were correctly trimmed, hot-water bottles were forbidden, feet were examined every day, and loose and air-permeable foot-gear was selected.

The flow of network follow-up is shown in Fig. 1.

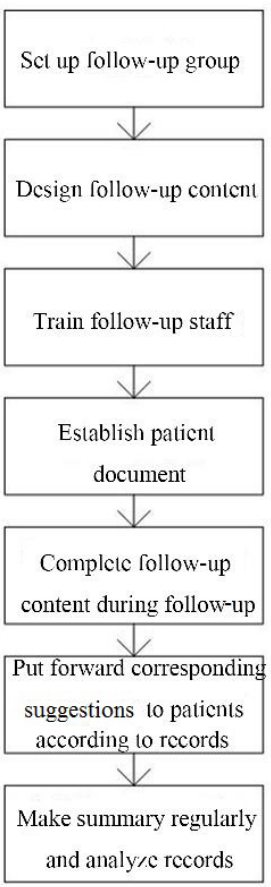

Fig. 1. *The procedures of indirect follow-up.*

Table I. *Comparison of general data between the two groups*

General data		Intervention group n=40 (%)	Control group n=40 (%)	P
Sex	Male	21(52.5)	22(55)	0.726
	Female	19(47.5)	18(45)	
Age	Under 40 years old	5(12.5)	4(10)	0.854
	40-60	17(42.5)	16(40)	
	Above 60 years old	18(45)	20(50)	
Job	On the job	17(42.5)	16(40)	0.685
	Retired/unemployed	23(57.7)	24(60)	
Educational background	Junior middle school or lower	10(25)	11(27.5)	0.452
	Senior high school	15(37.5)	14(35)	
	University or higher	15(37.5)	15(37.5)	
Marital status	Unmarried	7(17.5)	6(15)	0.652
	Married	19(47.5)	20(50)	
	Divorced/ widowed	14(35)	14(35)	
Medical expenses	Self-paying	11(27.5)	9(22.5)	0.741
	Medical insurance	29(72.5)	31(77.5)	
Income situation	Lower than 1000	5(12.5)	4(10)	0.623
	1000-3000	5(12.5)	6(15)	
	3000-5000	17(42.5)	15(37.5)	
	Higher than 5000	13(32.5)	15(37.5)	
Inhabiting information	Live alone	11(27.5)	10(25)	0.897
	Live with family	29(72.5)	30(75)	

Health education

Records were kept for each patient. Detailed records were established for patients in the intervention group, and the contents included general data, treatment course, date of discharge and information regarding fasting blood glucose, 2-hour post-meal blood glucose, cholesterol and blood pressure. Comprehensive knowledge of patient information could help nursing staff give effective suggestions.

Nurses provided patients with scientific information related to diabetes care, including scientific diet, correct medication, appropriate exercise, foot care, correct insulin injection.

The nurses organized weekly health lectures on diabetes, which included basic knowledge of diabetes, diet and exercise, management of hypoglycemia or hyperglycemia, proper insulin injection, and introduction

Table II. *Questionnaire.*

Item		Score
Diet	Whether can follow diet plan?	
	Whether can persist in eating fruit and vegetables?	
Drug use	Whether can take drugs and receive injection of insulin timely?	
	Whether can go to hospital for reexamination regularly?	
Sports	Whether can persist in exercise (at least four times per week and 30 min each time)?	
	Whether can carry candy and emergency card during sports?	
Blood glucose monitoring	Whether can persist in measuring blood glucose at least three times every week?	
	Whether can deal with the condition when the level of blood glucose is slightly high or low?	
Foot nursing	Whether can persist in foot nursing?	
	Whether can ensure comfortable shoes and footgear ?	

Table III. *Comparison of self-nursing ability between the intervention and control groups.*

	Intervention group(n=40)	Control group (n=40)	P
Diet	18.27±0.21	15.21±1.02	0.001*
Medication	18.69±0.34	15.37±1.12	0.000*
Exercise	18.11±0.52	14.67±1.25	0.000*
Monitoring of blood glucose	17.96±0.28	12.97±1.04	0.000*
Foot nursing	18.06±0.61	12.19±1.35	0.000*
Total score	89.64±1.64	72.68±2.47	0.000*

** $p < 0.001$, i.e., the difference was extremely significant.*

of diabetic complications.

Psychological guidance was given to the patients. The regular nursing staff understood the psychological status of patients, and encouraged them to face the disease bravely, maintain a positive and optimistic attitude, deal with physical emergencies timely and calmly, encourage patients with better physical condition to carry out more outdoor activities, timely answers to patients' questions, and pacify patients' emotions.

Home visits

A home visit can help to directly understand the patient's self-care condition and improve his consciousness through direct communication. Home visits were conducted at the first, fourth, eighth and twelfth week after discharge, 30 min each time. The visit helped the staff to understand the patient's self-care condition, evaluate medication and insulin injections, monitor diet and exercise, understand foot care and evaluate the monitoring of blood glucose.

Observational indicators

The self-nursing ability and blood glucose control of the patients were taken as observational indicators. Self-nursing ability was evaluated via a questionnaire.

Content of questionnaire

To ensure the accuracy of the survey results, the questionnaire was completed one-on-one by investigators and patients, and filled out by investigators. The questionnaire included five aspects of content, diet, medication, exercise, blood glucose monitoring and foot care, as shown in Table II.

The questionnaire had ten items, 10 points for each item. Patients evaluated themselves by giving a score between 6 and 10 for each item.

Statistical analysis

SPSS ver. 18.0 was used for statistical analysis. Count data was processed by *Chi*-squares test, and *t*-test was used for measurement data. $P < 0.05$ meant statistical significance, and $P > 0.05$ meant no statistical significance.

RESULTS

Comparison of self-nursing ability

The score of self-nursing ability of patients in the two groups is shown in Table II. It can be seen that the score of self-care ability of the intervention group was 89.64±1.64, and that of the control group was 72.68±2.47. There was a significant difference between the two groups ($P < 0.001$). The self-care ability of patients in the intervention group was superior to that in the control group. Among the five aspects of self-care ability, the two groups scored the highest in drug use, 18.69±0.34 and 15.37±1.12 respectively, and the score of blood glucose monitoring was the lowest, 17.96±0.28 and 2.97±1.04, respectively. It may be because drug use is the most effective way to control the disease and can take effect directly and rapidly, and blood glucose monitoring is difficult for patients. Nontheless, the score of blood glucose monitoring of the intervention group was significantly higher than that of the control group,

Table IV. *Comparison of blood glucose control condition between the intervention and control groups.*

	Intervention group (n=40)	Control group (n = 40)	P
Fasting blood glucose (MMOL/L)	6.62±0.86	7.85±1.01	0.000*
2-hour post-meal blood glucose level (MMOL/L)	8.47±1.32	9.27±1.04	0.047**

indicating that continuous nursing improved the patients' attention to blood glucose monitoring, and scientific guidance was of great help to the monitoring of blood glucose. In other aspects, the intervention group was also better than the control group, which suggested the effectiveness of continuous nursing.

Comparison of blood glucose control

Table III and Fig. 2 show that there were differences in the fasting blood glucose levels and 2-hour post-meal blood glucose levels between the intervention group and control group. The fasting blood glucose levels of the control group were 7.85±1.01 MMOL/L, and those of the intervention group were 6.62±0.86 MMOL/L, suggesting an extremely significant difference ($P < 0.001$). The 2-hour post-meal blood glucose level of the intervention group was 8.47±1.32 MMOL/L, which was significantly different from that of the control group (9.27±1.04 MMOL/L, $P < 0.05$). This indicated that continuous nursing improved the self-nursing ability of the patients and helped patients to control the level of blood glucose, but the blood glucose level of patients in the observation group was not strictly controlled after leaving the hospital because of the insufficient attention in daily life. All the findings suggested the effectiveness of continuous nursing for better recovery of patients.

DISCUSSION

Diabetes is a common chronic disease, and the control of chronic diseases is inseparable from the patient's self-management. Continuous nursing can provide patients with professional guidance, help them have a better grasp of disease condition (7) after leaving the hospital, effectively improve their quality of life (8, 9), adjust their emotions (10), ensure mental health (11), and strengthen their self-management skills (12). Receiving scientific guidance for diet and drug use is beneficial to recovery. It was found after three months of continuous nursing that the control ability of the intervention group was significantly superior to that of the control group in aspects of diet, sports and drug use; self-nursing ability of patients in the intervention group was significantly higher, and the fasting blood glucose levels and 2-hour post-meal blood glucose levels of the intervention group were significantly lower than those of the control group, which indicates that continuous nursing can effectively promote recovery of patients and improve the level of blood glucose, suggesting high application values.

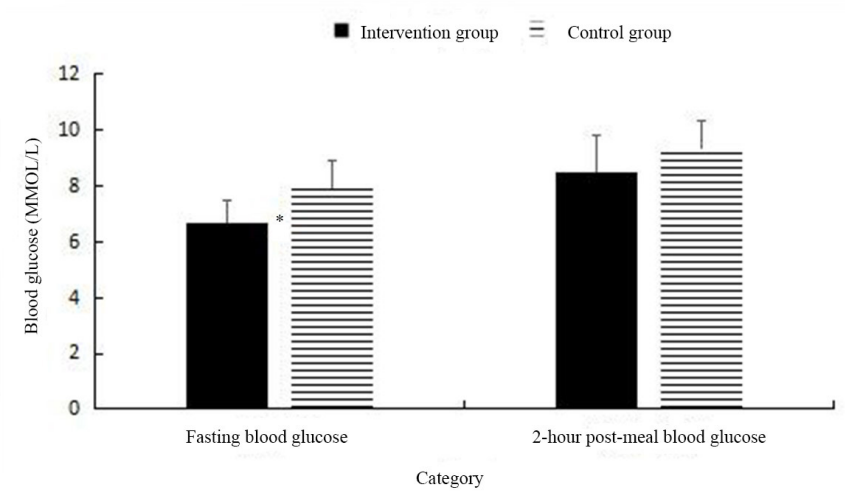

Fig. 2. *Comparison of blood glucose between the intervention and control groups. * $P < 0.01$, i.e., the difference was extremely significant; ** $P < 0.05$, i.e., the difference was statistically significant.*

REFERENCES

1. Perez-Rivera DT, Torres-Torres VL, Torres-Colon AE, Cruzaponte M. Development of a computational model of glucose toxicity in the progression of diabetes mellitus. Math Biosci Eng 2017; 13(5):1043-58.
2. Sayin N, Kara N, Pekel G. Ocular complications of diabetes mellitus. World J Diabet 2015; 6(1):92.
3. Asmat U, Abad K, Ismail K. Diabetes mellitus and oxidative stress-A concise review. Saudi Pharm J 2016; 24(5):547-53.
4. Zhang JR, Li Y, Zhang JX, Wang KP, Fang JR. Continuing care in patients with hypertensive intracerebral hemorrhage and its effects on life ability. J Int Neurol Neurosurg 2015; 0(1):37-40.
5. Li XX. Effect of continuing nursing on self-care ability of elderly patients with diabetes mellitus. Chin Mod Doct 2017; 55(18):151-53.
6. Otaghi M, Bastami M, Borji M, Tayebi A, Azami M. The effect of continuous care model on the sleep quality of hemodialysis patients. Nephrourol Mon 2016; 8(3):e35467.
7. Dong YJ, Shang S, Yao L. The progress of continuing care in foreign countries. Chin Nurs Manag 2012; 12(9):20-23.
8. Borji M, Tavan H, Azami M, Otaghi M. The effect of continuous care model on blood pressure and quality of life in patients on hemodialysis. Biomed Pharmacol J 2016; 9(2):689-95.
9. Li JZ, Zhang LJ, You TH. Influence of continuing care intervention on the quality of life for postoperative patients with breast cancer. Mod Prev Med 2014; 4:624-26.
10. Curtis K, Kuluski K, Bechsgaard G, Ridgway J, Katz J. Evaluation of a specialized yoga program for persons admitted to a complex continuing care hospital: a pilot study. Evid Based Complement Alternat Med 2016; 2016(3):6267879.
11. Chao JJ, Xue YZ. Effect of a new health education model on continuous nursing in elderly patients with diabetes mellitus. Chin Nurs Res 2018; 5(1):69-74.
12. Lin NJ, Zhao Y. Influence of network interactive continuous nursing intervention on life quality of patients with gestational diabetes mellitus. Tianjin J Nurs 2017; 25(2):102-5.

LETTER TO THE EDITOR

CONTRIBUTIONS OF VSX1 GENE TO KERATOCONUS

G. KALASIDOU[1], I. FRYDAS[2], A. KOZEI[3], P. SYRMAKESI[4], E. LOUKOVITIS[5], K. SFAKIANAKIS[6], M. BALIDIS[7], Z. ZACHARIADIS[7], P. TRANOS[7], N. KOZEIS[7] and G. ANOGEIANAKIS[7,8]

[1]Ippokrateion Hospital, Thessaloniki, Greece; [2]Laboratory of Environmental Engineering, Department of Chemical Engineering, Aristotle University of Thessaloniki, Greece; [3]School of Pharmacology, University of Nicosia, Nicosia, Cyprus; [4]AHEPA University Hospital, Thessaloniki, Greece and Ophthalmica Eye Institute, Thessaloniki, Greece; [5]Hellenic Army Medical Corps and Ophthalmica Eye Institute, Thessaloniki, Greece; [6]Division of Surgical Anatomy, Laboratory of Anatomy, Medical School, Democritus University of Thrace, University Campus, Alexandroupolis, Greece; [7]Ophthalmica Eye Institute, Thessaloniki, Greece; [8]Association for Training in Biomedical Technology, Thessaloniki, Greece

Received September 2, 2108 – Accepted September 25, 2018

Keratoconus (KC) is a complex, genetically heterogeneous, multifactorial degenerative corneal disorder, with incidence of approximately 1 per 2000 of the population. KC follows an autosomal recessive or dominant pattern of inheritance and is, apparently, associated with genes which interact with environmental, genetic and/or other factors. The present report focuses on the VSX1 gene, for which there is general agreement that it is involved in KC and other corneal pathologies, and critically details the evidence for its involvement in KC.

To the Editor,

Keratoconus (KC) is a bilateral, progressive ectatic disorder of the cornea characterized by thinning of the central cornea leading to protrusion which results in reduced vision, progressive, irregular astigmatism and cornea scarring (1). KC prevalence is almost 1 in 2000 subjects, and it is higher in the Asian and Middle Eastern populations (2). It usually occurs in the second decade (mean age at onset is 15.39 years) and progresses until the third or fourth decade of life. It is more prevalent in women and affects all ethnicities (1). KC is mostly sporadic, but in 6-10% cases there is positive family history (1).

KC is inherited with both autosomal and recessive forms, with incomplete penetrance in over 90% of autosomal dominant inheritance (1). KC is a complex heterogeneous disorder with variable clinical expression and risk factors, such as atopy and eye rubbing, while oxidative stress induced by ultraviolet light significantly contributes to its development (1). Inflammatory molecules, matrix metalloproteinase 9 (MMP9), interleukin 6 (IL-6), and tumor necrosis factor-α (TNF-a) are more abundant in the tear film of KC patients (3), indicating the role for chronic inflammation to KC pathogenesis.

Whole genome/exome sequencing identified causal mutations in KC families (3), and linkage analysis and candidate gene screening identified

Key words: keratoconus, VSX1 gene, *keratoconus risk factors, keratoconus comorbidities*

Mailing address:
Prof. G. Anogeianakis,
Ophthalmica Eye Institute,
Vas Olgas 196 & Ploutonos 27,
54655 Thessaloniki, Greece
Tel: +30 6976637334
e-mail: anogian@auth.gr

0393-974X (2018)

DISCLOSURE: ALL AUTHORS REPORT NO CONFLICTS OF INTEREST RELEVANT TO THIS ARTICLE.

several genomic loci on different chromosomes in KC families, pointing to its genetic heterogeneity (1). In total, more than 60 genes/loci have been associated with KC; however, the associations were inconsistent across different study cohorts and the roles of most genes/loci are inconclusive; among them are VSX1 (which encodes Visual system homeobox 1), SOD1 (superoxide dismutase 1), and ZNF469 (which encodes Zinc finger protein 469). Other genes that are putatively associated with KC are HGF (Hepatocyte Growth Factor), COL6A1 (which encodes the alpha 1 subunit of type VI collagen), COL8A1 (which encodes one of the alpha 1 subunit of type VIII collagen), LOX (lysyl oxidase), FOXO1 (which encodes Forkhead box protein O1), FNDC3B (Fibronectin Type III Domain Containing 3B), DOCK9 (Dedicator of Cytokinesis), TGFBI (Transforming Growth Factor, Beta Induced), STK24 (Serine/Threonine-protein kinase 24), IPO5 (Importin 5), and MIR184 (microRNA 184) (3). Genome-wide association study (GWAS) also associated KC with more than 150 polymorphisms, however only few of them are associated significantly with KC and thus the number is inflated (3). In conclusion, meta-analysis proved that KC in white human populations is associated with 8 SNPs in 6 genes/loci, including BANP-ZNF469 rs9938149, FOXO1 rs2721051, FNDC3B rs4894535, RXRA-COL5A1 rs1536482, COL4A4 rs2228557 and rs2229813 and IMMP2L rs214884 and rs757219, and 10 genes/loci with suggestive evidence of association with KC (3). In view of there being no definite or consistent results regarding the role of most of the genes implicated in KC (3), apparently owing to the many coding variations in the KC-related genes among different ethnicities (1), the present report focuses on VSX1 for which there is general agreement that it is involved in KC and other corneal pathologies.

The VSX1 gene

VSX1 mutations have been identified in KC and posterior polymorphous corneal dystrophy (PPCD) (1, 4, 5) and the pathogenic role of this gene is widely accepted even though several studies have failed to confirm the association between KC and VSX1 variants/polymorphisms (5, 6). Given the ethnic variation found in various parts of the world (7), and the multifactorial/polygenic character of KC (6), it is possible that some VSX1 mutations are not responsible for KC (5). Thus, VSX1 plays a significant role in KC development in Italian, Iranian and Chinese people, while no pathogenic mutations in VSX1 were found in KC patients from Slovenia, South India, Saudi Arabia and Ecuador (8). A similar situation is observed among Indian and Korean people (8).

VSX1 is expressed in the cornea but also in the retina (6). Although not overly expressed in resting or quiescent human keratocytes, VSX1 is expressed by keratocytes in wounded corneas, or in corneas cultured in serum that mimic wound conditions and contribute to the fibroblastic transformation of corneal stromal cells into myofibroblasts. This supports the hypothesis that VSX1 has a role in the wound healing response that contributes to the underlying pathology of corneal disease (6) as, e.g., in abnormal stromal repair (9).

The VSX1 is localized to chromosome 20p11-q11 (3). A homeodomain transcription protein is encoded by this gene and is responsible for cone opsin expression during the early ocular development and for cellular differentiation during craniofacial development (7, 9). Mutations in VSX1 trigger developmental abnormalities in craniofacial tissues, retinal cells, the sella turcica and in the corneal endothelium (6). VSX1 is also expressed in several ocular tissues and in the core of the locus which controls the red-green visual pigment gene cluster (10). The VSX1 consists of a paired-like homeodomain (HD) with a highly conserved CVC domain in the C-terminal. It has a vital role in the proliferation and survival of retinal progenitor cells and bipolar interneurons (1). There are also six transcripts and five variants which encode a truncated protein, while two of them retain the DNA binding domain (4). The five exons of VSX1 encode a 365 amino-acid protein with a homeobox DNA binding and a ceh-10 domain and the highly conserved among vertebrates Chx10/VSX1 domain (1, 7).

Five exons in the VSX1 span 6.2kb of the coding sequence (4). Other reports mention that the exons

of VSX1 span 6.7 kb of DNA on chromosome 20 with an additional two exons characterized that encode two isoforms of the VSX1 transcript; transcript 1 (NM_014588) encodes protein isoform A (NP_199452.1) and transcript 2 (NM_199425) encodes protein isoform B (NP_955457) (6). Two more exons of VSX1 produce four previously unknown VSX1 transcripts (4). Therefore, VSX1 spans 10.65 kb of genomic DNA and has 7 exons producing six transcripts (via different splicing patterns). According to Genbank (11), these are NM_199425 (or DQ854808), NM_014588 (or DQ854807), DQ854809, DQ854810, DQ854811, and DQ854812. Exons 2,3 and 4 of VSX1 apparently have an increased probability of being mutated (4), even though (as already mentioned) not all VSX1 mutations are causally connected to KC.

Variants of VSX1 such as G160D, L17P, P247R, G160V, L159M, N151S, H244R, D144E and R166W are possibly associated with KC (4). Two VSX1 mutations (R166W and L159M) were initially identified in KC patients, as was the variant H244R, although it is not confirmed that they cause KC (5). For example, the G160D variant is pathogenic while P247R is not pathogenic (4); however, P247R seems to co-segregate with KC (4) since the G160D alone is associated with mild to moderate PPD, while P247R alone does not cause any corneal abnormalities. Also, abnormal electroretinographic function of the inner retina, where VSX1 is also expressed, is detected with either the G160D or P247R mutation. (5)

The role of D144E mutation in KC is also confusing. Some studies support that it is pathogenic whereas others do not (5). The H244R mutation, which is located in exon 4 of the gene (in the CVC domain) and is essential for the repressive transcriptional action of VSX1, is present in 2% of the patients (4). Hence, the role of mutations H244R, L159M, R166W and D144E in VSX1 in KC are disputed (4). Two other variants, G160V and N151S, have been identified in the Korean population but not in any other population (5). Mutations D144N and D295Y may have a role in the pathogenesis of KC and attempts to associate Q195H in VSX1 with KC are inconclusive (4, 5).

Other VSX1 variants identified in KC patients are c.432CAG (Asp144Glu), c.475T4A (Leu159Met), c.496C4T(Arg166Trp), c.731A4G(His244Arg) (12). Three of these, (i.e., Asp144Glu, Leu159Met and Arg166Trp), as well as Pro247Arg and Gly160Asp (also in VSX1 gene), are possibly associated with KC and PPCD (12). The p.His244Arg has been associated with PPCD, macular degeneration and bipolar cell dysfunction (1). Other mutations in VSX1 like Leu17Pro (3), the missense mutations Asn151Ser and Gly160Val, and one intragenic polymorphism are associated with KC only (12).

Regarding the relationship between VSX1 pathogenic variations and sporadic KC (7), recent studies report that sporadic KC in Chinese and Indian populations is associated with four nucleotide variations, i.e., the missense p.Arg131Pro (c.5427G>C) (heterozygous), nucleotide c.8326G>A sequence variation (in both heterozygous and homozygous forms) and the missense p.Gly160Val sequence variant (heterozygous) (7). However, the pathogenic effects of most missense substitutions in the VSX1 are not confirmed (1).

VSX1 και PPCD

Apart from KC, VSX1 is associated with the pathogenesis of endothelial corneal dystrophy Fuchs and PPCD (12). Thus, VSX1 SNPs rs2071376, rs12480307 and rs56157240 increase the risk PPCD and KC apparently because these disorders share a common mode of involvement in Descemet's membrane (6). However, SNP rs6050307 has a protective effect in the Han Chinese population (3).

PPCD is a frequently asymmetric autosomal dominant, mostly bilateral corneal dystrophy characterized by abnormalities in Descemet's membrane and the corneal endothelium (6, 12) and is associated with mutations in the PPCD3 locus, in the ZEB1 (that encodes Zinc finger E-box-binding homeobox 1) gene (6). PPCD is also affected by the COL4A3 gene (which encodes collagen type IV alpha 3 chain) associated with KC (12); it is genotypically heterogeneous (6). Similarly, mutations in COL8A2 are also associated with PPCD and Fuchs endothelial corneal dystrophy (6, 12). Finally, chromosome 20p11-q11 is associated with PPCD1 (cytogenetic location 20p11.23) while VSX1

mutations (genetic locus VSX1; MIM#605020) and (genetic locus KTCN1; MIM#148300) are involved in PPCD1 and in KC, respectively (12). Therefore, the association between PPCD and KC is considered well documented, with many of the cases described co-occurring in the same cornea (6).

In conclusion, the present review consolidates evidence of the involvement of the VSX1 gene in KC manifestation and development. It also identifies other genes that are putatively associated with KC, such as SOD1, ZNF469, HGF, COL6A1, LOX, FOXO1, FNDC3B, DOCK9, TGFBI, STK24, IPO5, and MIR184. Despite the fact that these associations apparently are still not well established and that differences among them are evident from study to study, a case can be made for exploring the genetic make-up of comorbidities that share these genes with KC in the hope that the resultant genetic association profiles may also shed light on the different expression of familiar and sporadic KC.

REFERENCES

1. Shetty R, Nuijts RM, Nanaiah SG, et al. Two novel missense substitutions in the VSX1 gene: clinical and genetic analysis of families with Keratoconus from India. BMC Med Genet 2015; 16(1):33.
2. Valgaeren H, Koppen C, Van Camp G. A new perspective on the genetics of keratoconus: why have we not been more successful? Ophthalmic Genet 2018; 39(2):158-74.
3. Rong SS, Ma STU, Yu XT, et al. Genetic associations for keratoconus: a systematic review and meta-analysis. Sci Rep 2017; 7(1):4620.
4. Paliwal P, Singh A, Tandon R, Titiyal JS, Sharma A. A novel VSX1 mutation identified in an individual with keratoconus in India. Mol Vis 2009; 15:2475-79.
5. Tang YG, Picornell Y, Su X, Li X, Yang H, Rabinowitz YS. Three VSX1 gene mutations, L159M, R166W, and H244R, are not associated with keratoconus. Cornea 2008; 27(2):189–92.
6. Vincent AL, Jordan C, Sheck L, Niederer R, Patel DV, McGhee CN. Screening the visual system homeobox 1 gene in keratoconus and posterior polymorphous dystrophy cohorts identifies a novel variant. Mol Vis 2013; 19:852-860.
7. Guan T, Wang X, Zheng LB, Wu HJ, Yao YF. Analysis of the VSX1 gene in sporadic keratoconus patients from China. BMC Ophthalmol 2017; 17(1):173.
8. Karolak JA, Polakowski P, Szaflik J, Szaflik JP, Gajecka M. Molecular screening of keratoconus susceptibility sequence variants in VSX1, TGFBI, DOCK9, STK24, and IPO5 genes in Polish patients and novel TGFBI variant identification. Ophthalmic Genet 2016; 37(1):37-43.
9. Barbaro V, Iorio ED, Ferrari S, Bisceglia L, Ruzza A, Luca MD, Pellegrini G. Expression of VSX1in human corneal keratocytes during differentiation into myofibroblasts in response to wound healing. Invest Opthalmol Vis Sci 2006; 47(12):5243-50.
10. VSX1 gene - Genetics Home Reference - NIH [Internet]. U.S. National Library of Medicine. National Institutes of Health; [cited 2018Aug26]. Available from: https://ghr.nlm.nih.gov/gene/VSX1
11. GenBank Overview [Internet]. Advances in pediatrics. U.S. National Library of Medicine; [cited 2018 Aug26]. Available from: https://www.ncbi.nlm.nih.gov/genbank/
12. Lechner J, Dash DP, Muszynska D et al. Mutational spectrum of the ZEB1 gene in corneal dystrophies supports a genotype–phenotype correlation. Invest Opthalmol Vis Sci 2013; 54(5):3215-23.

JOURNAL OF BIOLOGICAL REGULATORS & HOMEOSTATIC AGENTS Vol. 32, no. 6, 1519-1523 (2018)

LETTER TO THE EDITOR

THE p75 NEUROTROPHIN RECEPTOR IN CELLS OF ORAL MUCOSAL EPITHELIUM

A. BRYJA[1], M. JANKOWSKI[1], M. DYSZKIEWICZ-KONWIŃSKA[1,2], H. PIOTROWSKA-KEMPISTY[3], P. ANTOSIK[4], D. BUKOWSKA[4], M. BRUSKA[1], M. NOWICKI[5] and B. KEMPISTY[1,5,6]

[1]Department of Anatomy, Poznan University of Medical Sciences, Poznan, Poland; [2]Department of Biomaterials and Experimental Dentistry, Poznan University of Medical Sciences, Poznan, Poland; [3]Department of Toxicology, Poznan University of Medical Sciences, Poznan, Poland; [4]Veterinary Center, Nicolaus Copernicus University in Torun, Torun, Poland; [5]Department of Histology and Embryology, Poznan University of Medical Sciences, Poznan, Poland; [6]Department of Obstetrics and Gynecology, University Hospital and Masaryk University, Brno, Czech Republic

Received July 10, 2018 – Accepted October 19, 2018

The p75 neurotrophin receptor ($p75^{NTR}$) can play different roles in cells. This protein can on the one hand act in the regulation of cell growth and survival, while being an apoptosis inducing factor in different contexts. $p75^{NTR}$ regulates cell cycle not only in nerve cells but also in epithelial oral mucosal cells. In the former, neurotrophin–$p75^{NTR}$ signaling affects cell growth and survival. Recent studies showed that $p75^{NTR}$ is expressed in basal cells of oral mucosal epithelium and can be used as one of the markers of epithelial stem/progenitor cells. This role of $p75^{NTR}$ can be utilised in aspects such as tissue engineering and gene therapy. One of the examples of clinical use of cultivated oral mucosal cells is ocular surface reconstruction. $p75^{NTR}$ can be a significant marker of stem cells in studies of epithelial tissues, especially when the cells will exhibit other specific markers, such as CK13, CK14 and PCNA.

To the Editor,

Structure and role of the p75 neurotrophins receptor

Neurotrophins are secreted in small amounts under physiological conditions. They are responsible for maintaining nerve cells alive. The group consists of Nerve Growth Factor (NGF), Brain-Derived Neurotrophic Factor (BDNF), Neurotrophin-3 (NT-3), and Neurotrophin-4 (NT-4). These proteins bind to and signal through two cell surface receptors. The first is a tyrosine kinase receptor (Trk) that has a tyrosine kinase domain in its cytoplasmic region, and the second one is a low-affinity nerve growth factor receptor, known as the p75 Neurotrophin Receptor ($p75^{NTR}$). $p75^{NTR}$ is also known as CD271 and p75 Nerve Growth Factor ($p75^{NGF}$) or p75 Nerve Growth Factor Receptor ($p75^{NGFR}$) (1). $p75^{NTR}$ receptor was identified for the first time in 1973 and is a member of the Tumor Necrosis Factor Receptor (TNFR) superfamily and can mediate cell survival and cell death in response to NGF. $p75^{NTR}$ is a type I transmembrane protein that has molecular weight of 75 kDa and is coded by genes located on chromosome 17q21. Human $p75^{NTR}$ is synthesized as a precursor, containing a 28-amino acid signal peptide, that is

Key words: $p75^{NTR}$, oral mucosa epithelium, neurotrophins, OSCC

Mailing address:
Bartosz Kempisty PhD,
Department of Histology and Embryology,
Department of Anatomy, Poznań University of Medical Sciences,
6 Święcickiego St., 60-781 Poznań, Poland
Tel./Fax: +48 61 8546418/+48 61 8546440
e-mail: bkempisty@ump.edu.pl

0393-974X (2018)

DISCLOSURE: ALL AUTHORS REPORT NO CONFLICTS OF INTEREST RELEVANT TO THIS ARTICLE.

cleaved from molecule upon insertion of $p75^{NTR}$ into the membrane. This receptor has an extracellular domain (ECD) that includes four modules containing six cysteines. Its intracellular domain contains an 80-amino acid death domain (DD) module.

$P75^{NTR}$ has several functions and plays a role in the development and injury-induced apoptosis, the growth of neurons and cell migration.

All neurotrophins bind to $p75^{NTR}$, while each NT is specific for different Trk receptor subtypes (A, B and C) (2). The TrkA ECD contains a canonical LLR consisting of three leucine-rich repeats capped, at either end, with cysteine-rich domains, followed by an Ig-C1 and an Ig-C2 domain.

It is postulated that these two receptors may cooperate in transducing NGF signals (2). The expression patterns of $p75^{NTR}$ and Trk receptors overlap extensively, and in some instances, TrkA is exclusively expressed with $p75^{NTR}$ (2). Some authors also showed interactions between $p75^{NTR}$, NGF and TrkA (2). Wehrman et al. proposed that NGF can create a "high-affinity" TrkA/NGF/p75 complex (2).

Nakamura et al. analysed the role of neurotrophin signaling in $p75^{NTR}$ positive oral keratinocytes. They used UV-induced apoptosis assay (TUNEL) in an *in vitro* culture. Without UV conditions, neurotrophins did not seem to influence cell death in an *in vitro* culture. Under UV conditions, NGF exerts a positive effect against UV-induced apoptosis. Other neurotrophins (BDNF, NT3, NT-4) did not affect cells (3). The researchers, using BrdU assay, indicated that NGF and NT-3 stimulated proliferation of p75(+) keratinocytes, while not confirming, in immunohistochemical results, that neurotrophins influence cell differentiation (3).

The pattern of $p75^{NTR}$ expression in oral mucosa epithelium

It was observed that, in mucosal keratinocytes, mRNA coding NGF and its receptors, TrkA and $p75^{NTR}$, was expressed (4). Hayashi et al., in their study, immunostained normal oral mucosa and oral lichen (OL) with antibodies against NGF, proNGF, $p75^{NTR}$ (4). In normal tissue proNGF protein and mRNA staining was seen in all epithelial cell layers, and a similar situation was observed in OL. Cytoplasmic staining for NGF was detected in the granular cells and spinous cell layers in both normal epithelium and OL. Staining for $p75^{NTR}$ was observed only in the cell membrane of basal cell layers. In OL basal keratinocytes showed no or only weak cytoplasmic staining for $p75^{NTR}$ (4). The Authors summarized that increased expression of TrkA and decreased expression of $p75^{NTR}$ in OL might be factors that alleviate early cell death and support cell survival in OL (4).

Nakamura et al. demonstrated that $p75^{NTR}$ was expressed in the tips of the papillae in the buccal mucosa (3). They also found that in the gingiva, $p75^{NTR}$ was expressed in the tips of the papillae and in the deep rete edge (3). The cells with positive expression of the p75 receptor were smaller and possessed higher *in vitro* proliferative potential (3). Similar results were presented by Chen et al. The expression of $p75^{NTR}$ was strictly confined to the basal layer (5). In another study, also employing human oral keratinocytes from oral buccal or gingival tissue, it was confirmed that expression of $p75^{NTR}$ was limited to the basal layer cells. The expression of $p75^{NTR}$ was more intense in the tip of the papillae. Contrary to the above results, Gemenetzidis et al. described that expression of $p75^{NTR}$ in deep rete ridges was less intense (6). They used FACS to isolate two types of keratinocytes. The first type exhibited low expression of $p75^{NTR}$ (low-$p75^{NTR}$). Differentiating/non-clonogenic cells belonged to this fraction. The second type of cells, showing high expression of $p75^{NTR}$ (high-$p75^{NTR}$), contains stem and early progenitor cells which are clonogenic, or can form holoclones *in vitro* (6). The cells that expressed $p75^{NTR}$ alone represented the majority of clonogenic stem/progenitor cells, compared to cells with co-expression of $p75^{NTR}$ and integrin β1 (epidermal stem cell marker) that demonstrated only a marginal advantage in clonogenic potential (6).

Slow cycling is one of the unique features of adult stem cells (SCs). Okumura et al. checked the *in vivo* cell cycle status in human oral mucosal epithelium. They used Ki67 as a marker for actively cycling cells. In their results, the number of p75(+) cells with high expression of Ki67 was scientifically lower than p75(+)/Ki67(-) cells. This indicated that *in vivo*, most p75(+) cells were not actively cycling cells (3).

Summarizing the above results, it is known

that p75^{NTR} in oral mucosa is expressed in cell membrane area of basal cells and it was confirmed that keratinocytes located in the basal layer that express p75^{NTR} belong to oral epithelial stem cells (1). Ishii et al. investigated the expression of p75^{NTR} in mouse buccal mucosa epithelium during wound healing and postulated that p75NTR(+)/PCNA(+) or p75NTR(+)/BrdU(+) cells taking part in the re-epithelialization process might be epithelial stem cells (ESCs) (1). The results of these study suggested that p75 receptor can be used as oral keratinocyte stem/progenitor cell markers (3).

Ishii et al. also presented results stating that the number of cells with positive expression of p75^{NTR} was reduced in the wound site, from the early stage of wound healing in comparison to control groups. The number of p75(+) cells was recovered after the epithelium completely closed the irradiated area (1). They concluded that regenerated epithelial cells might move from the wound margin to the wound surface, but these cells are not proliferative and do not act as progenitor cells at the wound area (1).

The biological role of p75^{NTR} in oral mucosa diseases

The high-level expression of p75^{NTR} was observed in oral mucosal melanoma and cutaneous melanoma. In reference to these observations, it was postulated that the invasion-inducing role of p75^{NTR} is similar in both oral mucosal and skin melanomas. Boiko et al., in their study, used p75^{NTR} as a cancer stem cell

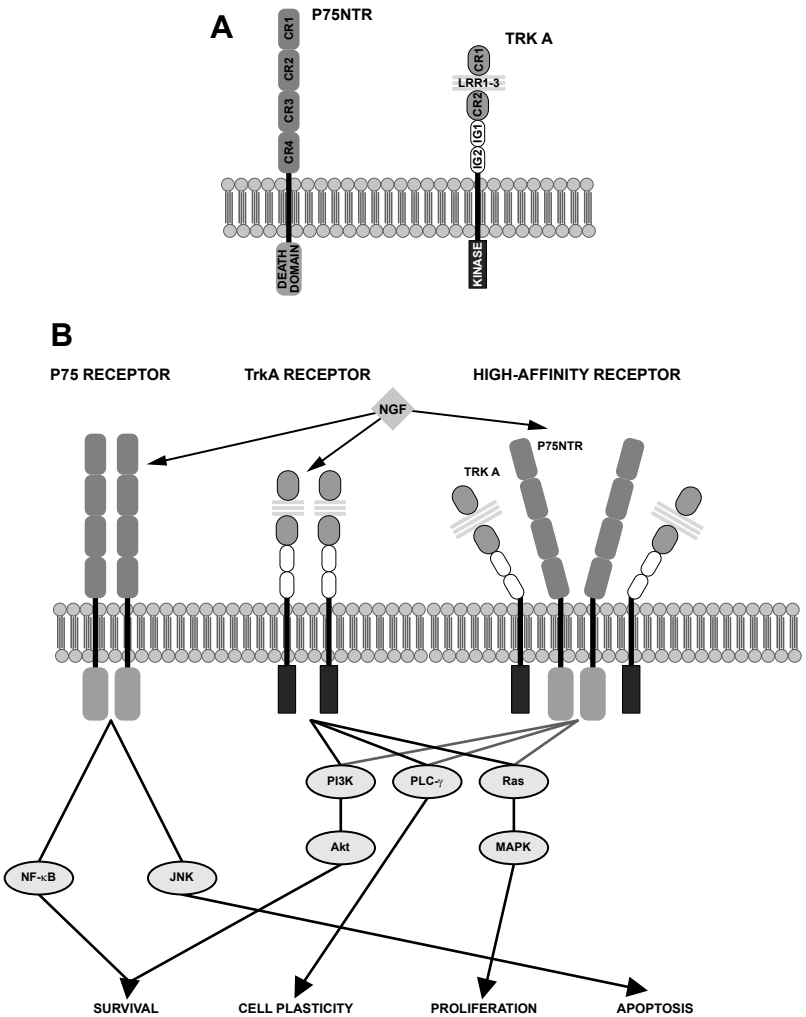

Fig. 1. *Structures and functions of p75^{NTR} and TrkA in cells. **A)** Structures of p75^{NTR} and TrkA. **B)** Signaling pathways of p75^{NTR} and TrkA.*

marker that allowed identification and prospective isolation of melanoma cancer stem cells (7). Transplantation of isolated p75(+) melanoma cells into engrafted human skin or bone in mice resulted in melanoma. In the case when isolated p75(-) cells were used for transplantation, melanoma did not develop in mice (7).

It is generally considered that cancer stem cells play a role in tumor initiation and growth. Oral squamous cell carcinoma (OSCC) often arises from dysplastic lesions (8). In a recent study, CD44, $p75^{NTR}$, CD24 and ALDH were used as potential cancer stem cell markers (9). Dalley et al., in their work, used 3D organotypic culture to investigate cancer stem cell involvement in the progression of oral dysplasia to OSCC (8). To produce Human Oral Mucosa Equivalent (HOME) they used de-epidermised dermis (DED) as a base for culture of 4 cell lines: normal tissue (OKF6-TERT2), mild dysplasia (DOK), severe dysplasia (POE-9n) and oral squamous cell carcinoma (PE/CA PJ15) (8). Their experiment with the HOME culture system showed that loss of hierarchical coordination of CD44 and $p75^{NTR}$ discriminated carcinoma delivered cells from non-cancerous cells when grown as HOME cultures (8).

Soland et al. in their study presented that high expression and the pattern of invasion of $p75^{NTR}$ were associated with a poor prognosis in oral squamous cell carcinoma (9). $p75^{NTR}$ can be used as a prognostic and recurrence marker for OSCC (9). Similar results were shown in esophageal squamous cell carcinoma (ESCC) by Okumura et al. They concluded that $p75^{NTR}$ is necessary for survival and maintenance of ESCC tumors (10). Similarly, Huang et al. described that cells with positive expression of $p75^{NTR}$ can self-renew and are chemotherapy resistant (10).

$p75^{NTR}$ as a marker of stem cells in the reconstructive medicine

Oral mucosa contains two tissue layers: the epithelium and the underlying lamina propria. In development, interactions between stem/progenitor cells and mesenchyme are important to morphogenesis of oral mucosa. These interactions are significant in transplantation and regeneration of oral mucosa. The stem cells play a role in wound healing and tumorigenesis. Their identification is important for therapeutic use in tissue engineering, gene therapy and in various diseases (3). $p75^{NTR}$ is often used as stem/progenitor cells marker in reconstructive medicine.

Oral mucosa epithelial cells have been used as an autologous cell source for corneal epithelium reconstruction in bilateral ocular surface diseases (11) and limbal stem cell deficiency (11). The ocular surface is composed of three types of epithelial cells: conjunctival, limbal and corneal epithelium (11). The ocular surface disease is marked by the conjunctival invasion of the corneal surface, neovascularization, chronic inflammation, loss of vision and severe dry eye (11). Limbal stem cell transplantation (LSCT) or conjunctival limbal autograft (CLAU) can be used in its reconstruction, but these techniques have limitations, especially in bilateral ocular surface disease. These limitations can be minimalized by using oral mucosal epithelial cells as transplant material (11). One of the important factors for ocular surface reconstruction is $p75^{NTR}$ expressed in human corneal epithelium, oral mucosa epithelium, skin and neurons (11).

RT-qPCR analysis detected expression of $p75^{NTR}$ in the cultured oral epithelium. Cultured cells were also checked by immunohistochemistry. Only a few cells expressed p75 in the cultured oral cells, in contrast to the large proportion of cells from cultured limbal and conjunctival cultures, which expressed $p75^{NTR}$. Authors suggested that $p75^{NTR}$ may be a more appropriate marker for stem cells of the oral epithelium, hence in culture, the number of stem cells may not be very high. They also confirmed the expression of $p75^{NTR}$ in limbal and conjunctival cultures (12).

In conclusion, the interaction between neurotrophins and $p75^{NTR}$ was confirmed not only in nerve cells but also in epithelial cells. Neurotrophins can promote p75(+) keratinocyte growth. The influence of neurotrophin on cell differentiation was not confirmed. It is known that in oral mucosa, cells with positive expression of $p75^{NTR}$ were localized in the basal layer, and $p75^{NTR}$ can be used as a marker of epithelial stem cells.

REFERENCES

1. Ishii A, Muramatsu T, Lee J-M, Higa K, Shinozaki N, Jung H-S, Shibahara T. Expression of p75(NGFR), a proliferative and basal cell marker, in the buccal mucosa epithelium during re-epithelialization. Acta Histochem Cytochem 2014; 47:145-53.
2. Wehrman T, He X, Raab B, Dukipatti A, Blau H, Garcia KC. Structural and mechanistic insights into nerve growth factor interactions with the TrkA and p75 receptors. Neuron 2007; 53:25-38.
3. Nakamura T, Endo K-i, Kinoshita S. Identification of human oral keratinocyte stem/progenitor cells by neurotrophin receptor p75 and the role of neurotrophin/p75 signaling. Stem Cells 2007; 25:628-38.
4. Hayashi K, Karatsaidis A, Schreurs O, Bjornland T, Sugisaki M, Schenck K. NGF and its receptors TrkA and p75NTR in the epithelium of oral lichen. J Oral Pathol Med 2008; 37:241-48.
5. Chen H-CJ, Chen H-L, Lai J-Y, et al. Persistence of transplanted oral mucosal epithelial cells in human cornea. Invest Ophthalmol Vis Sci 2009; 50:4660-68.
6. Gemenetzidis E, Elena-Costea D, Parkinson EK, Waseem A, Wan H, Teh MT. Induction of human epithelial stem/progenitor expansion by FOXM1. Cancer Res 2010; 70:9515-26.
7. Boiko AD, Razorenova OV, van de Rijn M, et al. Human melanoma-initiating cells express neural crest nerve growth factor receptor CD271. Nature 2010; 466:133-37.
8. Dalley AJ, AbdulMajeed AA, Upton Z, Farah CS. Organotypic culture of normal, dysplastic and squamous cell carcinoma-derived oral cell lines reveals loss of spatial regulation of CD44 and p75 NTR in malignancy. J Oral Pathol Med 2013; 42:37-46.
9. Soland TM, Brusevold IJ, Koppang HS, Schenck K, Bryne M. Nerve growth factor receptor (p75 NTR) and pattern of invasion predict poor prognosis in oral squamous cell carcinoma. Histopathology 2008; 53:62-72.
10. Huang S-D, Yuan Y, Liu X-H, et al. Self-renewal and chemotherapy resistance of p75NTR positive cells in esophageal squamous cell carcinomas. BMC Cancer 2009; 9:9.
11. Sen S, Sharma S, Gupta A, et al. Molecular characterization of explant cultured human oral mucosal epithelial cells. Invest Ophthalmol Vis Sci 2011; 52:9548-54.
12. Madhira SL, Vemuganti G, Bhaduri A, Gaddipati S, Sangwan VS, Ghanekar Y. Culture and characterization of oral mucosal epithelial cells on human amniotic membrane for ocular surface reconstruction. Mol Vis 2008; 14:189-96.

LETTER TO THE EDITOR

CORRELATION BETWEEN SPARC, TGFβ1, ENDOGLIN AND ANGIOGENESIS MECHANISM IN LUNG CANCER

B. WANG[1], Z. ZHANG[2], J. TANG[3], H. TAO[1] and Z. ZHANG[1]

[1]Department of Respiratory Medicine, First Affiliated Hospital of Hebei Northern College, Zhangjiakou City, Hebei, China; [2]Department of Radiotherapy, First Affiliated Hospital of Hebei Northern College, Zhangjiakou City, Hebei, China; [3]Department of Clinical Pharmacology, First Affiliated Hospital of Hebei Northern College, Zhangjiakou City, Hebei, China

Received August 28. 2018 – Accepted September 19, 2018

To study the relationship between Secreted protein, acidic and rich in cysteine (SPARC), Transforming growth factorβ1 (TGFβ1), Endoglin and angiogenesis in lung cancer, 40 cases of lung cancer specimens and 40 adjacent normal lung tissues specimens were collected and 10 cases from each were selected for preparation of tissue chip. CD34 (endothelial cell marker), Endoglin human α-Smooth muscle actin, and (α-SMA) markers were performed by immunohistochemical staining, and the immuno-phenotype and the relationship between different morphologies of the microvascular wall components were evaluated. The expression of SPARC mRNA and protein, TGFβ1 mRNA and protein and Endoglin in the remaining 30 cases of lung cancer were detected by immunohistochemistry and in-situ hybridization. The result shows that the positive rates of SPARC, TGFβ1 and Endoglin in lung cancer tissues were significantly higher than those in adjacent normal lung tissues (P < 0.05). The expression of SPARC and TGFβ1 was negatively correlated with lung cancer. When the positive expression of SPARC increased, the micro-vessel density (MVD) marked by Endoglin decreased gradually; while the positive expression of TGFβ1 increased, MVD increased gradually, and SPARC, TGFβ1 and MVD were correlated (P<0.05). High SPARC mRNA expression in lung cancer tissues could inhibit the progression of lung cancer, while high TGFβ1 mRNA expression can promote the progression of lung cancer and participate in the metastasis of lung cancer. To sum up, the angiogenesis of lung cancer may be related to the interaction of SPARC, TGFβ1 and Endoglin.

To the Editor,

Blood supply is essential for tumor growth. Angiogensis, the process of new blood vessels sprouting from pre-existing vessels, is essential to tumor growth and metastasis (1, 2). The new vessels firstly provide transport channels for oxygen, nutrients and cytokine supply as well as metabolic waste excretion to sustain the tumor growth. Secondly, the neo-vessels provide access for tumor cells to enter the circulation. However, the mechanism of tumor angiogenesis may be different in different tumor cells and different organ growth sites (3).

SPARC (secreted protein, acidic and rich in cysteine) is a low molecular glycoprotein rich in cysteine (4), which reduces the proliferation and migration of endothelial cells, leading to cell morphological changes and inhibition of cell adhesion (5). TGFβ1 (transforming growth factorβ1) is a multifunctional polypeptide cytokine, which has

Key words: lung cancer, SPARC, TGFβ1, Endoglin, angiogenesis mechanism

Mailing address:
Dr Zhihua Zhang,
Department of Respiratory Medicine,
First Affiliated Hospital, Hebei Northern College,
No.12 Changqing Road, Zhangjiakou City,
075000, Hebei, China
e-mail: zhangzhihua1989@126.com

0393-974X (2018)

been proved to play an important role in regulating cell growth (6). Endoglin is a component of the TGFβ receptor complex and is mainly expressed in human vascular endothelial cells, especially on the surface of microvascular endothelial cells (7). Some studies show that Endoglin can protect hypoxic endothelial cells from apoptosis through TGFβ1, thereby promoting angiogenesis (8). However, the correlation of SPARC, TGFβ1 and Endoglin remains largely unknown. Therefore, in this study, we aim to elucidate the relationship between SPARC, TGFβ1 and Endoglin in lung cancer tissue and its relationship with neovascularization, through detecting SPARC, TGFβ1 and Endoglin expression in lung cancer and adjacent normal lung tissues.

MATERIALS AND METHODS

Preparation of tissue chips

A total of 40 patients with lung cancer were enrolled from March 2016 to June 2018 at the First Affiliated Hospital of Hebei Northern College. Patients did not receive radiotherapy or chemotherapy prior to surgery. Forty cases of adjacent normal lung tissues were collected. Ten cases of lung cancer patients and 10 cases of corresponding adjacent lung tissues were selected to observe the blood vessel distribution of the tumor and prepare tissue chips. The other 30 cases of lung cancer were designated as the experimental group, and the remaining 30 cases of the corresponding adjacent normal lung tissue (>5cm from the tumor margin) were designated as the control group to study the relationship between SPARC, TGFβ1, Endoglin and the invasion and metastasis of lung cancer. Informed consent was signed by all groups of patients and the study was approved by the Hospital Ethics Committee of First Affiliated Hospital of Hebei Northern College, China.

Immunohistochemistry staining

The lung tissues from patients were fixed in 10% formalin for 24 hours. The fixed tissues were embedded with paraffin and the tissue blocks were sliced into 4 μm paraffin sections. The sliced sections were collected on slides, baked at 70°C for 1 hour, deparaffinized with xylene (10 mins, twice) and rehydrated in gradient alcohol of 100%, 95%, 85%, 80% and 70% ethanol for 2 min each. Slides were further washed with PBS (5 min, 3 times) and were subjected to antigen retrieval (pressure cooker at 120°C for 4 min) with corresponding buffer (Endoglin and CD34 were retrieved in Tris-EDTA buffer, PH= 9.0; CD34 was retrieved in citrate buffer , PH= 6.0). The α-SMA did not need to be repaired. Afterwards, tissue sections were washed with PBS (3 min, 3 times) and incubated with 3% H_2O_2 for 10 min to inactivate the endogenous peroxidase, followed by incubation with primary antibodies: mouse anti-human monoclonal anti-Endoglin (1:200, Biolegend, USA), mouse anti-human monoclonal anti-CD34 (1:200, Biolegend, USA), mouse anti-human monoclonal anti-α-SMA (1:200, Biolegend, USA), mouse anti-human monoclonal anti-Endoglin (1:200, Biolegend, USA), rabbit anti-human SPARC polyclonal antibody (1:150, Cell signaling, USA), rabbit anti-human TGFβ1 polyclonal antibody(1:100, Cell signaling, USA), rabbit anti-human polyclonal antibody (working solution, cell signaling, USA) overnight at 4°C. PBS solution was used to replace primary antibody as blank control to exclude false positive results. The slides were further washed with PBS (3 min, 3 times) and incubated with secondary antibody goat anti-mouse IgG (1:2,000, Abcam, Cambridge, UK) for 20 m at 37ºC. Sections were rinsed in PBS (3 min, 3 times), incubated in avidin–biotin complex (Vecta stain Elite ABC Kit, Vector Laboratories) for 1 h at 20°C and rinsed with PBS (10 min X 3). Finally, sections were developed in diaminobenzidine substrate (DAB, P0203-1, Beyotime, China) for 5 min at 25°C and counterstained with hematoxylin (SH8390, Solarbio, Beijing, China). The sections were further differentiated in 0.1% HCl, dehydrated in gradient alcohol, cleared by xylene and mounted with resinous media. Images were taken under a bright field microscope and the area of positive staining was analyzed by Image Pro Plus 7.0 (Media Cybernetics).

In-situ hybridization

Routine deparaffinization and rehydration was conducted on paraffin section. Tissue sections were washed with PBS (3 min, 3 times) and incubated with 3% H_2O_2 for 10 min to inactivate the endogenous peroxidase. Following twice rinsing for 5 min with PBS and distilled water, slides were incubated with freshly diluted pepsin in 3% citric acid at 37ºC for 30 min. Slides were then washed (PBS, 5 min, 3 times and distilled water, 5 min) and fixed in the stationary solution containing

1% paraformaldehyde and 0.1% diethyl pyrocarbonate (DEPC) at room temperature for 10 min. After extensive washing (PBS, 5 min, 5 times), slides were incubated with 20 μL hybrid buffer and incubated at 40ºC for 3 h. Afterwards, the slides were covered with the special cover glass for in situ hybridization and were placed at 40ºC overnight. The wet box and the cover slides were removed, washed with 2×SSC (5 min, twice) at 37ºC, 0.5×SSC at 37ºC for 15 min and 0.2×SSC at 37ºC for 15min. One drop (about 50 uL) of sealing fluid was added to each slice and incubated at 37ºC for 30 min. One drop (about 50 uL) of biotinylated rat anti-digoxin was added to each slice and incubated at 37ºC for 60 min for in-situ hybridization. After extensive washing with PBS (5 min, 4 times), slides were incubated with one drop (about 50 uL) of biotinylated peroxidase at 37ºC for 20 min. Afterwards, slides were washed with PBS (5 min, 4 times) and dripped with 50 uL freshly made DAB reagent. The staining effect was controlled under a microscope. In general, the DAB reaction was terminated after 10 min incubation by immersing with tap water. The sections were further counterstained with hematoxylin (SH8390, Solarbio, Beijing, China), differentiated in 0.1% HCl, dehydrated in gradient alcohol, cleared by xylene and mounted with resinous media. Images were taken under a bright field microscope and the area of positive staining was analyzed by Image Pro Plus 7.0 (Media Cybernetics).

MVD calculation

Vascular endothelial cells (VECs) labeled with Endoglin monoclonal antibodies were used to count the number of microvessels per unit area, namely MVD (Mircrovessel density). At low magnification, the region with the most abundant tumor microvasculature was selected, and the number of blood vessels in different regions was counted under 400 X magnification, and the mean value was taken as MVD. A single endothelial cell or an endothelial cell cluster was considered a microvessel, as long as they were separated from adjacent microvessels, tumor cells or other connective tissue. Once the thickness of the muscular layer and the diameter of the lumen was larger than 8 red blood cells, it was not counted as a microvessel.

Statistical analysis

SPSS19.0 software was used for statistical analysis, and the count data used χ^2 test; the measurement data were analyzed by *t*-test and variance analysis and MVD was expressed in the form of $\bar{x} \pm s$. The correlation between SPARC and TGFβ1 was analyzed by Spearman grade correlation, and the correlation between MVD and SPARC and TGFβ1 was analyzed by Mann-Whitney U test. The test standard $P<0.05$ indicated statistical significance.

RESULTS

Observation of vascular morphology in lung cancer

Eight tissue chips were successfully constructed. The main manifestations of microvascular morphology in the chips were punctate microvessels, linear microvessels, circular microvessels and strip microvessels.

CD34 and Endoglin were expressed in the cytoplasm of microvascular endothelial cells, in which CD34 labeled linear, circular and strip-like microvessels, mostly branching, sinusoidal and spore-like (no lumen) (Fig. 1A); Endoglin labeled microvessels were mainly punctate microvessels, small in diameter, mosaic or circular, part without lumen (Fig. 1B). α-SMA was expressed in the cytoplasm of microvascular pericytes (Fig. 1C).

In summary, CD34 staining of blood vessels were more extensive and less specific, thus it was impossible to distinguish between mature blood vessels and neovascularization. Compared with the CD34 labeled vessels, Endoglin could be more specific to mark the neovascularization of the tumor. However, α-SMA could be accurately expressed in the perivascular cells of neo-microvessels, therefore α-SMA was selected as a specific marker of perivascular cells of lung cancer.

Expression of SPARC, TGFβ1 and Endoglin factors

The SPARC factor was mainly expressed in the cytoplasm of interstitial fibroblasts, with fewer expression in the nucleus. Positive expression could be detected in cancer cells and vascular endothelial cells. The positive expression rate (56.67%) in lung cancer tissues was significantly higher than that in adjacent lung tissues (20%) ($P < 0.01$).TGFβ1 protein staining was mainly located in the cytoplasm, and its

positive expression rate (60%) in lung cancer was significantly higher than that in adjacent lung tissues (30%) (P < 0.01).Endoglin protein was mainly expressed on the cell membrane or cytoplasm of tumor vascular endothelial cells, with irregular arrangement and less obvious cavity formation. Endoglin was not expressed in large vessels, and was extremely weak or even not expressed in normal tissues. The mean MVD in lung cancer was 12.15±5.87, and that in adjacent lung tissues was 0.35±0.18. The difference was statistically significant (P < 0.01).

Expression of SPARC, TGFβ1 and Endoglin factors and its relationship with clinic-pathological features

The expression of SPARC factor in lung cancer was correlated with clinical stage and lymph node metastasis (P<0.05), but irrelevant with age, gender, tumor size, differentiation and clinical classification (P>0.05). The expression of TGFβ1 was correlated with tumor size, clinical stage and lymph node metastasis (P<0.05), but irrelevant with age, gender, differentiation and clinical classification of lung cancer patients (P>0.05). Endoglin factor was associated with clinical stage and lymph node metastasis of lung cancer (P<0.05), but irrelevant with age, gender, tumor size, differentiation and clinical classification of lung cancer patients (P>0.05). Specific data are shown in Table I.

Correlation between the expression of SPARC, TGFβ1 and Endoglin in lung cancer tissues

In 17 cases of lung cancer tissues with positive expression of SPARC factor, 8 cases of TGFβ1 were positive and 9 were negative. In 13 cases of lung cancer tissues with negative SPARC factor expression, 10 cases of TGFβ1 factor were positive

Table I. *Expression of SPARC, TGFβ1 and Endoglin factors and its relationship with clinic-pathological features.*

Parameters		Cases (n)	SPARC		TGFβ1		Endoglin	
			+	P	+	P	($\bar{x} \pm s$)	P
Age (years)	<60	18	9	0.246	12	0.137	13.22±7.12	0.281
	≥60	12	8		6		11.35±6.35	
Gender	Male	22	13	0.487	12	0.312	11.52±5.33	0.062
	Female	8	4		6		14.83±8.15	
Tumor size (cm^3)	<3	6	4	0.356	1	0.000	11.92±4.25	0.683
	≥3	24	13		17		12.59±6.84	
Differentiation	Well-moderately	20	11	0.414	12	0.747	12.73±6.77	0.674
	Poorly-undifferentiated	10	6		6		11.74±5.83	
Clinical classification	Adc	20	12	0.636	14	0.131	13.25±7.11	0.392
	Sqcc	6	4		4		11.69±4.54	
	SC	1	1		1		12.63±5.02	
	Carcinoid	1	1		1		11.53±6.11	
	Sclc	2	2		2		9.08±4.02	
TNM stage	I~II	17	13	0.001	8	0.005	10.92±5.13	0.018
	III~IV	13	4		10		14.53±7.64	
Lymph node metastasis	Yes	17	8	0.012	13	0.002	14.27±7.34	0.002
	No	13	9		5		9.85±3.75	

and 3 were negative. There was a negative correlation between the two expressions (r=-0.251, P=0.037).

In 30 cases of lung cancer tissues, the number of neovascularization decreased when SPARC factor was positively expressed in lung cancer, and there was a correlation between SPARC factor and MVD (P<0.05).

In 30 cases of lung cancer tissues, the number of tumor neovascularization increased with the increase of positive expression of TGFβ1 factor in lung cancer, and there was a significant correlation between TGFβ1 factor and MVD (P<0.01).

Expression of SPARC mRNA and TGFβ1 mRNA

SPARC mRNA signals were mainly expressed in the cytoplasm of stromal fibroblasts (Fig. 2A). A

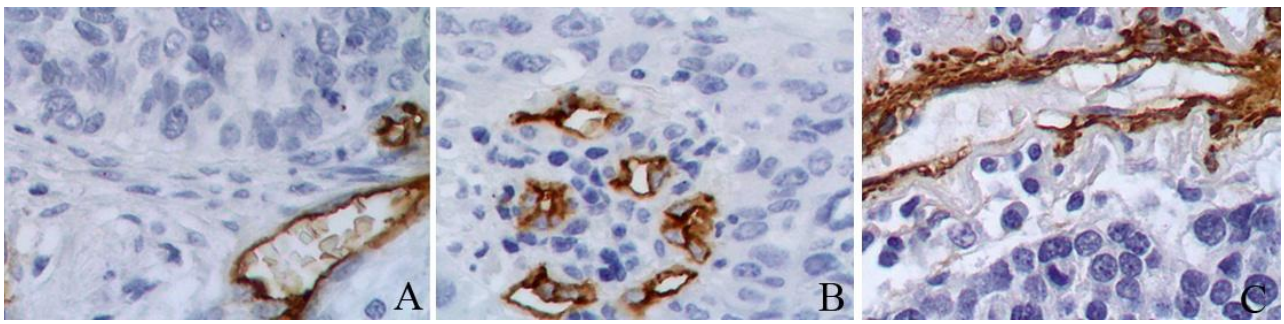

Fig. 1. ***A)*** *positive expression of CD34 in lung cancer;* ***B)*** *positive expression of Endoglin in lung cancer;* ***C)*** *positive expression of α-SMA in lung cancer (*400).*

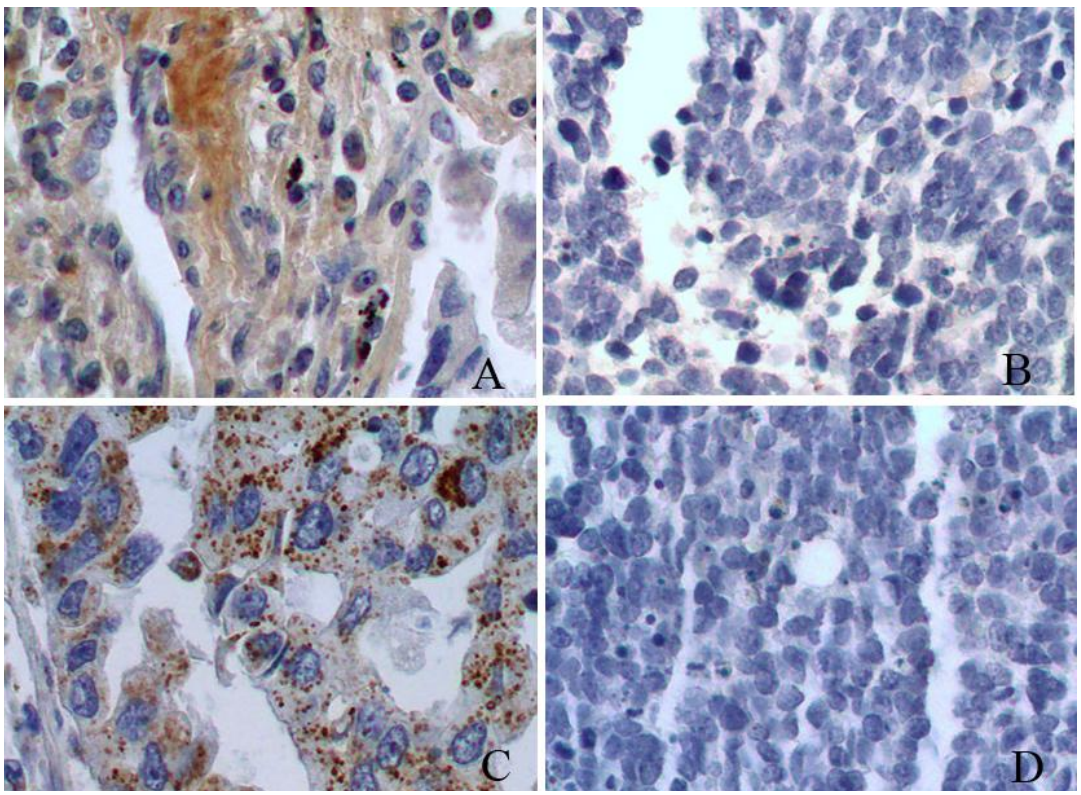

Fig. 2. *Expression of SPARC mrna and TGFβ1 mRNA in lung cancer and adjacent normal lung tissues.* ***A)*** *expression of SPARC mRNA in lung cancer tissues;* ***B)*** *expression of SPARC mRNA in adjacent normal lung tissues;* ***C)*** *expression of TGFβ1 mrna in lung cancer tissues;* ***D)*** *expression of TGFβ1 mRNA in adjacent normal lung tissues) (*400).*

small number of SPARC expression could also be detected in the nucleus, less positively expressed in cancer cells, and the positive signal was brown-yellow diffuse or granular. The positive expression rate in lung cancer tissues was significantly higher than that in adjacent normal lung tissues (Fig. 2B) ($P<0.05$).

TGFβ1 mRNA signals staining was mainly located in the cytoplasm, as the positive signal shown as granular brown yellow (Fig. 2C). The positive expression rate of TGFβ1 mRNA in lung cancer was significantly higher than that in adjacent normal lung tissues (Fig. 2D) ($P<0.05$).

Expression of SPARC mRNA and TGFβ1 mRNA in lung cancer and its relationship with clinic-pathological features

Results obtained from this study demonstrated that the expression of SPARC mRNA in lung cancer tissues was related to clinical stage and lymph node metastasis ($P<0.05$). In clinical stage, the expression of SPARC mRNA in stage I~II was higher than that in stage III~IV ($P<0.05$), and its expression in non-lymph node metastasis was higher than that in patients with lymph node metastasis ($P<0.01$). However, the expression was not correlated with age, gender, tumor size, differentiation or clinical classification ($P > 0.05$).

The expression of TGFβ1 mRNA in lung cancer tissues was related to tumor size, clinical stage and lymph node metastasis ($P<0.05$). The expression of TGFβ1 mRNA in tumor volume$\geq 3cm^3$ was higher than that in tumor volume$<3cm^3$ ($P<0.05$). The expression of TGFβ1 mRNA in stage III-IV was higher than that in stage I-II ($P<0.01$), and the expression in lymph node metastasis is higher than that of non-lymph node metastases. It was irrelevant with age, gender, tumor differentiation or clinical classification ($P>0.05$).

Correlation between SPARC mRNA and TGFβ1 mRNA expression in lung cancer tissues

Eight patients showed positive expression for SPARC mRNA and TGFβ1 mRNA, 3 cases showed negative. Ten patients showed positive in SPARC mRNA and negative in TGFβ1 mRNA, and 9 patients showed negative in SPARC mRNA and positive in TGFβ1 mRNA. mRNA expression of SPARC and TGFβ1were negatively correlated with lung cancer ($r=-0.361$, $P=0.002$).

Consistency analysis of the results of SPARC and TGFβ1 in lung cancer

Of 30 cases of lung cancer tissues, SPARC protein and SPARC mRNA were positively correlated in lung cancer ($r = 0.525$, $P=0.000$). It indicated that the two methods of immunohistochemistry and in-situ hybridization were highly consistent. The expression of TGFβ1 and TGFβ1 mRNA in lung cancer was positively correlated ($r=0.331$, $P=0.005$), which indicated that the two methods of immunohistochemistry and in-situ hybridization were highly consistent.

DISCUSSION

SPARC protein is closely related to embryonic development, angiogenesis, cell regeneration, tissue repair and remodeling (9, 10). SPARC is mainly expressed in stromal fibroblasts, which may inhibit the progression and metastasis of lung cancer. The expression of SPARC in lung cancer may be related to the formation of antitumor angiogenesis. In addition, the expression of SPARC mRNA and SPARC protein is positively correlated in lung cancer, suggesting that the expression of SPARC is consistent at gene and protein levels. These results suggest that the high expression of SPARC mRNA and SPARC protein may inhibit the progression, invasion, metastasis and angiogenesis of lung cancer. The results show that as TGFβ1 expression in lung cancer increases, the number of neovascularization also gradually increases. Furthermore, the expression of TGFβ1 mRNA and TGFβ1 protein is positively correlated in lung cancer which suggests that the expression of TGFβ1 is consistent at gene and protein levels. While the expression of TGFβ1 mRNA is up-regulated, the TGFβ1 protein is increased.

SPARC and TGFβ1 can interact with each other (11, 12). Endoglin is also correlated with SPARC and TGFβ1. With the increase of Endoglin-labeled neovascularization, the expression of SPARC in

lung cancer decreases, while the expression of TGFβ1 increases. These results suggest that SPARC can inhibit angiogenesis in lung cancer, and TGFβ1 can promote angiogenesis. This study speculates that SPARC has an anti-angiogenesis effect in lung cancer, which may impact TGFβ1 pathway by regulating Endoglin.

ACKNOWLEDGEMENTS

This work was supported by 2018 Self-financing project of science and technology plan in Zhangjiakou, Hebei Province (Project No.: 1821039D);2017 Science and technology plan financial assistance project in Zhangjiakou, Hebei Province (Project No.: 1712008D); 2017 Key project of medical science research in Hebei Province in 2017 (Project No.: 20170185).

REFERENCES

1. Uramoto H, Yamada S, Tanaka F. Angiogenesis of lung cancer utilizes existing blood vessels rather than developing new vessels using signals from carcinogenesis. Anticancer Res 2013; 33(5):1913-16.
2. Micu GV, Stăniceanu F, Sticlaru LC, et al. Correlations between the density of tryptase positive mast cells (DMCT) and that of new blood vessels (CD105+) in patients with gastric cancer. Rom J Intern Med 2016; 54(2):113-20.
3. Demircioglu F, Hodivala-Dilke K. αvβ3 Integrin and tumour blood vessels - learning from the past to shape the future. Curr Opin Cell Biol 2016;42:121-27.
4. Gore B, Izikki M, Mercier O, et al. Key role of the endothelial TGF-β/ALK1/endoglin signaling pathway in humans and rodents pulmonary hypertension. Plos One 2014; 9(6):e100310.
5. Kieć-Wilk B, Stolarz-Skrzypek K, Sliwa A, Zdzienicka A, Kawecka-Jaszcz K. Peripheral blood concentrations of TGFβ1, IGF-1 and bFGF and remodelling of the left ventricle and blood vessels in hypertensive patients. Kardiol Pol 2010; 68(9):996-1002.
6. Song W, Wang X. The role of TGFβ1 and LRG1 in cardiac remodelling and heart failure. Biophys Rev 2015; 7(1):91-104.
7. Rivera LB, Brekken RA. SPARC promotes pericyte recruitment via inhibition of endoglin-dependent TGF-β1 activity. J Cell Biol 2011; 193(7):1305-19.
8. Maring JA, van Meeteren LA, Goumans MJ, Ten Dijke P. Interrogating TGF-β Function and Regulation in Endothelial Cells. Methods Mol Biol 2016; 1344:193-203.
9. Chlenski A, Liu S, Guerrero LJ, et al. SPARC expression is associated with impaired tumor growth, inhibited angiogenesis and changes in the extracellular matrix. Int J Cancer 2006; 118(2):310-16.
10. Charest A, Pépin A, Shetty R, et al. Distribution of SPARC during neovascularisation of degenerative aortic stenosis. Heart 2006; 92(12):1844-49.
11. Said N, Frierson HF Jr, Chernauskas D, Conaway M, Motamed K, Theodorescu D. The role of SPARC in the TRAMP model of prostate carcinogenesis and progression. Oncogene 2009; 28(39):3487-98.
12. Cutroneo KR, White SL, Phan SH, Ehrlich HP. Therapies for bleomycin induced lung fibrosis through regulation of TGF-β1 induced collagen gene expression. J Cell Physiol 2007; 211(3):585-89.

LETTER TO THE EDITOR

COMPARATIVE ASSESSMENT OF ATHEROSCLEROSIS OF RABBIT FEMORAL ARTERY BY DUPLEX ULTRASOUND SCANNING, OPTICAL COHERENCE TOMOGRAPHY AND FRACTIONAL FLOW RESERVE

J.M. YANG[1*], J.T. YAO[2*], J.Y. ZHANG[2], Y. WANG[2], X. SUN[2], K.K. WANG[3] and Y. TIAN[1,2]

[1]Cardiac Ultrasonography Room, the First Affiliated Hospital, Cardiovascular Institute, Harbin Medical University, Harbin, P.R. China; [2]Department of Cardiology, the First Affiliated Hospital, Cardiovascular Institute, Harbin Medical University, Harbin, P.R. China; [3]Department of Ultrasound, the First Affiliated Hospital, Harbin Medical University, Harbin P.R. China

Received September 1, 2018 – Accepted October 12, 2018

[*]These authors contributed equally to this work and should be considered co-first authors

Duplex Ultrasound Scanning (DUS), Frequency-domain optical coherence tomography (FD-OCT) and fractional flow reserve (FFR) remarkably shape our understanding of the significance of coronary stenosis. The present study aimed to compare the assessment results of the atherosclerotic lesions in rabbit superficial femoral artery by DUS with that of FD-OCT and FFR. A total of 20 atherosclerotic lesions were analyzed. Morphological assessments were prospectively compared through DUS, FD-OCT and quantitative superficial femoral angiography (QFA). In addition, the correlation between DUS-derived lesion parameters and FFR was determined. The results show that, compared with FD-OCT and QFA, DUS detected larger reference diameter and higher percent stenosis. However, the minimal lumen diameter (MLD) and distance from profunda femoris to MLD were equivalent measured by the three imaging modalities. There was a poor correlation between FFR and DUS-derived percent diameter stenosis (R^2=0.198, P=0.049). In conclusion, hemodynamic significance of lesions assessed by FFR was only related with percent diameter stenosis measured by DUS.

To the Editor,

Duplex ultrasound scanning (DUS) provides extensive noninvasive information on arterial morphology and hemodynamics, which is widely used for preintervention assessment, surgical procedure monitoring and postrevascularization surveillance in peripheral arterial disease (1). Frequency-domain optical coherence tomography (FD-OCT) is a newly developed near-infrared light-based imaging technology. FD-OCT can provide morphological details (e.g. plaque erosion, dissection, stent malapposition), which are helpful to guide the procedure of percutaneous coronary intervention (PCI) (2). Fractional flow reserve (FFR) is a better technique for physiological assessment of coronary artery disease, which can identify ischaemia- generating stenoses and predict patients' clinical outcome during follow-up (3). However, both methods are invasive and have risks of complication.

Validation of DUS has been reported on the

Key words: *Duplex Ultrasound Scanning (DUS), Optical Coherence Tomography (OCT), Fractional Flow Reserve (FFR), atherosclerotic lesions*

Mailing address:
Dr Ye Tian,
Cardiac Ultrasonography Room,
The First Affiliated Hospital, Cardiovascular Institute,
Harbin Medical University,
Harbin 150001, P.R. China
e-mail: yetian1@yeah.net

0393-974X (2018)

comparison with angiography, intravascular ultrasound, histology and intra-arterial pressure gradient (4-6). However, there are few studies in which DUS has been compared with FD-OCT and FFR in the evaluation of lower limb artery disease. In this study, an atherosclerotic model in the rabbit superficial femoral artery was established to compare the lumen measurements by DUS with those by FD-OCT and quantitative superficial femoral angiography (QFA), and reveal the relationship between DUS and FFR. This study is helpful to better understand the measurement difference between these diverse imaging modalities and reduce unnecessary invasive procedures.

MATERIALS AND METHODS

Animal model preparation

Twenty five New Zealand white adult male rabbits with the body mass of 2.5-3.0 kg were used for the study. All the animal procedures were approved by the Ethics Committee for Animal Experiments in Harbin Medical University and rigorously conformed to Animal Research: Reporting In Vivo Experiments (ARRIVE) guidelines (7).

All the rabbits were fed a 2% high-cholesterol diet for 1 week before and 4 weeks after endothelium denudation of the right superficial femoral artery. Before the intervention, the rabbits were given 100 IU/kg heparin intravenously. Then, the animals were anaesthetized by intravenous injection of pentobarbital sodium (30mg/kg). A 2.75×14mm balloon catheter (JW Medical Systems, Shangdong, China) was introduced through the left common carotid artery and advanced over a 0.014-inch guidewire under fluoroscopic guidance into the initial segment of the right superficial femoral artery. The balloon was inflated to 6-8 atm for three 30-second intervals. At the end of the procedure, the balloon catheters were removed, the common carotid arteries were ligated, and the surgical incisions were repaired. All the animals were recovered and housed for 4 weeks.

Ultrasound scanning

All the rabbits were examined prior to angiography by one experienced vascular sonographer blinded to intravascular imaging using MyLab-60 (Esaote S.p.A, Genova, Italia) equipped with the 6-18 MHz linear array transducer. The images were acquired in supine position. The smallest lumen size in the injured right superficial femoral artery was identified and the distance from profunda femoris to minimum lumen diameter (MLD) was recorded. The reference was defined as the most "normal-appearing" segment within 10 mm distal to the worst lesion. The percentage area and diameter stenosis were calculated using the following expressions:

Area stenosis% =(1-minimal lumen area/reference lumen area)×100%

Diameter stenosis%=(1-minimallumen diameter/reference lumen diameter)×100%

After Doppler angle correction (less than or equal to 60°), the peak systolic velocity (PSV, cm/s) was measured at the site of the worst stenosis and reference segment. The PSV ratio was calculated from the PSV within the worst stenosis to the PSV within the reference segment. All the measurements were repeated three times and the average values were recorded for further analysis.

Quantitative superficial femoral angiography

A 6F guiding catheter (Terumo, Japan) was introduced through the right common carotid artery and advanced over a 0.014-inch guidewire under fluoroscopic guidance into the ostium of the common iliac artery. The quantitative superficial femoral angiography (QFA) was obtained after injection of nitroglycerin (0.2 mg). All the angiograms were obtained from posteroanterior projection. After calibration using the guiding catheter, the analysis [minimum lumen diameter (MLD), distal reference lumen, percent diameter stenosis and distance from profunda femoris to MLD] was determined (Innova2100-IQ, GE medical systems, Connecticut, USA).

FD-OCT image acquisition and analysis

FD-OCT imaging of the atherosclerotic lesion was obtained using the commercially available C7-XR OCT imaging system and 2.7F DragonFly catheter (LightLab Imaging, St. Jude Medical, Westford, Massachusetts, USA). The automated pullback device was set at 20 mm/s while the blood was removed by a short injection of preheated Iohexol (Yangtze River Pharmaceutical Group, Jiangsu, China) through the guiding catheter. The images were digitally recorded for offline analysis by an experienced reader, blinded to QFA and FFR data.

The offline analysis was performed using the

validated software (LightLab Imaging) and in adaptation to the published consensus for quantitative assessment of atherosclerotic lesion. The reference cross-section was defined as the frame with the largest lumen within 10 mm distal to the worst stenosis without any side branch. As described in duplex ultrasound scanning, the lumen dimension and percentage of luminal stenosis were calculated.

FFR measurement

The pressure wire (St. Jude Medical, St. Paul, Minnesota, USA), which was calibrated, was introduced through a 6F guiding catheter and advanced to the right superficial femoral artery as far as possible. The maximal hyperaemia was induced by bolus injection of adenosine (40 μg). FFR was calculated as the ratio between superficial femoral artery and aortic pressure. The measurement was repeated twice and the average value of both measurements was recorded for analysis.

Statistical analysis

The continuous variables were expressed as the standard errors of mean values. The comparison between two or more groups was analyzed by the paired *t*-test or one-way analysis of variance, followed by the Turkey's multiple comparison test. The agreement between the measurements (DUS *vs* FD-OCT, DUS *vs* QFA) was expressed in the Bland-Altman plot. The linear regression

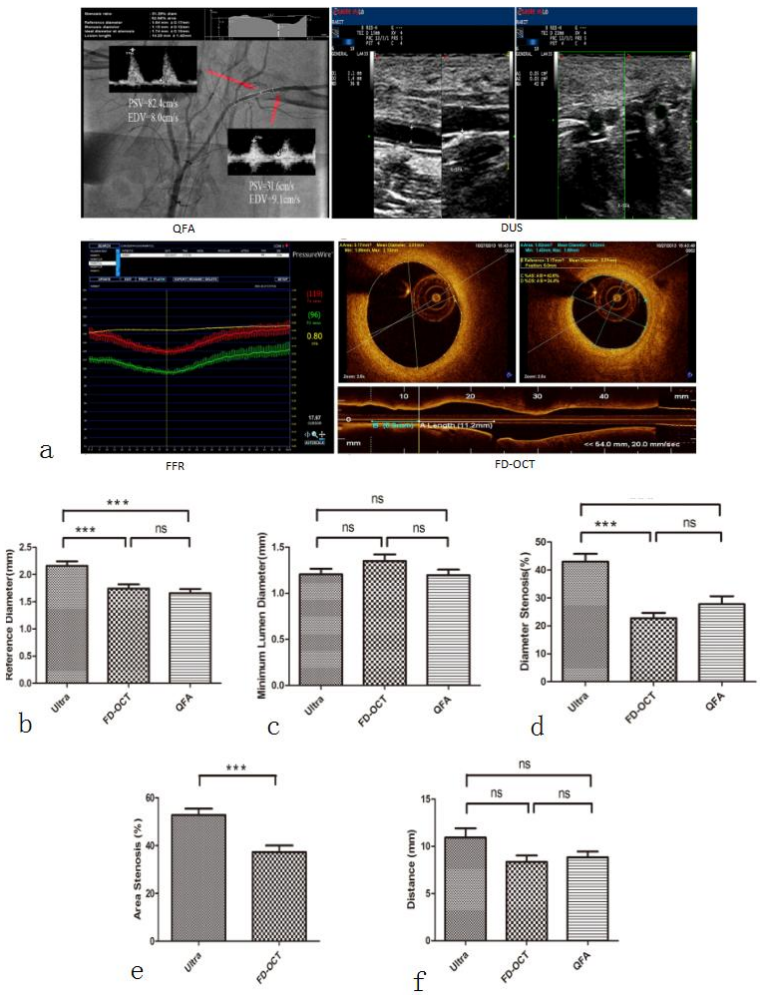

Fig. 1. *Representative example of measured images (**a**) and mean values (SEM) for (**b**) reference diameter, (**c**) minimum lumen diameter (MLD), (**d**) diameter stenosis, (**e**) area stenosis and (**f**) distance from profunda femoris to MLD derived from DUS, D-OCT and QFA in the rabbit superficial femoral artery stenosis. ***P<0.001; ns: not significant (Paired t-test, One-way analysis of variance and Tukey's multiple comparison test).*

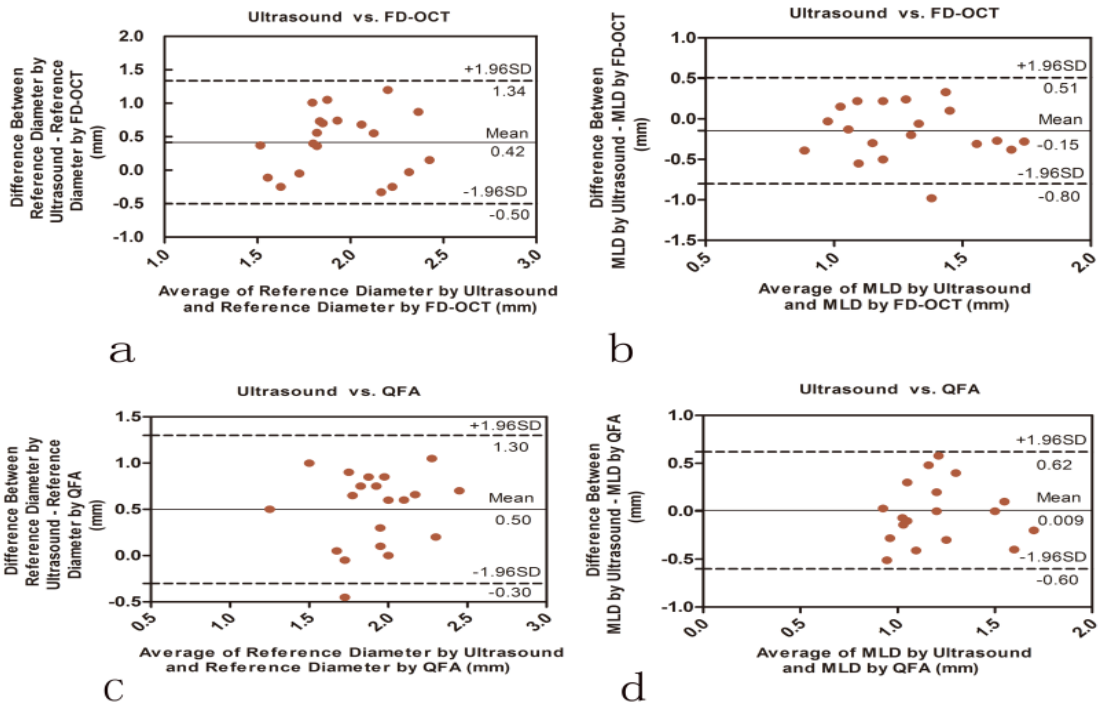

Fig. 2. *Bland-Altman plots for the differences in reference diameter and minimum lumen diameter (MLD) measurements between DUS and FD-OCT (**a**, **b**), and between DUS and QFA (**c**, **d**).*

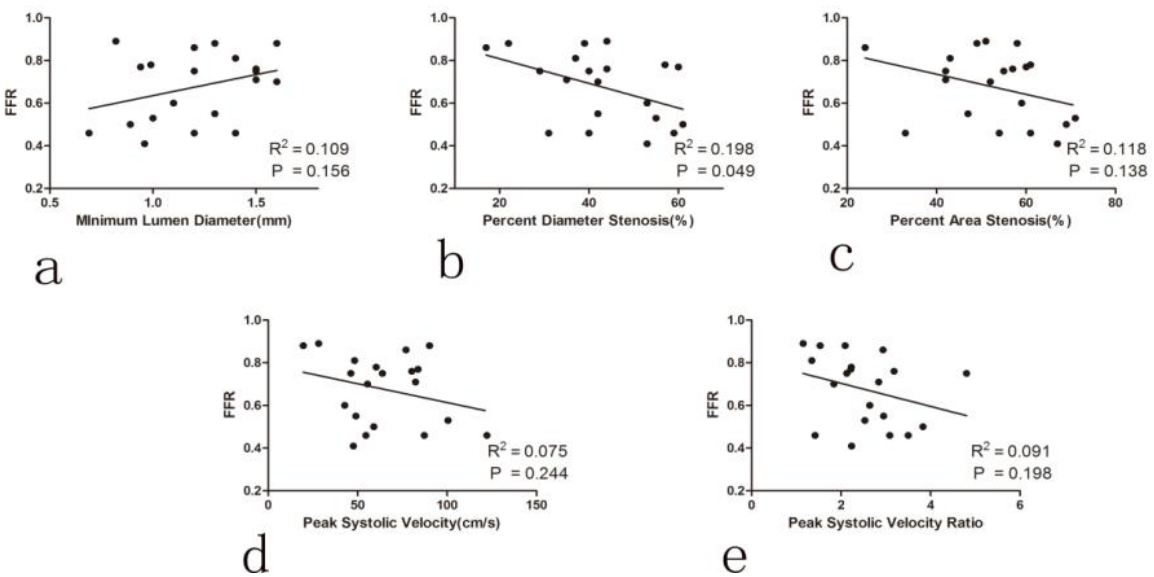

Fig. 3. *Correlation between FFR and measurements by duplex ultrasound scanning (DUS) (Linear regression analysis).*

analysis was performed to determine the correlation between the FFR and DUS-derived parameters. The statistical analysis was performed using the SPSS software (v13.0; IBM Corporation, Armonk, NY, USA). P <0.05 was considered to be statistically significant.

RESULTS

Atherosclerotic lesions in the right superficial femoral arteries were confirmed successfully in 20 rabbits, and 5 rabbits were excluded from the analysis because of thrombus formation. Fig. 1a shows a representative example of the angiographic, FFR, DUS and FD-OCT measurements.

Comparison of measurements with DUS, FD-OCT and angiography

All the DUS, FD-OCT, and angiography-derived morphometric parameters for identifying atherosclerotic lesions were compared (Fig. 1b). The reference diameter was significantly larger by ultrasound (ANOVA, P<0.0001) compared with FD-OCT and QFA (2.16±0.08 *vs* 1.74±0.08, 1.66±0.07 mm; P<0.001). No significant difference was found in the minimum lumen diameter (MLD) measured by DUS, FD-OCT and QFA (1.20±0.06 *vs* 1.35±0.07, 1.20±0.06 mm; P=0.18). The diameter stenosis was also larger by DUS (ANOVA, P< 0.0001) compared with FD-OCT and QFA (43.00±2.81% *vs* 22.72±1.95%, 27.79±2.82%; P<0.001). DUS detected higher percent area stenosis than FD-OCT (52.75±2.65% *vs* 37.29±2.75%; Paired *t*-test, P=0.0003). In addition, there was no difference regarding the distance from profunda femoris to MLD in any of the 3 techniques (10.93±0.99 *vs* 8.36±0.67, 8.84±0.62mm; P=0.0545).

Fig. 2 shows the Bland-Altman analysis for the measurement of reference diameter and MLD between DUS, FD-OCT and QFA. The mean differences between DUS and FD-OCT for reference diameter and MLD were 0.42±0.47 mm (limits of agreement of -0.5 to 1.34 mm) and -0.15±0.33 mm (limits of agreement of -0.8 to 0.51 mm), respectively. The mean differences between DUS and QFA were 0.5±0.4 mm (limits of agreement of -0.3 to 1.3 mm) and 0.009±0.31 mm (limits of agreement of -0.6 to 0.62 mm), respectively.

Correlation of measurements between DUS and FFR

The FFR of all the stenoses was 0.68±0.04. The linear regression analysis showed a significant but poor correlation between the percent diameter stenosis by DUS and FFR (R^2=0.198, P<0.049, Fig. 3b). However, the other parameters, such as MLD (R^2=0.109, P=0.156), percent area stenosis (R^2=0.118, P=0.138), peak systolic velocity (R^2=0.075,P=0.244) and peak systolic velocity ratio (R^2=0.091, P=0.198, Fig. 3, a, c, d and e), showed no correlation with the FFR values.

DISCUSSION

Compared with FD-OCT and QFA, DUS detected larger reference diameter and higher percent stenosis, possibly due to the following causes: Firstly, the axial resolution of FD-OCT was 10 μm, which possessed much higher resolution than that of DUS and thus could delineate the lumen geometry more precisely. Secondly, the 6F guiding catheter occupied additional space in the relatively small ostium of common iliac artery. This partial occlusion became evident in reference segments of superficial femoral vessels which were liable to change in blood flow and pressure, leading to smaller dimensions detected by FD-OCT and QFA (8). Finally, rapid injection of contrast media increased shear stress and thus induced vasoconstriction.

FFR considered the major determinants of coronary stenosis severity, such as the viability, microcirculatory status of the subtended myocardium and the presence of collateral circulation. Several large clinical trials (9-11) indicated that compared with angiographic guidance, patients with stable coronary artery disease could benefit from the FFR-guided PCI. DUS was frequently used in the lower limb disease because of its safe and non-invasive characteristics. However, linear regression analysis showed no significant correlation between FFR value and Ultrasonic measurements (MLD, percent area stenosis, peak systolic velocity, peak systolic velocity ratio), which may be partially ascribe to small sample size in this study. The hemodynamic

significance of lesions assessed by FFR was only related to the percent diameter stenosis measured by DUS. Therefore, it was necessary to establish FFR threshold (12) for inducible ischaemia and thus improve clinical outcomes on lower limb artery disease in the future.

In summary, DUS generated larger reference diameter and higher degrees of disease severity compared with FD-OCT and QFA. The hemodynamic significance of lesions assessed by FFR was only related to the percent diameter stenosis measured by DUS.

ACKNOWLEDGEMENTS

This work was supported by the National Natural Science Foundation of China (81171483, 81371709, 81101164) and the Scientific and Technical Key Task of Heilongjiang Province, China (GC10C306). This work was also supported by the National key clinical specialist construction Programs of China.

REFERENCES

1. Tendera M, Aboyans V, Bartelink ML, et al. ESC guidelines on the diagnosis and treatment of peripheral artery diseases: document covering atherosclerotic disease of extracranial carotid and vertebral, mesenteric, renal, upper and lower extremity arteries: The Task Force on the Diagnosis and Treatment of Peripheral Artery Diseases of the European Society of Cardiology (ESC). Eur Heart J 2011; 32(22):2851-906.
2. Waksman R, Kitabata H, Prati F, Albertucci M, Mintz GS. Intravascular ultrasound vs optical coherence tomography guidance. J Am Coll Cardiol 2013; 62(17S1):S32-S40.
3. Van de Hoef TP, Meuwissen M, Escaned J, Davies JE, Siebes M, Spaan JAE, Piek JJ. Fractional flow reserve as a surrogate for inducible myocardial ischaemia. Nat Rev Cardiol 2013; 10(8):439-52.
4. Favaretto E PC, Amato A, Conti E, et al. Analysis of agreement between duplex ultrasound scanning and arteriography in patients with lower limb artery disease. J Cardiovasc Med (Hagerstown) 2007; 8(5):337-41.
5. Sheikh KH DC, Kisslo KB, Harrison JK, Himmelstein SI, Kisslo J, Bashore TM. Comparison of intravascular ultrasound, external ultrasound and digital angiography for evaluation of peripheral artery dimensions and morphology. Am J Cardiol 1991; 67(9):817-22.
6. Pan XM SD, Reilly LM, Bowersox JC, et al. Assessment of carotid artery stenosis by ultrasonography, conventional angiography, and magnetic resonance angiography: correlation with ex vivo measurement of plaque stenosis. J Vasc Surg 1995; 21(1):82-89.
7. Eisen JA, Baker D, Lidster K, Sottomayor A, Amor S. Two years later: journals are not yet enforcing the ARRIVE guidelines on reporting standards for pre-clinical animal studies. PLoS Biol 2014; 12(1):e1001756.
8. Bezerra HG, Attizzani GF, Sirbu V, et al. Optical coherence tomography vs intravascular ultrasound to evaluate coronary artery disease and percutaneous coronary Intervention. JACC Cardiovasc Interv 2013; 6(3):228-36.
9. De Bruyne B, Pijls NHJ, Kalesan B, et al. Fractional flow reserve–guided PCI vs medical therapy in stable coronary disease. N Engl J Med 2012; 367(11):991-1001.
10. Pijls NHJ, Fearon WF, Tonino PAL, et al. Fractional flow reserve vs angiography for guiding percutaneous coronary intervention in patients with multivessel coronary artery disease. J Am Coll Cardiol 2010; 56(3):177-84.
11. Pijls NHJ, van Schaardenburgh P, Manoharan G, et al. Percutaneous coronary intervention of functionally nonsignificant stenosis. J Am Coll Cardiol 2007; 49(21):2105-11.
12. Lotfi AS, Sivalingam SK, Giugliano GR, Ashraf J, Visintainer P. Use of fraction flow reserve to predict changes over time in management of superficial femoral artery. J Interv Cardiol 2012; 25(1):71-77.

LETTER TO THE EDITOR

CORRELATION OF HYPERTENSION AND F2RL3 GENE METHYLATION WITH PROGNOSIS OF CORONARY HEART DISEASE

BF. GAO, ZC. SHEN, WS. BIAN, SX. WU, ZX. KANG and Y. GAO

Department of Vasculocardiology, The Third People's Hospital of Linyi City, Linyi, Shandong, China

Received August 24, 2018 – Accepted October 2, 2018

The aim of this work was to investigate the correlation between methylation of F2RL3 gene and coronary heart disease (CHD) with or without hypertension, secondary cardiovascular events and mortality. Sixty patients with CHD who underwent a cardiovascular rehabilitation program were recruited. Group A included 30 patients with hypertension and CHD, and group B included 30 patients with non-hypertensive CHD, followed-up for more than 8 years. F2RL3 gene methylation was characterized by Sequenom matrix assisted laser desorption ionization time flight mass spectrometry. The correlation between methylation of the F2RL3 gene, hypertension and secondary cardiovascular events and all-cause mortality was analyzed by multivariate Cox, regression models that estimated confounders to control risk ratios. The results showed that during the follow-up, 3 patients in Group A developed non-fatal stroke, 2 patients died of cardiovascular disease, 1 patient died of other causes, and 4 patients in Group B developed non-fatal myocardial infarction. After adjusting for known prognostic factors, Cox model analysis showed that methylation of F2RL3 gene was closely related to hypertension and mortality. After F2RL3 included in the regression model, the correlation between hypertension and all prognostic outcomes increased. In conclusion, the methylation of F2RL3 can affect the prognosis of different types of acute coronary syndrome and is closely related to mortality.

To the Editor,

Coronary heart disease (CHD), featured by myocardial ischemia, hypoxia or cardiomyocytes necrosis, is frequently caused by the accumulation of atherosclerotic plaque which leads to vascular cavity stenosis or occlusion (1, 2). With the rapid aging of the Chinese population, the incidence of coronary heart disease has increased rapidly, with younger onset age (3-5).

F2RL3 is a receptor which belongs to a protease activated family. Some studies suggested that this gene may play an important role in human blood coagulation, in the pain response and inflammation. F2RL3 is activated by thrombin, and trypsin may be associated with lung cancer in human patients (6).

Despite the recent advancement in understanding pathophysiological mechanisms of hypertension and therapeutic strategies, hypertension remains one of the world's largest public health problems (7). Studies have shown that abnormal DNA methylation plays an important role in the occurrence and development of diseases such as colorectal cancer, breast cancer, coronary heart disease and schizophrenia (8).

DNA methylation levels have been significantly reduced in hypertensive patients, and the trend continues with the progress of hypertension.

Key words: hypertension, F2RL3 methylation, CHD, prognosis

Mailing address:
Dr Bingfeng Gao,
Department of Vasculocardiology,
The Third People's Hospital Linyi City,
No. 117 Huaxia Road, Hedong District, Linyi,
Shandong, 276023, China
e-mail: gaobf0518@163.com

0393-974X (2018)

Currently, studies have found that methylation of F2RL3 gene has a certain correlation with cardiovascular diseases, but there is still a lack of relevant data on how to regulate it (9). This study aimed to determine whether hypertension affects the expression of F2RL3 in CDH and the relationship between secondary cardiovascular events and mortality.

MATERIALS AND METHODS

Patients

A total of 60 patients (aged 45±4.67) who had received cardiovascular rehabilitation treatment for acute coronary syndrome in The Third People's Hospital of Linyi City from September 2009 to September 2017 were recruited in the study. Group A included 30 patients who had been diagnosed with CHD and grade 3 hypertension (Grade 3 hypertension: systolic blood pressure over 180 mm Hg or diastolic pressure over 110 mm Hg.). Group B included 30 patients who had been diagnosed with non-hypetension CHD. The patient acceptance period meant that the survival time was from the beginning of the study to the end of the study. Exclusion criteria: patients with cancer, mental illness, serious infectious disease, chronic obstructive pulmonary disease, heart valve disease, autoimmune diseases, various types of cardiomyopathy, application of mechanical ventilation or shock patients, within 3 months of trauma or surgery, within 2 weeks of drug use which may affect liver function (such as benzene oxygen aromatic acids, antibiotics, bile acid chelating agent, etc.), age under 40, pregnancy, breast-feeding, or with child bearing plan in the near future. None of the participants smoked. This study was approved by the ethics committees of The Third People's Hospital of Linyi City and each participant gave written informed consent..

Table I. *Different influencing factors F2RL3 methylation baseline*

	AHD with hypertension		AHD without hypertension		P value
Risk factor	Number	Methylation intensity Median(Q1-Q3)	number	Methylation intensity Median(Q1-Q3)	
Sex(female/man)	15/15	0.68(0.65-0.71)/0.58(0.51-0.75)	15/15	0.69(0.55-0.69)/0.78(0.61-0.75)	0.000
Primary diabetes	3	0.57(0.51-0.75)	10	0.61(0.43-0.66)	0.000
secondary diabetes	5	0.66(0.54-0.66)	8	0.59(0.55-0.61)	
Discharge prescriptions ACE-inhibitor					
Prescribed	17	0.61(0.57-0.75)	7	0.71(0.63-0.79)	0.821
Not prescribed	13	0.54(0.49-0.61)	23	0.65(0.49-0.61)	
Lipid-lowering drugs					
Prescribed	16	0.54(0.48-0.63)	5	0.62(0.55-0.65)	0.012
Not prescribed	14	0.63(0.59-0.72)	25	0.66(0.61-0.71)	
ASS					
Prescribed	16	0.53(0.47-0.65)	6	0.57(0.55-0.64)	0.135
Not prescribed	14	0.69(0.56-0.77)	24	0.71(0.59-0.78)	
β-Blocking drugs					
Prescribed	25	0.52(0.51-0.63)	3	0.63(0.58-0.71)	0.337
Not prescribed	5	0.68(0.63-0.79)	27	0.76(0.69-0.81)	

Methylation intensity at F2RL3 by gender, medicine status during the follow-up period. Median methylation is slightly lower in men than in women of the two groups, but is consistent across age groups. By far, the largest change in methylation intensity is based on the condition of diabetes. Current levels of methylation in CHD are much lower than in non-hypertensive CHD participants.

Table II. *Spearman correlation coefficients of two different CHD and methylation intensity of F2RL3 with risk factors at baseline.*

Risk factors	R_s [1)]	P value	R_s [2)]	P value
Age	0.051	0.024	0.065	0.014
Reaction C protein	-0.235	0.000	-0.152	0.000
Interleukin(IL-6)	-0.215	0.000	0.102	0.000
Albumin	0.155	0.000	-0.001	0.000
ADiponectin	-0.011	0.568	0.000	0.321
N-terminal Pro-B-ratriuretic peptide	-0.123	0.000	-0.051	0.000
High-density lipoprotein cholesterol	0.022	0.457	-0.001	0.954
Total cholesterol	-0.085	0.000	-0.051	0.033
Triglycerides	-0.075	0.000	-0.012	0.458
Free fatty acids	0.023	0.456	0.011	0.554
Cholesteryl ester transfer protein	0.021	0.321	0.024	0.546
Lipoprotein-associated phospholipase A2	-0.051	0.095	-0.068	0.087
Fasting glucose	-0.056	0.874	-0.037	0.897
Fetuin A	0.008	0.874	0.046	0.069
Adipocyte fatty acid-binding protein	0.016	0.655	0.002	0.994
Retinol-binding protein-4	0.024	0.477	0.046	0.152
CKD-EP1	-0.066	0.041	-0.010	0.788
Arnal-Dade	0.077	0.019	0.071	0.031
Alcohol consumption during rehabilitation	-0.058	0.124	-0.047	0.129
Alcohol consumption during pass year	-0.031	0.412	0.017	0.621
γ-Glutamyltransferase activity	-0.059	0.078	-0.088	0.007

[1)]After adjustment for age and gender, the relationship between the status of methylation and the vascular risk factors of hypertension ACS; [2)]After adjustment for age and gender, the relationship between the status of methylation and the vascular risk factors of non-hypertensive ACS.

Date and sample collected

At the end of the inpatient rehabilitation stage, blood was collected from the patients. Serum was isolated after centrifugation and stored at -80□ (freezer from haier, China, Qingdao). Standard routine clinical parameters (such as serum levels of glutamine transferase, muscle coordination, fasting blood glucose, high-density lipoprotein, total cholesterol, and triphthalein) were obtained from inpatient Medical Records. After rehabilitation, the patients were contacted by email 1, 3, 4, 5, 6 and 8 years after discharge from the hospital, and information regarding non-fatal cardio-cerebrovascular events (myocardial infarction and stroke) was obtained through standardized questionnaires.

Methylation assessment

Desorption ionization time was detected by flight mass spectrometry. Initially, the DNA sample was bisulfite-converted using Ez-96 DNA methylation gold kit (http://www.integratedsci.com.au/) according to the manufacturer's instructions. Subsequently, the primers containing cg03636183 amplifiers and the adjacent 6 plus CpG sites were amplified with the prespecified bisulfite. After the treatment of alkaline phosphatase (SAP), the RNase A was cut and the resin was cleaned. MassARRAY EpiTyper v1.0 software and 384 spectroCHIPs were used to transfer the PCR product fragments (10).

Statistical analysis

SPSS 19.0 statistical software was used to analyze the data, and the non-normal measurement data was represented by median number (q1-q3). Rank sum test was used for comparison, Spearman's test and the Kaplan-Meier method were used for correlation analysis and for drawing the survival curve, and log-rank test was used for comparison.

RESULTS

A total of 60 patients were included in this study. Methylation at one or more CpG sites was detected in 99.9% of the subjects. During the follow-up period, 3 patients in group A developed non-fatal stroke, 2 patients died of cardiovascular diseases, 1 died of other causes, and 4 patients in the group developed non-fatal myocardial infarction (Table I).

Correlation between methylation level of hypertension in F2RL3 and risk markers of coronary heart disease

The methylation levels of two different types of coronary heart disease was positively correlated with age and gender. Hypertensive ACS patients showed much higher levels of F2RL3 methylation. The methylation level of F2RL3 gene was significantly different in the subjects with hypertension and acute cardiovascular events. By adjustment of age and gender, the correlations between the two coronary heart disease risk indexes were: on the level of methylation of F2RL3 gene, the correlation coefficient of hypertension and serum albumin Spearman >0.10, and the correlation coefficient of N-terminal Pro-B-ratriuretic peptide, Reaction C protein and interleukin-6 Spearman was <-0.10. (Table II)

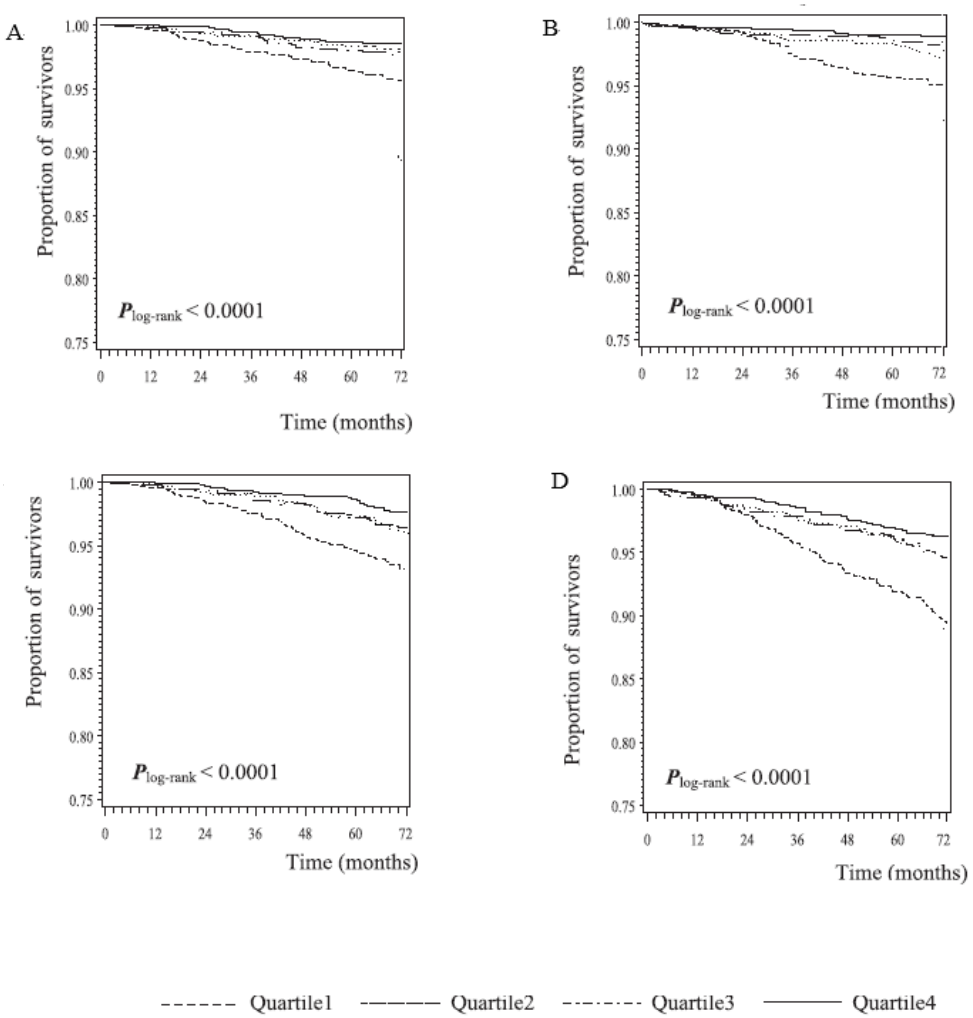

Fig. 1. *Kaplan–Meier estimates of survival. **A)** Adjusted for gender and age; **B)** Adjust for the incidence of diabetes; **C)** Model 1,2 + adjusted for the interaction between risk indicators such as hypertension history, nt-pro BNP (log), hypersensitive c-reactive protein (log) and albumin and methylation level. **D)** is consistent with model 3 except that the hypersensitive creative protein (log) and albumin are not adjusted.*

Correlation between methylation level of F2RL3, hypertension and the prognosis of patients

According to F2RL3 methylation degree with four-digit stratification, the Kaplan-Meier curve was used to analyze the differences in survival between the 4 groups (Fig. 1). Compared to the two groups with the lowest methylation of F2RL3, the two groups with the highest methylation quartile of F2RL3 had better prognosis. At the end of the follow-up period, mortality from all causes was increased in the F2RL3 methylated quartile group. Patients in the lowest methylated quartile showed a three-fold higher risk of all-cause mortality compared with those in the highest methylated quartile. After adjusting the methylation of F2RL3, the effect ratio of hypertension was significantly reduced.

DISCUSSION

The results of this study indicated that the degree of hypomethylation of F2RL3 gene in patients with coronary heart disease was associated with hypertension, and it could affect mortality and other prognostic indexes to a certain extent. Some researchers suggested that hypertension is accompanied by mild inflammation in the cardiovascular system, and the inflammatory marker C-reaction protein level in serum was altered in hypertensive patients (11). Therefore, it is not surprising that methylation of F2RL3 gene is associated with the prognosis of cardiovascular patients. In this study, C-reactive protein and IL-6 were used as risk factors for the study, and F2RL3 methylation level was compared between the two groups. The results showed that the methylation correlation of IL-6 in different groups varied. Previous studies reported that innate immune cells can release reactive oxygen species and reactive nitrogen, both important signaling molecules in the cardiovascular system (12).

In the present study, after the methylation of F2RL3 was corrected, the correlation between hypertension and various death outcomes was weakened, suggesting that hypertension could be correlated with F2RL3 methylation and affect the prognosis and development of coronary heart disease.

In summary, F2RL3 methylation level is correlated with hypertension. Hypertension has a certain effect on the methylation degree of F2RL3 and coronary heart disease. The prognosis of coronary heart disease with hypertension is more dangerous.

REFERENCES

1. Noriega FJ, Vives-Borrás M, Solé-González E, et al. Influence of the extent of coronary atherosclerotic disease on ST-segment changes induced by ST elevation myocardial infarction. Am J Cardiol 2014; 113(5):757-64.
2. Zhu KF, Wang YM, Zhu JZ, et al. National prevalence of coronary heart disease and its relationship with human development index: A systematic review. Eur J Prev Cardiol 2016; 23(5):530-43.
3. Ge L, Ge J. The reasons coronary heart disease mortality has increased in China. Am Heart Hosp J 2007; 5(2):97-99.
4. Esteghamati A, Hafezi-Nejad N, Zandieh A, et al. Homocysteine and metabolic syndrome: from clustering to additional utility in prediction of coronary heart disease. J Cardiol 2014; 64(4):290-96.
5. Kim SY, Guevara JP, Kim KM, et al. Hyperuricemia and coronary heart disease: a systematic review and meta-analysis. Arthritis Care Res (Hoboken) 2010; 62(2):170-80.
6. Navar-Boggan AM, Peterson ED, D'Agostino RB Sr, et al. Hyperlipidemia in early adulthood increases long-term risk of coronary heart disease. Circulation 2015; 131(5):451-58.
7. Touyz RM. Advancement in hypertension pathogenesis: some new concepts. Curr Opin Nephrol Hypertens 2011; 20(2):105-6.
8. Breitling LP, Salzmann K, Rothenbacher D,et al. Smoking, F2RL3 methylation, and prognosis in stable coronary heart disease. Eur Heart J 2012; 33(22):2841-48.
9. Besingi W, Johansson A. Smoke-related DNA methylation changes in the etiology of human disease. Hum Mol Genet 2014; 23(9):2290-7.
10. Montecucco F, Pende A, Quercioli A, et al. Inflammation in the pathophysiology of essential hypertension. J Nephrol 2011; 24(1):23-34.

11. Nagai T, Anzai T, Kaneko H, et al. C-reactive protein overexpression exacerbates pressure overload-induced cardiac remodeling through enhanced inflammatory response. Hypertension 2011; 57(2):208-15.
12. Adar T, Edden Y, Shteingart S, et al. Portal hypertension is associated with modulation of regulatory T cells. Eur J 2016; 14(1):40-47.

LETTER TO THE EDITOR

EFFICACY OF COMMERCIAL VACCINES AGAINST THE PREVALENT STRAINS OF NEWCASTLE DISEASE AND AVIAN INFLUENZA (H9N2) INFECTIONS IN BROILERS IN PAKISTAN

I. IRSHAD[1], A. ASLAM[1], M.Y. TIPU[1], K. ASHRAF[2], B. ZAHID[1] and A. IRSHAD[3]

[1]Department of Pathology, University of Veterinary and Animal Sciences, Lahore-Pakistan;
[2]Department of Parasitology, University of Veterinary and Animal Sciences, Lahore-Pakistan;
[3]Centre of Excellence in Molecular Biology, University of the Punjab, Lahore-Pakistan

Received August 8, 2018 – Accepted September 21, 2018

The efficacy of the two commonly used commercial vaccines for Newcastle disease (ND) and low path avian influenza (LPAI) H9N2 were evaluated against field virus in broiler chicks. One hundred one-day-old commercial broiler chicks were divided into four groups (A to D) with an equal number of birds per group. Group A and B were vaccinated against H9N2 and NDV, respectively, at day 7 of age while group C served as positive infected control for H9N2 and group D for NDV. Serum samples from birds in all groups were tested for presence of antibodies against H9N2 and NDV at day 21 of age. Subsequently, on day 28 of age, groups A and C were challenged with the field strain of H9N2 virus, and Group B and D with NDV. Birds were monitored for a period of 2 weeks for development of any clinical signs and mortality. The geometric mean titer were high in groups A (4.90) and B (7.3), and low in the unvaccinated groups C (0.7) and D (1.1). The highest and lowest value of H9N2 antibody titer detected through ELISA were 1.498 and 0.502, respectively. The S/P ratios greater than 0.5 were considered positive. The highest and lowest value for NDV antibody titer detected through ELISA were 783 and 882, respectively. Serum samples with titer greater than 396 were considered positive and indicated vaccination or other exposure to NDV. On histological examination severe congestion, necrosis, degeneration, hemorrhages and leukocyte infiltration were observed in intestine, lungs, trachea and bursa of Fabricius of the non-vaccinated group post-infection. Mild tissues changes were observed in the vaccinated group. It can be concluded from the findings that the commonly used commercial vaccines may provide effective protection against the circulating H9N2 and ND virus in broiler birds by producing protective antibody titer.

To the Editor,

Newcastle disease and avian influenza viruses are the members of paramyxoviride and orthomyxoviride family responsible for significant economic losses to the poultry industry globally (1). ND is considered endemic in Pakistan and despite regular vaccination, the outbreaks of this disease are frequently reported in commercial and backyard poultry (2). Likewise, H9N2 subtype of avian influenza (AI) which is considered a less pathogenic virus is being detected in poultry farms even when the birds are immunized against it. H9N2 is an emerging public health pathogen as it has been linked to human illness in Hong Kong, China and recently in Bangladesh (3). ND exists endemically almost all year round. This scenario challenged the efficacy of the ongoing programs regarding vaccination against the disease. Some questions were triggered after the failure of

Key words: Newcastle disease, low path avian influenza (LPAI), broiler, ELISA

Mailing address:
Dr. Asma Irshad,
Centre of Excellence in Molecular Biology,
University of the Punjab,
Lahore, 54000-Pakistan
e-mail: asmairshad76@yahoo.com

0393-974X (2018)

the vaccination programs; is there any difference between the field virus strain and vaccine strains, inappropriate methodology or plan of action, creation of new genotypes under the more elevated immune response which are resistant to current vaccines (4). Poultry provides protective conditions to the H9N2 virus to develop into the strains which could affect the wild species of birds. According to some modern research reports, similarities have been detected in the viral genome of H7N3, H5N1 and H9N2 (Pakistani) as a consequence of antigenic drifts. Therefore, H9N2 could be a potential pandemic problem for human health in the future, hence there is a need to regularly test the genome for any mutations and improve the vaccines accordingly (5). Despite vaccination, these viruses are still circulating in poultry, therefore the current study was designed to test the immunoprophylactic potential of two commonly used commercial vaccines against the field viruses.

MATERIALS AND METHODS

Experimental design

One hundred, one-day-old commercial broiler chicks were procured from a local hatchery and evenly divided into four groups A, B, C and D, 25 in each group. Birds were reared under standard management conditions and were offered feed and water ad libitum. On day 7 of age, the birds in group A were vaccinated (0.25 mL subcutaneously) with an inactivated oil-based Avian influenza (H9N2) vaccine (Otto Fluvac, EID_{50} 9.2/mL. HA 264 HAU/50 μL). while group B was vaccinated (0.3 mL subcutaneously, Gallimune) against Newcastle disease virus. Birds in group C and D did not receive any immunization and served as positive control for H9N2 and NDV.

Serum antibody titer

Serum samples were collected from birds in all groups on day 21 of age, and tested for the presence of antibodies against NDV and H9N2 using HI (6) and ELISA (IDEXX, USA) used per manufacturers guidelines; the S/P ratios greater than 0.5 were considered positive for presence of antibodies against AIV, and NDV serum samples with titer greater than 396 were considered positive and indicated vaccination to NDV. From the HI test GMT was calculated and values between 4-6 indicated protection.

Challenge trial

On day 28 of age, groups A and C were challenged with the H9N2 virus ($10^{7.7}$ EID50) isolated from the suspected poultry flocks and groups B and D with field isolate of NDV ($10^{8.6}$ EID50). Birds were monitored until two weeks post-infection i.e. 42 days of age for development of clinical signs of disease and mortality.

Histological examination

Five birds from each group were sacrificed on days 28 and 35 to evaluate the histological changes. The tissue samples of intestine, lungs, kidney, trachea, thymus and bursa of Fabricius were collected and processed

Table I. *ELISA and HI antibody titer against AI (H9N2) and NDV in vaccinated groups (A and B) and HI antibody titer in control groups (C and D).*

Sample ID	ELISA for AIV titer	Results	Antibody titer against AI (H9N2)		ELISA for NDV titer	Results	Antibody titer against NDV (Log^2)	
			Vaccinated Birds (Group A)	Control Birds (Group C)			Vaccinated birds (Group B)	Control birds (Group D)
1	0.541±0.01^{a}	Positive	4±0.02^{a}	1±0.01^{cd}	1552±0.03^{bc}	Positive	8±0.03^{c}	2±0.2^{c}
2	0.575±0.03^{a}	Positive	4±0.03^{ab}	1±0.02^{c}	1714±0.01^{d}	Positive	8±0.01^{c}	2±0.01^{c}
3	0.627±0.01^{ab}	Positive	5±0.01^{ab}	0±0.01^{a}	1724±0.02^{d}	Positive	8±0.01^{c}	1±0.03^{ab}
4	1.498±0.04^{d}	Positive	6±0.06^{c}	0±0.02^{a}	882±0.01^{a}	Positive	4±0.03^{a}	0±0.01^{a}
5	0.511±0.01^{a}	Positive	4±0.03^{ab}	1±0.01^{c}	1735±0.1^{d}	Positive	8±0.02^{c}	0±0.02^{a}
6	1.052±0.01^{c}	Positive	6±0.01^{c}	2±0.04^{d}	1578±0.05^{bc}	Positive	7±0.01^{b}	1±0.01^{ab}
7	0.502±0.03^{a}	Positive	3±0.06^{a}	0±0.01^{a}	1468±0.01^{b}	Positive	7±0.05^{b}	2±0.06^{c}
8	0.661±0.02^{ab}	Positive	5±0.01^{ab}	0±0.06^{a}	1783±0.01^{d}	Positive	8±0.04^{c}	1±0.1^{ab}
9	0.738±0.1^{ab}	Positive	6±0.02^{c}	1±0.01^{c}	1537±0.04^{bc}	Positive	7±0.02^{b}	0±0.02^{a}
10	1.026±0.01^{c}	Positive	6±0.05^{c}	1±0.01^{ab}	1647±0.02^{c}	Positive	8±0.01^{c}	2±0.01^{c}

Values are mean±SD of triplicate experiments. Furthermore, mean carrying different superscript letters (a-d) exhibit significant difference among means at ($p<0.05$) with 95% confidence. HI: hemagglutination inhibition; AIV: avian influenza virus; NDV: Newcastle disease virus.

in the Histopathology Lab., Department of Pathology, University of Veterinary and Animal Sciences, Lahore, Pakistan.

Statistical analysis

Minitab software was used for computation and analysis of different parameters. Differences were analyzed by considering $p<0.01$ statistically significant. The collected data was analyzed by means and standard deviation.

RESULTS

The results of the current study indicated the development of an effective antibody response after vaccination with otto Fluvac® and Gallimune® (Table I). Birds in both vaccinated groups showed no signs of illness and no mortality recorded. In comparison, 10% of the birds died in the non-vaccinated group challenged with H9N2 virus, whereas 80% of the birds died in the group challenged with NDV. The GMT was 4.90, 7.3, 0.7, and 1.1 for groups A, B, C and D respectively. S/P ratio of ELISA for H9N2 in the vaccinated group varied between 0.502-1.498 while antibody titer as measured by ELISA for NDV ranged between 882-1783. On day 28 of age, no histological changes were observed in tissue samples of the treated groups. On the 35th day, group C showed moderate changes, trachea and lung were inflamed with severe sloughing of epithelial cells (Fig. 1a). The lungs were severely congested and emphysematous. There was infiltration of inflammatory cells in the lungs (Fig. 1b) in group D. Severe degeneration and necrotic foci were also observed in the lungs and spleen. Necrosis with infiltration of inflammatory

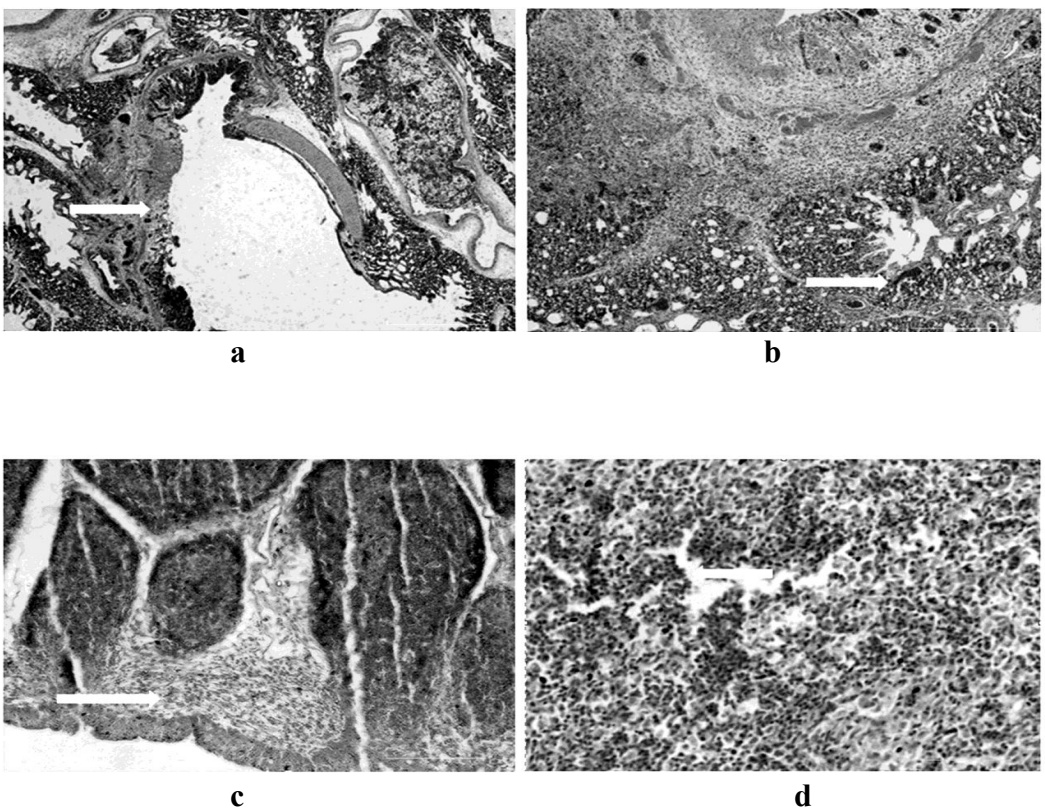

Fig. 1. *Histological results of treated groups at different magnification using hematoxylin & eosin staining.* ***a****) Group C showing sloughed off epithelium in lungs on (35th day of age) 7th day post-infection (10X).* ***b****) Group D bird showing Infiltration of hetero-phils in lungs on (35th day of age) 7th day post-infection (10X).* ***c****) Group D bird challenged with NDV showing infiltration of inflammatory cells in bursa on (35th day of age) 7th day post-infection (20X).* ***d****) Spleen of group D on (35th day of age) 7th day post-infection showing hemorrhages of spleen (40X).*

cells in kidney and tubuinterstitial nephritis was seen in the left kidneys. Leukocytic infiltration and cellular degeneration was observed in the bursa of Fabricius (Fig. 1c). Group D showed congestion, necrosis, degeneration, hemorrhages and dead tissue mass in intestine and spleen (Fig. 1d). Congestion, degeneration and atrophy were observed in the bursa of Fabricius as compared to group A and B.

DISCUSSION

This study demonstrated that Gallimune ND® can provide over 90% protection against the NDV genotype VII challenge in broiler birds under experimental conditions. However, there are several studies which report continuous outbreaks of avian influenza (7) and Newcastle disease in Pakistan (2). This persistence of disease despite vaccination may be due to the difference in vaccine efficacy under field and experimental conditions (8). There are several infectious and non-infectious factors, e.g. high levels of ammonia, fungal toxins in feed, and poor nutrition, along with infectious diseases such as infectious bursal disease, chicken infectious anemia, and Marek's disease, which can interfere with both innate and acquired vaccinal immunity (9). The results of the current study are in agreement with the findings of a previous study (10) which reported that locally produced avian influenza vaccines including otto-flu generate high antibody titers against avian influenza. Gross and histological changes, including congestion, hemorrhages and necrosis, were observed on kidney and intestine. Similar findings were reported by other Authors (9, 11, 12). Severe hemorrhages and atrophy of bursa were also observed. Pazhani et al. (13) reported necrosis with infiltration of inflammatory cells in kidneys, and tubuinterstitial nephritis were seen in kidneys which coincides with our results.

It can be concluded from the present study that despite of reports of genetic reassortments and emergence of new genotypes of H9N2 and NDV, vaccines are still providing effective antibody titer under experimental conditions, and other environmental and infectious problems may be associated with poor vaccine efficacy and disease outbreaks.

ACKNOWLEDGEMENTS

The authors are grateful to the Higher Education Commission, Pakistan and Prof. Dr. Shafqat from the WTO, University of Veterinary and Animal Sciences, Lahore-Pakistan for their support.

REFERENCES

1. Wang G, Zhu R, Yang L, et al. Non-thermal plasma for inactivated-vaccine preparation. Vaccine 2016; 34:1126-32.
2. Shabbir MZ, Zohari S, Yaqub T, Nazir J, Shabbir MAB, Mukhtar N, Munir M. Genetic diversity of Newcastle disease virus in Pakistan: a countrywide perspective. Virol J 2013; 10:170. http://doi.org/10.1186/1743-422X-10-170.
3. Parvin R, Heenemann K, Halami M, Chowdhury E, Islam MR, Vahlenkamp T. Full genome analysis of avian influenza virus h9n2 from Bangladesh reveals internal gene reassortments with two distinct highly pathogenic avian influenza viruses. Arch Virol 2014; 159:1651-61.
4. Muzaffar A, Yaqub T, Mukhtar N, et al. Prevalence and phylogenentics of H9N2 in backyard and commercial poultry in Pakistan. Avian Dis 2017; In press.
5. Umar S, Rehman A, Younus M, et al. Effects of Nigella sativa on immune responses and pathogenesis of avian influenza (H9N2) virus in turkeys. J Appl Poult Res 2015; 2:1-9.
6. Thayer SG, Beard CW, Zavala LD, et al. A Laboratory Manual for the Isolation, Identification and Characterization of Avian Pathogens, 5th ed. Jacksonville, FL: Ameri Asso Avi Pathol 2008:222-29.
7. Abid M, Yaqub T, Mehboob A, Shabbir MZ. Characterization and phylogenetic analysis of avian influenza virus subtype H9N2 in Pakistan. Hosts and Viruses 2017; 4(4):62-69.
8. Perozo F, Marcano R, Afonso CL. Biological and phylogenetic characterization of a genotype VII Newcastle disease virus from Venezuela: efficacy of field vaccination. J Clin Microbiol 2012; 50(4):1204-8.
9. Hoerr FJ. Clinical aspects of immunosuppression in poultry. Avian Dis 2010; 54(1):2-15.
10. Shaukat S. Management of epidemics in Tropical Countries. J Trop Dis 2016; 4:3.
11. Anis Z, Morita T, Azuma K, Ito H, Ito T, Shimada A.

Histopathological alterations in immune organs of chickens and ducks after experimental infection with virulent 9a5b Newcastle disease virus. J Comp Pathol 2013; 149:82-93.

12. Dai Y, Cheng X, Liu M, Shen X, Li J, Yu S, Ding C. Experimental infection of duck origin virulent Newcastle disease virus strain in ducks. BMC Vet Res 2014; 10(1):164.
13. Pazhani GP, Niyogi SK, Singh AK, et al. Molecular characterization of multidrug resistance Shigella species isolated from epidemic and endemic cases of shigellosis in India. J Med Microbiol 2008; 57(7):856-63.

JOURNAL OF BIOLOGICAL REGULATORS & HOMEOSTATIC AGENTS Vol. 32, no. 6, 1551-1556 (2018)

LETTER TO THE EDITOR

ELECTROSPUN PROBIOTICS: AN ALTERNATIVE FOR ENCAPSULATION

Z. AKBAR[1], T. ZAHOOR[1], N. HUMA[1], A. JAMIL[2], H. AYESHA[3] and J.M. KUMAR IRUDAYARAJ[4]

[1]NIFSAT, University of Agriculture, Faisalabad, Pakistan; [2]Department of Biochemistry, University of Agriculture, Faisalabad, Pakistan; [3]Punjab Medical College, Faisalabad, Pakistan; [4]Micro and Nanotechnology Lab., Purdue University, West Lafayette, Indiana, U.S.A.

Received June 15, 2018 – Accepted October 11, 2018

Electrospinning has emerged as a potential method to fabricate nonwoven nanofibers. It has application in different fields of biomedicine as it has potential to carry antimicrobial and bioactive agents. The present investigation was conducted to optimize the process conditions and determine the viability of probiotics after being electrospun in fibers. Poly(vinyl alcohol) (PVA) was utilized as electrospun material because it possesses generally recognized as safe (GRAS) status and in dry form it acts as a high oxygen barrier and has high water solubility. This characteristic allows the easy recovery of the bacteria from electrospun fibers. The viability tests, carried out at three different temperatures (room temperature, 4°C and -20°C) showed *Bifidobacterium animalis* subsp. Lactis Bb12 (probiotic 1) and combination of *Streptococcus thermophilus* (TH-4®), *Lactobacillus paracasei* 431® and Bb-12 (probiotic 2) within the electrospun PVOH fibers remained viable after 1 week at room temperature and refrigeration temperature. The nanofibers containing probiotics prepared with 9% poly venyl alcohol showed homogenous, uniform, bead-free and smooth texture. Probiotic 1 demonstrated growth as 1.85×10^8, 1.57×10^8 and 1.71×10^8 before, 0 hour and after 1 week of encapsulation. While probiotic 2 exhibited a growth of 2.1×10^8 before electrospinning, 1.3×10^8 at 0 hour and 1.97×10^8 after one week of electrospinning. There was no change in CFU/mL count and remained 10^8 CFU/mL. The encapsulation efficiency was 84.07% and 85.73% at 0 and one week, respectively, for Probiotic 1, while probitic 2 showed 90.09% and 93.59 % encapsulation efficiency before and after one week, respectively. Considering the prolonged viability of nanofibers containing probiotics noted at room temperature, this technology can be implemented for prolonged viability of probiotics.

To the Editor,

Recently, an increase in nutritional awareness has fueled a generation to use probiotics due to their immense benefits. The intestinal flora contributes to human wellness by hindering the pathogenic colonization, enhancing immune system of host, by metabolizing the nutrients and producing good by-products. Different strains of bifidobacteria, either separately or a mixture of different strains, have been employed for human consumption. *Bifidobacterium animalis* subsp. lactis Bb12, *Streptococcus thermophilus* (TH-4®) and *Lactobacillus paracasei* 431® have been widely used in the pharmaceutical and food industries as well as in infant formulae

Key words: electrospinning, PVA, electrospun fibers

Mailing address:
Dr Zainab Akbar,
Biotechnology and Microbiology Lab.,
National Institute of Food Science and Technology (NIFSAT),
University of Agriculture, Faisalabad, Pakistan
Tel.: +923317276902
e-mail: zainabfst@gmail.com

0393-974X (2018)

(1). It is recommended that at least 10^{8-9} CFU/g of bacteria should be present in each product. However, the viability of bacteria is adversely affected due to numerous factors including technological processes, high and low temperature, gastrointestinal conditions, pre- and post-fermentative pH, digestive enzymes, bile acids and gastric juices. Different techniques, such as spray drying (2), coacervation (3) and emulsifying crosslinking (4), have been used for encapsulation, but there is involvement of organic solvents, fluctuated temperatures and drying methods which consequently disturb the viability of bacteria. and some organic agents lead to toxicity issues (5). Electrospinning is considered as an alternate solution for this issue. Basically, it is a high voltage spinning used to produce fibers in nano and micro ranges. An electrospinning setup comprises of a syringe, a syringe pump, a high-voltage power and a collector but no specific temperature is required during this process. After optimizing the process parameters (flow rate, molecular weight of polymer, viscosity, concentration of polymer, distance and voltage) an aqueous solution can be drawn after addition of additives to form nanofibers (6-7). The present study was designed with the objective to optimize and make electrospun fibers containing probiotics by using poly(vinyl alcohol) (PVA) to check the appropriateness and viability of the probiotics.

MATERIALS AND METHODS

This study was carried out in Bindley Bioscience center, Purdue University, IN, U.S.A. to prepare the probiotics containing electrospun fibers.

Poly vinyl alcohol (PVA) with an average molecular weight of 80 KDa to 100 KDa and utilized with a degree of hydrolysis of 99% was acquired from Sigma Aldrich Co. (Spain).

Optimization of process parameters for electrospinning

For optimization of electrospinning process parameters 6%, 9% and 12% PVA solutions were utilized. These solutions were prepared by dissolving the polymer in distilled water at 80°C under magnetic stirring to get a complete dissolution. However, a complete dissolution of polymer was not observed even after 2 h, therefore autoclave at 121°C with liquid cycle was utilized for complete dissolution and sterility of solutions.

Electrospinning equipment setup

The electrospinning set up equipped with an adjustable high-voltage 0-30 kV power supply was assembled. The anode was connected to a stainless-steel needle through PTFE wires, of 5 mL plastic syringe. The syringe was located horizontally in the cradle of a manually controlled syringe pump which could deliver flow rates within in the range of 10-3 to 10 mL h-1 (KD Scientific Inc., Holliston, U.S.A.). The cathode was attached with a collector drum to create a high electric field.

Preparation of polymer solution

The autoclaved solutions were electrospun at 25°C to produce nanofibers. For the collection of electrospun fibers, the grounded collector was creased with aluminum foil and later rotary drum. For optimization of process, different conditions were utilized such as; voltage, 12 kV, 20 and 25 kV; tip to collector distance, 15, 11 cm and flow rate, 0.4, 0. 75 and 0.1 mL/h. The collected nanofibers were then dried and evaluated by SEM. From Scanning Electron Microscopy (SEM) results, conditions were finalized for further processing of nanofibers.

Bifidobacterial containing solution

B. lactis cells were added to 9% PVA solution (selected after performing SEM) under sterile conditions and were pumped through the needle (L 0.8 mm). The experimental setup was retained in a laminar flow safety cabinet.

Preparation of PVA/Bb12 fibers

For the collection of the PVA electrospun fibers comprising *Bifidobacterium animalis* subsp. lactis Bb12, *Streptococcus thermophilus* (TH-4®) and *Lactobacillus paracasei* 431®, the rotary drum was used as collector. The electrospinning conditions were as follow; voltage 25 kV; tip to collector distance 11 cm and flow rate 0.75 mL/hr and 1000 rpm for roller. By using these conditions, a stable jet mode was achieved. The electrospun nanofibers were dried for a whole night before SEM observation.

Scanning Electron Microscopy

SEM analyses were performed on a FEI Nova NanoSEM 200, Hitachi microscope (Hitachi S-4100) at a

voltage of 5 kV and spot size 3 with working distance of 20 mm. Coating of electrospun fibers was done by using a gold-palladium mixture under vacuum before their morphological studies. Fiber diameters of the electrospun fibers were measured by means of the Adobe Photoshop CS3 extended software from the SEM micrographs in their original magnification.

Viability of Bifidobacteria in nanofibers

Electrospun fibers were detached from roller. Weighing and storage of aliquots of the PVA/Bb12 fibers was carried out (room temperature and 4°C) for viability studies, and a small sample was kept for SEM. Nanofibers containing probiotics Bb12 cells were also stored at room temperature and 4°C, and their ability to grow was also determined. For viability studies, one fresh PVA/ Bb12 aliquot was diluted in PBS at room temperature for 1 h, to dissolve the polymeric fibers, and serial 10-fold dilutions were prepared and plated on MRS agar. After incubation at optimal conditions for 48 h, the viability of electrospun Bb12 cells to growth was determined.

RESULTS

Morphological characteristics of fibers prepared during optimization and after optimization containing probiotics

The nanofibers made of poly vinyl alcohol (PVA) (at the concentration of 6, 9 and 12 %) were used to check the viability of probiotics. These fibers containing probiotics were studied under SEM and images were taken at different resolutions.

Fig. 1a. shows the fibers prepared from 6, 9 and 12% PVA solution. This figure demonstrates that with 6% PVA the sputtering of solution was observed, resulting in the formation of non-uniform fibers with droplets of solution. The morphology of nanofibers prepared with 9% PVA solution is presented in Fig. 1b which shows homogenous, uniform, bead-free and smooth formations of long ultrathin fibers. The nanofibers prepared from 12% of PVA solution (Fig. 1c) exhibit the formation of non-uniform, coarse and beaded nanofibers. This solution was

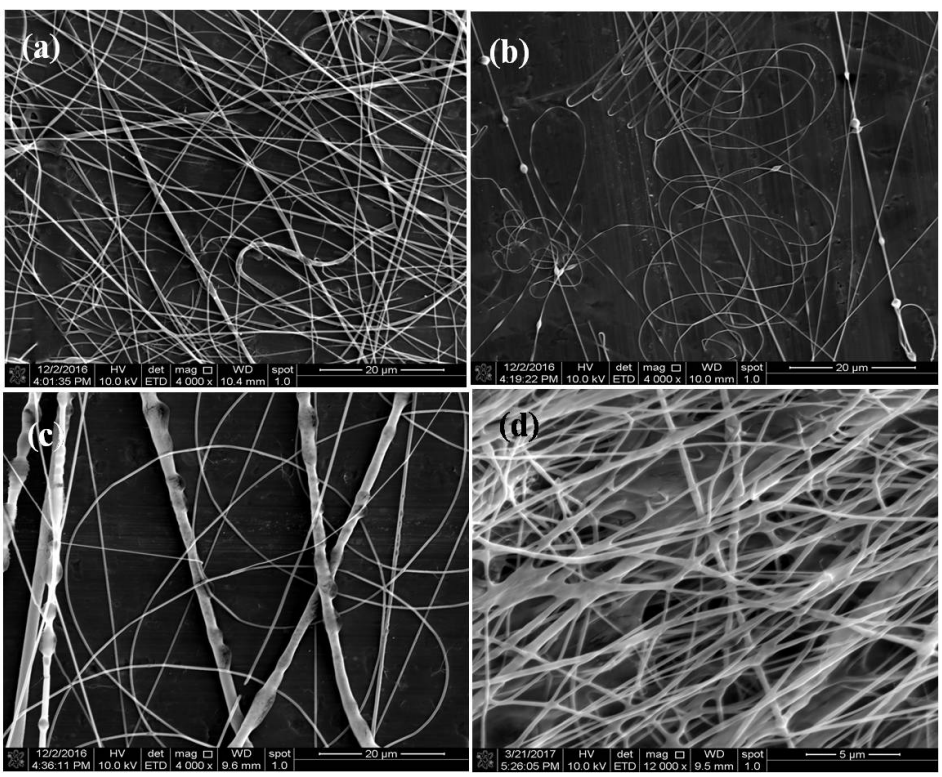

Fig. 1. *Images of nanofibers taken at 4000x magnification power for 6% (**a**), 9% (**b**), 12% (**c**) without probitics and (**d**) optimized 9% PVA solution with probiotics.*

sufficiently viscous to be drawn from needle outlet. Fig. 1d shows the morphology of electrospun fibers containing probiotics within their structure. An entangled chain of long fibers can be easily seen in the figure. PVA is a hydrophilic polymer and confers a barrier for oxygen and the bioactivity of probiotics is not affected.

Viability of encapsulated bifidobacteria

Electrospun ultrathin fibers were detached and the viability of probiotics were assessed during storage at room temperature. The survivability of probiotics in electrospun fibers was determined before and after electrospinning by plate counting method.

Fig. 2a shows the effect of time on the viability of probiotics before, at 0 hour and after one week of nanofabrication. There was a statistically non-significant difference on the viability of probiotics with the passage of time. It shows that viability of probiotics was preserved and not lost after electrospinning.

The growth for probiotic 1 was found 1.85×10^8, 1.57×10^8 and 1.71×10^8 before, 0 hour and after 1 week of encapsulation. While probiotic 2 exhibited a growth of 2.1×10^8 before electrospinning, 1.3×10^8 at 0 hour and 1.97×10^8 after one week of electrospinning. The overall CFU/mL count was not changed and remained 10^8 CFU/mL.

Fig. 2b presents the graphical description of entrapment efficiency of probiotics by using electrospinning. The encapsulation efficiency was 84.07 and 85.73% at 0 and one week for P1, while for P2 demonstrated 90.09 and 93.5 %, respectively.

DISCUSSION

Concentration of polymer solution plays a considerable role for the process of electrospinning. If the concentration is low then it results in electrospray instead of electrospinning as the solution has high surface tension and less viscosity (9). Lower concentration of PVA results in nonuniform fibers with defects such as junctions and beads (8). Moreover, the formation of smooth and continuous fibers cannot be achieved in very low viscosity (10).

It was reported by Son et al. (11) that by increasing the amount of PVA in the solution resulted in stabilized and consistent flow of solution from the needle and consequently formed the long uniform fibers, which were entangled in chain. The smooth nanofibers are formed at suitable concentration of polymer solution (12-13).

As the concentration of polymeric concentration goes a little higher, a mixture of beads and fibers will be attained (14) while a very high viscosity results in the hard ejection of polymeric solution, therefore, it is necessary to standardize the suitable viscosity for electrospinning (15).

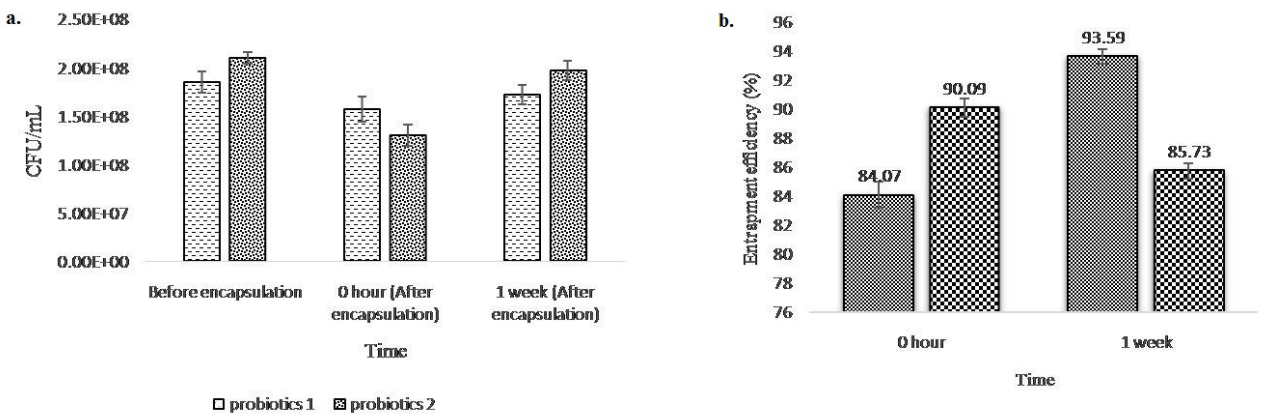

Fig. 2. ***a)*** *Effect of time on viability of probiotics in electrospun nanofibers.* ***b)*** *Effect of time on on entrapment efficiency of electrospun nanofibers.*

The nanofibers having no beads and homogenous structure are suitable for encapsulation of *Bifidobacterium animalis*. Considering the prolonged viability of nanofibers containing probiotics at room temperature, it is recommended to use nanofiber technology in the preparation of therapeutic diets for the children (16).

The encapsulation potential of poly vinyl alcohol (PVOH) for probiotics was explored because it is generally recognized as safe (GRAS), and allows easy recovery of the bacteria for viability determination (17). No decrease or loss in viability of *B. animalis* Bb12 after electrospinning assay was reported when compared to other encapsulation techniques, such as spray drying, which resulted in decreased viability of probiotic bacteria. The probiotic survivability was observed for 40 days at room temperature and for 130 days at refrigeration temperature. The results for the viability of probiotics during the present investigation are supported by these findings because there was no viability loss after one week of electrospinning. Moreover, PVA was used to make fibers as it is water soluble and acts as a good oxygen barrier when dry, thus resulted in the preservation of viability.

Different probiotics, such as *Lactobacillus casei*, *Lactobacillus acidophilus*, *Bifidobacterium longum* and *Lactobacillus rhamnosus* were microencapsulated to evaluate the effect of homogenization (encapsulation technique) on beads size and viability of the probiotics. Reduction of bead sizes was observed due to three different homogenization techniques. The entrapment efficiency was found 64.4% to 47.7% (18) which is comparably less than nanofabricated probiotics investigated in the present study.

The entrapment efficiency of probiotics during this study is supported by a previous work (19) which utilized soluble dietary fiber from agrowastes, oil palm trunk, oil palm frond and okara (soybean solid waste), along with 8% PVA solution for the nano-encapsulate of *Lactobacillus acidophilus*. *L. acidophilus* was merged into the solution to synthesize the nanofiber-encapsulated probiotic, measuring 229-703 nm. A significant bacterial viability 78.6-90% was observed under electrospinning conditions and sustained it at 4ºC for 21 days of storage.

From the present study, it is concluded that electrospun nanofibers have the potential to preserve and extend the viability of probiotics to get beneficial effect from probiotics with comparably better entrapment efficiency. Due to these reasons nanofibers are good alternate for encapsulation. By using biodegradable material such fibers can be utilized directly in food and metabolized by the body while the viability at room temperature can also be extended for a longer time, as supported by the present and previous works. Any antimicrobial agent can also be carried to the body or food system by the biodegradable fibers in order to prevent disease or to enhance the shelf life of product. These fibers also open an era for the pharmaceutical industry as they have the potential to carry a drug into the body or exactly to the site of action.

REFERENCES

1. Saxelin M, Tynkkynen S, Mattila-Sandholm T, De Vos WM. Probiotic and other functional microbes: from markets to mechanisms. Curr Opin Biotechnol 2005; 16:204-11.
2. Bruschi ML, Cardoso ML,Lucchesi MB, Gremião MP. Gelatin microparticles containing propolis obtained by spray-drying technique: preparation and characterization. Int J Pharm Pharm Res 2003; 264:45-55.
3. Mauguet MC, Legrand J, Brujes L, Popineau YJ. Gliadin Matrices for microencapsulation processes by simple coacervation method. J Microencapsul 2002; 19:377-84.
4. Ishizaka T, Endo K, Koishi M. Preparation of egg albumin microcapsules and microspheres. J Pharm Sci Exp Pharmacol 1981; 70:358-63.
5. Birnbaum DT, Kosmala JD, Henthorn DB, Brannon-Peppas L. Controlled release of [beta]-estradiol from PLAGA microparticles: the effect of organic phase solvent on encapsulation and release. J Control Release 2000; 65:375-87.
6. López-Rubio A, Sanchez E, Sanz Y, Lagaron JM. Encapsulation of living *bifidobacteria* in ultrathin PVOH electrospun fibers. Biomacromolecules 2009; 10:823-29.

7. Torres-Giner S, Martinez-Abad A, Ocio MJ, Lagaron JM. Stabilization of a nutraceutical omega-3 fatty acid by encapsulation in ultrathin electrosprayed zeinprolamine. J Food Sci 2010; 75:69-79.
8. Deitzel JM, Kleinmeyer J, Harris D, Beck Tan NC. The effect of processing variables on the morphology of electrospun nanofibers and textiles. Polym 2001; 42:261-72.
9. Fung WY, Yuen KH, Liong M. Agrowaste-based nanofibers as a probiotic encapsulant: fabrication and characterization. J Agri Food chem 2011; 59:8140-47.
10. Larrondo L, Manley SJR. 1981. Electrostatic fiber spinning from polymer melts. I. Experimental observations on fiber formation and properties. J Polym Sci: Polym Phy 1981; 19:909-20.
11. Son WK, Youk JH, Lee TS, Park WH. Effect of pH on electrospinning of poly (vinylalcohol). Mater Lett 2005; 59:1571-75.
12. Fong H, Chun I, Reneker DH. Beaded nanofibers formed during electrospinning. Polym 1999; 40:4585-92.
13. Lee KH, Kim HY, Bang HJ, Jung YH, Lee SG. The change of bead morphology formed on electrospun polystyrene fibers. Polym 2003; 44:4029-34.
14. Eda G, Shivkumar S. Bead-to-fiber transition in electrospun polystyrene. J Appl Polym Sci 2007; 106:475-87.
15. Sukigara S, Gandhi M, Ayutsede J, Micklus M, Ko F. Regeneration o Bombyx mori silk by electrospinning-part 1: Processing parameters and geometric properties. Polym 2003; 4:5721-27.
16. Rubio A, Sanchez E, Sanz Y, Lagaron JM. Encapsulation of living bifidobacteria in ultrathin PVOH electrospun fibers. Biomacromole 2009; 10:2823-29.
17. Capela P, Hay TKC, Shah NP. Effect of homogenisation on bead size and survival of encapsulated probiotic bacteria. Food Resear Inter 2007; 40:261-69.
18. Fung WY, Yuen KH, Liong M. Agrowaste-based nanofibers as a probiotic encapsulant: fabrication and characterization. J Agri Food chem 2011; 59:8140-47.

JOURNAL OF BIOLOGICAL REGULATORS & HOMEOSTATIC AGENTS Vol. 32, no. 6, 1557-1563 (2018)

LETTER TO THE EDITOR

SHORT-TERM EFFECTS OF A DIETARY SUPPLEMENT ON LOWER URINARY TRACT SYMPTOMS

V. COSENTINO[1], A. MILITELLO[2] and G. LAURIA[3]

[1]Private Practice, Caltanissetta, Italy; [2]Private Practice, Roma, Italy; [3]Andrological Urological Private Practice, Palermo, Italy

Received July 10, 2018 – Accepted September 14, 2018

Benign prostatic hyperplasia (BPH) is one of the most common conditions affecting men over 40 years of age, typically manifesting itself with lower urinary tract symptoms (LUTS). Recently, research interest has focused in discovering a viable nutraceutical alternative to the drugs that are currently the first line of treatment for BPH. The aim of this study was to investigate the efficacy and safety of a dietary supplement containing curcumin, beta-sitosterol and oligomeric proanthocyanidins in a group of BPH/LUTS patients. One-hundred men with LUTS caused by BPH were enrolled in this study and agreed to take one tablet a day of the test dietary supplement for three months. Several parameters, such as International Prostate Symptom Score (IPSS), degree of urinary obstruction and average urinary flow were evaluated at different time points. Significant improvement in LUTS was seen after one month of treatment and a significant decrease in mean IPSS index was evident after three months of treatment. Moreover, a comparison of the mean urinary flow and of the number of subjects with bladder obstruction at three months versus one month of treatment shows a significant improvement. The study results suggest that the dietary supplement is effective for almost all the symptoms investigated, including the reduction of IPSS score and the increase of urinary flow. Moreover, the dietary supplement proved to be safe and well tolerated by the great majority of the enrolled subjects.

To the Editor,

Benign prostatic hyperplasia (BPH) is a disorder that affects 15% to 60% of men above 40 years of age (1), characterized by enlargement of the prostate and a decreased maximum urinary flow rate (Q_{max}), and clearly related to lower urinary tract symptoms (LUTS) (2). LUTS are a variety of symptoms that can be obstructive (e.g., hesitancy, poor and/or intermittent stream, straining, prolonged micturition), irritating (e.g., frequent urination, urgency, urge incontinence, nocturia), and/or related to post-micturition (e.g., feeling of incomplete emptying and post-micturition dribble). The main risk factors for BPH are age, genetic factors, high levels of dihydrotestosterone (DHT), lifestyle and inflammatory events (3). Currently, the approach used to limit LUTS is mainly symptomatic, and consists of treatment with α-adrenergic receptor blockers or 5-α reductase inhibitors (4). These drugs can cause several side effects, such as impotence, libido reduction, ejaculation disorders and gynecomastia. Since BPH is a chronic disease requiring long-term treatment, alternatives are much needed. Curcumin, an active compound contained in turmeric, is a good candidate, orally bioavailable and highly safe in humans. Its natural chemical components can block

Key words: benign prostatic hyperplasia, lower urinary tract symptoms, urinary flow, nutraceutical compound, food supplement, curcumin

Mailing address:
Dr Giuseppe Lauria,
Andrological Urological Private Practice,
Via Paolo Paternostro, 62
90141 Palermo, Italy
Tel:. +39 3339122324
e-mail: dottgiuseppelauria@virgilio.it

0393-974X (2018)

DISCLOSURE: ALL AUTHORS REPORT NO CONFLICTS OF INTEREST RELEVANT TO THIS ARTICLE.

the inflammation processes acting on tumor necrosis factor-alpha (TNF-α) (5): β-sitosterols act as a well-tolerated 5-α reductase inhibitor (6) and Oligomeric proanthocyanidins (OPC) are oligomeric flavonoids with powerful antioxidant properties, especially useful in improving erectile and sexual performance dysfunctions (7, 8). These natural substances can slow down the hypertrophic process, hence reducing the associated LUTS without significant side effects. The aim of this study was to investigate the efficacy and the safety of a dietary supplement composed by curcumin, β-sitosterols and OPC in BPH/LUTS subjects.

MATERIALS AND METHODS

Study design

An observational, prospective, multicenter study was conducted in accordance with the Harmonized Tripartite Guidelines for Good Clinical Practice (ICH-GCP) and the set of ethical principles laid down in the Declaration of Helsinki. Study subjects were enrolled in three different Italian Clinical Centers, after signing and endorsing the informed consent form for the study participation.

All subjects underwent clinical and instrumental assessments as per standard clinical practice, such as an urological visit with digital rectal examination (DRE), ultrasound of the urinary tract with post-voiding residual (PVR), total PSA and PSA ratio evaluation, LUTS evaluations, in addition to filling in the International Prostate Symptom Score (IPSS) questionnaire. The presence of the following LUTS was assessed: difficulty in micturition, poor and/or intermittent stream, straining, frequent urination, urgency, urge incontinence, nocturia, feeling of incomplete emptying and post-micturition dribble. The IPSS questionnaire asks seven questions concerning urinary symptoms, each answer with a 0-5 score, resulting in a total score ranging from 0 (asymptomatic) to 35 (severe symptoms) (9). Based on their IPSS index, study subjects were classified into three groups according to their symptom severity: mild (IPSS 0-7 points), moderate (8-20 points), and severe (20-35 points); the effect of the test food supplement was then evaluated on each of those symptom severity groups.

After enrollment, all subjects were instructed to take one tablet of the study product daily, for 3 months.

The primary objectives of this study were the efficacy and the safety of a new dietary supplement in patients with BPH. The primary outcomes were the improvement of both the IPSS questionnaire score and the urinary flow rate. Secondary outcomes were the improvement of the above-mentioned symptoms (i.e., their presence/absence in the following visits) and the evaluation of efficacy and tolerability of the product.

In this observational study only within-subjects comparisons were planned, and a sample size of one hundred patients was considered large enough to obtain reliable information on the effect of the study product on LUTS.

Inclusion and exclusion criteria

The eligible population were men aged between 45 and 85 years, with clinical diagnosis of BPH related LUTS. An essential selection criterion was that subjects were included in the study at the first observation of disease, as such, they were drug-naïve for LUTS.

Patients with BPH complications (e.g., bladder calculus, bladder diverticulitis disease, prostatitis, bladder neck obstruction, PVR higher than 80 cc) were excluded from the study.

Study and treatment

One hundred men, aged 59±9 years, diagnosed for the first time with LUTS due to BPH, were enrolled in three Italian Clinical Centers in an outpatient setting. Study subjects were observed for three months, during which they were taking one tablet a day of a dietary supplement called LENITUS (formulated by UROBASP® technology to make the active ingredients bioavailable). Each tablet was composed of 135 mg of pine bark (*Pinus ssp.*), with a minimal beta-sitosterol content of 94.5 mg, 105 mg of turmeric, with a curcuminoid content of 99.75 mg and 21 mg of pine bark (*Pinus massoniana*), with an oligomeric proantocianidine content of 19.95 mg.

During the study each subject attended three clinical visits. During the first visit, the patients' baseline conditions were assessed as per standard clinical practice. Moreover, the IPSS questionnaire was administered and the study treatment was dispensed to the patients.

The second visit was performed after 30 days of treatment, to evaluate the efficacy and safety of the dietary supplement: the presence of the symptoms was

reassessed and, in case of need, the Investigators could decide to prescribe an alpha-lytic drug in addition to the study product.

The final visit was performed at the end of the treatment period to evaluate the product tolerance and effectiveness, by newly administering the IPSS questionnaire to the patients, measuring the urinary flow and assessing the presence of LUTS. These symptoms can be grouped into three types: obstructive (hesitancy, poor and/or intermittent stream, straining, prolonged micturition, feeling of incomplete bladder emptying), irritating (frequent urination urgency, urge incontinence, and nocturia) and post-micturition (feeling of incomplete emptying and post-micturition dribble).

Table I. *Improvement of main symptoms between Visit 1 (V1) and Visit 2 (V2).*

Symptom	V1			V2			Improved /worsened	p-value[a]
	Occurence	No.	%	Occurence	No.	%		
Frequent urination	N	25	25.00	N	32	32.99	9 / 1	**0.0114**
	Y	75	75.00	Y	65	67.01		
Nocturia	N	41	41.00	N	50	51.02	10/ 0	**0.0016**
	Y	59	59.00	Y	48	48.98		
Urgency	N	39	39.00	N	52	53.06	15 / 1	**0.0005**
	Y	61	61.00	Y	46	46.94		
Urge incontinence	N	96	96.00	N	85	92.39	0 / 3	0.0833
	Y	4	4.00	Y	7	7.61		
Hesitancy	N	48	48.00	N	57	58.76	13 / 1	**0.0013**
	Y	52	52.00	Y	40	41.24		
Dysuria	N	41	41.00	N	51	53.68	12 / 0	**0.0005**
	Y	59	59.00	Y	44	46.32		
Poor and/or intermittent stream	N	24	24.00	N	34	34.69	11 / 0	**0.0009**
	Y	76	76.00	Y	64	65.31		
Feeling of incomplete bladder emptying	N	47	47.47	N	60	64.52	16/ 1	**0.0003**
	Y	52	52.53	Y	33	35.48		
Post-micturition dribble	N	36	36.00	N	44	46.32	10 / 1	**0.0067**
	Y	64	64.00	Y	51	53.68		

[a] *McNemar's test. Bolded values are statistically significant at p<0.05.*

Table II. *Improvement of urinary flow and obstruction between Visit 2 (V2) and Visit 3 (V3).*

Urinary obstruction[a]	V2		V3		Improved/worsened	
	No.	%	No.	%		p-value[b]
Obstructed	7	7.22	4	4.49	*24 / 1*	**<0.0001**
Borderline	62	63.92	42	47.19		
Not obstructed	28	28.87	43	48.31		

[a] *Obstructed: "maximum urinary flow rate < 10 ml/sec."*
Borderline: "maximum urinary flow rate between 10 and 15 ml/sec."
Not obstructed: "maximum urinary flow rate > 15 ml/sec."
[b] *Bowker's test of symmetry. Bolded values are statistically significant at p<0.05.*

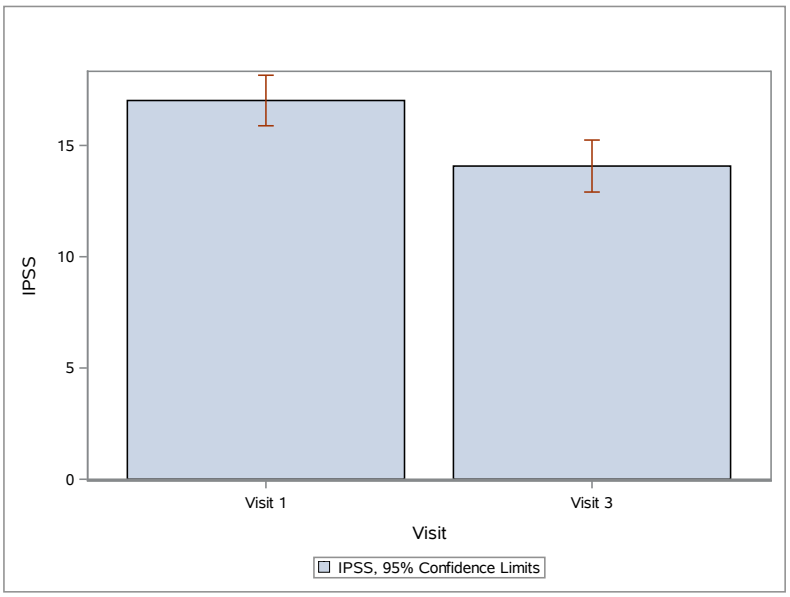

Fig. 1. *International Prostate Symptom Score (IPSS) values at Visit 1 and Visit 3.*

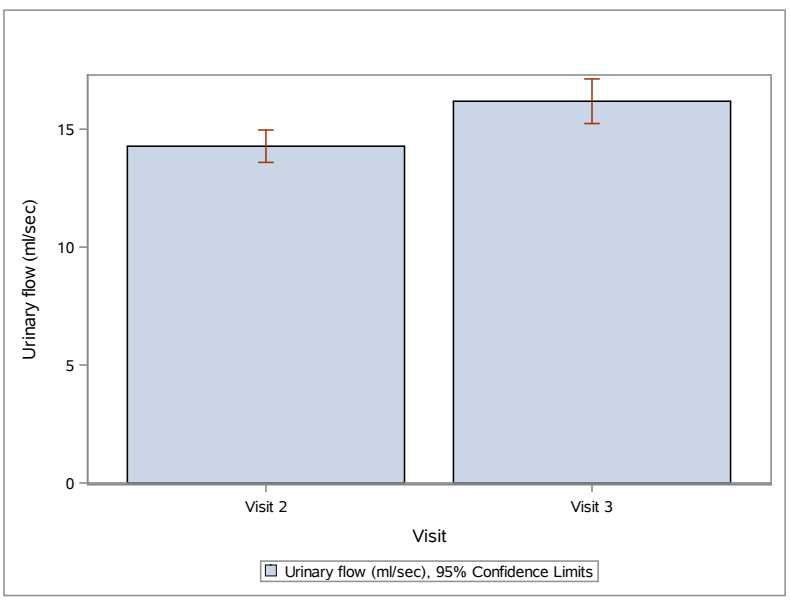

Fig. 2. *Urinary flow at Visit 2 and Visit 3.*

During the treatment period, the side effects were recorded to evaluate the safety of the study product.

Statistical analysis

Mean and standard deviations were calculated for continuous variables, and frequencies and percentages for discrete variables. Changes in continuous variables between visits were assessed using paired *t*-test. Changes in dichotomous variables between visits (2X2 tables) was assessed using McNemar's test. For square tables that have more than two response categories (levels, example 3X3), Bowker's test of symmetry was used. Statistical tests were considered statistically significant when p was lower that 0.05 ($p < 0.05$). Exact p-values are reported.

RESULTS

In this study, 100 men took one tablet a day of the test dietary supplement. Eight patients discontinued the study product before the study end: four subjects withdrew due to the adverse event reported below and four for personal reasons.

The following baseline features were evaluated in the study population: familiarity for prostate cancer (PCa) (30.61% had positive familiarity) and BPH (45.36% had positive familiarity); erectile dysfunction (55% was positive); premature ejaculation (11% was positive) and decreased libido (44% positive).

Several LUTS were evaluated and compared between Visit 1 (V1) and Visit 2 (V2). Significant improvement was observed in most of the symptoms investigated. For instance, frequent urination was present in 75% of the patients at V1 and in 67% of the patients at V2: in detail, 9 patients improved (i.e. frequent urination disappeared) while 1 patient worsened (i.e. previously absent frequent urination appeared during the study). Significant improvement was observed also for nocturia, urgency, hesitancy, dysuria, poor and/or intermittent stream, feeling of incomplete bladder emptying, and post-micturition dribble. Each of these symptoms disappeared in ten to sixteen patients. Urgency, hesitancy, feeling of incomplete bladder emptying, and post-micturition dribble appeared at V2 in one patient for each symptom, when they were not present at baseline, while urge incontinence appeared in three patients, who did not report it at baseline (Table I).

Mean IPSS decreased by 3.20 points between V1 and Visit 3 (V3) (from 17.02±5.72 to 14.07±5.70) and the difference was statistically significant ($p<0.0001$) (Fig. 1). Analyzing the improvement for each IPSS severity group separately, IPSS decreased by 0.8 points (from 6.29±0.49 to 5.40±1.82, not statistically significant), by 3.23 points (from 14.28±3.81 to 11.15±4.44, $p<0.0001$) and by 3.46 points (from 21.95±2.66 to 18.56±3.43, $p<0.0001$) in the mild, moderate and severe category, respectively.

Mean urinary flow increased by 2.06 ml/sec between V2 and V3 (from 14.28±3.41 to 16.18±4.49 ml/sec) and the increase was statistically significant ($p<0.0001$) (Fig. 2). Looking at each IPSS severity group, mean urinary flow increased by 1.83 ml/sec (from 18.23±2.13 to 19.90±5.10 ml/sec, not statistically significant), by 1.94 ml/sec (from 15.24±3.70 to 17.12±5.43 ml/sec, $p<0.0001$) and by 2.22 ml/sec (from 12.65±2.16 to 14.82±2.55 ml/sec, $p<0.0001$) in the mild, moderate and severe category, respectively. Even when categorizing the patients in obstructed, borderline and not obstructed, the improvement was statistically significant: 24 patients improved their urinary flow and only one worsened (Table II). In particular, obstruction was present in 7 patients at V2 and in 4 patients at V3. Borderline was present in 62 patients at V2 and in 42 patients at V3. 28 patients were not obstructed at V2 and 43 at the end of the treatment.

Subjective evaluation of the efficacy of the food supplement showed an increase in the confidence in the product between V2 and V3, with 45% of the subjects considering the study product effective or very effective.

Looking at the safety of the product, its tolerability was positively judged by the majority of the patients: only three patients did not tolerate well the product, while for the others the tolerability evaluated at V3 was at least good (excellent for 65% of the patients).

During the study, only eight subjects out of 100 experienced an adverse event: decreased libido (3), diarrhea/dysentery (2), gastrointestinal disturbances (2) and urticaria (1). Four events were considered as related to the study treatment: urticaria, two

events of decreased libido and one event of diarrhea/dysentery. The four subjects experiencing these events withdrew from the study. The relationship with the study product of the other events was considered unlikely.

Twenty-eight patients (28%) used 5-alpha reductase inhibitors after V2, as the improvement of the symptoms was judged by the Investigator not satisfactory.

DISCUSSION

In this observational, prospective, multicenter study, the administration of a dietary supplement containing curcumin, β-sitosterols and OPCs led to a decrease of mean IPSS and an increase of urinary flow in BPH/LUTS patients. In addition, almost all LUTS improved and only eight subjects reported an adverse event. Curcumin is known to have mainly anti-inflammatory and antioxidant properties (10). β-sitosterols act as 5-α reductase inhibitors, resulting in a decrease of circulating DHT, the increase of which is associated with BPH. According to the literature, β-sitosterols play a role in counteracting the hyperplasia of prostate cells (11) and improve urinary symptoms and urinary flow (12). The intake of OPCs can lead to an improvement of erectile dysfunction and sexual performance (7, 8). Thanks to the effects of the dietary supplement administered, BPH/LUTS patients enrolled in this study have experienced several improvements. First, the Q_{max} increased between one and three months of treatment. Several LUTS improved after only one month of treatment. In addition, the limited use of 5-alpha reductase inhibitors (28%) can be considered a proof of the efficacy of this dietary supplement. The urinary symptoms were evaluated also through IPSS, resulting in improvement after three months of intake of the dietary supplement. Overall, the clinical pattern of the patients enrolled in this study improved considerably, showing that curcumin, β-sitosterols and OPC are good candidates for BPH/LUTS treatment. The study had a number of limitations that could have led to uncontrolled bias: the small population, the lack of a control group and the concomitant use of alpha-lythic drugs. Despite these limitations, the study product had a positive effect on all the symptoms investigated, reduced the IPSS score and increased the urinary flow, and it was considered efficient and tolerable by both patients and investigators.

REFERENCES

1. Girman CJ, Jacobsen SJ, Guess HA, Oesterling JE, Chute CG, Panser LA, Lieber MM. Natural history of prostatism: relationship among symptoms, prostate volume and peak urinary flow rate. J Urol 1995; 153:1510-15.
2. Madersbacher S, Alivizatos G, Nordling J, Sanz CR, Emberton M, de la Rosette JJ. EAU 2004 guidelines on assessment, therapy and follow-up of men with lower urinary tract symptoms suggestive of benign prostatic obstruction (BPH guidelines). Eur Urol 2004; 46:547-54.
3. Parsons JK. Benign Prostatic Hyperplasia and Male Lower Urinary Tract Symptoms: Epidemiology and Risk Factors. Curr Bladder Dysfunct Rep 2010; 5:212-18.
4. Oelke M, Bachmann A, Descazeaud A, et al. European Association of Urology. EAU guidelines on the treatment and follow-up of non-neurogenic male lower urinary tract symptoms including benign prostatic obstruction. Eur Urol 2013; 64:118-40.
5. Zhang L, Wu C, Zhao S, et al. Demethoxycurcumin, a natural derivative of curcumin attenuates LPS-induced pro-inflammatory responses through down-regulation of intracellular ROS-related MAPK/NF-kappaB signaling pathways in N9 microglia induced by lipopolysaccharide. Int Immunopharmacol 2010; 10:331-38.
6. Cabeza M, Bratoeff E, Heuze I, Ramírez E, Sánchez M, Flores E. Effect of beta-sitosterol as inhibitor of 5 alphareductase in hamster prostate. Proc West Pharmacol Soc 2003; 46:153-55.
7. Schmitt CA, Dirsch VM. Modulation of endothelial nitric oxide by plant-derived products. Nitric Oxide 2009; 21:77-91.
8. Kobori Y, Suzuki K, Iwahata T, et al. Improvement of seminal quality and sexual function of men with oligoasthenoteratozoospermia syndrome following supplementation with L-arginine and Pycnogenol®. Arch Ital Urol Androl 2015; 87:190-93.

9. Barry MJ, Fowler FJ Jr, O'Leary MP, Bruskewitz RC, Holtgrewe HL, Mebust WK, Cockett AT. Measurement Committee of the American Urological Association. The American Urological Association Symptom Index for Benign Prostatic Hyperplasia. J Urol 2017; 197:S189-97.
10. Cho JW, Lee KS, Kim CW. Curcumin attenuates the expression of IL-1ß, IL-6, and TNF- α as well as cyclin E in TNF-α-treated HaCaT cells; NF-κB and MAPKs as potential upstream targets. Int J Mol Med 2007; 19:469-74.
11. Hirano T, Homma M, Oka K. Effects of stinging nettle root extracts and their steroidal components on the Na+,K(+)-ATPase of the benign prostatic hyperplasia. Planta Med 1994; 60:30-33.
12. Berges RR, Windeler J, Trampisch HJ, Senge T. Randomised, placebo-controlled, double-blind clinical trial of beta-sitosterol in patients with benign prostatic hyperplasia. Beta-sitosterol Study Group. Lancet 1995; 345:1529-32.

LETTER TO THE EDITOR

PEDICLED PALATAL FLAP FOR SURGICAL REPAIR OF ORO-NASAL FISTULA

R. RAUSO[1], G. TARTARO[1], L. CALIFANO[2], L. RUGGE[1], F. CHIRICO[1] and G. COLELLA[1]

[1]Maxillo-Facial Surgery Department, University of Campania "Luigi Vanvitelli", Naples, Italy; [2]Maxillo-Facial Surgery Department, University Federico II, Naples, Italy

Received July 26, 2018 – Accepted August 27, 2018

Oronasal fistula can occur secondary to various pathologies, but cleft surgery is the most common. The authors propose a pedicled palatal flap technique for surgical repair of small oronasal fistula (0.5-0.8 cm), derived from their experience in the treatment of 7 patients between March 2003 and December 2007. In one case, the fistula was induced by prolonged snorting of cocaine. In the other cases, the fistulas developed after excision of a benign tumor of the palate. For the cocaine-induced fistula, failure of the repair attempt was apparent within 7 days of surgery. In all other cases, complete fistula closure was obtained, and no complications occurred.

To the Editor,

Oronasal fistula is often observed after palatal surgery. The defect also may arise after surgical removal of a benign or malignant tumor, from continuous snorting of cocaine, and for other reasons (1, 2). Although these lesions are not necessarily symptomatic, conditions such as fluid reflux, rhinorrhea, and speech disorders are common presenting signs, which also can affect the size and severity of the fistula. In general, larger fistulas are accompanied by more severe symptoms. Various surgical options, based on fistula size, have been proposed to treat palatal fistulas, including local flaps, regional intraoral and extraoral flaps, free flaps, and prosthetic obturators (3-9).

One of the most common surgical techniques is the single palatal flap, which is usually the preferred flap for small (<1.0 cm) recurrent fistulas (1). For larger fistulas (over 1 cm), the island flap technique is usually effective (8). This flap is positioned above the palatal vascular bundle, and after its release, substantial flap mobility can be attained, reducing the traction and tension of the flap (8). For very large fistulas or subsequent attempts to address palatal flap failure, other techniques may be considered, such as free flaps, but this type of surgery is much more complex (5, 7).

We propose an alternative technique to repair small oronasal fistula – the pedicled palatal flap – which is easy to perform and has a low rate of failure.

MATERIALS AND METHODS

From March 2003 to December 2007, 7 patients with oronasal fistula (5 women, 2 men; aged 28-67 years) underwent surgery in the Department of Head and Neck Surgery of the Second University of Naples (actual University of Campania "Luigi Vanvitelli"). All patients signed a consent form before the surgery was performed. In one patient, the fistula was induced by prolonged snorting of cocaine. In the other 6 patients, the fistula arose after excision of a benign tumor of the palate

Key words: palatal fistula, palatal flap, oronasal communication

Mailing address:
Prof Raffaele Rauso, MD PhD MSc,
Maxillo-Facial Unit,
University of Campania "Luigi Vanvitelli",
Piazza Miraglia, 80138 Naples, Italy
e-mail: raffaele.rauso@unicampania.it

0393-974X (2018)

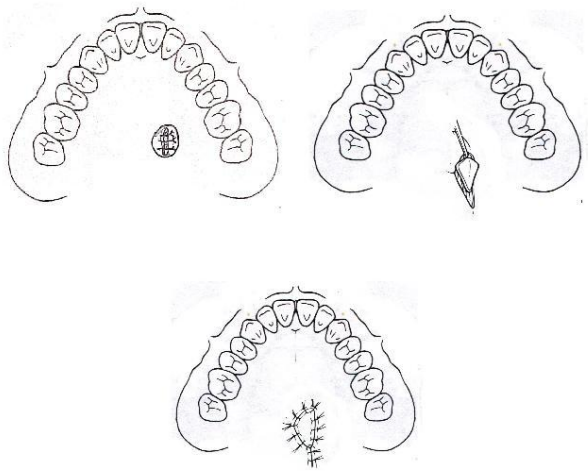

Fig. 1. *Graphic representation of the proposed surgical technique.*

(pleomorphic adenoma).

The size of oronasal communications in these patients was small, ranging from 0.5 to 0.8 cm. In the patient whose fistula was induced by cocaine use, the communication was purulent. This patient was instructed to start antibiotic therapy 3 days prior to surgery; all other patients began antibiotic therapy on the day of surgery.

In all cases, fistula closure was performed while the patient was under general anesthesia. In addition, xylocaine (0.5%) with epinephrine (1:100,000) was injected in the area around the fistula. Twelve minutes later, the surgical procedure began. A partial-thickness incision of the palatal mucosa was made around the fistula. After elevating the submucosa, the prepared flaps were reversed and sutured to provide a mucosal lining for the nasal cavity. Following this, a small pedicled flap of mucosa and submucosa was harvested immediately below the fistula, and was mobilized to cover the defect completely (Fig. 1). The flap was fixed with resorbable sutures. Patients were discharged after 3 days (on average).

RESULTS

All patients were prescribed antibiotic therapy (amoxicillin and clavulanic acid, 1 g every 12 hours for 5 days) and were instructed to apply a gel consisting of amino acids and sodium hyaluronate (3 times daily for 15 days).

Seven days postoperatively, early failure of the repair was evident for the fistula that had been induced by cocaine snorting. The patient refused further surgical repair, and a palatal obturator was used instead. In the other 6 cases, there were no complications, and complete fistula closure was obtained (Fig. 2). The follow-up period ranged from 6 months to 24 months (median, 10.8 months).

DISCUSSION

Various surgical techniques have been employed to repair palatal fistula, including creation of local mucoperiosteal flaps or utilization of additional tissue such as tongue flaps, buccal mucosa flaps, and free flaps (3-9). For surgical repair of a small

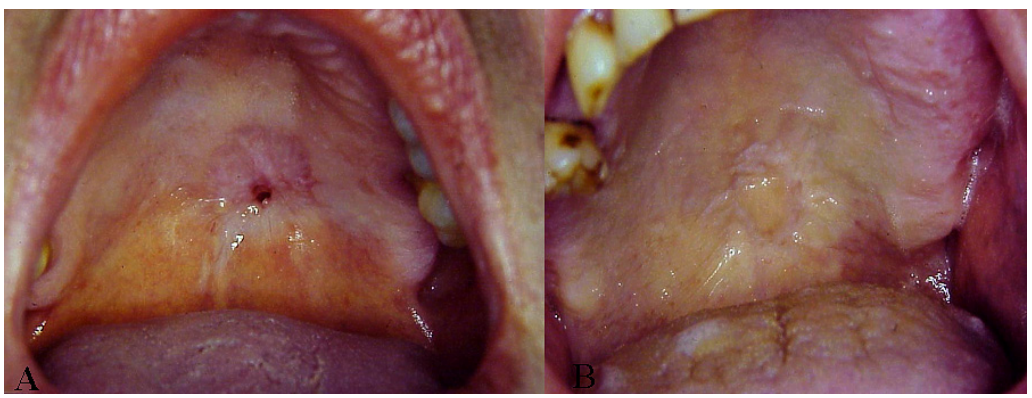

Fig. 2. *Left: preoperative view of a case of palatal fistula. Right: postoperative control, 50 days after surgery.*

fistula (<1 cm), local flaps are commonly used (6). In particular, 3 factors affect the success of repair: the extent of the defect (e.g., size, diameter), the amount of time that has elapsed since the defect first appeared, and the condition of the palatal and nasal mucosa (1).

For a new defect (<1 week old) with limited diameter (<0.5 cm), it has been recommended to wait for potential spontaneous closure; however, for chronic and/or larger defects, surgical repair is required (1). When surgery is recommended, Axhausen's principles must still be considered, even though they originated early in the 20th century (10). These principles are: i. the flap must be mobilized without traction or tension; ii. the flap must be adapted so as to cover the defect with a surplus of 0.5 to 0.75 cm; and iii. there should be no residual dehiscence at the wound site.

Although many techniques have been used for surgical closure of oronasal fistulas (3-9), none has proven superior to the others; however, certain advantages and disadvantages do exist.

In the present case series, a mucoperiosteal flap was elevated distally at the entrance to the neurovascular bundle, and was positioned so that it covered the entire area of communication. After elevating the submucosa, the prepared flap was reversed and sutured to provide a mucosal lining for the nasal cavity. Failure occurred in only one case, which likely was attributable to the cause of the fistula (cocaine snorting). Surgical treatment for oronasal fistula repair induced by snorting cocaine is still controversial; a palatal obturator may be a viable option, especially in patients who are chronic cocaine users (11).

The surgical technique proposed by the authors is recommended for select cases in which the oronasal fistula is smaller than 0.8 cm. Even though the number of patients in this case series is small, results demonstrate that the surgical technique is easy to perform, safe, and provides optimal blood perfusion for the flap.

REFERENCES

1. Sahoo NK, Desai AP, Roy ID, Kulkarni V. Oro-nasal communication. J Craniofac Surg 2016; 27(6):e529-33.
2. Hardwicke JT, Landini G, Richard BM. Fistula incidence after primary cleft palate repair: a systematic review of the literature. Plast Reconstr Surg 2014; 134(4):618e-27e.
3. Denny AD, Amm CA. Surgical technique for the correction of post palatoplasty fistulae of the hard palate. Plast Reconstr Surg 2005; 115(2):383-87.
4. Sodhi SP, Kapoor P, Kapoor D. Closure of anterior palatal fistula by tongue flap: a prospective study. J Maxillofac Oral Surg 2014; 13(4):546-49.
5. Gupta V, Cohan DM, Arshad H, Kuriakose MA, Hicks WL Jr. Palatal reconstruction. Curr Opin Otolaryngol Head Neck Surg 2012; 20(4):225-30.
6. Freda N, Rauso R, Curinga G, Clemente M, Gherardini G. Easy closure of anterior palatal fistula with local flaps. J Craniofac Surg 2010; 21(1):229-32.
7. Ariffuddin I, Arman Zaharil MS, Wan Azman WS, Ahmad Sukari H. The use of facial artery musculomucosal (FAMM) readvancement flap in closure of recurrent oronasal fistula. Med J Malaysia 2018; 73(2):112-13.
8. Abdel-Aziz M, Kamel A, Fawaz M, Rezk I, Kamel M. Closure of fistula of the hard palate with two layers of mucoperiosteum. Int J Pediatr Otorhinolaryngol 2018; 104:43-46.
9. Honnebier MB1, Johnson DS, Parsa AA, Dorian A, Parsa FD. Closure of palatal fistula with a local mucoperiosteal flap lined with buccal mucosal graft. Cleft Palate Craniofac J 2000; 37(2):127-29.
10. Axhausen G. Uber den plastischen Verschlub von Mund-Antrum-Verbindungen. Dtsch Mschr Zahnheilk 1930; 3:193-98.
11. Tartaro G, Rauso R, Bux A, Santagata M, Colella G. An unusual oronasal fistula induced by prolonged cocaine snort: case report and literature review. Minerva Stomatol 2008; 57:203-10.

JOURNAL OF BIOLOGICAL REGULATORS & HOMEOSTATIC AGENTS Vol. 32, no. 6, 1569-1572 (2018)

LETTER TO THE EDITOR

PERCUTANEOUS HEADLESS SCREWS AND WIDE-AWAKE ANESTHESIA TO FIX METACARPAL AND PHALANGEAL FRACTURES: OUTCOMES OF THE FIRST 56 CASES

A.M. NUCCI[1], A. DEL CHIARO[1], F. ADDEVICO[1], A. RASPANTI[2] and A. POGGETTI[3]

[1]AOU Pisana, Orthopaedic and Trauma Unit, University of Pisa, Italy; [2]Orthopaedic and Trauma Unit ASL 3, Pistoia, Italy; [3]AOU Careggi, Hand and Microsurgery Reconstruction Unit, Florence, Italy

Received February 5, 2018 – Accepted September 20, 2018

Phalangeal (P) and metacarpal (MC) fractures are very common injuries, with potentially disabling, residual impairment, deformities or stiffness. Conservative treatment represents the strategy of choice in most cases, but in unstable fractures and/or high-demanding patients, surgical fixation could be required. Ideally, the best treatment choice will be the intramedullary fixation systems, if possible without the implant protruding from the skin. Intramedullary headless screw fixation could be the reliable option to achieve a primary fixation, allowing an early active movement, with regard to the fractures site. The Authors analyzed the results achieved after 56 extra-articular unstable fractures (31 phalangeal fracture and 25 metacarpal fracture) treated with intramedullary headless compression screws. After surgery, patients underwent early mobilization without splinting. The results of the study suggest that this technique could be a reliable therapeutic option in order to obtain early mobilization and quick return to work after a phalangeal or metacarpal fracture, especially for high-demanding patients.

To the Editor,

Phalangeal and metacarpal fractures are the second most common fractures of the hand, after wrist fractures (1, 2). Even if small bone segments are involved, these types of fracture are potentially disabling, because of possible residual deformities and stiffness. Conservative treatment (splints and casts) represents the strategy of choice in most cases, but in cases of unstable fractures and/or high-demanding patients a surgical approach may be required. Different fixation techniques are available (percutaneous K-wires, screws and plates), but the best management has still to be defined.

Recent studies have presented intramedullary headless screw fixation as a new reliable option in the treatment of oblique and transverse of phalanges and metacarpals fractures.

MATERIALS AND METHODS

From March 2014 to December 2015, 56 consecutives extra-articular, oblique or transverse, metacarpal and phalangeal, unstable fractures in 50 consecutive adult patients were treated (informed consent was routinely achieved). The patients included 44 men and 6 women with a mean age of 37.4 years (range 18–84). Eighteen fractures were initially treated conservatively, but secondary displacement occurred after first X-ray control (1 week later). The other 38 fractures were judged primary unstable. Thirty-three fractures were to the dominant hand

Key-words: hand fractures, wide-awake surgery, intramedullary screw fixation

Mailing address:
Andrea Poggetti, MD,
AOU Careggi, Hand and Microsurgery Reconstruction Unit,
Largo Palagi 2, 50039, Florence, Italy
Tel.: +39 3272031697
e-mail: poggetti.andrea@gmail.com

0393-974X (2018)

DISCLOSURE: ALL AUTHORS REPORT NO CONFLICTS OF INTEREST RELEVANT TO THIS ARTICLE.

and 23 to the non-dominant hand. There were 5 open fractures and 2 pathological fractures (enchondromas). A total of 46 patients had an isolated fracture in a single ray. Five patients had concomitant fractures in multiple digits. There were 25 metacarpal fractures, 24 fractures of the proximal phalanx (P1) and 7 fractures of the middle phalanx (P2). The mean time from injury to surgical intervention was 4 days (range 1–13). A total of 36 patients had wide-awake anaesthesia without tourniquet, while 14 patients underwent regional or general anaesthesia under tourniquet. Wide-awake anaesthesia was carried out through a modification of the original technique proposed by Lalonde (3). An infiltration was performed with 0.5% bupivacaine and 1:100,000 epinephrine (20 ml for metacarpal and 10 ml for phalangeal segment) injected 30 min before surgery. A single injection was used around the dorsal aspect of the fractured bone segment.

During pre-operative surgical planning, the diameter of the intramedullary canal was measured on the true lateral X-ray. For the phalangeal fractures, the average diameter was 2.43 mm (2.6-2.17 mm) and a 2.2 or 2.4 mm headless screw (SpeedTip CCS Medartis® in 26 cases/ HCS DePuy Synthes® in 5 cases) was chosen. For metacarpal fractures, in all cases the diameter resulted larger than 3 mm, and a 3 mm headless screw was always adopted (SpeedTip CCS Medartis® in 8 cases and HCS DePuy Synth® in 17 cases). The fractures were reduced under fluoroscopy and temporarily fixed with Kirschner wire, used as a guide to the screw implantation. In all cases, a percutaneous technique was used, with a 3-mm skin incision without drilling.

The osteosynthesis technique changed on the basis of the side and the type of the fracture. In the metacarpal fractures an intra-articular retrograde fixation technique was adopted (in one patient a anterograde screw insertion was used). The dorso-radial or dorso-ulnar metacarpal head access was chosen according to the fracture position. In order to avoid extensor tendon iatrogenic lesion, the metacarpophalangeal joint (MPJ) was maintained with 90° degrees of flexion throughout the operation (Fig. 1).

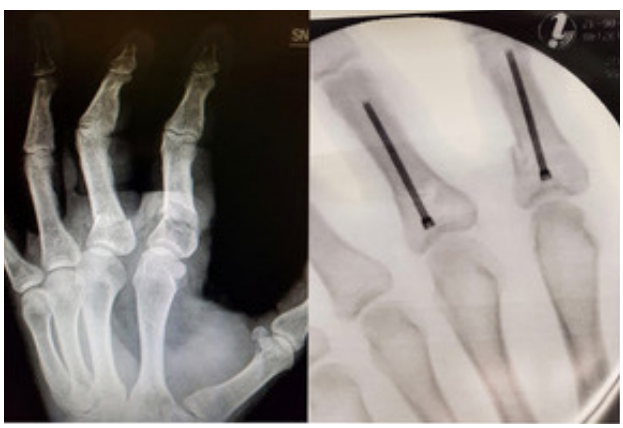

Fig. 1. *Unstable extrarticular P1 fractures. The intramedullary screws achieve the anatomical bone fixation.*

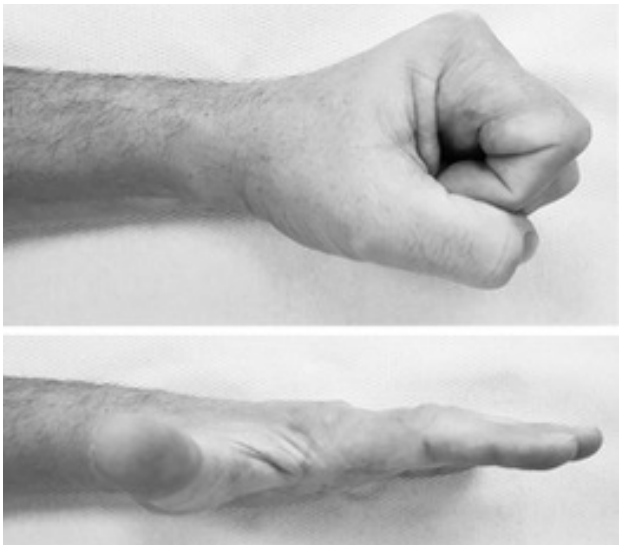

Fig. 2. *After long-term follow-up with full functional recovery.*

For the phalangeal fractures, a retrograde insertion was used in 3 cases of middle phalanx fractures. All the other phalangeal fractures were synthetized with the anterograde technique. The intra-articular technique was adopted for 17 fractures of the P1 and 5 of the P2. In these cases, the guide wire was inserted through the dorsal central portion of the phalangeal base; a gentle dorsal translation of P1 was performed in order to increase the space available for screw insertion. In the other 7 fractures of P1 and 2 of the P2 the Kapandji trans-articular technique was performed. This technique resulted more practical in cases where the fracture line involved the proximal portion of the P1 with fragment was difficult to control with an intra-articular technique. The trans-articular technique consisted of inserting the wire from the dorsal aspect of the head of the more proximal bone passing, it through the articular space, and then in the base of the fractured bone. Afterwards, the correct position of the screw was checked under fluoroscopy. After the surgical procedure, the involved ray was dressed with buddy strapping to the adjacent fingers. Patients were encouraged to actively

move the finger immediately after surgery. The follow-up was scheduled 7, 15 30, 60 and 90 days after surgery. Except for the first two follow-ups, X-ray control was carried out. The patients were followed-up for an average of 16 weeks (range 8-36). At each control, the Total Active Motion (TAM) of the digit was calculated, and at the final follow-up the grip strength was measured in both hands by means of a Jamar dynamometer (Patterson Medical Holding, Warrenville, IL, USA) (Fig. 2).

RESULTS

All fractures were clinically and radiographically healed on average within 31 days (range 28-43) after surgery, except for one case of long oblique fracture of the proximal phalanx, which presented with a loss of reduction after 9 days, so a new synthesis with two lag screws was performed.

After 4 months, the mean TAM values were 222° and 250°, respectively, for phalangeal and metacarpal fractures, while the Jamar grip strength was 25 Kg and 42 Kg, respectively, for phalangeal and metacarpal fractures. Except for one case of pathological fracture that showed a limited extension requested a tenolysis to improve function, all the other patients healed without major complications. No mal-unions, non-unions, rotational deformities or infections were observed. In the first case treated, a protrusion of the proximal portion of the screw from the P1 base was noted. The complication was observed at the end of surgical procedure with fluoroscopy and the screw was removed.

DISCUSSION

Metacarpal and phalangeal fractures are the second most frequent fractures of the upper extremity after distal radius fractures. This type of lesion is particularly frequent among the active population (18-35-year-old age group) (1).

Facing a metacarpal or phalangeal fracture, the orthopaedic surgeon has to choose the most appropriate treatment from a wide array of different techniques on the basis of the characteristics of the patient and of the fracture. Regardless of the method employed, the principles of the treatment must be always the same: restoration of articular anatomy, avoiding angular or rotational deformities, stabilization of the fracture, minimal surgical insult and rapid mobilization (4).

Many fractures can be successfully managed with a conservative treatment like a splint or a cast followed by rehabilitation, but in cases of fracture instability, multiple fractures, open fractures or high-demanding patients, a surgical treatment should be preferred. Nowadays the main surgical options include: Kirschner wires, screws and plate, lag screw, tension band wiring and external fixation. Each of these methods of treatment has its own advantages and disadvantages, therefore there is uncertainty regarding what is the best way to treat these fractures (4, 5). Percutaneous fixation with Kirschner wires is a simple and less invasive technique, but it must be followed by a prolonged immobilization that can lead to articular stiffness. Furthermore, there is a risk of pin track infection, pin loosening, mal-union and non-union. Plates and screws can provide a stable fixation and allow an early mobilization, but they require an extensive dissection and they can cause the formation of tendon adhesions (6, 7).

Recently, new surgical techniques have been proposed. In particular, Del Piñal et al. described the use of intramedullary cannulated headless compression screws as a minimal invasive technique that permits to obtain an immediate stability in cases of phalangeal and metacarpal fractures. In this study, the screws were always introduced in a retrograde manner (8). In cases of phalangeal fractures, we prefer to use an anterograde introduction that has been demonstrated to damage a smaller relative articular surface. Furthermore, there is a real risk of lesion of the central slip of the extensor tendon at the level of the proximal interphalangeal articulation with the retrograde technique.

The anterograde synthesis can be realized using an intra-articular technique or a trans-articular technique. The first one consists of introducing the guide wire dorsally through the metacarpophalangeal joint into the base of the proximal phalanx, while in the second case the guide wire is inserted into the metacarpal head and then into the phalangeal base. In a cadaver

study, Borbas et al. demonstrated that the intra-articular introduction should be preferred as with this technique less cartilage damage was observed, the correct entry point was easier to find and little damage to extensor tendons was seen (9, 10).

In our study, intramedullary headless compression screws proved to be an advantageous alternative in the treatment of extra-articular unstable fractures of metacarpals and phalanges, especially if associated with wide-awake anaesthesia. This type of anaesthesia, based on local infiltration of bupivacaine and epinephrine, has many advantages: cost efficiency, no preoperative testing, no tourniquet pain, less time in hospital to undergo surgery, the ability to speak to their surgeon during the surgery, prolonged pain control, and no sedation at home after surgery (11).

REFERENCES

1. Karl JW, Olson PR, Rosenwasser MP. The epidemiology of upper extremity fractures in the United States. J Orthop Trauma 2015; 29:242-44. doi:10.1097/BOT.0000000000000312.
2. Cepni SK, Aykut S, Bekmezci T, Kilic A. A minimally invasive fixation technique for selected patients with fifth metacarpal neck fracture. Injury 2016; 47:1270-75. doi:10.1016/j.injury.2016.01.034.
3. Lalonde DH. "Hole-in-One" local anesthesia for wide-awake carpal tunnel surgery. Plast Reconstr Surg 2010; 126:1642–4. doi:10.1097/PRS.0b013e3181f1c0ef.
4. Meals C, Meals R. Hand fractures: a review of current treatment strategies. J Hand Surg Am 2013; 38:1021–31, quiz1031. doi:10.1016/j.jhsa.2013.02.017.
5. Cheah AE-J, Yao J. Hand fractures: indications, the tried and true and new innovations. J Hand Surg Am 2016; 41:712-22. doi:10.1016/j.jhsa.2016.03.007.
6. Kawamura K, Chung KC. Fixation choices for closed simple unstable oblique phalangeal and metacarpal fractures. Hand Clinics 2006; 22:287-95. doi:10.1016/j.hcl.2006.02.018.
7. Başar H, Başar B, Başçı O, Topkar OM, Erol B, Tetik C. Comparison of treatment of oblique and spiral metacarpal and phalangeal fractures with mini plate plus screw or screw only. Arch Orthop Trauma Surg 2015; 135:499-504. doi:10.1007/s00402-015-2164-3.
8. del Piñal F, Moraleda E, Rúas JS, de Piero GH, Cerezal L. Minimally invasive fixation of fractures of the phalanges and metacarpals with intramedullary cannulated headless compression screws. J Hand Surg Am 2015; 40:692-700. doi:10.1016/j.jhsa.2014.11.023.
9. Borbas P, Manuel M, Poggetti A, Calcagni M, Giesen T. Treatment of proximal phalangeal fractures with an antegrade intramedullary screw: a cadaver study. J Hand Surg Eur Vol 2016. doi:10.1177/1753193416641319.
10. Giesen T, Gazzola R, Poggetti A, Giovanoli P, Calcagni M. Intramedullary headless screw fixation for fractures of the proximal and middle phalanges in the digits of the hand: a review of 31 consecutive fractures. J Hand Surg Eur 2016. doi:10.1177/1753193416641330.
11. Lalonde DH, Wong A. Dosage of local anesthesia in wide awake hand surgery. J Hand Surg Am 2013;38:2025-28. doi:10.1016/j.jhsa.2013.07.017.

LETTER TO THE EDITOR

ASSESSMENT OF NUTRITIONAL STATUS AND THERAPY IN EMERGENCY MEDICINE SETTINGS

G.M. GIORGETTI[1], P. DE TOMA[2], E. DI PIETRO[2], Y.M. KHAZRAI[2], F. FABIOCCHI[1], M.C. TROTTA[1], E. MIRANTE[2], P. BARLETTA[3], E. CASTALDO[3], W. ELISEI[4], M. PICCHIO[5] and A. TURSI[6]

[1]Clinical Nutrition Unit, "Sant'Eugenio" Hospital, ASL Roma 2, Roma, Italy; [2]Master's Degree Course in Food Science and Human Nutrition (SANUM), "Campus Biomedico" University, Roma, Italy; [3]Emergency Medicine Unit, "Sant'Eugenio" Hospital, ASL Roma 2, Roma, Italy; [4]Division of Gastroenterology, ASL RM6, Albano Laziale, Roma, Italy; [5]Division of Surgery, "P. Colombo" Hospital, ASL RM6, Velletri, Roma, Italy; [6]Territorial Gastroenterology Service, ASL BAT, Andria (BT), Italy

Received June 4, 2018 - Accepted October 10, 2018

Hospital malnutrition is becoming a clinical concern. Our aim was to determine the prevalence of hospital malnutrition through Nutritional Risk Screening 2002 (NRS) and to evaluate nutritional risk through a prospective study. Nutritional status was assessed collecting anthropometric parameters together with the data relating to the diseases in the medical records of patients admitted to the Department of Emergency Medicine of the "Sant'Eugenio" Hospital. One hundred and sixty patients were retrospectively enrolled during a 3-month observational period. The risk of malnutrition was detected in 52% of patients (of whom 38% at risk and 62% at serious risk). The NRS score was positively correlated with patient age, days between hospital admission and nutritional assessment, disease severity, length of hospital stay and catabolism ($p<0.05$); Basal Energy Expenditure (BEE) and mean arm circumference (MUAC) were negatively correlated with positive outcome ($p<0.05$). No correlations were found in the NRS score, gender, height, weight, Body Mass Index (BMI) and Total Energetic Expenditure (TEE) (p=n.s). A high prevalence of the risk of malnutrition may be detected in the emergency medicine setting, particularly in the geriatric population. The NRS score is not strictly related to BMI, but rather is an excellent tool for disease prognosis, as well as nutritional screening.

To the Editor,

It is well known that malnutrition is an underestimated problem throughout the health system. From a clinical standpoint, hospital malnutrition can contribute to amplifying disease complications, such as morbidity and mortality (1). Malnutrition arises as the result of an imbalance between the intake and the expenditure of energy and nutrients.

Approximastely 20-50% of all hospitalized patients are at risk of malnutrition, depending on the definition, clinical setting, and screening tool used to make the diagnosis (2). Most of these patients are at nutritional risk already at the time of admission and, malnutrition even develops during hospital stay (3) in up to 48.7% of patients (4). Moreover, elderly patients and those with chronic diseases are more prone to nutritional risk than others (5, 6). Aging, illness, and inadequate nutrition contribute to sarcopenia, frailty, loss of functions, and progression

Key words: emergency department, malnutrition, nutritional assessment, Nutritional Risk Screening 2002.

Mailing address:
Antonio Tursi MD,
Servizio di Gastroenterologia Territoriale,
Via Torino, 49, 76123 Andria, Italy
Tel.: +39 0883 551094
Fax: +39 0883 1978210
e-mail: antotursi@tiscali.it

0393-974X (2018)

DISCLOSURE: ALL AUTHORS REPORT NO CONFLICTS OF INTEREST RELEVANT TO THIS ARTICLE.

of the disease in the elderly population. Aging is often associated with a decrease in food intake, an increased risk of malnutrition, and weight and muscle mass loss (7). Chronic or acute disease, low protein intake, chewing problems, poor appetite and physical inactivity cause sarcopenia: the energy requirement (Total Energetic Expenditure, TEE) is reduced because sarcopenia leads to a decrease in the resting metabolic rate (RMR) (8).

Despite current recommendations, the rate of malnutrition does not seem to decrease significantly. The European Society for Clinical Nutrition and Metabolism (ESPEN) guidelines for nutritional screening in patients admitted to hospital (9, 10) recommend a multistep approach to in-hospital malnutrition in order to identify and treat malnutrition adequately. The aim of the present study was to determine the nutritional status and related therapy in the Emergency Medicine settings by using Nutritional Risk Screening (NRS-2002) score.

Table I. *The Nutritional Risk Screening (NRS) 2002 System Scoring.*

	Altered nutritional status		**Severity of the disease (increase in needs)**
Absent Score: 0	Normal nutritional status	**Absent Score: 0**	Normal nutritional needs
Mild Score: 1	Weight loss> 5% in 3 months or food intake between 50-75% of the normal needs in the previous weeks	**Mild Score: 1**	Trauma with fractures or Chronic patient, in particular with acute complications: cirrhosis, COPD. Chronic hemodialysis, diabetes, oncology
Moderate Score: 2	Weight loss> 5% in 2 months or BMI 18.5-20 + altered general conditions or food intake between 25-50% of normal needs in the previous weeks	**Moderate Score: 2**	Major abdominal surgery, Stroke, Severe pneumonia, onco-hematology
Severe Score: 3	Weight loss> 5% in 1 month (> 15% in 3 months) or BMI <18.5 + altered general conditions or food receipts between 0-25% of the normal needs in the previous weeks	**Severe Score: 3**	Head trauma Marrow transplantation Intensive care patients (APACHE> 10)
Score:	**…… +**	**Score:……..**	**= Total Score**
Age: If ≥ 70 years old add 1 to the above score			**= Age Adjusted Score**

Score ≥ 3: the patient is at nutritional risk and a nutritional program must be developed.

Score < 3: weekly re-assessment of the patient. If the patient is to undergo major surgery, a nutritional program should be drawn up to prevent a nutritional risk.

Table II. *Patient stratification based on risk: No Risk vs Risk patients.*

SCORE < 3 48%(n = 76)	Age (Mean): 67±17 years
	BMI (Mean): 26±5.5 kg/m²
	Average hospitalization: 5±4 days
	TEE (Mean): 1780±480 kcal
SCORE ≥ 3 52% (n = 84)	Age (Mean): 76±15 years
	BMI (Mean): 24±6 kg/m²
	Average hospitalization: 7±7 days
	TEE (Mean): 1611±408 kcal

MATERIALS AND METHODS

This 3-month retrospective observational study was conducted in the Department of Emergency Medicine of the "Sant'Eugenio" Hospital of Rome, Italy (Azienda Sanitaria Locale Roma 2), which serves a population of >500.000 inhabitants located in the South of Rome, and having >200,000 admissions to the emergency department every year.

All the enrolled patients underwent nutritional assessment and screening for nutritional risk through the Nutritional Risk Screening 2002 (NRS 2002) (11) (Table I). The evaluation of the nutritional status included recording the anthropometric parameters and the diseases documented in the patients' medical records. For patients who were bedridden and unable to move, the patient's height was estimated from the length of the ulna while the average arm circumference (Mild Upper Arm Circumference, MUAC) was used to estimate the BMI interval (and thus, indirectly, the weight of the patient).

RESULTS

From April to June 2016, 160 patients (58% women, 42% men, with an average age of 72±17 years) were included in this study. As far as age distribution of the sampled population is concerned, 7% were aged between 20-40 years, 15% between 41-60 years, 39% between 61-80 years and 39% ≥80 years, with a clearly high presence of a geriatric population in the hospital (78% over ≥61 years of age). Cardiovascular diseases (20%), respiratory diseases (17%), gastroenterological diseases (13%), traumas and fractures (11%) were the main causes of hospital admission. The average hospital stay of this population was 6±6 days (range 0-42 days): at the end of the hospitalization, 52% of the patients were transferred, 40% discharged, 7% died, 1% was discharged against medical advice. Seven patients who left the study following discharge, were later readmitted for hospitalization.

The nutritional status was recorded and showed that 42% of patients were normal weight (BMI 18.5-24.9), 34% were overweight (BMI 25-28.9) and

Table III. *NRS correlations.*

	P value	Pearson's Coefficient
Age	0.000	0.336
Days before evaluation	0.025	0.177
Outcome	0.001	-0.267
Hospital stay	0.001	0.266
Comorbity	0.034	0.167
BEE	0.000	-0.33
Catabolism	0.001	0.23
Arm circumference	0.000	-0.32
Gender	0.211	-0.099
Heyght	0.146	-0.115
Weigth	0.072	-0.143
Body Mass Index (BMI)	0.180	-0.107
TEE	0.180	-0.10

17% obese (BMI ≥30). Thus, the overweight/obese population constituted 51% of the total sample.

NRS score showed the absence of nutritional risk in 76 patients, corresponding to 48% of the population, while it was present in 84 patients, i.e. 52% of the sample. Of these 52%, 38% were at risk, with NRS score=3, while 62% were at serious risk, with NRS score ≥4. An increase in the NRS score, average hospitalization times and BMI was found in patients who had a worse outcome (transfer and death). Table II summarizes the outcome of patients at risk or not at risk.

Regarding the nutritional requirements of patients and the possible use of artificial nutrition during hospitalization, Oral Nutritional Supplement (ONS) was prescribed in 7% of patients, enteral nutrition (EN) in 5%, total parenteral nutrition (TPN) in 2% and oral feeding with diet or disease-specific diets in 86% of patients. Table III shows the factors influencing the NRS score.

DISCUSSION

This study was performed in an Emergency department, and confirms that there was an increasing and underestimated risk of malnutrition in this setting. In fact, we found that the NRS detected the presence of nutritional risk in 52% of patients, of whom 38% were at risk and 62% at serious risk. Significantly, we found a large presence of the geriatric population (78%), who are considered a population at risk of malnutrition (5). Moreover, we found that patients at risk had a higher average age and longer hospital stay, with lower mean values of BMI and TEE. The correlation between the NRS score and the days of hospitalization, the severity of the outcome, the catabolism and the BEE was significant. This confirms that NRS score 2002 is really predictive of the disease outcome in patients with chronic and severe diseases (12).

However, it shows also that nutritional support in those people is still not appropriate to the needs of the patient. This may also be due to the difficulties in compiling the food diary in the ward and in verifying the actual intake of oral nutritional supplements by patients, especially those not self-sufficient. Our data confirm therefore that it is extremely difficult to assess the food intake and compliance to treatment in hospitalized patients.

In conclusion, this study confirms that NRS is a useful screening tool to identify patients at nutritional risk in Emergency Departments, is more efficient than simple BMI assessment, and identifies patients needing a closer monitoring program, nutritional therapy (diet) and possibly artificial nutrition (ONS, NE, TPN). Moreover, we found that NRS score may be a significant predictor of disease severity and outcome, which operates independently from the BMI, since a total score of ≥ 3 can predict a transfer (continuation of treatment) or death of the patient.

REFERENCES

1. Cederholm T, Barazzoni R, Austin P, et al. ESPEN guidelines on definitions and terminology of clinical nutrition. Clin Nutr 2017; 36:49-64.
2. National Alliance for Infusion Therapy and the American Society for Parenteral and Enteral Nutrition Public Policy Committee and Board of Directors (2010). Disease-related malnutrition and enteral nutrition therapy: a significant problem with a cost-effective solution. Nutr Clin Pract 2010; 25:548-54.
3. Keller HH, Ostbye T. Nutritional risk and time to death; predictive validity of SCREEN (Seniors in the Community Risk Evaluation for Eating and Nutrition). J Nutr Health Aging 2003; 7:274-79.
4. Kami AA, Fernandes R, de Quadros Camargo C, Corsi DM, de Salles RK, de Moraes Trindade EB. Nutrition risk screening in patients admitted to an adult emergency department of a Brazilian university hospital. Nutr Clin Pract 2017; 32:84-91.
5. Bernabeu-Wittel M, Jadad A, Moreno-Gaviño L, et al. Peeking through the cracks: an assessment of the prevalence, clinical characteristics and health-related quality of life (HRQoL) of people with polypathology in a hospital setting. Arch Gerontol Geriatr 2010; 51:185-91.
6. Edington J, Boorman J, Durrant ER, et al. The Malnutrition Prevalence Group. Prevalence of malnutrition on admission to four hospitals in England. Clin Nutr 2000; 19:191-95.

7. Pirlich M, Schütz T, Kemps M, et al. Social risk factors for hospital malnutrition. Nutrition 2005; 21:295-300.
8. Suominen MH, Jyvakorpi SK, Pitkala KH, et al. Nutritional guidelines for older people in Finland. J Nutr Health Aging 2014; 18:861-7.
9. Volkert D, Berner YN, Berry E, et al. ESPEN Guidelines on Enteral Nutrition: geriatrics. Clin Nutr 2006; 25:330–60.
10. Kondrup J, Allison SP, Elia M, Vellas B, Plauth M. Educational and Clinical Practice Committee, European Society of Parenteral and Enteral Nutrition (ESPEN). ESPEN guidelines for nutrition screening 2002. Clin Nutr 2003; 22:415–21.
11. Kondrup J. Nutritional-risk scoring systems in the intensive care unit. Curr Opin Clin Nutr Metab Care 2014; 17:177-82.
12. Cui J, Wan Q, Wu X, et al. Nutritional Risk Screening 2002 as a predictor of outcome during general ward-based noninvasive ventilation in chronic obstructive pulmonary disease with respiratory failure. Med Sci Monit 2015; 21:2786-93.

JOURNAL OF BIOLOGICAL REGULATORS & HOMEOSTATIC AGENTS Vol. 32, no. 6, 1579-1582 (2018)

LETTER TO THE EDITOR

ADDITIVE MANUFACTURING AND BIOMIMETIC MATERIALS IN ORAL AND MAXILLOFACIAL SURGERY: A TOPICAL OVERVIEW

A. PACIFICI, A. POLIMENI and L. PACIFICI

Department of Oral and Maxillofacial Sciences, Sapienza University of Rome, Italy

Received September 10, 2018 – Accepted October 1, 2018

The Authors contributed equally to this work

Additive manufacturing (AM) is the term used for different and complex techniques to manufacture products with complex morphology, often referred to as "custom-made". The product is made without needing to melt the material into pre-formed molds, nor to remove it from an initial mass, as happens in subtractive processes. The additive methodology gives the AM enormous potential in the widest fields of application, from aerospace to biomedical, from dental to maxillofacial. This wide range of AM technologies can be applied to different types of polymeric materials such as plastics, resins and biopolymers that are processed to obtain optimal scaffolds. The most common synthetic and biocompatible polymeric materials for the production of biocompatible scaffolds are: polylactic acid (PLA), polycaprolactone acid (PLC) and polylactic-co-glycolic acid (PLGA); such materials interact effectively with cell behavior and tissue development. These materials are degradable in the physiological environment and the degradation products do not have harmful effects. In conclusion, new biomaterials are increasingly being studied as possible therapeutic remedies. Advances in tissue engineering are leading to the development of new scaffolds useful for bone regeneration and therefore potentially valid for applications in maxillofacial surgery.

To the Editor,

Additive Manufacturing (AM) is an industrial technique that allows to convert a 3D digital model into a solid clinical model, printing it layer by layer. Three-dimensional printing offers a method of personalizing surgical devices that improves patient outcome. In oral and maxillofacial surgery, anatomical models printed in 3D and surgical guides have led to a reduction in operative times and increased surgical precision (1).

AM is a process divided into four basic phases: the imaging-stage which consists of the acquisition of images by CBTC conical beam computed tomography; image processing; computer-aided design (CAD); and the prosthesis production by additive manufacturing. The additive manufacturing is more operator-dependent in respect to subtractive technology: to obtain a good product, it is important to have skilled operators and surgeons, working together for the final result (2).

Currently, the AM techniques provide a solution for the production of customized micro- and nano-structured biodegradable constructs to be used in reconstructive bone surgery for the reconstruction of large and complex defects. Surgical bone replacement is typically needed when the bone defects are large enough not to regenerate on their own, and this implies the use of scaffolds or synthetic grafting

Key words: additive manufacturing, regenerative dentistry, biomaterials, prosthetics

Mailing address:
Prof. Luciano Pacifici,
Department of Oral and Maxillofacial Sciences,
Sapienza University of Rome, Italy
e-mail: prof.lucianopacifici@libero.it

0393-974X (2018)

materials that offer good mechanical properties and interfacial biocompatibility (3-5).

AMs for scaffold production are conventionally classified into four categories: (i) stereolithography (SLA); (ii) selective laser sintering (SLS); (iii) three-dimensional printing (3DP); and (iv) fused deposition modeling (FDM). As a result of these technologies, tissue engineered scaffolds are made with complex geometries and with a micrometric distribution of spaces, allowing the optimal seeding of cells and growth factors (6).

This wide range of additive manufacturing technologies can be applied to different types of polymeric materials such as plastics, resins and biopolymers that are processed to obtain optimal scaffolds. In particular, an ideal scaffold must have three fundamental characteristics: it must be osteogenic, osteoconductive and osteoinductive, therefore it must support cell survival, proliferation and differentiation. The biomaterial must be 90% porous with an appropriate pore diameter to allow cells to penetrate the biomaterial, thus ensuring the growth of new bone tissue and optimal vascularization. Furthermore, it must guarantee an efficient resorption as the bone regenerates.

The most common synthetic and biocompatible polymeric materials for the production of scaffolds are polylactic acid (PLA), polycaprolactone acid (PLC) and polylactic-co-glycolic acid (PLGA) that interact positively with cells. These materials are degradable in the physiological environment and the degradation products do not have harmful effects. Furthermore, the degradation rate, hydrophilicity and mechanical strength can be controlled by manipulating their chemical composition.

Polylactic acid (PLA) is a thermoplastic polymer that can be used as a new material in additive manufacturing. PLA has well-controlled degradation times and has a manufacturing process that allows the formation of every imaginable shape, offering excellent biocompatibility. In fact, new *in vitro* study has shown that PLA disks obtained by FDM additive technique do not show cytotoxic effects on human osteoblasts (7, 8).

The latest advances in tissue engineering aim to regenerate tissues using more biological approaches and the use of stem cells in combination with scaffolds to create more stable systems. In fact, a study conducted by Diomede et al. evaluated *in vitro* and *in vivo* regeneration of the bone defect of three-dimensional PLA scaffolds enriched with human gingival mesenchymal stem cells (hGMSCs) and complexed with EV (membrane vesicles containing functional proteins, lipids and nucleic acids, such as mRNA and micro-RNA). A polyethyleneimine (PEI) coating was used to activate PLA scaffolds, demonstrating that the increase of PLA degradation by-products over time did not result in an increase in cytotoxic response and that the enriched biomaterial induced the upregulation of all the 31 genes identified and involved in the regulation of ossification as well as in ossification processes. Thus, the EVs and the PEI-EV combination may be used in future with PLA scaffolds to promote bone regeneration (9).

Another important polymer used in bone regeneration is PLGA which is a copolymer obtained from the combination of lactic acid and glycolic acid by foreign bonds. The composition of the final polymer chains influences the degradation time, extending the half-life of the polymer once applied *in situ*.

PLGA is used in various forms, such as in the shaping of porous scaffolds, hydrogels or microspheres. By evaluating the different process parameters and the physical properties of PLGA, SLS proved to be the best technique for making the scaffolds.

Currently, this polymeric bone substitute is widely used for dental bone regeneration in dentistry and has been combined with growth factors and MSC to achieve even more promising results. Recent developments have highlighted the potential of porous hydroxyapatite (HAp) as a synthetic bone graft. The addition of HAp into PLGA scaffolds (PLGA/HA-Alos) has led to better manipulation and biocompatibility and the creation of stem cell complexes that can better adapt to bone defects (10).

Polycaprolactone (PLC or PCL) is an aliphatic polyester less well known among synthetic polymers. It has good mechanical characteristics and degrades through hydrolysis of foreign bonds. PCL is used in the biomedical field thanks to its biocompatibility,

mechanical resistance and its biodegradation over time. However, PCL is a hydrophobic material, and this leads to cell failure. To overcome this problem, collagen has been added to the PCL, which allows increased cell adhesion.

The interest in biodegradable polymer matrices has increased in recent years. In fact, a recent study aimed to verify the effects of hydroxyapatite-reinforced PCL demonstrating *in vitro* that the new scaffolds were not toxic to human osteosarcoma cells (11). Therefore, the prepared scaffolds could be promising for bone regeneration and potentially useful for orthopedic applications and maxillofacial surgery.

Recently, biodegradable hybrid scaffolds of PCL and Mg have shown that the incorporation of Mg microparticles into PCL scaffolds greatly improves its mechanical properties and bioactivity. Roh et al. carried out preliminary *in vitro* studies to evaluate the effects of the PCL/HAp /MgO scaffold produced by the 3D printing technique. They demonstrated that the addition of MgO and HAp nanoparticles and plasma treatment improved cell adhesion, proliferation and differentiation in PCL scaffolds (12).

Hydrogels are another class of scaffolds commonly used for tissue engineering applications. Fibrin, hyaluronic acid (HyA), gelatin, chitosan and alginate are natural polymers which, through intense hydration, lead to the formation of hydrogel. Hydrogels represent an important class of biomaterials in biotechnology and medicine as they show excellent biocompatibility.

However, hydrogels are deficient in mechanical strength, in fact, it is for this reason that they are used in association with other substances that give them stability. In particular, a new hybrid system was studied and developed in which ceramic scaffolds, consisting of biphasic calcium phosphate (BCP) or HAp and tricalcium phosphate (TCP) phases, were loaded with hydrogel of porous HyA, improving the resistance to compression and providing good biodegradability of the final scaffolds (13).

Tatullo et al. also discovered an important correlation among scaffolds to be used in bone regeneration and systemic inflammatory pathologies: it may be important to control inflammation before regenerating large defects with scaffolds; moreover, a careful clinical and surgical management is strictly suggested for patients with systemic pathologies or reporting smoking habits (14, 15).

Scaffolds are currently used as injectable bone substitutes (IBS), typically composed of beta-tricalcium phosphate (β-TCP) and combined with hydrogels: IBS are particularly able to contribute to bone regeneration by acting as a scaffold-like structure displaceable in complex-shape defects, and results have been verified both clinically and radiologically (16-18).

DISCUSSION

In conclusion, new biomaterials are increasingly being studied as possible therapeutic remedies. Advances in tissue engineering are leading to the development of new scaffolds useful for bone regeneration and therefore potentially valid for application in maxillofacial surgery. The AM technologies available today are able to use both metallic and polymeric materials, thus allowing an excellent versatility in the production of prostheses that are both resistant and of a complex shape.

3D scaffolds require an even more complex shape and different consistencies, moreover, the inner structure is currently made with interconnected pores, in order to ensure transport of nutrients. These specific characteristics are particularly useful in bone regeneration. SLS is currently the most useful and replicable technique able to create customized large-sized models from composite powders. The only criticism is related to the mechanical strength of such SLS-made scaffolds.

Selective Laser Melting technology is one of the most promising in the field of additive manufacturing of metal products and consists in the point-to-point fusion of a metal in powders through focused laser light: this technique is currently able to reach micrometric dimensions, so obtaining highly personalized macroscopic and microscopic forms adaptable to the anatomy of the facial mass. The prosthesis of the future is based on the defects extrapolated from the radiological analysis of bone

defects. The versatility of AM and the biomimicking of new materials will allow in the future to have reconstructions of complex and wide traumas in shorter surgical times and with a quicker follow-up as well as with minor complications.

ACKNOWLEDGEMENTS

The authors are grateful to the Department of Odontostomatological and Maxillofacial Sciences, of the University of Rome "Sapienza" for its technical and scientific support.

REFERENCES

1. Diment LE, Thompson MS, Bergmann JHM. Clinical efficacy and effectiveness of 3D printing: a systematic review. BMJ Open 2017; 7(12):e016891.
2. Marrelli M, Gentile S, Palmieri F, Paduano F, Tatullo M. Correlation between surgeon's experience, surgery complexity and the alteration of stress related physiological parameters. PLoS One 2014; 9(11):e112444.
3. Aulino P, Costa A, Chiaravalloti E, et al. Muscle extracellular matrix scaffold is a multipotent environment. Int J Med Sci 2015; 12(4):336-40.
4. Marrelli M, Maletta C, Inchingolo F, Alfano M, Tatullo M. Three-point bending tests of zirconia core/veneer ceramics for dental restorations. Int J Dent 2013; 2013:831976.
5. Perniconi B, Coletti D, Aulino P, et al. Muscle acellular scaffold as a biomaterial: effects on C2C12 cell differentiation and interaction with the murine host environment. Front Physiol 2014; 5:354.
6. Mota C, Puppi D, Chiellini F, Chiellini E. Additive manufacturing techniques for the production of tissue engineering constructs. J Tissue Eng Regen Med 2015; 9(3):174-90
7. Annibali S, Cristalli MP, Tonoli F, Polimeni A. Stem cells derived from human exfoliated deciduous teeth: a narrative synthesis of literature. Eur Rev Med Pharmacol Sci 2014; 18(19):2863-81
8. Paduano F, Marrelli M, Palmieri F, Tatullo M. CD146 expression influences periapical cyst mesenchymal stem cell properties. Stem Cell Rev 2016; 12(5):592-603.
9. Diomede F, Gugliandolo A, Cardelli P, et al. Three-dimensional printed PLA scaffold and human gingival stem cell-derived extracellular vesicles: a new tool for bone defect repair. Stem Cell Res Ther 2018; 9(1):104
10. Ceccarelli G, Presta R, Lupi SM, et al. Evaluation of poly(lactic-co-glycolic) acid alone or in combination with hydroxyapatite on human-periosteal cells bone differentiation and in sinus lift treatment. Molecules 2017; 22(12).
11. Tatullo M, Simone GM, Tarullo F, et al. Antioxidant and antitumor activity of a bioactive polyphenolic fraction isolated from the brewing process. Sci Rep 2016; 6:36042.
12. Roh HS, Lee CM, Hwang YH, Kook MS, Yang SW, Lee D, Kim BH. Addition of MgO nanoparticles and plasma surface treatment of three-dimensional printed polycaprolactone/hydroxyapatite scaffolds for improving bone regeneration. Mater Sci Eng C Mater Biol Appl 2017; 74:525-35.
13. Paduano F, Marrelli M, Alom N, Amer M, White LJ, Shakesheff KM, Tatullo M. Decellularized bone extracellular matrix and human dental pulp stem cells as a construct for bone regeneration. J Biomater Sci Polym Ed 2017; 28(8):730-48.
14. Tatullo M, Marrelli M, Amantea M, Paduano F, Santacroce L, Gentile S, Scacco S. Bioimpedance detection of oral lichen planus used as preneoplastic model. J Cancer 2015; 6(10):976-83.
15. Tatullo M, Gentile S, Paduano F, Santacroce L, Marrelli M. Crosstalk between oral and general health status in e-smokers. Medicine (Baltimore) 2016; 95(49):e5589.
16. Annibali S, Iezzi G, Sfasciotti GL, et al. Histological and histomorphometric human results of HA-Beta-TCP 30/70 compared to three different biomaterials in maxillary sinus augmentation at 6 months: a preliminary report. Biomed Res Int 2015; 2015:156850.
17. Di Carlo G, Saccucci M, Ierardo G, et al. Rapid maxillary expansion and upper airway morphology: a systematic review on the role of cone beam computed tomography. Biomed Res Int 2017; 2017:5460429.
18. Annibali S, Bignozzi I, Cristalli MP, Graziani F, La Monaca G, Polimeni A. Peri-implant marginal bone level: a systematic review and meta-analysis of studies comparing platform switching versus conventionally restored implants. J Clin Periodontol 2012; 39(11):1097-113.

JOURNAL OF BIOLOGICAL REGULATORS & HOMEOSTATIC AGENTS Vol. 32, no. 6, 1583-1587 (2018)

LETTER TO THE EDITOR

EFFECT OF SELF-ADJUSTING FILE AND WAVEONE RECIPROCATING FILE ON THE FILLING ABILITY OF OVAL-SHAPED CANALS WITH THERMOPLASTICIZED GUTTA-PERCHA

L. GENERALI[1], F. CAVANI[2], E. RIGHI[2], A. MURRI DELLO DIAGO[1], E. SPINAS[3] and L. GIANNETTI[1]

[1]Department of Surgery, Medicine, Dentistry and Morphological Sciences with Transplant Surgery, Oncology and Regenerative Medicine Relevance (CHIMOMO), University of Modena and Reggio Emilia, Modena, Italy; [2]Department of Biomedical, Metabolic and Neural Sciences, University of Modena and Reggio Emilia, Modena, Italy; [3]Department Surgical Sciences, University of Cagliari, Cagliari, Italy

Received September 17, 2018 – Accepted October 11, 2018

The aim of the study was to compare the effect of Self-Adjusting Files (SAF) and WaveOne Primary file with syringe and needle irrigation on the filling ability of oval-shaped root canals obturated with thermoplasticized gutta-percha. Twenty-four single root teeth with single oval-shaped root canals were distributed into two experimental homogeneous groups. One group was instrumented and cleansed using the SAF system while in the other group the WaveOne system with syringe and needle irrigation was used. After instrumentation, the roots were filled by Thermafil Obturators and TopSeal sealer. Specimens were transversally sectioned at 2-, 5- and 7-mm levels from the apex and observed under light microscope. The percentage of gutta-percha filled area (PGFA), the percentage of sealer filled area (PSFA) and the percentage of voids area (PVA) were measured for each section, moreover the percentage of completely filled sections was evaluated. At all levels, no significant differences in terms of PGFA, PSFA, PVA and percentage of completely filled canals between groups were obtained ($P > 0.05$). On the contrary, when the data were pooled, the mean PGFA in the SAF group was 95.8%, whereas it was 93.2% in the WaveOne group ($P < 0.05$). The percentage of sections completely filled was 77.8% in the SAF group, and 52.8% in the WaveOne group ($P < 0.05$). Overall, the use of the SAF system in oval canals allows to obtain a significantly greater complete filling than the use of the WaveOne system.

To the Editor,

Rotating and reciprocating nickel-titanium (NiTi) endodontic instruments have improved root canal shaping by reducing procedural errors (1). Root canals often have areas inaccessible to manual and NiTi endodontic instruments (2, 3). Rotating and reciprocating systems show similar shaping ability with respect to the percentage of non-instrumented root-canal wall and leave considerable areas of unprepared dentin. In particular, in the oval canals the instruments are unable to contact all canal walls according to the width of the canal and this causes the packing of dentine debris and the uncomplete removal of the pulp residues (4).

Instrumentation and three-dimensional obturation of oval canals are a challenge for dentists. The permanence of hard and soft tissue in non-shaped walls and the irregular canal shape can compromise root canal obturation. The filling material and sealer remain separated from the root canal due to

Key words: filling ability, oval canal, self adjusting file, Thermafil, WaveOne

Mailing address:
Dr Luigi Generali,
Department of Surgery,
Medicine, Dentistry and Morphological Sciences with Transplant Surgery, Oncology and Regenerative Medicine Relevance (CHIMOMO),
University of Modena and Reggio Emilia,
Via del Pozzo, 71 - 41124 Modena, Italy
Tel.: +39 059 4224324
e-mail: luigi.generali@unimore.it

0393-974X (2018)

the permanence of tissues and debris, preventing inactivation of the remaining bacteria and providing a potential recontamination space (5, 6). The Self-Adjusting File (SAF) (ReDent Nova, Ra'anana, Israel) is a hollow and flexible file that adapts itself three-dimensionally to the root canal (5). It is a thin-walled pointed cylinder either 1.5 or 2.0 mm in diameter composed of 120-µm-thick NiTi lattice. The slightly abrasive surface of the instrument and the vibrating movement combined with the contact along the entire circumference and length of the canal allow to remove a layer of dentin. During shaping, the file allows continuous irrigation which, with the vibrating motion, improves the cleaning of the canal (7).

The aim of the present study was to compare the effect of the SAF system and the WaveOne (WO) primary (Dentsply Maillefer, Baillagues, Switzerland) file with syringe and needle irrigation on the filling ability of oval-shaped root canals obturated with thermoplasticized gutta-percha. The null hypotheses tested were the following:

i. there is no difference in the percentage of gutta-percha filled area (PGFA), percentage of sealer filled area (PSFA) and percentage of voids area (PVA) between canals shaped with the SAF system or with the WO reciprocating files;

ii. there is no difference in the percentage of completely filled canals between SAF system and WO files.

MATERIALS AND METHODS

Seventy-three teeth with a single straight mature root (central incisors, canines, low premolars) were selected from a pool of extracted human permanent teeth. Teeth had been stored in 0.1% thymol solution at 4°C until use. Teeth that showed more than one canal, previous root canal treatment, calcifications, resorption and cracks were discarded (n = 7). Two radiographs were taken in mesio-distal and bucco-lingual plane to select teeth with a short cross-sectional diameter ratio ≥ 2.5 (oval shape) at 5 mm from the apex (2) (n = 24).

The coronal portion of each tooth was removed at the cement-enamel junction using a high-speed fissure bur under water spray to obtain a root length of 13±1 mm from the apex. A 21-mm #10 K-file (Dentsply, Maillefer, Baillagues, Switzerland) was inserted into the canal until its tip appeared at the apical foramen under microscopic vision (OPMI PICO; Carl Zeiss Meditec Inc., Jena, Germany) at 10x. The working length (WL) was established by subtracting 0.5 mm from the total root length. Each root was pre-flared with using Gates-Glidden drills (Dentsply, Maillefer, Baillagues, Switzerland) size 1 to 4 inserted in the middle and coronal third and a glide path was created by using PathFile 1, 2 and 3 (size 13, 16, 19 and 2% taper) (Dentsply, Maillefer) to the WL mounted on an X Smart plus engine (Dentsply, Maillefer) at 300 rpm. After the use of each instrument, the root canals were irrigated with 1 mL of 5.25% sodium hypochlorite (NaOCL) (Niclor, Ogna, Muggiò, Italy) using a syringe with a 30-gauge side-vented needle (Max-i-Probe; Dentsply Rinn, Elgin IL) placed before the binding point but no closer than 2 mm from the WL. The 24 selected teeth were divided into two experimental groups (n = 12 each) according to the type of shaping: SAF system (SAF group) and WaveOne primary system (WO group). The groups had similar canal width, measured on radiographs at 5 mm from the apex, using the Student's *t*-test ($P > 0.05$). In the SAF group, each root was prepared by using the SAF file for 4 min with an in-and-out manual motion (0.4 mm amplitude and 5000 vibrations per minute) with continuous irrigation by using 5.25% NaOCl provided by a VATEA peristaltic pump (ReDent-Nova) at a rate of 2mL/min. After 4 min the SAF file reached the WL. At the end of the shaping the SAF system was used for a final irrigation using 17% EDTA (Ogna, Muggiò, Italy) for two min.

In the WO group, each root was shaped by using NiTi WaveOne Primary reciprocating files (size 25 and 8% taper) up to 1 mm to the WL, then the WL was re-checked with a #10 K-file and eventually the WaveOne Primary file was brought to the full WL (8). The WaveOne Primary files were used in a slow in-and-out pecking motion using a dedicated reciprocating engine (X Smart plus, Dentsply, Maillefer) with the manufacturer's setup configuration. Every time the WaveOne Primary was pulled out, the canal was irrigated with 1 mL of 5.25% NaOCl (Ogna, Muggiò, Italy) using a syringe with a 30-gauge side-vented needle (Max-i-Probe; Dentsply Rinn, Elgin IL) placed 2 mm from the WL. At the end of the canal preparation, an irrigation of 4 mL of 17% EDTA (Ogna, Muggiò, Italy) left in place

for two min was performed. The needle was placed 2 mm from the WL. For both groups a final irrigation with 3 mL of 5.25% NaOCl was performed.

All roots were dried with paper points and filled by Thermafil Obturators #25 (Dentsply, Tulsa Dental Specialties, Johnson City, TN, USA) with TopSeal sealer (Dentsply, Tulsa Dental Specialties, Johnson City, TN, USA). All specimens were stored at 37°C for 36 h. A single operator was responsible of all the experimental procedures.

All roots were embedded in methacrylate resin (Technovit 3040, Heraeus Kulzer, Wehrheim, Germania) and transversally sectioned at 2, 5 and 7 mm from the apex with a saw microtome (Leica SP 1600, Wetzlar, Germania) to obtain 200-μm thick sections.

The specimens were examined under a light microscope Axiophot (Carl Zeiss Vision, Hallbergmoos, Germany) at 25 and 50X magnification. Digital images were acquired with the AxioCam ERc 5s (Carl Zeiss, Göttingen, Germany) camera.

A blinded operator measured the total area of each canal and the areas of gutta-percha, sealer and voids in metric system with the ImageJ software (National Institutes of Health, Bethesda, MD) and converted to percentages (PGFA, PSFA and PVA) of the total area.

Statistical analysis

The Shapiro-Wilk test was used to evaluate the normal distribution of the data. When data were not normally distributed, the Mann-Whitney test was used to compare means between groups and the Kruskal-Wallis test to compare within group data. The number of sections (expressed as percentage in Table II) that showed a complete (100%) filling of the canal was compared between groups with the Fisher's exact test. SPSS Statistic (Armonk, NY, USA) software was used, the level of significance was set at $P < 0.05$.

RESULTS

Fig. 1 shows representative images from each experimental group at 2-, 5- and 7-mm levels of the gutta-percha filled areas. No significant differences ($P > 0.05$, Table I) were found in terms of PGFA, PSFA and PVA between groups at all levels. On the other hand, when data were pooled together PGFA and PVA values were significantly ($P < 0.05$) higher and lower, respectively, in the SAF group with respect to the WO one. The PSFA values were close to significativity ($P = 0.056$). No significant

Table I. *Means and standard deviations of PGFA, PSFA and PVA (%).*

	PGFA		PSFA		PVA	
	WO	SAF	WO	SAF	WO	SAF
2-mm	94.8±7.2	95.8±11.1	4±5.1	3.8±9.6	1.2±2.5	0.4±1.5
5-mm	92.6±9.6	95.3±7.9	5.9±8.4	3.7±5.8	1.5±2.2	1±2.6
7-mm	92.2±11.4	96.5±5.6	2.2±3	1.9±3.1	5.6±10.4	1.6±3.6
pooled	93.2±9.3	95.8±8.3*	4±5.9	3.2±6.6	2.8±6.5	1±2.7*

**P < 0.05 vs WO, Mann-Whitney test*

Table II. *Percentage of sections completely filled.*

	2-mm	**5-mm**	**7-mm**	**pooled**
WO	66.7%	41.7%	50%	52.8%
SAF	91.7%	75%	66.7%	77.8%*

**P < 0.05 vs WO, Fisher's exact test*

differences (P > 0.05) were found between 2-mm, 5-mm and 7-mm levels within each group.

Table II reports the percentage of sections showing a complete filling of the canal according to level and treatment. No significant differences (p < 0.05) were found between WO and SAF files when each level was compared, but when data were pooled together the percentage of sections completely filled was significantly higher in the SAF group in respect to the WO one.

DISCUSSION

For geometric reasons, the buccal and lingual recesses of oval canals cannot be adequately shaped by rotating or reciprocating NiTi instruments. In order to shape these recesses, it would be necessary to increase the size of the instruments considerably, thus compromising the structural resistance of the root due to the significant amount of dentin removed (7). The smear layer and the debris produced during the shaping tend to be pushed into these recesses, preventing the flow of the filling material. The SAF system represents a different approach in the way of operating and has been designed to overcome this problem (7). Several micro-CT studies (9-10) have shown a significantly better shaping of oval and C-shaped canals using the SAF instruments, compared to the NiTi rotary instruments, even if in all cases the complete circumferential preparation of the canal is not achieved. The use of the SAF instrument compared to rotating NiTi instruments significantly reduces the amount of dentinal residues accumulated in the buccal and lingual recesses of oval canals (11). The gutta-percha is stable over time, whilst the sealer tends to reabsorb (12). Therefore, in the present

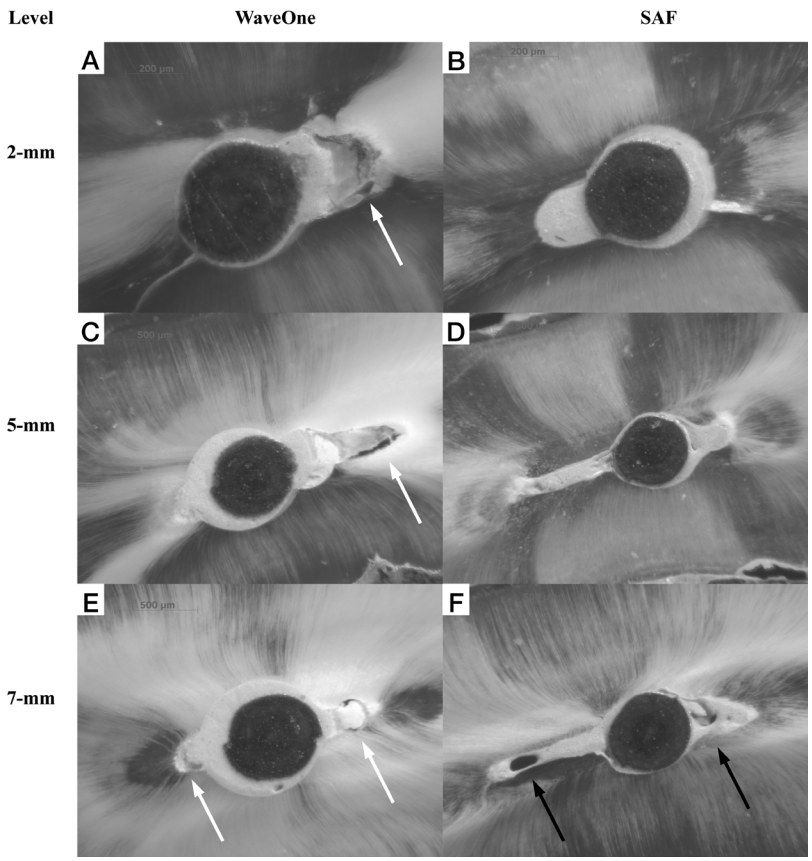

Fig. 1. *Representative light microscope images of sections at different levels from the WaveOne group (**A**, **C**, **E**) and the SAF group (**B**, **D**, **F**) filled with Thermafil Obturators. In A, C, E the debris into the recesses (white arrows) prevents the complete filling of the canal. In F note the presence of voids (black arrows).*

study, the PGFA and PSFA were used to evaluate the quality of root canal filling. No significant differences were found between the groups when each level was compared. On the other hand, when the data from each group were pooled, the PGFA and the PVA were significantly higher in the SAF group, while there was no difference between the groups for the PSFA, therefore the first null hypothesis was rejected. These results are in agreement with those of a previous study (11). In the present study, no significant differences were found between the groups regarding the percentage of sections completely filled when each level is compared, but, again, by pooling the data of the sections in each group, the SAF was significantly better for a greater number of sections completely filled (77.8% SAF *vs* 52.8% WO), therefore the second null hypothesis was rejected. Within the limitation of this study, it is possible to conclude that none of the techniques used guarantees 100% complete canal filling. The use of the SAF system allows to have a greater complete filling with thermoplasticized gutta-percha compared to the instrumentation with WaveOne with syringe and needle irrigation.

ACKNOWLEDGEMENTS

This research was funded by the FAR project (University of Modena and Reggio Emilia Funds for Research) entitled “Microstructural and Mechanical investigation of Nickel-Titanium Endodontic instruments – MMiNTEndo”.

REFERENCES

1. Iacono F, Pirani C, Generali L, et al. Wear analysis and cyclic fatigue resistance of electro discharge machined NiTi rotary instruments. G It Endo 2016; 30:64-68.
2. De Deus G, Barino B, Marins J, Magalhaes K, Thuanne E, Kfir A. Self-adjusting file cleaning-shaping-irrigation system optimizes the filling of oval-shaped canals with thermoplasticized gutta-percha. J Endod 2012; 38:846-49.
3. Giannetti L, Murri A. Clinical evidence and literature to compare two different therapeutic protocols in tooth avulsion. Eur J Paediatr Dent 2006; 3:122-30.
4. De Deus G, Belladonna FG, Silva EJNL, et al. Micro-CT evaluation of non-instrumented canal areas with different enlargements performed by NiTi systems. Braz Dent J 2015; 26:624-29.
5. Generali L, Cavani F, Serena V, Pettenati C, Righi E, Bertoldi C. Effect of different irrigation systems on sealer penetration into dentinal tubules. J Endod 2017; 43:652-56.
6. Generali L, Prati C, Pirani C, Cavani F, Gatto MR, Gandolfi MG. Double dye technique and fluid filtration test to evaluate early sealing ability of an endodontic sealer. Clin Oral Investig 2017; 21:1267-76.
7. Metzger Z, Teperovich E, Zary R, Cohen R, Hof R. The self-adjusting file (SAF). Part 1: respecting the root canal anatomy--a new concept of endodontic files and its implementation. J Endod 2010; 36:679-90.
8. Generali L, Righi E, Todesca MV, Consolo U. Canal shaping with WaveOne reciprocating files: influence of operator experience on instrument breakage and canal preparation time. Odontology 2014; 102:217-22.
9. Versiani MA, Pecora JD, de Sousa-Neto MD. Flat-oval root canal preparation with self-adjusting file instrument: a micro–computed tomography study. J Endod 2011; 37:1002-7.
10. Solomonov M, Paqué F, Fan B, Eilat Y, Berman LH. The challenge of C-shaped canal systems: a comparative study of the self-adjusting file and ProTaper. J Endod 2012; 38:209-14.
11. De-Deus G, Souza EM, Barino B, et al. The self-adjusting file optimizes debridement quality in oval-shaped root canals. J Endod 2011; 37:701-5.
12. Schäfer E, Zandbiglari T. Solubility of root canal sealers in water and artificial saliva. Int Endod J 2003; 36:660-69.

JOURNAL OF BIOLOGICAL REGULATORS & HOMEOSTATIC AGENTS Vol. 32, no. 6, 1589-1592 (2018)

LETTER TO THE EDITOR

A NOVEL TECHNIQUE TO PREVENT SINUS MEMBRANE COLLAPSE DURING MAXILLARY SINUS FLOOR AUGMENTATION WITHOUT BONE GRAFT: TECHNICAL NOTE

A. SCARANO[1,2], G. MURMURA[1], F. MASTRANGELO[3], F. LORUSSO[1], A. GRECO LUCCHINA[4] and F. CARINCI[5]

[1]Department of Medical, Oral and Biotechnological Sciences University of Chieti-Pescara, Italy; [2]Center for Research on Ageing and Translational Medicine (CeSI-MeT), University of Chieti-Pescara, Italy; [3]Deptartment of Medical Science and Biotechnology, University of Foggia, Italy; [4]Oral Surgery Unit, University of Eastern Piedmont, Novara, Italy; [5]Chief of Maxillofacial Surgery, University of Ferrara, Italy

Received June 27, 2018 – Accepted October 11, 2018

Different surgical techniques have been developed to reconstruct the posterior maxilla without bone graft. A barrier membrane usually placed internal to the sinus, without stabilizer or bone window, pushed inside the sinus cavity as the "roof" of the sinus cavity to preserve the space and help bone regeneration has been used with success. In the present technical report, the heterologous cortical lamina is used for the mechanical support of sinus membranes. The membrane is placed through two lines of 2-3 mm, mesial and distal, created at the top of the antrostomy. The half heterologous membrane is positioned on these lines and pushed to the nose wall of the sinus, and the other half is folded to cover the window. In this way the bone lamina is stable. Cone Beam Computed Tomography was used to evaluate the efficacy of bone lamina to preserve the space in sinus lifting which contributes positively to wound healing and is effective in bone formation without biomaterials.

To the Editor,

Rehabilitation of the edentulous posterior maxilla with dental implants may be a problem for buccolingual and/or apical occlusal atrophy of the edentulous alveolar crest and pneumatization of the maxillary sinus (1). In this anatomical situation, it can be very difficult to obtain primary stability because of the absence of a useful quantity of cortical bone and for the loose structure of type IV spongious bone, which prevents an implant migration into the sinus (2, 3).

The grafting materials that are utilized in floor augmentation could provide for a bone formation process, by replacing the bone materials, due to capillary infiltration, and support of the implants (3). These grafting materials help to maintain space between the basal bone and membrane.

A new bone formation is achieved in the sinus after bone grafting making implant placement possible. However, the possibility of new bone formation with a membrane elevation without bone graft in the maxillary sinus has been reported in human studies (4, 5). Spontaneous bone formation inside the maxillary sinus has been noted after removal of a cyst (6), removal of a displaced implant (7) and in an extraction socket (8). The use of the sinus

Key words: bone graft, without bone graft, resorbable barrier, sinus lift, heterologous cortical lamina, bone regeneration

Mailing address:
Antonio Scarano, M.D., D.D.S.
Department of Medical, Oral and Biotechnological Sciences,
University of Chieti-Pescara,
Via dei Vestini 31, 66100 Chieti, Italy
Fax: +39 0871 3554099
e-mail: ascarano@unich.it

0393-974X (2018)

DISCLOSURE: ALL AUTHORS REPORT NO CONFLICTS OF INTEREST RELEVANT TO THIS ARTICLE.

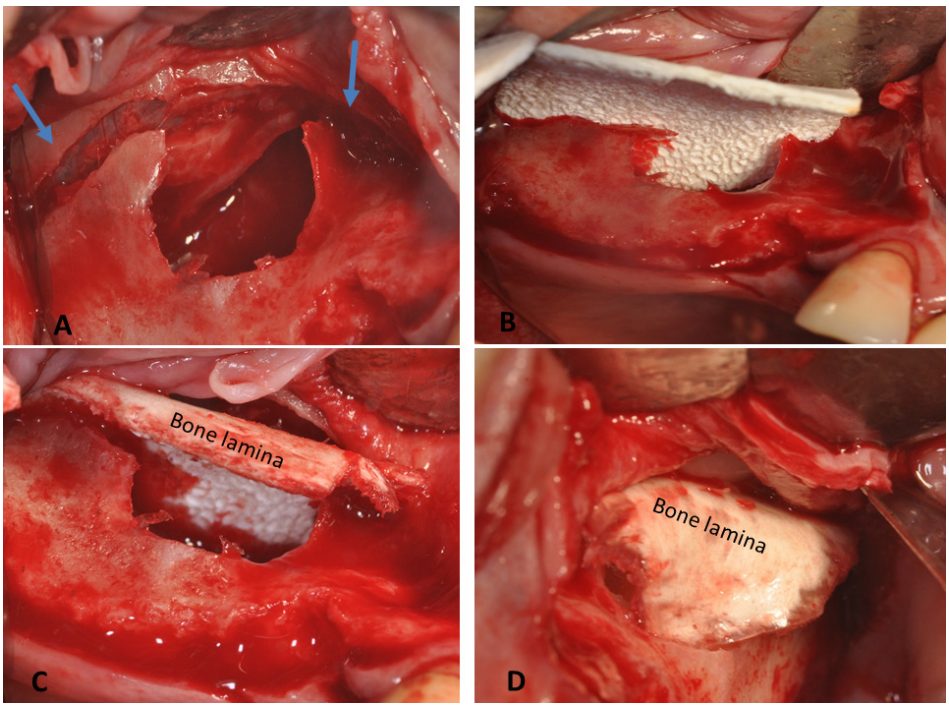

Fig. 1. ***A****) Schneiderian membrane was elevated and two lines of 2-3 mm, mesial and distal (Arrows), was created at the top of the antrostomy.* ***B*** *and* ***C****) The half heterologous membrane was positioned on lines and pushed to the nose wall of the sinus.* ***D****)The other half was folded to cover the window.*

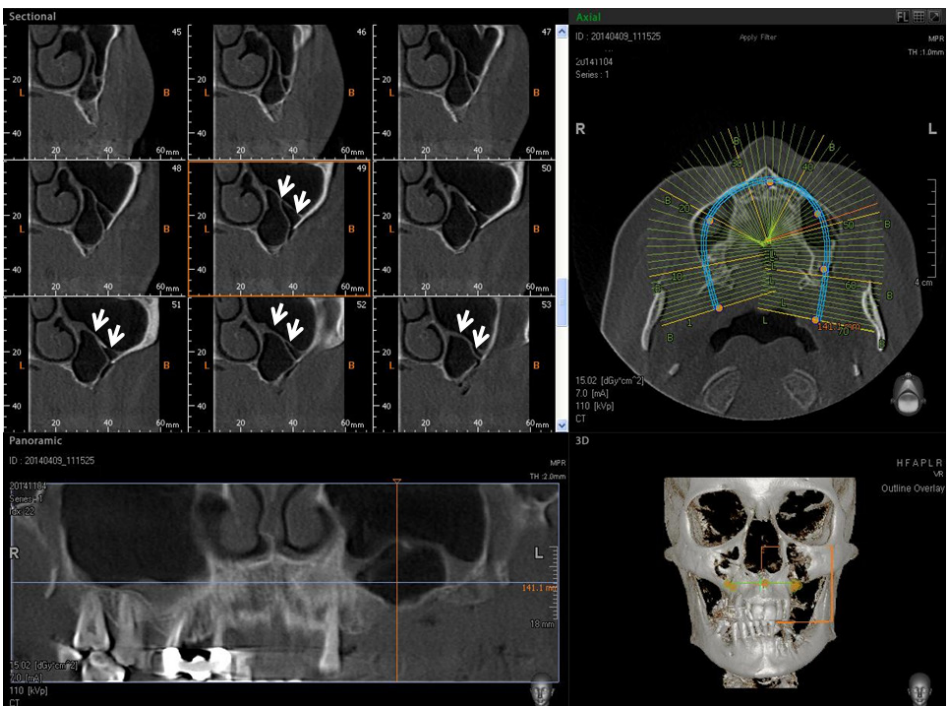

Fig. 2. *CBCT after sinus lifting with bone lamina to preserve the space (arrows).*

membrane elevation technique was investigated in patients referred for sinus augmentation (4, 9). Sinus membrane stabilization is a requirement for bone formation. It must be pointed out that maxillary sinus pneumatization could be the result of positive intrasinus air pressure caused by respiration, and this pressure might promote resorption and new pneumatization after maxillary sinus augmentation (10). To avoid this, Borges et al. (11) pushed the lateral bone window inside the sinus cavity, using this thin bone as the ''roof'' of the secluded cavity. The limitation of this technique is the distance between the antrostomy and the nose wall; in fact, in the case of a large distance the bone window is insufficient to support the sinus membranes (12).

To avoid sinus membrane collapse in maxillary sinus floor augmentation without bone graft, a novel technique for placing a bone lamina (Lamina, OsteoBiol, Turin, Italy) in antrostomy is presented.

This technique uses a cortical bone lamina of 2-3 mm thickness, modelled and positioned in the sinus as a new sinus. This membrane is rigid, and stability improves through the two lines from 2-3 mm, mesial and distal created at the top of the antrostomy. After accomplishing elevation of the Schneiderian membrane, two lines of 2-3 mm, mesial and distal, were created at the top of the antrostomy (Fig. 1A). The antrostomy was measured with a periodontal probe for cutting the membrane to size.

This heterologous barrier was washed with saline solution for 10 min. After water contact the bone lamina softens and it is possible to shape it, allowing to fit the anatomic curvature of the sinus. The cortical laminar membrane is first softened and then imbibed with the patient's blood for 2-3 minutes. The half heterologous membrane was positioned on these lines and pushed to the nose wall of the sinus (Fig. 1B); when the coagulum was observed underneath the elevated sinus mucosa, the other half was folded to cover the window (Fig. 1 C-D). This procedure was performed carefully to avoid tearing or folding of the bone lamina. Fig. 2 shows CBCT after sinus lifting with bone lamina to preserve the space. The bone lamina used in the present research was rigid and allowed organization of the clot. The fibrin network of the blood clot acted as a scaffold for fibrocellular invasion, and hence was beneficial to bone formation. The bone lamina is made of cortical bone of porcine origin, has an elastic consistency, nevertheless maintaining the typical compactness of the bone tissue from which it originates. This property is particularly useful when it is necessary to obtain a space-making effect in bone regeneration.

The heterologous cortical lamina is a valid technique for mechanical support of the sinus membrane to help only bone tissue formation and not as a mix with bone graft. It is the experience of the authors that this procedure prevents sinus membrane collapse.

REFERENCES

1. Scarano A, Perrotti V, Carinci F, Shibli JA. Removal of a migrated dental implant from the maxillary sinus after 7 years: a case report. Oral Maxillofac Surg 2011; 15:239-43. doi:10.1007/s10006-010-0243-8.
2. Fürst G, Gruber R, Tangl S, et al. Sinus grafting with autogenous platelet-rich plasma and bovine hydroxyapatite. A histomorphometric study in minipigs. Clin Oral Impl Res 2003; 14:500-508.
3. Froum SJ, Tarnow DP, Wallace SS, Rohrer MD, Cho SC. Sinus floor elevation using anorganic bovine bone matrix (OsteoGraf/N) with and without autogenous bone: a clinical, histologic, radiographic, and histomorphometric analysis--Part 2 of an ongoing prospective study. Int J Periodontics Restorative Dent 1998; 18:528-43.
4. Lundgren S, Andersson S, Gualini F, Sennerby L. Bone reformation with sinus membrane elevation: a new surgical technique for maxillary sinus floor augmentation. Clin Implant Dent Relat Res 2004; 6:165-73.
5. Scarano A, de Oliveira PS, Traini T, Lorusso F. Sinus membrane elevation with heterologous cortical lamina: a randomized study of a new surgical technique for maxillary sinus floor augmentation without bone graft. Materials (Basel) 2018; 17:11(8). doi: 10.3390/ma11081457
6. Lundgren S, Andersson S, Sennerby L. Spontaneous bone formation in the maxillary sinus after removal of a cyst: coincidence or consequence? Clin Implant Dent Relat Res 2003; 5:78-81.

7. Scarano A, Piattelli A, Iezzi G, Varvara G. Spontaneous bone formation on the maxillary sinus floor in association with surgery to remove a migrated dental implant: a case report. Minerva Stomatol 2014; 63:351-59.
8. JungY-S, Chung S-W, Nam W, Cho I-H, Cha I-H, Park H-S. Spontaneous bone formation on the maxillary sinus floor in association with an extraction socket. Int J Oral Maxillofac Surg 2007; 36:656-57. doi:10.1016/j.ijom.2007.01.013.
9. Scarano A, Lorusso F, Arcangelo M, D'Arcangelo C, Celletti R. Lateral sinus floor elevation performed with trapezoidal and modified triangular flap designs: a randomized pilot study of post-operative pain using thermal infrared imaging. Int J Environ Res Public Health 2018; 15(6). doi: 10.3390/ijerph15061277.
10. Testori T, Weinstein R, Wallace S. Maxillary sinus surgery and alternatives in treatment. Quintessence Publ. 2009.
11. Borges FL, Dias RO, Piattelli A, et al. Simultaneous sinus membrane elevation and dental implant placement without bone graft: a 6-month follow-up study. J Periodontol 2011; 82:403-12. doi:10.1902/jop.2010.100343.
12. Scattarella A, Ballini A, Grassi FR, et al. Treatment of oroantral fistula with autologous bone graft and application of a non-reabsorbable membrane. Int J Med Sci 2010; 7:267.

LETTER TO THE EDITOR

EFFICACY OF A COMBINED SEA SALT-BASED ORAL RINSE WITH XYLITOL AGAINST DENTAL PLAQUE, GINGIVITIS, AND SALIVARY *STREPTOCOCCUS MUTANS* LOAD

S. CANTORE[1,2,3*], A. BALLINI[1*], R. SAINI[4*], D. DE VITO[1], V. ALTINI[4], S.R. SAINI[4], T. PUSTINA-KRASNIQI[5], E. XHAJANKA[6], C. GARGIULO ISACCO[4], G. DIPALMA[4*] and F. INCHINGOLO[4*]

[1]Department of Basic Medical Sciences, Neurosciences and Sense Organs, University of Bari Aldo Moro, Bari, Italy; [2]City Unity College, Athens, Greece; [3]POLYPHENO S.r.l., Accredited Spin Off, University of Bari Aldo Moro, Bari, Italy; [4]Department of Interdisciplinary Medicine, School of Medicine, University of Bari Aldo Moro, Bari, Italy; [5]Faculty of Medicine, Prishtina, University of Prishtina "Hasan Prishtina", Kosovo; [6]Faculty of Dentistry, University of Medicine, Tirana, Albania

Received September 6, 2018 – Accepted October 22, 2018

Dental plaque is a biofilm which forms on the non-shedding surfaces of the oral cavity. If left untreated, the succession of dental plaque development can lead to serious complications, such as caries, gingivitis, and periodontitis. The control of dental plaque on tooth surfaces is vital for the prevention of dental plaque related diseases. In this context, antimicrobial agents may serve as a valuable complement to mechanical plaque removal. Therefore the present study was aimed to evaluate the action of a combined rinsing solution containing different antimicrobials (sea salt, xylitol and lysozyme) used individually, for the reduction of a salivary specific bacteria *(S. mutans)* colonizing oral environment.

To the Editor,

It is generally accepted that the development of dental plaque surrounding the tooth/gingiva interface is one of the major causes of gingival inflammation and caries (1-3). Chemical methods of reducing plaque, such as mouthwashes, are therefore appealing as they can provide significant benefits to patients who cannot maintain adequate mechanical plaque control (4, 5). Various chemical mouthwashes are available on the market, but are associated with side-effects such as immediate hypersensitivity reactions, toxicity, tooth staining, etc. (6).

Several studies have shown that natural products i.e. polyphenols and xylitol have biological activity most notably as a constituent of dietary products (2, 7). Frequent use of xylitol chewing gum has been shown to prevent caries, biofilm formation and *Streptococcus mutans (S. mutans)* level in the oral micro-environment. A wide range of experiments *in vitro* has shown that the majority of oral microorganisms cannot metabolise xylitol to acidic products (2, 5, 6). Nevertheless, xylitol in the forms of chewing gum and candies may not be practical for young children or elderly adults. In these situations, an aqueous solution or mouthrinse may be useful. However, clinical evidence of the efficacy of xylitol in mouthrinses is very limited (2).

Therefore, the aim of the present study was to compare the plaque control efficacy of the new formula H2Ocean Sea Salt Mouthwash on salivary

Key words: gingivitis, randomised controlled trial, Streptococcus mutans

Mailing address:
Dr Stefania Cantore,
University of Bari Aldo Moro,
P.zza Giulio Cesare, 11,
70124, Bari, Italy.
Tel./fax: +39 0805448514.
e-mail: stefaniacantore@pec.omceo.bari.it

0393-974X (2018)

DISCLOSURE: ALL AUTHORS REPORT NO CONFLICTS OF INTEREST RELEVANT TO THIS ARTICLE.

S. mutans count, plaque and gingival scores of young adults.

MATERIALS AND METHODS

Subjects and study schedule

The present study was conducted at the Dentist Education Institute in collaboration with the Dental Institute of the City Unity College, Greece, from February 2018 to June 2018 as a double-blind parallel-group clinical trial. Twenty gingivitis patients between the ages of 18 and 25 years were enrolled in the study and all gave written informed consent in accordance with the Declaration of Helsinki .

The patients received a verbal description of the clinical protocol to be followed, and in order to have unbiased and accurate clinical data, a double-blind protocol was followed for enrolment of the patients in terms of treatment plan and further categorization into the study group. All the enrolled patients underwent scaling and polishing to get the baseline score to nil.

All the subjects were advised to brush twice daily for 5 min using a modified bass technique (which was demonstrated to each subject). Medium bristle tooth brushes and tooth paste were provided to each subject during the study course to maintain standardization.

Sample size and blinding

The subjects were then categorized into two treatment regime groups in groups. Group I (n = 10): combined mouth rinse containing sea salt and xylitol (H2Ocean Sea Salt Mouthrinse, a new mouthwash formula that contains sea salt, xylitol and lysozyme with no harsh chemicals, alcohol or fluoride). Group II (n = 10): placebo mouth rinse (physiologic saline solution - no mouthwash dilution added).

Subjects in both groups were instructed to rinse their mouth with 10 ml of mouthwash twice daily (for the first 30 days, then once per day for the following 60 days), after breakfast and again after lunch for 60 days for 1 min, and not to rinse with water thereafter for the following 30 min. Both the mouth rinses had similar bottle appearance.

Inclusion criteria

Patients aged between 18 and 25 years, and suffering from gingivitis with good to fair oral hygiene were selected for the study.

Exclusion criteria

Patients who presented less than 20 sound permanent teeth with a minimum of 5 teeth present in each arch quadrant, or who had received antibiotics or nonsteroidal antiinflammatory drugs (such as Ibuprofen) in the previous 9–11 weeks or periodontal treatment in the previous 6 months; pregnancy or breast-feeding; presenting artificial prosthesis; smoking or tobacco consumption in any form; suffering from any systemic diseases; female patients using intrauterine birth control devices or birth control pills; and subjects not willing to participate in the study.

Table I. *Baseline characteristics of study population.*

Population	Group 1	Group 2	Total
Total participants (N)	10	10	20
Males	4	3	7
Females	6	7	13
Mean age(years)	23.7	22.1	p = 0.29
Mean DMFT	2.16	2.18	p = 0.184

Clinical parameters

Clinical Recording Protocol Clinical parameters evaluated were gingival index (GI) and plaque index (PI), by the same blinded trained examiner at baseline and 30, 60 and 90 days. The measurements were recorded of central incisors, canines and second premolars of four quadrants (8). A mean value of each parameter was calculated in each pre- and post-rinse measurement.

Microbiologic examination

For microbial evaluation, saliva samples were collected by chewing on a piece of sterile paraffin wax in order to test whether there were variations in the numbers of bacteria due to the laboratory methods. A paired cultivation of 20 samples was carried out. Samples were transferred to the Microbiology Laboratory of University of Bari Aldo Moro, Italy, for further processing. The transport of samples to the lab was done via express courier and the use of tryptic-soy-serum-bacitracin-vancomycin transport media, and the samples were analyzed within 24 h (4). Then, 50 µL of the specimen were cultured on blood agar. After 48-hr incubation at 37°C, colony counts were enumerated. Total bacterial count was determined by visual counting and the latter was multiplied by 20 to express as colony forming units (CFU)/mL.

Statistical analysis

The statistical analyses were performed by using Two-way ANOVA, and Tukey's multiple comparisons test were performed to assess statistical differences using the GraphPad Prism software (version 7.0; San Diego, California, USA). The probability (p) of <0.05 was considered to indicate statistical significance.

RESULTS

The baseline characteristics of all the subjects who participated in the study are shown in Table I.

Clinical measurements

The clinical results were encouraging, and patients provided positive feedback on the use of this protocol. All subjects (N = 20) completed the trial, and there were no missing values. The amounts of mouthwashes used indicated good compliance with the instructions. No adverse events or side effects were reported or observed. The plaque and gingival scores for the test and control groups at the end of the experimental period are shown in Fig. 1 A-B.

Microbiologic examination

As reported in Table II, the mean reduction in colony forming units, before brushing and after H2Ocean Sea Salt Mouthwash were 87.5% and 32.5%, respectively, with a highly significant difference of 55.0% ($P<0.001$). Large variations in inter- and intra-individual measurements were observed. Both examinations showed a significant decrease from the baseline.

Compliance

Compliance with the course of the intake of the tested product from the participants was also documented. All subjects returned the medication bottles. All subjects from both groups (100%) completed the course of mouthwash protocol as indicated.

Table II. *Colony-forming units (CFUs) before and after treatment.*

	Before	**After**	**Difference**
Range	65-110	25-40	-
Mean	87.5	32.5	55.0
"p" Value	-	-	<0.001

A

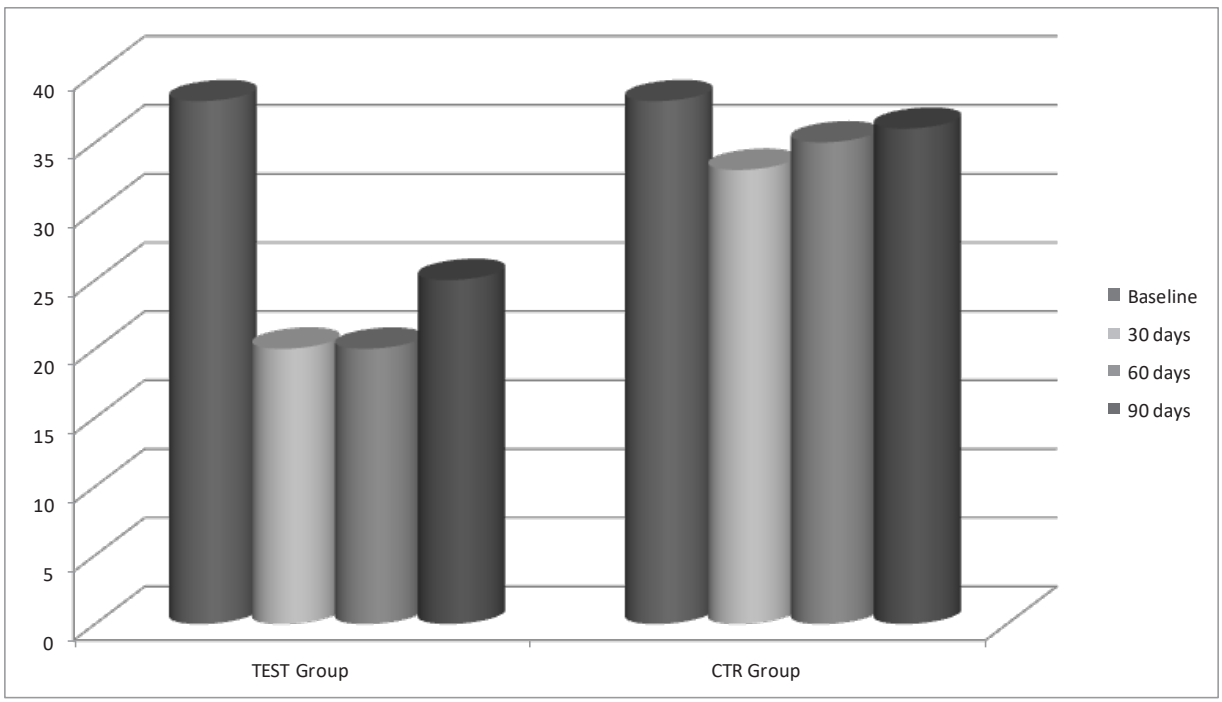

B

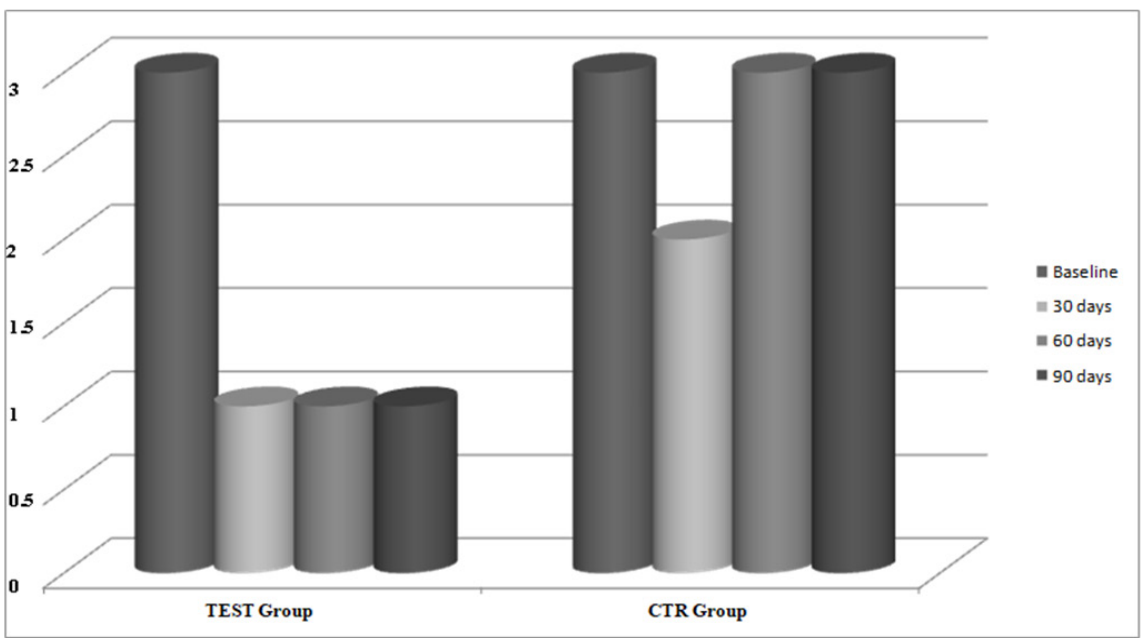

Fig. 1. *Plaque (**A**) and Gingival (**B**) scores for the test and control groups at the end of the study period.*

DISCUSSION

Microbial biofilms are complex communities of bacteria present in the environment and human body (1). If not removed regularly and adequately, dental plaque matures into a pathogenic bacterial complex which can lead to caries, gingivitis, periodontitis and peri-implantitis, ultimately resulting in impaired oral function (9-11).

Although different mechanical tooth cleaning methods are considered the most reliable means of plaque control worldwide, various chemotherapeutic agents have always been sought as adjuvants (4). Thus, mouth rinses are frequently recommended for chemical control of dental biofilm, especially in areas which are inaccessible to tooth brushing (3).

The findings of the present study are in accordance with Shyama et al. (12) who assessed the effect of xylitol candies on gingival indices in physically disabled pupils, and discovered a statistically significant reduction in gingival index scores of the study participants when they consumed xylitol candies thrice daily.

However, this research was a relatively short clinical study and the findings may be different to a prolonged one. Studies of longer duration with cross-over study design and wash-out period in gingivitis patients would have been more authenticating as they would eliminate the bias of viable host relating to the use of H2Ocean Sea Salt Mouthwash. Finally, it should be noted that natural agents such as mouth rinses are not substitutes for through brushing and flossing, but they should be used as adjunct.

A larger-scale, longer-term clinical trial using mouthwashes is needed which could demonstrate the feasibility of H2Ocean Sea Salt Mouthwash in different populations with different dietary and oral hygiene patterns, and establish the minimum daily frequency of use.

REFERENCES

1. Marsh PD. Dental plaque as a biofilm: The significance of pH in health and caries. Compend Contin Educ Dent 2009; 30:76-78.
2. Council on scientific Affairs. Acceptance Program Guidelines - Chemotherapeutic Products for Control of Gingivitis. [Internet]: ADA. [Last accessed on 2018 Jul 23]. Available from: http://www.ada.org/sections/scienceAndResearch/pdfs/guide_chemo_ging.pdf .
3. Gunsolley JC. A meta-analysis of six-month studies of antiplaque and antigingivitis agents. J Am Dent Assoc 2006; 137:1649-57.
4. Cantore S, Ballini A, Mori G, et al. Anti-plaque and antimicrobial efficiency of different oral rinse in a 3-days plaque accumulation Model. J Biol Regul Homeost Agents 2016; 30:1173-78.
5. Davey ME, O'Toole GA. Microbial biofilms: from ecology to molecular genetics. Microbiol Mol Biol Rev 2000; 64:847-67.
6. Gupta P, Gupta N, Prakash A, Birajdar S, Natt A, Singh H. Role of sugar and sugar substitutes in dental caries: a review. ISRN Dentistry 2013; 2013:1-5.
7. Tatullo M, Simone GM, Tarullo F, et al. Antioxidant and antitumor activity of a bioactive polyphenolic fraction isolated from the brewing process. Sci Rep 2016; 27: 36042.
8. Ballini A, Scattarella A, Crincoli V, et al. Surgical treatment of gingival overgrowth with 10 years of follow-up. Head Face Med 2010; 6:19.
9. Lovreglio P, Bukvic N, Fustinoni S, et al. Lack of genotoxic effect in workers exposed to very low doses of 1,3-butadiene. Arch Toxicol 2006; 80:378-81.
10. Dohan Ehrenfest DM, Del Corso M, Inchingolo F, Charrier JB. Selecting a relevant in vitro cell model for testing and comparing the effects of a Choukroun's platelet-rich fibrin (PRF) membrane and a platelet-rich plasma (PRP) gel: tricks and traps. Oral Surg Oral Med Oral Pathol Oral Radiol Endod 2010; 110:409-11.
11. Ballini A, Tetè S, Scattarella A, et al. The role of anti-cyclic citrullinated peptide antibody in periodontal disease. Int J Immunopathol Pharmacol 2010; 23:677-81.
12. Shyama M, Honkala E, Honkala S, Al-Mutawa SA. Effect of xylitol candies on plaque and gingival indices in physically disabled school pupils. J Clin Dent 2006; 17:17-21.

LETTER TO THE EDITOR

SERUM 25-HYDROXY VITAMIN D LEVELS IN ESSENTIAL HYPERTENSION

T. GRANATO[1], E. ANASTASI[2], V. VIGGIANI[2], F. OCCHIUZZI[3], A. ANGELONI[4], R. GRADINI[4] and M. SUPPA[3]

[1]CNR-IBPM, National Research Council, Rome. Italy; [2]Department of Molecular Medicine, "Sapienza" University of Rome, Italy; [3]Emergency Department, "Sapienza" University of Rome, Italy; [4]Department of Experimental Medicine" Sapienza" University of Rome, Italy

Received June 21, 2018 – Accepted October 29, 2018

Vitamin D may have prognostic value in hypertension patients and, in addition to conventional biomarkers, could be a valuable tool for disease management. The aim of this study was to assess the association of vitamin D status in patients with essential hypertension and to evaluate its prognostic utility. Forty-eight consecutive patients (40 Caucasian and 8 Asian) aged between 30 and 80 years (mean 61.5, range 34-84 years), were enrolled in the study. The main exclusion criteria were age < 18 years, kidney failure, onco-hematologic disease, hypo-hyperparathyroidism, osteoporosis, treatment with bisphosphonate or 25(OH) vitamin D supplementation. Of the 48 patients included in the study, hyperlipidemia was described in 28, diabetes type 2 in 8, and ischemic heart disease in 14. Serum electrolytes, calcium, sodium, and potassium concentrations were within normal range. Low 25(OH) vitamin D levels inversely correlated with essential hypertension values ($p < 0.001$) were considered extremely significant. The determination of 25(OH) vitamin D levels in patients with essential hypertension could improve the research for possible underlying conditions, which should be managed meticulously according to current guidelines.

To the Editor,

For decades, 25(OH) vitamin D has been considered a dynamic steroid hormone exerting its action as a transcription factor regulating the expression of various genes (1). Vitamin D is a cluster of fat-soluble molecules analogous to steroids. Numerous forms of vitamin D exist; cholecalciferol (or vitamin D3) is synthesized in reaction to ultraviolet (UV) irradiation of the skin consequential to the photochemical cleavage of 7-dehydrocholesterol, a precursor of cholesterol in the skin. A second form of vitamin D, ergocalciferol (or vitamin D2), is formed by irradiation of ergosterol, a membrane sterol found in the Ergot fungus. Nutritional sources of vitamin D comprise fish oils (D3), egg yolks (D3), and mushrooms (D2), as well as unnaturally prepared cereals and dairy products (D2 or D3). Epidemiological studies established improved risks of chronic morbid disorders with lower levels of serum 25-OH D. More recently, 25(OH) vitamin D deficiency has been considered as an independent risk factor for cardiovascular disease and mortality in the general population. Biologic effects of 25(OH) vitamin D result largely from its binding to the nuclear steroid hormone 25(OH) vitamin D receptor (VDR), which is found in almost all tissues and is closely related to the thyroid, retinoid, and peroxisome proliferator-activator receptors. While all 25(OH) vitamin D metabolites bind the VDR, most biological effects are probably mediated by calcitriol

Key words: hypertension, 25(OH) vitamin D, biomarkers, diagnosis

Mailing address:
Dr Teresa Granato,
CNR-IBPM,
National Research Council
Viale Regina Elena 324, 00161 Rome, Italy
Tel.: +39 0649970317
e-mail: teresa.granato@uniroma1.it

0393-974X (2018)

DISCLOSURE: ALL AUTHORS REPORT NO CONFLICTS OF INTEREST RELEVANT TO THIS ARTICLE.

because of its greater receptor similarity(2). Vitamin D plays a considerable function in the physiology of the cardiovascular system and its insufficiency has been allied to extensive complications, such as cardiovascular events, hypertension, obesity, metabolic syndrome, type 2 diabetes, immune disorders and numerous types of cancer (3,4). The indisputable potential inverse relationship between vitamin D deficiency and elevated blood pressure (BP) suggests involvement of vitamin D metabolism in the pathogenesis of hypertension. A cause-and-effect relationship is hypothesized on the source of the key modulating effects of 25(OH) vitamin D on the Renin-Angiotensin-Aldosterone System (RAAS) axis whereby 25(OH) vitamin D deficiency may promote sustained RAAS activation, whereas sufficient levels may afford "endogenous" proximal inhibition. Population studies demonstrate an unequivocal association between vitamin D deficiency and the prevalence of many chronic morbid conditions, including cardiovascular disease (CVD) and its risk factors (5, 6). Notable examples include the third National Health and Nutrition Examination, as well as large European cohorts that showed a cross-sectional inverse relationship between 25-OH D levels and the prevalence of hypertension, insulin resistance, type 2 diabetes mellitus (DM), and dyslipidemia. 25(OH) Vitamin D deficiency has been implicated as an independent risk factor for the prospective development of CVD and hypertension or its risk factors (7). The objective of this study was to assess the association of 25(OH) vitamin D status in patients with hypertension and to evaluate its prognostic utility.

MATERIALS AND METHODS

Study population

Between November 2015 and March 2016, 48 consecutive outpatients (40 Caucasian and 8 Asian), aged between 30 and 80 years (mean 61.5, range 38-84 years), were enrolled in the study. The evaluation was performed in compliance with the Declaration of Helsinki. Written informed consent was given by all patients whose samples were used in all parts of this evaluation. In order to decrease the risk of possible bias, in 25(OH) vitamin D due to different latitude and global solar radiation on the ground, only patients who had been living in Rome for at least 1 year before blood collection were chosen. In addition, all patients underwent blood sampling in the same season (winter period).

Exclusion criteria included, chronic diseases, coeliac disease or other causes of malabsorption or any disorder that may impact calcium or vitamin D metabolism (hepatic, parathyroid and renal dysfunction).

The patients were divided into two subgroups, females (n=12) and males (n=36), respectively. The main exclusion criteria were age<18 years, kidney failure, onco-hematologic disease, hypo- hyperparathyroidism, hypo/hyperthyroidism, osteoporosis, treatment with bisphosphonate or 25 (OH) vitamin D supplementation.

The clinical characteristics of the patients included in

Table I. *Patient characteristics.*

	Female (n. 12)	**Male (n. 36)**
Type 2 Diabetes	2	6
CAD	2	10
Hypercholesterolemia	10	18

the study are described in Table I. On enrolment, medical history was taken and peripheral blood samples were taken from all patients and immediately sent for analysis of the serum levels of 25(OH) vitamin D.

Sample collection

Blood samples were drawn immediately after admission by direct venipuncture of an antedecubital vein, applying a minimum of stasis. Laboratory tests were carried out on the serum concentration of 25(OH) vitamin D of all patients.

25-OH Vitamin D determination

25(OH) Vitamin D levels were measured with the Lumipulse® G1200 (Fujirebio, Japan), an automated assay system that allows quantitative measurements in specimens and is based on chemiluminescent enzyme immunoassay (CLEIA) technology. Lumipulse® G1200 uses a novel two-step sandwich method (Innogenetics-Fujirebio, Belgium). The assay utilizes a solid-phase and alkaline phosphatase (ALP)-labeled monoclonal antibodies immobilized on the particles that specifically bind to the analyte, forming antigen–antibody immunocomplexes. Particles are then washed and rinsed in order to remove unbound materials. ALP-labeled monoclonal antibody specifically binds to the antigen of the immunocomplexes. After a second wash, substrate solution is added. Adamantyl-1,2-dioxetane phosphate (AMPPD) contained in the substrate solution is dephosphorylated by the catalysis of ALP indirectly conjugated to the particles. A luminescent signal is generated by the cleavage reaction of dephosphorylated AMPPD and reflects the amount of antigen in the sample. The cut off value between sufficient and insufficient 25(OH) vitamin D was chosen corresponding to 20.2 ng/mL, according to the WHO.

Statistical analysis

All analyses were performed using MedCalc® statistical software version 15.8. (MedCalc Software bvba, Ostend, Belgium).

RESULTS

In this study patients showed the following characteristics: 58.3% (28 patients) had

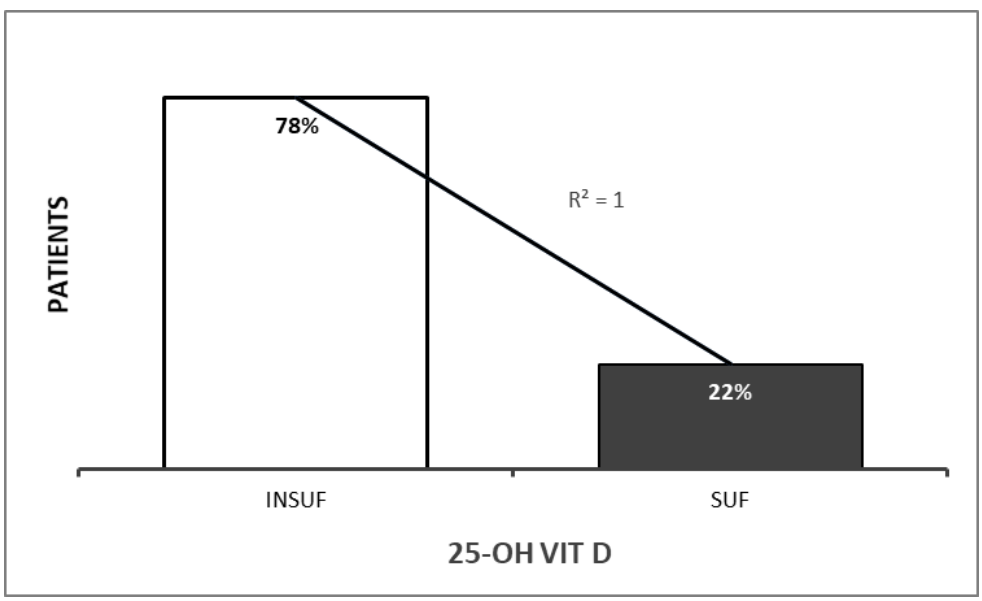

Fig. 1. *White bar represents the percentage of patients with insufficient level of 25-OH Vitamin D. Black bar represents the percentage of patients with insufficient level of 25-OH Vitamin D (P = 0.0001 considered extremely significant).*

hypercholesterolemia,16.6% (8 patients) diabetes mellitus type 2 and 25% (12 patients) with coronary artery disease; all 48 patients included in the study presented hypertension.

Deficiency of 25-OH- vitamin D was observed in 78% of these patients. Figs. 1 and 2 show the good correlation of deficiency of 25-OH vitamin D levels *vs* the presence of hypertension (p=0.0001). No relationship was found between 25-OH vitamin D concentrations and sex, age, diabetes, dyslipidemia or cardiovascular disease.

In addition, the evaluation of biochemical parameters showed that serum electrolytes, sodium, potassium, calcium levels were within normal range.

DISCUSSION

The association of vitamin D status and hypertension is particularly solid. Both controlled trials and meta-analyses have revealed a protective effect of high calcium intake for both pregnancy-related and essential hypertension (8, 9), but risk for incident hypertension is inversely associated to antecedently calculated serum 25(OH)D concentration (10).

Experimental studies sustain the notion that 25(OH) vitamin D exerts anti-hypertensive effects and has a positive impact on the overall cerebrovascular risk profile and on stroke outcome. Some small randomized controlled trials (RCTs) have already shown a modest blood pressure decrease by vitamin D treatment, but this has not been consistently observed in all studies. Published RCTs did not show a significant 25(OH) vitamin D effect on stroke incidence but have not been properly considered to address this issue (11). While the data is promising on potentially 25(OH) vitamin D effects on arterial hypertension and cerebrovascular disease, it should also be pointed out that patients with arterial hypertension and stroke are at moderately high risk for 25(OH)vitamin D deficiency and those with linked musculoskeletal diseases. This final consideration can provide a motivation for the assessment, prevention and treatment of 25(OH) vitamin D deficiency in individuals with arterial hypertension and stroke. Numerous mechanisms have been proposed on how vitamin D could be implicated in blood pressure regulation and the pathophysiology of arterial hypertension which is a major risk factor for stroke. 25(OH) vitamin D effects on the Renin-Angiotensin-Aldosterone System (RAAS) have been extensively investigated

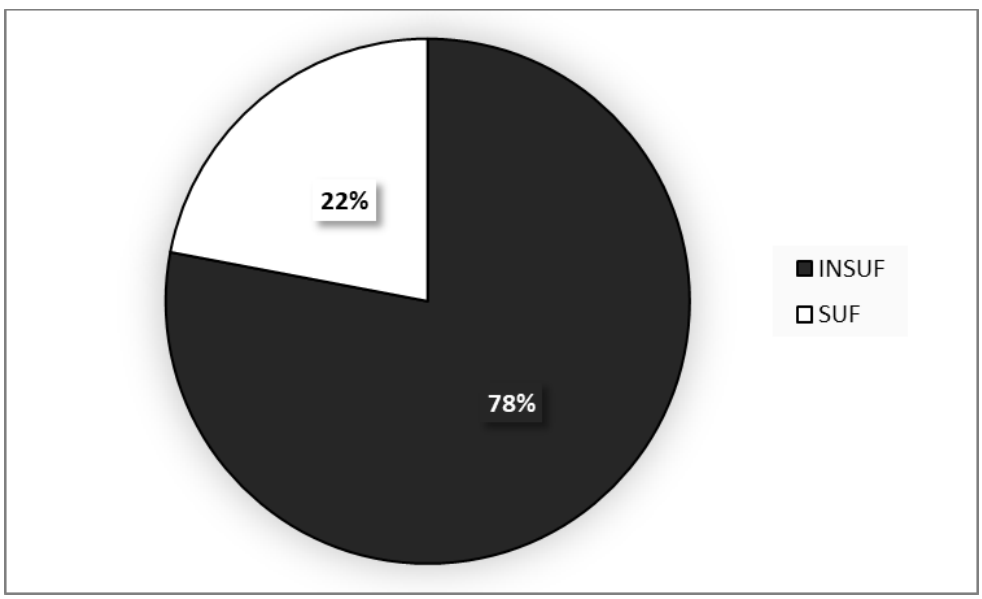

Fig. 2. *Distribution of 25(OH) vitamin D in patients with essential hypertension.*

by experimental studies. VDR knockout mice show an increased rennin expression, arterial hypertension and myocardial hypertrophy (12). Further studies established the molecular mechanisms by which VDR activation down-regulates renin expression, but it is not clear whether these important effects observed *in vitro* are also of relevance *in vivo*, in a clinical setting (13).

One study was conducted by Vimal Karan et al. at the Institute of Child Health at University College, London. Researchers acquired and analyzed data provided by D-CarDia collaboration based on 35 studies involving more than 155,000 people and several centers in Europe and North America. The data collected showed that those with high 25(OH) vitamin D concentrations had low blood pressure and therefore a reduced risk of hypertension. The study showed that there is a cause/effect relationship between the concentration of Vitamin D in blood and blood pressure values: high (or regular) levels of 25(OH) vitamin D, equal to low or standard blood pressure; low levels of vitamin D lead to high blood pressure or hypertension

As reported in The Lancet Diabetes & Endocrinology, the researchers found that for each 10% increase in the 25(OH)vitamin D concentration, diastolic blood pressure was reduced by 0.29 mmHg (-0.52 to -0.07; p = 0.01) and systolic pressure was 0.37 mmHg (-0.73 to 0.003, p = 0.052). Moreover, for each increase of 10% in 25(OH) vitamin D there was a decrease of 8.1% (OR 0.92, 0.87-0.97, p = 0.002) of the probability of developing hypertension (14, 15).

An inappropriate increased activation of the Renin-Angiotensin-Aldosterone (RAAS) system has been reported in VDR and 1α-hydroxylase knockout mice. These animals developed hypertension and myocardial hypertrophy even after the normalization of calcium homeostasis. Instead, blocking the RAAS system with ace inhibitors normalized blood pressure and heart abnormalities, similar to 25 (OH)vitamin D treatment. The molecular effects of 25(OH)vitamin D on RAAS were also clarified by the finding that the VDR ligand suppresses the expression of renin, by linking to CREB (cAMP-response element-binding protein). As a result, stimulation of renin transcription is inhibited because CREB is no longer able to stimulate transcription, binding to cAMP response elements in the renin gene promoter region: hypertensive renin activity was inversely associated with the levels of 25 (OH) vitamin D (16, 17).

In several studies, after treatment, decreased renin and angiotensin II levels were observed. In addition, the vitamin's protective effects on the kidneys are also related to its ability to counteract the loss of podocytes and reduce their hypertrophy, but also to suppress the proliferation of mesangial cells. All this would be a valid antagonism to the development of arterial hypertension, especially in the course of renal failure.

Our findings, according to latest scientific observations, show that low levels or 25(OH) vitamin D can be a risk factor for CVD development. This data is reinforced by the close association of inverse correlation between the values of blood pressure and the blood concentration of 25(OH) vitamin D. The estimation of 25(OH) vitamin D levels in combination with hypertension could develop research for possible underlying conditions which should be managed meticulously according to current guidelines to improve the clinical outcome.

The results of this study highlight the role of Vitamin D as a possible modifiable risk factor for CVD and its symptoms, although a cause-effect relationship is not yet clear.

Further studies are needed to confirm this association, also in order to suggest vitamin D supplementation in selected subjects with insufficiency/deficiency of the vitamin associated with symptomatic hypertension. Multicenter randomized controlled studies must be conducted to identify the safe dose of vitamin D before recommending vitamin D supplementation for these patients.

ACKNOWLEDGEMENTS

This study was supported by the University of Rome Sapienza. The Authors are grateful to Giuseppina Gennarini, Barbara Colaprisca and Silvestra Tudini for their excellent technical assistance.

REFERENCES

1. Holick MF. Vitamin D Deficiency. N Engl J Med 2007; 57:266-81.
2. Adams JS, Hewison M. Update in vitamin D. J Clin Endocrinol Metab 2010; 95:471-78.
3. de Boer IH, Kestenbaum B, Shoben AB, Michos ED, Sarnak MJ, Siscovick DS. 25-hydroxyvitamin D levels inversely associate with risk for developing coronary artery calcication. J Am Soc Nephrol 2009; 20:1805-12.
4. Al MheidI RS, Quyyumi AA. Vitamin D and cardiovascular disease: controversy unresolved. J Am Coll Cardiol 2017; 4:70:89-100.
5. Al Mheidl RS, Patel V, Tangpricha A, Quyyumi AA. Vitamin D and cardiovascular disease: is the evidence solid? Eur Heart J 2013; 34:3691-98.
6. Anastasi E, Suppa M, Viggiani V, Tartaglione S, Angeloni A, Granato T. Serum 25-hydroxy vitamin D concentration in acute coronary syndrome. J Biol Regul Homeost Agents 2017; 31(3):823-27.
7. Anastasi E, Capoccia D, Granato T, et al. Assessing the association between 25-OH vitamin D levels and ROMA score in a population of obese women. J Biol Regul Homeost Agents 2016; 30(4):1165-71.
8. Anderson JL, May HT, Horne BD, et al. Inter mountain Heart Collaborative (IHC) Study Group. Am J Cardiol 2010; 106(7):963-68.
9. Burgaz A, Orsini N, Larsson SC, Wolk A. Blood 25-hydroxyvitamin D concentration and hypertension: a meta-analysis. J Hypertens 2011; 4:636-45.
10. Vimaleswaran S, Cavadino A, Berry DJ, et al. +97 additional authors. Association of vitamin D status with arterial blood pressure and hypertension risk: a mendelian randomisation study. The Lancet Diabetes Endocrinol 2014; 2:719-29.
11. Shin JH, Lee HT, Lim YH, et al. Defining Vitamin D deficiency and its relationship to hypertension in postmenopausal Korean women. J Womens Health (Larchmt) 2015; 24(12):1021-29.
12. Forman JP, Giovannucci E, Holmes MD, et al. Plasma 25-hydroxyvitamin D levels and risk of incident hypertension. Hypertension 2007; 49:1063-69.
13. Wang TJ, Pencina MJ, Booth SL, et al. Vitamin D deficiency and risk of cardiovascular disease. Circulation 2008; 117:503-11.
14. Binkley N, Krueger D, Cowgill CS, et al. Assay variation confounds the diagnosis of hypovitaminosis D: a call for standardization. J Clin Endocrinol Metab 2004; 89:3152-57.
15. Li YC . Molecular mechanism of vitamin D in the cardiovascular system. J Investig Med 2011; 59:868-71.
16. Vaidya A, Williams JS. Vitamin D in the pathophysiology of hypertension, kidney disease, and diabetes: examining the relationship between Vitamin D and the renin-angiotensin system in human diseases. Metabolism 2012; 61(4):450-58.
17. Yang T, Xu C. Physiology and pathophysiology of the intrarenal renin-angiotensin system: an update. J Am Soc Nephrol 2017; 28(4):1040-49.

LETTER TO THE EDITOR

SPIDER ZYGOMA: A NEW IMPLANT REHABILITATION TECHNIQUE FOR ATROPHIC MAXILLA

M. ZANNA[1], M. MASCITTI[2], E. COCCIA[2], L. LO MUZIO[3] and A. SANTARELLI[2,4]

[1]"Casa di cura E. Montanari" Private Hospital, Morciano di Romagna, Italy; [2]Department of Clinical Specialistic and Dental Sciences, Marche Polytechnic University, Ancona, Italy; [3]Department of Clinical and Experimental Medicine, University of Foggia, Foggia, Italy; [4]National Institute of Health and Science of Aging, INRCA, Ancona, Italy

Received June 18, 2018 – Accepted September 4, 2018

Atrophic maxilla is a challenge in dental implant surgery, and new strategies are needed. We present a new minimally-invasive approach, called "Spider Zygoma", consisting of implant-supported prosthesis with the addition of customized maxillofacial plates and screws on surface of zygomatic bone. A 3D-model of the edentulous upper jaw was used as preoperative model. Two customized bone plates were created and used as guide for placement of implants and zygomatic screws. Although this is only a pilot study, this new surgical technique seems to be safe and accurate, confirmed by the maintenance of good aesthetic and functional results after 5-year follow-up.

To the Editor,

Implant-based rehabilitation has shown high long-term success rate, but one of the current challenges remains the treatment of patients with atrophic maxilla. This condition is not unusual, due mainly to pneumatization of maxillary sinus and alveolar resorption (1).

To solve this problem, the use of several surgical procedures and materials for ridge augmentation have emerged (2). Despite maxillary sinus augmentation procedures have proven to be effective, a range of adverse events were reported. Furthermore, a major contraindication is the presence of pathological processes in maxillary sinuses (3). Regarding the use of specific implant strategies, zygomatic implants have provided a solution for treatment of extremely atrophied maxilla as an alternative to sinus augmentation or bone graft (4). Unfortunately, this procedure is significantly more invasive and is associated with several types of complications, such as maxillary sinus infection and ocular complications (5). The necessity for less invasive and, therefore, less risky surgical technique has led to the development of new implant strategies, such as tilted implants and mini-implants (2). These techniques have proven to have a good load distribution and a significative reduction of the stress level in immediate loading rehabilitation of edentulous jaw (6). The major limitation is the lack of long-term survival analysis and comparative studies between mini-implants and standard implants (2).

With the aim of continuing the path of minimally-invasive strategies and better distribution of occlusal forces, we have developed a new solution to provide further bone support. In this report we present a case of severely resorbed upper jaw, which was treated

Key words: dental implants, zygomatic implants, atrophic maxilla, bone plates, new technique

Mailing address:
Prof. Andrea Santarelli.
Via Tronto 10,
60126 Ancona, Italy
Tel.: +39 071 2206226
Fax: +39 071 2206221
e-mail: andrea.santarelli@staff.univpm.it

0393-974X (2018)

DISCLOSURE: ALL AUTHORS REPORT NO CONFLICTS OF INTEREST RELEVANT TO THIS ARTICLE.

using a minimally-invasive approach, called "Spider Zygoma", consisting of implant-supported prosthesis with the addition of customized maxillofacial plates and screws on surface of zygomatic bone (Fig. 1, A-B).

Case report

A 56-year-old Caucasian female presented to "Casa di cura E. Montanari" Private Hospital with the desire "to solve her dental problem". Indeed, the patient was not satisfied with the dental function and appearance of her denture. Her medical history included the diagnosis of bilateral chronic hyperplastic sinusitis starting 3 years previously. She did not smoke or consume alcohol. On clinical examination, the patient showed maxillary total edentulism and a fixed complete denture in the mandible. The patient stated that she had been edentulous in the upper jaw for about 10 years. The removable maxillary denture showed lack of retention due to severe atrophy. Upon clinical and computed tomography (CT) evaluation, the maxilla was classified ACP PDI for Complete Edentulism Class III. The patient was informed about surgical alternatives and the "Spider Zygoma" procedure and provided written consent. A 3D model of the edentulous maxillary arch and the surrounding bone was made and used as the preoperative model. CAD/CAM technology was used to create two customized bone plates (Fig. 1, C-D). A total of 16 implants (GiEsse Technology srl, Cogoleto, Italy) were placed using the following protocol ("Spider Zygoma" protocol). After supra-crestal incision, four 2.9 x 8 mm implants and four 2.9 x 6 mm implants were placed in the maxilla and torqued to 40 Ncm (Fig. 2, A-B). Furthermore, six 2.9 x 6 mm implants and two 2.7 x 11 mm zygomatic screws were placed from the maxillary premolar area to the zygomatic surface, using the customized titanium bone plates (35 x 1 mm) as guides. The implants were torqued to 60 Ncm, and the connection between plates and implants was ensured by interference fit (Fig. 2C-D). After suturing the soft tissues, the maxillary denture was inserted and, after occlusal adjustment, was fixed with prosthetic retaining screws (Fig. 2, E-F).

The patient was given proper oral hygiene instructions and scheduled for follow-up every 3 months. At the follow-up appointments, there were no discernable clinical or radiographic changes

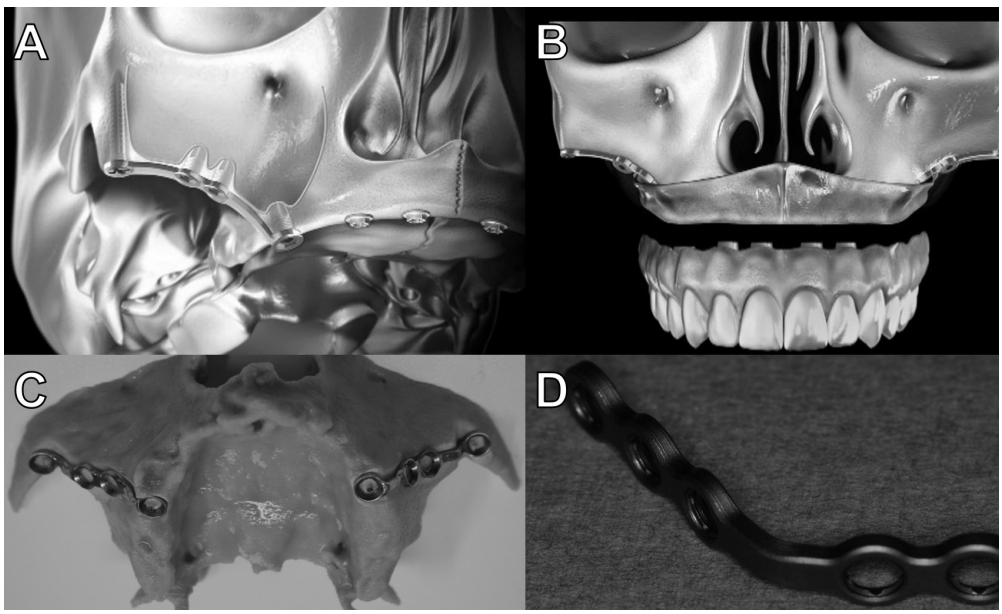

Fig. 1. ***A, B****) Spider Zygoma treatment concept, using customized titanium plates and screws on surface of zygomatic bone.* ***C****) 3D model of the edentulous maxillae and (****D****) customized titanium bone plates.*

around the dental implants. Furthermore, bone formation at the maxillary sinus floor following implants placement was observed, as highlighted by transparent 3D CT image protocol (Fig. 3, A-B). After a 5-year follow-up period, the patient maintained a good aesthetic and functional result.

DISCUSSION

To date, the major limitation in maxillary rehabilitation with dental implants is the lack of bone volume, due to the resorption of the alveolar process and the pneumatization of the maxillary sinuses (1). Furthermore, several reports demonstrate low bone density in maxilla (7, 8). Several surgical techniques have been proposed to overcome these limitations in severely atrophied upper jaws: elevation of the sinus floor, bone grafting, and zygomatic implants. Sinus lift surgery was avoided due to the presence of bilateral chronic sinusitis, considered a contraindication (3). The use of bone grafting was avoided as the patient was uncomfortable with the exploitation of extraoral sites. Regarding the use of zygomatic implants, several disadvantages were considered, such as the invasiveness of this approach and the risk of severe complications (5, 9). To increase the support surface area, thus providing a better distribution of occlusal forces, we developed the Spider Zygoma protocol, consisting of using two custom-made titanium plates, fixed on both zygomatic surfaces with screws. Spider Zygoma offers a series of advantages: i) a less invasive surgical procedure; ii) a lower risk of complications; and iii) the use of cortical screw anchorage of zygomatic bone (10).

In conclusion, this new surgical technique seems to be safe and accurate, confirmed by the

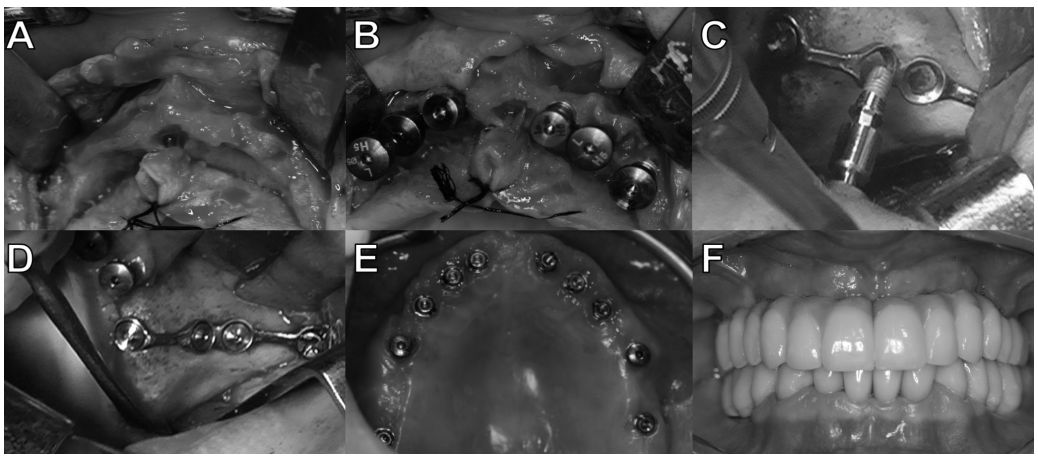

Fig. 2. *Surgical steps of Spider Zygoma protocol. **A**) Supra-crestal incision, (**B**) implant placement, (**C**, **D**) placement of implants, zygomatic screws, and bone plates from maxillary premolar area to zygomatic surface, (**E**, **F**) prosthodontic phases.*

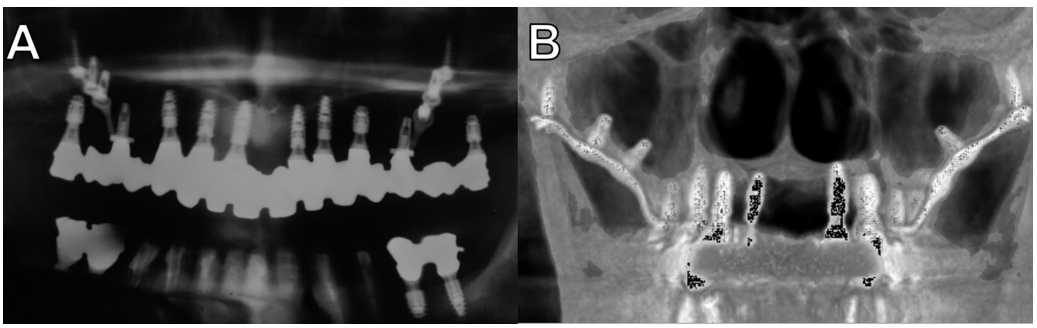

Fig. 3. *A) Panoramic radiograph after implant placement. **B**) Transparent 3D CT image protocol highlights bone formation at the maxillary sinus floor.*

absence of clinical or radiographic changes and the maintenance of good aesthetic and functional results after a 5-year follow-up. However, due to the novelty of this technique, we take a cautious approach, using a greater number of implants in the distal area. Future prospective studies are needed to compare this technique with other well-established implant strategies, especially with zygomatic implants. Indeed, recent development in zygomatic implant protocols makes this technique less susceptible to complications (11, 12). For these reasons, other spatial configurations of the Spider Zygoma system will need to be studied.

REFERENCES

1. Sorni M, Guarinos J, Garcia O, Penarrocha M. Implant rehabilitation of the atrophic upper jaw: a review of the literature since 1999. Med Oral Patol Oral Cir Bucal 2005; 10(Suppl 1):E45-56.
2. Ali SA, Karthigeyan S, Deivanai M, Kumar A. Implant rehabilitation for atrophic maxilla: a review. J Indian Prosthodont Soc 2014; 14:196-207.
3. Chiapasco M, Casentini P, Zaniboni M. Bone augmentation procedures in implant dentistry. Int J Oral Maxillofac Implants 2009; 24(Suppl):237-59.
4. Candel-Marti E, Carrillo-Garcia C, Penarrocha-Oltra D, Penarrocha-Diago M. Rehabilitation of atrophic posterior maxilla with zygomatic implants: review. J Oral Implantol 2012; 38:653-57.
5. Tran AQ, Reyes-Capo DP, Patel NA, Pasol J, Capo H, Wester ST. Zygomatic dental implant induced orbital fracture and inferior oblique trauma. Orbit 2018:1-4.
6. Menini M, Signori A, Tealdo T, et al. Tilted implants in the immediate loading rehabilitation of the maxilla: a systematic review. J Dent Res 2012; 91:821-27.
7. Wakimoto M, Matsumura T, Ueno T, Mizukawa N, Yanagi Y, Iida S. Bone quality and quantity of the anterior maxillary trabecular bone in dental implant sites. Clin Oral Implants Res 2012; 23:1314-19.
8. Santarelli A, Mascitti M, Orsini G, et al. Osteopontin, osteocalcin and OB-cadherin expression in Synthetic nanohydroxyapatite vs bovine hydroxyapatite cultured Osteoblastic-like cells. J Biol Regul Homeost Agents 2014; 28:523-29.
9. Sharma A, Rahul GR. Zygomatic implants/fixture: a systematic review. J Oral Implantol 2013; 39:215-24.
10. Nkenke E, Hahn M, Lell M, et al. Anatomic site evaluation of the zygomatic bone for dental implant placement. Clin Oral Implants Res 2003; 14:72-79.
11. Balan I, M DIG, Lauritano D, Carinci F. Treatment of severe atrophic maxilla with zygomatic implants: a case series. Oral Implantol (Rome) 2017; 10:317-24.
12. Grecchi F, Bianchi AE, Siervo S, Grecchi E, Lauritano D, Carinci F. A new surgical and technical approach in zygomatic implantology. Oral Implantol (Rome) 2017; 10:197-208.